SISSA
Scuola
Internazionale
Superiore di
Studi Avanzati

Physics Area — PhD course in
Statistical Physics

STOCHASTIC DYNAMICS IN COMPLEX LANDSCAPES
From fluctuating fields to quenched disorder

Candidate:
Davide Venturelli

Advisor:
Prof. Andrea Gambassi

Academic Year 2022-2023

Acknowledgements

My first thought goes to my supervisor Andrea, who most of all succeeded in passing me a scientific method — as well as his attention for the details and for a clear and effective communication. Thanks for being a great teacher, and for promoting my scientific growth and independence.

A huge thanks goes to my family and friends, scattered between Brescia, Roma, and elsewhere: you have always been the pillars of my happiness and my mental health, and always remained close in spite of the geographical distance that most of the time separates us. Thanks in particular to Giovanni, Alessandro, Stefano, Luca, Davide, Silvia, Filippo, Giacomo, Mattia, Andrea, and Luca. Thank you Inês, for always being here for me.

Thank you Benjamin, for being not only a friend and a great office mate, but also a guide and an example, especially at the beginning of my PhD (when I most needed one). Thanks to my other office mates — last but not least Daria — for always maintaining a cheerful and welcoming working environment, and for tolerating my unnerving mumbling in Italian. Thank you Alessandro and Guido, for your frankness and for taming my unjustified enthusiasm.

Thanks to all the wonderful people I met in SISSA and in Trieste, who made it a place I will cherish. The list is long and I will not attempt sketching it, lest I forget someone, but I especially thank Lorenzo and Luca for sharing in so many everyday experiences and emotions. Thanks Sarah, because since your appearance you have remained a solid example of determination.

Thank you Angelo Rosa, for letting me assist you in your Quantum Mechanics course — for reasons I only partly understand, teaching gives me an immense pleasure. Thanks to the SISSA Student Council, which felt to me like the most rewarding political endeavour I have ever been part of. Many thanks to Morgana, Elisa, Marko, Luca, and Elisa, for sharing the joys of music.

Thank you Leticia F. Cugliandolo, Marco Tarzia and Greg Schehr, for your warm and kind hospitality during my visiting periods in LPTHE and LPTMC, at Sorbonne Université. I also thank all those who made my staying in Paris a formidable experience — among which Brieuc, Vincent, Jade, Zachary, Andrei, Francesco, Marc, David — and who made me wish to return.

Thanks to my other scientific collaborators, among which are Irene Giardina, Emanuele Loffredo, Édgar Roldán, Asja Jelic, and Pierluigi Muzzeddu. Dealing with the pandemic has been harsh overall, but I found it both peculiar and rewarding to write a paper with Markus Gross only through epistolary exchanges, without ever meeting in person (at least so far).

I acknowledge Stack Exchange, where countless silly doubts on Wolfram Mathematica were settled, and my local gym, where a surprisingly large chunk of my scientific progress took place.

Finally, I thank Ignacio A. Martínez for inviting me to visit his experimental soft-matter lab, thus giving me a concrete idea of what I am talking about in this thesis — it is reassuring to be occasionally reminded that this is not pure mathematics.

This page intentionally not left blank.

Contents

Introduction

Stochastic dynamics describes the temporal evolution of systems that are subject to the action of *random* forces, possibly along with other deterministic forces which are more familiar from classical mechanics. It hinges on the idea that a large number of deterministic forces to which a system may be subject — e.g., due to the interaction with a larger system — may be replaced by a single, stochastic term [1, 2]. This idea is revolutionary, and understanding it requires a conceptual leap which is central in modern physics: namely the inclusion, in our descriptions of the physical reality, of *effective* variables that do not have a direct counterpart in terms of physical observables, but which are rather instrumental to the prediction of the behavior of the latter.

In statistical physics, which aims at understanding the behavior of systems made up of a large number of microscopic units, the construction of effective descriptions passes through *coarse-graining*. Indeed, quite generally, even admitting that one could write down exact equations of motion for each of the individual units that compose a many-body physical system, still the simultaneous solution of such equations would remain elusive. This is both due to computational limitations, and to uncertainties in the knowledge of the initial conditions — the latter being inherent in the quantum case, and whose propagation is typically unconstrained. This humble realization has arguably lain at the bottom of statistical physics from its very foundations [3], and is sufficient to wash away any *reductionist* claim that Nature could be completely understood (and reconstructed) once we grasp the fundamental laws governing its smallest units [4]. Physicists have thus long since devised methods to reduce the number of variables required to characterize a system, focusing only on a few *effective* ones by discarding irrelevant information, and this way progressing towards mesoscopic (coarse-grained) descriptions. The very idea of renormalization, one of the pillars of modern theoretical physics [5, 6], ultimately stems from the realization that the large-scale critical properties of a system may not be affected by its microscopic details, but depend merely on its symmetries and spatial dimensionality. It is upon coarse-graining that such emergent universality becomes manifest. Similarly, emergent collective properties — which do not pertain to the behavior of each single unit — only become evident when subsuming the (numerous) initial microscopic variables into a small number of appropriate *order parameters*.

Within the realm of stochastic dynamics, coarse-graining often refers to the practice of focusing on the dynamics of a small subset of the initial dynamical degrees of freedom of the system, typically by integrating/projecting out the others, which yields effective evolution equations for the former [7–10]. One often considers the dynamics of only one amongst the initial dynamical variables, calling it the *tracer*, while all the other variables constitute the *bath*. A paradigmatic example is that of a tracer colloidal particle immersed in a fluid substrate, and thus subject to

frequent collisions with the fast-moving molecules that constitute the substrate. Within a description based on Brownian motion [1, 2, 11] — which may be viewed as the most extreme form of coarse-graining for this type of systems — the substrate is represented as a spatially structureless bath. Furthermore, it is assumed that the bath relaxes rapidly (in comparison to the time scale that characterizes the motion of the tracer particle), allowing to neglect the feedback reaction of the tracer on the bath itself. In view of the central limit theorem, the overall effect of the bath variables on the tracer then becomes statistically equivalent to a white Gaussian random variable [11]. This way the trajectory of the tracer gets described by a *stochastic process*, while the initial multitude of bath variables is replaced by a single, effective noise, whose values at different space-time points are mutually uncorrelated. This latter simplification allows for a powerful mathematical description in terms of a *Markovian* process, i.e., the Langevin equation [12], in which the current state of the tracer determines its subsequent stochastic evolution, without retaining memory of its past trajectory.

In nature, however, the motion of colloidal particles immersed in real fluid media often defies a description based on Brownian motion. Indeed, as the particle acquires momentum from the surrounding fluctuating molecules, it also induces a displacement of the adjacent fluid. In turn, the displaced fluid exerts a feedback effect on the particle — this has been referred to as *hydrodynamic memory* in the literature [13], and it generally gives rise to correlations which are not accounted for by Brownian motion [14, 15]. Accordingly, when they are probed over sufficiently small time scales, all media are expected to reveal spatio-temporal correlations. In some media the time scale that characterizes these correlations can be particularly large, eventually comparable to the one characterizing the particle motion: this is the case, for instance, of viscoelastic fluids [16], which feature macroscopically long structural stress-relaxation times. Spatio-temporal correlations of the environment are also known to affect the dynamics of diverse physical systems such as inclusions in lipid membranes [17–21], microemulsions [22–25], as well as defects in ferromagnetic systems [26–31]. These correlations become long-ranged and particularly relevant when the environment is close to a critical point, as in the case of colloidal particles in binary liquid mixtures [32–37], which have recently received significant attention (for reasons that we will soon clarify).

To overcome some of the assumptions underlying Brownian motion — in particular the requirement that the medium relaxes instantaneously — particles in contact with a thermally fluctuating complex environment have often been described by using the generalized Langevin equation, in which the interaction with the medium is encoded in a friction memory kernel [7, 38]. However, this framework still relies on the absence of spatial structure within the medium, and thus it cannot describe the spatial distribution of the work and energy flows that are expected to take place between the medium and the particles. Moreover, it is unable to account for the *fluctuation-induced* forces experienced by objects that are immersed in a correlated medium, and which thus modify its fluctuations. A prominent example of these forces is provided by the *critical Casimir forces* felt by colloidal particles in near-critical binary liquid mixtures (which we

[1] In conjunction with a viscous friction term — see, c.f., Section 1.1.

mentioned above [32–37]). The properties of these forces, which are the thermal counterpart of the celebrated Casimir force in electromagnetism [39], are relatively well understood in equilibrium [40–45], while much remains to be unveiled about their nonequilibrium properties. Indeed, field-mediated forces do not propagate instantaneously, and this becomes relevant when the included objects are displaced faster than the typical relaxation time scales that characterize the fluctuating medium.

As will be argued in this thesis, a lot can be learned by analyzing the simplified setting of one or more Brownian particles coupled to a thermally fluctuating scalar field, which influence each other along their stochastic evolution. In this setting, the medium is no longer described solely in terms of a structureless white noise, but rather by the combination of noise with a spatially-resolved (and time-evolving) order parameter field $\phi(\mathbf{x}, t)$. A spatially confining potential can then be assumed to act on the particle, eventually injecting work into the system and driving it out of equilibrium. This provides a cartoon for an optically trapped colloid immersed in a fluid close to its bulk critical point, and thus mimics the setup adopted in microrheology experiments [32–36, 46]. Focusing on the effective dynamics of the tracer particle(s) then reveals numerous interesting dynamical features, which reflect the (critical) properties of the underlying medium — e.g., its spatial and temporal correlations — and which are already evident when the coupling between the particle and the field is weak. This paradigm, which was introduced a decade ago to tackle the diffusion of a Brownian particle in a fluctuating environment (and in particular to compute the corrections to its diffusion coefficient [28–31]), will be revisited in Chapters 2 to 5 to address nonequilibrium settings, to analyze the field-mediated forces exchanged between particles, to extend concepts of stochastic thermodynamics in the presence of spatio-temporal correlations, and finally to assess the effects of spatially confining boundaries. In particular, after providing some theoretical background in Chapter 1, the rest of the thesis is structured as follows:

- In Chapter 2 we consider a particle in contact with a fluctuating scalar Gaussian field and confined by a harmonic potential. We will show that, when the particle is displaced from its equilibrium position, its average position during relaxation displays algebraic tails, which we characterize in terms of the critical properties of the underlying medium.

- In Chapter 3 we consider two trapped particles in contact with the same fluctuating field. Mimicking the setting of an experiment with colloidal particles in a binary liquid mixture reported in Ref. [35], we assume that one of the two traps is oscillated periodically, and we characterize the field-induced response of the particle sitting in the other, fixed trap.

- In Chapter 4 we extend the formalism of stochastic thermodynamics to give a unified description of the energy and entropy flows for a particle in a correlated environment, with special focus on the case in which work is injected into the system by a steadily-driven harmonic trap. In passing, we analyze the average relaxation trajectory of the particle when it is initially displaced from its steady-state position (similarly to Chapter 2, but in a moving trap), and demonstrate that it displays oscillations — in contrast to Markovian

overdamped systems, but analogously to recent experimental observations in viscoelastic media [47].

- In Chapter 5 we analyze the effective particle dynamics and the resulting steady state when the field is spatially confined by boundaries, which impose specific boundary conditions. We do so by developing an *ad hoc* adiabatic elimination method, hinging on the field being fast (or even *quenched*) in comparison to the time scale characterizing the tracer particle. The lowest order in this adiabatic approximation corresponds to the tracer diffusing in a static field-induced potential, which is nontrivial due to the presence of boundaries.

Finally, another fundamental instrument used in statistical physics to represent static disordered landscapes — as well as another example in which stochastic noise plays a role in the effective modeling of large interacting systems — is provided by *random matrices* [48, 49], to which Chapter 6 is devoted. Random matrix theory is a fascinating and active field of research, whose origins are usually traced back to Wigner's suggestion to use an effective Hamiltonian with randomly distributed entries to reproduce the spectra observed in heavy atoms nuclei [50]. Although actual coarse-grained derivations are only available in a few cases, it is believed that many physical systems — ranging from quantum systems to wave scattering, complex ecosystems, and financial markets — admit an effective description in terms of random matrices. Like field theories, random matrix models are also grouped into universality classes which reflect the symmetries of the underlying physical system. The simplest example is provided by the Gaussian orthogonal ensemble (GOE): in this case, the entries of the matrix which is assumed to describe the interactions between the system components are taken to be Gaussian random variables. In turn, the spectral properties of a matrix ensemble (e.g., the presence of gaps in their spectra) can affect the dynamical evolution of a system that has such a matrix as its Hamiltonian. In the last decades, a host of analytical techniques have thus been developed to assess the spectral properties of these ensembles [49]. In this respect, fruitful parallelisms have been established with the techniques used in the fields of spin glasses and disordered systems, due to the formal analogy between random matrix ensembles, and the Hamiltonian of spin systems in the presence of quenched disorder. One notable example is the *replica* method [51], which will be widely employed in Chapter 6 to analyze the spectral statistics of a modified GOE ensemble, known as the generalized Rosenzweig-Porter model.

Each Chapter of this thesis is accompanied by an Appendix, where we provide details of the derivations to support the findings illustrated in the main text, and by a summary, where the latter are recapitulated. Finally, a few open questions and future perspectives are outlined in the general concluding section.

List of publications

This thesis is based on the following publications and preprints:

(i) **Davide Venturelli**, Francesco Ferraro, and Andrea Gambassi,
Nonequilibrium relaxation of a trapped particle in a near-critical Gaussian field,
Phys. Rev. E **105**, 054125 (2022) — published 16 May 2022;

(ii) **Davide Venturelli** and Andrea Gambassi,
Inducing oscillations of trapped particles in a near-critical Gaussian field,
Phys. Rev. E **106**, 044112 (2022) — published 11 October 2022;

(iii) **Davide Venturelli** and Markus Gross,
Tracer particle in a confined correlated medium: an adiabatic elimination method,
J. Stat. Mech. (2022) 123210 — published 29 December 2022;

(iv) **Davide Venturelli**, Leticia F. Cugliandolo, Grégory Schehr, and Marco Tarzia,
Replica approach to the generalized Rosenzweig-Porter model,
SciPost Phys. **14**, 110 (2023) — published 12 May 2023;

(v) **Davide Venturelli** and Andrea Gambassi,
Memory-induced oscillations of a driven particle in a dissipative correlated medium,
2023 New J. Phys. **25** 093025 — published 12 September 2023;

(vi) **Davide Venturelli**, Sarah A. M. Loos, Benjamin Walter, Édgar Roldán, and Andrea Gambassi,
Stochastic thermodynamics of a probe in a fluctuating correlated field,
arXiv:2305.16235 — submitted 25 May 2023.

During my PhD I also co-authored the following publication — resulting from a collaboration on *active matter* topics with Prof. Irene Giardina (Sapienza, Rome), building upon the project I had initiated during my Master's thesis [52] — but, in order to keep the coherence of the presentation, it will not be discussed here:

(vii) Emanuele Loffredo, **Davide Venturelli**, and Irene Giardina,
Collective response to local perturbations: how to evade threats without losing coherence,
2023 Phys. Biol. **20** 035003 — published 11 April 2023.

1

Theoretical background

In this Chapter we provide some background on the theory of stochastic processes, with the primary aim of setting the notation for the rest of this thesis. Most derivations will thus be omitted for the sake of conciseness.

1.1 Langevin and Fokker-Planck equations

In this thesis we will often deal with stochastic differential equations of the form

$$\dot{\mathbf{X}}(t) = \nu \mathbf{F}(\mathbf{X}(t), t) + \xi(t), \tag{1.1}$$

where the *white noise* term $\xi(t)$ is a Gaussian variable with zero mean and variance

$$\left\langle \xi_i(t)\xi_j(t') \right\rangle = \Omega_x \delta_{ij}\delta(t \quad t') \equiv 2\nu T \delta_{ij}\delta(t \quad t'). \tag{1.2}$$

To understand its significance, let us first consider the Newton equation for an isolated particle of mass m at position $\mathbf{X}(t)$, i.e., $m\ddot{\mathbf{X}} = \mathbf{F}$, where

$$\mathbf{F}(\mathbf{X}(t), t) = \quad \nabla_{\mathbf{X}} \mathcal{U}(\mathbf{X}, t) + \mathbf{F}_{\text{ext}}(\mathbf{X}, t) \tag{1.3}$$

may represent a force arising from a conservative potential $\mathcal{U}(\mathbf{X}, t)$ and/or an external drive $\mathbf{F}_{\text{ext}}(\mathbf{X}, t)$. Within (underdamped) Brownian motion, one amends the Newton equation by a friction and a noise term,

$$m\ddot{\mathbf{X}}(t) = \mathbf{F}(\mathbf{X}(t), t) + \nu^{\ 1} \left[\quad \dot{\mathbf{X}}(t) + \xi(t) \right], \tag{1.4}$$

which phenomenologically account for the overall, coarse-grained effect of all the fast variables that have not been included in the description above [11, 12]. The latter are assumed to evolve on much shorter timescales than the one characterizing the dynamics of the particle at $\mathbf{X}(t)$, and thus they act on it as an equilibrium *thermal bath* at temperature T — i.e., the one appearing in the noise variance in Eq. (1.2). The Gaussian character of the noise $\xi(t)$ follows as a natural consequence of the central limit theorem [11]. Above, $\nu^{\ 1}$ is a friction coefficient, and its inverse ν is called the *mobility* of the particle. In the *overdamped* limit in which inertial effects are negligible, we can discard the term on the left-hand-side of Eq. (1.4), so that the latter reduces to Eq. (1.1).

Each realization of the stochastic noise $\xi(t)$ in the Langevin equation (1.1) generates a different trajectory $\mathbf{X}(t)$. One may rather be interested in the one-point probability density

$$P_1(\mathbf{X}, t) = \langle \delta(\mathbf{x} \quad \mathbf{X}(t)) \rangle , \tag{1.5}$$

[1] Here and henceforth we adopt units in which the Boltzmann constant $k_B \equiv 1$, so as to omit it from the noise variances such as $\Omega_x = 2\nu k_B T$.

where the *ensemble* average $\langle \dots \rangle$ is understood over all possible realizations of $\xi(t)$. The evolution of $P_1(\mathbf{X}, t)$ is ruled by the Fokker-Planck equation corresponding to the Langevin equation (1.1), namely [53, 54]

$$\partial_t P_1(\mathbf{x}, t) = \nabla_{\mathbf{x}} \cdot \left[\nu \mathbf{F}(\mathbf{x}, t) + \frac{\Omega_x}{2} \nabla_{\mathbf{x}} \right] P_1(\mathbf{x}, t). \tag{1.6}$$

A derivation of such Fokker-Planck equation along the lines of Ref. [54] is provided in Appendix C.2.1 for a more general case. In the absence of external driving and for a time-independent potential — i.e., $\mathbf{F}_{\text{ext}}(\mathbf{X}, t) \equiv 0$ and $\mathcal{U}(\mathbf{x}, t) = \mathcal{U}(\mathbf{x})$ in Eq. (1.3) — the dynamics prescribed by Eqs. (1.1) and (1.2) satisfies detailed balance. Accordingly, upon setting $\partial_t P_1(\mathbf{x}, t) = 0$ in Eq. (1.6), it is simple to check that the latter admits the equilibrium solution $P_1^{(\text{eq})}(\mathbf{x}) \propto \exp\left[\frac{1}{T} \mathcal{U}(\mathbf{x}) \right]$, corresponding to the canonical distribution of the particle in the potential $\mathcal{U}(\mathbf{x})$.

Note that, upon replacing $\xi(t)$ by $g(\mathbf{X}(t))\xi(t)$ in Eq. (1.1), the noise term becomes *multiplicative* rather than *additive*. To give meaning to the so-obtained equation, one needs to specify the rule of stochastic calculus (e.g., Itô or Stratonovich), which fixes the discretization convention adopted for the Gaussian white noise [11]. Accordingly, the corresponding Fokker-Planck equation becomes sensitive to the choice of the calculus, and acquires new *spurious drift* terms for any convention other than Itô[2]. In this thesis, however, any occurrence of a multiplicative noise will be in conjunction with *colored*, rather than white, Gaussian noise — see, c.f., Section 1.4. In the presence of colored noise, any ambiguity due to the choice of the discretization convention is lifted [53, 56, 57]; however, the system becomes non-Markovian, and thus it is in general no longer possible to write a closed equation for $P_1(\mathbf{x}, t)$ which is local in time [58]. We will come back to this point in Section 3.2.1.

Two examples of Langevin equations that will be largely employed in this thesis are presented in the next two sections.

1.2 The Ornstein-Uhlenbeck process

The motion of an overdamped Brownian particle in a harmonic potential of stiffness κ

$$\mathcal{U}(\mathbf{x}, t) = \frac{\kappa}{2} [\mathbf{x} \quad \mathbf{x}_F(t)]^2 \tag{1.7}$$

(whose center is possibly moving deterministically according to $\mathbf{x}_F(t)$) is ruled by the Ornstein-Uhlenbeck process. Its Langevin equation reads

$$\dot{\mathbf{X}}(t) = \quad \nu \nabla_{\mathbf{X}} \mathcal{U}(\mathbf{X}, t) + \xi(t) = \quad \nu\kappa \, [\mathbf{X}(t) \quad \mathbf{x}_F(t)] + \xi(t) \,, \tag{1.8}$$

with the noise variance given in Eq. (1.2). Each component X_j of the particle position $\mathbf{X}$ is ruled by an independent Gaussian and Markovian process. The propagator $P_{1|1}(\mathbf{X}, t|\mathbf{X}_0, t_0)$ is thus Gaussian [53], with

$$P_{1|1}(\mathbf{X}, t|\mathbf{X}_0, t_0) = \left[\frac{1}{\sqrt{2\pi}\sigma(t)} \right]^d \exp\left[\frac{|\mathbf{X} \quad \mathbf{m}(t)|^2}{2\sigma^2(t)} \right], \tag{1.9}$$

[2] See, e.g., Chap. 6 in Ref. [55].

where the symbol $(\dots|\dots)$ indicates a conditional average, and d is the spatial dimensionality. This expression contains the expectation value $\mathbf{m}(t)$ of the particle position

$$\mathbf{m}(t) \equiv \langle \mathbf{X}(t)|\mathbf{X}(t_0) = \mathbf{X}_0\rangle = \mathbf{X}_0 e^{\ \gamma(t\ \ t_0)} + \gamma \int_{t_0}^{t} \mathrm{d}s\, e^{\ \gamma(t\ \ s)} \mathbf{x}_F(s)\,, \tag{1.10}$$

and its variance which is, by the isotropy of the problem, the same for each component X_j:

$$\sigma^2(t) \equiv \left\langle X_j^2(t)|X_j(t_0) = (\mathbf{X}_0)_j \right\rangle \quad m_j^2(t) = \frac{T}{\kappa}\left[1 \quad e^{\ 2\gamma(t\ \ t_0)}\right]. \tag{1.11}$$

Above we introduced the (inverse) relaxation timescale

$$\tau_\kappa{}^1 = \nu\kappa \equiv \gamma, \tag{1.12}$$

and we assumed the particle to start at time $t = t_0$ at position $\mathbf{X}(t = t_0) = \mathbf{X}_0$. Note that, in general, $P_{1|1}(\mathbf{X}, t|\mathbf{X}_0, t_0) \neq P_{1|1}(\mathbf{X}, t \quad t_0|\mathbf{X}_0, 0)$, because the explicit time dependence in $\mathbf{x}_F(t)$ breaks the time-translational invariance of the problem. By means of the Langevin equation (1.8), one can finally compute the connected two-time correlation function

$$\begin{aligned} C(t_1, t_2) &\equiv \left\langle X_j(t_1)X_j(t_2)\right\rangle_c = \left\langle \left[X_j(t_1) \quad \langle X_j(t_1)\rangle\right]\left[X_j(t_2) \quad \langle X_j(t_2)\rangle\right]\right\rangle \\ &= \frac{T}{\kappa}\left[e^{\ \gamma|t_2\ \ t_1|} \quad e^{\ \gamma(t_1+t_2\ \ 2t_0)}\right] \underset{t_0\to\ \infty}{\longrightarrow} \frac{T}{\kappa} e^{\ \gamma|t_2\ \ t_1|}, \end{aligned} \tag{1.13}$$

which, again, is independent of the value of j, while correlations $\langle X_j(t_1)X_{i\neq j}(t_2)\rangle_c$ vanish. At long times (e.g., $t_0 \to \ \infty$), $C(t_1, t_2)$ becomes time-translational invariant, and the system attains the thermal equilibrium described by the probability distribution

$$P_1^{\mathrm{st}}(\mathbf{x}) = (2\pi T/\kappa)^{\ d/2} \exp\left[\ \kappa x^2/(2T)\right]. \tag{1.14}$$

1.3 The free Gaussian) field

Equation (1.8) describes the stochastic evolution of each of the d spatial components of the position $\mathbf{X}(t)$ of a particle. In this Section we focus instead on the evolution of a scalar *field*, whose value $\phi(\mathbf{x}, t) \in \mathbb{R}$ is defined in correspondence of every spatial point $\mathbf{x} \in \mathbb{R}^d$ (which form a continuum). We thus consider its stochastic evolution when subject to the Langevin equation

$$\partial_t \phi(\mathbf{x}, t) = \quad D(i\boldsymbol{\nabla}) \ \frac{\delta \mathcal{H}_\phi}{\delta\phi(\mathbf{x}, t)} + \eta(\mathbf{x}, t) = \quad D(i\boldsymbol{\nabla}) \ \left[(r \quad \nabla^2)\phi(\mathbf{x}, t)\right] + \eta(\mathbf{x}, t) \tag{1.15}$$

(where $\delta/\delta\phi$ indicates a functional derivative), and to the quadratic Hamiltonian

$$\mathcal{H}_\phi[\phi] = \int \mathrm{d}^d\mathbf{x} \left[\frac{1}{2}(\boldsymbol{\nabla}\phi)^2 + \frac{r}{2}\phi^2\right]. \tag{1.16}$$

In the latter, the parameter r measures the deviation from the *critical point* $r = 0$, at which the *correlation length* $\xi = r^{\ 1/2}$ diverges (its role will be elucidated shortly). In the Langevin equation (1.15), the parameter takes the value $= 0$ for a non-conserved dynamics of the order

parameter ϕ, or $\quad = 2$ if ϕ is subject to local conservation during the evolution, in the sense that Eq. (1.15) can then be cast in the form $\partial_t \phi(\mathbf{x}, t) = \quad \boldsymbol{\nabla} \quad \mathbf{J}(\mathbf{x}, t)$ for a suitable current $\mathbf{J}(\mathbf{x}, t)$. These two choices of $\quad$ correspond to model A and model B in the classification of Ref. [59], in which the self-interaction term $\sim \phi^4$ is neglected, i.e., within the Gaussian approximation. Note that, for $\quad = 0$, Eq. (1.15) formally resembles the Langevin equation (1.8) for $\mathbf{X}(t)$, upon replacing the gradient operator $\boldsymbol{\nabla}_{\mathbf{X}}$ by a functional derivative. Finally, $\eta(\mathbf{x}, t)$ is a white Gaussian noise field with zero mean and variance

$$\langle \eta(\mathbf{x}, t)\eta(\mathbf{x}', t')\rangle = 2DT(i\boldsymbol{\nabla}) \quad \delta^d(\mathbf{x} \quad \mathbf{x}')\delta(t \quad t'), \tag{1.17}$$

with D and T denoting, respectively, the mobility of the field and the temperature of the bath.

The Fokker-Planck equation corresponding to Eq. (1.15) is analogous to Eq. (1.6), i.e. [60, 61],

$$\partial_t P_1([\phi], t) = \int \mathrm{d}^d x \, \frac{\delta}{\delta\phi(\mathbf{x})} \left[D(i\nabla) \quad \frac{\delta \mathcal{H}_\phi}{\delta\phi(\mathbf{x})} + DT(i\nabla) \quad \frac{\delta}{\delta\phi(\mathbf{x})} \right] P_1([\phi], t). \tag{1.18}$$

In particular, Eq. (1.18) admits as its equilibrium solution the canonical distribution

$$P_1^{(\mathrm{eq})}[\phi] \propto \exp\left\{ \quad \frac{1}{T}\mathcal{H}_\phi[\phi] \right\} = \exp\left\{ \quad \frac{1}{2T} \int_{\mathbb{R}} \frac{\mathrm{d}^d q}{(2\pi)^d} \phi_{\mathbf{q}} (q^2 + r) \phi \quad _{\mathbf{q}} \right\}, \tag{1.19}$$

where we introduced the Fourier convention $f(\mathbf{x}) = \int [\mathrm{d}^d q \,/(2\pi)^d] \exp(i\mathbf{q}\cdot\mathbf{x}) f_{\mathbf{q}}$. Since $\mathcal{H}_\phi$ is Gaussian, the equilibrium fluctuations of ϕ can be simply obtained by first constructing the generating functional [62]

$$\mathcal{Z}[j] = \int \mathcal{D}\phi \, \exp\left\{ \quad \frac{1}{T}\mathcal{H}_\phi[\phi] \quad \int \mathrm{d}^d x \, j(\mathbf{x})\phi(\mathbf{x}) \right\} \propto \exp\left(\frac{T}{2} \int \frac{\mathrm{d}^d q}{(2\pi)^d} \frac{j_{\mathbf{q}} j \quad _{\mathbf{q}}}{q^2 + r} \right), \tag{1.20}$$

and thus

$$\left\langle \phi(\mathbf{x})\phi(\mathbf{0}) \right\rangle = \int_{\mathbb{R}} \frac{\mathrm{d}^d q}{(2\pi)^d} e^{i\mathbf{q}\cdot\mathbf{x}} \left. \frac{\delta^2 \mathcal{Z}[j]}{\delta j_{\mathbf{q}} \delta j \quad _{\mathbf{q}}} \right|_{j=0} = T \int_{\mathbb{R}} \frac{\mathrm{d}^d q}{(2\pi)^d} \frac{e^{i\mathbf{q}\cdot\mathbf{x}}}{q^2 + r} \equiv T\xi^{2 \quad d} g(x/\xi), \tag{1.21}$$

with $x \equiv |\mathbf{x}|$. In the last step we rescaled momenta as $\quad \equiv q\xi$, thus identifying the scaling function

$$g(y) \equiv \int_{\mathbb{R}} \frac{\mathrm{d}^d}{(2\pi)^d} \frac{e^{i\mathbf{z}\cdot\mathbf{y}}}{^2 + 1} = \frac{y^{1 \quad d/2}}{(2\pi)^{d/2}} K_{d/2 \quad 1}(y) \underset{y \gg 1}{\simeq} \frac{(\pi y)^{(1 \quad d)/2}}{2^{(1+d)/2}} e^{\quad y}, \tag{1.22}$$

where K_ν is a modified Bessel function of the second kind[3] [63]. In general, $\langle \phi(\mathbf{x})\phi(\mathbf{0})\rangle$ in Eq. (1.21) rapidly decays to zero for large values of x/ξ, and in this sense the parameter $r = \xi^{\quad 2}$ in the Hamiltonian $\mathcal{H}_\phi$ in Eq. (1.16) controls the spatial range of the field fluctuations at equilibrium. In particular, ξ diverges at the critical point $r = 0$, and the large-x behavior of $\langle \phi(\mathbf{x})\phi(\mathbf{0})\rangle$ thus becomes algebraic [62].

We now rewrite Eqs. (1.15) and (1.17) in Fourier space, which gives[4]

$$\dot{\phi}_{\mathbf{q}}(t) = \quad _q \phi_{\mathbf{q}}(t) + \eta_{\mathbf{q}}(t), \tag{1.23}$$

$$\langle \eta_{\mathbf{q}}(t)\eta_{\mathbf{q}'}(t')\rangle = \Omega_\phi(q)\delta^d(\mathbf{q} + \mathbf{q}')\delta(t \quad t') \equiv 2DTq \quad \delta^d(\mathbf{q} + \mathbf{q}')\delta(t \quad t'), \tag{1.24}$$

[3] In $d = 1$ and 3, for instance, Eq. (1.22) simplifies to $g(y) = \exp(\quad y)/2$ and $g(y) = \exp(\quad y)/(4\pi y)$, respectively.

[4] The common habit of carrying around $(2\pi)^d$ factors in these formulas can be avoided by normalizing the delta distribution in Fourier space as $\int [\mathrm{d}^d q \,/(2\pi)^d] \delta^d(\mathbf{q}) = 1$. In this thesis we will adopt this definition.

where we introduced the (inverse) relaxation timescale of the field

$$\tau_\phi^{-1}(q) = \quad _q \equiv Dq \ \ (q^2 + r). \tag{1.25}$$

This shows that the relaxation time $\tau_\phi(q \sim 0)$ for the long-wavelength Fourier modes of the field may become arbitrarily large for model A dynamics ($= 0$) at $r = 0$. The same happens for model B dynamics ($= 2$) for generic values of r, i.e., also off-criticality, due to the presence of the conservation law for which $\tau_\phi^{-1}(q \to 0) = 0$. These long-wavelength modes are always present in the bulk, while they are cut-off in a confined geometry such as that considered in Refs. [64, 65], and here in, c.f., Chapter 5.

The Green function of Eq. (1.23), i.e., the average solution $\langle \phi_{\mathbf{q}}(t) \rangle$ of

$$\dot{\phi}_{\mathbf{q}}(t) = \quad _q \phi_{\mathbf{q}}(t) + \eta_{\mathbf{q}}(t) + \delta(t), \tag{1.26}$$

is called the *response propagator* of the free field, and it reads

$$G_q(t) = e \quad ^{_q t} \Theta(t), \tag{1.27}$$

where $\Theta(t)$ is the Heaviside step function. To compute the two-point function, we note that Eq. (1.23) is formally identical to that of the Ornstein-Uhlenbeck particle in Eq. (1.8), so it is easy to derive [66]

$$\langle \phi_{\mathbf{q}}(s_1)\phi_{\mathbf{p}}(s_2) \rangle = \delta^d(\mathbf{p} + \mathbf{q}) C_q^D(s_1, s_2) + G_q(s_1 \quad t_0) G_p(s_2 \quad t_0) \phi_{\mathbf{q}}(t_0)\phi_{\mathbf{p}}(t_0), \tag{1.28}$$

for times s_1, s_2 larger than the initial time t_0. Here

$$C_q^D(s_1, s_2) = \frac{T}{q^2 + r} \left[e \quad ^{_q |s_2 \ \ s_1|} \quad e \quad ^{_q (s_1 + s_2 \ \ 2t_0)} \right] \tag{1.29}$$

is the correlation function corresponding to the case of Dirichlet initial condition $\phi_{\mathbf{q}}(t_0) \equiv 0$ (to be compared with Eq. (1.13)), such that $C_q^D(s_1, s_2 = t_0) = C_q^D(s_1 = t_0, s_2) = 0$. It also coincides with the connected correlation function $\langle \phi_{\mathbf{q}}(s_1)\phi_{\mathbf{p}}(s_2) \rangle_c$ computed with any other *fixed* initial condition $\phi_{\mathbf{q}}(t_0)$. For $t_0 \to \quad \infty$ we recover from Eq. (1.28) the correlation function in the stationary state, i.e., $\langle \phi_{\mathbf{q}}(s_1)\phi_{\mathbf{p}}(s_2) \rangle \to \delta^d(\mathbf{p} + \mathbf{q}) C_q(s_2 \quad s_1)$ with the equilibrium correlator

$$C_q(\tau) = \frac{T}{q^2 + r} e \quad ^{_q |\tau|}, \tag{1.30}$$

which is time-translational invariant, as expected. Alternatively, if we assume that $\phi_{\mathbf{q}}(t_0)$ is randomly drawn from the stationary distribution of the field in Eq. (1.19) and we average the correlation function in Eq. (1.28) over all possible initial conditions, we get $\langle \phi_{\mathbf{q}}(t_0)\phi_{\mathbf{p}}(t_0) \rangle_{\text{i.c.}} = \delta^d(\mathbf{p} + \mathbf{q}) T/(q^2 + r)$, and again it follows that $\langle \phi_{\mathbf{q}}(s_1)\phi_{\mathbf{p}}(s_2) \rangle_{\text{i.c.}} = \delta^d(\mathbf{p} + \mathbf{q}) C_q(s_2 \quad s_1)$.

The linear susceptibility $\chi_q(t)$ of the free field is usually defined by adding to $\mathcal{H}_\phi$ a linear coupling $\mathcal{H}_\phi \to \mathcal{H}_\phi \quad \int \mathrm{d}^d x \, h(\mathbf{x})\phi(\mathbf{x})$, so that from Eq. (1.15) it follows

$$\chi_q(t, t_0) = \chi_q(t \quad t_0) \equiv \frac{\delta \langle \phi_{\mathbf{q}}(t) \rangle}{\delta h_{\mathbf{q}}(t_0)} = Dq \ \ G_q(t \quad t_0). \tag{1.31}$$

Moreover, $\chi_q(t)$ is linked to the equilibrium correlator $C_q(t)$ in Eq. (1.30) by the fluctuation-dissipation theorem [54]

$$T\chi_q(\tau) = \quad \Theta(\tau)\frac{\partial}{\partial\tau}C_q(\tau). \tag{1.32}$$

It is also straightforward to derive the relation

$$C_q^D(s_1, s_2) = \Omega_\phi(q)\int_{t_0}^{\min(s_1,s_2)} \mathrm{d}u\, G_q(s_1 \quad u)G_{\ q}(s_2 \quad u), \tag{1.33}$$

which becomes, in equilibrium and in Fourier space (with $\tilde{f}(\omega) \equiv \int_{\mathbb{R}} \mathrm{d}t \exp(\ \ i\omega t)f(t)$),

$$\tilde{C}_q(\omega) = \Omega_\phi(q)\tilde{G}_q(\ \ \omega)\tilde{G}_{\ q}(\omega). \tag{1.34}$$

It is instructive to compare χ_q and C_q to the general scaling form of the dynamical susceptibility and two-time function expected to hold near criticality [54], by the scaling hypothesis:

$$\chi_\phi(q,t) = |q|^{\ 2+\eta+}\ \chi_\pm\left(q\xi, \frac{ta_0}{\tau_0\xi^{\ }}\right), \qquad C_\phi(q,t) = |q|^{\ 2+\eta}C_\pm\left(q\xi, \frac{ta_0}{\tau_0\xi^{\ }}\right). \tag{1.35}$$

Here ξ is the correlation length of the field, $\ $ is its dynamical critical exponent, and η its anomalous dimension; finally, τ_0 and a_0 represent some microscopic time and length scales, respectively. The scaling functions $\chi_\pm$ and $C_\pm$ are well behaved at the critical point, where they take a constant value — depending in general on whether the critical point is approached from above (+) or from below ( ). Comparing with Eqs. (1.27), (1.30) and (1.31), and using $r = \xi^{\ -2}$, one deduces that $\ = 2 + \ $ and $\eta = 0$ in the case of model A ($\ = 0$) and model B ($\ = 2$) within the Gaussian approximation [54].

1.4 Colored noise and generalized Langevin equation

So far we have considered examples of Markovian models; however, to quote Van Kampen, *"non-Markov is the rule, Markov is the exception"* [67]. The Langevin equation (1.1) was written under the assumption that the variables that compose the thermal bath relax *instantaneously* to their equilibrium configuration, which is an idealization valid when the typical time scale of the bath particles is much smaller than the one characterizing the tracer particle. If this separation of time scales breaks down, one expects *memory* terms to appear in the equation that governs the evolution of $\mathbf{X}(t)$, which thus becomes non-Markovian. Explicit coarse-grained derivations of the effective particle dynamics can be performed in some simple settings (e.g., a particle coupled linearly to a bath made of harmonic oscillators [10, 68]), allowing to derive the (linear) *generalized* Langevin equation [7, 38]

$$\int_{\infty}^{t} \mathrm{d}u\, \mathcal{K}(t \quad u)\dot{\mathbf{X}}(u) = \mathbf{F}(\mathbf{X}(t), t) + \quad (t). \tag{1.36}$$

Here, $\mathbf{F}$ again includes the forces exerted on the particle at position $\mathbf{X}$, while the effect of the interaction between the particle and the medium is encoded in a friction kernel $\mathcal{K}(t)$ acting on the

particle velocity. Finally, is a *colored* Gaussian noise, meaning that it exhibits nontrivial temporal correlations. If the system is at equilibrium, a generalized Einstein relation (or fluctuation-dissipation relation of the first type [7]) still holds, i.e.,

$$\left\langle \zeta_i(t)\zeta_j(t') \right\rangle = \delta_{ij} T \mathcal{K}(|t \quad t'|). \tag{1.37}$$

In some cases, memory kernels and/or colored noises can themselves be thought of as if generated by stochastic differential equations, such as the OU process described in Section 1.2. In such cases, one can extend the space of variables from $\mathbf{X}(t)$ alone to $\{\mathbf{X}(t), \quad (t)\}$, so as to obtain again a Markovian process. In Appendix A we present an example of this *Markovian embedding*, which is relevant for the model we will later introduce in Chapter 2. Generally speaking, given a kernel $\mathcal{K}(t)$ characterized by n relaxation time scales, one needs to introduce n new dynamical variables to make the system Markovian [10]. If, on the contrary, $\mathcal{K}(t)$ decays as a power law (i.e., scale-free), then there is no finite-dimension space in which the process is Markovian. Since a power-law decay can be obtained by summing an infinite number of exponentials, each with its typical decay time (e.g., $\int_0^\infty \mathrm{d}\gamma\, e^{\quad \gamma t} = 1/t$), one can envision that a Markovian embedding can be obtained in this case by coupling $\mathbf{X}(t)$ to a continuum of dynamical variables — or in other words, to a *field* such as the one described in Section 1.3.

1.5 Functional representations

The Langevin equation (1.1) (as well as its generalization discussed in the previous sections) admits useful functional representations [69–72], which we briefly discuss here. Quite generally, we start from [73]

$$\mathcal{L}\phi(\mathbf{x}, t) = F[\phi] + \eta(\mathbf{x}, t), \tag{1.38}$$

where $\mathcal{L}$ is a differential operator (e.g., $\mathcal{L} = \partial_t \quad \nabla^2_{\mathbf{x}}$), and $F[\phi]$ is a forcing term; finally, $\eta(\mathbf{x}, t)$ is a stochastic noise described by the probability density functional $\mathcal{P}[\eta]$, normalized as $\int \mathcal{D}\eta\, \mathcal{P}[\eta] = 1$, and with zero mean[5]. We denote by $\phi_s = \phi_s(\mathbf{x}, t|\eta)$ a single trajectory of the stochastic process $\phi(\mathbf{x}, t)$ — i.e., a solution of Eq. (1.38) given a certain realization of the noise η. Expectation values of observable quantities such as $\mathcal{O}(\phi)$ can be evaluated as

$$\begin{aligned}\left\langle \mathcal{O}(\phi) \right\rangle &= \int \mathcal{D}\eta\, \mathcal{P}[\eta] \mathcal{O} \quad \phi_s(\mathbf{x}, t|\eta)) = \int \mathcal{D}\eta\, \mathcal{P}[\eta] \int \mathcal{D}\phi\, \mathcal{O} \quad \phi)\, \delta\left[\phi \quad \phi_s(\mathbf{x}, t|\eta)\right] \\ &= \int \mathcal{D}\eta\, \mathcal{P}[\eta] \int \mathcal{D}\phi\, \mathcal{O} \quad \phi)\, \delta\left[\mathcal{L}\phi \quad F[\phi] \quad \eta\right] |\mathcal{J}|,\end{aligned} \tag{1.39}$$

where in the last step we used Eq. (1.38), and we introduced the Jacobian[6]

$$\mathcal{J} = \det\left(\mathcal{L} \quad \frac{\delta F}{\delta \phi}\right). \tag{1.40}$$

[5] Here we only consider additive noise for simplicity, but generalizations are possible [56, 57, 74]. Note that $\langle \eta \rangle \neq 0$ can be reabsorbed into the definition of $F[\phi]$ in Eq. (1.38).

[6] In general we indicate by $|\mathcal{J}| \equiv \sqrt{\mathcal{J}\mathcal{J}^\dagger}$, with the adjoint $\mathcal{J}^\dagger = \det\left(\mathcal{L}^\dagger \quad \delta F^\dagger/\delta\phi\right)$.

Integrating over η immediately yields

$$\langle O(\phi)\rangle = \int \mathcal{D}\phi\, \mathcal{P}\left[\mathcal{L}\phi \quad F[\phi]\right] |\mathcal{J}|\, O \quad \phi)\,, \tag{1.41}$$

where $\mathcal{P}\left[\mathcal{L}\phi \quad F[\phi]\right] \sim e^{\quad \mathcal{S}_{\rm OM}[\phi]}$ is known as the generalized Onsager-Machlup functional [69]. If the noise η is Gaussian, then

$$\mathcal{P}[\eta] = \frac{1}{\sqrt{\det\, 2\pi G_\eta)}} \exp\left[\ \frac{1}{2}\iint \mathrm{d}\vec{x}\,\mathrm{d}\vec{y}\ \ \eta(\vec{x}) {G_\eta}^{1}(\vec{x},\vec{y})\eta(\vec{y})\right], \tag{1.42}$$

where we collectively indicated by $\vec{x} \equiv (\mathbf{x}, t)$ the spatial and temporal coordinates, and we called $G_\eta(\vec{x},\vec{y}) \equiv \langle\eta(\vec{x})\eta(\vec{y})\rangle$. We can thus write

$$\langle O(\phi)\rangle = \frac{1}{\sqrt{\det\, 2\pi G_\eta)}} \int \mathcal{D}\phi\, |\mathcal{J}|\, e^{\quad \mathcal{S}_{\rm OM}[\phi]}\, O(\phi), \tag{1.43}$$

with the Onsager-Machlup functional

$$\mathcal{S}_{\rm OM}[\phi] \equiv \frac{1}{2}\iint \mathrm{d}\vec{x}\,\mathrm{d}\vec{y}\ \ \mathcal{L}\phi \quad F[\phi])_{\vec{x}}\, {G_\eta}^{1}(\vec{x},\vec{y})\ \ \mathcal{L}\phi \quad F[\phi])_{\vec{y}}\,. \tag{1.44}$$

If $\mathcal{P}[\eta]$ is chosen Gaussian, however, a more convenient choice is to construct the *response function* formalism [70–72] as follows. Starting from Eq. (1.39), before integrating over η we insert the following representation of the delta function:

$$\delta\left[\mathcal{L}\phi \quad F[\phi] \quad \eta\right] = \int \mathcal{D}[i\tilde{\phi}]\, \exp\left\{\ \int \mathrm{d}\vec{x}\, \tilde{\phi}(\vec{x})\ \ \mathcal{L}\phi \quad F[\phi] \quad \eta)_{\vec{x}}\right\}, \tag{1.45}$$

where we introduced the conjugate variable (or response field) $\tilde{\phi}$. Computing the Gaussian functional integral over η in Eq. (1.39) then yields

$$\langle O(\phi)\rangle = \iint \mathcal{D}\phi\, \mathcal{D}[i\tilde{\phi}]\, |\mathcal{J}|\, e^{\quad \mathcal{S}_{\rm MSR}[\phi,\tilde{\phi}]}\, O(\phi), \tag{1.46}$$

$$\mathcal{S}_{\rm MSR}[\phi,\tilde{\phi}] = \int \mathrm{d}\vec{x}\, \tilde{\phi}(\vec{x})\ \ \mathcal{L}\phi \quad F[\phi])_{\vec{x}} \quad \frac{1}{2}\iint \mathrm{d}\vec{x}\,\mathrm{d}\vec{y}\ \ \tilde{\phi}(\vec{x}) {G_\eta}^{1}(\vec{x},\vec{y})\tilde{\phi}(\vec{y}). \tag{1.47}$$

The issue of the Jacobian in Eq. (1.40) is discussed, e.g., in Chap. 4 of Ref. [75], where it is shown that it reduces to a ϕ-dependent term proportional to $\Theta(0)$, which turns out not to affect the expectation value of physical observables. We do not enter here its interpretation, but we merely note that such a term can be neglected upon adopting the Itô convention for which $\Theta(0) \equiv 0$.

In particular, for the case of the OU particle and free field described in Sections 1.2 and 1.3, the corresponding dynamical actions read

$$\mathcal{S}_x[\mathbf{X},\widetilde{\mathbf{X}}] = \int \mathrm{d}t \left\{\widetilde{\mathbf{X}}(t)\cdot\left[\dot{\mathbf{X}}(t) \quad \mathbf{F}(\mathbf{X}(t),t)\right] \quad \frac{\Omega_x}{2}|\widetilde{\mathbf{X}}(t)|^2\right\}, \tag{1.48}$$

$$\mathcal{S}_\phi[\phi,\tilde{\phi}] = \int \mathrm{d}t \int \frac{\mathrm{d}^d q}{(2\pi)^d}\left[\tilde{\phi}\ _{\mathbf{q}}(t)\ \ \partial_t + \ _q)\,\phi_{\mathbf{q}}(t) \quad \frac{\Omega_\phi(q)}{2}\tilde{\phi}^2_{\mathbf{q}}(t)\right]. \tag{1.49}$$

We will comment further on the latter in Appendix C.9.

2

Relaxation in a near-critical environment

As we outlined in the introduction, in the first few Chapters of this thesis we aim at describing the dynamics of a tracer particle in a fluctuating correlated medium. In general, studying the motion of colloidal particles in contact with thermally fluctuating environments provides a tool to probe the rheological properties of soft-matter systems [76, 77]. Although past studies have mostly focused on the behavior of tracer particles passively carried by a fluctuating solvent, in recent years increasing attention has been paid to cases in which the particle and the solvent affect each other dynamically [26–31, 78, 79]. The case in which the medium is a fluid near a critical point, thus displaying long-range spatial correlations and long relaxation times, is particularly interesting because it defies a description based on the (generalized) Langevin equation — and calls instead for more sophisticated models which are able to account for the spatial structure of the medium, and for the field-mediated forces it induces between enclosed objects. Here we wish to start filling this gap by analyzing a simple setup and by predicting the dynamics of quantities that are (in principle) easily accessible in experiments. The paradigm we have in mind is that of a near-critical fluid such as a binary liquid mixture [35, 36], in which a colloidal particle is trapped by optical tweezers; we then look for signatures of the correlations of the underlying medium in the resulting dynamics of the particle, in particular by inspecting the average and correlation functions of its position.

In this Chapter we thus study the non-equilibrium dynamics of a probe particle in contact with a fluctuating medium close to the bulk critical point of a continuous phase transition, and trapped in a harmonic potential. The medium is modeled as a scalar order parameter $\phi(\mathbf{x}, t)$ subject to a dissipative or conserved relaxational dynamics within the Gaussian approximation (model A and B, as discussed in Section 1.3). This may represent the relative concentration of the two species in a binary liquid mixture, or the deviation of the local fluid density ρ from its critical value ρ_c in a single-component fluid (i.e., $\phi(\mathbf{x}) \propto \rho \quad \rho_c$). The probe represents instead an overdamped colloidal particle interacting with the scalar field via a translationally invariant linear coupling. Because of this coupling, the particle and the field affect each other dynamically along their stochastic evolution, in such a way that detailed balance is fulfilled at all times. A velocity field $\mathbf{v}(\mathbf{x}, t)$ should be included to allow for the hydrodynamic transport of the field and the particle, but we will neglect it here for simplicity [59]. Nonetheless, this minimal model already displays nonlinear and non-Markovian effects in the resulting dynamics of the particle, which make analytical predictions difficult beyond perturbation theory.

Here we focus on the effective dynamics of the probe particle, and we study how it is affected

by the presence of the field. A series of works [28–31] analyzed the dynamics of an unconfined particle stochastically diffusing in contact with a scalar Gaussian field, studying the resulting effective diffusion constant. A recent work [80] investigated instead the auto-correlation function of a particle fluctuating in a harmonic trap in contact with a Gaussian field with conserved dynamics (model B), a problem which was tackled within the weak-coupling approximation. In particular, this proved the emergence of algebraic tails in the auto-correlation at long times (superimposed to its usual exponential decay), the exponent of which depends only on the spatial dimensionality of the system. These results do not depend on the details of the chosen interaction potential between the particle and the medium, provided that it is linear and translationally invariant — in this sense, they are characterized by a certain degree of universality. A similar setup was analyzed in Ref. [64], where the steady state and effective dynamics of a particle in contact with a critical Gaussian field were investigated in the presence of spatial confinement for the field. In the case of a linear coupling between the fluctuating field and the particle, an effective Fokker-Planck equation was obtained under the assumption of rapid relaxation of the field for each position of the particle. This allowed for the adiabatic elimination of the field degrees of freedom, given by its eigenmodes in a finite box subject to certain boundary conditions, from the coupled equations of motion of the system — we will come back to this problem in, c.f., Chapter 5.

As a first step towards the analysis of nonequilibrium scenarios within the model described above, in this Chapter we analyze the relaxation of the particle after it is released far from its position of mechanical equilibrium in the harmonic trap. Within a weak-coupling expansion, in Section 2.2 we first show that the average position of the particle itself displays an algebraic behavior at long times. Its decay exponents, which can be expressed solely in terms of the spatial dimensionality of the system and the dynamical critical exponent of the field, turn out to be related to those of the auto-correlation function of the position of the particle by the fluctuation-dissipation theorem. Our analysis additionally reveals a transient algebraic behavior which is entirely due to the nonlinearity of the effective particle dynamics, and which is therefore out of the reach of linear response theory.

In the same spirit as in Ref. [64] (see also, c.f., Chapter 5), in Section 2.3 we derive an effective Fokker-Planck equation for the motion of the particle in the adiabatic limit by integrating out the field degrees of freedom, which are a continuum of variables in the bulk. We use this effective equation to study again the problem of relaxation towards equilibrium, and thus we investigate the possible matching between the perturbative and the adiabatic predictions; this allows us to locate precisely the point at which the adiabatic approximation breaks down. In particular we find, as expected, that the latter fails close to criticality, and even far from criticality when the field dynamics is conserved.

In Section 2.4 we finally test our perturbative, analytical predictions against numerical simulations, so as to exclude the possibility that higher-order corrections in the coupling constant λ become increasingly relevant at long times; this way we prove that the qualitative features of our analytical predictions, based on a perturbative expansion in λ, remain valid beyond perturbation theory. The predictions of this Chapter are summarized in Section 2.5.

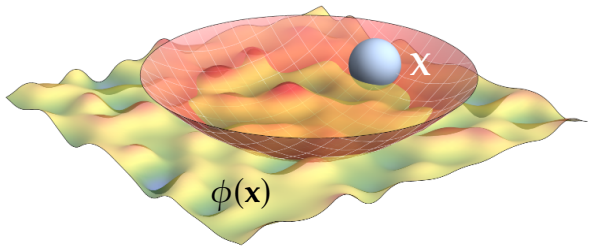

Figure 2.1: Pictorial representation of the model: a particle is in contact with a fluctuating scalar field $\phi(\mathbf{x})$ and trapped by a harmonic potential.

The content of this Chapter has been published as "D. Venturelli, F. Ferraro, and A. Gambassi, *Nonequilibrium relaxation of a trapped particle in a near-critical Gaussian field*, Phys. Rev. E **105**, 054125 (2022)" [81].

2.1 The model

As anticipated above, the system considered here consists of a harmonically trapped particle coupled to a scalar order parameter field, as schematically represented in Fig. 2.1. The total Hamiltonian of the system reads [80]

$$\mathcal{H}[\phi, \mathbf{X}] = \mathcal{H}_\phi[\phi] + \mathcal{H}_{\rm int}[\phi, \mathbf{X}] + \mathcal{U}(\mathbf{X}). \tag{2.1}$$

First, the medium is modeled by a scalar Gaussian field $\phi(\mathbf{x}, t)$ in d spatial dimensions, with Hamiltonian $\mathcal{H}_\phi[\phi]$ as given in Eq. (1.16). Second, the term

$$\mathcal{U}(\mathbf{X}) = \frac{\kappa}{2}|\mathbf{X}|^2 \tag{2.2}$$

represents a confining harmonic potential with elastic constant κ, while the d-dimensional vector $\mathbf{X}$ denotes the position of a reference point on the probe particle, e.g., its center. Last, the interaction term in Eq. (2.1) is chosen as

$$\mathcal{H}_{\rm int} = \lambda \int \mathrm{d}^d\mathbf{x}\, \phi(\mathbf{x}) V(\mathbf{x} - \mathbf{X}). \tag{2.3}$$

This coupling between the particle and the field is linear and translational invariant: this may physically model, for example, a colloid displaying a preferential adsorption towards one of the two components of a binary mixture. The interaction potential $V(\mathbf{x})$ is a function that models the shape of the particle, in the sense that the field interacts with the particle within its spatial extent, determined by the support of $V(\mathbf{x})$. For spherically symmetric tracers, it can be chosen as $V(\mathbf{x}) = \delta(\mathbf{x})$ in the case of a point-like particle; more generally, we will assume that $V(\mathbf{x}) = \overline{V}(x/R)$ is isotropic and characterized by a single length scale, namely the "radius" R of the particle, and is rapidly decaying for large $|\mathbf{x}|/R$; for instance,

$$V_G(\mathbf{x}) = \left(\sqrt{2\pi}R\right)^{-d} \exp\left[-|\mathbf{x}|^2/(2R^2)\right]. \tag{2.4}$$

We choose $V(\mathbf{x})$ to be normalized so that its integral over all space is equal to unity: this way the strength of the interaction is set only by the coupling constant λ. If λ and $V(\mathbf{x})$ in Eq. (2.1) are chosen to be positive, then configurations are favored in which the field ϕ is enhanced and assumes preferentially positive values in the vicinity of the particle.

Adopting the minimal model in Eq. (2.1) is physically motivated as follows. Upon approaching the critical point, the spatial correlations across the medium and consequently the characteristic timescale of its dynamics grow arbitrarily large — see Section 1.3. The system thus displays universal features, which are increasingly independent of its microscopic details, and therefore a minimal description of the medium in terms of a suitably-chosen, coarse-grained order parameter is sufficient as long as one is interested in its large-distance and long-time behaviour. Moreover, we expect the microscopic degrees of freedom of the medium to evolve much faster than a mesoscopic colloidal particle which is in contact with it. We thus identify the particle coordinate and the order parameter as the slow degrees of freedom of the system, while all the other degrees of freedom effectively constitute a thermal bath (see also Section 1.1). In this simplified model, we neglect hydrodynamic effects and other slow variables that should be taken into account when describing real fluids or binary liquid mixtures [54, 59]. Another clear limitation of the model is that the field essentially permeates the particle, whereas in a more realistic scenario, the interaction between the field and the particle should be designed to exclude the field from the physical extent of the particle. However, we expect that the long-time properties of the system (which we focus on in this Chapter) will not be drastically affected by the microscopic details of the interaction — as evidenced, for instance, by the fact that most of the qualitative conclusions presented below and in the next Chapters are essentially independent of the particle size R, and robust against changing the functional form of the interaction potential $V(\mathbf{x})$ in Eq. (2.3).

Let us now discuss the joint stochastic dynamics of the particle and the field. We assume a purely relaxational dynamics for the field as in Eq. (1.15), which we specialize here to $\mathcal{H}$ in Eq. (2.1):

$$\partial_t \phi(\mathbf{x}, t) = \quad D(i\boldsymbol{\nabla}) \quad \left[(r \quad \nabla^2)\phi(\mathbf{x}, t) \quad \lambda V(\mathbf{x} \quad \mathbf{X})\right] + \eta(\mathbf{x}, t). \tag{2.5}$$

As explained in Section 1.3, the choices $\quad = 0$ or 2 correspond to a non-conserved or locally conserved dynamics of the order parameter ϕ, respectively — i.e., model A or B within the Gaussian approximation [59]. The variance of the Gaussian noise $\eta(\mathbf{x}, t)$ is given in Eq. (1.17), with D and T denoting, respectively, the mobility of the field and the temperature of the environment. We recall that the parameter $r \geq 0$ measures the deviation from criticality, and controls the spatial correlation length $\xi = r^{\quad 1/2}$ of the field fluctuations at equilibrium.

The dynamics of the probe particle is assumed to be described by the overdamped Langevin equation (see Section 1.1)

$$\dot{\mathbf{X}}(t) = \quad \nu \boldsymbol{\nabla}_X \mathcal{H} + \boldsymbol{\xi}(t) = \quad \nu\kappa \mathbf{X} + \nu\lambda \mathbf{f} + \boldsymbol{\xi}(t), \tag{2.6}$$

where ν is the mobility of the probe, while the force $\mathbf{f}$ acting on the particle is given by the

gradient of the interaction energy

$$\mathbf{f}(\mathbf{X},\phi;t) \equiv \nabla_{\mathbf{X}} \int \mathrm{d}^d x\, \phi(\mathbf{x},t) V(\mathbf{x} \quad \mathbf{X}(t)) = \int \frac{\mathrm{d}^d q}{(2\pi)^d} i\mathbf{q}\phi_{\mathbf{q}}(t) V \ _q e^{i\mathbf{q}\cdot\mathbf{X}(t)}. \tag{2.7}$$

The particle and the field are assumed to be in contact with the same thermal bath at temperature T, so that $\boldsymbol{\xi}(t)$ is also a white Gaussian noise with zero mean and correlations as in Eq. (1.2).

The Langevin equation for the field in Fourier space reads

$$\dot{\phi}_{\mathbf{q}} = \quad _q \phi_{\mathbf{q}} + D\lambda q \ V_q e^{\ i\mathbf{q}\cdot\mathbf{X}} + \eta_{\mathbf{q}}, \tag{2.8}$$

with $_q \equiv Dq\ (q^2+r)$ as in Eq. (1.25), and noise correlations as in Eq. (1.24). It must be noted that an unbounded growth of the zero mode $\phi_{\mathbf{q}=\mathbf{0}}$ is implied by Eq. (2.8) for model A dynamics when $r = 0$. While this has no consequence on the particle dynamics (see Eq. (2.7)), in a more realistic system one would need to counteract this growth by adding a suitable chemical potential — e.g., $\mathcal{H}_\phi \mapsto \mathcal{H}_\phi + \lambda \int \mathrm{d}\mathbf{x}\, \phi(\mathbf{x})$.

Upon switching off the coupling between the particle and the field, i.e., by setting $\lambda = 0$, the two stochastic processes $\mathbf{X}(t)$ and $\phi(\mathbf{x},t)$ are non-interacting, and their solution is the one summarized in Sections 1.2 and 1.3. They are characterized by the (inverse) relaxation timescales τ_κ and $\tau_\phi(q)$ given in Eqs. (1.12) and (1.25), respectively; in particular, the relaxation time $\tau_\phi(q \sim 0)$ for the long-wavelength modes of the field may become arbitrarily large for model A dynamics at $r = 0$, and for model B dynamics for generic values of r, i.e., also off-criticality.

Since the dynamics in Eqs. (2.5) and (2.6) satisfies detailed balance, the joint equilibrium distribution of the field and the particle is the canonical one, $P_{\mathrm{eq}}[\phi,\mathbf{X}] \propto \exp\ \ \beta\mathcal{H}[\phi,\mathbf{X}]\big)$, where $\beta = 1/T$. Accordingly, the equilibrium distribution $P_{\mathrm{eq}}(\mathbf{X})$ of the particle is found by marginalizing $P_{\mathrm{eq}}[\phi,\mathbf{X}]$ as

$$P_{\mathrm{eq}}(\mathbf{X}) \propto \int \mathcal{D}\phi\, e^{\ \beta\mathcal{H}[\phi,\mathbf{X}]}. \tag{2.9}$$

A first somewhat unexpected result, which we prove in Appendix B.2, is that $P_{\mathrm{eq}}(\mathbf{X})$ is actually not affected by the presence of the field, and one still finds $P_{\mathrm{eq}}(\mathbf{X}) \propto \exp(\ \beta\mathcal{U}(\mathbf{X}))$ — i.e., the stationary statistics of the particle is solely and entirely determined by the trapping potential. The argument we invoke is completely general: it relies neither on the linearity of the coupling nor on the choice of a free field theory, and not even on the use of a quadratic particle potential. The only requirement is that the dynamics occurs in the bulk (i.e., there must be no boundaries), and that the coupling between the field and the particle is translationally invariant. We emphasize that the equilibrium distribution of the particle would indeed depend on the kind of coupling and boundary conditions if we had considered a system in a confined geometry, thus breaking translational invariance — see Refs. [64, 65] and, c.f., Chapter 5. Moreover, even in the bulk considered here, the marginal equilibrium distribution $P_{\mathrm{eq}}[\phi]$ of the field alone *does* indeed get modified by the presence of $\mathbf{X}$.

Interesting aspects of the field-particle interaction can instead be deduced by investigating the dynamical properties of the probe. In this Chapter we thus set out to predict the dynamics of the average particle position as it relaxes towards the center of the harmonic trap, being initially displaced from the position of mechanical equilibrium corresponding to $\mathbf{X} = 0$.

2.2 Weak-coupling approximation

The coupled nonlinear equations (2.5) and (2.6) for the dynamics of the particle and the field are not exactly solvable, and thus we resort to a perturbative expansion in the coupling strength λ, computing the relevant observables at the lowest nontrivial order in this parameter [80]. It must be noted that λ is not dimensionless: dimensional analysis of the Hamiltonian in Eq. (2.1) gives

$$[\phi] = \mathcal{E}^{1/2}\mathcal{L}^{1-d/2}, \qquad [\lambda] = \mathcal{E}^{1/2}\mathcal{L}^{d/2-1} \tag{2.10}$$

for the dimensions $[\phi]$ and $[\lambda]$ of the field and the coupling, in units of energy $\mathcal{E}$ and length $\mathcal{L}$. We consider the following formal expansions of the field and of the coordinates of the particle:

$$\phi(\mathbf{x},t) = \sum_{n=0}^{\infty} \lambda^n \phi^{(n)}(\mathbf{x},t), \qquad \mathbf{X}(t) = \sum_{n=0}^{\infty} \lambda^n \mathbf{X}^{(n)}(t), \tag{2.11}$$

and use them to compute the lowest order correction to the average particle position

$$\langle \mathbf{X}(t) \rangle = \langle \mathbf{X}^{(0)}(t) \rangle + \lambda^2 \langle \mathbf{X}^{(2)}(t) \rangle + O\left(\lambda^4\right). \tag{2.12}$$

Indeed, one can argue — on the basis of the invariance of the equations of motion under $\{\lambda \leftrightarrow -\lambda, \phi \leftrightarrow -\phi\}$ — that $\langle \mathbf{X}^{(1)}(t) \rangle = 0$, hence the first nontrivial term is of $O\left(\lambda^2\right)$. One can then insert the expansion in Eq. (2.11) into the equations of motion (2.5) and (2.6), and require that they are satisfied order by order in λ. This is done in Appendix B.3, where we derive

$$\begin{aligned} \langle X_j^{(2)}(t) \rangle = \nu \int \frac{\mathrm{d}^d q}{(2\pi)^d} i q_j \left|V_q\right|^2 \int_{t_0}^{t} \mathrm{d}s_2 \, e^{-\gamma(t-s_2)} \\ \times \int_{t_0}^{s_2} \mathrm{d}s_1 \left[\chi_q(s_1,s_2) + \nu q^2 e^{-\gamma(s_2-s_1)} C_q(s_1,s_2)\right] Q_{\mathbf{q}}(s_1,s_2). \end{aligned} \tag{2.13}$$

The functions C_q and χ_q are the stationary correlator and susceptibility of the Gaussian field in the absence of the particle discussed in Section 1.3, see Eqs. (1.30) and (1.31). We also introduced

$$Q_{\mathbf{q}}(s_1,s_2) \equiv \left\langle e^{i\mathbf{q}\cdot[\mathbf{X}^{(0)}(s_2) - \mathbf{X}^{(0)}(s_1)]} \right\rangle, \tag{2.14}$$

where the averages are taken over the non-interacting processes with $\lambda = 0$; they are computed by standard methods in Appendix B.1. To derive Eq. (2.13) we assumed for simplicity that the initial condition of the field $\phi_{\mathbf{q}}(t_0)$ is extracted from its stationary distribution reached *before* the particle is put in contact with the field — this does not affect the long-time properties of the particle which we focus on in this Chapter (see Appendix B.3).

We first specialize Eq. (2.13) to the case of a particle that is released, at time $t = t_0$, from the initial position $\mathbf{X}(t_0) = \mathbf{X}_0 \neq 0$ (the above expression for $\langle X_j^{(2)}(t) \rangle$ would remain valid if the initial condition $\mathbf{X}^{(0)}(t_0)$ were drawn instead from a random distribution). The asymptotic behavior of the resulting $\mathbf{X}(t)$ at long times is then examined in Appendix B.4, where we consider the general case in which $V_q \sim q^n$. Although we have assumed $V(\mathbf{x})$ to be normalized to unity in

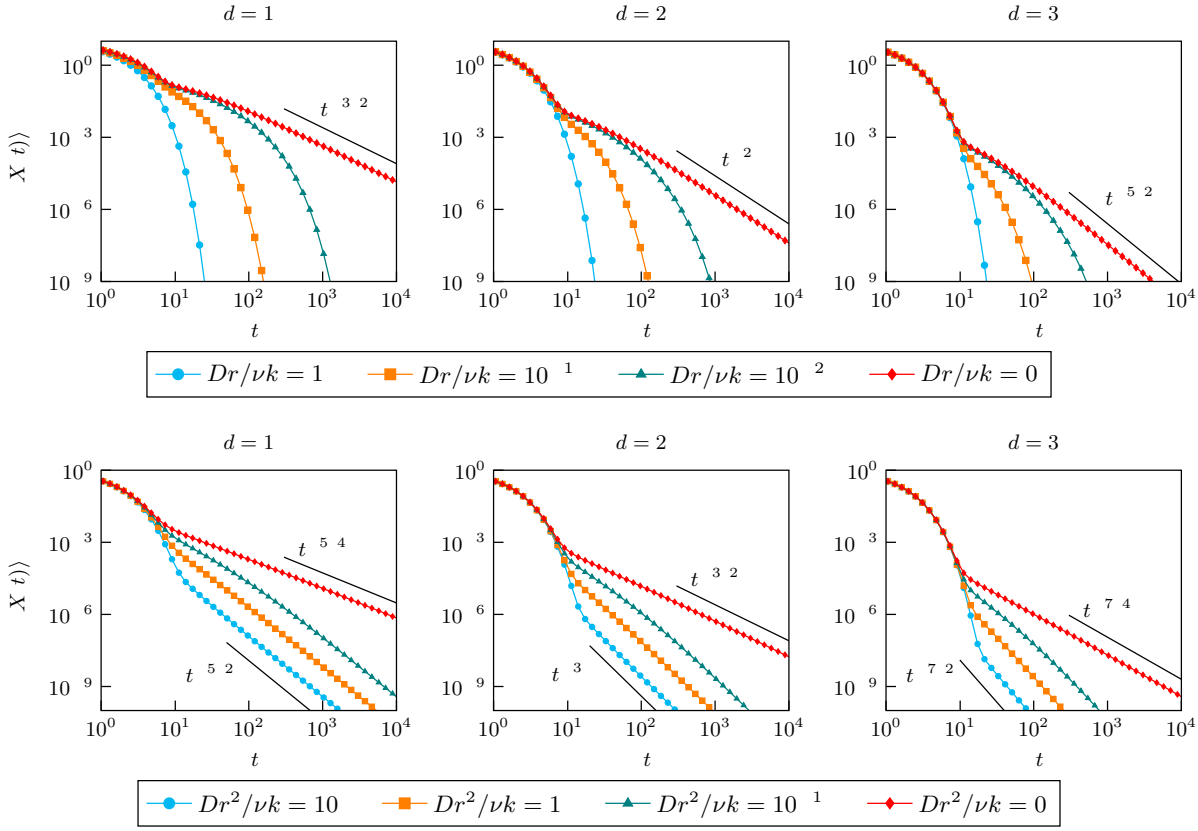

Figure 2.2: Evolution of the average position $\langle X(t)\rangle$ of a harmonically trapped particle initially released out of equilibrium and coupled to a field evolving with model A (top row) or model B (bottom row) dynamics, for various decreasing distances r from the critical point. The plot points are obtained from the numerical integration of the analytical prediction up to $O(\lambda^2)$ given in Eq. (2.13), and they are joined by a linear interpolation to guide the eye. The exponents of the power-law decays agree with those predicted in Eqs. (2.16) and (2.17). In these plots λ, T, D are set to unity, and the interaction potential is Gaussian with $R = 1$. In the top row we set $\nu = 10$, $k = 0.1$, and $X_0 = 10$, while in the bottom row these parameters are also set to unity.

real space (hence $V_{q=0} = 1$), this may model the case in which the particle is linearly coupled to the n-th (even) derivative of the field via an interaction term of the form

$$\mathcal{H}_{\rm int} = \lambda \int \mathrm{d}^d\mathbf{x}\, V(\mathbf{x} \quad \mathbf{X})\nabla^n \phi(\mathbf{x}) \tag{2.15}$$

in the Hamiltonian in Eq. (2.1). Below we summarize the main results of this analysis. In order to lighten the notation, we will often omit the suffix j from $\langle X_j(t)\rangle$, since its only non-zero component is the one along the initial displacement $\mathbf{X}_0$.

2.2.1 Long-time behavior of the position

By direct inspection of Eq. (2.13) in the case of model A and B dynamics (see Appendix B.4), we find the long-time asymptotics of the mean particle position $\langle X(t)\rangle$ to be given in model A by

$$\langle X(t)\rangle \sim \begin{cases} te^{-\gamma t} & \text{for} \quad r > \gamma/D, \\ t^{-(1+d/2)} e^{-Drt} & \text{for} \quad r < \gamma/D, \end{cases} \tag{2.16}$$

and in model B by

$$\langle X(t)\rangle \sim \begin{cases} t^{-(2+d/2)} & \text{for} \quad r > 0, \\ t^{-(1+d/4)} & \text{for} \quad r = 0. \end{cases} \tag{2.17}$$

These results have a clear physical interpretation: the long-time dynamics of the particle is practically determined by the slowest timescale characterizing the system. The two competing timescales are given by $\tau_\kappa = \gamma^{-1}$ and $\tau_\phi(q)$ in Eqs. (1.12) and (1.25), where we set $q = 0$ in the latter in order to account for the longest wavelength mode, which is infinite in the bulk. Consider first the case of model A dynamics, for which $\tau_\phi^{-1}(q = 0) = Dr$. Sufficiently away from the critical point — i.e., for large r, where the field evolves more rapidly than the particle — the motion of the latter is essentially unaffected. Upon approaching criticality — i.e., by reducing the value of r towards 0 — the dynamics of the field becomes instead increasingly slower and eventually it represents the longest timescale: this determines the change in the rate of exponential decay observed in Eq. (2.16). Finally, at criticality ($r = 0$) the divergence of the timescale characterizing the field dynamics induces correspondingly a scale-free behavior of the tracer particle. In model B, on the other hand, $\tau_\phi(q \to 0)$ is infinite even away from criticality, due to the presence of a conservation law: as a result, the dynamics of the tracer particle is always controlled by the field for any value of the parameter r.

The prediction in Eq. (2.13) is plotted in Fig. 2.2, which show an initial exponential decay followed by a crossover towards the algebraic behavior, once the leading order contribution $\langle X^{(0)}(t)\rangle = X_0 \exp(-\gamma t)$ has faded out. In Appendix B.5 we link the decay exponents for $r = 0$ with the dynamical critical exponent $= 2 +$ of the underlying Gaussian model; there we also derive the asymptotics of the average position at long times

$$\langle X_j(t)\rangle \simeq \frac{\sqrt{2\pi}\lambda^2}{e\nu k^2} t^{-(d+2)/} \int \frac{\mathrm{d}^d p}{(2\pi)^d} p_j |V_{pt^{-1/}}|^2 (\mathbf{p}\cdot\mathbf{X_0})\, \chi_{pt^{-1/}}(t - 1/\gamma). \tag{2.18}$$

At criticality, $r = 0$, this gives generically

$$\langle X(t)\rangle \simeq \frac{\lambda^2 c_1 X_0}{k} (\gamma t)^{-1} (Dt)^{-(d+2n)/} \sim t^{-1-(d+2n)/}, \tag{2.19}$$

where c_1 is a numerical constant (see Eq. (B.59) in Appendix B.5), and the even integer n indicates a coupling to the n-th derivative of the field, as in Eq. (2.15). For $n = 0$, we recover from Eq. (2.19)

[1] The long-time behavior for the off-critical case in model A was reported incorrectly in Ref. [81].

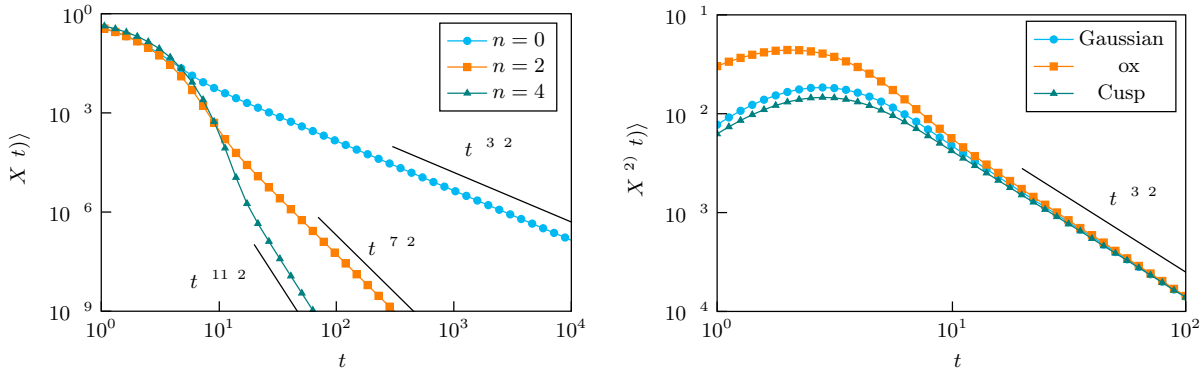

Figure 2.3: **a)** Average particle position $\langle X(t)\rangle$ in the presence of a coupling to the n-th derivative of the field, as in Eq. (2.15). The plot shows the case of critical model A in $d = 1$, and the observed decay exponents agree with those predicted in Eq. (2.19) for $= 2$. In this plot the interaction potential is Gaussian with $R = 1$. **b)** Independence of the long-time behaviour of the average position of the particle from the particular choice of the interaction potential $V(\mathbf{x})$. The plot shows the correction $\langle X^{(2)}(t)\rangle$ for model A in $d = 1$ (the leading order exponential term is irrelevant at long times). The exponent of the algebraic decay is not affected by the specific form of $V(\mathbf{x})$, but only by the behavior of its Fourier transform V_q for $q \to 0$, in agreement with the asymptotic expression in Eq. (2.18). On the contrary, the short-time behavior is sensitive to the particular choice of $V(\mathbf{x})$. The forms of the interaction potential reported here are Gaussian $V_q = \exp \quad R^2q^2/2)$, box $V_q = \mathrm{sinc}(Rq/2)$, cusp $V_q = 1/(1 + R^2q^2)$, where R indicates the linear size of the particle. In these plots we set $r = 0$, while λ, ν, k, T, D, and X_0 are set to unity.

the critical exponents in Eqs. (2.16) and (2.17) by setting $= 2$ (model A) or $= 4$ (model B), respectively. Specializing Eq. (2.18) to the non-critical case of model B renders, instead,

$$\langle X(t)\rangle \simeq \frac{\lambda^2 c_2 X_0 D}{k\gamma} (Dr)^{(2+n+d/2)} t^{2\ (d+n)/2}, \tag{2.20}$$

where the numerical constant c_2 is given in Eq. (B.60). This dependence is, as expected, generically algebraic with a temporal decay that is faster than in the critical case. Figure 2.3a shows how the value of n changes the decay exponent of the asymptotic behavior in agreement with Eq. (2.19). Moreover, Eq. (2.18) reveals that the details of the interaction potential V_q do not affect the large-t behavior of the particle: indeed, the interaction potential only enters Eq. (2.18) via $V_{pt^{1/}} \simeq V_{p\simeq 0}$, meaning that two distinct potentials with the same behavior for $p \simeq 0$ yield exactly the same asymptotic expression for the average position. This is verified in Fig. 2.3b, where the average position is plotted for various choices of $V(\mathbf{x})$ and the corresponding curves become indistinguishable at long times.

In Section 2.4.2 we will comment on how to amplify the long-time algebraic decay (which is most relevant at $r = 0$) in possible experimental realizations of the system.

One may ask the extent to which the results we obtained via a weak-coupling expansion could be retrieved by using a simpler linear response analysis. The linear response (LR) is formally

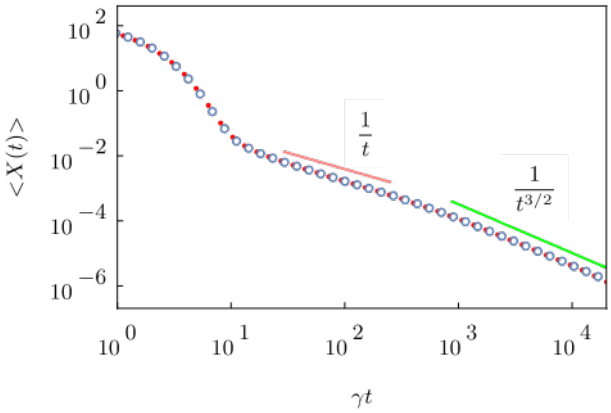

Figure 2.4: Relaxation of the average position $\langle X(t)\rangle$ towards equilibrium in $d = 1$ critical model A when the initial position X_0 is chosen sufficiently large so as to emphasize the nonlinear response. Open blue circles represent the theoretical prediction in Eq. (2.13), while red filled circles are the results of numerical simulations performed at $T = 0$ (we justify this choice and describe the simulation method in Section 2.4 and Appendix B.8). Straight lines indicate the intermediate and asymptotic power-law decays (see text). The parameters used in the simulation are $\nu = 1$, $k = 0.1$, $X_0 = 150$, $D = 1$, $R = 1$, $\lambda = 0.25$, integration timestep $\Delta t = 0.01$, and lattice size $L = 2048$.

recovered from Eq. (2.13) as

$$\langle X_j(t)\rangle_{\rm LR} \equiv X_0 \, \frac{\mathrm{d}}{\mathrm{d}X_0} \langle X_j^{(2)}(t)\rangle \Big|_{X_0=0} \tag{2.21}$$

(the zeroth-order term trivially vanishes) and it turns out, with hindsight, that the long-time asymptotic expression in Eq. (2.18) for the average position is indeed linear in $\mathbf{X}_0$. At short and intermediate times, however, nonlinear contributions arise which are encoded in the full response in Eq. (2.13), but they would be missed if we truncate it to the linear order. A simple way to highlight them is to choose $\mathbf{X}_0$ large enough so as to leave the linear response regime: Fig. 2.4 shows the emergence of an intermediate algebraic behavior with different decay exponents, which is correctly described by Eq. (2.13) and is actually observed in numerical simulations presented further below in Section 2.4. We give a semi-phenomenological description of this transient behavior in Section 2.4.1 and in Appendix B.6; our analysis allows us to predict the amplitude and the slope of the average position in this regime, as well as an estimate of the crossover time t_c at which the decay exponents in Eqs. (2.16) and (2.17) are recovered.

2.2.2 Comparison with the auto-correlation function

The predictions presented above are to be compared with the long-time behavior of the auto-correlation function $C(t) \equiv \langle \mathbf{X}(t) \cdot \mathbf{X}(0)\rangle$. The case of model B dynamics is discussed in Ref. [80], where it was shown that

$$\langle X(t) \cdot X(0)\rangle \sim \begin{cases} t^{\,d/4} & \text{for} \quad r = 0, \\ t^{\,(1+d/2)} & \text{for} \quad r > 0. \end{cases} \tag{2.22}$$

This result can be re-derived within the same perturbative framework as we did for the average position, as discussed in Appendix F of Ref. [81]. The calculation can then be extended to model A, for which we find [81]

$$\langle X(t) \cdot X(0) \rangle \sim \begin{cases} t^2 e^{\ \gamma t} & \text{for} \quad r > \gamma/D, \\ t^{\ d/2} e^{\ Drt} & \text{for} \quad r < \gamma/D. \end{cases} \tag{2.23}$$

The similarities between the two sets of exponents (see Eqs. (2.16) and (2.17)) appear to be a manifestation of the fluctuation-dissipation theorem at long times. Indeed, one could write for the particle a linearized effective equation [80] in the form

$$\dot{X}(t) = F[X] + h(t) + \xi(t), \tag{2.24}$$

where $\xi(t)$ is white Gaussian noise, $h(t)$ is an external forcing term, and $F[X]$, possibly nonlocal in time, contains the effects of the interaction with the field. The knowledge of the response function $R(\tau)$ would allow one to express, within the linear response regime,

$$\langle X(t) \rangle = \int_{t_0}^{t} \mathrm{d}t' \, R(t \quad t') h(t'). \tag{2.25}$$

Now, studying the relaxation of $X(t)$ starting from an initial condition $X_0 \neq 0$ is tantamount to setting $h(t) = X_0 \delta(t \quad t_0)$ into the effective equation (2.24), thus one concludes that $\langle X(t) \rangle = X_0 R(t)$. Then it is clear that at long times, i.e., sufficiently close to equilibrium, the fluctuation-dissipation theorem holds, relating the linear response in Eqs. (2.16) and (2.17) with the correlation function $C(t)$ in Eqs. (2.23) and (2.22) according to

$$R(t > 0) = \frac{1}{k_B T} \frac{\mathrm{d}C(t)}{\mathrm{d}t}. \tag{2.26}$$

2.3 Adiabatic approximation

In this Section we carry out a first-order adiabatic elimination of the field degrees of freedom that are assumed to be fast compared to the motion of the particle: this way we obtain an effective equation for the dynamics of the particle alone. Note that projecting the fast degrees of freedom over the dynamics of the tracer particle adopting the Mori-Zwanzig scheme [7, 8], which renders a linear equation, may lead to uncontrolled results in the present case, because the effective particle dynamics is actually nonlinear [82, 83]. We follow instead Ref. [9] and we *integrate out* the field degrees of freedom using a transparent and physically intuitive procedure. In the process, we generalize the approach of Refs. [9, 84, 85] to the case in which a continuum of fast variables are coupled to a single slow variable (see Appendix B.7 for further details).

As it is customary in this context [9], we will initially choose as a small parameter for the adiabatic expansion the ratio ν/D of the mobility of the particle to that of the field. However, it is clear from the discussion in Section 2.1 that the true time scale for the relaxation of the field variables is expressed by Eq. (1.25), so that the long-wavelength Fourier modes exhibit slow

relaxation close to criticality (or even far from criticality for a conserved dynamics, i.e., model B). We thus expect the adiabatic approximation to eventually break down; in the following, we will be interested in locating when this breakdown occurs and possibly matching the adiabatic approximation with the weak-coupling solution in Eq. (2.13).

2.3.1 Effective Fokker-Planck equation

Let us go back to the coupled equations of motion (2.6) and (2.8) for the particle and the field, respectively. We observe that the equations for the Fourier components $\phi_{\mathbf{q}}(t)$ decouple over the modes $\mathbf{q}$: this holds true because we are considering the Gaussian model, which renders linear equations of motion. One should however bear in mind that the field $\phi(\mathbf{x}, t)$ is real, which implies $\phi^*_{\mathbf{q}} = \phi_{\ \mathbf{q}}$; this suggests to separate its real and imaginary parts $\phi^R_{\mathbf{q}} \equiv \mathrm{Re}\{\phi_{\mathbf{q}}\}$ and $\phi^I_{\mathbf{q}} \equiv \mathrm{Im}\{\phi_{\mathbf{q}}\}$ [61]. We then rewrite Eqs. (2.6) and (2.8) as

$$\dot{\mathbf{X}} = \quad \gamma\mathbf{X} + \nu\lambda \int \frac{\mathrm{d}^d q}{(2\pi)^d} \mathbf{q} \left(\phi^R_{\mathbf{q}} g^I_{\mathbf{q}} \quad \phi^I_{\mathbf{q}} g^R_{\mathbf{q}} \right) + \boldsymbol{\xi}(t), \tag{2.27}$$

$$\dot{\phi}^{R,I}_{\mathbf{q}} = \quad {}_q\phi^{R,I}_{\mathbf{q}} + D\lambda q \ \ g^{R,I}_{\mathbf{q}} + \eta^{R,I}_{\mathbf{q}}, \tag{2.28}$$

where we defined $g_{\mathbf{q}}(\mathbf{X}) \equiv V_q \exp(\ \ i\mathbf{q}\cdot\mathbf{X})$, and the noise correlations read

$$\langle \eta^{R,I}_{\mathbf{q}}(t) \eta^{R,I}_{\mathbf{q}'}(t') \rangle = \frac{\phi}{2} \left[\delta^d(\mathbf{q} \quad \mathbf{q}') \pm \delta^d(\mathbf{q} + \mathbf{q}') \right] \delta(t \quad t'), \qquad \langle \eta^R_{\mathbf{q}}(t) \eta^I_{\mathbf{q}'}(t') \rangle = 0, \tag{2.29}$$

with $_\phi \equiv 2DTq\ $. The equations of motion for $\phi^{R,I}_{\mathbf{q}}$ are now completely decoupled, and thus their time-dependent probability distribution factorizes into

$$\mathcal{P}\left[\phi, \mathbf{X}, t\right] = \prod_{\mathbf{q}\in\mathbb{R}^d} P\left(\phi^R_{\mathbf{q}}; \mathbf{X}, t\right) P\left(\phi^I_{\mathbf{q}}; \mathbf{X}, t\right). \tag{2.30}$$

Clearly, this $\mathcal{P}$ does not factorize into an $\mathbf{X}$-dependent and a ϕ-dependent part, if not possibly at the initial time t_0. Note that the noise term in Eq. (2.29) still correlates $\phi^\sigma_{\mathbf{q}}$ with $\phi^\sigma{}_{\mathbf{q}'}$, for $\sigma = R, I$. When we write the Fokker-Planck equation corresponding to the set of Langevin equations (2.27) and (2.28), this produces mixed derivatives in the form $\delta^2/(\delta\phi^\sigma_{\mathbf{q}}\delta\phi^\sigma{}_{\mathbf{q}})$, which can nonetheless be dealt with by noting that $\phi^R{}_{\mathbf{q}} = \phi^R_{\mathbf{q}}$ and $\phi^I{}_{\mathbf{q}} = \quad \phi^I_{\mathbf{q}}$. We thus obtain

$$\partial_t \mathcal{P} = \left[\mathcal{L}_X + \int \frac{\mathrm{d}^d q}{(2\pi)^d} \left(\mathcal{L}^R_{\mathbf{q}} + \mathcal{L}^I_{\mathbf{q}} \right) \right] \mathcal{P}, \tag{2.31}$$

where, calling $\boldsymbol{\nabla} \equiv \boldsymbol{\nabla}_X$ and $_x \equiv 2\nu T$, we introduced the operators

$$\mathcal{L}_X = \boldsymbol{\nabla} \ \left[\gamma\mathbf{X} \quad \nu\lambda \int \frac{\mathrm{d}^d q}{(2\pi)^d} \mathbf{q} \left(\phi^R_{\mathbf{q}} g^I_{\mathbf{q}} \quad \phi^I_{\mathbf{q}} g^R_{\mathbf{q}} \right) \right] + \frac{x}{2} \nabla^2 \tag{2.32}$$

and

$$\mathcal{L}^\sigma_{\mathbf{q}} = \frac{\delta}{\delta\phi^\sigma_{\mathbf{q}}} \left[\ {}_q\phi^\sigma_{\mathbf{q}} \quad D\lambda q \ \ g^\sigma_{\mathbf{q}}(\mathbf{X}) \right] + \frac{\phi}{2} \frac{\delta^2}{\delta(\phi^\sigma_{\mathbf{q}})^2}. \tag{2.33}$$

The second consideration is that the coupling with the field in the equation of motion for $\mathbf{X}$ is linear. The problem of the adiabatic elimination of a fast variable from a system of two stochastic differential equations was addressed, e.g., in Ref. [9] and generalized in Refs. [84, 85] to the case of a multi-dimensional Fokker-Planck equation linear in the fast variables. We sketch in Appendix B.7 how the same method can be naturally extended to Eq. (2.31), which contains a continuum of fast variables. The resulting Fokker-Planck equation for the slow variable $\mathbf{X}(t)$ turns out to be

$$\partial_t P(\mathbf{X}, t) = \mathcal{L}_X^{\text{eff}} P(\mathbf{X}, t), \tag{2.34}$$

where, in the case of an isotropic interaction potential,

$$\mathcal{L}_X^{\text{eff}} = \boldsymbol{\nabla} \quad (\chi\gamma\mathbf{X}) + \chi\nu T\nabla^2 + \mathcal{O}\left(\left(\frac{\nu}{D}\right)^2\right), \tag{2.35}$$

with $\chi \equiv 1 \quad \lambda^2\mu$ and

$$\mu \equiv \frac{\nu}{Dd}\int_{\mathbb{R}} \frac{\mathrm{d}^d q}{(2\pi)^d} \frac{q^2}{(q^2+r)^2} |V_q|^2. \tag{2.36}$$

This integral converges, at finite values of r, provided that the interaction potential V_q decays sufficiently fast for large q, thus providing some form of ultra-violet cutoff. We may identify, *a posteriori*, the coefficient $\lambda^2\mu$ as the actual dimensionless small parameter in the adiabatic expansion which emerges naturally from the calculation.

Equation (2.34) is markedly Markovian; non-Markovian effects would appear at the next perturbative order, here neglected [9]. It shows that, up to the second order in the adiabatic approximation, the only effect of the interaction with the field is to renormalize the drift and diffusion coefficients by the same amount in the equation of motion for an otherwise diffusing particle in a potential: this, in turn, is equivalent to rescaling time according to $t \to \chi t$. This is expected in order for Eq. (2.34) to render the correct steady state distribution $\mathcal{P}_{\text{eq}}(\mathbf{X}) \propto \exp \quad \beta k X^2/2\big)$ of the particle, which does not depend on λ (Appendix B.2). Such a dependence emerges instead during relaxation: in fact, Eq. (2.34) implies straightforwardly that a particle initially displaced from its equilibrium position at time $t_0 = 0$ will relax back as

$$\langle X_{\text{ad}}(t)\rangle = X_0 e^{\ \chi\gamma t}. \tag{2.37}$$

2.3.2 Comparison with the perturbative solution

It is natural at this point to investigate if and when the perturbative solution in Eq. (2.13) matches the adiabatic approximation in Eq. (2.37). To address this issue, we consider their ratio

$$\eta \equiv \frac{\langle X_{\text{ad}}(t)\rangle}{\langle X(t)\rangle} \quad 1 = \lambda^2 \left[\mu\gamma t \quad \frac{\langle X^{(2)}(t)\rangle}{X_0} e^{\gamma t}\right] + \mathcal{O}\left(\lambda^4\right), \tag{2.38}$$

which vanishes when the adiabatic approximation gives the same result as the weak-coupling expression at this perturbative order. Note that η can be computed analytically by choosing, for instance, a Gaussian or δ-like potential, as detailed in Appendix H of Ref. [81]. In order for η to vanish for some time t, and therefore for the adiabatic approximation to be accurate, we need

$\langle X^{(2)}(t)\rangle\, e^{\gamma t}$ to be linear in t. One might expect this to be the case at long times t: indeed, the particle moves faster initially, when it is released, while it slows down as it reaches the bottom of the harmonic trap, thus making heuristically the adiabatic approximation more reliable. We have already analyzed the behavior of $\langle X^{(2)}(t)\rangle$ in this regime both for model A in Eq. (2.16), and model B in Eq. (2.17), so we conclude that:

(i) The adiabatic approximation is never accurate in model B: indeed, $\langle X^{(2)}(t)\rangle$ always decays algebraically at large t and there is no way that it can counterbalance the term $e^{\gamma t}$, thus causing $|\eta|$ to grow without bounds. This is not surprising, because in the whole adiabatic elimination procedure we have used the ratio of the two mobilities ν/D as a small adiabaticity parameter; however, the actual timescale τ_ϕ for the relaxation of the field is given in Eq. (1.25), which shows that, for any choice of D and r, there are always long-wavelength Fourier modes in model B that relax slower than the particle.

(ii) By the same token, the timescale for relaxation in model A is given by Eq. (1.25) with $= 0$, so that the slowest mode is characterized by ${\tau_\phi}^{1}(q = 0) = Dr$. We are led to the conclusion that $\langle X^{(2)}(t)\rangle\, e^{\gamma t}$ can only possibly behave linearly in t when $Dr > \gamma$, as it is clear by looking at Eq. (2.16). Being ${\tau_\kappa}^{1} = \gamma$ the timescale of relaxation of the particle in the trap, this implies that even the slowest field mode must relax faster than the particle.

In Appendix H of Ref. [81] we determine, for the case of model A, the linear growth coefficient a defined as $\langle X^{(2)}(t)\rangle\, e^{\gamma t} \simeq at$, for $t \gg \tau_\kappa$, which enters the definition of η in Eq. (2.38); we then compare it to the values of μ in Eq. (2.36) computed with the same interaction potential (which is chosen to be Gaussian for definiteness). This way we prove that the balancing in Eq. (2.38) does occur, thus making $\eta = 0$ at long times: this provides a matching between the perturbative and the adiabatic solutions for $\tau_\phi \ll \tau_\kappa$.

2.4 Numerical simulation

In order to verify the validity of our analytical predictions beyond the various approximations considered, we numerically simulate the system by direct integration of the coupled Langevin equations of motion for the field and the particle, Eqs. (2.5) and (2.6), respectively. To this end, we discretize the field over a lattice of size L and we adopt periodic boundary conditions, as described in Appendix B.8. A great simplification arises by noticing that the long-time asymptotic expression we found in Eq. (2.18) for the average position of the particle does not depend on the temperature T (which affects instead the dynamics at intermediate times and the amplitude of the thermal fluctuations). At long times and close to the equilibrium position $\mathbf{X} = 0$, noise fluctuations make it challenging to observe clearly the algebraic decay predicted in Eqs. (2.16) and (2.17). In addition, it is well known that very large systems are needed in order to sample the vicinity of a bulk critical point without incurring in finite-size effects. Accordingly, we first simulate the noiseless equations of motion, corresponding to setting $T = 0$, in large systems in $d = 1$ and $d = 2$, finding excellent agreement with the analytical prediction in Eq. (2.13) and its

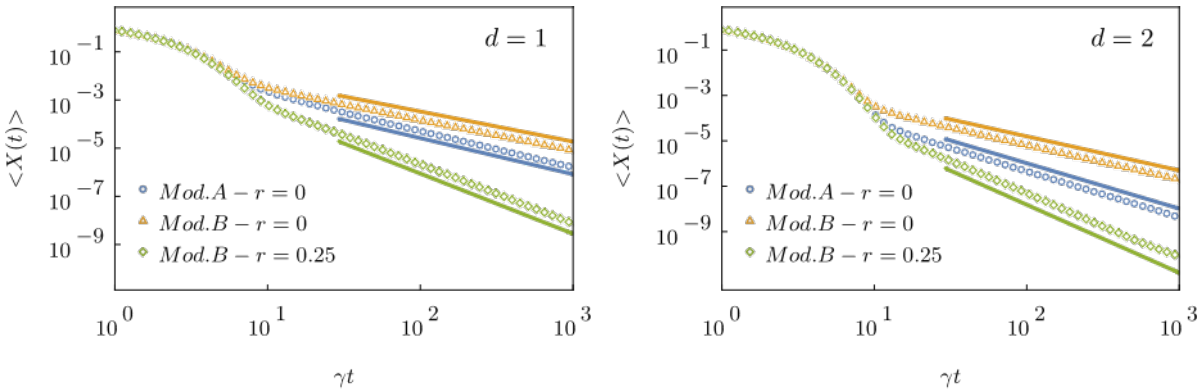

Figure 2.5: Average position $\langle X(t) \rangle$ of the particle in numerical simulations of the noiseless equations of motion, corresponding to $T = 0$, in $d = 1$ (left) and $d = 2$ (right). All the simulations are in excellent agreement with the long-time behavior predicted in Eqs. (2.16) and (2.17) (corresponding to the slopes indicated by the solid straight lines). We do not show here the full prediction in Eq. (2.13) for graphical clarity, as it is almost indistinguishable from the simulation points (but we do present such a comparison in Figs. 2.4 and 2.6a). The parameters used in the simulation are $\nu = 1$, $k = 0.1$, $X_0 = 2$, $D = 1$, $R = 0.5$, $\lambda = 0.25$, and $\Delta t = 0.01$. The system size is chosen to be $L = 2048$ in the $d = 1$ case, and $L = 512$ in the $d = 2$ case.

long-time algebraic behavior. This is presented in Fig. 2.5, which shows the average position in simulations performed at small values of the coupling λ (solid lines represent the slope of the long-time algebraic behavior predicted by Eqs. (2.16) and (2.17)). We then focus on one of these curves and we re-introduce the noise by considering $T \neq 0$, showing that in fact the effect of thermal fluctuations on the average particle displacement is negligible provided that one averages over a sufficiently large number N of realizations. Indeed, we show in Fig. 2.6a that even the *noisy* curve agrees with the prediction in Eq. (2.13), with scarce dependence on the specific choice of the interaction potential V_q, provided that its characterizing length scale R is of the same order as the one used in the simulation (which is performed by adopting a Gaussian interaction potential, see Appendix B.8).

2.4.1 Analysis of the transient behavior for large X_0

As anticipated in Section 2.2.1, by choosing a sufficiently large value of the initial displacement X_0 one observes an intermediate, algebraic behavior in the average particle position, highlighted in Fig. 2.4. This would not be captured by a linear response analysis of the system, but it is correctly described by the perturbative prediction in Eq. (2.13). In this Section we use such analytical prediction together with numerical simulations of the system in order to provide a phenomenological description of this transient behavior within the small-λ regime, where Eq. (2.13) agrees well with numerical data. By inspecting several relaxation curves corresponding to different values of the initial displacement X_0, one can observe the following:

(i) For short times $t \ll \tau_\kappa = \gamma^{-1}$, the dynamics is dominated by the initial exponential decay determined by the force exerted by the harmonic trap. If one insists on isolating the $O(\lambda^2)$

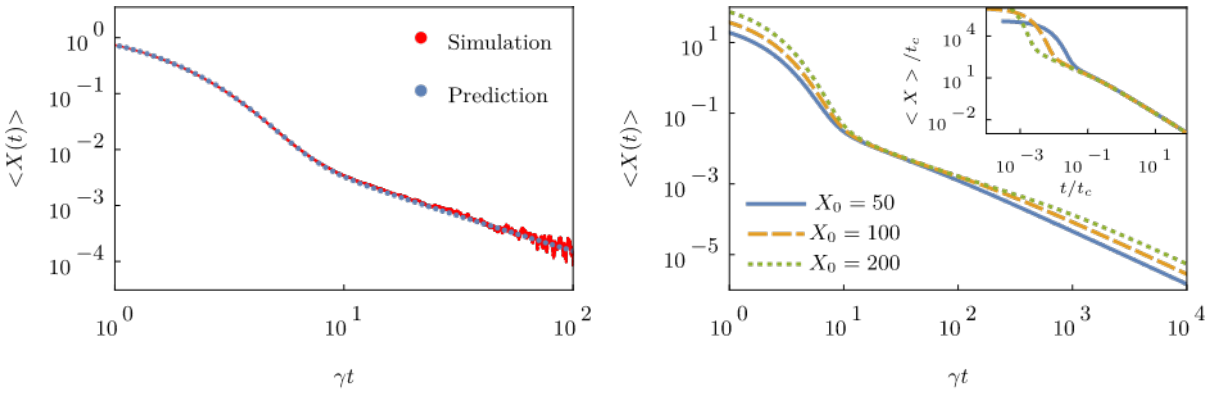

(a) (b)

Figure 2.6: **a)** Average particle position $\langle X(t) \rangle$ during the relaxation to equilibrium in $d = 1$ critical model B, in the presence of noise. Simulation results are plotted as a solid red line, while the blue dots represent the theoretical prediction in Eq. (2.13); they are shown to be in complete agreement. The parameters used in the simulation are $r = 0$, $X_0 = 2$, $\Delta t = 0.01$, $T = 0.1$, $L = 128$, and $N = 7.7 \times 10^8$ realizations. **b)** Average particle position $\langle X(t) \rangle$ during its relaxation towards equilibrium in $d = 1$ critical model A, when the initial position X_0 is chosen sufficiently large so as to emphasize the nonlinear response. In the main plot, the various curves correspond to increasing values of X_0, and the associated crossover time t_c is seen to shift towards larger times. In the inset, the same curves are collapsed according to the scaling form in Eq. (2.39) (see the main text). In the simulation we used $T = 0$, $\Delta t = 0.01$, and $L = 8192$. In both (a) and (b) we set $\lambda = 0.25$, and $k = 0.1$, while the parameters R, ν, and D were set to unity.

correction to the average position by subtracting the leading order exponential decay, they would observe an initial growth (qualitatively analogous to Fig. 2.7a) whose precise form is influenced by all the microscopic details of the confining potential and of the interaction potential, such as γ, R and the functional form of $V(\mathbf{x})$ (see, e.g., Fig. 2.3b).

(ii) For $t \quad \tau_\kappa$ and up to a crossover time which we denote by t_c, the average displacement of the particle decays algebraically with an exponent that does not coincide with the one eventually displayed at longer times. This exponent shows some universal features, as it only depends on the spatial dimensionality of the system and on the critical properties of the field (i.e., on its dynamical critical exponent). Moreover, quite surprisingly, the amplitude of $\langle X(t) \rangle$ in this regime turns out to be independent of the value of X_0 itself, a clear example of nonlinear response.

(iii) For $t > t_c$, we recover the asymptotic decay exponents predicted by Eqs. (2.16) and (2.17), in agreement with linear response analysis. The crossover time t_c becomes larger upon increasing X_0.

The problem is analyzed in full details in Appendix B.6. We start by identifying the crossover time t_c with the relaxation timescale of the field over length scales comparable with X_0: this timescale can be read in Eq. (1.25) by setting $q \sim 1/X_0$, which yields in the critical case $t_c \sim X_0/D$. The physical motivation is the following. At time $t = 0$ the particle is released in position X_0

and enters in contact with the field; since the latter has a nonzero relaxation time, at short times $t \lesssim \tau_\kappa$ we expect the particle to be dragged primarily by the restoring force of the harmonic trap, $\dot{X} \simeq \gamma X_0$. On a timescale given by $\tau_\kappa = \gamma^{-1}$ the particle covers a distance of the order of $\Delta X \sim X_0$, so that it becomes relevant to consider the time $t_c(X_0)$ taken by the field in order to rearrange over such a distance. Once the field has reached a state close to its equilibrium configuration around the particle (which is by now close to the center of the harmonic trap), then the dynamics is captured by linear response and we recover the asymptotic results of Section 2.2.1. Of course the transient regime cannot be appreciated if one chooses a small value of X_0, simply because correspondingly $t_c \ll \tau_\kappa$.

Motivated by the phenomenological observation stated above that the behavior of the particle is algebraic within the transient region $t \lesssim t_c$, while the amplitude is independent of X_0, we propose for times $t \gg \tau_\kappa$ the scaling ansatz

$$\langle X(t) \rangle \simeq c_0 t^{\theta_0} f(t/t_c), \tag{2.39}$$

where $f(\tau)$ is a scaling function with the property that

$$f(\tau) \sim \begin{cases} \tau^{\beta_0} & \text{for} \quad \tau \gg 1, \\ \text{const.} & \text{for} \quad \tau \lesssim 1. \end{cases} \tag{2.40}$$

The intermediate exponent θ_0 and the coefficient c_0 (the latter up to some numerical constant) can now be determined from an asymptotic matching of Eq. (2.39) with the long-time expression $\langle X_j(t) \rangle \simeq c_\infty X_0 t^{\theta_\infty}$, where c_∞ and θ_∞ are known from our previous asymptotic calculation, Eqs. (2.18) and (2.19). This gives at criticality

$$\theta_0 = 1 + \frac{d - 1}{2}, \qquad \text{and} \qquad c_0 \propto \frac{\lambda^2}{\gamma k} D^{(1-d)/2}. \tag{2.41}$$

A similar analysis can be repeated for the off-critical case in model B, yielding for $\xi \ll X_0$ a crossover time $t_c \sim X_0^2/(Dr)$ with intermediate exponent and proportionality factor

$$\theta_0 = 2 + \frac{d - 1}{2}, \qquad \text{and} \qquad c_0 \propto \frac{\lambda^2 D}{\gamma k} (Dr)^{(d+3)/2}. \tag{2.42}$$

In Fig. 2.6b we plot the average position of the particle in the case of critical model A ($d = 1$) for three values of the initial displacement X_0. In the main plot we observe that the three curves share the same amplitude within the transient region $\tau_\kappa \ll t \lesssim t_c$, with t_c becoming larger as X_0 is increased. In the inset we exhibit the collapse of the three curves according to the scaling ansatz in Eq. (2.39), which can equivalently be written as $\langle X_j(t) \rangle \simeq c_0 t_c^{\theta_0} f_2(\tau)$ upon defining $\tau = t/t_c$ and $f_2(\tau) \equiv \tau^{\theta_0} f(\tau)$. Plotting $t_c^{-\theta_0} \langle X_j(t) \rangle$ vs (t/t_c) shows indeed that a single curve $f_2(\tau)$ well describes the dynamics for $t \gg \tau_\kappa$.

2.4.2 How to amplify the long-time algebraic decay

Here we address the question of how to control the overall amplitude of the algebraic decay predicted for the average particle position. Indeed, although our model is not meant to describe

the dynamics of an actual colloid in a fluid, it still makes sense to check whether it would be in principle possible to amplify it and make it comparable with the length scale of the colloid radius R. A naive look at the asymptotic expressions in Eqs. (2.19) and (2.20), which are linear in X_0, would lead to the (wrong) conclusion that the algebraic decay can be enhanced by increasing X_0. However, we have checked in Section 2.4.1 that the crossover time t_c at which the asymptotic algebraic decay starts to be seen increases upon increasing X_0. Accordingly, one should better ask: how large is the average position at time t_c, when the decay assumes its asymptotic algebraic form? Interestingly, plugging the various estimates for t_c given in Section 2.4.1 into Eqs. (2.19) and (2.20) leads to the same expression for the position at the crossover time, i.e.,

$$\langle X(t_c)\rangle = \frac{\lambda^2 c D}{k\gamma} X_0^{1\ \ d} \quad , \tag{2.43}$$

where the numerical constant c is either c_1 or c_2 for the critical or off-critical cases, respectively. This expression tells us that the optimal value of X_0 should be chosen as small as possible in order to amplify the effect, but still sufficiently large so as to satisfy the assumption $t_c > \tau_\kappa$ introduced in Section 2.4.1.

We now recall that the coupling parameter λ is not dimensionless (see Eq. (2.10)), so that the notion of "small λ" we have often adopted in the previous sections has to be made more precise. To do this, we now choose to measure lengths in units of the particle radius R. The position at time t_c can then be conveniently expressed as[2]

$$\langle X(t_c)\rangle = g^2 R\,(X_0/R)^{1\ \ d} \quad , \tag{2.44}$$

where the dimensionless coupling $g^2 \equiv c\lambda^2 D/(k\gamma R^{d+}\ )$ emerges naturally as the actual small parameter for our perturbative expansion in Eq. (2.11).

In Appendix B.9 we focus on the case of the non-critical model B, which is the closest to experimental realizations among the models we considered in this Chapter. Choosing for the various parameters of the model the typical values corresponding to experiments with silica particles immersed in binary fluid mixtures [35, 43], we show that the amplitude of the effect we predicted in Eq. (2.43) is in principle well within the reach of digital video microscopy.

2.4.3 A hint at the large-λ behavior

The agreement between the perturbative solution in Eq. (2.13) and the numerical simulations justifies the weak-coupling approximation we adopted throughout this Chapter, and ensures that the higher-order contributions that we have systematically neglected do not become increasingly relevant at long times, at least as long as the coupling constant λ is small. Now we can use the numerical simulation to explore the regime in which λ becomes larger. We will consider for definiteness the case of critical model B in $d = 1$ and choose values of the coupling $\lambda \in [0.25 \quad 2.00]$. With the choice of parameters $k = 0.1$ and D, γ, and R set to unity, this corresponds to taking the dimensionless coupling g defined in Section 2.4.2 within the range $g \in [0.55 \quad 4.42]$.

[2] An upper bound on the value of λ can in principle be obtained by requiring $\langle X(t_c)\rangle \ll X_0$ from Eq. (2.43). However, this bound is generally too loose to be of practical use.

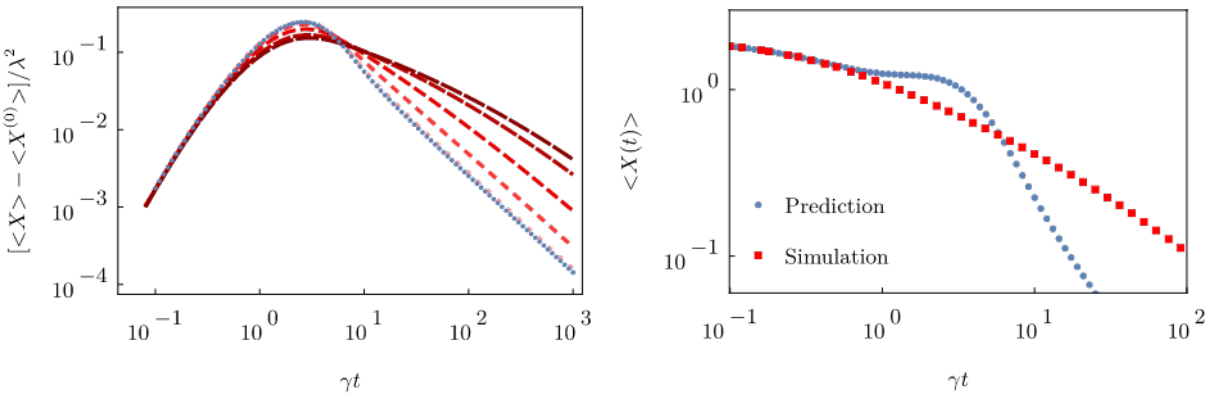

(a) (b)

Figure 2.7: **a)** Perturbative correction to the average position $\langle X(t)\rangle$ during the relaxation to equilibrium in $d = 1$ critical model B. Blue dots represent the theoretical prediction of $\langle X^{(2)}(t)\rangle$ in Eq. (2.13), while we plotted in different shades of red (and different dashing) the quantity $[\langle X\rangle \quad \langle X^{(0)}\rangle]/\lambda^2$ estimated in numerical simulations for increasing values of $\lambda \in [0.25 \quad 2.00]$, from lightest to darkest (and from shortest to longest dashing). For each curve we subtracted from the data the purely exponential decay and divided by λ^2. For large values of λ, one observes qualitatively the same power-law decay at long times, whose onset is nonetheless delayed as λ increases. **b)** Average particle position $\langle X(t)\rangle$ during its relaxation to equilibrium in $d = 1$ critical model B. We chose a large value of the coupling constant λ, well beyond the perturbative regime where agreement is observed between simulation data and our analytical prediction. Here the theoretical prediction indeed fails to describe even the qualitative behavior of the average position at short times (see main text). In the simulation we used $\lambda = 2$. In both (a) and (b) we chose $T = 0$, $k = 0.1$, $X_0 = 2$, $\Delta t = 0.01$, and $L = 128$, while the parameters v, D, R were set to unity.

Figure 2.7a compares the prediction in Eq. (2.13) with the corresponding total correction to the average position, including higher-orders, which we can extract from the simulation data by subtracting from the measured trajectory $\langle X(t)\rangle$ the purely exponential decay $\left\langle X^{(0)}(t)\right\rangle$ predicted at $O\ \lambda^0)$, and therefore dividing by λ^2. One observes that at long times the exponent of the algebraic decay does not change upon increasing λ, but the amplitude predicted by Eq. (2.18) acquires positive corrections coming from higher-order contributions. The time at which the onset of the power-law behavior occurs also shifts towards longer times as the value of λ increases.

A common feature in all the curves shown in Fig. 2.7a is that the $O\ \lambda^2)$ correction, which vanishes at $t = 0$, grows up to a maximum value before decaying algebraically to zero. One can envision that, for large enough λ, the correction $\lambda^2\,\langle X^{(2)}(t)\rangle$ would become larger than the leading term $\langle X^{(0)}(t)\rangle$, thus affecting its monotonic behavior. Of course such a scenario is well beyond the reach of the asymptotic expansion in Eq. (2.11), and in fact it is proven wrong in the numerical simulations performed at large λ which we report in Fig. 2.7b, where a clear departure from the weak-coupling prediction is observed even at short times.

In passing, we observe that the initial growth of the correction $\langle X^{(2)}(t)\rangle$ to the average position shown in Fig. 2.7a also presents an algebraic behavior (although, of course, the effect is masked by the leading exponential contribution in this short-time regime). However, the characterizing

exponents are found in this case to depend on the specific choice of the interaction potential $V(\mathbf{x})$, while they are in general insensitive to the value of r quantifying the distance from criticality.

2.5 Summary of this Chapter

In this Chapter we analyzed the relaxation towards equilibrium of a particle linearly coupled to a scalar Gaussian field, both following a stochastic evolution which satisfies detailed balance. Working within a weak-coupling expansion, we have shown that, due to the coupling with the field, the average position of the particle displays an algebraic decay at long times (see Eqs. (2.16) and (2.17)) if the field is close to its bulk critical point (see Fig. 2.2), and also far from criticality for a conserved field dynamics (model B). At criticality, we related these decay exponents with the dynamical critical exponent of the underlying Gaussian dynamical field theory, see Eq. (2.19). These exponents exhibit a certain degree of universality, in the sense that they depend only on the spatial dimensionality of the system but not on the specific form of the coupling potential between the field and the particle, provided that it is linear and translationally invariant. We supported these predictions beyond the perturbative approximation through numerical integration of the Langevin equations of motion, as shown in Figs. 2.5 and 2.6.

In the adiabatic limit, we derived an effective Fokker-Planck equation for the particle by integrating out the field degrees of freedom from the coupled equations of motion; then we used it in order to obtain an adiabatic approximation of its relaxation towards equilibrium. The matching of the adiabatic solution with that obtained via the weak-coupling approximation is only possible for a dissipative field dynamics (model A), and sufficiently far from criticality so that $\tau_\phi \ll \tau_\kappa$ — being τ_ϕ and τ_κ the relaxation timescales of the noninteracting field and of the particle, respectively (see Eqs. (1.25) and (1.12)). In particular, since τ_ϕ can become arbitrarily large at the critical point due to the presence of long-wavelength modes, the adiabatic approximation can *never* be applied for a critical field in the bulk, as it was heuristically expected. Moreover, in the case of a conserved field dynamics (model B) the adiabatic approximation fails also away from criticality, because of the presence of such slow modes for any value of the parameter r.

Finally we showed that, by choosing a sufficiently large value of the initial displacement X_0, a transient algebraic regime is observed in the average position of the particle. This would be entirely missed if one had adopted a linear response analysis, while it is correctly described by our perturbative prediction in Eq. (2.13). The main features of this intermediate regime are encoded in the scaling form we proposed in Eq. (2.39).

We emphasize that the conclusions we reached in this Chapter are in principle qualitatively testable with currently available experimental setups, for instance by microscopic observation of silica particles trapped by optical tweezers and immersed in a binary liquid mixture close to the critical point of its demixing transition [35, 36].

A question we left open in this Chapter is whether the inclusion in the Hamiltonian of additional terms which are nonlinear in the field ϕ may have an effect on the decay exponents of the average particle position. We expect the latter to depend in general on the static and dynamic universality classes of the bulk field Hamiltonian, so that additional terms involving

ϕ (but not $\mathbf{X}$) should play a role whenever they are relevant in the renormalization group sense. On the other hand, nonlinear couplings such as $\sim \phi^3(\mathbf{x})V(\mathbf{x} \quad \mathbf{X})$ (which have the same symmetry as those considered in this Chapter) may turn out to provide subleading contributions at long times. Various related problems can be addressed within this model, and some of them will be explored in the following Chapters. Some future perspectives will instead be illustrated in the Conclusions.

3

Nonequilibrium field-mediated interactions

Objects immersed in a fluctuating medium experience induced interactions due to the constraints they impose on its fluctuating modes. Among these interactions [39, 41, 86–90] are the critical Casimir forces [40, 42–44, 91] observed in classical systems close to the critical point of a second-order phase transition: they are the thermal and classical counterpart of the well-known Casimir effect in quantum electrodynamics [39]. Compared to other effective forces acting, e.g., in soft matter and colloidal dispersions, critical Casimir forces are characterized by a range which can be conveniently controlled by acting on the thermodynamic distance from the critical point [43]. Even when fluctuations are negligible, particles deforming a correlated elastic medium still experience field-mediated interactions [92, 93].

The static properties of these forces in equilibrium are by now widely understood in terms of the free energy of the system, and of its dependence on the separation between the confining surfaces [40–42]. However, this framework is generally unable to describe the forces arising in nonequilibrium conditions, such as those determined by a moving object (but also by temperature gradients [94], or in active systems [95–98]). In order to circumvent the difficulties that arise when imposing boundary conditions on moving surfaces, one can alternatively introduce in the total Hamiltonian of the system some suitable interaction potentials between the field and the included objects: actual boundary conditions might be eventually recovered in the formal limit in which the interaction strength becomes infinite [99–101]. This approach is particularly suited for studying the effects of boundary conditions imposed on randomly fluctuating surfaces, such as those of Brownian particles interacting with a correlated medium [93, 102].

As in the previous Chapter, here we are particularly interested in the case in which the medium under consideration is a fluid near a critical point, which displays long-range spatial correlations and long relaxation times. In this Chapter we thus study the dynamics of two probe particles, trapped and kept at a certain distance by two confining harmonic potentials, and in contact with a fluctuating medium close to the bulk critical point of a continuous phase transition. As in Chapter 2, we characterize the medium by a scalar order parameter $\phi(\mathbf{x}, t)$ subject to a dissipative or conserved relaxational dynamics, while we neglect hydrodynamic effects. The two overdamped Brownian particles are then made to interact with the scalar field via a translationally invariant linear coupling. Since this coupling appears in the system Hamiltonian, the particles and the field affect each other dynamically along their stochastic evolution, in such a way that detailed balance holds at all times.

A recent experiment [35] reported the observation of a temperature-controlled synchronization of the motion of two colloidal particles immersed in a binary liquid mixture close to the critical point of its demixing transition. In particular, the two colloids were trapped by two optical tweezers, and their distance was periodically modulated by spatially moving one of the two traps: the synchronization then occurred upon approaching the critical temperature of the fluid. Since the electrostatic and hydrodynamic forces acting on the system turned out to be insensitive to its critical state, they could not be responsible for the observed synchronization. These results were then explained in terms of the instantaneous action of the static critical Casimir force arising between the two colloids at equilibrium (i.e., the one computed from the equilibrium force within the Derjaguin approximation [33, 103]).

Motivated by this experimental study, we aim here at investigating the possible emergence of this behaviour in our minimal model, and how it is affected by the possible retardation in the "propagation" of the force [102]. In particular, we analyze the simple setup in which the center of one of the two harmonic traps is driven periodically with a tunable frequency Ω, so that the system eventually reaches a nonequilibrium periodic state. Our analysis follows the same lines as in the previous Chapter. Working within a weak-coupling expansion, we first derive a master equation which fully describes the motion of the particle in the spatially fixed trap. We then obtain, in the adiabatic limit, an effective Langevin equation for its motion by integrating out the field degrees of freedom. As we stressed in Chapter 2, upon approaching criticality the relaxation timescale of the field grows increasingly large, thus undermining the assumption of fast relaxation which the previous adiabatic approximation scheme hinges on. Accordingly, we first analyze the dynamics in the weak-coupling approximation and then compare it to the adiabatic solution, thus determining the limits of validity of the latter and characterizing the dynamical properties of the former.

The rest of the presentation is organized as follows. In Section 3.1 we introduce the model and the notation. In Section 3.2 we study, within a weak-coupling expansion, the induced motion of one of the trapped particles when the other particle is forced periodically, while in Section 3.3 we study the same quantity but within the adiabatic approximation. In Section 3.4 we characterize the weak-coupling solution and compare it with to adiabatic approximation; a comparison with numerical simulations is presented in Section 3.5. In Section 3.6 we extend our framework to the case in which more than two particles are immersed in the field. We finally summarize our results in Section 3.7.

The content of this Chapter has been published as "D. Venturelli and A. Gambassi, *Inducing oscillations of trapped particles in a near-critical Gaussian field*, Phys. Rev. E **106**, 044112 (2022)" [104].

3.1 The model

The system composed by the two particles and the field considered in this Chapter is described by the Hamiltonian

$$\mathcal{H} = \mathcal{H}_\phi + \mathcal{U} + \mathcal{U}_y + \mathcal{H}_{\rm int}, \tag{3.1}$$

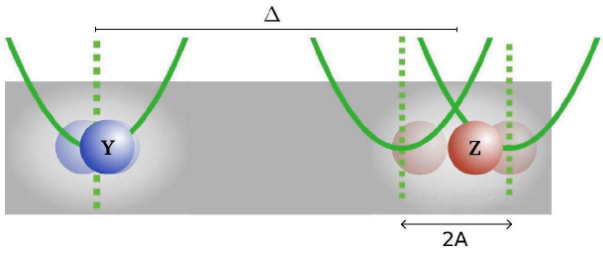

Figure 3.1: Two particles of radius R (blue and red spheres) are trapped in two distinct harmonic potentials spaced apart by a distance $\Delta \gg R$. The particles are immersed in a medium (grey background) represented here by a scalar Gaussian field (see Hamiltonian in Eq. (3.1)), and they interact with it. The centre of the trap containing the particle $\mathbf{Z}$ is driven periodically in time according to Eq. (3.12), with a driving amplitude $A \ll \Delta$.

and it is schematically represented in Fig. 3.1. First, the medium is modeled by a scalar Gaussian field $\phi(\mathbf{x}, t)$ in d spatial dimensions, as in Chapter 2, with the Hamiltonian $\mathcal{H}_\phi$ given in Eq. (1.16). The terms

$$\mathcal{U}_y(\mathbf{Y}) = \frac{\kappa_y}{2}|\mathbf{Y}|^2 \quad \text{and} \quad \mathcal{U}\ (\mathbf{Z}) = \frac{\kappa}{2}|\mathbf{Z} \quad \mathbf{z}_F(t)|^2 \tag{3.2}$$

in Eq. (3.1) represent two confining harmonic potentials with elastic constants κ_y and κ for the two particles. The d-dimensional vectors $\mathbf{Y}$ and $\mathbf{Z}$ denote the position of the centers of the particles; we will sometimes refer to them collectively as $\mathbf{X}_a$, with $a = y,\ $. The position of the center of the second trap is externally controlled and is given by $\mathbf{z}_F(t)$.

Finally, the interaction term in Eq. (3.1) is given by

$$\mathcal{H}_{\text{int}}\left[\phi, \mathbf{Y}, \mathbf{Z}\right] = \lambda \int \mathrm{d}^d x\, \phi(\mathbf{x})[V^{(\ )}(\mathbf{x} \quad \mathbf{Z}) + V^{(y)}(\mathbf{x} \quad \mathbf{Y})], \tag{3.3}$$

generalizing the one in Eq. (2.3) to the case of two particles. In the following, we will mostly choose for the shape functions $V^{(\ )}$ and $V^{(y)}$ a Gaussian with variance R (see Eq. (2.4)), the latter representing the "radius" of both particles.

The field is assumed to evolve according to a relaxational dynamics [59] involving the Hamiltonian in Eq. (3.1):

$$\partial_t \phi(\mathbf{x}, t) = D(i\boldsymbol{\nabla}) \frac{\delta \mathcal{H}}{\delta \phi(\mathbf{x}, t)} + \eta(\mathbf{x}, t) = D(i\boldsymbol{\nabla}) \left[(r \quad \nabla^2)\phi \quad \lambda \sum_a V^{(a)}(\mathbf{x} \quad \mathbf{X}_a(t))\right] + \eta, \tag{3.4}$$

or equivalently in Fourier space

$$\dot{\phi}_{\mathbf{q}} = \quad {}_q\phi_{\mathbf{q}} + \lambda D q \sum_a V_q^{(a)} e^{\ i\mathbf{q}\cdot\mathbf{X}_a} + \eta_{\mathbf{q}}, \tag{3.5}$$

where ${}_q$ was introduced in Eq. (1.25), and with the variance of the noise η given in Eqs. (1.17) and (1.24). The two particles evolve instead according to the overdamped Langevin equations

$$\dot{\mathbf{Y}}(t) = \nu_y \boldsymbol{\nabla}_Y \mathcal{H} + \boldsymbol{\xi}^{(y)}(t) = \gamma_y \mathbf{Y} + \lambda \nu_y \mathbf{f}_y + \boldsymbol{\xi}^{(y)}, \tag{3.6}$$

where we introduced $\gamma_y \equiv \nu_y \kappa_y$, and

$$\dot{\mathbf{Z}}(t) = \nu\ \boldsymbol{\nabla}_Z \mathcal{H} + \boldsymbol{\xi}^{(\ )}(t) = \gamma\ [\mathbf{Z} \quad \mathbf{z}_F(t)] + \lambda \nu\ \mathbf{f}\ + \boldsymbol{\xi}^{(\ )}. \tag{3.7}$$

The constants ν_a denote the mobilities of the two particles, while the force $\mathbf{f}_a$ on each particle is given by the gradient of the interaction potential

$$\mathbf{f}_a(\mathbf{X}_a, \phi; t) \equiv \nabla_{X_a} \int \mathrm{d}^d x \, \phi(\mathbf{x}) V_a(\mathbf{x} \quad \mathbf{X}_a(t)) = \int \frac{\mathrm{d}^d q}{(2\pi)^d} i\mathbf{q} V_q^{(a)} \phi_{\mathbf{q}}(t) e^{i\mathbf{q}\cdot\mathbf{X}_a(t)}. \tag{3.8}$$

Both particles are assumed to be in contact with a thermal bath at the same temperature T as the field, so that $\boldsymbol{\xi}^{(a)}(t)$ are also Gaussian uncorrelated white noises satisfying the Einstein relation

$$\langle \xi_i^{(a)}(t) \xi_j^{(b)}(t') \rangle = 2\nu_a T \delta_{ab} \delta_{ij} \delta(t \quad t'). \tag{3.9}$$

Note that, with this choice of variances for η and $\boldsymbol{\xi}^{(a)}$, one expects the system to relax to a Gibbs state with the total Hamiltonian given in Eq. (3.1), i.e.,

$$\mathcal{P}_{\mathrm{eq}}[\phi, \mathbf{Y}, \mathbf{Z}] \propto e^{\ \beta \mathcal{H}[\phi, \mathbf{Y}, \mathbf{Z}]}. \tag{3.10}$$

By setting $\lambda = 0$, we obtain three non-interacting stochastic processes whose evolution was summarized in Section 1.1; they are characterized by the relaxation timescales

$$\tau_a{}^{1} = \nu_a k_a \equiv \gamma_a, \qquad \text{with} \qquad a \in \{y, \ \}, \tag{3.11}$$

and $\tau_\phi(q)$ given in Eq. (1.25).

In the following, we will be interested in the nonequilibrium periodic state attained at long times by the system when we apply an external periodic forcing to the center $\mathbf{z}_F(t)$ of the harmonic trap of the second particle:

$$\mathbf{z}_F(t) = \boldsymbol{\Delta} + \mathbf{A} \sin(\Omega t). \tag{3.12}$$

Here represents the average separation between the two traps, as depicted in Fig. 3.1. When not specifically interested in the motion of the center $\mathbf{Z}(t)$ of the driven particle, we will often adopt the *deterministic* limit $\kappa \to \infty$ in which the particle follows the motion of the trap with no delay and no fluctuations, i.e., with $\mathbf{Z}(t) = \mathbf{z}_F(t)$ (see also Appendix C.1).

3.2 Weak-coupling approximation

The coupled nonlinear equations (3.4), (3.6) and (3.7) for the field and the two particles do not lend themselves to an analytic solution. We will then resort to a perturbative expansion of the equations of motion in powers of the coupling constant λ, and calculate the relevant observables at the lowest nontrivial order in this parameter. One way to proceed (which has been successfully pursued in Refs. [80, 81] in the case of a single particle, see Chapter 2) is to formally expand the field and the particle coordinates in a series for small λ, as in Eq. (2.11). One then substitutes these expansions into the equations of motion for the field and the particles, and computes the desired observables order by order in λ; we follow this approach in Appendix B of Ref. [104], and derive the average position $\langle \mathbf{Y}(t) \rangle$ for the sake of illustration. However, since we are mainly interested in the nonequilibrium periodic state attained by the system at long times when the particle denoted by $\mathbf{Z}$ is subject to a periodic external driving, it will be convenient to work, instead, at the level

of a master equation: this will make it easier to identify transient terms which play no role in the periodic state, and calculations will simplify significantly. Moreover, if one is able to derive an evolution equation for the one-point probability distribution $P_1(\mathbf{y}, t)$, then the expectation value of any one-time observable (e.g., the variance) can be computed straightforwardly and without requiring the calculation of the corresponding perturbative series. While one generically expects the effective dynamics of the particle to be non-Markovian, and therefore not necessarily captured by a master equation for $P_1(\mathbf{y}, t)$, we will see below that this description is however viable within the weak-coupling approximation.

3.2.1 Master equation

Here we derive a master equation for the probability density function of the position $\mathbf{Y}(t)$ which is valid up to $O\ \lambda^2)$. To this aim, we start from the Langevin equation (3.5) for the field. Using the response propagator of the free field given in Eq. (1.27), we can solve for $\phi_{\mathbf{q}}(t)$ in Eq. (3.5) as

$$\phi_{\mathbf{q}}(t) = \int_{t_0}^{t} \mathrm{d}s\ G_q(t \quad s) \left[\lambda D q \quad \sum_a V_q^{(a)} e^{\ i\mathbf{q}\cdot\mathbf{X}_a(s)} + \eta_{\mathbf{q}}(s) \right], \tag{3.13}$$

where we set the initial condition $\phi_{\mathbf{q}}(t = t_0) = 0$ for simplicity, as we are interested in the long-time properties of the system. Substituting Eq. (3.13) into Eq. (3.6), we obtain an effective Langevin equation for the position $\mathbf{Y}(t)$ of the particle moving in the *fixed* harmonic trap. A master equation for the associated probability distribution $P_1(\mathbf{y}, t)$ can then be derived from its very definition $P_1(\mathbf{y}, t) = \langle \delta(\mathbf{y} \quad \mathbf{Y}(t)) \rangle$, where the average is understood over all possible realizations of the stochastic noises $\eta_{\mathbf{q}}(t)$ and $\xi^{(y,\ )}(t)$. The equation is formally obtained as

$$\partial_t P_1(\mathbf{y}, t) = \quad \boldsymbol{\nabla}_{\mathbf{y}} \cdot \left\langle \delta(\mathbf{y} \quad \mathbf{Y}(t)) \dot{\mathbf{Y}}(t) \right\rangle, \tag{3.14}$$

and by substituting $\dot{\mathbf{Y}}(t)$ from the effective Langevin equation (3.6) in which $\phi(\mathbf{x}, t)$ has been replaced by Eq. (3.13). We provide the details of the calculation in Appendix C.2.1 and we report here only the final result:

$$\begin{aligned} \partial_t P_1(\mathbf{y}, t) = {} & \mathcal{L}_0 P_1(\mathbf{y}, t) + \lambda^2 \mathcal{L}\ (t) P_1(\mathbf{y}, t) \\ & + \lambda^2 \int_{t_0}^{t} \mathrm{d}s \int \mathrm{d}\mathbf{x}\, \mathcal{L}(\mathbf{y}, \mathbf{x}; t, s) P_2(\mathbf{y}, t; \mathbf{x}, s) + O\left(\lambda^4\right). \end{aligned} \tag{3.15}$$

Here

$$\mathcal{L}_0 \equiv \boldsymbol{\nabla}_{\mathbf{y}} \cdot \ \gamma_y \mathbf{y} + \nu_y T \boldsymbol{\nabla}_{\mathbf{y}}) \tag{3.16}$$

is the Fokker-Planck operator for an Ornstein-Uhlenbeck particle [53], while

$$\mathcal{L}\ (t) \equiv \boldsymbol{\nabla}_{\mathbf{y}} \cdot \nu_y \int \frac{\mathrm{d}^d q}{(2\pi)^d} i\mathbf{q} V_q^{(y)} V_q^{(\ )} e^{\ i\mathbf{q}\cdot\mathbf{y}} F_{\mathbf{q}}^{(\ )}(t), \tag{3.17}$$

with

$$F_{\mathbf{q}}^{(\ )}(t) \equiv \int_{t_0}^{t} \mathrm{d}s\ \chi_q(t \quad s) \left\langle e^{i\mathbf{q}\cdot\mathbf{Z}(s)} \right\rangle_0, \tag{3.18}$$

where the free-field susceptibility χ_q was given in Eq. (1.31). The quantity $F_{\mathbf{q}}^{(\ )}(t)$ represents an additional, nonlinear drift force due to the presence of the second particle in position $\mathbf{Z}$. The average $\langle \ldots \rangle_0$ in Eq. (3.18) is intended over the independent ($\lambda = 0$) process, and is computed in Appendices B.1 and C.1. Finally, we note that Eq. (3.15) involves a convolution of the two-time probability distribution $P_2(\mathbf{y}, t; \mathbf{x}, s)$ with a memory kernel $\mathcal{L}(\mathbf{y}, \mathbf{x}; t, s)$. This is typical in non-Markovian problems, where one usually obtains a hierarchy of master equations linking the n-point distribution $P_n(\mathbf{x}_n, t_n; \mathbf{x}_{n\ \ 1}, t_{n\ \ 1}; \ldots; \mathbf{x}_1, t_1)$ with P_{n+1} (see for instance Refs. [58, 105]). This kernel reads (summation over the repeated indices j and k is implied)

$$\mathcal{L}(\mathbf{y}, \mathbf{x}; t, s) \equiv \nu_y \nabla_{\mathbf{y}}^k \int \frac{\mathrm{d}^d q}{(2\pi)^d} i q_k |V_q^{(y)}|^2 e^{\ i\mathbf{q}\cdot(\mathbf{y}\ \ \mathbf{x})} \left[\chi_q(t \quad s) \quad i\nu_y C_q(t, s; t_0) e^{\ \gamma_y(t\ \ s)} q_j \nabla_{\mathbf{y}}^j \right], \quad (3.19)$$

where $C_q(s_1, s_2; t_0)$ is the field correlator for $\lambda = 0$ (see Eq. (1.29)). At long times, by taking the formal limit $t_0 \to \quad \infty$, the latter renders the equilibrium form $C_q(t \quad s)$ in Eq. (1.30), and the memory kernel $\mathcal{L}$ becomes time-translational invariant, i.e., $\mathcal{L}(\mathbf{y}, \mathbf{x}; t, s) = \mathcal{L}(\mathbf{y}, \mathbf{x}, t \quad s)$. Finally, in Eq. (3.19) the notation $\boldsymbol{\nabla}_{\mathbf{y}}^j$ is shorthand for $\partial/\partial y_j$.

As expected, Eq. (3.15) can be expressed as $\partial_t P_1(\mathbf{y}, t) = \quad \boldsymbol{\nabla}_{\mathbf{y}} \cdot \mathbf{J}(\mathbf{y}, t)$ for a suitably chosen current $\mathbf{J}(\mathbf{y}, t)$, so that probability conservation is guaranteed. Moreover, looking at Eq. (3.17) one immediately observes that:

(i) The contribution of the second particle in position $\mathbf{Z}$ to the evolution equation of the first is only mildly non-Markovian: indeed, while $\mathcal{L}\ (t)$ depends on the complete past history of $\mathbf{Z}(t)$, it is however independent of the past history of $\mathbf{Y}(t)$. In the limit $\kappa \to \infty$ in which the motion of $\mathbf{Z}(t)$ becomes deterministic, the history $\mathbf{Z}(t) = \mathbf{z}_F(t)$ is known and the drift term in Eq. (3.17) becomes Markovian.

(ii) The contribution of the second (and possibly of any other additional) particle enters linearly in the master equation for $P_1(\mathbf{y}, t)$.

These observations may appear surprising, but in fact they apply only to the effective dynamics up to $O\ \lambda^2)$. Indeed, as discussed in Appendix C.2.1, $P_2(\mathbf{y}, t; \mathbf{x}, s)$ at the next perturbative order in λ satisfies a master equation completely analogous to Eq. (3.15) involving both $\mathbf{Z}(t)$ and $P_3(\mathbf{y}, t; \mathbf{x}, s; \mathbf{x}', s')$.

3.2.2 Nonequilibrium periodic state

We are interested in the nonequilibrium periodic state reached at long times by the system when a periodic forcing is applied to the particle with position $\mathbf{Z}(t)$, as in Eq. (3.12). The task is significantly simplified when one realizes that the term containing the memory kernel $\mathcal{L}(t, s)$ in the master equation (3.15) can be discarded in the periodic state: we prove this fact in Appendix C.2.2. We are thus left with the (Markovian) master equation

$$\partial_t P_1(\mathbf{y}, t) = \mathcal{L}_0 P_1(\mathbf{y}, t) + \lambda^2 \mathcal{L}\ (t) P_1(\mathbf{y}, t) + O\left(\lambda^4\right), \quad (3.20)$$

with $\mathcal{L}\ (t)$ defined in Eq. (3.17) and

$$F_{\mathbf{q}}^{(\ )}(t) \equiv \int_0^\infty \mathrm{d}u\ \chi_q(u)\ \langle e^{i\mathbf{q}\cdot\mathbf{Z}(t\ \ u)}\rangle_0\,. \tag{3.21}$$

The latter coincides with Eq. (3.18) after taking the limit for $t_0 \to\ \ \infty$. A perturbative solution of Eq. (3.20) can now be found by expanding in powers of the coupling constant

$$P_1(\mathbf{y},t) = P_1^{(0)}(\mathbf{y},t) + \lambda^2 P_1^{(2)}(\mathbf{y},t) + O\Big(\lambda^4\Big). \tag{3.22}$$

This is done in Appendix C.2.3, where we derive an expression for $P_1^{(2)}(\mathbf{y},t)$ which can be used to compute expectation values of quantities such as the average particle displacement from the trap center, i.e.,

$$\langle \mathbf{Y}(t)\rangle = \ \ \nu_y\lambda^2 \int \frac{\mathrm{d}^d q}{(2\pi)^d} i\mathbf{q}v(\mathbf{q}) e^{\ Tq^2/(2\kappa_y)} \int_{\ \infty}^{t} \mathrm{d}t'\, F_{\mathbf{q}}^{(\ )}(t') e^{\ \gamma_y(t\ \ t')} + O\Big(\lambda^4\Big), \tag{3.23}$$

where we introduced for brevity

$$v(\mathbf{q}) \equiv V_q^{(y)} V^{(\ )}_{\ q}. \tag{3.24}$$

When a periodic external forcing is applied to the particle in $\mathbf{Z}(t)$, we expect the induced response of the particle in $\mathbf{Y}(t)$ to be in general nonlinear (as it is clear from Eq. (3.21)) and therefore anharmonic, but still periodic. This suggests to look for an expression of $\langle \mathbf{Y}(t)\rangle$ in the form of a Fourier series: this is done in Appendix C.2.3, where we compute, up to $O\ \lambda^2\big)$, the cumulant generating function of the particle position

$$\log\Big\langle e^{\ i\mathbf{p}\cdot\mathbf{Y}(t)}\Big\rangle = \ \ \frac{Tp^2}{2\kappa_y}\ \ \nu_y\lambda^2 \sum_{n\in\mathbb{Z}} \left[\int \frac{\mathrm{d}^d q}{(2\pi)^d} e^{\ \frac{Tq^2}{2\kappa_y}} v(\mathbf{q}) a_n(\mathbf{q}) A_n(\mathbf{p}\cdot\mathbf{q})\right] e^{in\Omega t}, \tag{3.25}$$

where $a_n(\mathbf{q})$ is the n-th Fourier coefficient of the function $F_{\mathbf{q}}^{(\ )}(t)$ defined in Eq. (3.21), while $A_n(\mathbf{p}\cdot\mathbf{q})$ reads

$$A_n(\mathbf{p}\cdot\mathbf{q}) \equiv (\mathbf{p}\cdot\mathbf{q}) \int_0^\infty \mathrm{d}\tau \exp\left[\ \ in\Omega\tau\ \ \ \gamma_y\tau\ \ \ \frac{T}{\kappa_y}(\mathbf{p}\cdot\mathbf{q}) e^{\ \gamma_y\tau}\right]. \tag{3.26}$$

When a pure sinusoidal forcing is applied to the system as in Eq. (3.12), the expectation value that appears in Eq. (3.18) takes the simple form (see Appendices B.1 and C.1)

$$\langle e^{i\mathbf{q}\cdot\mathbf{Z}(t)}\rangle_0 = \exp\left\{\ \ \frac{Tq^2}{2\kappa} + i\mathbf{q}\cdot[\ \ + \mathbf{A}\sin(\Omega t\ \ \ \theta\ )]\right\}. \tag{3.27}$$

For later convenience we have introduced the phase shift

$$\theta_a = \arctan(\Omega/\gamma_a), \tag{3.28}$$

here with $a \equiv\ \ $, which is a measure of the delay accumulated by the particle at point $\mathbf{Z}$ while following the motion of the center $\mathbf{z}_F(t)$ of its harmonic trap of finite strength $\kappa\ $. We can then use

the cumulant generating function in Eq. (3.25) to compute the expectation value of the position and the variance of the particle $\mathbf{Y}$, which read

$$\langle \mathbf{Y}(t) \rangle = \lambda^2 \sum_{n\in\mathbb{Z}} \frac{i\nu_y D}{\gamma_y + in\Omega} \left[\int \frac{\mathrm{d}^d q}{(2\pi)^d} \frac{\mathbf{q} q \;\; v(\mathbf{q}) J_n(\mathbf{q}\cdot\mathbf{A})}{\;\; q + in\Omega} e^{\;\; Tq^2/(2k_p) + i\mathbf{q}\cdot} \right] e^{in(\Omega t \;\; \theta\;)} + \mathcal{O}\left(\lambda^4\right), \tag{3.29}$$

$$\left\langle Y_j^2(t) \right\rangle_c = \frac{T}{\kappa_y} \left\{ 1 \quad \lambda^2 \sum_{n\in\mathbb{Z}} \frac{\nu_y D}{2\gamma_y + in\Omega} \left[\int \frac{\mathrm{d}^d q}{(2\pi)^d} \frac{q_j^2 q \;\; v(\mathbf{q}) J_n(\mathbf{q}\cdot\mathbf{A})}{\;\; q + in\Omega} e^{\;\; \frac{Tq^2}{2k_p} + i\mathbf{q}\cdot} \right] e^{in(\Omega t \;\; \theta\;)} \right\} + \mathcal{O}\left(\lambda^4\right), \tag{3.30}$$

where J_n is the modified Bessel function of the first kind. In the expressions above we introduced k_p such that $1/k_p = 1/\kappa \;\; + 1/\kappa_y$; in the *deterministic* limit $\kappa \;\; \to \infty$, one has $k_p \to \kappa_y$ and $\theta \;\; \to 0$ (see Eq. (3.28)). One can also check that, since the integrand functions in Eqs. (3.29) and (3.30) have a definite parity in $\mathbf{q}$, then the resulting expressions are real-valued.

3.2.3 Effective field interpretation

The form of the master equation (3.15), obtained in the limit of small coupling λ, lends itself to a simple physical interpretation. The original problem consisted of two particles whose reciprocal interactions are mediated by the field ϕ, and the strength of such interactions is controlled by the coupling λ. Applying a periodic driving of $\mathcal{O}\;\lambda^0)$ on the particle $\mathbf{Z}$ induces a displacement of $\mathcal{O}\;\lambda^2)$ on the particle $\mathbf{Y}$, as shown by Eqs. (3.29) and (3.30). By the same token, any feedback reaction of $\mathbf{Z}$ due to $\mathbf{Y}$ will be at least of $\mathcal{O}\;\lambda^4)$ and, as such, it will not contribute to the expressions discussed here, which are valid up to and including $\mathcal{O}\;\lambda^2)$. We also noted above that the motion of the particle $\mathbf{Z}$ does not affect the memory kernel in the master equation (3.15), whose presence is thus only to be ascribed to the self-interaction of the particle $\mathbf{Y}$, again mediated by the field ϕ. Once this contribution has faded out and the long-time periodic state is reached (see the discussion in Appendix C.2.2), the particle $\mathbf{Y}$ is essentially moving within the mean effective field $\langle \phi^{\mathrm{eff}} \rangle$ obtained by treating the particle $\mathbf{Z}$ as a source term, i.e.,

$$\left\langle \phi^{\mathrm{eff}}_{\mathbf{q}}(t) \right\rangle = \lambda \int_{\infty}^{t} \mathrm{d}s \; \chi_q(t \quad s) V_q^{(\;)} \left\langle e^{\;\; i\mathbf{q}\cdot\mathbf{Z}(s)} \right\rangle, \tag{3.31}$$

where again $\chi_q(u)$ is the linear susceptibility of the field reported in Eq. (1.31). Indeed, we show in Appendix C.3 how Eqs. (3.29) and (3.30) for the average displacement and variance of the particle $\mathbf{Y}$ can be retrieved by studying the dynamics of $\mathbf{Y}$ as if it were immersed into the mean effective field in Eq. (3.31), but in the absence of the second particle $\mathbf{Z}$.

We can build an analogy with Casimir force calculations [41], in which the Casimir energy in the presence of two surfaces can be computed by taking into account the multiple scatterings of the freely propagating field between the two surfaces — i.e., by first considering its free propagator, which propagates fluctuations from one surface to the other, and then summing over all possible numbers of round-trip reflections [106]. Our perturbative calculation up to $\mathcal{O}\;\lambda^2)$ corresponds to restricting this sum to the first scattering.

By extension, one can convince oneself that, within this weak-coupling expansion where multiple scatterings are neglected, the effect of the presence of any other particle within the same medium would simply add up to that of the particle **Z** in generating the effective field in Eq. (3.31). This is in contrast with other types of fluctuation-induced interactions such as Casimir forces [41], which have a non-additive nature. Although we have drawn here this conclusion on the basis of a weak-coupling expansion, we will in fact verify in Section 3.6 that this pairwise additivity persists beyond the perturbative regime.

3.2.4 A physical bound on the value of λ

The coupling constant λ around which we constructed a perturbative expansion is not dimensionless — see Eq. (2.10). It is thus useful to clarify what we mean by weak coupling. Hereafter, let us choose for definiteness a Gaussian interaction potential $V^{(a)}(\mathbf{x})$ as in Eq. (2.4) for both particles; assume that they have the same radius R, so that $v(\mathbf{q}) = \exp\left(-q^2R^2\right)$ (see Eq. (3.24)). In fact, the specific choice of the interaction potential is in general largely irrelevant [80, 81] and what really matters is its characteristic length scale R, which sets a UV cutoff on the field fluctuations (see also Appendix C.5).

In order to obtain an upper bound on the value of the coupling constant λ for which the perturbative expansion leads to reliable predictions, we may inspect the variance derived in Eq. (3.30) which, by definition, cannot become negative. A simple calculation (see Appendix E in Ref. [104]) shows that this requirement is always fulfilled if one chooses

$$\lambda^2 \leq 2d\kappa_y \left(2\sqrt{\pi}\widetilde{R}\right)^d, \tag{3.32}$$

where we introduced the effective particle radius

$$\widetilde{R}^2 \equiv T/(2k_p) + R^2. \tag{3.33}$$

Note that, in fact, this effective radius appears in Eq. (3.29) rather than R or T separately. This implies that the only effect of temperature on the average particle position $\langle \mathbf{Y}(t) \rangle$ is that of renormalizing the radius R of the particle by the average mean square displacement of the particle in the trap alone, which follows from equipartition theorem as $\langle Y_j^2 \rangle_0 \sim T/k_p$.

3.3 Adiabatic approximation

Any adiabatic elimination scheme [53, 81] of the field degrees of freedom $\phi_{\mathbf{q}}(t)$ from the coupled equations of motion (3.4), (3.6), and (3.7) relies on the assumption that the motion of the two particles is much slower than the relaxation timescales of the field. Note that, due to critical slowing down, this is expected to happen only sufficiently far from criticality (we will make this statement more precise later). When this is the case, the field effectively equilibrates around the instantaneous positions of the two particles, hence distributing according to

$$\mathcal{P}_{\mathrm{st}}\left[\phi|\mathbf{Y},\mathbf{Z}\right] = \frac{1}{\mathcal{Z}_{\mathrm{st}}(\mathbf{Y},\mathbf{Z})} e^{-\beta\left(\mathcal{H}_\phi + \mathcal{H}_{\mathrm{int}}\right)}, \tag{3.34}$$

where $\mathcal{H}_\phi$ and $\mathcal{H}_{\rm int}$ were given in Eqs. (1.16) and (3.3), respectively, and where we introduced the partition function

$$\mathcal{Z}_{\rm st}(\mathbf{Y},\mathbf{Z}) \equiv \int \mathcal{D}\phi\, e^{\beta(\mathcal{H}_\phi+\mathcal{H}_{\rm int})}. \tag{3.35}$$

An effective Hamiltonian $\mathcal{H}_{\rm eff}(\mathbf{Y},\mathbf{Z})$ describing the distribution of the particles alone can thus be obtained by marginalizing the equilibrium Boltzmann distribution in Eq. (3.10) over the field degrees of freedom, i.e.,

$$\mathcal{P}_{\rm eq}(\mathbf{Y},\mathbf{Z}) \propto e^{\beta\mathcal{H}_{\rm eff}(\mathbf{Y},\mathbf{Z})} \equiv \int \mathcal{D}\phi\, e^{\beta\mathcal{H}[\phi,\mathbf{Y},\mathbf{Z}]} = e^{\beta(\mathcal{U}_y+\mathcal{U}\ )} \int \mathcal{D}\phi\, e^{\beta(\mathcal{H}_\phi+\mathcal{H}_{\rm int})}, \tag{3.36}$$

where the last integral is nothing but $\mathcal{Z}_{\rm st}(\mathbf{Y},\mathbf{Z})$ in Eq. (3.35). From this partition function one can naturally derive the effective interaction potential $V_c(\mathbf{x})$ as

$$\mathcal{Z}_{\rm st}(\mathbf{Y},\mathbf{Z}) \propto e^{\beta\lambda^2 V_c(\mathbf{Z}\ \ \mathbf{Y})}, \tag{3.37}$$

and therefore from Eq. (3.36) it follows that

$$\mathcal{H}_{\rm eff}(\mathbf{Y},\mathbf{Z}) = \mathcal{U}_y(\mathbf{Y}) + \mathcal{U}\ (\mathbf{Z}) + \lambda^2 V_c(\mathbf{Z}\quad \mathbf{Y}). \tag{3.38}$$

The coupling to the field in the exponential of Eq. (3.35) is linear, so the Gaussian integral can be performed easily (see Appendix C.5), resulting in

$$V_c(\mathbf{x}) = \int \frac{\mathrm{d}^d q}{(2\pi)^d} \frac{v(\mathbf{q})}{q^2+r} e^{i\mathbf{q}\cdot\mathbf{x}}. \tag{3.39}$$

In this expression we have already subtracted the self-energy contributions, i.e., the energy needed to bring each of the two particles (separately) from an infinite distance into the field: as a result, $V_c(\mathbf{x}\to\infty) = 0$. An analysis of the latter is presented in Appendix C.5 for the case of particles with rotationally invariant interaction with the field. The effective potential $V_c(\mathbf{x})$ is plotted in Fig. 3.2a, together with the corresponding induced force $\mathbf{F}_c(\mathbf{x}) = \lambda^2\boldsymbol{\nabla}_{\mathbf{x}} V_c(\mathbf{x})$, in one spatial dimension and for the choice of identical Gaussian interaction potentials $V^{(a)}(\mathbf{x})$ between the field and the particles. A similar qualitative behavior is observed in higher spatial dimensions and for different interaction potentials characterized by the same cutoff scale R. The induced force $\mathbf{F}_c(\mathbf{x})$ features a maximum at a distance $x_{\rm max}$ implicitly defined by the condition in Eq. (C.68), while it decays to zero both for small and large values of $x = |\mathbf{x}|$. Both $V_c(\mathbf{x})$ and $\mathbf{F}_c(\mathbf{x})$ decay as $\exp(-x/\xi)$ when x is large compared to the correlation length $\xi = r^{1/2}$ (see Eq. (C.65)). One expects in general $V_c(\mathbf{x})$ and $\mathbf{F}_c(\mathbf{x})$ to exhibit an algebraic decay for $r = 0$ (see Appendix C.5), but we will not explore this issue further since we will assume that the medium has a finite (although possibly very small) correlation length ξ.

The particle dynamics at the lowest order in the adiabatic approximation is then obtained by averaging the equations of motion (3.6) and (3.7) for $\mathbf{Y}(t)$ and $\mathbf{Z}(t)$ over the stationary distribution $\mathcal{P}_{\rm st}\left[\phi;\mathbf{Y},\mathbf{Z}\right]$ of the field ϕ for fixed $\mathbf{Y}$ and $\mathbf{Z}$, given in Eq. (3.34). The resulting effective *adiabatic* Langevin equation for the particle $\mathbf{Y}$ subject to the fixed trap, derived in Appendix C.6, is

$$\dot{\mathbf{Y}}(t) = -\nu_y\kappa_y\mathbf{Y} - \nu_y\lambda^2\nabla_y V_c(\mathbf{Z}\quad \mathbf{Y}) + \boldsymbol{\xi}^{(y)} = -\nu_y\nabla_y\left[\mathcal{U}_y(\mathbf{Y}) + \lambda^2 V_c(\mathbf{Z}\quad \mathbf{Y})\right] + \boldsymbol{\xi}^{(y)}, \tag{3.40}$$

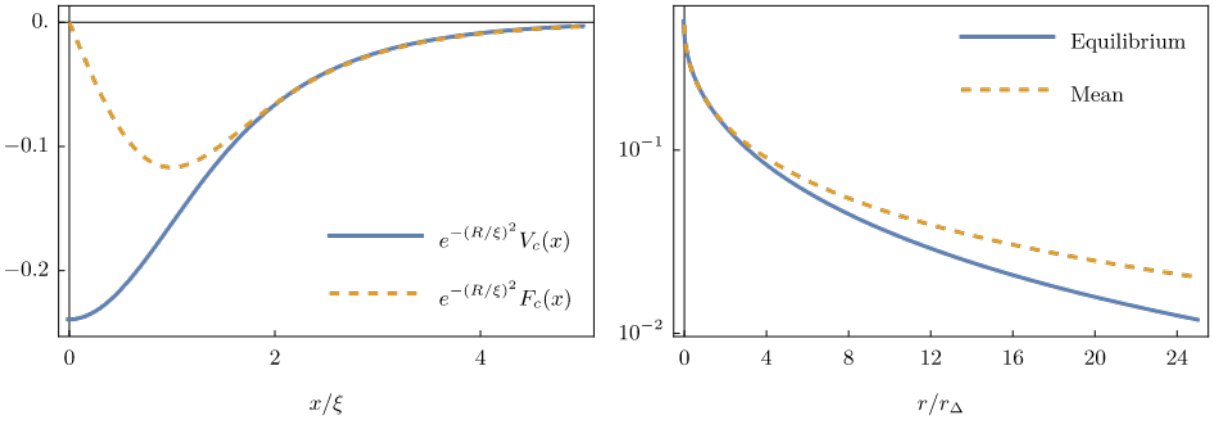

(a) (b)

Figure 3.2: **a)** Field-induced effective potential $V_c(x)$ and force $F_c(x)$ within the adiabatic approximation (in spatial dimension $d = 1$), as a function of the "center-to-center" distance x between the particles. They are plotted in units of the field correlation length $\xi = r^{1/2}$ and rescaled by the R-dependent part of their asymptotic amplitude computed in Eq. (C.65). Here R corresponds to the linear size of the particles which characterizes the interaction potentials $V^{(a)}(\mathbf{x})$, chosen to be Gaussian as in Eq. (2.4). The force shows a maximum at a distance $x_{\max}$ implicitly defined by the condition in Eq. (C.68), while it approaches zero for both small and large values of x/ξ. The parameters used in the plot are $R = 0.5$ and $r = 1$. **b)** Equilibrium position of the particle $\mathbf{Y}$ in the fixed-traps limit (solid line), and temporal mean value of the average position $\langle Y(t)\rangle$ of the particle in the fixed trap (dashed line, indicated by b_0 and c_0 in, c.f., Section 3.3.3.1). The two curves refer to one spatial dimension, and show the behavior as a function of $r/r_\Delta = (\Delta/\xi)^2$ (see Eq. (3.44)). The position of the particle $\mathbf{Y}$ when it is only subject to the equilibrium attraction to the particle $\mathbf{Z}$ is described by Eq. (3.42). The temporal mean value $\langle Y(t)\rangle$ is the same in the adiabatic (b_0) and in the dynamical response (c_0), as predicted by Eq. (3.51), and it is Ω-independent. The parameters used in the plot are $\gamma_y = 1$, $D = 10$, $\widetilde{R} = 0.7$, $\Delta = 3$, and $A = 1$.

which (as expected) we recognize as an overdamped Langevin dynamics computed as if the two particles interact via the effective, field-independent Hamiltonian computed in Eq. (3.38). We will denote as $\mathbf{Y}_{\rm ad}(t)$ the solution of the Langevin equation (3.40), which reads, for small λ (see the details in Appendix C.6),

$$\langle \mathbf{Y}_{\rm ad}(t)\rangle = \lambda^2 \nu_y \int \frac{\mathrm{d}^d q}{(2\pi)^d} \frac{i\mathbf{q} v(\mathbf{q})}{q^2 + r} e^{-Tq^2/(2\kappa_y)} \int_0^\infty \mathrm{d}u\, e^{-\gamma_y u} \left\langle e^{i\mathbf{q}\cdot\mathbf{Z}(t-u)} \right\rangle_0 + \mathcal{O}\left(\lambda^4\right). \tag{3.41}$$

This expression should be compared to the actual solution of the dynamics in Eq. (3.29). In Appendix C.6.2 we show how we may recover this result starting from the dynamical expression in Eq. (3.23) and taking the formal limit $D \to \infty$ of extremely fast field relaxation, which however is only meaningful if we assume $q\ (q^2 + r) \neq 0$ (see Eq. (1.25)). Clearly this last condition is not fulfilled in the presence of slow modes: recalling the discussion about timescales in Section 1.3, these modes appear in model A at criticality, but also off-criticality in model B.

3.3.1 Fixed traps

In the absence of a time-dependent external forcing, both the dynamical expression in Eq. (3.23) and the adiabatic expression in Eq. (3.41) describe the simple equilibrium attraction between the two particles, mediated by the field. This can be seen explicitly by fixing the position of the particle in $\mathbf{Z}(t)$ to a constant value $\mathbf{Z} \equiv$: in both equations, the time integral can be simply computed and we get

$$\langle \mathbf{Y}(t) \rangle \, , \langle \mathbf{Y}_{\rm ad}(t) \rangle \underset{\mathbf{Z}\equiv}{\longrightarrow} \frac{\lambda^2}{\kappa_y} \int \frac{\mathrm{d}^d q}{(2\pi)^d} \frac{\mathbf{q}\, e^{\widetilde{R}^2 q^2}}{q^2 + r} \sin(\mathbf{q} \cdot \quad), \tag{3.42}$$

for both model A and B. This expression can be alternatively obtained (up to $O(\lambda^2)$) by requiring that the total force $\mathbf{F}_{\rm tot}$ acting on the particle at position $\mathbf{Y}$ vanishes, i.e.,

$$\mathbf{F}_{\rm tot} = \kappa_y \mathbf{Y} \quad \lambda^2 \boldsymbol{\nabla}_{\mathbf{y}} V_c(\mathbf{Z} \quad \mathbf{Y}) \equiv 0, \tag{3.43}$$

which corresponds to the condition of mechanical equilibrium reached when the force derived from the field-induced potential V_c given in Eq. (3.39) counterbalances the restoring attraction of the harmonic trap of strength κ_y. In Fig. 3.2b we plot the resulting equilibrium position of the particle $\mathbf{Y}$ as a function of $r/r_\Delta = (\Delta/\xi)^2$, having defined

$$r_\Delta \equiv \Delta^{\ 2}. \tag{3.44}$$

The plot shows that the attraction is maximum at criticality and it decays monotonically as we increase the parameter r.

3.3.2 Periodic driving

Let us specialize Eq. (3.41) to the case in which a sinusoidal forcing is applied to one of the particles ($\mathbf{Z}$) as in Eq. (3.12). As for the dynamical case, we expect the response of the other particle ($\mathbf{Y}$, in the static trap) to be periodic, but not harmonic. We can then expand $\langle \mathbf{Y}_{\rm ad}(t) \rangle$ in Fourier series as

$$\langle \mathbf{Y}_{\rm ad}(t) \rangle = \sum_{n=\ \infty}^{\infty} \mathbf{b}_n e^{in\Omega t} = \mathbf{b}_0 + 2 \sum_{n=1}^{\infty} |\mathbf{b}_n| \cos(n\Omega t + \theta_n), \tag{3.45}$$

where $|\mathbf{b}_n|$ and θ_n indicate the complex modulus and the phase, respectively, of the Fourier coefficients

$$\mathbf{b}_n \equiv \frac{\Omega}{2\pi} \int_0^{\frac{2\pi}{\Omega}} \mathrm{d}t\, e^{\ in\Omega t} \langle \mathbf{Y}_{\rm ad}(t) \rangle \, , \tag{3.46}$$

with the property $\mathbf{b}_{\ n} = \mathbf{b}_n^*$. These coefficients can be easily computed by means of Eqs. (3.27) and (C.41), yielding

$$\mathbf{b}_n = \frac{i\lambda^2 e^{\ in\theta}}{\kappa_y (1 + in\Omega/\gamma_y)} \int \frac{\mathrm{d}^d q}{(2\pi)^d} \frac{\mathbf{q} J_n(\mathbf{q} \cdot \mathbf{A})}{q^2 + r} e^{\ q^2 \widetilde{R}^2 + i\mathbf{q}\cdot\Delta}, \tag{3.47}$$

where $\widetilde{R}$ is the effective particle radius defined in Eq. (3.33). They are to be compared with the analogous coefficients $\mathbf{c}_n$ of the expansion of the *dynamical* response $\langle \mathbf{Y}(t) \rangle$ which we can read from Eq. (3.29), i.e.,

$$\mathbf{c}_n = \frac{i\lambda^2 D e^{\ in\theta}}{\kappa_y(1 + in\Omega/\gamma_y)} \int \frac{\mathrm{d}^d q}{(2\pi)^d} \frac{\mathbf{q} q \ J_n(\mathbf{q}\cdot\mathbf{A})}{_q + in\Omega} e^{\ q^2\widetilde{R}^2 + i\mathbf{q}\cdot\Delta}. \tag{3.48}$$

We discuss this comparison in Section 3.4, while we focus below on the adiabatic response. In the following, we will indicate for brevity $b_n \equiv \|\mathbf{b}_n\|$, $c_n \equiv \|\mathbf{c}_n\|$; however, one can check that their only nonzero component is the one along the direction of $\mathbf{A}$ and .

3.3.3 Analysis of the adiabatic response

We are interested here in studying the behavior of the adiabatic response in Eq. (3.41) as we vary the external driving frequency Ω. To this end, it is useful to rewrite the corresponding Fourier coefficients $\mathbf{b}_n$ in Eq. (3.47) as

$$\mathbf{b}_n(\Omega) = \frac{\mathbf{b}_n(\Omega = 0)}{1 + in\Omega/\gamma_y}, \tag{3.49}$$

where $\mathbf{b}_n(\Omega = 0) = \ i\lambda^2 e^{\ in\theta}\ \mathcal{I}_n/\kappa_y$, having defined

$$\mathcal{I}_n \equiv \int \frac{\mathrm{d}^d q}{(2\pi)^d} \mathbf{q} \frac{e^{\ q^2\widetilde{R}^2}}{q^2 + r} J_n(\mathbf{q}\cdot\mathbf{A}) e^{i\mathbf{q}\cdot\Delta}. \tag{3.50}$$

3.3.3.1 Mean value

The temporal mean value $\mathbf{b}_0 \equiv \mathbf{b}_0(\Omega) = \mathbf{b}_0(\Omega = 0)$ around which the oscillations occur is the same in the adiabatic and dynamical response, i.e., $\mathbf{c}_0 = \mathbf{b}_0$: from Eqs. (3.48) and (3.49), it reads

$$\mathbf{b}_0 = \mathbf{c}_0 = \frac{\lambda^2}{\kappa_y} \int \frac{\mathrm{d}^d q}{(2\pi)^d} \mathbf{q} \frac{e^{\ q^2\widetilde{R}^2}}{q^2 + r} J_0(\mathbf{q}\cdot\mathbf{A}) \sin(\mathbf{q}\cdot\Delta). \tag{3.51}$$

This quantity is plotted in Fig. 3.2b as a function of the correlation length ξ of the field: the average is maximum at criticality, $r = 0$, and it decays monotonically as $\sim r^{\ 1}$ as one moves away from the critical point.

We note that the temporal mean value $\mathbf{b}_0$ of the (anharmonic) oscillations is Ω-independent, but it does *not* coincide with the position of mechanical equilibrium in Eq. (3.42) as long as the driving amplitude $\mathbf{A}$ does not vanish. This is expected, since the field-induced attraction is nonlinear (see, c.f., Eq. (C.61) in Appendix C.5 and Fig. 3.2a). Indeed, let us analyze a single oscillation in one spatial dimension, and consider the second derivative of the induced force $h \equiv \partial_x^2 F_c(x)\big|_{x=x_{\mathrm{eq}}} \neq 0$ computed in correspondence of the equilibrium interparticle distance $x = x_{\mathrm{eq}}$ (see Eq. (3.43)). When the two particles approach each other, if $h < 0$ ($h > 0$), they experience a stronger (weaker) attraction which is not completely counterbalanced by a proportionally weaker (stronger) attraction felt while they are further away from each other. The net result is that they spend more (less) time close to one another than they would if the attraction were the same during the two phases of the oscillation (as it happens in a linear force gradient, for which $h = 0$).

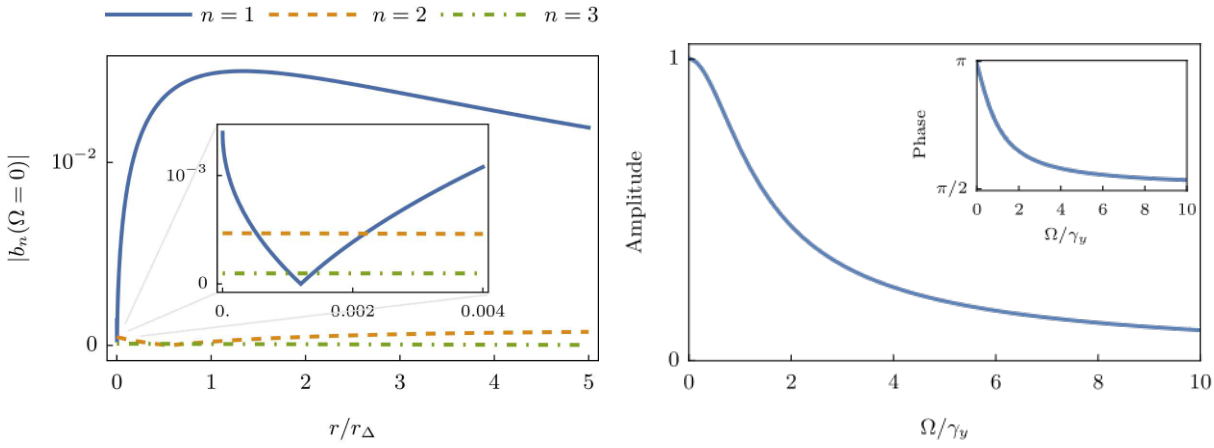

(a) (b)

Figure 3.3: **a)** Amplitude of the first three Fourier harmonics (indexed by n) of the adiabatic response in Eq. (3.47), in spatial dimension $d = 1$ and for $\Omega = 0$. This provides an indication on the ratio of their magnitudes also for $\Omega \neq 0$, see Eq. (3.52). They are plotted as a function of $r/r_\Delta = (\Delta/\xi)^2$ (see Eq. (3.44)). The adiabatic response is in general dominated by the first harmonic, but the latter is suppressed in correspondence of a specific value r_1 of r (see the main text). The parameters used in the plot are $\gamma_y = 1$, $\widetilde{R} = 0.7$, $\Delta = 3$, and $A = 0.5$. **b)** Amplitude $|\mathbf{b}_1|$ and relative phase $\delta\theta$ of the first Fourier harmonic in the adiabatic response, see Eq. (3.47). The amplitude is normalized by $|\mathbf{b}_1(\Omega = 0)|$, see Eq. (3.52), and $\delta\theta$ is the phase difference with respect to the mean position of the driven particle $\langle \mathbf{Z}(t) \rangle_0$, see Eq. (3.56). The curves in this plot are then independent of all the other parameters.

In Appendix H of Ref. [104] we derive again, using linear response theory, the value of the temporal average of the oscillations for small driving amplitudes $\mathbf{A}$: its expression is given in Eq. (H2) therein, and it does not coincide with the value of $\mathbf{b}_0$ in Eq. (3.51) if not for $\mathbf{A} = 0$. Indeed, linear response theory cannot capture the effect of the dynamical perturbation on the mean value of the oscillations, which is quadratic in $\mathbf{A}$ (being $J_0(x) \simeq 1 \quad x^2/4$ for small x in Eq. (3.51)).

3.3.3.2 Amplitude

The amplitude of the n-th harmonic of $\langle \mathbf{Y}_{\text{ad}} \rangle$ is found by inspecting Eq. (3.49), and it reads

$$|\mathbf{b}_n(\Omega)| = \frac{|\mathbf{b}_n(\Omega = 0)|}{\sqrt{1 + (n\Omega/\gamma_y)^2}}. \tag{3.52}$$

It is interesting first to compare the relative magnitude of $|\mathbf{b}_n(\Omega = 0)|$ for various n: they are plotted in Fig. 3.3a as a function of the ratio $r/r_\Delta = (\Delta/\xi)^2$ (see Eq. (3.44)). For $r \simeq r_\Delta$ the amplitude of the first harmonic attains a maximum: this corresponds to the correlation length ξ being of the same order as the average separation Δ between the two traps, i.e., $\xi \sim \Delta$.

In general, it appears from Fig. 3.3a that the adiabatic response is essentially and generically determined by its dominant first harmonic. Although higher harmonics become more relevant when the amplitude A of the driving is much larger than the effective particle radius $\widetilde{R}$, they still remain small compared to the first harmonic as long as A and $\widetilde{R} \ll \Delta$. As an exception, however,

Fig. 3.3a shows that the first harmonic is significantly reduced at a small value of r which we denote by r_1. Expanding for small forcing amplitudes $\mathbf{A}$ the equation $|(\mathbf{b}_1)_i| \equiv 0$ that defines r_1, one finds

$$A^j \int \frac{\mathrm{d}^d q}{(2\pi)^d} \frac{e^{-q^2\widetilde{R}^2}}{q^2 + r_1} q_i q_j e^{i\mathbf{q}\cdot} \equiv 0. \tag{3.53}$$

This equation turns out to be the same as the condition in Eq. (C.55), which defines the distance $\mathbf{x}_{\max}$ at which the field-induced interparticle force $\mathbf{F}_c(\mathbf{x})$ is maximum (see Fig. 3.2a), as it is clear by identifying $\mathbf{x} \equiv$ and $v(\mathbf{q}) \equiv \exp\left(-q^2\widetilde{R}^2\right)$. The physical interpretation is the following: for $r = r_1$ and small $\mathbf{A}$, the average interparticle distance actually coincides with the distance $\mathbf{x} = \mathbf{x}_{\max}$ at which the field-induced force $\mathbf{F}_c(\mathbf{x})$ is maximum. Expanding $\mathbf{F}_c(\mathbf{x})$ at the leading order around $\mathbf{x} = \mathbf{x}_{\max}$ gives a force gradient which is at least quadratic in $|\mathbf{x} \quad \mathbf{x}_{\max}|$, so that the response loses its linear component (i.e., the first harmonic in its Fourier expansion — for example, feeding $\sin(\Omega t)$ into a quadratic force gradient would render $\sin^2(\Omega t)$, whose frequency is doubled). Note that the identification between Eqs. (3.53) and (C.55) is not accidentally due to the choice of a Gaussian interaction potential $V_q = \exp(-q^2R^2/2)$: the generalization to another interaction potential V_q' is straightforwardly obtained by replacing $\exp\left(-q^2\widetilde{R}^2\right) \mapsto |V_q'|^2 \exp(-q^2T/2\kappa_p)$ in Eq. (3.53) (see Eqs. (3.24) and (3.33)). In both cases, we see that the only effect of the temperature T is to renormalize the parameter R (which characterizes V_q) by the mean-square displacement of the particle in the trap; in the case in which V_q is Gaussian, R gets simply replaced by $\widetilde{R}$ defined in Eq. (3.33).

In Appendix C.6.3 we determine the value r_1 of r at which this frequency doubling occurs for the case $d = 1$ (see Eq. (C.84)). However, from the above discussion it emerges that a similar qualitative behavior holds also for $d > 1$, as we check within linear response theory in Appendix H of Ref. [104]. Indeed, the occurrence of frequency doubling relies only on the existence of a local maximum in the induced force (see Fig. 3.2a), a feature which goes possibly beyond our particular choice of a Gaussian interaction potential $V(\mathbf{x})$ (see, for instance, the analysis of the theta-potential in Appendix C.5 and that of the critical Casimir force in Ref. [107]). We anticipate here that frequency doubling is actually a feature of the adiabatic response which is observed in the full dynamical response only when the adiabatic approximation is applicable — this will be shown below in Section 3.4.1.

Finally, for any given value of r, Eq. (3.52) shows that the amplitude $|\mathbf{b}_n|$ is maximum at low driving frequencies Ω, while it decays as $\sim \Omega^{-1}$ upon increasing Ω beyond values that are larger than $\tau_y^{-1} \equiv \gamma_y$: this is shown in Fig. 3.3b, where the amplitude $|\mathbf{b}_1|$ of the first harmonic is plotted as a function of Ω/γ_y. We recall that τ_y is the timescale that characterizes the relaxation of the particle $\mathbf{Y}$ in its harmonic trap.

3.3.3.3 Phase

When $r > r_1$ the adiabatic response is dominated by its first harmonic, which is completely characterized by its amplitude $|\mathbf{b}_1|$ studied above and by its phase θ_1 (see Eq. (3.45)), which we

analyze here. This phase can be extracted from the complex Fourier coefficient $\mathbf{b}_1$ in Eq. (3.49) as

$$\theta_1 = \quad \theta_y + \theta \quad + \pi/2\big) + \pi \times \mathrm{sign}(\mathcal{I}_1), \tag{3.54}$$

where θ_a is given in Eq. (3.28) and $\mathrm{sign}(\mathcal{I}_1) = \pm 1$, depending on the sign of $\mathcal{I}_1$ given in Eq. (3.50). In $d = 1$ and for $r > r_1$, the integral $\mathcal{I}_1$ is negative: this can be checked via a numerical evaluation of Eq. (3.50) within a range of parameters compatible with our physical setting in Fig. 3.1, i.e., $\Delta \gg A, \widetilde{R}$. We recall that the average motion of the driven particle is given, at lowest order in λ, by (see Appendix C.1)

$$\langle \mathbf{Z}(t) \rangle_0 = \mathbf{\Delta} + \mathbf{A} \cos(\Omega t \quad \theta \quad \pi/2), \tag{3.55}$$

where the average is computed over the independent ($\lambda = 0$) process. By comparing Eqs. (3.54) and (3.55) with Eq. (3.45), we can extract the actual phase difference $\delta\theta$ between $\langle \mathbf{Y}(t) \rangle$ and $\langle \mathbf{Z}(t) \rangle_0$, i.e.,

$$\delta\theta \equiv \theta_1 \quad (\quad \theta \quad \pi/2) = \quad \theta_y \quad \pi. \tag{3.56}$$

In the slow-forcing limit $\Omega \ll \gamma_y$ it is $\theta_y \to 0$, and from Eq. (3.56) we deduce that the particle $\mathbf{Y}(t)$ moves in counterphase with respect to $\mathbf{Z}(t)$. This is physically expected, as the particle $\mathbf{Y}$ feels a stronger attraction when the particle $\mathbf{Z}$ is closer to it than when it is further apart. In the fast-forcing limit $\Omega \gg \gamma_y$, where $\theta_y \to \pi/2$, we get instead $\delta\theta = \quad 3\pi/2$: the particle $\mathbf{Y}(t)$ develops a $\pi/2$ phase shift with respect to the driven particle $\mathbf{Z}(t)$. The situation is depicted in Fig. 3.3b (inset), where we plot the phase difference $\delta\theta$ and we show that it varies smoothly by $\pi/2$ over a scale determined by γ_y.

We mention that a richer phenomenology is expected in spatial dimension $d > 1$, where the direction of the driving $\mathbf{A}$ could in principle be chosen to be orthogonal to that of the average separation between the two traps. In this setup, one can check that the sign of the integral $\mathcal{I}_1$ in Eq. (3.50) is positive, so that Eq. (3.56) reads $\delta\theta = \quad \theta_y$. In the slow-forcing limit in which $\theta_y \to 0$, the two particles would then move in phase ($\delta\theta = 0$), as physically expected by arguing again that their attraction is stronger when they are spatially close to one another, than when they are further apart.

3.4 Analysis of the dynamical response

In this section we analyze the dynamical response $\langle \mathbf{Y}(t) \rangle$ of the particle in the fixed well, within the weak-coupling approximation given in Eq. (3.29). All the figures we present and discuss below refer for simplicity to the case $d = 1$, but the main qualitative features of the response persist in higher spatial dimensions.

We start by focusing on the Fourier coefficients of the dynamical response given in Eq. (3.48) and by comparing them to those of the adiabatic response given in Eq. (3.47). First and not surprisingly, they coincide for a vanishing driving frequency, i.e., $\mathbf{c}_n(\Omega = 0) = \mathbf{b}_n(\Omega = 0)$: their difference is only manifest in the dynamics. Secondly, a common factor $(1 + in\Omega/\gamma_y)^{\ 1}$ multiplies both sets of coefficients, and this is the only place where the relaxation timescale $\tau_y{}^1 = \gamma_y$ of the fixed trap appears. We have seen in Section 3.3.3 how it is this factor alone that determines

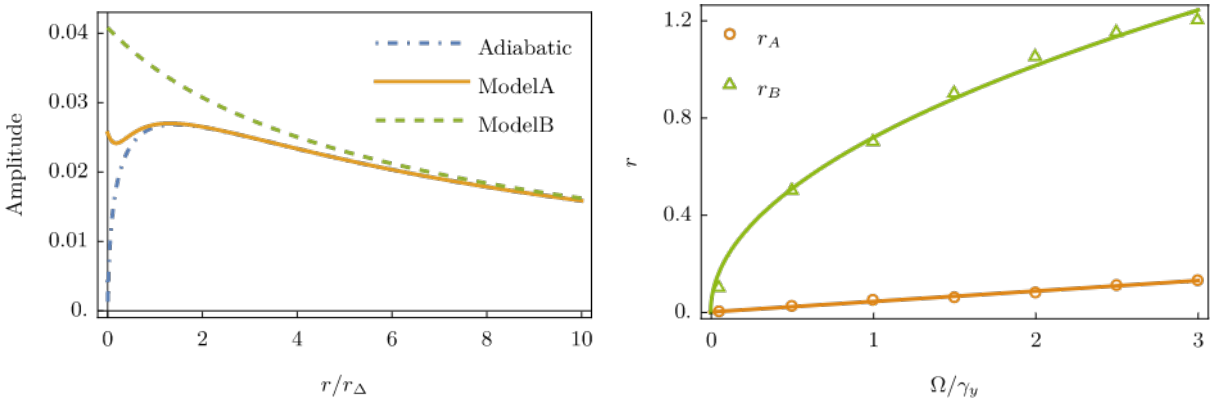

(a) (b)

Figure 3.4: **a)** Amplitude $|b_1|$ and $|c_1|$ of the first (and most relevant) Fourier components in the adiabatic and dynamical response for model A and B, plotted as a function of $r/r_\Delta = (\Delta/\xi)^2$ (see Eq. (3.44)). The amplitudes of the oscillations in the two cases are particularly different upon decreasing r for $r < r_\Delta$, where the adiabatic response reaches its maximum before decreasing towards zero (see also Fig. 3.3a and the discussion in Section 3.4.1). Here the amplitude is plotted for a driving frequency $\Omega < \Omega_{\text{peak}}$ (see discussion in Section 3.4.2.1). The parameters used in the plot are $\gamma_y = 1$, $D = 10$, $\widetilde{R} = 0.7$, $\Delta = 3$, $A = 1$, and $\Omega = 0.35$. **b)** Values $r_{A,B}$ of the parameter r such that, for a given value of the driving frequency Ω, the amplitude of the dynamical response in model A, B matches that of the adiabatic approximation (see the main text for further explanations). By scaling arguments, we expect $r_A \sim \Omega$ and $r_B \sim \sqrt{\Omega}$ (see Eq. (3.57)). The parameters used in the graph are $\gamma_y = 1$, $D = 100$, $\widetilde{R} = 0.7$, $\Delta = 3$, and $A = 1$.

the properties of the adiabatic response as a function of Ω, see Eq. (3.49); its qualitative features (amplitude, phase) are analogous to those of a low-pass filter in circuit electronics. Even though the dependence on Ω is more complicated in Eq. (3.48), this "filter" remains and it characterizes the dynamical response for frequencies $\Omega \geq \gamma_y$.

We noticed in Section 3.3.3.2 that, in general, the first Fourier harmonic dominates the adiabatic response (see Fig. 3.3a). One can check that this is also the case for the dynamical response, both at low Ω (which is not surprising, since for $\Omega = 0$ the two sets of Fourier coefficients $\mathbf{b}_n$ and $\mathbf{c}_n$ coincide) and for higher driving frequencies because, for large Ω, one has $|\mathbf{c}_n| \sim (n\Omega)^{-2}$ from Eq. (3.48). In the following, we will then focus mostly on the analysis of the first harmonic, bearing in mind that the zeroth harmonic, i.e., the average value around which the particle $\mathbf{Y}$ oscillates, is the same as that of the adiabatic approximation (see Eq. (3.51)), whose features have been described in Section 3.3.3.1.

3.4.1 Adiabatic limit

Let us first compare the dynamical response to the adiabatic one. Looking at Fig. 3.4a, which shows the amplitude of the first harmonic as a function of $r = \xi^{-2}$, it appears that for any fixed value of the driving frequency Ω there exists a threshold value r_A or r_B (depending on the model considered) such that for $r \geq r_{A,B}(\Omega)$ the system dynamics becomes effectively adiabatic. When

this happens, the amplitude of the dynamical response in model A/B is very well approximated by that of the adiabatic response, and the corresponding curves in Fig. 3.4a coincide.

This can be understood in terms of the competition between the relaxation timescale τ_ϕ of the field, which is given in Eq. (1.25), and the one set by the external periodic driving, i.e., $\tau_\Omega \sim \Omega^{-1}$. Typical field fluctuations are those with wavevector $q \sim \xi^{-1}$, where $\xi \sim r^{-1/2}$ is the field correlation length. We expect the adiabatic approximation to be accurate when the timescale τ_ϕ^{typ} of these typical fluctuations is much shorter than τ_Ω, i.e., $\tau_\phi^{\text{typ}} \equiv \tau_\phi(q \sim \xi^{-1}) \ll \tau_\Omega$: a simple calculation indicates that the threshold values $r_{A,B}$ are given by

$$r_A \sim \Omega/D, \qquad r_B \sim \sqrt{\Omega/D}. \tag{3.57}$$

This is verified in Fig. 3.4b, where we plot r_A and r_B as a function of the driving frequency Ω. The symbols correspond to numerical estimates of $r_{A,B}$ obtained by inspecting plots analogous to that of Fig. 3.4a, while the solid lines correspond to Eq. (3.57).

Note that the timescale $\tau_y \sim \gamma_y^{-1}$, which characterizes the relaxation of the particle **Y** in its harmonic trap, does not affect this interplay between τ_Ω and τ_ϕ. As anticipated above, it merely contributes a common scaling factor $[1 + (\Omega/\gamma_y)^2]^{-1/2}$ to the amplitude of the first harmonic and results into a phase shift θ_y given by Eq. (3.28). This is in fact consistent with the effective field interpretation we gave in Section 3.2.3: the particle **Y** moves under the effect of the excitations generated on the field ϕ by the motion of the particle **Z**. Any feedback of the particle **Y** on the field is neglected, because we are considering only the lowest nontrivial order in a perturbative expansion in the coupling λ. Accordingly, adiabaticity depends on how faithfully the field ϕ (which relaxes on a finite timescale) is able to transmit the excitation generated by the motion of the particle **Z**: the smaller the driving frequency Ω, the more accurate this transmission becomes. What happens to the particle **Y** after the "message" is received will only eventually depend on its characteristic timescale τ_y.

Outside the adiabatic regime, the adiabatic and dynamical responses are qualitatively different especially for $r < r_\Delta = \Delta^{-2}$, the latter being the value of r around which the adiabatic response reaches its maximum (see Fig. 3.4a and the discussion in Section 3.3.3.2). This also marks the point at which the correlation length of the field becomes of the same order of magnitude as the average separation between the two traps, i.e., $\xi \sim \Delta$. In Section 3.3.3.2 we described the phenomenon of frequency doubling in the adiabatic response: the amplitude of its first harmonic decreases upon decreasing r below r_Δ, and vanishes at $r = r_1$ (see Fig. 3.3b). We can conclude that, in general, frequency doubling is not observed in the dynamical response, unless the adiabatic approximation is accurate (i.e., at small driving frequency Ω and large field mobility D, according to the discussion above).

3.4.2 Frequency dependence of the dynamical response

The behavior of the actual dynamical response in Eq. (3.29) as a function of the driving frequency Ω is richer than that of the adiabatic response. The limiting cases of slow and fast driving are analytically accessible, while for intermediate values of the driving frequency Ω we can evaluate

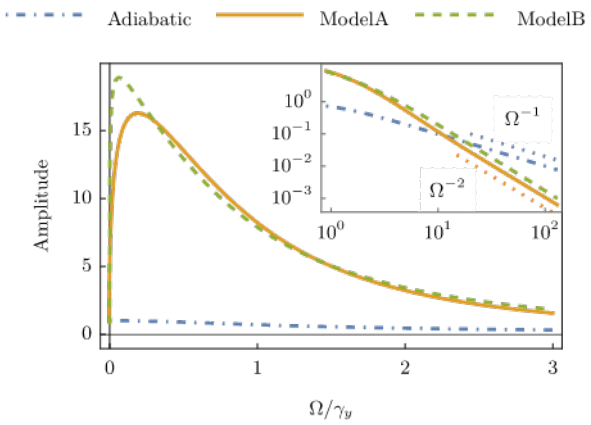

Figure 3.5: Amplitudes $|b_1|$ and $|c_1|$ of the first Fourier harmonic in the adiabatic and dynamical responses, respectively, shown as functions of the driving frequency Ω in $d = 1$, for both models A and B. For large Ω, the amplitude decays as Ω^{-1} for the adiabatic response and as Ω^{-2} in the dynamical case (see the inset in log-log scale, where we indicated the asymptotic behaviors with dotted lines). For small values of Ω, the dynamical response is typically larger than the one predicted by the adiabatic approximation, and it is peaked around Ω_{peak} given in Eq. (3.59). Close to $\Omega \sim 0$, both responses collapse on their static amplitude given in Eq. (3.58); all the curves in this plot are normalized by this value. The parameters used in the graph are $\nu_y = 1$, $\kappa_y = 1$, $D = 1$, $\widetilde{R} = 0.7$, $\Delta = 3$, $A = 1$, and $r = 10^{-4}$.

numerically the integrals that appear in Eq. (3.29). We can then use the insight we gained in Section 3.3.3 in order to rationalize the qualitative behavior observed in the plots.

In order to simplify the discussion by enforcing a separation of timescales, we consider in this Section a large value of the inverse timescale $\gamma_y = \tau_y^{-1}$. Indeed, as anticipated above, the amplitude of $\langle \mathbf{Y}(t) \rangle$ is significantly reduced at frequencies $\Omega \gg \gamma_y$, and this would make the features of the dynamical response hardly appreciable. Let us also set the parameter $r \ll r_\Delta$ (see Eq. (3.44)), a choice which we will motivate further below.

3.4.2.1 Amplitude

The main qualitative features of the dynamical response are displayed in Fig. 3.5, where we plot the amplitude $|\mathbf{c}_1|$ of the first Fourier harmonic (see Eq. (3.48)) as a function of Ω for models A and B, and we compare it to the amplitude of the adiabatic response. For vanishing Ω both responses collapse on a common quasi-static curve, which follows from Eqs. (3.45) and (3.47) to (3.50) as

$$2|\mathbf{b}_1(\Omega = 0)| = 2|\mathbf{c}_1(\Omega = 0)| = 2\lambda^2 \mathcal{I}_1/\kappa_y. \tag{3.58}$$

For small but nonzero Ω, on the other hand, the dynamical response is typically larger than the one predicted within the adiabatic approximation. The former appears to be peaked around a frequency Ω_{peak} which can be identified as the inverse relaxation timescale of the field ϕ over a distance comparable with the average separation Δ between the two traps. This can be obtained

from Eq. (1.25) by setting $q \simeq 1/\Delta$: for $r \ll r_\Delta = \Delta^{\ 2}$, we find

$$\Omega_{\text{peak}} \sim \tau_\phi^{\ 1}(q \simeq 1/\Delta) \simeq D/\Delta \ , \tag{3.59}$$

where $= 2 +$ is the dynamical critical exponent of the field ϕ (we recall that $= 0$ and 2 for model A and B respectively [54]). Accordingly, Ω_{peak} is different for model A and model B dynamics.

Finally, for large Ω, the amplitude of the dynamical response decays as $\Omega^{\ 2}$, at odds with the adiabatic response which decays as $\Omega^{\ 1}$, so that the former becomes eventually smaller than the latter. This is shown in the inset of Fig. 3.5, where the amplitude is plotted as a function of Ω in log-log scale, together with the asymptotic decays mentioned above.

Let us now motivate the choice $r \ll r_\Delta$. The argument we gave in Section 3.4.1 when discussing the adiabatic limit can be reversed: for every fixed value of the parameter r, there will be a driving frequency $\Omega_{A,B}(r)$ such that, when $\Omega \leq \Omega_{A,B}(r)$, the dynamics of the system is well approximated by the adiabatic one. Their value can be found by inverting Eq. (3.57), i.e.,

$$\Omega_A \sim Dr, \qquad \Omega_B \sim Dr^2. \tag{3.60}$$

Since the characteristic frequency scale of the dynamical response is given by Ω_{peak} (see Fig. 3.5), in order to appreciate the difference with respect to the adiabatic response we must require $\Omega_{A,B}(r) \ll \Omega_{\text{peak}}$. By choosing $r \ll r_\Delta$ this requirement is automatically satisfied, as it can be checked by using the definition of Ω_{peak} in Eq. (3.59). If, on the contrary, one chooses $r \quad r_\Delta$, then intermediate cases occur in which the peak shifts towards larger values of Ω, while still remaining far from the adiabatic limit.

Similarly, in plotting the amplitude of the dynamical response as a function of r in Fig. 3.4a we chose $\Omega \ll \Omega_{\text{peak}}$. In fact, had we chosen instead $\Omega \gg \Omega_{\text{peak}}$, the dynamical amplitude would have been smaller than the adiabatic amplitude, and it would have approached the latter from *below* in correspondence of $r_{A,B}(\Omega)$.

3.4.2.2 Phase

In analogy with what we did for the adiabatic response discussed in Section 3.3.3.3, from the Fourier coefficient $\mathbf{c}_1$ in Eq. (3.48) one can determine the phase of the dynamical response which we indicate by φ_1, so as to distinguish it from the phase θ_1 of the adiabatic response. In particular, one finds

$$\varphi_1 = \quad \theta_y + \theta \ + \pi/2) + \arg(I_1), \tag{3.61}$$

where $\arg(I_1)$ indicates the argument of the complex integral

$$I_1 \equiv \int \frac{\mathrm{d}^d q}{(2\pi)^d} \frac{q_{||} q \ J_1(\mathbf{q}\cdot\mathbf{A})}{_q + i\Omega} e^{\ q^2\widetilde{R}^2 + i\mathbf{q}\cdot\Delta}. \tag{3.62}$$

In the expression above $q_{||}$ indicates the component of $\mathbf{q}$ along $\mathbf{A}$ and . For $\Omega \to 0$, we note that $I_1 \simeq \mathcal{I}_1/D$ (see Eq. (3.50)) and we recover the adiabatic limit with $\varphi_1 \simeq \theta_1$. For $\Omega \to \infty$, instead, one finds

$$I_1 \simeq \frac{1}{i\Omega} \int \frac{\mathrm{d}^d q}{(2\pi)^d} q_{||} q \ J_1(\mathbf{q}\cdot\mathbf{A}) e^{\ q^2\widetilde{R}^2 + i\mathbf{q}\cdot\Delta}. \tag{3.63}$$

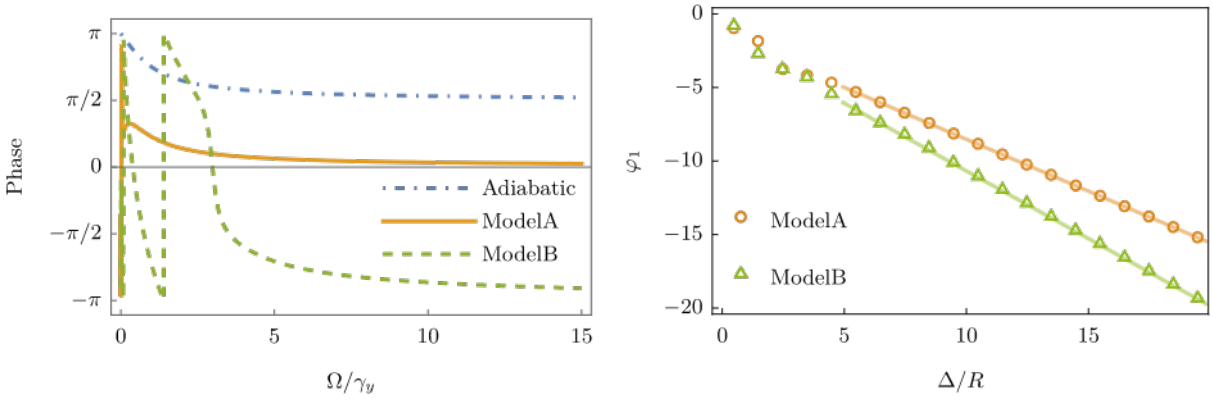

(a) (b)

Figure 3.6: **a)** Phase of the adiabatic and dynamic responses, shown as a function of the driving frequency Ω in $d = 1$. In both cases the relative phases $\delta\theta$ and $\delta\varphi$, respectively, are measured with respect to the motion of the driven particle $\langle \mathbf{Z}(t)\rangle_0$ (see Eqs. (3.56) and (3.64)). For large values of Ω, the response in model A is in phase with the motion of the driven particle (i.e., $\delta\varphi \to 0$), while in model B it is in counterphase (i.e., $\delta\varphi \to \pi$). They are both in contrast with the adiabatic approximation, which predicts a $\pi/2$ phase shift $\delta\theta$. For sufficiently small Ω, the three responses must coincide and we recover the physically familiar picture in which the motion is in counterphase with respect to $\langle \mathbf{Z}(t)\rangle_0$ with $\delta\varphi = \delta\theta = \pi$. For intermediate values of Ω, the phase in the dynamical response varies rapidly and non-monotonically, if $\widetilde{R} \ll \Delta$, before reaching its asymptotic value. The parameters used in the plot are $\gamma_y = 1$, $D = 10^{-3}$, $\widetilde{R} = 0.4$, $\Delta = 3$, $A = 0.1$, and $r = 10^{-3}$. **b)** Phase φ_1 of the dynamical response, shown as a function of the distance Δ between the two traps, for small values of the driving frequency Ω (see the main text). The behavior of φ_1 as a function of Δ is asymptotically linear, with a slope κ which is independent of the spatial dimensionality d; for the case of model A, it is predicted by Eq. (3.66). The parameters used in the graph are $\gamma_y = 1$, $D = 0.1$, $\widetilde{R} = 1$, $A = 0.1$, and $r = 10^{-3}$.

In analogy with Section 3.3.3.3, we focus on the phase difference $\delta\varphi$ with respect to the motion of the driven particle $\langle \mathbf{Z}(t)\rangle_0$, i.e.,

$$\delta\varphi \equiv \varphi_1 \quad (\quad \theta \quad \pi/2) = \quad \theta_y + \arg(I_1). \tag{3.64}$$

Recalling that $\theta_y \to \pi/2$ for large Ω, it follows from Eq. (3.63) that $\delta\varphi \simeq \pi/2 \pm \pi/2$, where the sign of the last term can be determined by performing the integration over $\mathbf{q}$ in Eq. (3.63) and it is in general different for model A or B (see Appendix C.7 — in $d = 1$, the plus sign corresponds to model A, and the minus sign to model B). The motion of $\mathbf{Y}$ for large Ω is thus either in phase or in counterphase with the motion of the driven particle, depending on the model: in both cases, this is in sharp contrast with the adiabatic approximation, which predicts a $\pi/2$ phase shift (see Fig. 3.3b in the same limit). However, the approximation we used to derive Eq. (3.63) can only be accurate if Ω is larger than all the physical frequencies involved in the problem. If we assume that the system is sufficiently close to criticality so that $\xi \gg \widetilde{R}$, then the effective particle radius $\widetilde{R}$ plays the role of a cutoff and the fastest timescale is represented by $\tau_\phi(q \sim 1/\widetilde{R})$. Accordingly,

we expect the dynamical phase to reach its asymptotic value for

$$\Omega \gg \Omega_{\text{cutoff}} \equiv \tau_\phi^{-1}(q \sim 1/\widetilde{R}) \sim D/\widetilde{R} \ . \tag{3.65}$$

Recall that the amplitude $|\mathbf{c}_1|$ of the dynamical response starts decreasing for $\Omega \gg \Omega_{\text{peak}}$ (see Section 3.4.2.1 and Eq. (3.59)), and within our setup of Fig. 3.1 with $\widetilde{R} \ll \Delta$ it is $\Omega_{\text{cutoff}} \gg \Omega_{\text{peak}}$. As a result, the asymptotic value of φ_1 will not be reached in practice if not for vanishing values of the amplitude $|\mathbf{c}_1|$, and one observes instead a phase which is rapidly changing as a function of Ω, different in general from the adiabatic phase θ_1 (if not by coincidence). This can be seen in Fig. 3.6a, which compares the relative phase $\delta\varphi$ of the dynamical response to that of the adiabatic response, $\delta\theta$, as a function of Ω.

Moreover, since $\widetilde{R}$ (which enters in I_1 defined in Eq. (3.62)) depends on the temperature T via Eq. (3.33), an interesting outcome of the analysis presented above is that the phase φ_1 itself is T-dependent in our model. This was not the case for the phase θ_1 within the adiabatic approximation, see Eq. (3.54).

Finally, in Fig. 3.6b we plot the phase φ_1 as a function of the average separation Δ between the traps and for small values of the driving frequency Ω: the dependence of φ_1 on Δ turns out to be linear for sufficiently large Δ. The corresponding slope k is independent of the spatial dimensionality d, and it can be extracted explicitly in the case of model A by using the method of steepest descent: this is done in Appendix C.7.2, where we show that

$$k \equiv \frac{\partial\varphi_1}{\partial\Delta} = \left[r^2 + (\Omega/D)^2\right]^{1/4} \sin\left(\frac{1}{2}\arctan\left(\frac{\Omega}{Dr}\right)\right). \tag{3.66}$$

This fact suggests an interesting interpretation within the effective field picture presented in Section 3.2.3. Indeed, the response of the particle $\mathbf{Y}$ to a small sinusoidal perturbation generated by the particle $\mathbf{Z}$ at a distance Δ apart effectively reads

$$\langle \mathbf{Y}(t) \rangle \simeq \mathbf{R}(\Omega)\cos(\Omega t \quad k\Delta + \varphi_k), \tag{3.67}$$

where the phase shift φ_k and $\mathbf{R}(\Omega) \simeq |\mathbf{c}_1|$ (see Eq. (3.48)) depend in general on the various parameters of the problem. Equation (3.67) describes a wave propagating out of the source $\mathbf{Z}(t)$, and in this analogy the parameter k plays the role of an effective wavenumber. This simplified picture does not apply when Ω becomes large compared to the other characteristic frequencies of the system, because then we have seen that φ_1 must saturate to a constant limiting value (which is, in particular, independent of Δ). Moreover, albeit small, the contribution of higher harmonics will still modify the first harmonic contribution described by Eq. (3.67).

3.5 Numerical simulation

In this Section we investigate the validity of our analytical predictions, derived within the weak-coupling expansion, by direct integration of the coupled Langevin equations of motion of the field in Eq. (3.4), and of the two particles in Eqs. (3.6) and (3.7). To this end, we discretize the field ϕ over a lattice of side L in $d = 1$ or $d = 2$ spatial dimensions, as described in Appendix C.8,

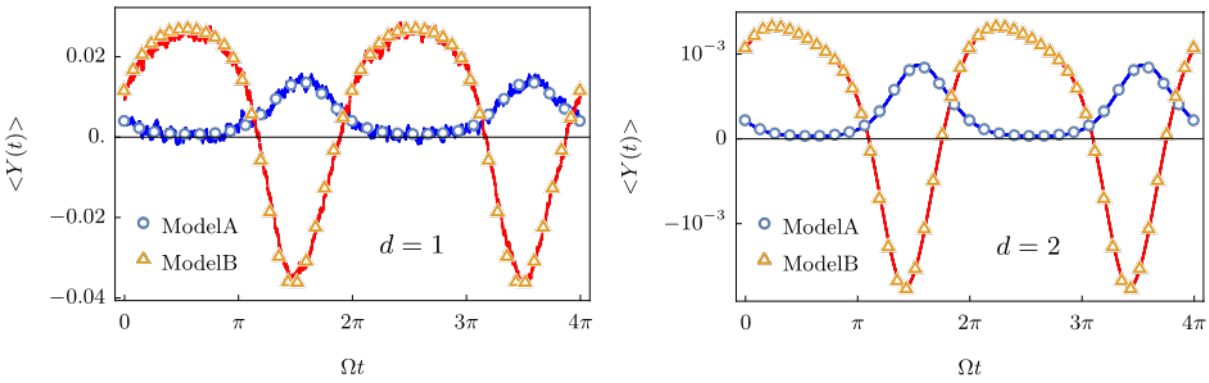

(a) (b)

Figure 3.7: Average position $\langle Y(t)\rangle$ of the particle in the fixed trap, (a) in $d = 1$, and (b) in $d = 2$. The results of the numerical simulations (colored lines) are reported together with the analytical prediction in Eq. (3.29) (symbols), showing excellent agreement. The parameters used in both graphs are $\nu_y = 1$, $D = 1$, $\kappa_y = 0.1$, $r = 0.1$, $\lambda = 0.5$, $\Delta = 20$, $A = 5$, $\Omega = 2\pi \times 10^{-3}$, lattice side $L = 128$, and integration time step $\delta t = 0.01$. In panel (a) we set $R = 1.5$, $T = 0.01$, and we averaged over $N = 10^5$ realizations of the thermal noise appearing in Eqs. (3.4) and (3.6). In panel (b) the noise is absent (corresponding to $T = 0$), and we take a single realization of the dynamics with the effective particle radius $\widetilde{R} = 1.5165$ (see the main text), corresponding to the values of R and T considered in panel (a) and as obtained from Eq. (3.33).

and we assume periodic boundary conditions. We consider, for simplicity, the limit $\kappa \to \infty$ for the driven particle $\mathbf{Z}(t)$, which thus evolves deterministically according to Eq. (3.12), while the second particle $\mathbf{Y}(t)$ undergoes Brownian diffusion under the effects of its fixed trap.

We first simulate the system in $d = 1$ in the presence of noise. Figure 3.7a compares the average over many realizations of the simulated trajectories of the particles with the analytical predictions in Eq. (3.29), showing a good agreement for both model A and model B. For this simulation we chose a set of parameters that poses model A close to the adiabatic regime, while model B is actually far from it. As a result, the curve corresponding to model A is (almost) in counterphase with respect to the external driving $\sim A \sin(\Omega t)$, while the curve corresponding to model B has a generic phase. We chose a large value of the driving amplitude A so as to emphasize also the contribution of higher Fourier harmonics, although the first harmonic still dominates the response, as expected.

A further conclusion we can draw from this agreement between theoretical predictions and numerical simulations is the following. As we emphasized in Section 3.2.4, the prediction for $\langle \mathbf{Y}(t)\rangle$ in Eq. (3.29) does not distinguish the separate effects of having a larger particle radius R from those of a higher temperature T, being them tangled into the effective radius $\widetilde{R}$ defined in Eq. (3.33). This observation actually simplifies the task of performing numerical simulations in higher spatial dimension d, where they become longer and more resource-demanding: we simply set $T = 0$ and simulate the noiseless (i.e., deterministic) equations of motion, correcting $\widetilde{R}$ accordingly. Figure 3.7b exemplifies this in $d = 2$, for the same set of parameters as those used in Fig. 3.7a. The curves we observe are qualitatively similar to those in $d = 1$, and again they

are in good agreement with the analytical prediction. In this second plot it appears even more evidently that the oscillations of the probe particle are not harmonic, as a result of the nonlinear interaction.

3.6 Extension to many particles

In Section 3.2 we noted that the contribution of any additional particle enters linearly in the master equation (3.15) which describes the one-point probability $P_1(\mathbf{y}, t)$ of the position $\mathbf{Y}(t)$ of the particle. In Section 3.2.3 we further commented that the *effective field* in which the particle $\mathbf{Y}$ evolves can be obtained by simply summing the contributions of all the other particles, which are acting as source terms for the field ϕ. It would thus appear that multi-body effects are absent in our model, and that the induced interactions are indeed pairwise-additive, at odds with other types of fluctuation-induced interactions such as Casimir forces. Similar conclusions have been recently reached in Ref. [92], where it was shown that field-mediated forces between point-like particles linearly coupled to a Gaussian field in *equilibrium* are indeed pairwise-additive, independently of the strength of the linear coupling. However, this is in principle not the case for nonequilibrium settings, such as the one considered in this Chapter. Since our analysis was based on a perturbative description valid for a small coupling λ, it is then natural at this point to ask whether pairwise-additivity holds beyond the perturbative regime. In order to answer this question, we now assume that N particles $\{\mathbf{X}_1, \mathbf{X}_2, \dots, \mathbf{X}_N\}$ are in contact with the field ϕ as in Section 3.1, so that

$$\mathcal{H} = \mathcal{H}_\phi + \sum_{a=1}^{N} \mathcal{U}_a(\mathbf{X}_a) + \mathcal{H}_{\text{int}}, \tag{3.68}$$

where $\mathcal{U}_a$ are generic confining potentials, and

$$\mathcal{H}_{\text{int}} = \lambda \sum_{a=1}^{N} \int \mathrm{d}^d\mathbf{x}\, \phi(\mathbf{x}) V^{(a)}(\mathbf{x} \quad \mathbf{X}_a) \tag{3.69}$$

generalizes Eq. (3.3) to many particles. The field ϕ still evolves according to Eq. (3.4), while the particles follow

$$\dot{\mathbf{X}}_a(t) = \mathbf{F}_a(\mathbf{X}_a, t) + \lambda v_a \mathbf{f}_a(\mathbf{X}_a, \phi) + \boldsymbol{\xi}^{(a)}(t), \tag{3.70}$$

where we denoted by v_a the mobility coefficients, $\boldsymbol{\xi}^{(a)}(t)$ are independent white Gaussian noises with the same variance as in Eq. (3.9), and $\mathbf{f}_a$ is defined as in Eq. (3.8). To make contact with Eq. (3.6) we can choose $\mathbf{F}_a(\mathbf{X}_a, t) \equiv \quad v_a \nabla_{X_a} \mathcal{U}_a(\mathbf{X}_a(t))$, so as to describe the equilibrium fluctuations of the particles in their confining potentials $\mathcal{U}_a(\mathbf{X}_a)$ and in contact with the field. However, $\mathbf{F}_a(\mathbf{X}_a, t)$ can also be explicitly time-dependent (e.g., as in Eq. (3.7)), so that the problem is in general out of equilibrium (and similar to the one discussed above).

In order to study the dynamics induced by the set of Langevin equations (3.4) and (3.70), it is convenient to consider the corresponding Martin–Siggia–Rose [29, 70–72] dynamical functional $\mathcal{S}[\phi, \tilde{\phi}, \{\mathbf{X}_a, \widetilde{\mathbf{X}}_a\}]$, as detailed in Appendix C.9. Here we indicated by $\tilde{\phi}(\mathbf{x}, t)$ and $\widetilde{\mathbf{X}}_a(t)$ the variables dynamically conjugate to $\phi(\mathbf{x}, t)$ and $\mathbf{X}_a(t)$, respectively. Integrating out the fields ϕ and

$\tilde{\phi}$ from the dynamical functional $\mathcal{S}$ formally yields an effective functional $\mathcal{S}_{\text{eff}}[\{\mathbf{X}_a, \widetilde{\mathbf{X}}_a\}]$: any expectation value over the realization of the noises of quantities such as $O[\{\mathbf{X}_a\}]$, involving the particles but not the field, can then be expressed as

$$\langle O[\{\mathbf{X}_a\}]\rangle = \int \left(\prod_{a=1}^{N} \mathcal{D}\mathbf{X}_a \, \mathcal{D}\widetilde{\mathbf{X}}_a\right) O[\{\mathbf{X}_a\}]\, e^{\ \mathcal{S}_{\text{eff}}[\{\mathbf{X}_a, \widetilde{\mathbf{X}}_a\}]}, \tag{3.71}$$

where $\mathcal{D}\mathbf{X}_a$ indicates a path integral over the realizations of $\mathbf{X}_a$ (and similarly for $\mathcal{D}\widetilde{\mathbf{X}}_a$).

The integration over the fields ϕ and $\tilde{\phi}$ in the dynamical functional $\mathcal{S}$ given in Eq. (C.100) is possible for any value of λ, because the field Hamiltonian $\mathcal{H}_\phi$ in Eq. (1.16) is Gaussian and the field-particles coupling is linear. This results in the effective functional

$$\mathcal{S}_{\text{eff}}[\{\mathbf{X}_a, \widetilde{\mathbf{X}}_a\}] = \mathcal{S}_0[\{\mathbf{X}_a, \widetilde{\mathbf{X}}_a\}] \quad \lambda^2 \mathcal{S}_\lambda[\{\mathbf{X}_a, \widetilde{\mathbf{X}}_a\}], \tag{3.72}$$

where the free part $\mathcal{S}_0$ can be expressed as a sum of single-particle contributions (see Eq. (C.99)),

$$\mathcal{S}_0[\{\mathbf{X}_a, \widetilde{\mathbf{X}}_a\}] = \sum_{a=1}^{N} \mathcal{S}_a[\mathbf{X}_a, \widetilde{\mathbf{X}}_a], \tag{3.73}$$

while the interacting part $\mathcal{S}_\lambda$ contains a sum over two-particle contributions (see Eq. (C.109)),

$$\mathcal{S}_\lambda[\{\mathbf{X}_a, \widetilde{\mathbf{X}}_a\}] = \sum_{a,b=1}^{N} \mathcal{S}_{ab}[\mathbf{X}_a, \widetilde{\mathbf{X}}_a, \mathbf{X}_b, \widetilde{\mathbf{X}}_b], \tag{3.74}$$

where the explicit form of $\mathcal{S}_{ab}$ is provided in Eq. (C.109). The dynamical action in Eq. (3.72) is markedly pairwise additive, as it is only written in terms of one- and two-body terms. Moreover, it is exact for any value of the coupling λ. We can thus conclude that higher-order corrections which we have not included in our perturbative calculation will have the effect of renormalizing the (pairwise) interaction potential, but they will not introduce any additional multi-body interaction. In this respect, the conclusions of Ref. [92] readily extend also out of equilibrium.

3.7 Summary of this Chapter

In this Chapter we considered two Brownian particles interacting with the same fluctuating field, which are therefore subject to field-mediated forces: these can be used to induce synchronization when one of the two particles is externally driven. In equilibrium, these forces can be obtained by integrating out the field degrees of freedom from the system composed by the particles and the field: within this *adiabatic* approximation, the effective Langevin dynamics of the particles remains Markovian. The same holds if the medium is not instantaneously in equilibrium, but still characterized by a relaxation timescale which is short compared to that characterizing the motion of the particles. However, if the relaxation time of the medium becomes longer, then the adiabatic approximation fails, and different techniques are needed to study the (nonequilibrium) dynamics of the particles.

We exemplified these facts by studying a simple, yet rich, model in which a scalar Gaussian field is linearly coupled to two overdamped Brownian particles kept spatially separated by two confining harmonic traps (Fig. 3.1). This is a natural extension of the model considered in Chapter 2 to the case of two particles. One of the two traps is driven periodically with a tunable frequency Ω, which allows us to probe the dynamical response of the other particle over a range of frequencies which spans across the various timescales of the system. As the field approaches its critical point $r = 0$, its relaxation timescale diverges, and one observes a gradual departure from the condition of adiabatic response presented above. Within a weak-coupling expansion, we first derived the master equation (3.20) that describes the dynamics of the non-driven particle in the nonequilibrium periodic state attained by the system at long times. This can be used to determine the cumulant generating function of the particle position reported in Eq. (3.25), from which one can deduce, inter alia, the average and variance of the actual *dynamical* response of the particle given in Eqs. (3.29) and (3.30), respectively.

The latter has to be compared to the adiabatic response in Eq. (3.41), which we derived in Section 3.3 under the assumption of fast field relaxation. Its behavior as a function of the driving frequency Ω is trivially analogous to that of a low-pass filter in circuit electronics (Fig. 3.3b), and therefore we focus on its dependence on the field correlation length $\xi = r^{1/2}$ (Fig. 3.3a): the amplitude of the oscillations induced on the particle in the fixed trap features a peak when $\xi \sim \Delta$, being Δ the average separation between the two traps, while it decays to zero for both larger and smaller values of ξ. Observing the response of such a particle then becomes a way to probe the equilibrium effective potential $V_c(\mathbf{x})$ induced between the two particles by the presence of the field, see Eq. (3.39) and Fig. 3.2a. Being $V_c(\mathbf{x})$ nonlinear, interesting phenomena such as frequency doubling can occur under periodic driving (see Section 3.3.3.2).

Conversely, the behavior of the actual dynamical response as a function of Ω is significantly richer and it is determined by the interplay between the various timescales characterizing the system. In particular, these are the relaxation time of the particle in its trap (see Eq. (3.11)), the timescale set by the external driving with frequency Ω, and the relaxation times of the field (see Eq. (1.25)) across the typical length scales of the system: the field correlation length ξ, the average separation Δ between the two traps, the radius R and the mean square displacement of the particle in the trap (see Eq. (3.33)). In Section 3.4 we studied in detail the amplitude (Figs. 3.4a and 3.5) and the phase (Figs. 3.6a and 3.6b) of this dynamical response. In particular, the amplitude of the oscillations displays a peak when the driving frequency Ω matches the relaxation timescale of the field over a length scale of the order of Δ (see Fig. 3.5). Moreover, for sufficiently slow driving, the phase φ_1 displays a linear dependence on Δ (see Fig. 3.6b and Eq. (3.66)). Both these features are not captured by the adiabatic response, whose amplitude decays monotonically upon increasing Ω, and whose phase θ_1 is Δ-independent. Finally, in the limit of fast driving (i.e., large Ω) the dynamical response predicts a $\pi/2$ phase shift with respect to the adiabatic approximation (see Fig. 3.6a), which is a clear effect of retardation.

In passing, we interpreted these results in terms of the *effective field* (see Section 3.2.3): within the weak-coupling approximation, one can study the dynamics of a tracer particle as if it were immersed in the effective field generated by the motion of all the other particles coupled to the

same field, which can be treated as source terms. In fact, it turns out that the excitations generated by each of these moving particles contribute additively to the average effective field given in Eq. (3.31). This feature persists beyond the perturbative regime, as we verified in Section 3.6 by determining the dynamical functional that describes the many-particle dynamics for any value of the coupling constant λ, and checking that it does not give rise to genuine many-body effects.

We finally tested the accuracy of the perturbative approach by comparing its analytical predictions with the results of the numerical integration of the coupled equations of motion of the particles and the field, finding in general a good agreement (see Fig. 3.7). We conclude by noting that not only the kind of systems investigated here are well within the reach of current experiments [36], but a similar setup has in fact already been studied in Ref. [35], where the motion of silica particles immersed in a near-critical binary liquid mixture was observed by digital video-microscopy, and synchronization of their motion under external driving was reported upon approaching the critical point.

4

Stochastic Thermodynamics and oscillating modes in correlated media

In this Chapter we elaborate further on the model discussed in the previous ones, and focus on the problem of a particle dragged at constant velocity through a correlated medium. The action of an external "agent", which pumps energy into the system by driving the particle, is expected to produce nontrivial energetic and entropic flows both within the medium, and between the medium and the particle. However, standard stochastic thermodynamics does not allow to describe such flows, because it relies on the assumption of a spatially structureless bath whose equilibrium is not perturbed by the presence of a driven probe. As we noted in the previous Chapters, these assumptions are generically violated in a medium that presents macroscopic spatio-temporal correlations.

In the first part of this Chapter (from Section 4.1 to Section 4.3) we thus extend the framework of stochastic thermodynamics [108, 109] to include the case in which the medium displays spatio-temporal correlations. We will discuss their implications on the statistics of the work injected in the system, and on the spatially-resolved heat dissipation density. Our construction naturally renders the standard stochastic thermodynamics for a probe in a white thermal bath upon setting $\lambda = 0$, where λ is the coupling between the probe and the fluctuating order parameter. With these new tools in hand, we will be in a position to analyze the problem of a particle dragged at constant velocity through the medium by a moving harmonic trap, which is a setup commonly used to study friction and viscosity in (active) microrheology experiments [46, 111, 112], and is prototypical in stochastic thermodynamics.

In the second part of this Chapter (from Section 4.4 to Section 4.6), we characterize further the particle statistics in the nonequilibrium steady state attained at long times in the driven trap. In particular, we will focus on the evolution of the average particle position after a small perturbation, and demonstrate that it can sustain oscillating modes due to the underlying correlated medium. This behavior is generically ruled out in Markovian overdamped systems, while it is reminiscent of recent observations with colloidal particles in viscoelastic media [47].

The content of this Chapter has been published as "D. Venturelli and A. Gambassi, *Memory-induced oscillations of a driven particle in a dissipative correlated medium*, 2023 New J. Phys. **25** 093025" [113], and in the preprint "D. Venturelli, S. A. M. Loos, B. Walter, É. Roldán, and A. Gambassi, *Stochastic thermodynamics of a probe in a fluctuating correlated field*, arXiv: 2305.16235" [114].

[1] Indeed, the driving considered here can be practically realized via optical tweezers [110].

4.1 Stochastic thermodynamics in a correlated medium

Stochastic thermodynamics provides a conceptual framework to investigate the entropic and energetic properties of fluctuating systems coupled to thermal baths, even far from equilibrium [108, 109, 115–118]. A crucial result in this context is the quantitative relation between the time-reversal asymmetry of the system fluctuations on the one hand, and the heat dissipated to the environment (and associated entropy production) on the other [119–122]. Most of the previous work relied on the assumption that the bath is at all times in equilibrium or in a nonequilibrium steady state, and displays no dynamical spatio-temporal correlations. In various contexts, however, the dynamics crucially hinges on spatio-temporal correlations of the environment — this is the case, e.g., for inclusions in lipid membranes [17–20], microemulsions [22–25], or defects in ferromagnetic systems [26–31]. As discussed in the previous Chapters, these correlations become long-ranged and particularly relevant when the environment is close to a critical point, as in the case, e.g., of colloidal particles in binary liquid mixtures [32–37]. Moreover, the simplified assumption of a structureless environment implies that all the information about local energy and entropy flows occurring within the environment is not taken into account. To generalize this paradigm, there is growing interest in extending concepts from stochastic thermodynamics towards systems with spatially extended correlations, such as pattern-forming statistical systems [123–126] or critical media [127–130]. Furthermore, a line of recent works discusses the irreversibility of active many-particle systems described by hydrodynamic field theories [126, 130–133]. These theoretical advances are driven by state-of-the-art experiments involving optical trapping, ultra-fast video-microscopy, or active particles [134–138].

In the following, we investigate the stochastic thermodynamics of a system consisting of a mesoscopic, externally driven probe coupled to a fluctuating medium. The latter is here represented by a scalar field obeying non-conserved or conserved dynamics [59], and the whole system (composed by the probe and the field) is immersed in a homogeneous heat bath at a fixed temperature T that induces thermal fluctuations. We provide suitable definitions for the heat, work and entropy exchanges between the probe, the field and the thermal bath, which are consistent with the first and second laws of stochastic thermodynamics. This approach is simpler than addressing a fully microscopic model, while it goes beyond a description based on a generalized Langevin equation [139–144] — which may capture temporal, but not spatial correlations of the environment (see Eq. (1.36)). Notably, our framework is particularly powerful when dealing with a fluctuating medium that is close to a critical point, where one can replace a complex microscopic dynamics with the simplest model belonging to the same universality class [6, 59]. Within the approach developed here, one can investigate the interplay between the probe, the spatio-temporal correlated field, and the heat bath under the light of stochastic thermodynamics. We illustrate the theory for the minimal yet insightful example in which the medium is represented by a fluctuating Gaussian field, as in Chapters 2 and 3.

Our starting point is a reference model similar to the one introduced in the previous Chapters: we consider a system formed by a mesoscopic probe located at $\mathbf{Y}(t) \in \mathbb{R}^d$ in d spatial dimensions and a scalar field, whose value at position $\mathbf{x} \in \mathbb{R}^d$ and time t is denoted by $\phi(\mathbf{x}, t) \in \mathbb{R}$. The

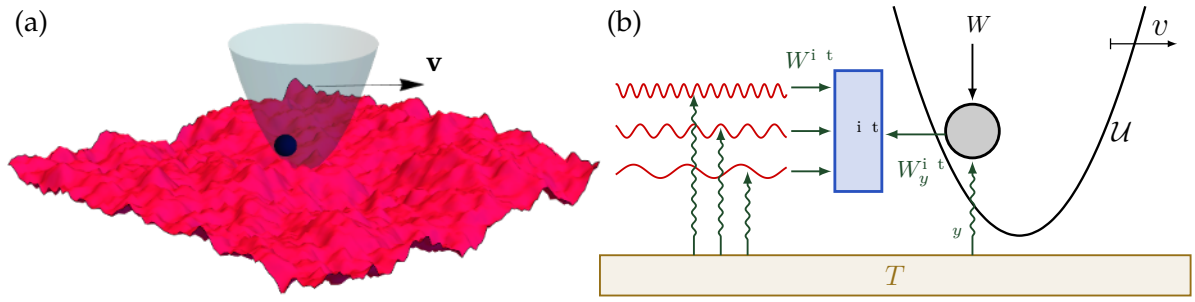

Figure 4.1: **a)** Sketch of a probe particle dragged by a trap with velocity $\mathbf{v}$ through a correlated field (red surface). **b)** Cartoon of the particle at position $\mathbf{Y}$, the modes of the field ϕ (red waves), and the particle–field interaction (blue box), which can store elastic energy $\mathcal{H}^{\rm int}$. Particle and field exchange heats $đQ_y$ and $đQ_\phi$, respectively, with a bath at temperature T. An external agent exerts work $đW$ on the particle. Particle and field may exchange energies $đW_y^{\rm int}$ and $đW_\phi^{\rm int}$, respectively, via their interaction. For clarity we do not indicate work exchanges between field modes. Heat fluxes are considered positive when they are supplied to the system.

Hamiltonian of the system is given by

$$\mathcal{H}[\phi, \mathbf{Y}, t] = \mathcal{H}_\phi[\phi] + \mathcal{H}^{\rm int}[\phi, \mathbf{Y}] + \mathcal{U}(\mathbf{Y}, t), \tag{4.1}$$

where $\mathcal{H}_\phi$ denotes the energy of the field, $\mathcal{U}$ is an external potential acting only on the probe, and $\mathcal{H}^{\rm int}$ encodes the interaction between the probe and the field. Notably, at this stage $\mathcal{H}_\phi$ needs not be Gaussian. The probe is assumed to follow the overdamped Langevin equation

$$\gamma_y \dot{\mathbf{Y}} = \quad \nabla_{\mathbf{Y}} \mathcal{H} + \mathbf{F}_{\rm ext} + \boldsymbol{\xi}, \tag{4.2}$$

where $\mathbf{F}_{\rm ext}(\mathbf{Y}, t)$ accounts for non-conservative external forces. Similarly, the scalar field is assumed to evolve as discussed in Section 1.3, i.e.,

$$\gamma_\phi \dot{\phi} = \quad (i\nabla) \ \frac{\delta \mathcal{H}}{\delta \phi} + \eta = \quad (\ \nabla^2) \ ^{/2} \frac{\delta \mathcal{H}}{\delta \phi} + \eta, \tag{4.3}$$

with $\quad = 0$ or 2 for locally non-conserved or conserved dynamics [54, 59]. Here $\gamma_{y,\phi}$ are friction coefficients, while η and ξ are independent Gaussian white noises satisfying the fluctuation-dissipation relations $\langle \xi_i(t)\xi_j(t')\rangle = 2\gamma_y T \delta_{ij}\delta(t \quad t')$ and $\langle \eta(\mathbf{x}, t)\eta(\mathbf{x}', t')\rangle = 2\gamma_\phi T(\ \nabla^2) \ ^{/2}\delta^d(\mathbf{x} \ \mathbf{x}')\delta(t \quad t')$, where $\langle \ldots \rangle$ denotes the average over various noise realizations. Accordingly, in the absence of external driving (i.e., for $\mathbf{F}_{\rm ext} = 0$ and time-independent $\mathcal{U}$), the system reaches a state of thermal equilibrium. Figure 4.1(a) is a sketch of the model with a harmonic potential $\mathcal{U}$.

Note that the model described above generalizes the one introduced in Section 2.1 and adopted throughout Chapters 2 and 3 to the case in which $\mathcal{H}_\phi$ and $\mathcal{U}$ are not necessarily quadratic, and $\mathcal{H}^{\rm int}$ is not yet specified. Here we made explicit use of the friction coefficients γ_ϕ and γ_y, as customary in stochastic thermodynamics. To make contact with the notation used in the previous Chapters, one needs to rescale $\eta \to \gamma_\phi \eta$, $\xi \to \gamma_y \xi$, and connect the field/probe friction coefficients to their respective mobilities as $\gamma_\phi = 1/D$, $\gamma_y = 1/\nu$.

4.2 Thermodynamic laws for the particle and the field

To investigate the thermodynamic properties of the system, we need to introduce suitable definitions of the energy flows and entropy changes associated with their stochastic dynamics. To this end, we utilize ideas from the framework of stochastic thermodynamics [108], and generalize them to the present case. In addition to the equations of motion, given by Eqs. (4.2) and (4.3), the only assumption we make is *energy conservation* for both the probe and field dynamics. We use Stratonovich stochastic calculus throughout [11]. The fluxes of energy and entropy between particle, field and thermal bath described below are summarized in Fig. 4.1(b).

First, we assume that the only systematic energy input into the system is due to the work done on the probe by the action of an external agent. This can either result from changing in time the potential $\mathcal{U}(\mathbf{Y}, t)$ — thereby increasing the potential energy of the probe — or from the application of an external force $\mathbf{F}_{\text{ext}}$. In agreement with classical mechanics, the work đW done on the probe within the time interval $[t, t + \mathrm{d}t]$ is simply given by [109]

$$đW = \frac{\partial \mathcal{U}(\mathbf{Y}, t)}{\partial t}\mathrm{d}t + \mathbf{F}_{\text{ext}} \circ \mathrm{d}\mathbf{Y}, \tag{4.4}$$

where đ denotes non-exact differentials, and $\circ$ indicates the usage of Stratonovich calculus throughout [109]. The total work W along a certain stochastic trajectory $\{\mathbf{Y}(t), \phi(\mathbf{x}, t)\}_{t_\text{i}}^{t_\text{f}}$ in the configuration space of the field and probe, from time t_i to t_f, is obtained by integrating over the infinitesimal increments, i.e., $W[\{\mathbf{Y}, \phi\}_{t_\text{i}}^{t_\text{f}}] = \int_{\{\mathbf{Y},\phi\}_{t_\text{i}}^{t_\text{f}}} đW$.

Next, we consider the total energy $\mathcal{U} + \mathcal{H}_\phi + \mathcal{H}^{\text{int}}$ of the system and how it may change, in order to identify all possible types of energy (ex-)changes within the system. First, the probe can store potential energy $\mathcal{U}(\mathbf{Y}, t)$. The latter can change due to a probe displacement, i.e., a change of $\mathbf{Y}$, or due to a variation of the confining potential itself, giving rise to the differential

$$\mathrm{d}\mathcal{U}(\mathbf{Y}, t) = \boldsymbol{\nabla}_\mathbf{Y}\mathcal{U}(\mathbf{Y}, t) \circ \mathrm{d}\mathbf{Y} + \frac{\partial \mathcal{U}(\mathbf{Y}, t)}{\partial t}\,\mathrm{d}t. \tag{4.5}$$

Note that the last term on the r.h.s. of this equation can be expressed, via Eq. (4.4), in terms of the work đW as (đW $\mathbf{F}_{\text{ext}} \circ \mathrm{d}\mathbf{Y}$). This fact will be used further below in Sec. 4.2.1.
Second, the field can store energy $\mathcal{H}_\phi$ in its configuration, characterized by its local energy density $h_\phi(\mathbf{x})$, such that $\mathcal{H}_\phi = \int \mathrm{d}^d\mathbf{x}\, h_\phi(\mathbf{x})$. Since we assume that $\mathcal{H}_\phi$ is not explicitly time-dependent, the total change $\mathrm{d}\mathcal{H}_\phi$ of the internal energy is accordingly given by

$$\mathrm{d}\mathcal{H}_\phi = \int \mathrm{d}^d\mathbf{x}\, \mathrm{d}h_\phi(\mathbf{x}), \qquad \text{with} \qquad \mathrm{d}h_\phi(\mathbf{x}) = \frac{\delta \mathcal{H}_\phi}{\delta\phi(\mathbf{x})} \circ \mathrm{d}\phi(\mathbf{x}). \tag{4.6}$$

Here $\mathrm{d}h_\phi(\mathbf{x})$ denotes the local change of internal energy of the field. Notably, depending on the choice of $\mathcal{H}_\phi$, the change $\mathrm{d}h_\phi(\mathbf{x})$ may contain contributions from the neighboring points $\phi(\mathbf{x}' \neq \mathbf{x})$. For example, for the Gaussian Hamiltonian given in Eq. (1.16), the Laplacian term induces energy exchanges between neighboring locations, as one realizes by discretizing space on a lattice.
Third, the interaction $\mathcal{H}^{\text{int}}$ between field and probe can store elastic energy. Again, one can define

the density $h^{\text{int}}(\mathbf{x})$ of interaction energy such that $\mathcal{H}^{\text{int}} = \int \mathrm{d}^d\mathbf{x}\, h^{\text{int}}(\mathbf{x})$, while the differential of $\mathcal{H}^{\text{int}}$ reads

$$\mathrm{d}\mathcal{H}^{\text{int}}(\mathbf{x},t) = \quad \text{đ}W_y^{\text{int}} \quad \int \mathrm{d}^d\mathbf{x}\, \text{đ}W_\phi^{\text{int}}(\mathbf{x}), \tag{4.7}$$

with

$$\text{đ}W_y^{\text{int}} := \quad \boldsymbol{\nabla}_{\mathbf{Y}}\mathcal{H}^{\text{int}} \circ \mathrm{d}\mathbf{Y}, \tag{4.8}$$

$$\text{đ}W_\phi^{\text{int}}(\mathbf{x}) := \quad \frac{\delta\mathcal{H}^{\text{int}}}{\delta\phi(\mathbf{x})} \circ \mathrm{d}\phi(\mathbf{x}). \tag{4.9}$$

Here we have defined $\text{đ}W_y^{\text{int}}$ and $\text{đ}W_\phi^{\text{int}}(\mathbf{x})$ — the latter being a *density*, or field — as the infinitesimal changes of the interaction energy due to the fluctuations of $\mathbf{Y}$ or $\phi(\mathbf{x})$, respectively. We interpret these energy flows as the work done by $\mathbf{Y}$ and ϕ, respectively. From Eq. (4.7) it follows that, in general, $\text{đ}W_y^{\text{int}} \neq \int \mathrm{d}^d\mathbf{x}\, \text{đ}W_\phi^{\text{int}}(\mathbf{x})$, because $\mathcal{H}^{\text{int}}$ itself can store energy.

4.2.1 First law of stochastic thermodynamics

As a final step, we connect the various energy flows, thereby obtaining the balance equations and the appropriate expressions for the heat. We start from $\mathrm{d}\mathcal{U}(\mathbf{Y},t)$ given in Eq. (4.5): using Eq. (4.4) and then Eq. (4.2), one finds

$$\begin{aligned}\mathrm{d}\mathcal{U}(\mathbf{Y},t) &= [\boldsymbol{\nabla}_{\mathbf{Y}}\mathcal{U}(\mathbf{Y},t) \quad \mathbf{F}_{\text{ext}}] \circ \mathrm{d}\mathbf{Y} + \text{đ}W = \quad \xi \quad \gamma_y\dot{\mathbf{Y}} + \boldsymbol{\nabla}_{\mathbf{Y}}\mathcal{H}^{\text{int}}) \circ \mathrm{d}\mathbf{Y} + \text{đ}W \\ &= \quad \xi \quad \gamma_y\dot{\mathbf{Y}}) \circ \mathrm{d}\mathbf{Y} + \text{đ}W_y^{\text{int}} + \text{đ}W,\end{aligned} \tag{4.10}$$

where in the last line we identified $\text{đ}W_y^{\text{int}}$ given by Eq. (4.8). Since we assume energy conservation for the probe dynamics, all the work $\text{đ}W_y^{\text{int}} + \text{đ}W$ done on the system that is not used to increase the potential energy of the probe (by an amount $\mathrm{d}\mathcal{U}$) must be dissipated into the heat bath in the form of the heat $\quad \text{đ}Q_y$. Thus, it follows from Eq. (4.10) that the first law for the probe reads

$$\mathrm{d}\mathcal{U} = \text{đ}Q_y + \text{đ}W_y^{\text{int}} + \text{đ}W, \tag{4.11}$$

with the heat flow $\text{đ}Q_y$ defined as

$$\text{đ}Q_y = (\xi \quad \gamma_y\dot{\mathbf{Y}}) \circ \mathrm{d}\mathbf{Y}. \tag{4.12}$$

Note that the latter is identical to the Sekimoto expression [115] for a single particle in a heat bath (i.e., with $\mathcal{H}^{\text{int}} = 0$).

We now turn to the energetics of the field. We start with $\mathrm{d}h_\phi(\mathbf{x})$ given in Eq. (4.6) and we insert the equation of motion (4.3) of the field, finding

$$\begin{aligned}\mathrm{d}h_\phi(\mathbf{x}) &= \frac{\delta\mathcal{H}_\phi}{\delta\phi(\mathbf{x})} \circ \mathrm{d}\phi(\mathbf{x}) = \left\{(\ \nabla^{\ 2})^{\ /2}\left[\eta(\mathbf{x}) \quad \gamma_\phi\dot{\phi}(\mathbf{x})\right] + \frac{\delta\mathcal{H}^{\text{int}}}{\delta\phi}\right\} \circ \mathrm{d}\phi(\mathbf{x}) \\ &= \left\{(\ \nabla^{\ 2})^{\ /2}\left[\eta(\mathbf{x}) \quad \gamma_\phi\dot{\phi}(\mathbf{x})\right]\right\} \circ \mathrm{d}\phi(\mathbf{x}) + \text{đ}W_\phi^{\text{int}}(\mathbf{x}),\end{aligned} \tag{4.13}$$

where in the last step we recognized $\text{đ}W_\phi^{\text{int}}$ given in Eq. (4.9). Again, energy conservation requires that all the work $\text{đ}W_\phi^{\text{int}}$ that is locally done on the field is either stored in the field configuration

in the form of a $\mathrm{d}h_\phi(\mathbf{x})$ (its "bending"), or otherwise it is dissipated by the field in the form of heat $\text{đ}Q_\phi(\mathbf{x},t)$. Accordingly, the (local) first law for the field, valid at any point in space, reads

$$\mathrm{d}h_\phi(\mathbf{x}) = \text{đ}Q_\phi(\mathbf{x}) + \text{đ}W_\phi^{\mathrm{int}}(\mathbf{x}). \tag{4.14}$$

We note that the l.h.s. of the previous equation describes the total change of internal energy of the field at a given point $\mathbf{x}$, which generally also contains nonlocal contributions, as mentioned after Eq. (4.6). These terms can be interpreted as the energy exchanges within the field, i.e., between ϕ at different points in space. The integral form of Eq. (4.14) follows as

$$\mathrm{d}\mathcal{H}_\phi = \int \mathrm{d}^d\mathbf{x}\left[\text{đ}Q_\phi(\mathbf{x}) + \text{đ}W_\phi^{\mathrm{int}}(\mathbf{x})\right]. \tag{4.15}$$

This first law allows us to identify from Eqs. (4.3) and (4.13) the local heat dissipation density (or field) of ϕ as

$$\text{đ}Q_\phi(\mathbf{x}) = \left\{(\quad\nabla\quad^2)\quad^{/2}\left[\eta(\mathbf{x})\quad\quad\gamma_\phi\dot{\phi}(\mathbf{x})\right]\right\}\circ\mathrm{d}\phi(\mathbf{x}), \tag{4.16}$$

which generalizes the Sekimoto expression [109]. For $\quad = 0$, Eq. (4.16) formally resembles the heat exchange of a single particle. For conserved dynamics ($\quad = 2$), the differential operator further introduces terms that are nonlocal in space.

4.2.2 Second law of stochastic thermodynamics

In accordance with the framework of stochastic thermodynamics for a finite number of degrees of freedom coupled to a heat bath, and with the framework of irreversibility for fields [131, 132], we define the total entropy production along a trajectory $\{\mathbf{Y}(t),\phi(\mathbf{x},t)\}_{t=t_\mathrm{i}}^{t_\mathrm{f}}$ of the system from time t_i to t_f as [109]

$$\Delta S_{\mathrm{tot}}[\{\mathbf{Y},\phi\}_{t_\mathrm{i}}^{t_\mathrm{f}}] = \ln\frac{\mathcal{P}[\{\mathbf{Y},\phi\}_{t_\mathrm{i}}^{t_\mathrm{f}}]}{\mathcal{P}^{\mathrm{R}}[\{\mathbf{Y}^{\mathrm{R}},\phi^{\mathrm{R}}\}_{t_\mathrm{i}}^{t_\mathrm{f}}]}. \tag{4.17}$$

Here $\mathcal{P}$ denotes the path probability of the forward path of the joint trajectory of field and probe, starting from the probability density field $\rho_{\mathbf{Y},\phi}[\mathbf{Y}(t_\mathrm{i}),\phi(\mathbf{x},t_\mathrm{i})]$, while $\mathcal{P}^{\mathrm{R}}$ denotes the probability of the corresponding backward path in the time-reversed process, initialized with $\rho_{\mathbf{Y},\phi}[\mathbf{Y}(t_\mathrm{f}),\phi(\mathbf{x},t_\mathrm{f})]$. In the time-reversed process, the time-dependent external driving protocols $\mathcal{U}(\mathbf{x},t)+\mathbf{F}_{\mathrm{ext}}(t)$ are reversed in time. The path probabilities are interpreted within the Onsager-Machlup formalism (see Ref. [69] and Section 1.5); by construction, the second law $\langle\Delta S_{\mathrm{tot}}\rangle \geq 0$ holds, as detailed in Appendix D.1.

A central result of this Chapter, which is proved in Appendix D.1, is that the irreversibility ΔS_{tot} defined in Eq. (4.17) is equivalent to the total thermodynamic entropy production

$$\Delta S_{\mathrm{tot}} = \frac{Q_y}{T} \quad \int \mathrm{d}^d\mathbf{x}\,\frac{Q_\phi(\mathbf{x})}{T} + \Delta S_{y,\phi}^{\mathrm{sh}}, \tag{4.18}$$

with the heat dissipation Q_y and Q_ϕ defined in Eqs. (4.12) and (4.16), respectively — indicating the thermodynamic consistency of our framework. Here $\Delta S_{y,\phi}^{\mathrm{sh}}$ denotes the change of the Shannon

entropy, $S^{\mathrm{sh}}_{y,\phi} \propto \ln \rho_{\mathbf{Y},\phi}$, which is the entropy associated with the choice of the initial/final condition, and thus quantifies the entropy production due to configurational changes of the system. In contrast, the contributions Q_y and $Q_\phi(\mathbf{x})$ depend on the entire trajectory, and thus quantify the entropy production in the medium associated with heat dissipation [145].

4.2.3 Steady states

If the system admits a steady state, then $\langle \mathrm{d}\mathcal{H}^{\mathrm{int}} \rangle$, $\langle \mathrm{d}\mathcal{H}_\phi \rangle$, and $\langle \mathrm{d}\mathcal{U} \rangle$ vanish. Thus, the first laws for the probe and field given in Eqs. (4.11) and (4.14), respectively, simplify to

$$\langle đW \rangle = \left\langle đQ_y \right\rangle \left\langle đW_y^{\mathrm{int}} \right\rangle, \qquad \text{and} \qquad \left\langle đQ_\phi(\mathbf{x}) \right\rangle = \left\langle đW_\phi^{\mathrm{int}}(\mathbf{x}) \right\rangle. \tag{4.19}$$

Moreover, from Eq. (4.7) we find

$$\left\langle \int \mathrm{d}^d\mathbf{x}\, đW_\phi^{\mathrm{int}}(\mathbf{x}) \right\rangle = \left\langle đW_y^{\mathrm{int}} \right\rangle. \tag{4.20}$$

This equation implies, by using Eq. (4.19), that the total dissipation of the entire process is given by the work applied to the probe, i.e.,

$$\left\langle \dot{W} \right\rangle = \left\langle \dot{Q}_y \right\rangle \int \mathrm{d}^d\mathbf{x} \left\langle \dot{Q}_\phi(\mathbf{x}) \right\rangle = T \left\langle \Delta \dot{S}_{\mathrm{tot}} \right\rangle \geq 0, \tag{4.21}$$

with $\dot{Q} := đQ/\mathrm{d}t$, $\dot{W} := đW/\mathrm{d}t$, and $\Delta \dot{S}_{\mathrm{tot}} \simeq \Delta S_{\mathrm{tot}}/(t_{\mathrm{f}} \quad t_{\mathrm{i}})$. (Indeed, in steady states the Shannon entropy $S^{\mathrm{sh}}_{y,\phi}$ is on average a conserved quantity, so $\langle \Delta S^{\mathrm{sh}}_{y,\phi} \rangle = 0$.) Accordingly, in steady states, $\langle \Delta \dot{S}_{\mathrm{tot}} \rangle$ is proportional to the average power $\langle \dot{W} \rangle$ injected into the system, which indicates the physical consistency of our approach.

4.3 The case of a particle dragged through a Gaussian field

Within the framework developed above, we consider the typical setup [46] in which a probe particle is dragged at constant velocity $\mathbf{v}$ by a harmonic trap of stiffness κ. The corresponding potential is $\mathcal{U}(\mathbf{Y}, t) = \kappa\,(\mathbf{Y} \quad \mathbf{v}t)^2/2$, and the dissipation rate follows from Eq. (4.4) as

$$\dot{W} = \quad \kappa \mathbf{v} \cdot (\mathbf{Y} \quad \mathbf{v}t). \tag{4.22}$$

In the long-time limit, the system reaches a steady state in the comoving reference frame with velocity $\mathbf{v}$. As a minimal model for a near-critical medium — and as the simplest approximation of various complex systems — we consider a Gaussian field with Hamiltonian as in Eq. (1.16), as we already did in Chapters 2 and 3. We model the particle–field interaction $\mathcal{H}^{\mathrm{int}}$ as in Eq. (2.3), in which the interaction potential $V(\mathbf{x})$ is as usual characterized by a single length scale R, representing the size of the particle.

4.3.1 Steady state in the comoving frame

To make contact with the notation introduced in Section 2.1 and adopted throughout Chapters 2 and 3, in the following we rescale $\eta \to \gamma_\phi \eta$, $\xi \to \gamma_y \xi$, and rename $\gamma_\phi = 1/D$, $\gamma_y = 1/\nu$. We will also use $\gamma = \nu\kappa$ for brevity, as in the previous Chapters.

We start by measuring the position $\mathbf{Z} \equiv \mathbf{Y} \quad \mathbf{v}t + \mathbf{v}/\gamma$ of the particle in the reference frame that is comoving with the harmonic trap. In terms of the coordinate $\mathbf{Z}$, the equations of motion (4.2) and (4.3) become

$$\dot{\mathbf{Z}} = \quad \gamma \mathbf{Z} \quad \nu \nabla_Z \mathcal{H}_{\rm int}[\varphi, \mathbf{Z}] + \xi, \tag{4.23}$$

$$(\partial_t \quad \mathbf{v} \cdot \nabla)\varphi(\mathbf{x}, t) = \quad D(i\nabla) \ \frac{\delta \mathcal{H}[\varphi, \mathbf{Z}]}{\delta \varphi(\mathbf{x}, t)} + \eta(\mathbf{x}, t), \tag{4.24}$$

where we introduced the translated field $\varphi(\mathbf{x}, t) \equiv \phi(\mathbf{x} + \mathbf{v}t \quad \mathbf{v}/\gamma, t)$. Note that $\mathcal{H}_\phi[\varphi] = \mathcal{H}_\phi[\phi]$ and $\mathcal{H}_{\rm int}[\varphi, \mathbf{Z}] = \mathcal{H}_{\rm int}[\phi, \mathbf{Y}]$, by translational invariance (which applies also to the white noises ξ and η). In Fourier space, these equations can be written as

$$\dot{\mathbf{Z}} = \quad \gamma \mathbf{Z} + \lambda \nu \int \frac{\mathrm{d}^d q}{(2\pi)^d} i\mathbf{q} V \ _q \varphi_{\mathbf{q}} e^{i\mathbf{q}\cdot\mathbf{Z}} + \xi, \tag{4.25}$$

$$(\partial_t \quad i\mathbf{q} \cdot \mathbf{v} + \ _q)\varphi_{\mathbf{q}} = \lambda D q \ V_q e^{\ i\mathbf{q}\cdot\mathbf{Z}} + \eta_{\mathbf{q}}, \tag{4.26}$$

with $_q$ given in Eq. (1.25). Note that, for $\lambda = 0$, the evolution equation (4.26) for $\varphi_{\mathbf{q}}$ (with $\mathbf{v} \neq \mathbf{0}$) is formally the same as that for $\phi_{\mathbf{q}}$ in a fixed reference frame (i.e., with $\mathbf{v} = \mathbf{0}$ — see Eq. (1.23)), up to a shift $_q \mapsto (\ _q \quad i\mathbf{q}\cdot\mathbf{v})$. Accordingly, its solution in the steady state is the same as in equilibrium (see Section 1.3), upon replacing the free-field equilibrium correlator $C_q(t)$, propagator $G_q(t)$, and susceptibility $\chi_q(t)$ with

$$C^{(\mathbf{v})}_{\mathbf{q}}(t) = \frac{T}{q^2 + r} e^{\ (\ _q \ \ i\mathbf{q}\cdot\mathbf{v})|t|} \equiv e^{i\mathbf{q}\cdot\mathbf{v}|t|} C_q(t), \tag{4.27}$$

$$G^{(\mathbf{v})}_{\mathbf{q}}(t) = e^{\ (\ _q \ \ i\mathbf{q}\cdot\mathbf{v})t} \Theta(t) = e^{i\mathbf{q}\cdot\mathbf{v}t} G_q(t), \tag{4.28}$$

and similarly $\chi^{(\mathbf{v})}_{\mathbf{q}}(t) = Dq \ \ G^{(\mathbf{v})}_{\mathbf{q}}(t)$. We will make use of these expressions in what follows.

At long times, we expect the system to reach a stationary state with $\langle \dot{\mathbf{Z}} \rangle_{\rm ss} = 0$ and $\left\langle \partial_t \varphi_{\mathbf{q}} \right\rangle_{\rm ss} = 0$ in which, according to Eqs. (4.25) and (4.26),

$$\langle \mathbf{Z} \rangle_{\rm ss} = \frac{\lambda}{\kappa} \int \frac{\mathrm{d}^d q}{(2\pi)^d} i\mathbf{q} V \ _q \left\langle \varphi_{\mathbf{q}} e^{i\mathbf{q}\cdot\mathbf{Z}} \right\rangle_{\rm ss}, \qquad \left\langle \varphi_{\mathbf{q}} \right\rangle_{\rm ss} = \frac{\lambda D q \ \ V_q \left\langle e^{\ i\mathbf{q}\cdot\mathbf{Z}} \right\rangle_{\rm ss}}{_q \quad i\mathbf{q} \cdot \mathbf{v}}. \tag{4.29}$$

Note that $\mathbf{Z} = 0$ is the mean steady-state position for $\lambda = 0$.

Due to the coupling between the field $\varphi_{\mathbf{q}}$ and the particle coordinates $\mathbf{Z}$, it is difficult in general to evaluate the terms $\left\langle \varphi_{\mathbf{q}} e^{i\mathbf{q}\cdot\mathbf{Z}} \right\rangle_{\rm ss}$ and $\left\langle e^{\ i\mathbf{q}\cdot\mathbf{Z}} \right\rangle_{\rm ss}$ which appear in Eq. (4.29). In Refs. [80, 81, 104] and in the previous Chapters, this has been achieved by a perturbative expansion in increasing powers of the weak coupling λ: following the same approach and using numerical simulations, in the following sections we will investigate quantitatively the properties of the nonequilibrium stationary state of the system. However, we anticipate here some of the qualitative features that emerge from such analysis, because they are useful to gain a physical insight into the problem.

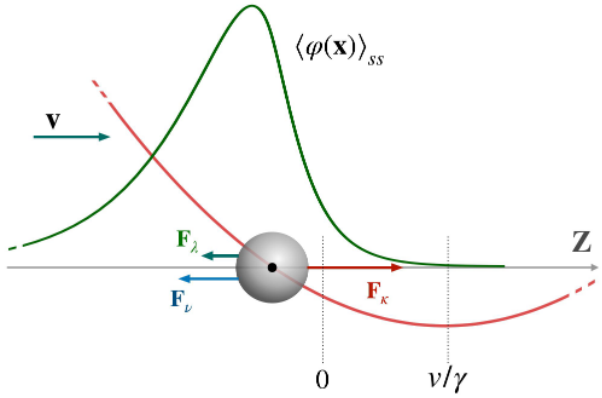

Figure 4.2: Sketch of the system in its nonequilibrium steady state, attained at long times in the comoving frame of reference with $\mathbf{Z} = \mathbf{Y} \quad \mathbf{v}t + \mathbf{v}/\gamma$. The field rearranges around the particle forming a *shadow* (see Eq. (4.29)), represented here in spatial dimensionality $d = 1$ (green line). The particle is subject to the attractive force $\mathbf{F}_\lambda(\mathbf{Z})$ directed towards the shadow (and due to the field, see Eq. (4.25)), to the friction force which is, on average, $\langle \mathbf{F}_\nu \rangle = \quad \mathbf{v}/\nu$, and to the restoring force $\mathbf{F}_\kappa = \quad \kappa\mathbf{Z}$ due to the harmonic trap (red parabola). The steady-state position of the particle (see Eq. (4.29)) results from the balance $\langle \mathbf{F}_\kappa \rangle = \langle \mathbf{F}_\nu \rangle + \langle \mathbf{F}_\lambda \rangle$. For $\lambda = 0$ the field and the particle are decoupled, so that $\mathbf{F}_\lambda = 0$ and the steady-state position reduces to $\langle \mathbf{Z} \rangle = \mathbf{0}$.

In the steady state, the average field profile $\langle \varphi(\mathbf{x}) \rangle_{\rm ss}$ — obtained from the inverse Fourier transform of $\langle \varphi_{\mathbf{q}} \rangle_{\rm ss}$, see Appendix D.4.1 — turns out to be enhanced in correspondence of the particle position, and is stretched in the direction opposite to the particle motion: we will refer to this field configuration as the *shadow*, and we represent it schematically in Fig. 4.2. Note that, by using Eq. (2.3), the term $\propto \lambda$ on the r.h.s. of Eq. (4.23) can be written as $\lambda\nu \int \mathrm{d}^d\mathbf{z}\, \nabla\varphi(\mathbf{z}) V(\mathbf{z} \quad \mathbf{Z})$. Accordingly, for $\lambda \neq 0$, the particle is subject to a force which pushes it towards the maximum of the shadow. In the stationary state, this force adds up to the friction force in counterbalancing the restoring force exerted by the harmonic trap. Using perturbative arguments, in Section 4.3.3 we will deduce that in general the field is responsible for the emergence of an additional (non-linear) friction acting on the dragged particle. Accordingly, the equilibrium position of the particle is further displaced to the *left* with respect to the value $\langle \mathbf{Z} \rangle = 0$ it would have in the absence of the field (i.e., for $\lambda = 0$ — see Eq. (4.29)). Note that the formation of the shadow is due to the response of the field to the passage of the particle, an aspect which is usually neglected in models used to describe the passive advection of a particle by a fluid flow [146, 147].

4.3.2 Heat dissipation field

The first thermodynamic quantity we analyze is the spatially resolved heat dissipation Q_φ in the comoving reference frame. In Fig. 4.3 we show numerical results for $\langle \dot{Q}_\varphi \rangle$ of a field in $d = 2$ with $= 0$ (see the details in Appendix D.5). For small values of the correlation length ξ [see panel (a)], we observe that $\langle \dot{Q}_\varphi \rangle$ is essentially negligible (within numerical uncertainties) and displays no discernible spatial structure. In contrast, if ξ grows and becomes comparable to the particle size R [panel (b)], regions of average heat dissipation ($\langle \dot{Q}_\varphi \rangle < 0$) or absorption ($\langle \dot{Q}_\varphi \rangle > 0$) start

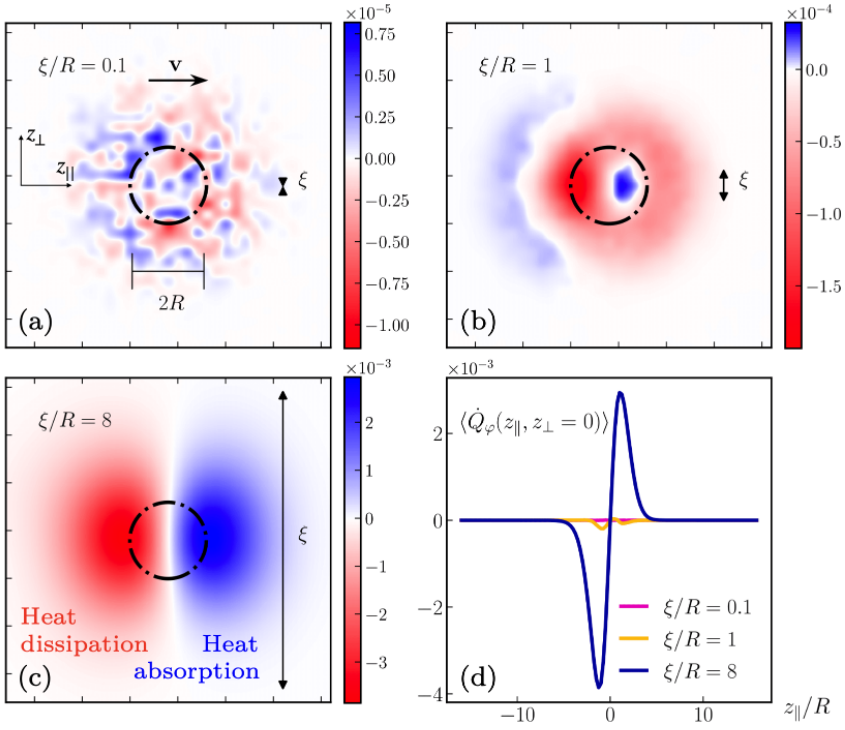

Figure 4.3: Average local heat dissipation rate $\langle \dot{Q}_\varphi(\mathbf{z})\rangle$ by the field into the bath, in a frame comoving at velocity $\mathbf{v}$ with the harmonic trap (see Fig. 4.1). These results of numerical simulations (see Appendix D.5) refer to a Gaussian field in $d = 2$ with non-conserved dynamics and, from (a) to (c), increasing values of ξ/R, where ξ is the correlation length and R the probe size (indicated with dash-dotted circles). Panel (d) shows $\langle \dot{Q}_\varphi(\mathbf{z})\rangle$ along the drag direction $_\parallel$, for $_\perp = 0$ and the values of ξ considered in (a–c). We used $L = 128$, $\Delta t = 10^{-2}$, $\lambda = 5$, $v = 5$, a Gaussian potential V with variance $R = 4$, and set all the other parameters to unity.

developing. Close to criticality, with $\xi \gg R$ [panel (c)], a dissipation dipole forms, with a region of heat absorption in front of the particle, whose spatial extent is approximately given by ξ. Hence, surprisingly, in front of the particle the heat bath supplies net energy as if it was coupled to a cooler object. Note that the second law [see Eq. (4.21)] implies $\langle \dot{Q}_y \rangle + \int \mathrm{d}^d\mathbf{x} \langle \dot{Q}_\varphi(\mathbf{x})\rangle < 0$, but it does not preclude local heat absorption, i.e., $\langle \dot{Q}_\varphi(\mathbf{x})\rangle > 0$ for some $\mathbf{x}$. To further elucidate the origin of this effect, below we analytically investigate the statistics of particle and field for various values of $v = |\mathbf{v}|$ and ξ, and the dissipated power.

4.3.3 Particle statistics and bending of the field

We now assume λ to be small, and use it as a perturbative parameter [64, 80, 81, 104, 113]. From Eq. (4.26) we can calculate the mean stationary profile $\langle \varphi_{\mathbf{p}} \rangle_{\mathrm{st}}$, i.e., the shadow described above — this is detailed in Appendix D.4.1. The shadow is shown in Fig. 4.4(a) for a field in $d = 1$ with $= 0$: the field is strongly bent around the particle, while $\langle \varphi(\ )\rangle_{\mathrm{st}} \propto \exp(-|\ |/\ell_\pm)$ for $\to \pm\infty$,

with (see Appendix D.4.1)

$$\ell_{\pm} = \xi \left[\sqrt{1 + \left(\frac{\xi v}{2D}\right)^2} \mp \left(\frac{\xi v}{2D}\right) \right]. \tag{4.30}$$

Far from criticality ($\xi \to 0$, see inset), the shadow vanishes, rationalizing the corresponding vanishing of $\langle \dot{Q}_{\varphi}(\mathbf{z}) \rangle$ in Fig. 4.3(a).

Via a perturbative approach, we can investigate the particle fluctuations analytically. The moment generating function $g(\mathbf{q}) \equiv \langle \exp(\ i\mathbf{q} \cdot \mathbf{Z}) \rangle$ of the particle position at the lowest nontrivial order in λ reads (see Appendix D.3)

$$\ln g(\mathbf{q}) = \ \frac{q^2 T}{2\kappa} + \frac{i\lambda^2}{\kappa} \int_0^{\infty} \frac{\mathrm{d}u}{\sigma_2^2(u)} \int \frac{\mathrm{d}^d p}{(2\pi)^d} \frac{(\mathbf{p} \cdot \mathbf{v})}{p^2 + r} |V_p|^2 G_{\mathbf{p}}^{(\mathbf{v})}(u) e^{\ p^2 \sigma_2^2(u)} \left[1 \quad e^{\ (\mathbf{p}\cdot\mathbf{q})\sigma_2^2(u)} \right], \tag{4.31}$$

with $\sigma_2^2(u) \equiv T\,(1 \quad e^{\ \gamma u})\,/\kappa$, and $G_{\mathbf{p}}^{(\mathbf{v})}(u)$ as in Eq. (4.25). Interestingly, Eq. (4.31) predicts a non-Gaussian statistics of the particle position. In addition, the variance $\langle Z_l Z_m \rangle_c \propto \delta_{lm}$ changes anisotropically compared to the case $\mathbf{v} = \mathbf{0}$, so that the position distribution is elongated in the direction parallel to $\mathbf{v}$ [148]. Furthermore, $i\nabla_{\mathbf{q}} g|_{\mathbf{q}=\mathbf{0}}$ gives the average displacement

$$\langle \mathbf{Z} \rangle = \ \frac{\lambda^2}{\kappa} \int \frac{\mathrm{d}^d p}{(2\pi)^d} \frac{\mathbf{p}\,(\mathbf{p} \cdot \mathbf{v})}{p^2 + r} |V_p|^2 \int_0^{\infty} \mathrm{d}u\, G_{\mathbf{p}}^{(\mathbf{v})}(u) e^{\ p^2 \sigma_2^2(u)}, \tag{4.32}$$

which turns out to be directed along $\mathbf{v}$; hence, the field induces a shift of the probability density of the particle position, which lags behind the average stationary value in the absence of the field [see the inset of Fig. 4.4(b)]. Such a lag is the footprint of an underlying additional source of dissipation, which we analyze next.

4.3.4 Power fluctuations

From the generating function in Eq. (4.31), we can access the distribution of the dissipated power. Indeed, rewriting Eq. (4.22) in terms of $\mathbf{Z}$ gives $\dot{W} = \nu \ {}^1v^2 \quad \kappa\mathbf{v} \cdot \mathbf{Z}$, and thus

$$\ln \left\langle \exp \quad i\mu \dot{W} \right\rangle = \ i\mu\nu \ {}^1v^2 + \ln g(\ \mu\kappa\mathbf{v}), \tag{4.33}$$

encoding all moments of the dissipated power. To study the impact of the field, we focus on the average power

$$\langle \dot{W} \rangle = \nu \ {}^1v^2 \quad \kappa\mathbf{v} \cdot \langle \mathbf{Z} \rangle \equiv \langle \dot{W} \rangle_0 + \langle \dot{W} \rangle_{\lambda}\,, \tag{4.34}$$

where we identify the dissipation rate $\langle \dot{W} \rangle_0 = \nu \ {}^1v^2 \geq 0$ in the absence of the field, while $\langle \dot{W} \rangle_{\lambda} = \ \kappa\mathbf{v} \cdot \langle \mathbf{Z} \rangle \geq 0$ encodes the additional dissipation due to the field. According to Eq. (4.21), these are further equal to the entropy production at $\lambda = 0$ and $\lambda > 0$, i.e., $\langle \dot{W} \rangle_0 = T \left\langle \dot{S}_{\mathrm{tot}} \right\rangle_0$ and $\langle \dot{W} \rangle_{\lambda} = T \left\langle \dot{S}_{\mathrm{tot}} \right\rangle_{\lambda}$, respectively. In Fig. 4.4(b) we show the perturbative prediction for $\langle \dot{W} \rangle_{\lambda}$ as a function of v, and the corresponding numerical data from simulations (see Appendix D.5), which are in good agreement. We find that $\langle \dot{W} \rangle_{\lambda}$ generally displays three distinct regimes[2] upon

[2]The first and the third among these regimes are consistent with the scaling of drag forces reported in Refs. [26–28], where particles moving with constant velocity (i.e., without positional fluctuations) were studied.

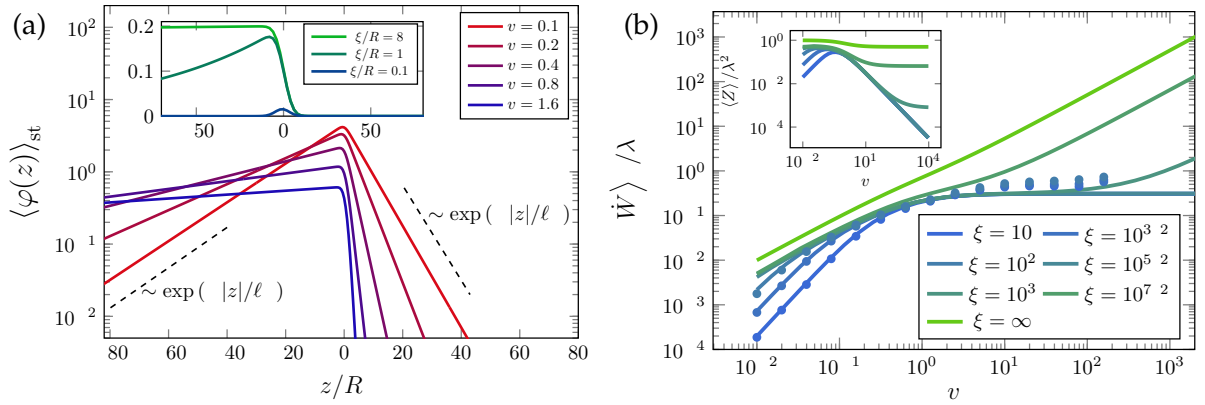

Figure 4.4: **a)** Steady-state expectation value $\langle\varphi(\ )\rangle_{\rm st}$ of the field in the comoving frame, for various drag velocities $v > 0$, in $d = 1$ and with non-conserved dynamics. The *shadow* $\langle\varphi(\ )\rangle_{\rm st}$ flattens upon increasing v (at fixed correlation length $\xi = 10$, main plot) or upon decreasing ξ (at fixed $v = 5$, inset). $\langle\varphi(\ )\rangle_{\rm st}$ decays exponentially upon increasing $|\ |$ with different decay lengths $\ell_\pm$ in front of or behind the particle — see Eq. (4.30). We used $V_q = \exp\ q^2R^2/2)$ and $R^2 + T/\kappa = 1$, while the other parameters were set to unity. **b)** Additional dissipation rate [see Eq. (4.34)] as a function of v, for various values of ξ (with $T = 0.1$, while the other parameters were set to one). Symbols correspond to simulations. Inset: scaled correction $\langle Z\rangle/\lambda^2$ to the average particle position [see Eq. (4.32)].

increasing v: first, $|\langle Z\rangle|$ grows linearly [see Fig. 4.4(b), inset], so that $\langle\dot{W}\rangle_\lambda \propto v^2$, as it would be the case for usual Stokes friction. After a crossover, in the second regime $|\langle Z\rangle| \propto 1/v$, and therefore $\langle\dot{W}\rangle_\lambda$ plateaus at intermediate v, which indicates a constant energetic cost associated with the particle–field interaction. Finally, in the third regime, $|\langle Z\rangle|$ saturates and thus $\langle\dot{W}\rangle_\lambda \propto v$. We remark that the second and third *non-Stokesian* regimes cannot be captured by a linear GLE — see Appendix D.2.

We present a thorough analysis of these regimes in Appendix D.4.1, for the case $= 0$, and summarize it here. First, by inserting into Eq. (4.25) the formal solution of Eq. (4.26) for $\varphi_{\mathbf{p}}(t)$, an effective equation for $\mathbf{Z}(t)$ can be obtained, which is non-Markovian and nonlinear. However, in the limit of small v, the field is sufficiently fast to equilibrate around the particle at each instant in time [64, 104]. Conversely, for large v, the evolution of the field is so slow that the particle encounters an effectively static field configuration. Accordingly, the first two regimes can be quantitatively captured by adiabatically replacing the field $\varphi_{\mathbf{p}}(t)$ in Eq. (4.25) with its mean (comoving) profile $\langle\varphi_{\mathbf{p}}\rangle_{\rm st}$, i.e., with the shadow shown in Fig. 4.4(a), resulting in an approximately Markovian evolution of $\mathbf{Z}(t)$. In contrast, at intermediate values of v, the timescales of the particle dynamics are comparable with

$$\tau_\xi \equiv 1/(Dr) = \xi^2/D, \tag{4.35}$$

which quantifies the relaxation timescale of the field φ over its correlation length $\xi = r^{1/2}$ (see Eq. (1.25) with $q \simeq \xi^{-1}$ and $= 2$). As a result, the adiabatic approximation is no longer accurate: the particle dynamics within the crossover between the first two regimes is dominated by the memory effects caused by the mutual influence of the particle and the field. Finally, in the third

regime, the shadow becomes negligible compared to the (critical) fluctuations of the field, and the particle effectively encounters a rough landscape resulting from them. Notably, as the field approaches criticality ($\xi \to \infty$), the amplitude of its fluctuations diverges [54], and thus the last (non-Stokesian) regime extends to small values of v.

4.4 Memory-induced oscillations

Having developed a stochastic thermodynamics framework for a probe in a correlated medium, which we exemplified for a dragged particle, we now turn to the study of the dynamics of the latter, and we analyze an intriguing analogy with the dynamics of a probe in a *viscoelastic* medium. In general, the storage and dissipation of energy within the complex microstructure of viscoelastic fluids translate into a macroscopically long stress-relaxation time, which gives rise to non-Newtonian behavior [16]. Dragging a colloidal particle through such a fluid — as it is typically done in active microrheology experiments [76, 111, 149–152] — thus drives the medium out of equilibrium, unlike the case of Brownian motion. In turn, this affects the statistics of the particle position [153]. At a coarse-grained level, the resulting particle dynamics is often phenomenologically described by an overdamped generalized Langevin equation (GLE, see Section 1.4): here the effect of the interaction between the particle and the medium is encoded in a friction kernel $\mathcal{K}(t)$ acting on the particle velocity as $\int_{-\infty}^{t} \mathrm{d}u\, \mathcal{K}(t-u)\dot{X}(u) = F(X,t) + \zeta(t)$, where F includes the forces exerted on the particle at position X, while ζ is a colored Gaussian noise.

Recently, it has been experimentally shown that viscoelasticity can give rise to oscillating modes in the overdamped motion of colloidal particles driven through the medium [47]. This is somehow unexpected and noteworthy, because oscillations (which typically occur in systems with underdamped dynamics) are strictly forbidden at equilibrium, as shown, e.g., in Ref. [47]. Heuristically, one may note that integrating by parts the retarded friction in the GLE above formally renders a term $\int_{-\infty}^{t} \mathrm{d}u\, \mathcal{M}(t-u)\ddot{X}(u)$, where $\mathcal{M}(t) \sim \int^{t} \mathrm{d}u\, \mathcal{K}(u)$ can be readily interpreted (if positive) as a memory-induced *inertia* [7], which is generally absent from the description of Markovian overdamped systems.

Memory terms in the effective evolution equation of a particle actually appear quite naturally in many physical systems, after integrating the slow degrees of freedom out of the original, microscopic dynamics in which they are coupled to those describing the tracer particle [8, 154, 155]. For example, above and in the previous Chapters we formulated a minimal model for diffusion in a thermally fluctuating correlated medium in terms of the joint overdamped dynamics of a particle and a scalar Gaussian field $\phi(\mathbf{x}, t)$, the latter being characterized by a correlation length ξ and a finite relaxation time. If the coupling between the field and the particle is chosen to be linear, then the field can be integrated out exactly, resulting into an effective evolution equation for the particle — see, c.f., Eq. (4.63). This equation provides insights on the connection between the emerging memory kernel and the features of the original microscopic model, as we will show in the following.

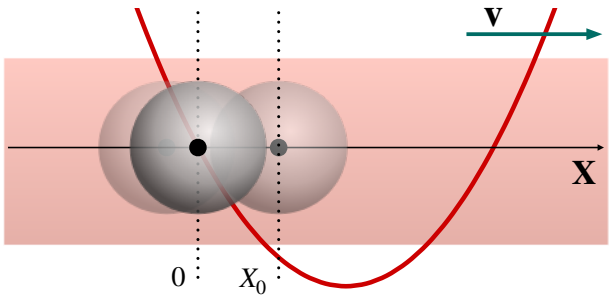

Figure 4.5: Setup of the problem. A particle is spatially confined by a harmonic potential, the center of which is dragged at constant velocity $\mathbf{v}$. The particle interacts with a thermally fluctuating order parameter ϕ (red background) according to the Hamiltonian in Eq. (1.16). The particle position $\mathbf{X}(t)$ is measured in a comoving frame of reference, chosen so that $\langle \mathbf{X} \rangle = 0$ in the steady state (see Section 4.5 for details). At time $t = 0$ the particle is suddenly displaced by a small amount $\mathbf{X}_0$ from its current position, and the ensuing relaxation is observed.

In this context, it is natural to ask whether the memory kernel in the effective evolution equation of the tracer particle, which originates from the spatio-temporal correlations of the field, may give rise to oscillating modes similar to those observed in viscoelastic fluids [47] — which, instead, are primarily due to the mechanical response of the medium. To address this question, we consider again the setting of a particle driven at constant velocity through a fluctuating Gaussian field, as discussed in Section 4.3. We first integrate out the field degrees of freedom, thus obtaining an effective (non-linear) equation which describes the motion of the particle in the steady state reached by the system at long times. By linearizing this equation and inspecting the analytic structure of the field-induced memory kernel, we demonstrate that damped oscillations are indeed displayed by the particle during the relaxation that occurs after it has been displaced from its steady-state position. These oscillations are confirmed via numerical simulations of the model. The simplicity of our model allows us to study in detail how the interplay between the various timescales of the system dictates the emergence of the particle oscillations, and to determine their frequency and typical decay time.

In the following, we will be primarily interested in exploring the effect of the field when the coupling λ is relatively strong, and thus we will adopt a different approach compared to the perturbative one used in the previous sections. In particular, in Section 4.5 we first analyze the relaxation of a particle initially displaced from its steady-state position, under the assumption that thermal fluctuations are negligible. This allows one to determine an analytic expression of the particle trajectory $\mathbf{X}(t)$ for generic values of λ. The effect of thermal noise when $T \neq 0$ is then assessed in Section 4.6, where we also compare our analytical predictions with numerical simulations.

4.5 Noiseless limit

In this Section we will focus on the *noiseless* limit of the dynamics, i.e., the limit in which the amplitude T of the stochastic noises $\xi(t)$ and $\eta(\mathbf{x}, t)$ is set to zero. In the absence of thermal noise,

the equations of motion (4.25) and (4.26) become deterministic and no fluctuations occur. Accordingly, $\langle \mathbf{Z} \rangle_{\rm ss} = \mathbf{Z}^{(\rm ss)}$, $\langle \varphi_{\mathbf{q}} \rangle_{\rm ss} = \varphi_{\mathbf{q}}^{(\rm ss)}$, while $\langle \varphi_{\mathbf{q}} e^{i\mathbf{q}\cdot\mathbf{Z}} \rangle_{\rm ss} = \varphi_{\mathbf{q}}^{(\rm ss)} e^{i\mathbf{q}\cdot\mathbf{Z}^{(\rm ss)}}$ and $\langle e^{\ i\mathbf{q}\cdot\mathbf{Z}} \rangle_{\rm ss} = e^{\ i\mathbf{q}\cdot\mathbf{Z}^{(\rm ss)}}$. Then, by using Eq. (4.29) in the steady state, one readily finds that

$$\mathbf{Z}^{(\rm ss)} = \frac{\lambda^2 D}{\kappa} \int \frac{\mathrm{d}^d q}{(2\pi)^d} i\mathbf{q} \frac{q \ \ |V_q|^2}{_q \quad i\mathbf{q}\cdot\mathbf{v}}, \tag{4.36}$$

$$\varphi_{\mathbf{q}}^{(\rm ss)} = \frac{\lambda D q \ \ V_q \exp\big[\ \ i\mathbf{q}\cdot\mathbf{Z}^{(\rm ss)}\big]}{_q \quad i\mathbf{q}\cdot\mathbf{v}}. \tag{4.37}$$

Equation (4.37) provides the expression of the shadow in the absence of thermal noise. As anticipated in Section 4.4, we aim to describe the motion of the particle after it is suddenly displaced, at time $t = t_0$, from the position it assumes in the stationary state — a schematic representation is provided in Fig. 4.5. In order to do this, one can solve Eq. (4.26) (where $\eta_q = 0$ in the limit we are interested in) by assuming that the field configuration at time $t = t_0$ is the one of the stationary state — i.e., $\varphi_{\mathbf{q}}(t = t_0) = \varphi_{\mathbf{q}}^{(\rm ss)}$ is used as the initial condition of the dynamics. The resulting evolution of the field thus reads

$$\varphi_{\mathbf{q}}(t) = G_{\mathbf{q}}^{(\mathbf{v})}(t \quad t_0)\varphi_{\mathbf{q}}^{(\rm ss)} + \lambda V_q \int_{t_0}^{t} \mathrm{d}s \, \chi_{\mathbf{q}}^{(\mathbf{v})}(t \quad s) e^{\ i\mathbf{q}\cdot\mathbf{Z}(s)}. \tag{4.38}$$

Equation (4.36) suggests the natural change of reference frame, in which the origin of the coordinate system corresponds to $\mathbf{Z}^{(\rm ss)}$. Accordingly, we introduce $\mathbf{X} \equiv \mathbf{Z} \quad \mathbf{Z}^{(\rm ss)}$, so that the resting position of the particle is $\mathbf{X} = 0$ in the stationary state (as depicted in Fig. 4.5). By substituting $\varphi_{\mathbf{q}}(t)$ found in Eq. (4.38) into Eq. (4.25) with $\boldsymbol{\xi} = \mathbf{0}$, we obtain the (noiseless) effective equation

$$\begin{aligned} \dot{\mathbf{X}}(t) = \quad & \gamma \left[\mathbf{X}(t) + \mathbf{Z}^{(\rm ss)}\right] + \lambda^2 \nu \int \frac{\mathrm{d}^d q}{(2\pi)^d} \frac{i\mathbf{q}|V_q|^2}{_q \quad i\mathbf{q}\cdot\mathbf{v}} \chi_{\mathbf{q}}^{(\mathbf{v})}(t \quad t_0) e^{i\mathbf{q}\cdot\mathbf{X}(t)} \\ & + \lambda^2 \nu \int_{t_0}^{t} \mathrm{d}u \int \frac{\mathrm{d}^d q}{(2\pi)^d} i\mathbf{q}|V_q|^2 \chi_{\mathbf{q}}^{(\mathbf{v})}(t \quad u) e^{i\mathbf{q}\cdot[\mathbf{X}(t) \ \ \mathbf{X}(u)]}. \end{aligned} \tag{4.39}$$

This non-linear equation with memory cannot be generically solved. However, further analytical progress can be made by assuming that the particle is actually perturbed by a small, sudden displacement $\mathbf{X}_0$ away from its resting position, as sketched in Fig. 4.5. Under this assumption, it is possible to linearize Eq. (4.39) around $\mathbf{X} = 0$, which leads (upon using Eq. (4.36)) to

$$\dot{X}_j(t) = \quad X_j(t) \left[\gamma + \lambda^2 \nu D \int \frac{\mathrm{d}^d q}{(2\pi)^d} \frac{q_j^2 q \ \ |V_q|^2}{_q \quad i\mathbf{q}\cdot\mathbf{v}} \right] + \lambda^2 \nu \int_{t_0}^{t} \mathrm{d}u \int \frac{\mathrm{d}^d q}{(2\pi)^d} q_j^2 |V_q|^2 \chi_{\mathbf{q}}^{(\mathbf{v})}(t \quad u) X_j(u), \tag{4.40}$$

for $j = 1, \ldots, d$. Let us now introduce the memory kernel

$$_j(t) \equiv \lambda^2 \nu \int \frac{\mathrm{d}^d q}{(2\pi)^d} q_j^2 |V_q|^2 \chi_q(t) \tag{4.41}$$

and its Laplace transform $\hat{\ }_j(s) = \int_0^\infty \mathrm{d}t \, e^{\ st} \ _j(t)$; in terms of these quantities, the linearized equation of motion (4.40) can be written in the compact form

$$\dot{X}_j(t) = \quad X_j(t) \left[\gamma + \hat{\ }_j(0) \right] + \int_{t_0}^{t} \mathrm{d}u \quad _j(t \quad u) X_j(u). \tag{4.42}$$

We recognize Eq. (4.42) as the noiseless limit of an overdamped generalized Langevin equation — see Section 1.4. By setting $t_0 = 0$, the solution of the latter equation with initial condition $X_j(t = 0) = X_0$ can be conveniently expressed in Laplace space as

$$\hat{X}_j(s) = \frac{X_0}{s + \gamma \quad \left[\hat{\ }_j(s) \quad \hat{\ }_j(0)\right]}, \tag{4.43}$$

where, as in the case of $\hat{\ }_j$ after Eq. (4.41), $\hat{X}_j(s)$ stands for the Laplace transform of $X_j(t)$.

4.5.1 The memory kernel (t)

The dynamics of $X_j(t)$ is determined by the analytic structure of the function $\hat{\ }_j(s)$ in the complex plane, which we discuss here. For later convenience, we introduce the following timescales:

$$\tau_R \equiv R \ /D, \tag{4.44}$$

$$\tau_v \equiv R/v. \tag{4.45}$$

The first timescale τ_R is the time taken by a critical field in order to relax over a distance of order R: this can be seen by using Eq. (1.25) with $r = 0$, $q \simeq 1/R$, and $\equiv 2 +$. We recall that R enters as a length scale in $V(\mathbf{x})$, and plays the role of the radius of the particle described by $V(\mathbf{x})$; in the following, we will often choose an exponentially decaying potential

$$V(\mathbf{x}) = \frac{1}{\Omega_d \ _E(d)R^d} \exp(\ \|\mathbf{x}\|/R), \tag{4.46}$$

where Ω_d is the d-dimensional solid angle, and $_E(\ )$ is the Euler gamma function. The second timescale τ_v in Eq. (4.45) represents, instead, the time taken by the moving trap to cover a distance of order R; equivalently, $\tau_v{}^{1}$ estimates the shear rate near the driven particle [47].

By rescaling momenta as $p = qR$ in Eq. (4.41) and evaluating the Laplace transform, we obtain

$$\hat{\ }_j(s) = \frac{\lambda^2\nu}{R^d} f(s; \tau_R, \tau_v, R, \xi) = \frac{\lambda^2\nu}{R^d} \tilde{f}(s\tau_R, \tau_R/\tau_v, R/\xi), \tag{4.47}$$

where the prefactor $\lambda^2\nu/R^d$ has the physical dimensions of an inverse time, while $\tilde{f}$ is a dimensionless scaling function defined as

$$\tilde{f}(\theta_1, \theta_2, \theta_3) = \int \frac{\mathrm{d}^d y}{(2\pi)^d} \frac{y_j^2 y \ |V_{y/R}|^2}{\theta_1 + y \quad y^2 + \theta_3^2) \quad i\theta_2 \mathbf{y} \cdot \mathbf{v}}. \tag{4.48}$$

Note that $V_{y/R}$ is in fact R-independent by construction (see, e.g., Eq. (4.46)). Moreover, the timescale τ_κ (see Eq. (1.12)) which determines the relaxation time of the particle (decoupled from the field) in the harmonic trap does not enter the memory kernel, which thus describes solely the interaction between the medium and the particle. By substituting Eq. (4.47) into Eq. (4.43), one eventually finds

$$\hat{X}_j(s) = \frac{X_0/\gamma}{1 + s/\gamma \quad g\left[f(s) \quad f(0)\right]}, \tag{4.49}$$

where we introduced the dimensionless coupling constant

$$g \equiv \frac{\lambda^2}{\kappa R^d}, \tag{4.50}$$

and where we simplified the notation by explicitly indicating only the dependence on s of f introduced in Eq. (4.47). The coupling constant g can be used to quantify the effect of the interaction with the medium on the particle dynamics. We note that $\hat{X}(s)$ in Eq. (4.49) satisfies the initial value theorem for Laplace transforms [156], i.e.,

$$\lim_{s\to\infty} s\hat{X}(s) = X(t = 0^+) = X_0, \tag{4.51}$$

as expected — indeed, one can check that $f(s) \sim 1/s$ for large s.

In order to get physical insight into the dynamics of the particle, it is convenient to consider the case in which the timescales τ_R and τ_κ, which $\hat{X}_j$ depends on via f, are well separated. This is actually achieved in the *strong-confinement limit* [148], defined as the limit in which τ_κ, determined by the harmonic trap, is shorter than the typical relaxation time τ_R of the field, i.e., $\tau_R \gg \tau_\kappa$ or, equivalently,

$$\rho \equiv \tau_R/\tau_\kappa = \gamma\tau_R \gg 1. \tag{4.52}$$

In this limit we will focus on the dynamics for times $t \gg \tau_\kappa$, so that τ_κ is indeed the smallest timescale in the problem. A convenient way of singling out the behavior in this temporal regime is to consider, in Eq. (4.43), the formal limit $\gamma \to \infty$ and thus

$$\hat{X}^{(\mathrm{sc})}(s) \equiv \lim_{\gamma\to\infty} \gamma\hat{X}(s) = \frac{X_0}{1 \quad g\,[f(s) \quad f(0)]}, \tag{4.53}$$

the analysis of which is simplified by the fact that $\hat{X}^{(\mathrm{sc})}(s)$ depends on s only via the function $f(s)$. As a drawback of this approach, $\hat{X}^{(\mathrm{sc})}(s)$ defined above no longer satisfies the initial value theorem and, as a consequence, its inverse Laplace transform $X^{(\mathrm{sc})}(t)$ diverges in the initial temporal region $t \leq \tau_\kappa$. Beyond this initial regime, however, the functions $X^{(\mathrm{sc})}(t)$ and $\gamma X(t)$ are expected to agree quantitatively (as discussed in, c.f., Section 4.5.3).

4.5.2 The case of model A

To make further progress with our analysis, we focus here on the one-dimensional case $d = 1$, with the field poised at its critical point $r = 0$ (further below we consider also the case $r > 0$). In addition, we choose an exponential interaction potential as in Eq. (4.54), which takes a particularly simple form in Fourier space, namely

$$V_q = (1 + q^2R^2)^{\ 1}. \tag{4.54}$$

This choice renders the expressions below more amenable to analytical manipulation. In fact, the resulting memory kernel in Eq. (4.47) becomes

$$\hat{}(s) = \frac{\lambda^2\nu}{R}\int_{\mathbb{R}} \frac{\mathrm{d}q}{2\pi} \frac{q}{(1+q^2)^2(q \quad iq\tau_R/\tau_v + s\tau_R)}, \tag{4.55}$$

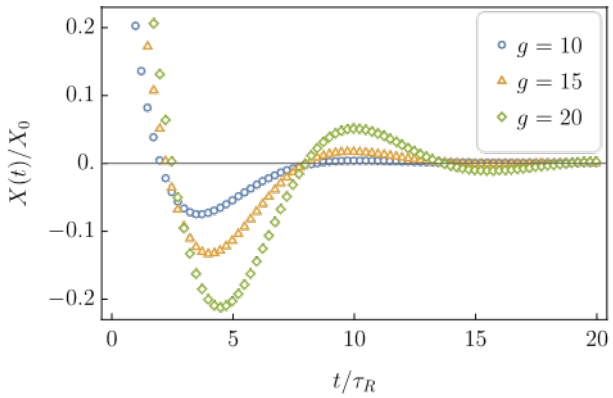

Figure 4.6: Evolution of the particle position $X(t)$ as a function of time t, in the noiseless limit. At $t = 0$ the particle is released from the position $X(t = 0^+) = X_0$ away from the steady-state position $X = 0$. The displayed symbols are obtained from the numerical Laplace inversion of $\hat{X}^{(\mathrm{sc})}(s)$ in Eq. (4.53), corresponding to the strong-confinement limit. The plot refers to model A at criticality in spatial dimensionality $d = 1$ (see Section 4.5.2), and was obtained by fixing the Weissenberg number $w = 0.75$ (see Eq. (4.57)), while varying the coupling strength g (see Eq. (4.50)), with $X_0 = 1$. The so-obtained $X^{(\mathrm{sc})}(t)$ differs from the actual $\gamma X(t)$ only at short times $t < \tau_\kappa$, where the former diverges (while the latter tends to γX_0 — see Eq. (4.51)).

where we dropped the subscript j from $\hat{}_j(s)$ since we are considering $d = 1$. In the Gaussian model A, the dynamical exponent equals 2, so that the integrand in $\hat{}(s)$ presents two simple poles in $q = \pm i$ and two additional poles in

$$q_\pm = i\left[\frac{\tau_R}{2\tau_v} \pm \sqrt{s\,\tau_R + \left(\frac{\tau_R}{2\tau_v}\right)^2}\right] \equiv i\,[w \pm \beta(s)]. \tag{4.56}$$

For later convenience, we parameterized these latter two poles as indicated above, with

$$w \equiv \frac{\tau_R}{2\tau_v} = \frac{vR}{2D}^{1} \tag{4.57}$$

(see Eqs. (4.44) and (4.45)), and $\beta(s) \equiv \sqrt{s\,\tau_R + w^2}$. In the context of microrheology experiments conducted in viscoelastic media, one usually identifies the Weissenberg number $\mathrm{Wi} \equiv \tau_s/(2\tau_v)$, where τ_s is the typical relaxation timescale of the medium. For a critical field this timescale is actually provided by τ_R (see Eq. (4.44)), and therefore the parameter w introduced in Eq. (4.57) above is readily identified with the Weissenberg number Wi of the system under investigation here. By using complex integration, one then finds that $\hat{}(s)$ in Eq. (4.55) can be expressed as

$$\hat{}(s) = \frac{\lambda^2\nu}{R}\,\frac{\beta(s)[1+\beta(s)]^2 \quad w^2[2+\beta(s)]}{4\beta(s)[1+\beta(s)+w]^2[1+\beta(s) \quad w]^2}. \tag{4.58}$$

This expression implies $\hat{}(s = 0) = \lambda^2\nu/[4R(1+2w)^2]$, which can be inserted into Eq. (4.43) together with $\hat{}(s)$ given above in order to obtain an analytical expression for $\hat{X}(s)$. The latter can then be inverted numerically to determine $X(t)$. An example of the resulting $X(t)$ is shown in Fig. 4.6, which refers to the strong-confinement limit, while a comparison with numerical

simulations is presented in, c.f., Section 4.6.2. The oscillatory character of this $X(t)$ is clearly visible from the figure and it can be amplified by increasing the coupling strength g (a systematic analysis of this dependence is presented in the next subsection).

By inspecting Eqs. (4.47) and (4.48), we finally note that the expression of $\hat{\ }(s)$ for model A away from criticality (i.e., with $r > 0$) can be obtained from Eq. (4.58) by means of the substitution

$$s \mapsto s + \tau_\xi{}^1, \tag{4.59}$$

where $\tau_\xi = 1/(Dr) = \xi^2/D$ (see Eq. (4.35)).

4.5.3 Relaxation in the strong-confinement limit

In the strong-confinement limit introduced in Eq. (4.53), the analytic properties of $\hat{X}^{(\mathrm{sc})}(s)$ are completely determined by those of the memory kernel $\hat{\ }(s)$ and, in particular, of the associated function $f(s)$ introduced in Eq. (4.47). This kernel was specialized in Eq. (4.58) to the case of model A at criticality ($r = 0$), while for $r > 0$ one can use the change of variable indicated in Eq. (4.59). The latter implies $\hat{X}^{(\mathrm{sc})}_r(s) = \hat{X}^{(\mathrm{sc})}_{r=0}(s + Dr)$, and therefore

$$X^{(\mathrm{sc})}_r(t) = \int_{c\ \ i\infty}^{c+i\infty} \frac{\mathrm{d}s}{2\pi i} e^{st} \hat{X}^{(\mathrm{sc})}_r(s) = e^{\ Drt} X^{(\mathrm{sc})}_{r=0}(t). \tag{4.60}$$

Above we highlighted the dependence of $X^{(\mathrm{sc})}(t)$ on r via a subscript. The inverse Laplace transform of $\hat{X}^{(\mathrm{sc})}(s)$ in the previous expression is obtained, as usual, by performing the Bromwich integral along a vertical line that is on the left of the leftmost pole of the integrand in the complex plane. Accordingly, in model A, the dynamical properties of $X^{(\mathrm{sc})}(t)$ in the off-critical case $r \neq 0$ are the same as in the critical case $r = 0$, up to an additional exponential decay factor $\exp(-t/\tau_\xi)$ (see Eq. (4.35)).

A second remarkable feature of $\hat{X}^{(\mathrm{sc})}(s)$ is that it depends on s only via the combination $s\,\tau_R$ — see Eqs. (4.47) and (4.48), and the definition of τ_R in Eq. (4.44). Taking the inverse Laplace transform of $\hat{X}^{(\mathrm{sc})}(s)$ as in Eq. (4.60) and changing the integration variable as $s' \equiv s\tau_R$, it follows that $X^{(\mathrm{sc})}(t) = \tau_R{}^1 X^{(\mathrm{sc})}(t/\tau_R)$. We deduce that rescaling $s\,\tau_R \mapsto s$ in $\hat{X}^{(\mathrm{sc})}(s)$ simply corresponds to measuring time t in units of τ_R. At criticality ($\xi \to \infty$), the explicit dependence on R of $\hat{\ }(s)$, which occurs in Eq. (4.47) only via R/ξ, is therefore lost. Accordingly, the resulting $\hat{X}^{(\mathrm{sc})}(s)$ eventually depends only on the pair of parameters (w, g) — see Eqs. (4.50) and (4.56) to (4.58).

Let us then focus on the analytic structure of $\hat{X}^{(\mathrm{sc})}(s)$ in the complex plane $s \in \mathbb{C}$, for $r = 0$ and with $\tau_R \equiv 1$. First, from Eq. (4.56) we infer the presence of a branch cut along the real axis for $\mathrm{Re}\{s\} < -w$, as shown in Fig. 4.7(a). The exact position of the poles of $\hat{X}^{(\mathrm{sc})}(s)$ in Eq. (4.53) cannot be determined analytically; however, they are easily found numerically. Indeed, the plot of $\mathrm{Re}\{\hat{X}(s)\}$ in the complex plane, shown in Fig. 4.7(a) as a colormap, reveals the presence of a pair of complex conjugate poles in $s_\pm = -\delta \pm i\Omega$, with $\Omega \geq 0$. The red dashed line in the plot indicates the trajectory of these poles upon varying g at fixed $w < 1$. The poles appear for a small $g = g^* > 0$, in the vicinity of the origin $s = -w$ of the branch cut, and have a vanishing imaginary part $\Omega = 0$; upon increasing g, they depart from the branch cut and acquire a nonzero

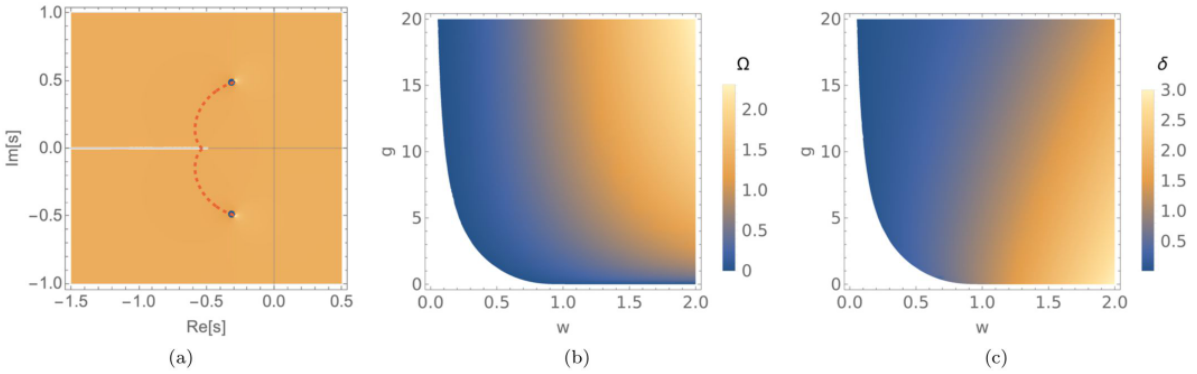

Figure 4.7: Analytic structure of the Laplace transform $\hat{X}(s)$ of $X(t)$ in the complex plane $s \in \mathbb{C}$, for model A in spatial dimension $d = 1$, at criticality $r = 0$, and in the strong-confinement limit (see Section 4.5.3). **a)** Plot of $\mathrm{Re}\{\hat{X}(s)\}$, which shows the presence of a branch cut for $\mathrm{Re}\{s\} < \quad w$, and a pair of complex conjugate poles $s_\pm = \quad \delta \pm i\Omega$ with nonzero imaginary part $\Omega > 0$. The latter determines the oscillatory frequency Ω of $X(t)$ after a short initial transient (see also Fig. 4.6). The plot corresponds to $w = 0.7$, and the red dashed lines indicate the trajectories of the poles in the complex plane, which emerge out of the branch cut and move away from it upon increasing the values of $g \in [0.32, 17]$. **b)** Imaginary part Ω of the upper pole s_+ as a function of w and g. Oscillations develop for any value of g as soon as $w \quad 1$, while they are absent within the white region, where there are no poles and the decay is controlled by the branch cut. The frequency Ω is measured in units of ${\tau_R}^1$ — see Eq. (4.44). **c)** Real part δ of the poles (which controls the rate of the exponential damping of the oscillation amplitude) as a function of w and g. Oscillations turn out to be increasingly damped upon increasing the value of w. As in panel (b), no poles emerge within the white region in this plane.

imaginary part $\Omega > 0$. As g is further increased, the two poles eventually move to the right of the branching point (i.e., $|\delta| < |w|$), and thus they become the *dominant* singularities. The presence of a dominant complex pole in the analytic structure of $\hat{X}^{(\mathrm{sc})}(s)$ implies the emergence of an oscillatory behavior of $X^{(\mathrm{sc})}(t)$ at long times, with frequency Ω (see Appendix D.6 for additional details). These are the oscillations featured in Fig. 4.6, where we plotted $X^{(\mathrm{sc})}(t)$ (obtained via numerical inversion of the analytical solution for $\hat{X}^{(\mathrm{sc})}(s)$) for increasing values of the coupling strength g, while keeping w fixed.

Figure 4.7(b) shows the oscillation frequency Ω as a function of the values of the parameters (w, g). Within the white region of the plot there are no poles, and thus no oscillations occur. Even for small values of g, instead, complex poles appear and oscillations are seen to develop as soon as $w \quad 1$; moreover, Ω is in general an increasing function of w, for any fixed value of g. We recall that $w = \mathrm{Wi}$ measures the ratio between the relaxation time of the medium and the timescale τ_v set by the moving trap (see Eq. (4.57)). This suggests a way to rationalize the "dynamical phase diagram" in Fig. 4.7(b). Indeed, for small g and sufficiently large values of the dragging speed $v \propto w$ (see Eqs. (4.45) and (4.57)), the field is no longer able to quickly rearrange around the instantaneous position assumed by the particle at a given time: the non-Markovian interplay between the dynamics of the particle and the shadow is then at the origin of the complex oscillatory behavior of $X(t)$. The effects of this interplay become increasingly prominent upon

increasing the coupling strength g, so that at large g one observes an oscillatory behavior even for $w \lesssim 1$.

Conversely, these oscillations are increasingly damped upon increasing the dragging speed, i.e., for $w \gg 1$. This is shown in Fig. 4.7(c), where we plot the real part δ of the dominant pole as a function of (w, g) — indeed, the latter controls the long-time exponential decay of $X(t)$ (see Appendix D.6). To understand the damping at large $w \propto v$, we first note that the shape of the shadow $\varphi^{(\mathrm{ss})}(\mathbf{x})$ is given by the Fourier transform of $\varphi^{(\mathrm{ss})}_{\mathbf{q}}$ in Eq. (4.29): upon inspection, the latter shows that the amplitude of the shadow itself decreases upon increasing v (see Fig. 4.4(a)). This is expected, since the finite relaxation time of the field φ does not allow φ to react instantaneously to the passage of the particle, and thus at a very large speed v the shadow cannot build up at all. The damping of the oscillations at large values of w thus simply reflects these facts.

We emphasize that no poles emerge in $\hat{X}(s)$ within the white region in the (w, g)-plane in Fig. 4.7(b,c). Correspondingly, the long-time behavior of $X(t)$ in that region is determined solely by the branch cut (see Fig. 4.7(a)): as we recall in Appendix D.6, this generically implies that $X(t)$ decays monotonically as $X(t) \sim t^{\ a} \exp(\ \ bt)$, for some positive constants a and b (see Eq. (D.62)). Conversely, upon increasing g far beyond the values that Fig. 4.7(a) refers to, the real part $\ \ \delta$ of the poles $s_\pm$ eventually becomes positive. This would imply an unbounded (oscillatory) growth of $X(t)$ at long times (see Appendix D.6 for details), and thus it signals the breakdown of the linear-response approximation within which such solution has been derived.

Beyond the strong-confinement limit discussed so far, i.e., upon decreasing the value of γ, new poles eventually appear in the complex-s plane shown in Fig. 4.7(a). Although the precise value of Ω at a certain point (w, g) of the plane is in general modified compared to the value it has in the strong-confinement limit $\rho \gg 1$ (see Eq. (4.52)), we find that the oscillatory nature of the solution $X(t)$ persists, within the same range of values as in Fig. 4.7(b), down to $\rho \quad 1$. Note that, after rescaling $s' \equiv s\,\tau_R$ in Eq. (4.49), the latter reads

$$\hat{X}_j(s'/\tau_R) = \frac{X_0/\gamma}{1 + s'/\rho \quad g\,[f(s'/\tau_R) \quad f(0)]}, \tag{4.61}$$

showing (as expected) that the strong-confinement limit becomes increasingly accurate as $\rho \gg 1$ — compare with Eq. (4.53). Moreover, Figs. 4.6 and 4.7 (together with the numerical simulations presented in, c.f., Section 4.6.2) show that $X(t)$ typically decays to zero on a scale of a few tens of τ_R. As a result, even for $\rho \lesssim 1$, the strong-confinement limit well approximates the behavior of $X(t)$ at times $t > \tau_\kappa = \gamma^{\ 1}$. Indeed, by taking the inverse Laplace transform of $\hat{X}_j(s)$ in Eq. (4.49) and calling $\ \equiv st$, one obtains

$$X_j(t) = (\gamma t)^{\ 1} \int_B \frac{\mathrm{d}}{2\pi i} \frac{e\ \ X_0}{1 + \ \ /(\gamma t) \quad g\,[f(\ \ /t) \quad f(0)]}, \tag{4.62}$$

where the integration is intended along the Bromwich contour as in Eq. (4.60). The term $\ \ /(\gamma t)$ at the denominator can be safely neglected as soon as $\gamma t \gg 1$, yielding in fact $X_j(t) \simeq X_j^{(\mathrm{sc})}(t)/\gamma$ (see Eq. (4.53)).

Away from the critical point (i.e., for $r > 0$), the damped oscillations of $X(t)$ persist, but they are additionally suppressed by the exponential factor $\exp(\ \ Drt) = \exp(\ \ t/\tau_\xi)$ (see Eqs. (4.35)

and (4.60)). Taking into account all the trends highlighted above, we expect that the oscillatory behavior of $X(t)$ is maximally amplified within the timescale window $\tau_\kappa < \tau_R < \tau_\xi$, where the second inequality corresponds to requiring $\xi > R$ (see Eqs. (4.35) and (4.44)). Note that increasing the trap strength κ has the effect of both increasing γ (thus pushing the system further into the strong-confinement regime), and decreasing the effective coupling g and therefore decreasing the amplitude of the oscillations (see Fig. 4.7(b,c)). Accordingly, oscillations generically develop at intermediate values of κ, while they vanish both at very large and very small values of κ. This was also the case in experiments performed on colloidal particles dragged in viscoelastic media (see Ref. [47] and Fig. 5 therein).

Figure 4.7 additionally confirms that no oscillations occur if the trap is not dragged, i.e., for $v = 0$ (hence $w = 0$). This was also the case in the experiments of Ref. [47] involving a viscoelastic medium (see Fig. 3 therein). This fact also agrees with the analytical and numerical results of Chapter 2, where the relaxation towards equilibrium of a trapped particle in contact with a near-critical Gaussian field was investigated perturbatively in the coupling λ [81]. In particular, we had found that $\langle X(t)\rangle$ decreases algebraically upon increasing time t for model A at criticality, and generically for model B. For completeness, in Appendix D.7 we reconsider this problem within the noiseless but non-perturbative approach presented in this Section, and we re-derive the exponents of the long-time algebraic decay of $\langle X(t)\rangle$ reported in Eqs. (2.16) and (2.17).

Finally, we note that in Ref. [47] an analogy with a stochastic underdamped harmonic oscillator was suggested, as it was shown that such a simplified model (with a positive, memory-induced mass term) is able to reproduce quantitatively the oscillations observed at long times in the dragged colloidal particle. While such an analogy turns out to be inappropriate in our case due to the non-analytic behavior of the memory kernel, in Appendix D.8 we discuss in detail its comparison with the theoretical model for viscoelastic fluids used in Ref. [47]. In particular, the memory kernels (t) emerging in the present case and in viscoelastic media appear to be both negative at long times t, confirming that the *negative response* of the surrounding medium (whose origin in our model has been clarified in the previous Sections) is responsible for the emergence of the oscillating modes exhibited by the overdamped particle.

4.6 Effects of thermal fluctuations

Thermal fluctuations act on the field and the particle, via the noise terms $\boldsymbol{\xi}(t)$ and $\eta_q(t)$ in Eqs. (4.25) and (4.26), whenever $T \neq 0$. The presence of the thermal noise represents an obstacle to the analytical derivation of the time-dependent relaxation of the particle, because it modifies the steady-state average of both the position $\langle \mathbf{Z} \rangle_{\rm ss}$ of the particle and the field $\langle \varphi_{\mathbf{q}} \rangle_{\rm ss}$ in Eq. (4.29). Once incorporated into the effective equation of motion of the particle, the field-induced fluctuations turn out to be non-Gaussian, as we will verify shortly; in order to account for them, we shall resort below to a perturbative expansion in the coupling constant λ. We emphasize that the (noiseless) effective equation (4.39) is actually *non-perturbative* in λ, and so is its solution in Eq. (4.49). Expanding the dynamics for small λ is just a computational tool to take fluctuations into account analytically, but the qualitative conclusions we reach are valid beyond the

perturbative regime, as we confirm in Section 4.6.2 by using numerical simulations.

4.6.1 Weak-coupling approximation

The effective equation (4.39) in Section 4.5 was determined first by choosing the shadow state in Eq. (4.37) as the initial condition for the field φ at time $t = t_0$, and then by moving to a reference frame in which the resting position of the particle corresponds to $\mathbf{X} = 0$. In this Section we adopt a different strategy: instead of explicitly determining the stationary shadow configuration (which is difficult in the presence of thermal fluctuations), we first solve for $\varphi_{\mathbf{q}}(t)$ as we did in Eq. (4.38), but we impose the flat initial condition $\varphi_{\mathbf{q}}(t = t_0) = 0$ at the initial time t_0 and we take into account the contributions due to the noise. Plugging the result into Eq. (4.25) then yields

$$\dot{\mathbf{Z}}(t) = \quad \gamma \mathbf{Z}(t) + \boldsymbol{\xi}(t) + \lambda \nu \int \frac{\mathrm{d}^d q}{(2\pi)^d} i\mathbf{q} V \;_q e^{i\mathbf{q}\cdot\mathbf{Z}(t)} \left[\zeta_{\mathbf{q}}(t) + \lambda V_q \int_{\infty}^{t} \mathrm{d}s \; \chi_{\mathbf{q}}^{(\mathbf{v})}(t \quad s) e^{\;i\mathbf{q}\cdot\mathbf{Z}(s)} \right], \tag{4.63}$$

where we introduced the colored Gaussian noise

$$\zeta_{\mathbf{q}}(t) \equiv \int_{\infty}^{t} \mathrm{d}s \; G_{\mathbf{q}}^{(\mathbf{v})}(t \quad s) \eta_{\mathbf{q}}(s), \tag{4.64}$$

which has zero mean and the correlator $C_{\mathbf{q}}^{(\mathbf{v})}(t)$ [see Eq. (4.27)]. Although we did not specify the stationary shadow configuration of the field (see Fig. 4.2) as the initial condition of its evolution, one can convince oneself that such a configuration is inevitably recovered by taking the limit $t_0 \to \quad \infty$, since it coincides with the nonequilibrium steady state of the system. The leading correction to the average particle position $\langle \mathbf{Z} \rangle$, due to thermal fluctuations, can in principle be accessed by first taking the average of Eq. (4.63), and then setting $\partial_t \langle \mathbf{Z} \rangle = 0$ to find the steady-state result $\langle \mathbf{Z} \rangle_{\mathrm{ss}}$ — see Appendix D.4.1. In fact, however, we have already calculated $\langle \mathbf{Z} \rangle_{\mathrm{ss}}$ in Eq. (4.32). In analogy with the derivation in Section 4.5, we now change reference frame to $\mathbf{X} \equiv \mathbf{Z} \quad \langle \mathbf{Z} \rangle_{\mathrm{ss}}$ in Eq. (4.63), we take the average over thermal fluctuations, and we linearize the resulting equation. This way we find the evolution of the *average* position $\langle \mathbf{X}(t) \rangle$ to be given by

$$\partial_t \left\langle X_j(t) \right\rangle = \quad \left\langle X_j(t) \right\rangle \left[\gamma + \hat{}_j(s = 0) \right] + \int_{\infty}^{t} \mathrm{d}u \quad _j(t \quad u) \left\langle X_j(u) \right\rangle, \tag{4.65}$$

which is formally the same as Eq. (4.42), but where $X_j(t)$ is replaced by $\left\langle X_j(t) \right\rangle$, the initial time t_0 is set to $\quad \infty$, and the memory kernel is replaced by

$$_j(t) \equiv \lambda^2 \nu \int \frac{\mathrm{d}^d q}{(2\pi)^d} q_j^2 |V_q|^2 e^{\;q^2 \sigma_2^2(t)} \left[\chi_{\mathbf{q}}^{(\mathbf{v})}(t) + \nu q^2 e^{\;\gamma t} C_{\mathbf{q}}^{(\mathbf{v})}(t) \right]. \tag{4.66}$$

As expected, compared to the memory kernel for the noiseless case in Eq. (4.41), which includes only the first term on the r.h.s. of Eq. (4.66), the present one includes a second term $\propto C_{\mathbf{q}}^{(\mathbf{v})}(t)$ due to thermal fluctuations. Note that the integration in the variable u in Eq. (4.65) runs from $\quad \infty$, and this fact prevents a direct solution of the equation of motion by using the Laplace transform [157]. However, in order to determine the response of the average particle position to a sudden displacement $\mathbf{X}_0$ imposed at time $t = 0$ from its stationary value $\langle \mathbf{X} \rangle = 0$, one can look for a

solution $\langle \mathbf{X}(t) \rangle$ of Eq. (4.66) with $\langle \mathbf{X}(t) \rangle \equiv 0$ for $t < 0$, and $\langle \mathbf{X}(t) \rangle = \mathbf{X}_0$ at $t = 0$. In this way, $\langle \mathbf{X}(t) \rangle$ for $t > 0$ follows immediately from a Laplace transform as in Eq. (4.43), with $\langle \hat{X}_j(s) \rangle$ in place of $\hat{X}_j(s)$, and with the memory kernel $\quad_j(t)$ given by the new expression in Eq. (4.66). In this case, an expression of the function $\hat{}_j(s)$ in closed form (such as the one found in Section 4.5.2 in the noiseless limit) cannot be obtained. In spite of this complication, studying the strong-confinement limit provides already valuable information concerning the main effects of thermal fluctuations. In fact, in Section 4.5.3 it was shown that this limit actually captures the particle evolution for times $t > \tau_\kappa$. Proceeding as in Eq. (4.53), we then inspect the formal limit $\gamma \to \infty$, which has the effect of suppressing the term proportional to the field correlator $C_{\mathbf{q}}^{(\mathbf{v})}(t)$ in the memory kernel given in Eq. (4.66). Accordingly, this results into

$$\langle \hat{X}^{(\mathrm{sc})}(s) \rangle = \frac{X_0}{1 \quad g\,[f(s) \quad f(0)]}, \tag{4.67}$$

where the function $f(s)$ is the same as in Eq. (4.48) upon replacing V_q with $\widetilde{V}_q \equiv V_q e^{\ Tq^2/(2\kappa)}$. Since the role of V_q is essentially that of providing a large-momentum cutoff for $q \quad 1/R$ [81, 104], we conclude that $\widetilde{V}_q$ represents an effective renormalization of the particle radius R, which is replaced by a combination of R and the *thermal length*

$$l = \sqrt{T/(2\kappa)}. \tag{4.68}$$

Note that l coincides with the mean squared displacement of the particle in its harmonic trap due solely to thermal fluctuations. For instance, a choice of V_q as in Eqs. (4.46) and (4.54) yields $|V_q|^2 \simeq 1 \quad 2q^2R^2$ for small q, so that $|\widetilde{V}_q|^2 \simeq 1 \quad 2q^2(R^2 + l^2)$, and therefore R is effectively renormalized as $R \mapsto \sqrt{R^2 + l^2}$.

4.6.2 Numerical simulations

In this section we present and discuss the results of numerical simulations of the system in one spatial dimension, which confirm our analytical predictions, also beyond the noiseless limit presented in Section 4.5 and the perturbation theory discussed in Section 4.6. In particular, the numerical data are obtained via a direct integration of the Langevin equations for the particle and the field, similarly to Section 2.4, but using the stochastic Runge-Kutta algorithm described in Ref. [158] (which is suited for investigating also cases with an explicitly time-dependent external drag). The field is initially prepared, at time $t = \quad \mathcal{T}$, in the flat configuration $\phi(\mathbf{x}, t = \quad \mathcal{T}) = 0$; the harmonic potential which traps the particle is dragged for a certain time $\mathcal{T}$ until the system reaches its steady state, in which the average particle position stops evolving in the comoving frame of reference. At time $t = 0$, the particle coordinate is suddenly displaced by an amount X_0 and its relaxation is recorded. Since the actual position of the particle at time $t = 0$ depends on the realization of the noise, it fluctuates. Accordingly, the result of this displacement is equivalent to extracting the initial particle position at time $t = 0^+$ from a distribution that is the same as the one in the steady state, but shifted in space by an amount X_0. We repeat the whole process (including thermalization) several times, and we finally take the average over the

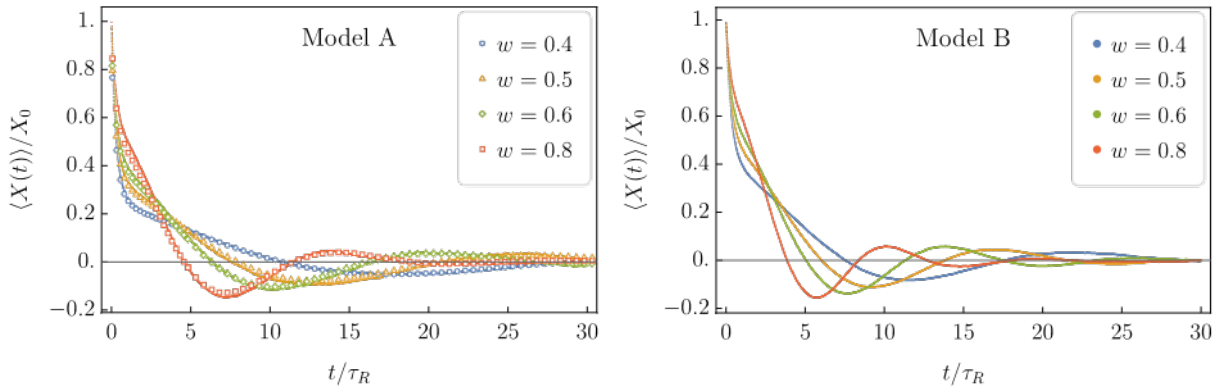

(a) (b)

Figure 4.8: Evolution of the average position $\langle X(t)\rangle$ of the particle, after a small displacement X_0 from its position in the steady state — see Fig. 4.5. **a)** Critical model A in spatial dimension $d = 1$. The data obtained from numerical simulations (solid lines, see the main text) are compared with the analytical prediction (symbols) calculated via the numerical inversion of the Laplace transform in Eqs. (4.49) and (4.58), showing good agreement. In the simulations, the interaction potential V_q was chosen to be exponential as in Eq. (4.54). We used the parameters $\lambda = 5$, $L = 2500$, $r = 0$, $R = 5$, $\nu = 5$, $\kappa = 0.2$, $D = 25$, and $v \in [4, 8]$, corresponding to $g = 25$, $\rho = 1$, and w as indicated in the legend. **b)** Non-critical model B in spatial dimension $d = 1$. In this case an analytical prediction in closed form is not available, and therefore we report only the curves obtained from numerical simulations: the qualitative behavior of the resulting evolution is similar to that of model A in panel (a). In particular, the frequency Ω of the damped oscillations increases upon increasing w. In this simulation the interaction potential was chosen to be Gaussian, i.e., $V_q = \exp\quad q^2R^2/2)$. We also set R, ν, κ, and D to unity, while we chose $\lambda = 6$, $L = 1024$, $r = 0.25$, and $v \in [0.8, 1.6]$, corresponding to $g = 36$ with w and ρ as in panel (a). In both panels (a) and (b), we chose $X_0 = 1$, $T = 10^{\ 2}$, an integration time step $\Delta t = 10^{\ 2}$, and we averaged over 10^4 realizations of the dynamics.

various realizations. Simulations are performed with periodic boundary conditions in order to approximate the behavior of the particle in the bulk. The lattice extension L is chosen sufficiently large so as to avoid *stirring* effects: in fact, a particle dragged along a ring of finite length L soon generates spurious field currents, which in general modify the particle statistics. The value of the particle displacement X_0 is chosen within the linear-response regime, which is verified a posteriori by comparing simulations performed for various (small) values of X_0, checking that the corresponding average particle trajectories $\langle X(t)\rangle$ collapse onto each other after their amplitude is rescaled by X_0.

Figure 4.8 presents the results of the numerical simulations described above. In particular, Fig. 4.8a corresponds to the case of critical model A, which we studied analytically in Section 4.5.2. For various values of the the drag velocity v (which determines the value of the Weissenberg number w indicated in the plot, see Eq. (4.57)), we plot $\langle X(t)\rangle$ (solid line) of a particle that is initially displaced from its steady-state position by an amount X_0, as a function of the time t elapsed from the displacement. These numerical curves are compared with our analytical prediction (symbols), which is obtained by numerical Laplace inversion of Eqs. (4.49) and (4.58),

and in which the particle radius R is replaced by the effective radius $(R^2 + l^2)^{1/2}$ to account for thermal fluctuations (see discussion at the end of Section 4.6.1). The plots show an overall agreement within the entire time range, including the fast initial decay displayed at short times. In general, this decay develops over a timescale $t \sim \tau_\kappa$, followed by an oscillating behavior which persists over a few tens of τ_R. Following our discussion at the end of Section 4.5.3, the latter region $t > \tau_\kappa$ in Fig. 4.8a is essentially described by the strong-confinement limit. This limit turns out to describe accurately the numerical data even when the choice of parameters is not strictly into the strong-confinement regime $\rho \gg 1$, as shown in Fig. 4.8a (see caption), which corresponds to $\tau_\kappa = \gamma^{-1} = 1$, $\tau_R = 1$, and therefore $\rho = 1$. This fact confirms the expectation that the phenomenology described by the dynamical phase diagram presented in Fig. 4.7 actually carries over moderately beyond the strong-confinement limit.

Our previous discussion in Section 4.5 revealed that the behavior of the *noiseless* model is completely determined by fixing the dimensionless numbers $g = \lambda^2/(\kappa R)$, $\rho = \gamma R^2/D$, and $w = Rv/(2D)$ — see Eqs. (4.50), (4.52) and (4.57), here specialized for model A in spatial dimension $d = 1$. Thermal fluctuations are, instead, perturbatively quantified by the ratio l/R of the thermal length l (see Eq. (4.68)) to the particle radius R — see Section 4.6.1. Note that the effective particle dynamics at criticality $r = 0$ has been written in the previous Sections in terms of $n = 10$ physical variables (i.e., X, t, κ, R, ν, λ, D, v, X_0, and T), but only $k = 4$ distinct physical units (i.e., mass, length, time and temperature). The physics of the model is thus actually captured by the mutual dependence of the $n - k = 6$ dimensionless parameters

$$\frac{X}{X_0} = F\left(\frac{t}{\tau_R}; w, \rho, g, \frac{l}{R}\right), \tag{4.69}$$

as suggested by dimensional analysis [159]. In the simulations, we chose $\rho = 1$ and a large effective coupling $g \simeq 25$, while we varied the Weissenberg number w within the range $0 < w \lesssim 1$. We finally added thermal fluctuations of moderate strength by tuning the noise temperature T so that $l/R \simeq 10^{-1} - 10^{-2}$. This choice facilitates the numerical computation and no significant qualitative change occurred at higher temperatures.

In Fig. 4.8b we show the results of simulations analogous to those presented in Fig. 4.8a, but for a field that evolves according to the conserved dynamics prescribed by model B. In addition, we chose here a finite correlation length $\xi \simeq 2R$, so that the system is off criticality. Although analytical predictions cannot be derived in closed form for model B, the simulations show a behavior similar to that of model A. This is interesting in view of possible experimental investigations of the effects qualitatively predicted in this Chapter, because off-critical model B more realistically represents, e.g., the case of colloidal particles immersed in a binary liquid mixture [34–36] (still assuming that hydrodynamics effects are negligible). Note that the parameters w, ρ and the ratio l/R used above are not far from those realistically achievable in experiments (see Appendix D.5.1); the magnitude of g depends, instead, on the specific mechanism that couples the medium with the particle and, from our discussion, one expects the overall effect to be enhanced if g can be made large in an experimental realization. Note also that the interaction potential $V(\mathbf{x})$ in Fig. 4.8b is chosen to be Gaussian with variance R, rather than exponential as

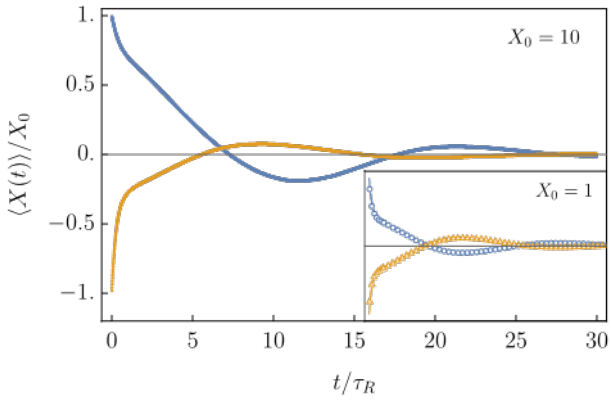

Figure 4.9: Evolution of the average position $\langle X(t)\rangle$ of the particle which is suddenly displaced at time $t = 0$ by an amount $\pm X_0$ from its actual position in the steady state. The solid lines in both the main panel and the inset are obtained from the numerical simulation of the system with model A dynamics in spatial dimension $d = 1$. The inset refers to the case $X_0 = 1$, so that the corresponding behavior is captured by the linear-response prediction in Eqs. (4.49) and (4.58) — the symbols correspond to its numerical Laplace inversion, and the scales on the axes are the same as in the main plot. This implies, inter alia, that $\langle X(t)\rangle$ starting from $+X_0$ is the opposite of $\langle X(t)\rangle$ starting from $-X_0$. The main plot, instead, refers to $X_0 = 10$, which turns out to be beyond the linear regime. In fact, the relaxation occurring from the initial values $+X_0$ and $-X_0$ are no longer related by the symmetry highlighted above. The remaining simulation parameters are the same as in Fig. 4.8a, with $w = 0.6$.

in Eq. (4.46). The overall qualitative behavior is thus shown to be robust against changing the details of $V(\mathbf{x})$, as expected [81].

Finally, we can use the numerical simulations to explore qualitative features that are not captured by the linear-response analysis. In particular, our analytical solution in Eq. (4.43) depends linearly on the initial particle displacement X_0, meaning that the evolution of $\langle X(t)\rangle$ after displacing the particle in the steady state by $+X_0$ is expected to be the opposite of that of $\langle X(t)\rangle$ after a displacement $-X_0$. This is indeed the case in our numerical simulations performed at small X_0, as we show in the inset of Fig. 4.9 (it is also mostly the case in the experiments of Ref. [47] — see Fig. 3 therein). However, the asymmetry between the two evolutions is expected to emerge upon increasing X_0, as it is clearly shown in Fig. 4.9. This asymmetry is a consequence of the non-linearity of the field-particle coupling, and therefore of the effective evolution equation for the particle position.

4.7 Summary of this Chapter

In this Chapter we characterized the effective dynamics and the stochastic thermodynamics of a probe in a spatio-temporally correlated medium, focusing on the case in which an external injection of work (exerted on the probe) drives the system into a nonequilibrium steady state.

First, in Section 4.2 we developed a thermodynamically consistent framework to study the energetic and entropic flows for a probe in a fluctuating medium with spatio-temporal correlations,

modeled here by a scalar field in contact with a heat bath. We showed that the mutual influence of the probe and the correlated environment leads to unusual thermodynamic properties, even for the simple example of a particle dragged by a harmonic trap through a Gaussian field, which we analyzed in Section 4.3. We showed that, close to criticality, a dipolar structure develops in the local heat dissipation of the field, with systematic heat absorption in front of the particle, and whose extent is determined by the spatial correlation length ξ of the field (see Fig. 4.3). Furthermore, in Section 4.3.4 we computed the cumulant generating function of the power needed to drag the particle — see Eqs. (4.31) and (4.33). In particular, we found that the additional power dissipated due to the presence of the field features three regimes with distinct scaling as a function of the drag speed v (see Fig. 4.4(b)), among which are two non-Stokesian regimes — a feature that cannot be captured by a linear GLE. Far from criticality ($\xi \to 0$), the medium is only weakly correlated, and indeed both the heat dipole and the additional dissipation vanish.

Next, in Section 4.4 we demonstrated that, when displaced from its steady-state position in the driven trap, the average position of the particle can exhibit oscillations during relaxation, in spite of the system dynamics being overdamped. This is reminiscent of the oscillatory modes recently observed with colloidal particles dragged through a viscoelastic fluid [47], except that the medium considered here is not viscoelastic. Accordingly, we have shown that oscillating modes can be found in overdamped media characterized by spatial and temporal correlations, which is typically the case for systems close to a second-order phase transition.

In particular, in Section 4.5 we first neglected thermal fluctuations and we derived an analytic solution of the effective equation of motion for the coordinate $X(t)$ of the particle, within the linear-response approximation, and when the particle is suddenly displaced at time $t = 0$ from its steady-state position — see Eq. (4.43). This approximation involves the field-induced memory kernel (t) which appears into the effective equation (4.42) of the particle, once the field has been integrated out. We then focused on the case $d = 1$ of model A dynamics, and we characterized the analytic structure of the memory kernel $\hat{}(s)$ in Laplace space (see Eq. (4.58) and Fig. 4.7), and its implications for the dynamics of $X(t)$. In particular, it turns out that $\langle X(t)\rangle$ generally exhibits oscillations if the relaxation timescale of the field τ_R — over distances of the order of the particle size R, see Eq. (4.44) — exceeds the typical timescale τ_κ set by the harmonic trap (see Section 4.5.3). These oscillations are damped (and eventually vanish) at large values of the trap strength κ and whenever the correlation length of the field ξ is much smaller than the particle radius R. Thermal fluctuations are then reinstated into the problem by using a perturbative expansion in the field-particle coupling λ — see Section 4.6. Their main effect on the late-time particle dynamics is a renormalization of the particle radius R by its thermal mean squared displacement l in the harmonic trap (see Eq. (4.68)), while the qualitative features of $\langle X(t)\rangle$ remain the same as in the absence of the noise.

The accuracy of our analytic predictions was tested via numerical simulations in Sections 4.3.3 and 4.6.2, finding good agreement (see Figs. 4.4(b) and 4.8). However, simulations can also be used to explore the range of parameters that are in principle out of reach of our analytical predictions. For example, in Fig. 4.8b we show that the qualitative features of $\langle X(t)\rangle$ obtained by using a conserved field dynamics, i.e., model B, are similar to those of model A. Moreover,

such features are robust against changing the particular shape of the field-particle interaction potential $V(\mathbf{x})$ (see Eq. (2.3)), as expected. In addition, by choosing a sufficiently large value of the initial particle displacement X_0, we can go beyond the linear-response approximation under which our analytical predictions were derived. In Fig. 4.9, the actual non-linearity of the field-particle coupling causes an asymmetry between the response of the system to a $+X_0$ or $-X_0$ initial particle displacement.

Finally, we note that other interesting features displayed by viscoelastic fluids — such as those observed in the *recoil* experiments performed in Ref. [150] — are found to emerge also within the minimal model for correlated (but not viscoelastic) media studied here. Other possible extensions and future perspectives will be described in the Conclusions.

5

The effects of boundaries: a tracer in a confined correlated medium

As discussed in the previous Chapters, determining effective equations of motion of a complex interacting system is a classic problem in statistical mechanics [11, 160–163]. A typical scenario of this kind is encountered when a tracer particle is immersed in a rapidly fluctuating medium. When there exists a clear separation between time scales, the fast degrees of freedom (medium) can be integrated out and subsumed into a reduced set of equations of motion for the slow degrees of freedom (particle). Several schemes have been proposed in the past to achieve this goal, generally starting form a set of (stochastic) differential equations which are phenomenologically assumed to describe the coupled system composed by the particle and its bath. Most of these schemes are based on the projection operator formalism [7, 8, 154, 155] or on the eigenfunction expansion of the Fokker-Planck equation corresponding to the original set of Langevin equations [9, 53, 84, 85].

In the previous Chapters we have focused on the case in which the tracer particle moves in a medium endowed with long-range correlations and large relaxation times. Theoretical descriptions of this type of systems (such as the one adopted above) often feature a scalar order parameter field $\phi(\mathbf{x})$; a possible enhancement or suppression of the field or its correlations at the tracer location $\mathbf{X}(t)$ (representing, e.g., critical adsorption [100]) can be modeled by including in the Hamiltonian terms proportional to $\phi(\mathbf{X})$ or $\phi^2(\mathbf{X})$, respectively, or derivatives thereof [28].

In order to obtain the effective dynamics of the tracer, a systematic method for the elimination of the field degrees of freedom coupled to $\mathbf{X}(t)$ from the dynamics is required — particularly in the case in which the field relaxation is *fast* (compared to the scale of the particle diffusion), but not instantaneous. The general problem of the elimination of N (non-interacting) fast variables from a system of $(N+M)$ stochastic differential equations is of course not new. The eigenfunction expansion method [9, 84, 85] has been successfully applied to the case in which the field-particle coupling is linear, both in a confined geometry [64, 164] and in the continuum — see the discussion in Section 2.3. In this setting, the fast variables correspond to the Fourier modes of the field, while the d-dimensional coordinates of the particle are the slow variables. The case of a coupling with the particle that is quadratic in the field has hitherto not been addressed within the above formalism: notably, the underlying hypothesis that the N fast variables are non-interacting is generally violated, because the quadratic coupling introduces an interaction between the Fourier modes of the field. Other methods [11, 165] require the specification of a steady-state distribution around which to construct a perturbative series in small powers of an appropriate *adiabaticity* parameter χ; however, such steady-state distribution is generally not known *a priori* when the

system is out of equilibrium.

In this Chapter we present an adiabatic elimination method for a tracer particle with linear or quadratic couplings to a stochastic background field subject to spatial confinement. The method consists in a systematic expansion in powers of a small adiabaticity parameter χ, which encodes the ratio of the field relaxation timescale to that of the particle diffusion. The procedure is transparent as it is based on a multiple-time-scale (or Chapman-Enskog-like) approach, where we project the dynamics over the *moments* of the joint probability distribution $P(\mathbf{X}, \phi, t)$: this way we obtain a hierarchy of equations for the various moments, which can be truncated by noting that the higher moments relax faster than the lower ones [166–168]. Notably, no assumption is made *a priori* about the equilibrium distribution of the tracer particle: the steady-state distribution is instead obtained from the method itself. As a result, the latter can be applied to systems violating detailed balance between tracer and field degrees of freedom. The main outcome of this method is an effective Fokker-Planck equation for the tracer position $\mathbf{X}(t)$, characterized by space-dependent drift and diffusion coefficients.

In the following, we will consider a point-like particle in contact with a scalar field $\phi(\mathbf{x}, t)$, whose Hamiltonian is Gaussian (but of various types, see below), and which undergoes a Langevin relaxational dynamics with or without local conservation. We consider a box with periodic boundary conditions (BCs) for the field and the tracer in all but the -direction, which has size L. In our actual calculations, we will mostly focus on a one-dimensional box of size L in order to arrive at analytically tractable expressions. The field is spatially confined by suitable boundary conditions at $= 0, L$; a Brownian particle is allowed to diffuse within the box (subject to reflective BCs at $= 0, L$), while coupled either linearly or quadratically to $\phi(\mathbf{X}, t)$, or to its derivatives $\nabla^n \phi(\mathbf{X}, t)$. The backreaction of the particle on the evolution of the field may or may not be taken into account. In the former case the tracer is termed *reactive*, and it can be viewed as a model for a colloidal particle in a critical fluid; detailed balance is satisfied along its evolution, so that the system reaches equilibrium by relaxing to the Gibbs state. Conversely, in the latter case, a *passive* tracer is carried by the medium without influencing it: it can be seen as an active particle driven by temporally correlated noise [64].

The rest of the presentation is organized as follows. In Section 5.1 we introduce the model and set the notation. In Section 5.2 we cast the dynamics in terms of the field eigenfunctions expansion, and we exemplify some choices of Hamiltonians and field-particle couplings by pointing out their significance in physical applications. In Section 5.3 we develop the adiabatic elimination method, carrying out the derivation for a reactive or a passive tracer separately. As an example, in Section 5.4 we apply the method to a few simple models, and we point out its qualitative predictions. Our results are summarized in Section 5.5.

The content of this Chapter has been published as "D. Venturelli and M. Gross, *Tracer particle in a confined correlated medium: an adiabatic elimination method*, J. Stat. Mech. (2022) 123210" [65].

5.1 The model

We consider the joint dynamics of a point-like tracer particle at position $\mathbf{X}(t)$ coupled to a fluctuating order parameter scalar Gaussian field $\phi(\mathbf{x}, t)$. The system is described by the Hamiltonian

$$\mathcal{H}(\mathbf{X}, [\phi]) \equiv \mathcal{H}_\phi[\phi] + \mathcal{H}_X(\phi(\mathbf{X})), \tag{5.1}$$

with

$$\begin{aligned} \mathcal{H}_X(\phi(\mathbf{X})) &\equiv \frac{c}{2}(\mathcal{K}_2\phi(\mathbf{X}))^2 \quad h\mathcal{K}_1\phi(\mathbf{X}), \\ \mathcal{H}_\phi[\phi] &\equiv \int_V \mathrm{d}^d x \left\{ \frac{1}{2}\phi(\mathbf{x})\Delta(\mathbf{x})\phi(\mathbf{x}) \quad h_1\phi(\mathbf{x})[\delta(\ ) + \delta(L\quad)] \right\}, \end{aligned} \tag{5.2}$$

where we take $\mathcal{K}_1$, $\mathcal{K}_2$, Δ to be generic self-adjoint differential operators (see Section 5.2.3 below for concrete examples), and the δ-functions are assumed to be located inside the volume V. The system is confined in the -direction, i.e., $\in [0, L]$, and the field is required to fulfill one of the following boundary conditions (BCs):

$$\text{Dirichlet:} \qquad \phi(\{\mathbf{x}_\parallel, \ \in \{0, L\}\}) = 0, \tag{5.3a}$$

$$\text{Neumann:} \qquad \partial\ \phi(\mathbf{x}_\parallel, \ )|_{\ \in\{0,L\}} = 0, \tag{5.3b}$$

$$\text{capillary:} \qquad \partial\ \left\langle \phi(\{\mathbf{x}_\parallel, \ \})\right\rangle |_{\ \in\{0,L\}} = \mp h_1, \tag{5.3c}$$

where $\mathbf{x} = \{\mathbf{x}_\parallel, \ \}$. The terms proportional to the boundary fields h_1 in Eq. (5.2) induce capillary BCs on the mean field [64].

Both the field and the particle are subject to a relaxational dynamics, ruled by the Langevin equations [29–31]

$$\dot{\mathbf{X}}(t) = \quad \gamma_x \nabla_{\mathbf{X}} \mathcal{H} + \sqrt{\gamma_x}\boldsymbol{\eta}(t), \tag{5.4a}$$

$$\dot{\phi}(\mathbf{x}, t) = \quad \gamma_\phi \Lambda \frac{\delta}{\delta\phi(\mathbf{x})}\left[\mathcal{H}_\phi[\phi] + \zeta\mathcal{H}_X(\phi(\mathbf{X}))\right] + \sqrt{\gamma_\phi}\xi(\mathbf{x}, t), \tag{5.4b}$$

where $\Lambda(\mathbf{x})$ is another self-adjoint differential operator, and the noise terms represent two independent Gaussian stochastic processes with zero average and variances

$$\left\langle \eta\ \ (t)\eta_\beta(t')\right\rangle = 2T_x\delta\ \ _\beta\delta(t \quad t'), \tag{5.5}$$

$$\langle \xi(\mathbf{x}, t)\xi(\mathbf{x}', t')\rangle = 2T_\phi\Lambda(\mathbf{x})\delta(\mathbf{x} \quad \mathbf{x}')\delta(t \quad t'). \tag{5.6}$$

The Fokker-Planck equation associated with Eq. (5.4) is given by [11]

$$\partial_t P = \int_V \mathrm{d}^d x\, \frac{\delta}{\delta\phi(\mathbf{x})}\left[\gamma_\phi\Lambda(\mathbf{x})\frac{\delta\mathcal{H}}{\delta\phi(\mathbf{x})} + T_\phi\gamma_\phi\Lambda(\mathbf{x})\frac{\delta}{\delta\phi(\mathbf{x})}\right] P + \gamma_x\nabla_{\mathbf{X}}\cdot(\nabla_{\mathbf{X}}\mathcal{H})\,P + T_x\gamma_x\nabla^2_{\mathbf{X}}P, \tag{5.7}$$

where we denoted for brevity $P \equiv P(\mathbf{X}, [\phi], t)$. Equation (5.4a) describes the dynamics of the particle under the influence of the field $\phi(\mathbf{X}, t)$. The parameter ζ in Eq. (5.4b) controls the back-reaction of the particle on the field: when $\zeta = 0$ the field dynamics is independent from that of the particle, which we will call "passive" (in the sense that the particle is passively carried by

the medium); for $\zeta = 1$, instead, the field is influenced by the tracer, called henceforth "reactive". In the first case ($\zeta = 0$), detailed balance is broken and the system is out of equilibrium for any choice of the temperatures T_x and T_ϕ; for all practical purposes, Eq. (5.4a) then describes an active particle driven by the (independent) stochastic process in Eq. (5.4b). Within the second scenario ($\zeta = 1$), on the other hand, setting $T_x = T_\phi \equiv T$ corresponds to a situation in which the particle and the field are in contact with the same thermal bath; the resulting steady-state probability distribution [which solves Eq. (5.7)] is then given by the Gibbs state

$$P_s(\mathbf{X}, [\phi]) = \frac{1}{\mathcal{Z}_0} \exp\left(\frac{1}{T} \mathcal{H}(\mathbf{X}, [\phi]) \right), \tag{5.8}$$

with $\mathcal{Z}_0 = \int_V \mathrm{d}^d X \int \mathcal{D}\phi \exp \quad \mathcal{H}(\mathbf{X}, [\phi])/T)$, and the functional measure $\mathcal{D}\phi$ is defined as

$$\int \mathcal{D}\phi \equiv \prod_n \int_\infty^\infty \mathrm{d}\phi_n \tag{5.9}$$

in terms of suitable field eigenmodes ϕ_n — see Section 5.2.1.

In the following, we will focus for simplicity on one spatial dimension, and we will be interested in the marginal dynamics of the tracer particle $\mathbf{X}(t)$ alone. Under the assumption of fast field relaxation (a notion we will make more precise in Section 5.2.5 below), we will write an approximate effective Fokker-Planck equation for the marginal probability distribution

$$\bar{P}(\mathbf{X}, t) \equiv \int \mathcal{D}\phi \, P(\mathbf{X}, [\phi], t), \tag{5.10}$$

which, due to global conservation of probability, fulfills $\int_V \mathrm{d}^d X \, \bar{P}(\mathbf{X}, t) = 1$. We choose for simplicity the initial joint probability distribution to be given by

$$P(\mathbf{X}, [\phi], t = t_0) = \delta(\mathbf{X} \quad \mathbf{X}_0) P_\phi(\mathbf{X}_0, [\phi]). \tag{5.11}$$

We assume the initial condition $\phi(\mathbf{x}, t = t_i) = 0$ to apply in the infinite past ($t_i = \quad \infty$), so that at $t = t_0 = 0$ the field has reached a steady state and its initial condition can be neglected. The initial condition for the particle is applied at $t = t_0 = 0$.

5.2 Preliminaries

5.2.1 Mode expansion of the field

Unless stated otherwise, we focus henceforth on a one-dimensional system with $\in [0, L]$. It is convenient to expand the field variable $\phi(x, t)$ in terms of a suitable eigenfunction basis. Assuming that the operators $\Delta(x)$ and $\Lambda(x)$ commute, we can find a set of common eigenfunctions σ_n satisfying the eigenvalue equations

$$\Delta\sigma_n \equiv \beta_n \sigma_n, \qquad \Lambda\sigma_n \equiv \frac{1}{T_\phi} L_n \sigma_n, \tag{5.12}$$

where n denotes the mode index [see Eq. (5.31) below for specific expressions]. We do not require that $\Delta(x)$, $\Lambda(x)$ commute with $\mathcal{K}_{1,2}(x)$; we thus define

$$u_n(\ ) \equiv \sqrt{c}\mathcal{K}_2\sigma_n(\ ), \qquad v_n(\ ) \equiv h\mathcal{K}_1\sigma_n(\ ), \tag{5.13}$$

where σ_n is not in general an eigenfunction of $\mathcal{K}_2$ or $\mathcal{K}_1$. We then introduce the following eigenfunction expansions of the order parameter and the noise fields:

$$\phi(\ ,t) = \sum_n \sigma_n(\ )\phi_n(t), \qquad \xi(\ ,t) = \sum_n \sigma_n(\ )\xi_n(t), \tag{5.14}$$

where the expansion coefficients are defined through the inverse relations

$$\phi_n(t) = \int_0^L \mathrm{d}\ \ \sigma_n^*(\ )\phi(\ ,t), \qquad \xi_n(t) = \int_0^L \mathrm{d}\ \ \sigma_n^*(\ )\xi(\ ,t). \tag{5.15}$$

The eigenfunctions $\sigma_n(\ )$ are taken to be orthonormal and to satisfy a completeness relation, i.e.,

$$\int_0^L \mathrm{d}\ \ \sigma_m^*(\ )\sigma_n(\ ) = \delta_{m,n}, \qquad \sum_n \sigma_n(\ )\sigma_n^*(\ ') = \delta(\qquad '). \tag{5.16}$$

Unless otherwise noted, we will consider in the following only real eigenfunctions σ_n (see also the discussion in Section 5.2.4).

5.2.2 Stationary distribution in the presence of detailed balance

Let us first introduce the notation

$$_{nm} \equiv \frac{\beta_n}{T_\phi}\delta_{nm} + \frac{1}{T_x}u_n(X)u_m(X), \tag{5.17}$$

$$\tau_n \equiv \frac{h_1}{T_\phi}[\sigma_n(0) + \sigma_n(L)] + \frac{\zeta}{T_x}v_n(X), \tag{5.18}$$

where β_n, u_n and v_n are defined as in Section 5.2.1. As we stressed above, the evolution equations (5.4) satisfy detailed balance in the reactive case ($\zeta = 1$) and provided that $T_x = T_\phi \equiv T$. In this case, the joint stationary distribution is the one given in Eq. (5.8), and it can be expressed in terms of the field modes as

$$P_s(X, \{\phi_n\}) = \frac{1}{\mathcal{Z}_0}\exp\left(\ \ \frac{1}{2}\sum_{nm}\phi_n\ \ _{nm}\phi_m + \sum_n \tau_n\phi_n\right). \tag{5.19}$$

The marginal stationary probability distribution of the particle at position X can be found by integrating out the field modes ϕ_n from the joint stationary distribution $P_s(X, \{\phi_n\})$ in Eq. (5.19). The latter is Gaussian in the ϕ_n's, so that a simple calculation renders (when $T_x = T_\phi \equiv T$)

$$P_s(X) \equiv \int \mathcal{D}\phi\, P_s(X, \{\phi_n\}) = \mathcal{N}\exp\left\{\ \ \frac{1}{T}[U(X) + W(X)]\right\}, \tag{5.20}$$

where $\mathcal{N}$ is a normalization constant, and where we introduced the effective potentials

$$U(X) \equiv \frac{T}{2}\ln(1+V(X)), \tag{5.21}$$

$$V(X) \equiv \sum_n \frac{u_n^2(X)}{\beta_n}, \tag{5.22}$$

$$W(X) \equiv \frac{T}{2}\tau_n \ {}^{1}_{nm}\tau_m, \tag{5.23}$$

stemming from the use of the matrix determinant lemma [169] — in partricular, $U(X)$ follows from the determinant of ${}_{nm}$ in Eq. (5.17). Note that $W(X)$ contains the effect of possible boundary fields $h_1 \neq 0$ through τ_n defined in Eq. (5.18), while the inverse matrix ^{1} can be explicitly computed by means of the Shermann-Morrison formula [169], yielding

$${}^{1}_{ij} = T\left\{\beta_i \ {}^{1}\delta_{ij} \quad \frac{u_i u_j}{\beta_i\beta_j[1+V(X)]}\right\}. \tag{5.24}$$

The effective potentials $V(X)$ and $W(X)$ are model-dependent, and they involve an infinite summation of terms containing the linear or quadratic coupling to the particle in their numerator (i.e., the functions $v_n(X)$ or $u_n(X)$, respectively), and the eigenvalue β_n of the field operator $\Delta(x)$ in their denominator. These sums can occasionally diverge, either because the denominator of the $n=0$ term is zero [called infrared (IR) divergence], or because the series does not converge to a finite result at large n [ultraviolet (UV) divergence]. IR divergences are typically related to the presence of zero modes in the field at criticality; we will see some examples of them in Section 5.4, and we will comment later on their meaning. In contrast, UV divergences are more subtle: they may either result in a flat stationary probability distribution (which is physically meaningful), or else prevent the said probability density function (PDF) from being normalized [64]. This second type of divergence generally indicates that the corresponding effective potential is *non-universal*, in the sense that it depends on other UV details that were not included in the original Hamiltonian. Indeed, these divergences are generally cured by including higher-order derivative terms in the field Hamiltonian $\mathcal{H}_\phi$ in Eq. (5.2), which in turn translates to the corresponding eigenvalue β_n being proportional to higher powers of the summation index n. In Section 5.4 we will exemplify the use of the adiabatic approximation procedure by applying it to models where the effective potentials in Eqs. (5.21) to (5.23) are not affected by UV divergences.

5.2.3 Some concrete examples

Many physical models fall within the class of Hamiltonians introduced in Eq. (5.2) when they are considered within their quadratic (Gaussian) approximation. The simplest is arguably the Landau-Ginzburg model endowed with model A/B dynamics [59], which we already considered in the previous Chapters, and which corresponds to the choice of operators [see Eq. (5.12)]

$$\Delta(\mathbf{x}) = \nabla^2_{\mathbf{X}} + r \quad \to \quad \beta_n = k_n^2 + r, \tag{5.25}$$

$$\Lambda(\mathbf{x}) = (\nabla^2_{\mathbf{X}})^{/2} \quad \to \quad L_n = T_\phi k_n. \tag{5.26}$$

As usual, the parameter can take the value = 0 (model A, dissipative dynamics) or = 2 (model B, conserved dynamics); the parameter r is linked to the correlation length ξ of the field by $r = \xi^{-2}$, so that for $r \to 0$ the system approaches a critical point characterized by the divergence of ξ (see also Section 1.3). For the sake of generality, we consider here again arbitrary dimension d and, accordingly, the squared wave number k_n^2 stands for $\sum_{i=1}^{d} k_{i,n}^2$ [see Eq. (5.31) below for expressions of $k_{,n}$ in the one-dimensional case].

Membranes are often described using the Helfrich Hamiltonian [21, 170–172], for which

$$\Delta(\mathbf{x}) = \kappa\nabla_{\mathbf{X}}^4 \quad \sigma\nabla_{\mathbf{X}}^2 \qquad \to \qquad \beta_n = \kappa k_n^2(k_n^2 + \tau), \tag{5.27}$$

where κ is the membrane bending modulus and σ its surface tension, and where we introduced $\tau = \sigma/\kappa$. Microemulsions (e.g., oil-water-surfactant mixtures) can instead be described in terms of the Gompper-Schick model [22, 23], where to the scalar order parameter $\phi(\mathbf{x}, t)$ one generically associates a free energy

$$\mathcal{F}[\phi] = f(\phi) + c_2(\nabla\phi)^2 + c_4(\nabla^2\phi)^2, \tag{5.28}$$

where $f(\phi)$ is a local polynomial in ϕ (typically of the 4th or 6th order). Choosing again model A/B dynamics leads to a 4th/6th order Allen-Cahn/Cahn-Hiliard evolution equation for the order parameter $\phi(\mathbf{x}, t)$, a problem that has been extensively covered in the mathematical literature [173–176]. When not specifically interested in studying phase coexistence, one can consider this model within the Gaussian approximation by truncating $f(\phi) \simeq \tau\phi^2$ to the quadratic order, again leading to

$$\Delta(\mathbf{x}) = c_4\nabla_{\mathbf{X}}^4 \quad c_2\nabla_{\mathbf{X}}^2 + \tau \qquad \to \qquad \beta_n = c_4 k_n^4 + c_2 k_n^2 + \tau. \tag{5.29}$$

In contrast to the Helfrich model, in the GS model the constant c_2 can take both positive or negative values: this can be used to describe the enhancement/reduction of the surface tension by the surfactant.

While the class of Hamiltonians in the form of Eq. (5.2) is broad, finding a simultaneous eigenbasis for the operators $\Lambda(\mathbf{x})$ and $\Delta(\mathbf{x})$ is not always straightforward (albeit unfortunately necessary in order to obtain closed-form results for the effective Fokker-Planck equation, as we will discuss later). For instance, the Helfrich Hamiltonian is often used in conjunction with a dynamics ruled by the Oseen hydrodynamic tensor [20, 172, 177]. In $d = 2$ and in Fourier space, the Oseen tensor takes the approximate form $\Lambda(\mathbf{q}) = 1/(4\eta|\mathbf{q}|)$, where η is the viscosity of the fluid surrounding the membrane [31, 178]. While in the bulk one can use plane waves $\exp(i\mathbf{q}\cdot\mathbf{x})$ to diagonalize $\Lambda(\mathbf{x})$ and $\Delta(\mathbf{x})$ simultaneously, in a confined geometry such as the one considered in this Chapter, the Fourier series coefficients of $\Lambda(\mathbf{q}) = 1/(4\eta|\mathbf{q}|)$ assume a cumbersome form which makes the calculation less practical. We will thus reserve the analysis of models involving the Oseen tensor for a future study.

Finally, a tracer particle can be coupled to the order parameter by means of the linear and/or quadratic terms contained in $\mathcal{H}_X$ in Eq. (5.2). Typical choices for the operators $\mathcal{K}_1$ and $\mathcal{K}_2$ are the identity , or else powers of $\nabla_{\mathbf{X}}$; we will sometimes denote the former case as *simple* linear or quadratic couplings, i.e.,

$$\mathcal{K}_1 = \quad , \quad \mathcal{K}_2 = \quad , \quad \mathcal{H}_X(\phi(\mathbf{X})) \equiv \frac{c}{2}\phi^2(\mathbf{X}) \quad h\phi(\mathbf{X}). \tag{5.30}$$

In the linear coupling case (e.g., $h\phi(\mathbf{X})$ or $h\nabla_{\mathbf{X}}\phi(\mathbf{X})$) and for $h > 0$, configurations are favored in which the field (or its derivative) are enhanced in the vicinity of the tracer particle. In the quadratic coupling case (e.g., $c\phi^2(\mathbf{X})$ or $c[\nabla_{\mathbf{X}}\phi(\mathbf{X})]^2$), on the contrary, the value of the field (or its derivative, respectively) are suppressed in the vicinity of the tracer particle; in the formal limit where $c \to \infty$, the coupling induces a point-like Dirichlet (or Neumann) boundary condition on ϕ in correspondence of the tracer's position $\mathbf{X}$ [28].

5.2.4 Choice of the eigenbasis

Local differential operators $\Lambda(\ )$, $\Delta(\ )$ like the ones listed above are diagonalized by the following eigenfunctions $\sigma_n(\ )$, which we specialize for the various BCs considered in Eq. (5.3):

$$\sigma_n^{(\mathrm{D})}(\ ) = \sqrt{\frac{2}{L}} \sin\left(k_n^{(\mathrm{D})}\ \right), \qquad k_n^{(\mathrm{D})} = \frac{\pi n}{L}, \qquad n = 1, 2, \ldots, \qquad \text{Dirichlet BCs,} \tag{5.31a}$$

$$\sigma_n^{(\mathrm{N})}(\ ) = \sqrt{\frac{2\ \ \delta_{n,0}}{L}} \cos\left(k_n^{(\mathrm{N})}\ \right), \qquad k_n^{(\mathrm{N})} = \frac{\pi n}{L}, \qquad n = 0, 1, 2, \ldots, \qquad \text{Neumann BCs.} \tag{5.31b}$$

Capillary BCs [see Eq. (5.3c)] can be imposed by choosing Neumann eigenfunctions, for which the averaged field profile can be shown to read [64]

$$\left\langle \phi(\ ) \right\rangle_{h_1} = h_1 L \left[\left(\frac{1}{2} \quad \frac{}{L} \right)^2 \quad \frac{1}{12} \right]. \tag{5.32}$$

We furthermore introduce, for future reference, the shorthand notation

$$\tilde{\sigma}_n(\ ) \equiv \frac{1}{k_n} \partial\ \sigma_n(\ ) = \begin{cases} \sqrt{\frac{2}{L}} \cos\left(k_n^{(\mathrm{D})}\ \right), & n = 1, 2, \ldots \qquad (\mathrm{D}) \\ \sqrt{\frac{2}{L}} \sin\left(k_n^{(\mathrm{N})}\ \right), & n = 1, 2, \ldots \qquad (\mathrm{N}) \end{cases} \tag{5.33}$$

and $\tilde{\sigma}_0^{(\mathrm{N})}(\ ) = 0$.

It must be noted that standard Dirichlet BCs generally entail a non-zero flux through the boundaries [179, 180], requiring to use suitable 'no-flux' basis functions in order to ensure global field conservation [181]. This is however technically rather involved, so in the following we will not consider conserved dynamics (model B) in conjunction with Dirichlet BCs. Moreover, in this Chapter we are mostly concerned with the effects of confinement on the dynamics of the tracer particle, and thus we will not focus explicitly on the case of periodic boundary conditions (PBCs), for which most of these effects have been found to trivialize [64]. However, the choice of eigenfunctions

$$\sigma_n^{(\mathrm{P})}(\ ) \equiv \begin{cases} \frac{1}{\sqrt{2}} \sigma_n^{(\mathrm{N})}(\ ), & n = 0,\ \ 1,\ \ 2, \ldots \\ \frac{1}{\sqrt{2}} \sigma_n^{(\mathrm{D})}(\ ), & n = 1, 2, 3, \ldots \end{cases} \tag{5.34}$$

formally corresponds to PBCs over the symmetric interval $\in [\ -L, L]$ (which is a convenient choice for later inspecting the *bulk* limit $L \to \infty$). These could be equivalently addressed by

adopting complex eigenfunctions $\sigma_n^{(\mathrm{p})}(\ ) = \frac{1}{\sqrt{2L}} \exp\left(\mathrm{i} k_n^{(\mathrm{p})}\ \right)$, $k_n^{(\mathrm{p})} = \pi n/L$, but then the Fokker-Planck-based method we present in Section 5.3 would require considering the joint probability distribution $\mathcal{P}(\ _R,\ _I, t)$ [or equivalently $\mathcal{P}(\ , \bar{\ }, t)$, with $\bar{\ } \equiv\ ^*$] for any complex dynamical variable $\ = \ _R + i\ _I$. While this is technically straightforward, the number of dynamical operators would double in our entire derivation. In order to limit the proliferation of terms and for the sake of clarity, we will assume in the following that the eigenfunctions σ_n are chosen real.

5.2.5 Dynamics

Let us rescale time as $t \to t/\gamma_x$ in the Langevin equations (5.4), and define appropriately rescaled fields [64]; this is equivalent to setting $\gamma_x \equiv 1$ in Eq. (5.4a) and replacing $\gamma_\phi \to \chi^{\ 1}$ in Eq. (5.4b), where we introduced the "adiabaticity" parameter

$$\chi \equiv \gamma_x/\gamma_\phi. \tag{5.35}$$

A dimensionless counterpart of χ in Eq. (5.35) can be introduced as follows:

$$\tilde{\chi} \equiv T_x L^{\ d_\Lambda} \chi, \tag{5.36}$$

where we denoted by $d_\Lambda \equiv [\Lambda(x)]$ the length dimension of the dynamical operator $\Lambda(x)$ introduced in Eq. (5.4b), and we have furthermore chosen T_x in order to account for the temperature dimension of χ. In the *adiabatic limit* $\tilde{\chi} \ll 1$, the field dynamics is much faster than the tracer dynamics.

The coupled Langevin equations (5.4a) and (5.4b) can now be rewritten in terms of the eigenfunctions σ_n as

$$\partial_t X = \ \sum_{nm} A_{nm}\phi_n\phi_m + \sum_n t_n\phi_n + \eta, \tag{5.37}$$

$$\partial_t \phi_n = \ \chi^{\ 1}\left[\sum_m B_{nm}\phi_m \quad s_n\right] + \chi^{\ 1/2}\xi_n. \tag{5.38}$$

Above we have introduced the vectors

$$t_n \equiv \partial_X v_n(X), \qquad s_n \equiv L_n\tau_n, \tag{5.39}$$

and the matrices

$$A_{ij} \equiv \frac{T_x}{2}\partial_X\ _{ij} \equiv \frac{1}{2}\partial_X(u_iu_j), \qquad B_{ij} \equiv b_i\delta_{ij} + c_{ij}, \tag{5.40}$$

where we denoted

$$b_i \equiv L_i\beta_i/T_\phi, \qquad c_{ij} \equiv \zeta L_i u_i u_j/T_x, \tag{5.41}$$

with β_i, L_i, $_{ij}$ and τ_n defined in Eqs. (5.12), (5.17) and (5.18), respectively (see Section 5.2.3 for specialization to the various models). The noise variances in Eq. (5.6) can also be expressed in terms of its expansion coefficients $\xi_n(t)$ as

$$\langle \xi_m(t)\xi_n(t')\rangle = 2L_n\delta_{mn}\delta(t \quad t'). \tag{5.42}$$

Equations (5.38) and (5.37) correspond to the following Fokker-Planck equation for the joint probability distribution $P(X, \{\phi_n\}, t)$:

$$\partial_t P = \partial_X \left[\sum_{mn} A_{nm}\phi_n\phi_m \quad \sum_n t_n\phi_n \right] P + T_x \partial_X^2 P$$
$$+ \chi^{-1} \sum_n \partial_{\phi_n} \left[\sum_m B_{nm}\phi_m \quad s_n \right] P + \chi^{-1} \sum_n L_n \partial_{\phi_n}^2 P. \tag{5.43}$$

Finally, in the reactive case ($\zeta = 1$) it follows from Eqs. (5.17) and (5.18) that ($L_{ij} \equiv L_i\delta_{ij}$)

$$B_{ij} = (L \circ \quad)_{ij}, \qquad t_n = T_x \partial_X \tau_n. \tag{5.44}$$

5.3 An adiabatic elimination method

In this Section we describe how the field coordinates ϕ_n can be eliminated from Eq. (5.43), thus yielding a Fokker-Planck equation which governs the dynamics of $X(t)$ alone, under the assumption that the field equilibrates faster than the particle. To this end, we define the following moments of $P(X, \{\phi_i\})$:

$$Q^{(0)}(X,t) = \int \mathcal{D}\phi\, P(X, \{\phi_i\}), \tag{5.45a}$$
$$Q_n^{(1)}(X,t) = \int \mathcal{D}\phi\, \phi_n(t) P(X, \{\phi_i\}), \tag{5.45b}$$
$$Q_{nm}^{(2)}(X,t) = \int \mathcal{D}\phi\, \phi_n(t)\phi_m(t) P(X, \{\phi_i\}), \tag{5.45c}$$
$$Q_{nmp}^{(3)}(X,t) = \dots, \tag{5.45d}$$

where $\int \mathcal{D}\phi$ indicates a multidimensional integral over the modes of ϕ [see Eq. (5.9)]. Note that $Q^{(0)}(X,t) = \bar{P}(X,t)$ [see Eq. (5.10)] is the time-dependent marginal probability distribution of the particle position, whose dynamics we are interested in. Integrating Eq. (5.43) over a mode ϕ_n as in Eq. (5.45) provides a hierarchy of equations for the evolution of these moments:

$$\partial_t Q^{(0)} = \partial_X \sum_{nm} A_{nm} Q_{nm}^{(2)} \quad \partial_X \sum_n t_n Q_n^{(1)} + T_x \partial_X^2 Q^{(0)}, \tag{5.46a}$$
$$\partial_t Q_n^{(1)} = \partial_X \sum_{ij} A_{ij} Q_{ijn}^{(3)} \quad \partial_X \sum_m t_m Q_{nm}^{(2)} + T_x \partial_X^2 Q_n^{(1)} \quad \chi^{-1} \left[\sum_m B_{nm} Q_m^{(1)} \quad s_n Q^{(0)} \right], \tag{5.46b}$$
$$\partial_t Q_{nm}^{(2)} = \partial_X \sum_{ij} A_{ij} Q_{ijnm}^{(4)} \quad \partial_X \sum_i t_i Q_{inm}^{(3)} + T_x \partial_X^2 Q_{nm}^{(2)} \tag{5.46c}$$
$$\chi^{-1} \sum_j \left[B_{nj} Q_{jm}^{(2)} + B_{mj} Q_{jn}^{(2)} \right] + \chi^{-1} \left[s_n Q_m^{(1)} + s_m Q_n^{(1)} \right] + 2\chi^{-1} L_n \delta_{nm} Q^{(0)},$$

and so on. By working in the adiabatic limit $\chi \ll 1$, we can formally expand the moments in powers of small χ:

$$Q_{nm\dots}^{(j)} = q_{nm\dots}^{(j)} + \chi \tilde{q}_{nm\dots}^{(j)} + \mathcal{O}(\chi^2). \tag{5.47}$$

The hierarchy of equations (5.46) can be closed by replacing the moments $Q^{(j)}_{nm\dots}$ by their expansion in Eq. (5.47), and then neglecting terms of $O(\chi^2)$ or higher. In the next Sections we will thus solve Eqs. (5.46b) and (5.46c), and plug the result back into Eq. (5.46a) in order to obtain an evolution equation for the marginal probability distribution $Q^{(0)}(X,t)$, i.e.,

$$\partial_t Q^{(0)} = \quad \partial_X[\mu(X)Q^{(0)}(X)] + \partial_X^2[D(X)Q^{(0)}(X)] + O(\chi^2), \tag{5.48}$$

where $\mu(X)$ and $D(X)$ represent the space-dependent effective drift and diffusion coefficients, respectively. In the following, we will consider separately the case of a reactive ($\zeta = 1$) and passive ($\zeta = 0$) tracer particle.

5.3.1 Reactive case

The lowest order in the adiabatic approximation is obtained by truncating the expansion in Eq. (5.47) to its leading order ($\chi = 0$); equivalently, we formally take the limit $\gamma_\phi \to \infty$ of the mobility of the field [see Eq. (5.35)]. The physical meaning of this is that the field instantaneously rearranges around the position $X(t)$ assumed at each time t by the particle — this is reminiscent of the Born-Oppenheimer approximation in condensed matter physics [182]. In the reactive case, setting $T_\phi = T_x = T$ implies that the steady-state probability distribution is given by $P_s(X,\{\phi_i\})$ in Eq. (5.19), because of detailed balance: accordingly, we can write

$$P(X,\{\phi_i\},t) = P_s(X(t),\{\phi_i\}) + O(\chi). \tag{5.49}$$

We thus deduce that we can obtain the lowest order terms $q^{(j)}_{nm\dots}$ in the expansion of $Q^{(j)}_{nm\dots}$ in Eq. (5.47) by taking the Gaussian expectation values

$$q^{(j)}_{nm\dots} = \int \mathcal{D}\phi\, \phi_n\phi_m \dots P_s(X(t),\{\phi_i\}) \equiv \left\langle \phi_n\phi_m\dots \right\rangle. \tag{5.50}$$

These are easily obtained by first constructing the generating functional [64]

$$\mathcal{Z}[\{J\}] = \int \mathcal{D}\phi\, P_s(X(t),\{\phi\}) \exp\left[\sum_n (J_n+\tau_n)\phi_n\right] = \mathcal{Z}[0]\exp\left[\frac{1}{2}\sum_{nm} J_n\ {}^{1}_{nm}J_m + \sum_{nm} J_n\ {}^{1}_{nm}\tau_m\right], \tag{5.51}$$

where $J(\ ) = \sum_n \sigma_n(\ )J_n$ is an auxiliary field, while ${}_{nm}$ and τ_n are defined in Eqs. (5.17) and (5.18), respectively. Note that $\mathcal{Z}[0] = P_s(X)$, i.e., the marginal stationary distribution given in Eq. (5.20). By using Wick's theorem, one can obtain the joint cumulants

$$\begin{aligned}
&Q^{(0)} = \mathcal{Z}[0], \qquad q^{(1)}_i = \mathcal{Z}[0]\ {}^{1}_{ij}\tau_j \equiv \mathcal{Z}[0]\langle i\rangle, \\
&q^{(2)}_{ij} = \mathcal{Z}[0]\left({}^{1}_{ij} + {}^{1}_{im}\ {}^{1}_{jn}\tau_m\tau_n\right) \equiv \mathcal{Z}[0]\langle ij\rangle \equiv \mathcal{Z}[0]\left[\langle ij\rangle_c + \langle i\rangle\langle j\rangle\right], \\
&q^{(3)}_{ijk} \equiv \mathcal{Z}[0]\langle ijk\rangle = \mathcal{Z}[0]\left[\langle i\rangle\langle j\rangle\langle k\rangle + \langle ij\rangle_c\langle k\rangle + (2\text{ perm.})\right], \\
&q^{(4)}_{ijkl} \equiv \mathcal{Z}[0]\langle ijkl\rangle = \mathcal{Z}[0]\left[\langle i\rangle\langle j\rangle\langle k\rangle\langle l\rangle + \langle ij\rangle_c\langle kl\rangle_c + (2\text{ perm.}) + \langle ij\rangle_c\langle k\rangle\langle l\rangle + (5\text{ perm.})\right],
\end{aligned} \tag{5.52}$$

where we have introduced the shorthand notation $\langle ij \rangle_c \equiv \ {}^1_{ij}$ and $\langle i \rangle \equiv \ {}^1_{ij}\tau_j$. In this notation, the Langevin equation (5.46a) reads at lowest order

$$\partial_t Q^{(0)} = \partial_X \left[U'(X) + W'(X) \right] Q^{(0)} + T \partial_X^2 Q^{(0)} + \mathcal{O}(\chi), \tag{5.53}$$

where the prime denotes a derivative with respect to X. Note that setting $\partial_t Q^{(0)} \equiv 0$ promptly yields the correct marginal stationary distribution given in Eq. (5.20). We will call the one in Eq. (5.53) the *super-adiabatic* approximation for the effective dynamics of the particle. Comparing Eq. (5.53) with Eq. (5.48) shows that, at the lowest order in the adiabatic approximation, the diffusion term is not modified, i.e., $D(X) = T$, while the drift term $\mu(X) = \ [U'(X) + W'(X)]$ is the one intuitively expected for a particle moving in the field-induced effective stationary potential given in Eq. (5.20). Although the latter seems to diverge for large c (see Eqs. (5.13), (5.21) and (5.22)), in fact its derivative does not, leading in the purely quadratic case ($h = h_1 = 0$) to an effective drift term

$$\mu(X) \underset{c \to \infty}{\to} \frac{T V'(X)}{2V(X)}, \tag{5.54}$$

with $V(X)$ given in Eq. (5.22).

We remark that it is possible to obtain Eq. (5.53) without resorting to the *quasi-static* assumption we made in Eq. (5.49), but instead by directly solving a Lyapunov matrix equation (see Appendix E.1). However, the latter route turns out to be computationally challenging when one tries to move beyond the $\mathcal{O}(\chi^0)$ result.

The $\mathcal{O}(\chi)$ correction in Eq. (5.53) is obtained by computing $\tilde{q}^{(1)}$ and $\tilde{q}^{(2)}$ from Eq. (5.46). Using Eq. (5.40) and the matrix relation [169, 183]

$$\partial_X \mathcal{M}^{\ 1}(X) = \ \mathcal{M}^{\ 1} \circ \partial_X \mathcal{M} \circ \mathcal{M}^{\ 1} \qquad \to \qquad \partial_X \ {}^1 = \ \frac{2}{T} \ {}^1 \circ A \circ \ {}^1, \tag{5.55}$$

a long but straightforward calculation renders

$$B_{nm} \tilde{q}^{(1)}_m = \left(\partial_X \langle n \rangle \right) \left[(U' + W') Q^{(0)} + T \partial_X Q^{(0)} \right], \tag{5.56a}$$

$$B_{nj} \tilde{q}^{(2)}_{jm} + B_{mj} \tilde{q}^{(2)}_{jn} = s_n \tilde{q}^{(1)}_m + s_m \tilde{q}^{(1)}_n + \left(\partial_X \langle nm \rangle \right) \left[(U' + W') Q^{(0)} + T \partial_X Q^{(0)} \right]. \tag{5.56b}$$

The terms $\tilde{q}^{(1)}$ and $\tilde{q}^{(2)}$ in general provide corrections both to the drift $\mu(X)$ and to the diffusion coefficient $D(X)$ in Eq. (5.48). Note that these contributions vanish when using for $Q^{(0)}$ the stationary distribution in Eq. (5.19), thus guaranteeing that the effective Fokker-Planck equation will still satisfy detailed balance.

In the next subsections we will solve Eqs. (5.56a) and (5.56b) in the cases where either a linear or a quadratic coupling to the particle are included in the Hamiltonian in Eq. (5.2). The most general case in which both couplings are included is reported in Ref. [65] — see Section 4.1.3 and Appendix B therein. The consistency of our results with those obtained in the bulk limit $L \to \infty$ in Refs. [29–31] will finally be explored in Appendix E.3.

5.3.1.1 Linear coupling

In this case, we set $c = 0$: this simplifies the calculation significantly, because then the matrices $B_{nm} = b_n \delta_{nm} = \delta_{nm} L_n \beta_n / T$ and $\ {}_{ij} = \beta_i / T \delta_{ij}$ are diagonal. Moreover, the matrix $A_{ij} = 0$, and

the quadratic part of the effective potential vanishes, i.e., $U(X) = 0$. From Eq. (5.46a) we see that $\tilde{q}^{(2)}_{nm}$ is actually not needed, and we just have to solve Eq. (5.56a) for

$$\tilde{q}^{(1)}_n = b_n{}^1 \left(\partial_X \langle n \rangle\right) \left[W' Q^{(0)} + T \partial_X Q^{(0)}\right], \tag{5.57}$$

and plug this back into Eq. (5.46a), together with $q^{(1)}_n$ given in Eq. (5.52). This yields an effective Fokker-Planck equation for the tracer particle in the form of Eq. (5.48), with the drift and diffusion coefficients given by

$$\mu(X) = \mu_0(X) + D'(X), \qquad \mu_0(X) = \quad [1 \quad \chi T M(X)]\, W'(X), \qquad D(X) = T \quad \chi T M(X), \tag{5.58}$$

where [see Eqs. (5.13) and (5.39) for the definitions of v_n, t_n, and s_n, respectively]

$$M(X) \equiv \frac{t_n}{b_n} \left(\partial_X \langle n \rangle\right) = \sum_n \frac{t_n^2}{\beta_n b_n} = T \sum_n \frac{[\partial_X v_n(X)]^2}{\beta_n^2 L_n}. \tag{5.59}$$

We note that the latter generalizes the quantity $m(X)$ defined in Ref. [64] for the particular case in which $\mathcal{K} =$, and the field Hamiltonian is of the Landau-Ginzburg type (see Section 5.4.1). The steady-state distribution of the resulting Fokker-Planck equation is by construction the one given in Eq. (5.20) — see the discussion after Eq. (5.56). Finally, in the absence of quadratic couplings, the effective potential in Eq. (5.23) reduces to

$$W(X) = \quad \frac{1}{2} \sum_n \frac{v_n^2(X)}{\beta_n} \quad h_1 \sum_n \frac{v_n(X)}{\beta_n} [\sigma_n(0) + \sigma_n(L)] + \text{const.}. \tag{5.60}$$

It is useful to note that $v_n \sim O(h)$, hence $M(X)$ and $W(X)$ are of $O(h^2)$.

5.3.1.2 Quadratic coupling

In this case the linear couplings (including boundary fields) are set equal to zero, $h = h_1 = 0$, so that also $s_n = t_n = 0$, and the linear part of the effective potential vanishes, i.e., $W(X) = 0$. In turn, this implies that the one-point cumulants $\langle n \rangle$ in Eq. (5.52) vanish as well. Starting from Eq. (5.56b), we denote the quantity on its r.h.s. as

$$\Omega_{nm} \equiv \left(\partial_X \langle nm \rangle\right) \left[U' Q^{(0)} + T \partial_X Q^{(0)}\right], \tag{5.61}$$

and thus rewrite

$$B_{nj} \tilde{q}^{(2)}_{jm} + B_{mj} \tilde{q}^{(2)}_{jn} = \Omega_{nm}. \tag{5.62}$$

The latter is a Lyapunov matrix equation (see also Appendix E.1), which, despite the fact that B_{ij}, Ω_{ij} and $\tilde{q}^{(2)}_{ij}$ are symmetric matrices, does not admit a straightforward analytic solution because in general $B\Omega \neq \Omega B$. Using the definition of B_{ij} in Eq. (5.40), we can however rephrase Eq. (5.62) as (no sum over n, m is intended)

$$(b_n + b_m) \tilde{q}^{(2)}_{nm} = \Omega_{nm} \quad c_{nk} \tilde{q}^{(2)}_{km} \quad c_{mk} \tilde{q}^{(2)}_{nk}, \tag{5.63}$$

which can be taken as a starting point for a recursive solution in orders of c, noting that $c_{ij} \sim O(c)$. Equation (5.63) resembles a Dyson sum, but it does not admit a straightforward exact resummation; however, its "bare" solution

$$\tilde{q}^{(2)}_{nm} \simeq \frac{\Omega_{nm}}{b_n + b_m} + O(c^2) \tag{5.64}$$

can already be adopted as a small-c approximation, which retains by construction the property of vanishing at equilibrium (i.e., in correspondence of the stationary distribution in Eq. (5.20)). Note that the correction in Eq. (5.64) is at least of $O(c^2)$, because Ω_{nm} itself contains contributions at least of $O(c)$ — see Eq. (5.61). Note also that c is a dimensionful quantity, so that the small-c regime is in fact defined by the smallness of a suitable dimensionless counterpart of the coupling parameter. The particular expression of this parameter is model-dependent — see, e.g., Eqs. (5.83) and (5.90) for the case of the Landau-Ginzburg and the Gompper-Schick models, respectively.

Inserting the approximate result reported in Eq. (5.64) into the evolution equation (5.46a), together with $q^{(2)}_{nm}$ found in Eq. (5.52), yields the effective Fokker-Planck equation

$$\begin{aligned}\partial_t Q^{(0)} &= \partial_X \left[Q^{(0)} \partial_X U + T \partial_X Q^{(0)} \right] + O(c^2) \\ &\chi T \partial_X \left[\frac{2}{1+V} \sum_{nm} \frac{A^2_{nm}}{(b_n + b_m)\beta_n \beta_m} + \left(\frac{1}{1+V} \right)' \sum_{nm} \frac{A_{nm} u_n u_m}{(b_n + b_m)\beta_n \beta_m} \right] \left[Q^{(0)} \partial_X U + T \partial_X Q^{(0)} \right].\end{aligned} \tag{5.65}$$

We can bring it to the form of Eq. (5.48) upon defining the drift and diffusion coefficients

$$\mu(X) = \mu_0(X) + D'(X), \qquad \mu_0(X) = \quad [1 \quad \chi T M_2(X)]\, U'(X), \qquad D(X) = T \quad \chi T M_2(X), \tag{5.66}$$

where we have introduced

$$M_2(X) \equiv T \left[\frac{2}{1+V} \sum_{nm} \frac{A^2_{nm}}{(b_n + b_m)\beta_n \beta_m} + \left(\frac{1}{1+V} \right)' \sum_{nm} \frac{A_{nm} u_n u_m}{(b_n + b_m)\beta_n \beta_m} \right]. \tag{5.67}$$

We recall that the expressions for A_{nm} and b_n are provided in Eqs. (5.40) and (5.41), those for β_n and L_n can be found in Section 5.2.3, while the potentials $U(X)$ and $V(X)$ are defined in Eqs. (5.21) and (5.22). At steady state, the associated Fokker-Planck equation is solved by P_s given in Eq. (5.20) [again by construction, see the discussion after Eq. (5.56)].

5.3.2 Passive case

Here we consider the situation in which the parameter $\zeta = 0$ in Eq. (5.4). In this case the interaction between the field and the particle is non-reciprocal: the field influences the particle, but not vice-versa. As explained in Section 5.1, this models a specific kind of "active" particle driven by the stochastic process in Eq. (5.4b), which can be correlated and induce non-trivial dynamics and steady states for the tracer. In this Section we disregard the possibility of adding boundary fields ($h_1 = 0$), which would be of limited physical significance; the relevant expressions for the evolution of the moments are then obtained by setting $s_n \equiv 0$ and $B_{nm} = b_n \delta_{nm} = \delta_{nm} L_n \beta_n / T_\phi$ in the coupled equations (5.46).

In the following we will consider the linear and the quadratic coupling cases separately. The comparison with previous results obtained in Refs. [29–31] in the absence of confinement will be commented on in Section 5.3.2.3, and further detailed in Appendix E.3.

5.3.2.1 Linear coupling

In this case we also have $A_{ij} = 0$. Grouping terms according to their order in χ in Eqs. (5.46b) and (5.46c) leads to

$$q^{(2)}_{nm} = \frac{T_\phi}{\beta_n}\delta_{nm}Q^{(0)}, \qquad q^{(1)}_n = 0, \qquad \tilde{q}^{(1)}_n = \frac{1}{b_n}\partial_X t_m q^{(2)}_{nm} = \frac{T_\phi^2}{\beta_n^2 L_n}\partial_X t_n Q^{(0)}, \tag{5.68}$$

where in the last result we used Eq. (5.46a). Inserting Eq. (5.68) back into Eq. (5.46a) then renders the effective Fokker-Planck equation for the reduced tracer distribution $Q^{(0)}$. This equation takes the same form as in Eq. (5.48), but with drift and diffusion coefficients given by

$$\mu(X) = \frac{1}{2}D'(X), \qquad D(X) = T_x + \chi T_\phi M(X), \tag{5.69}$$

and with $M(X)$ defined as in Eq. (5.59), upon replacing T with T_ϕ. Explicit expressions of the function $M(X)$ for some selected models are provided in Section 5.4 — see Eqs. (5.86), (5.95) and (E.33). Note that the correction to the diffusion coefficient $D(X)$ here has the opposite sign with respect to the one in the reactive case, see Eq. (5.58). One can easily check that the corresponding stationary distribution reads

$$P_{\rm s}(X) \propto D(X)^{\ 1/2}. \tag{5.70}$$

It is instructive to compare our results also to Refs. [29, 30], where a tracer particle linearly coupled to a fluctuating field has been analyzed in the *bulk*. While a quantitative comparison requires specialization of the above results to periodic BCs and performing the bulk limit (see Section 5.2.4 and the discussion in Appendix E.3), we focus here on the sign of the correction term $M(X)$ to $D(X)$ [see Eq. (5.69)]. In qualitative agreement with previous studies [see Eq. (E.15)], we find here that the effective diffusivity is generally reduced (enhanced) for a reactive (passive) tracer [see Eqs. (5.58), (5.59) and (5.69)]. Notably, it has been shown in Refs. [29, 30] that the diffusivity of a passive tracer coupled to a slowly relaxing field can even decrease below its bare value, an effect which is not captured within the adiabatic approximation.

5.3.2.2 Quadratic coupling

We leave the details of the calculation to Appendix E.2, and only report here the final effective Fokker-Planck equation, valid to $O(\chi c^2)$ (see below):

$$\partial_t Q^{(0)} = \frac{T_\phi}{2}\partial_X V'(X) Q^{(0)} + \partial_X^2\left[T_x + 2\chi T_\phi^2 \sum_{nm}\frac{A_{nm}^2}{(b_n+b_m)\beta_n\beta_m}\right]Q^{(0)} + \text{h.o.}\,. \tag{5.71}$$

We recall that A_{nm} and b_n are reported in Eqs. (5.40) and (5.41), while expressions for β_n and L_n for the various models can be found in Section 5.2.3. The potential $V(X)$ was defined in

Eq. (5.22), and explicit expressions for some selected models are reported in Section 5.4 below [see Eqs. (5.81), (5.82) and (5.89)]. We recognize

$$\mu(X) = \frac{T_\phi}{2} V'(X), \qquad D(X) = T_x + \chi T_\phi M_4(X), \tag{5.72}$$

with

$$M_4(X) = 2T_\phi \sum_{nm} \frac{A_{nm}^2}{(b_n + b_m)\beta_n \beta_m}, \tag{5.73}$$

while the corresponding stationary distribution is formally given by

$$P_s(X) \propto \frac{1}{D(X)} \exp\left[\int_0^X \mathrm{d}x \, \frac{\mu(x)}{D(x)}\right] \equiv e^{\ U_{\text{eff}}(X)/T_x}, \tag{5.74}$$

where we introduced the effective potential

$$U_{\text{eff}}(X) \equiv T_x \int_0^X \mathrm{d}x \, \frac{\mu(x)}{D(x)} + T_x \log D(X). \tag{5.75}$$

5.3.2.3 Discussion

First of all, we note that the correction to the diffusion coefficient $D(X)$ in Eq. (5.72) involves a (double) sum of positive terms, meaning that at $O(\chi)$ the diffusivity is enhanced due to the coupling with the (adiabatic) field. We remark that, in the bulk limit $L \to \infty$, we expect that $V(X) = \text{const.}$ by translational invariance: from Eqs. (5.66) and (5.67), this implies that $D(X)$ is then *reduced* in the reactive case. This qualitatively agrees with the findings in Ref. [31] — see Eq. (E.18), while in the rest of Appendix E.3 we show that their agreement is also quantitative. Similarly to the linear case, one expects that, for a very slowly evolving field (non-adiabatic regime), the bulk diffusivity of a passive tracer can even fall below its bare value [31].

Direct inspection of $V(X)$ for the case of the Landau-Ginzburg model with a simple quadratic coupling (see Section 5.4.1.1) shows that actually $V(X) \to 0$ for $L \to \infty$, meaning that the correction to the diffusion coefficient in the reactive case [see Eqs. (5.66) and (5.67)] becomes equal in modulus (but opposite in sign) to that of the passive case, Eq. (5.72). The correct limiting procedure involves taking the limit $L \to \infty$ by keeping ξ finite, which is why $V(X)$ presents instead a IR divergence for $L \to \infty$ in the critical models analyzed, e.g., in Section 5.4.2 and in Ref. [64]. At criticality ($\xi = \infty$), the adiabatic approximation breaks down as $L \to \infty$ because the field becomes infinitely slow [64, 81].

Secondly we note that, in contrast to the procedure of Section 5.3.1.2, in the passive case there was no need to expand for small c in order to obtain Eq. (5.71) (see Appendix E.2); indeed, in the passive problem the field is agnostic to the value of c, since the latter merely sets the strength of the influence of the field on the dynamics of the particle. However, Eq. (5.71) does not admit a significant limit for large c, the drift term being $\propto c$ and the diffusion coefficient $\propto c^2$. This suggests that the *effective* adiabaticity parameter in Eq. (5.71) is in fact proportional to χc^2, i.e., it involves both χ and the coupling constant c. Physically, by increasing c in the Langevin equation (5.4a) for $X(t)$, one is actually speeding up the stochastic evolution of the tracer. In contrast,

since the coupling constant c does not enter the Langevin equation (5.4b) for the field ϕ in the passive case, the relaxation timescale of the latter remains the same. Accordingly, increasing c eventually violates the assumption underlying the adiabatic approximation, namely that the field relaxes faster than the tracer particle; we must thus require c to remain sufficiently small within the adiabatic approach.

A third remark is that, in the adiabatic regime, Eq. (5.71) retains the form of a Fokker-Planck equation even though the stochastic process $\propto \phi^2(X)$ that drives $X(t)$ is non-Gaussian. Intuitively, this can be understood by considering the motion of the tracer along discrete time steps of length Δt (which is assumed to be smaller than the tracer relaxation time). Since the field relaxation time can be made arbitrarily small in the adiabatic limit, the tracer will pick up a set of uncorrelated random noises $\propto \phi^2$ during its motion over several time steps. According to the central limit theorem, the sum of these noises assumes a Gaussian character. Thus, this model is such that non-Markovian effects only appear at higher orders in the adiabaticity parameter χ (in contrast to other — even simpler — models featuring the square of a Gaussian process [184, 185]).

Next, in the case in which the coupling operator $\mathcal{K}_2$ in Eq. (5.2) is chosen to be the identity, the effective Fokker-Planck equation (5.71) can be compared to Eq. (4.31) in Ref. [64]. The latter was obtained within a small-c expansion and following the standard Gardiner/Stratonovich adiabatic elimination method [11, 165]. These methods generally assume (as we did in Section 5.3.1) that the fast variable relaxes to its equilibrium configuration around the slow variable, and then construct a perturbation series for small χ around this reference state. Note that no assumption in this sense has been invoked along the derivation of Eq. (5.71) outlined above. It turns out that the drift coefficient $\mu(X)$ in Eq. (4.32a) of Ref. [64] differs from Eq. (5.72) by a spurious drift term (compatible with a Stratonovich interpretation of the noise). However, including this term would render a steady-state particle distribution $P_s(X)$ which coincides, up to $O(c)$, with the stationary distribution in the presence of detailed balance given in Eq. (5.20) [see Eq. (4.33) in Ref. [64]] — this is not the correct stationary distribution, which is given instead by Eq. (5.74).

Following Ref. [64] we eventually note that, upon defining from Eq. (5.37) an effective field-induced noise (see Appendix E.4)

$$\Pi_c(X,t) \equiv \sum_{nm} A_{nm}(X)\phi_n(t)\phi_m(t), \tag{5.76}$$

the effective diffusion coefficient $D(X)$ reported in Eq. (5.72) can be expressed as a Green-Kubo relation:

$$D(X) = T_x + \int_{\infty}^{\infty} \mathrm{d}t\, \langle \Pi_c(X,t)\Pi_c(X,0)\rangle\,, \tag{5.77}$$

where the average is intended over the stochastic noises in Eq. (5.4). Moreover, by using the definition of A_{nm} in Eq. (5.40), we can rewrite

$$\Pi_c(\ ,t) \equiv \frac{c}{2}\partial\ [\mathcal{K}_2\phi(\ ,t)]^2, \tag{5.78}$$

which simplifies to $\Pi_c(\ ,t) \equiv \frac{c}{2}\partial\ \phi^2(\ ,t)$ in the case where $\mathcal{K}_2 =$ [64].

5.4 Application to specific models

Here we apply the adiabatic elimination method developed in the previous Sections to the Landau-Ginzburg (LG) and the Gompper-Schick (GS) models, which have been introduced in Section 5.2.3. In each of the cases considered below, we will discuss the stationary distribution $P_s(X)$ and the reduced diffusion coefficient

$$D_r(X) \equiv \frac{D(X) \quad D_0}{\chi D_0}, \tag{5.79}$$

where $D_0 = T_x$ denotes the bare diffusion coefficient [which is of $O(\chi^0)$]. Where possible, we provide analytic expressions for the reduced diffusivity or, correspondingly, for the functions $M_{1\ 4}(X)$, which are directly related to $D_r(X)$ via Eqs. (5.58), (5.66), (5.69) and (5.72). In the plots we will mostly set $T_x = 1$ and focus on the case $T_\phi = T_x$.

5.4.1 Landau-Ginzburg model

Turning first to the LG Hamiltonian, we consider in the following both dissipative (model A) and conserved (model B) field dynamics in the presence of simple linear and quadratic couplings (i.e., $\mathcal{K}_1 = \mathcal{K}_2 =$). Since many results for this model at the critical point (i.e., $r = 0$) have been reported in Ref. [64], we will focus here on the case $r \neq 0$, for which the field acquires a finite correlation length $\xi = 1/\sqrt{r}$.

5.4.1.1 Quadratic coupling

The choice of a simple (non-derivative) coupling $\propto \phi^2(X)$ gives $u_n = \sqrt{c}\sigma_n$ [see Eq. (5.13)]. The potential $V(X)$ introduced in Eq. (5.22) characterizes most static and dynamical properties in the quadratic case [see Sections 5.3.1.2 and 5.3.2.2]; here it becomes

$$V(X) = c \sum_n \frac{\sigma_n^2(X)}{\beta_n}, \tag{5.80}$$

where one can recognize $V(X) = \frac{c}{T} C_\phi(X, X)$ in terms of the field correlator [see Eq. (3.20) in [64]]. This quantity can in fact be computed even off-criticality, as detailed in Appendix E.5: for Dirichlet BCs, we find

$$V(X) = c\xi\, \mathrm{csch}(L/\xi) \sinh(X/\xi) \sinh\left(\frac{L \quad X}{\xi}\right). \tag{5.81}$$

For $\xi \to \infty$, the above expression reduces to a quadratic function in X [64], while it decays to zero upon decreasing ξ. Choosing Neumann BCs (including the zero mode), we find instead

$$V(X) = \frac{c\xi}{2} \mathrm{csch}(L/\xi) \left[\cosh(L/\xi) + \cosh\left(\frac{L \quad 2X}{\xi}\right)\right], \tag{5.82}$$

whose limit for $\xi \to \infty$ gives a X-independent diverging constant (which is removed by excluding the zero mode). Both Eqs. (5.81) and (5.82) show that $V(X) \to 0$ in the bulk limit $L \to \infty$ (with ξ kept finite — see the discussion in Section 5.3.2.3).

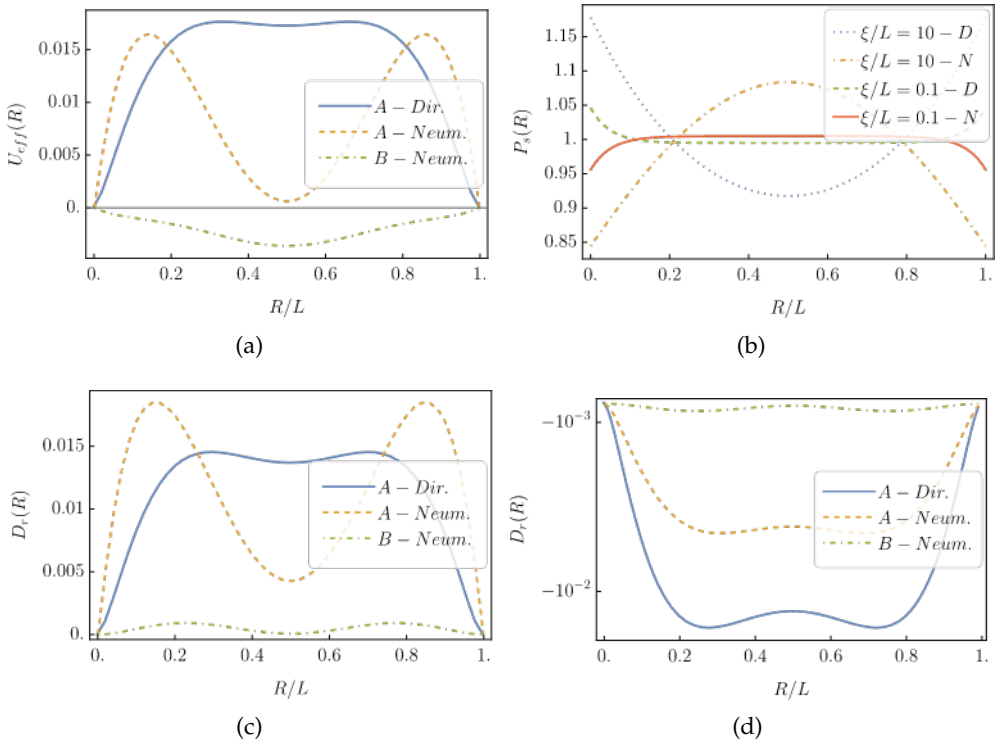

Figure 5.1: Landau-Ginzburg model with quadratic coupling. **a)** Effective potential $U_{\text{eff}}(X)$ given in Eq. (5.75) [with $V(X)$ given in Eqs. (5.81) and (5.82)] for a passive tracer with model A/B dynamics and Dirichlet/Neumann BCs. The correlation length is set to $\xi/L = 1$ and $\tilde{\chi} = 1$. **b)** Normalized stationary distribution $P_s(X)$ for a reactive tracer given in Eq. (5.20) and two distinct values of the correlation length ξ. The distribution becomes more flat upon decreasing ξ, with some residual structure in the proximity of the boundaries (limited in a layer of width ξ). (c,d) Reduced diffusion coefficient $D_r(X)$ [see Eq. (5.79)], with $\xi/L = 1$, for the (c) passive and (d) reactive case [see Eqs. (5.66) and (5.72)]. In the plots we set $h_1 = 0$, while we used $\varkappa_c = 0.1$ for the passive case and $\varkappa_c = 1$ for the reactive case.

Returning to the issue of finding a dimensionless counterpart of c (see Section 5.3.1.2), we note that dimensional analysis renders $[c] = [L]^{-1}$ in units of length. Following Ref. [64] (see Eq. (4.35) therein), we define the corresponding dimensionless parameter

$$\varkappa_c \equiv cL, \tag{5.83}$$

remarking that, sufficiently far from criticality, replacing L by ξ would render an equally admissible choice.

Finally, we can compute the stationary potential $W(X)$ in Eq. (5.23). In the quadratic case we have $h = 0$, so a non-vanishing $W(X)$ is only obtained in the presence of boundary fields ($h_1 \neq 0$). This case is described by capillary BCs (see Eq. (5.3)), for which

$$W(X) = \frac{c}{2(1+V(X))}\left\{\frac{h_1\xi}{\sinh(L/\xi)}\left[\cosh\left(\frac{L}{\xi}-\frac{X}{\xi}\right)+\cosh\left(\frac{X}{\xi}\right)\right]\right\}^2. \tag{5.84}$$

Again, this form suggests to introduce a dimensionless coupling describing the significance of

boundary fields as

$$\varkappa_{h_1} \equiv h_1\sqrt{L}. \tag{5.85}$$

For a quadratically coupled tracer, it is in general not possible to obtain analytical expressions for the drift and diffusion coefficients reported in Eqs. (5.66) and (5.72), apart from $\mu(X)$ in the passive case. In particular, the stationary distribution in the passive case [which is given in Eq. (5.74) in terms of $D(X)$] has to be evaluated numerically, while $P_s(X)$ for the reactive case is available in explicit form via Eq. (5.20). Both distributions are plotted in the first two panels of Fig. 5.1.

In the reactive case, the stationary distribution is independent of the type of dynamics (model A or B) due to detailed balance. Furthermore, the probability density of the tracer particle is peaked at the boundaries for Dirichlet BCs, or at the center of the interval for Neumann BCs, but both these features become less pronounced as we move away from the critical point, i.e., upon decreasing ξ. The difference between model A and B, however, becomes more evident in the passive case: in particular, for model A and Neumann BCs, the stationary distribution is no longer unimodal (see Fig. 5.1a). Similar features are shared by the (reduced) diffusion coefficients $D_r(X)$ in the passive and reactive case, which are plotted in the bottom row of Fig. 5.1. Notably, the effective diffusivity D_r is enhanced in the passive case due to the additional noise provided by the field. By contrast, in the reactive case, the diffusivity is reduced, which can be understood as a consequence of the suppression of field fluctuations due to the quadratic coupling. These findings are in qualitative agreement with the behavior of a tracer in a bulk medium [31].

5.4.1.2 Linear coupling

The analysis of the LG model with a linearly coupled particle was presented in Ref. [64] in the case of a critical field ($r = 0$). Here we extend it to the off-critical case, where the field acquires a finite correlation length $\xi = 1/\sqrt{r}$.

We start by computing the quantity $M(X)$ in Eq. (5.59), which characterizes the drift and diffusion coefficients both in the reactive and passive cases [see Eqs. (5.58) and (5.69), respectively], and, in particular, it determines the stationary distribution in the passive case [see Eqs. (5.69) and (5.70)]. Noting that the choice of a simple (non-derivative) coupling $\propto \phi(X)$ gives $v_n = h\sigma_n$ [see Eq. (5.13)], we find in the case of model B with Neumann BCs (see Appendix E.5)

$$M(X)_{\text{Neum}} = \frac{(h\xi)^2}{2\sinh^2(L/\xi)}\left[L\sinh^2\frac{X}{\xi} + \sinh\frac{L}{\xi}\cdot\left(X\sinh\frac{L}{\xi}\quad\frac{2X}{\xi}\quad\xi\sinh\frac{L}{\xi}\quad\sinh\frac{X}{\xi}\right)\right]. \tag{5.86}$$

(Recall that model B dynamics with a globally conserved field is incompatible with Dirichlet BCs — see Section 5.2.3). Similar expressions hold for model A (see Appendix E.5 and Eq. (E.33)). The critical point ($r = 0$) has already been considered in Ref. [64], in which case the function $M(X)$ simplifies to a polynomial form $m(X)$ (see, e.g., Eq. (3.26) in Ref. [64]). Note, however, that it is not directly possible to recover $m(X)$ from $M(X)$ by simply taking the limit for $\xi \to \infty$ in the latter: inspection of the relevant series for Neumann BCs reveals the presence of a constant,

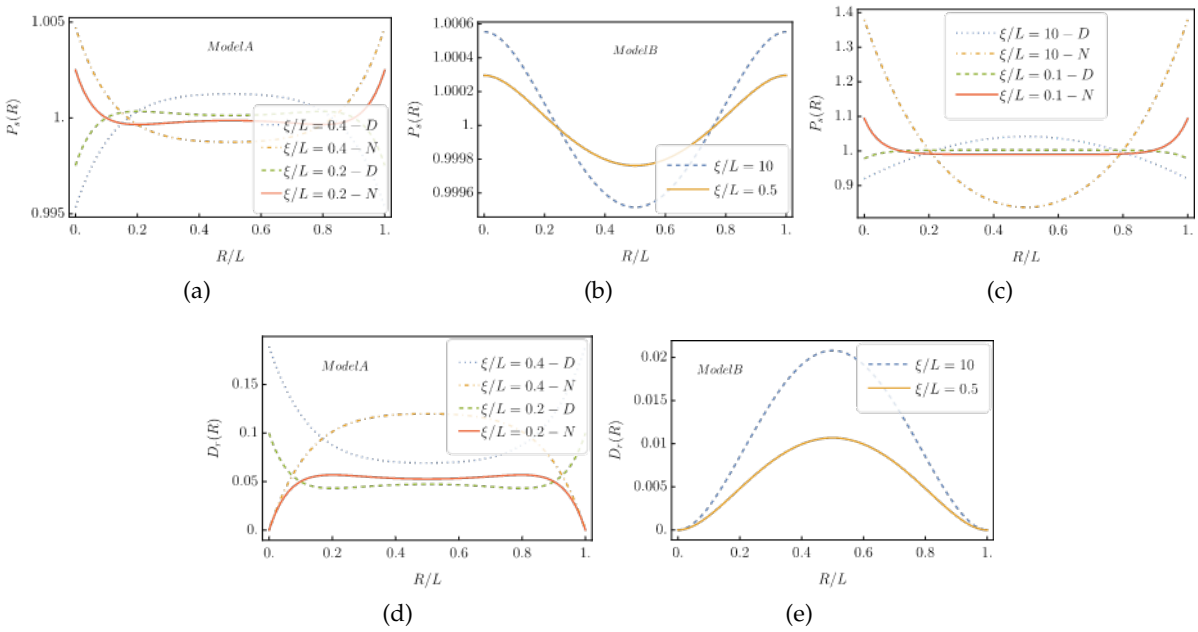

Figure 5.2: Landau-Ginzburg model with linear coupling. Stationary distribution $P_s(X)$ given in Eq. (5.70) [with the function $M(X)$ given in Eqs. (5.86) and (E.33)] for a passive tracer with **a)** model A and **b)** model B field dynamics (Neumann BCs only), using $\tilde{\chi} = 0.1$. **c)** Stationary distribution $P_s(X)$ given in Eq. (5.20) [with the function $W(X)$ given in Eq. (5.87)] for a reactive tracer and two different correlation lengths. **d,e)** Reduced diffusion coefficient $D_r(X)$ [see Eq. (5.79)] for a passive tracer with model A/B dynamics (which is equal in magnitude and opposite to that of the reactive case). In the plots we used $\varkappa_h = 1$ and $h_1 = 0$.

diverging zero mode which should be manually removed in order to yield meaningful results (see Appendix E.5). For any finite value of ξ, instead, the behavior of this zero mode is regular.

The stationary potential $W(X)$ given in Eq. (5.60) reduces to

$$W(X) = \frac{h^2}{2c}V(X) \quad \frac{hh_1\xi}{\sinh(L/\xi)}\left[\cosh\left(\frac{L \quad X}{\xi}\right) + \cosh\left(\frac{X}{\xi}\right)\right]. \tag{5.87}$$

Here the function $V(X)$ formally coincides with that given in Eqs. (5.81) and (5.82) (for the case of Dirichlet/Neumann BCs, respectively). Since $V(X)$ is proportional to c, the constant c (which is zero in the linear case) does not enter Eq. (5.87). The term proportional to h_1, which contains the effect of the boundary fields, implies the use of Neumann modes [Eq. (5.31b)] for the field. In this case, we can identify the dimensionless coupling $\varkappa_{h_1}$ to the boundary fields as in Eq. (5.85), and the dimensionless linear coupling to the tracer particle as

$$\varkappa_h = h\sqrt{L}. \tag{5.88}$$

The stationary distributions for the passive [Eq. (5.70)] and reactive [Eq. (5.20)] cases are plotted in Fig. 5.2 [panels (a-c)]. The case of passive model A is particularly interesting, as the qualitative character of the stationary distribution (i.e., the fact that it is peaked either at the boundaries or in the middle of the interval) drastically changes as we approach the critical point.

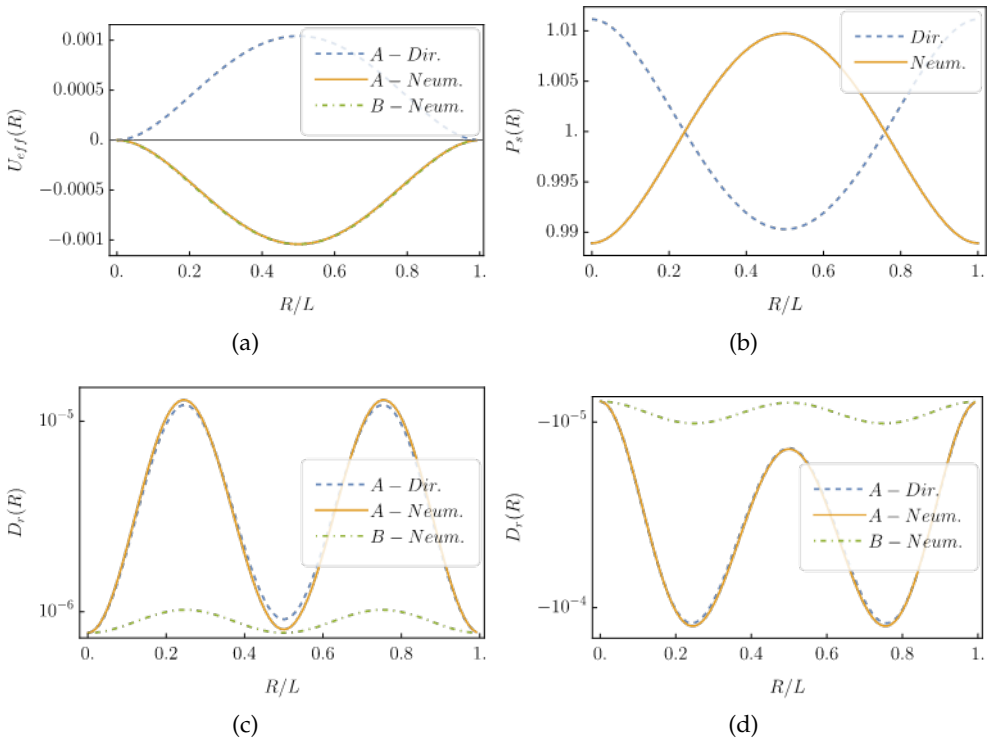

Figure 5.3: Critical Gompper-Schick model with quadratic coupling. **a)** Effective potential $U_{\text{eff}}(X)$ given in Eq. (5.75) [with $V(X)$ given in Eq. (5.89)] for a passive tracer with model A/B dynamics and Dirichlet and Neumann BCs ($\tilde{\chi} = 1$). **b)** Normalized stationary distribution $P_s(X)$ for a reactive tracer given in Eq. (5.20). **c,d)** Reduced diffusion coefficient $D_r(X)$ [see Eq. (5.79)] for the (c) passive and (d) reactive case. In the plots we set $h_1 = 0$, and used $\varkappa_c^{(\text{GS})} = 0.1$ in the passive and $\varkappa_c^{(\text{GS})} = 1$ in the reactive case [see Eq. (5.90)].

This is qualitatively confirmed by numerical simulations performed along the lines of Ref. [64] (not shown), and it is reflected in the behavior of the (reduced) diffusion coefficient $D_r(X)$ which is plotted in panels (d,e) of Fig. 5.2. We find that the effective diffusivity D_r is enhanced for a passive tracer when the field is near-critical ($\xi \gg L$), which is due to the additional noise provided by the field. Notably, before D_r vanishes as $\xi \to 0$, it acquires a bimodal character: indeed, the effect of the boundary conditions has a spatial extension of $O(\xi)$, which does not reach the center of the interval ($X = L/2$) when ξ is sufficiently small. In the reactive case, we obtain a D_r equal in magnitude but of opposite sign to the one in the passive case (not shown). The reduction of the diffusivity stems from to the creation of a field "halo" around the tracer as a direct consequence of the reactive coupling. The qualitative trends observed here are in agreement with the findings in Refs. [29, 30].

5.4.2 Critical Gompper-Schick model

Now we turn to the critical Gompper-Schick model, which differs from the LG model by the presence of higher order derivatives in its field Hamiltonian [see Eq. (5.28)]. We focus on the critical point, which corresponds to $\tau = 0$. In order to make the analytical computation of the

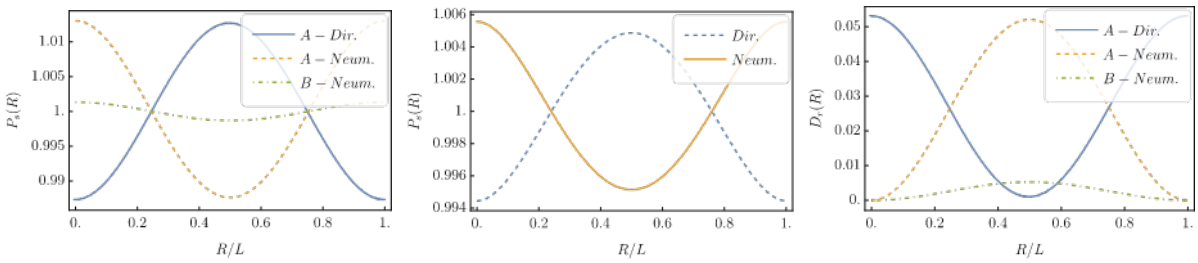

(a) (b) (c)

Figure 5.4: Critical Gompper-Schick model with linear coupling. **a)** Stationary distribution $P_s(X)$ given in Eq. (5.70) [with the function $M(X)$ given in Eq. (5.95)] for a passive tracer with model A/B dynamics ($\tilde{\chi} = 1$). **b)** Stationary distribution $P_s(X)$ for a reactive tracer given in Eq. (5.20) [with the function $W(X)$ given in Eq. (5.91)]. **c)** Reduced diffusion coefficient $D_r(X)$ [see Eq. (5.79)] for a passive tracer with model A/B dynamics. Note that D_r is equal in magnitude and opposite to the one of the reactive case (not shown). In the plots we set $h_1 = 0$, while we used $\varkappa_h^{(\mathrm{GS})} = 5$ in the passive case and $\varkappa_h^{(\mathrm{GS})} = 1$ in the reactive case [see Eq. (5.93)].

stationary potentials appearing in the effective Fokker-Planck equations tractable, we will retain here only $\Delta(\mathbf{x}) = c_4\nabla_{\mathbf{x}}^4$ in Eq. (5.29), and consequently $\beta_n = c_4 k_n^4$. This is expected to already capture the essential physics and the main differences with respect to the LG Hamiltonian. We will again consider simple linear and quadratic couplings, i.e., $\mathcal{K}_1 = \mathcal{K}_2 =$. We recall that, in the reactive case, the steady-state distribution is given by Eq. (5.20). The stationary distribution in the passive linear case is reported in Eq. (5.70) (and thus it is possible to write it analytically in terms of $M(X)$ computed below), while that of the passive quadratic case [which is formally stated in Eq. (5.74)] does not admit a straightforward analytic expression.

For the GS Hamiltonian, the effective potential defined in Eq. (5.22) for the quadratic coupling is given by (see Appendix E.5)

$$V(X) = \frac{c}{Lc_4}\left(\frac{L}{\pi}\right)^4\left[f_4(0) \mp f_4\left(\frac{2\pi X}{L}\right)\right], \tag{5.89}$$

where the function $f_n(x)$ is a n-th order polynomial (see Eq. (E.36)), and the signs $\mp$ correspond to Dirichlet or Neumann BCs, respectively (we have subtracted the zero mode in the Neumann case). Note that $V(X)$ in Eq. (5.89) does not admit a finite limit for $L \to \infty$ due to IR divergences related to criticality (see also the discussion in Section 5.3.2.3).

In this case, Eq. (5.89) suggests to identify a dimensionless coupling constant as

$$\varkappa_c^{(\mathrm{GS})} \equiv cL^3/c_4, \tag{5.90}$$

with $[c_4] = [L]^2$. Similarly, in the purely linear case ($c = 0$) we obtain

$$\begin{aligned} W(X) = \; & \frac{h^2}{2Lc_4}\left(\frac{L}{\pi}\right)^4\left[f_4(0) \mp f_4\left(\frac{2\pi X}{L}\right)\right] \\ & \frac{2hh_1}{Lc_4}\left(\frac{L}{\pi}\right)^4\left[f_4\left(\frac{\pi X}{L}\right) + \frac{1}{2}f_4\left(\pi(1 + X/L)\right) + \frac{1}{2}f_4\left(\pi(1 \quad X/L)\right)\right], \end{aligned} \tag{5.91}$$

while in the quadratic case with boundary fields ($h = 0$ and $h_1 \neq 0$) we find instead

$$W(X) = \frac{h_1^2 c}{2(1+V(X))} \left\{ \frac{2}{Lc_4} \left(\frac{L}{\pi}\right)^4 \left[f_4\left(\frac{\pi X}{L}\right) + \frac{1}{2} f_4\left(\pi(1+X/L)\right) + \frac{1}{2} f_4\left(\pi(1 \quad X/L)\right) \right] \right\}^2 . \quad (5.92)$$

In the last two expressions, the part proportional to h_1, which encodes the effect of boundary fields, is only present for Neumann BCs. Here, Eq. (5.91) suggests to define the dimensionless coupling constant

$$\varkappa_h^{(\mathrm{GS})} \equiv h L^{3/2}/\sqrt{c_4}. \quad (5.93)$$

Analogously, a dimensionless coupling quantifying the importance of the contribution of the boundary fields h_1 can be introduced as

$$\varkappa_{h_1}^{(\mathrm{GS})} \equiv h_1 L^{3/2}/\sqrt{c_4}, \quad (5.94)$$

such that $W(X)$ in Eq. (5.92) is $\propto \varkappa_c\, (\varkappa_{h_1}^{(\mathrm{GS})})^2$. Finally, the dynamical coefficient $M(X)$ of the linear case reads

$$M(X) = \frac{h^2}{Lc_4^2} \left(\frac{L}{\pi}\right)^{6+} \left[f_{6+}\ (0) \pm f_{6+}\ \left(\frac{2\pi X}{L}\right) \right], \quad (5.95)$$

where $a = 0, 1$ marks the distinction between model A/B dynamics.

The stationary distributions and diffusion coefficients corresponding to the quadratic or linear coupling cases are reported in Figs. 5.3 and 5.4, respectively. The (reduced) diffusion coefficient $D_r(X)$ of a quadratically coupled tracer is markedly bimodal (see Fig. 5.3), as the contribution of the field to the diffusion of the particle nearly vanishes both near the boundaries and at the center of the interval. Similarly to the LG model, both for a quadratically and a linearly coupled tracer (see Figs. 5.1 and 5.2), the diffusivity is enhanced (reduced) in the case of a passive (reactive) tracer. As before, one may understand these trends as a consequence of the additional field-induced noise imposed on a passive tracer, and of the slowing effect of the field halo created around a reactive tracer.

5.5 Summary of this Chapter

In this Chapter we presented a simple and systematic procedure to study the effective dynamics of a tracer particle coupled to a confined correlated medium within the adiabatic approximation. The medium is modeled as a scalar order parameter $\phi(\mathbf{x}, t)$ evolving under Langevin dynamics within the Gaussian approximation, and it is confined by the imposition of boundary conditions at the two extrema of a one-dimensional interval. The particle at position $\mathbf{X}(t)$ undergoes a stochastic motion and it is reflected at the boundaries. The interaction between the field and the particle is modeled by the addition of linear or quadratic coupling terms in the Hamiltonian in Eq. (5.2): in the former case the field $\phi(\mathbf{X}, t)$ (or its derivatives) are enhanced in the vicinity of the tracer particle, while in the latter they are suppressed. If detailed balance is satisfied by the dynamics [i.e., if $\zeta = 1$ and $T_x = T_\phi$ in Eqs. (5.4) and (5.6)], we call the particle *reactive*, as its feedback on the medium is taken into account. Conversely, if the influence of the particle on

the field dynamics is neglected, then the system is inherently out of equilibrium and we call the tracer *passive* — this case may alternatively be regarded as an *active* particle driven by temporally correlated noise.

The adiabatic elimination method presented here is particularly adapted to the case of a particle coupled to a strongly correlated and confined medium fluctuating on a fast (but still non-vanishing) time scale. In contrast to the approach of Refs. [84, 85], which employs a quantum mechanical operator formalism, our method works directly on the space of the actual dynamical variables. Furthermore, no additional assumptions on the steady-state distribution are required in our case.

The main outcome of the method described above (see Section 5.3) is a Fokker-Planck equation [Eq. (5.48)] that describes the effective Markovian tracer dynamics characterized by space-dependent drift and diffusion coefficients $\mu(X)$ and $D(X)$. The latter have been computed here up to their lowest non-trivial order in the adiabaticity parameter χ for the various cases discussed above, i.e., linear/quadratic field-particle coupling, dissipative or conserved dynamics, and passive/reactive tracer [see Eqs. (5.58), (5.66), (5.69) and (5.72)]. We also emphasized (when relevant) the effects of including boundary fields in the Hamiltonian of Eq. (5.2) (i.e., $h_1 \neq 0$). Our approach has allowed us to obtain, in a straightforward way, the effective equations of motion of a quadratically coupled tracer, including the spurious drift and higher-order corrections to the transport coefficients. We remark that, in general, an analysis based solely on the Langevin equation does not determine unambiguously the stochastic interpretation of the field-induced noise in the resulting effective equation for the tracer (see the discussion in Section 5.3.2.3) — except if the noise correlations trivially turn out to be independent of the position, as is the case in the bulk [29–31].

In Section 5.4 we applied our method to media described by Landau-Ginzburg or Gompper-Schick type Hamiltonians within the Gaussian approximation, to which the tracer particle is coupled via linear or quadratic (non-derivative) terms of the field. We obtained analytic expressions for the stationary distribution of the particle position and for the spatially dependent drift and diffusion coefficients (see Figs. 5.1 to 5.4). Notably, the spatial dependence is a consequence of the confinement of the correlated medium and it does not occur in the bulk, as we discussed in Chapter 2. The diffusivity is typically strongly influenced by the presence of a dynamical conservation law, as is the stationary distribution of a passive tracer. The consistency between our findings and those obtained in the bulk limit $L \to \infty$ in Refs. [29–31] is confirmed in Appendix E.3.

Our method may find application in the description of lipid membranes or microemulsions [17–25], as well as of colloidal particles in contact with a near-critical fluid medium [27–31, 44, 64, 78–81, 104]. In the latter case, a rapid order parameter field dynamics is obtained as a result of spatial confinement or a finite correlation length, which correspond to the typical experimental conditions [35, 36]. Future extensions of the present work should address the field dynamics beyond the Gaussian approximation, which could in principle be obtained by analyzing the nonlinear terms $\propto \phi^n$ within a suitable weak-coupling expansion. The same level of analytical complication is entailed by the inclusion of field-particle couplings higher than quadratic in the

Hamiltonian of Eq. (5.2), since both translate into nonlinearities in the Fokker-Planck equation for the field modes [see Eq. (5.43)]. Since the statistics of the critical Casimir force can be extracted from the tracer distribution function, the present approach could provide further insights into the dynamics of the critical Casimir force [102, 180, 186–190] and of its fluctuations [191], as well as on associated many-body effects [44, 192–195]. Finally, the extension of our results to higher spatial dimensions ($d = 2$ or $d = 3$) appears to be straightforward [64], and is very relevant for experimental applications; more refined models may in that case be devised to include the effects of the hydrodynamic transport of the tracer particle and the field.

6

Quenched disorder in a random matrix model

In Chapters 2 to 4 we analyzed a model in which a fluctuating field $\phi(\mathbf{x}, t)$ was used to represent a spatially complex landscape, whose features evolve in time. In Chapter 5 we then focused on the case in which the evolution of the field is fast compared to the time scales of interest — namely, those characterizing the motion of a tracer particle. In this case, it proved useful to compute the lowest adiabatic corrections around a configuration in which the field is assumed to equilibrate rapidly around the instantaneous position of the tracer: within this *super-adiabatic* approximation (see, e.g., Eq. (5.53)), the tracer thus effectively diffuses subject to a field-induced *quenched* potential.

This final Chapter deals with another prominent tool which is typically employed in statistical physics to model complex interaction patterns, in the presence of quenched disorder: namely, random matrices. As recalled in the Introduction, the field of random matrix theory has received considerable attention in the last decades, because it provides a powerful and versatile framework to describe a wide range of phenomena, from quantum many-body systems to financial markets. In random matrix models, stochastic variables are used to effectively describe the interactions between the individual components of large complex systems; the focus of their analysis then lies on the statistics of their eigenvalues, which are themselves stochastic variables, and particularly on their correlation functions. Moreover, the properties of the eigenvalue spectrum of a random matrix generally affect the dynamics of the corresponding physical system it represents. An intuitive example is provided by the seminal work of R. M. May on complex ecosystems [196], which we briefly recall in Appendix F.1.

In the following sections we will consider a well known random matrix ensemble — the generalized Rosenzweig-Porter model (GRP) — and derive new results about its eigenvalue statistics. Because of its relevance to the modeling of quantum many-body systems, this Chapter contains numerous references to many-body localization and fractality, which will be carefully explained in Section 6.1. Apart from its intrinsic interest and its significance for the above mentioned applications, the knowledge of the eigenvalue statistics of the GRP model also paves the way towards addressing its dynamical properties. Important steps in this direction have been moved in Ref. [197], to which we refer the reader, during the conception of the work presented in this Chapter.

The content of this Chapter has been published as "D. Venturelli, L. F. Cugliandolo, G. Schehr, and M. Tarzia, *Replica approach to the generalized Rosenzweig-Porter model*, SciPost Phys. **14**, 110 (2023)" [198].

6.1 The model and its context

Quantum non-interacting particles in a disordered potential undergo the Anderson localization transition as the disorder strength is increased [199]. In one and two spatial dimensions an infinitesimal amount of disorder is sufficient to localize all eigenstates of the Hamiltonian, while in dimension larger than two a critical value of the disorder strength separates a metallic phase, where the eigenstates are similar to plane waves and spread over the whole volume uniformly, from an insulating phase, where the eigenstates are instead exponentially localized around specific points in space, and thereby occupy a finite $O(1)$ portion of the total volume. It is well established that exactly at the Anderson localization critical point the wave-functions are *multifractal* [200, 201]. This means that they are neither fully delocalized (as in the metallic regime), nor fully localized (as in the insulating phase), since their support set grows with the system size but remains a vanishing fraction of the total volume. The *multi*-fractal character of the wave functions is due to the fact that the qth moments of their amplitudes decay with the size N as $\langle \sum_{i=1}^{N} |\psi_i|^{2q} \rangle \propto N^{(q-1)D_q}$, with different q-dependent exponents $0 \leq D_q \leq 1$.

In the last decade, the Hilbert space localization properties of quantum disordered many-body systems have attracted much interest. In this context, the emergence of multifractal states has been discussed as a key and robust feature of their phase diagram, and has been invoked to explain some of their unconventional properties beyond the single-particle limit. In the many-body setting, multifractal eigenstates that do not cover the whole accessible Hilbert space may lead to the violation of the eigenstate thermalization hypothesis (ETH) [202, 203]. Therefore, they are often called partially delocalized but *non-ergodic*, in contrast to the *ergodic* fully delocalized eigenstates, which are supposed to satisfy ETH.

In the context of many body localization (MBL), recent studies indicate that the many-body eigenstates are in fact multifractal in the whole insulating phase [204–211]. Furthermore, the seminal work by Basko, Aleiner and Altshuler [212] predicted the existence of a novel unconventional "bad metal" regime in between the fully ergodic metallic phase at low disorder and the insulating one at strong disorder. Following the pioneering ideas of Ref. [213], the unusual properties of the bad metal regime have also been put in relation with the possible multifractal nature of the many-body eigenstates. Recent investigations of the out-of-equilibrium phase diagram of the quantum random energy model [214–218] and Josephson junction arrays [219, 220] seem to support this scenario. The existence of partially extended but non-ergodic wave-functions is also believed to have relevant practical and conceptual implications in the efficient population transfer in the context of quantum computing [217, 218, 221]. Moreover, recent studies of the Sachdev-Ye-Kitaev model in high-energy physics and quantum gravity have reported evidence for the emergence of a non-ergodic, but partially extended phase when the model is perturbed by a single-body term [222, 223].

Matrix models have been an invaluable tool to describe and help understanding complex physical systems, in particular those with quenched randomness. The physical mechanism at the origin of the above-mentioned multiftactal eigenstates is one such problem, and specific matrix models have recently been used as proxies to capture the peculiar spectral properties

associated with them. In this respect, the Rosenzweig-Porter (RP) random matrix ensemble [224], originally introduced to reproduce the spectral properties of complex atomic spectra, provides an archetypal illustration of a system in which a partially extended phase featuring fractal eigenstates (along with other unconventional spectral properties that will be extensively discussed below) appears in an intermediate region of the phase diagram between a fully delocalized phase and a fully Anderson localized phase (see Fig. 6.1). For this reason the RP model has been the focus of a strong resurgence of attention over the last few years [225–233]. Although one cannot expect that simple random matrix models could capture all the properties of interacting quantum systems, they provide natural and powerful tools to understand the deep physical mechanisms behind some of their features, which are often elusive to analytical treatments in more realistic settings.

The Hamiltonian of the RP model $\mathcal{H} = A + c(N)B$ can be written as the sum of an $N \times N$ diagonal matrix A, whose entries a_i's are independent and identically distributed (i.i.d.) random variables drawn from a Gaussian distribution $p_a(a_i)$, and another $N \times N$ random matrix B belonging to the Gaussian orthogonal (or unitary) ensemble (GOE or GUE, respectively). If the variances of the matrix elements b_{ij} are chosen of $\mathcal{O}(1)$, then the width of the spectrum of B is of $\mathcal{O}(\sqrt{N})$: thus the matrix A (whose spectral width is of $\mathcal{O}(1)$) can produce significant deviations from the GOE/GUE behavior only if $c(N)$ decays sufficiently fast for large N. The properties of this model have been extensively studied by using different techniques, such as a mapping to the Dyson Brownian motion [234], supersymmetry [235, 236], resolvent methods [237, 238], and first order perturbation theory [239].

Due to the strong surge of attention towards multifractal states in quantum many-body disordered systems, a generalized version of the RP model in which the distribution $p_a(a_i)$ is not necessarily Gaussian has then been introduced in Ref. [225], and thoroughly investigated by using the techniques recalled above [226–233] — we will refer to this as the GRP model. In addition, new connections and applications have been pointed out in disordered elastic systems [240], many-body localization [207, 214–216], quantum gravity [222, 223], quantum information [217, 218, 221], models of theoretical ecology [241], and noise reduction in big data [242].

In this Chapter we revisit the generalized RP model by analyzing some properties of the energy levels and their correlations which have not been investigated in the literature yet. In particular, we perform a thorough study of the finite-N corrections to the average spectral density and compute the level compressibility in the intermediate phase, thereby providing a deeper understanding of the properties of the intermediate regime. Our analysis uses the replica method largely exploited in the analysis of spin glass models [51], but not only — for example, this tool has been recently applied to study the properties of the ground states in a deformed GOE ensemble [197]. Our replica study is developed for the case in which the entries of $\mathcal{H}$ are real numbers, so that $\mathcal{H}$ belongs to a deformed GOE ensemble (where the deformation is introduced by the addition of the diagonal random matrix A). However, and quite surprisingly, we show that the exact same behavior of the level compressibility applies to the crossover regime of the Hermitian GRP model [225] (in which the off-diagonal entries are complex).

In the rest of this introductory section we will present the RP model and some of its salient

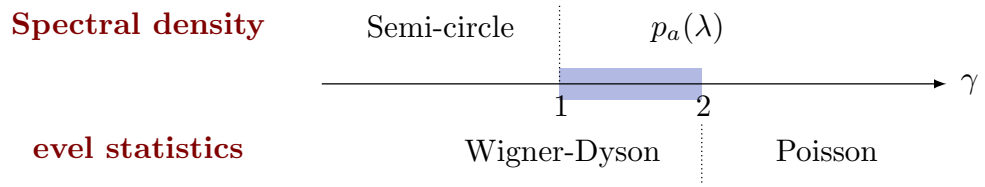

Figure 6.1: Sketch of the different phases of the RP model, depending on the value of the parameter γ in Eq. (6.1). Considering the average spectral density $\rho(\lambda)$, a transition is first observed at $\gamma = 1$ which separates a fully delocalized phase where $\rho(\lambda) = \rho_{\mathrm{GOE}}(\lambda)$ from a partially delocalized phase where $\rho(\lambda) = p_a(\lambda)$ in the thermodynamic limit (see the main text). Focusing instead on the local level statistics, another transition is found at $\gamma = 2$ from the partially delocalized phase characterized by the Wigner-Dyson statistics, to an Anderson-localized phase characterized by the Poisson statistics. The shaded region $1 < \gamma < 2$ indicates the intermediate phase studied in this Chapter.

properties (Section 6.1.1), and we will outline our study and main results (Section 6.1.2).

6.1.1 The generalized Rosenzweig-Porter model

We consider the Hamiltonian represented by the $N \times N$ matrix

$$\mathcal{H} = A + \frac{\nu}{N^{\gamma/2}} B, \tag{6.1}$$

where the matrix B belongs to the GOE ensemble: its elements are Gaussian random variables with zero mean and unit variance (i.e., $\langle b_{ii}^2 \rangle = 1$ and $\langle b_{ij}^2 \rangle = 1/2$ for $i \neq j$). With this choice, the spectrum of B in the limit $N \to \infty$ converges to a Wigner semicircle supported within $\lambda \in [-\sqrt{2N}, \sqrt{2N}]$, where we denote hereafter with λ the eigenvalues of $\mathcal{H}$. The parameter ν is of $O(1)$ and does not scale with N. The deformation matrix A is instead diagonal, with independent entries a_i's identically distributed according to a generic distribution $p_a(a)$, hence the name Generalized Rosenzweig-Porter model (GRP).

Following the analogy with disordered quantum many-body systems, each matrix index can be thought of as a site of the reference Hilbert space, which is connected to every other site with the transition rates distributed according to the Gaussian law. Different phenomenologies are expected depending on the value of the parameter γ, which renders one of the two matrices A or B subleading with respect to the other in the limit of large N. As summarized in Fig. 6.1, the model features three distinct phases (and two transition points between them): a fully delocalized phase for $\gamma < 1$, a fully Anderson localized phase for $\gamma > 2$, and an intermediate fractal phase for $1 < \gamma < 2$.

The transition from fully extended to fractal eigenstates at $\gamma = 1$ manifests itself as a transition for the average spectral density $\rho(\lambda)$, which reproduces the Wigner semicircle law for $\gamma < 1$ in the $N \to \infty$ limit, while it reduces to $\rho(\lambda) = p_a(\lambda)$ if $\gamma > 1$ and the same $N \to \infty$ limit is taken. At $\gamma = 1$, $\rho(\lambda)$ interpolates between $p_a(\lambda)$ and the Wigner semicircle as the value of the parameter ν is increased. This transition becomes sharp (i.e., it occurs at a particular value of $\nu = \nu_c$) provided that $p_a(a)$ has a compact support and vanishes sufficiently fast at its upper edge [240, 243].

The value $\gamma = 2$ corresponds instead to a genuine Anderson localization transition. Indeed, the region $\gamma < 1$ is characterized by the Wigner-Dyson statistics, meaning that the eigenvectors of $\mathcal{H}$ are uniformly delocalized on N sites in the large N limit, and the average level spacing follows the Wigner surmise [49], signaling level repulsion. Conversely, in the region $\gamma > 2$ the eigenvectors are completely localized over $O(1)$ sites and the mean level spacing exhibits Poisson statistics.

The intermediate region with $1 < \gamma < 2$ is particularly interesting, because the average spectral density tends to $p_a(\lambda)$, but the *local* level statistics remains of the Wigner-Dyson type. Here the eigenvectors are known to be delocalized over a large number of sites N^{D_γ}, which represent, however, a vanishing fraction of the total number of sites N in the thermodynamic limit, their fractal dimension being $D_\gamma = 2 \quad \gamma < 1$ [225].

The most intuitive way to understand the spectral properties in the intermediate region is provided by the Fermi golden rule. In the limit in which the off-diagonal matrix B is absent and all the eigenvectors are trivially localized on a single site, one has $|\psi_i\rangle = |i\rangle$, with corresponding eigenenergies $\lambda_i = a_i$. When the GOE perturbation $\nu N^{\ \gamma/2} B$ is turned on, the transition probability per unit time from a state i to another state j can be evaluated perturbatively as

$$_{i\to j} = \frac{2\pi\rho}{} \frac{4\eta}{N} |b_{ij}|^2, \tag{6.2}$$

where $\rho = \rho(\lambda)$ and, for future convenience, we have introduced the combination

$$\eta \equiv N^{1\ \gamma} \nu^2/4. \tag{6.3}$$

Hence, the average escape rate per unit time for a "particle" created in site i at time $t = 0$ reads

$$= \sum_{j\neq i} \langle\ _{i\to j}\rangle = \frac{2\pi\rho}{} 4\eta. \tag{6.4}$$

The quantity $\Delta E \sim$ can thus be interpreted as the bandwidth that can be reached in a time of $O(1)$ from a given site i. This implies that the eigenvectors within this energy window are hybridized by the GOE perturbation. For $1 < \gamma < 2$ such energy band decays with the system size as $\Delta E \propto N^{1\ \gamma}$ but is much larger than the mean level spacing

$$\delta_N \simeq [N\rho]^{\ 1}, \tag{6.5}$$

entailing that the system is not Anderson localized; still, ΔE remains much smaller than the total bandwidth, which is of $O(1)$. This signifies that the particle can only explore a sub-extensive portion of the total volume. The Anderson localization transition thus occurs when ΔE becomes smaller than the mean level spacing, i.e., for $\gamma \geq 2$: this implies that the average escape time from site i (i.e., $\Delta t \equiv \ /\Delta E$) grows at least linearly with N, and thus the eigenfunctions remain localized on $O(1)$ sites. Conversely, the transition to the fully delocalized phase takes place when ΔE becomes of the order of the total bandwidth, i.e., for $\gamma \leq 1$: this implies that, starting from site i, the wave-packet can reach any other site in a time of $O(1)$.

In the intermediate phase, $1 < \gamma < 2$, the support set of the eigenvectors (i.e., the number of sites that are hybridized by the perturbation) is simply given by the spreading of the energy interval divided by the average gap between adjacent energy levels, and thus scales as $\Delta E/\delta_N \sim N^{D_\gamma}$, with $D_\gamma = 2 \quad \gamma$. The partially extended but fractal eigenstates are therefore linear combinations of a bunch of N^{D_γ} localized states associated to nearby energy levels, i.e.,

$$|\psi_i\rangle \approx \sum_{\substack{i' \ s.t. \\ |a_i \ \ a_{i'}| \leq \Delta E}} c_{i'} |i'\rangle, \tag{6.6}$$

with coefficients $c_{i'}$ of order $N^{\ D_\gamma/2}$ to ensure normalization. These eigenstates give rise to the so-called *mini-bands* in the local spectrum [225]. The width of the mini-bands sets the energy scale

$$E_T \sim \Delta E \sim N^{D_\gamma \ 1} = N^{1 \ \gamma}, \tag{6.7}$$

often called the Thouless energy [244, 245], within which GOE-like spectral correlations (and in particular level repulsion) have been established. The moments of the wave-functions' coefficients (the so-called generalized *inverse participation ratios*, IPR) behave as

$$I_q = \sum_i |\langle i|\psi\rangle|^{2q} \propto N^{D_\gamma(1 \ \ q)} \qquad \Longrightarrow \qquad D_q = D_\gamma. \tag{6.8}$$

This implies that all the fractal dimensions D_q are degenerate and equal to D_γ for all positive integer q, i.e., that the intermediate phase of the GRP model is fractal but not multifractal.

As discussed above, the emergence of such fractal phase is particularly relevant in many physical contexts. Its existence was first suggested in Ref. [225] and then rigorously proven in Ref. [226]. In recent years several generalizations of the RP model have been put forward and analysed [246–251], and many other random matrix ensembles have been shown to have an intermediate partially delocalized phase with similar spectral properties [252–267]. Yet, the GRP setting is still a very useful playground to analyze the properties of fractal states in a controlled framework.

6.1.2 Outline of the calculation and summary of the main results

As explained above, the GRP model has been intensively investigated over the past few years with a great variety of analytical and numerical techniques. In this paper we tackle this model by applying yet another approach, namely the replica formalism [51], which allows us to obtain new results on the average spectral density, and the statistics of the number of energy levels within a finite interval.

In Section 6.2 we start by analyzing the average density of states $\rho(\lambda)$. When the size N of the matrix is large, we find the leading order estimate

$$\rho(\lambda) = \quad \frac{1}{\pi\eta} \lim_{\varepsilon \to 0^+} \mathrm{Re}\, C(\lambda_\varepsilon) + \mathcal{O}(1/N), \tag{6.9}$$

where $\lambda_\varepsilon = \lambda \quad i\varepsilon$, the parameter η depends on N and was introduced in Eq. (6.3), and the function $C(\lambda)$ is implicitly defined by the self-consistency equation

$$C(\lambda) = i\eta\, \mathcal{G}_a \left[\lambda + 2iC(\lambda)\right]. \tag{6.10}$$

Here $\mathcal{G}_a$ is the resolvent associated to the distribution $p_a(a)$ of the entries of A (c.f. Eq. (6.42)). In general, it is quite difficult to solve explicitly Eq. (6.10) for $C(\lambda)$ for any arbitrary distribution $p_a(a)$. However, we show in Section 6.2.4 that it can be solved explicitly for two special cases: (i) when $p_a(a)$ is a Wigner semicircle — which is expected, since it is stable under free convolution [268] — and (ii) when it is a Cauchy distribution, which is more surprising.

As we show in Section 6.2.3, by taking the limit $N \to \infty$ with η kept finite, Eqs. (6.9) and (6.10) reduce to the free addition formula [268], sometimes called the "Zee formula" in the physics literature [269]. However, as we show in Section 2.5 of Ref. [198], these equations contain more information and, in the case where $\eta = \eta(N) \ll 1$ defined in Eq. (6.3) with $1 < \gamma < 2$, they allow us to obtain the leading $1/N$ corrections to the limiting density $\rho(\lambda) = p_a(\lambda)$ in a controlled way, even when the resolvent $\mathcal{G}_a(\ )$ does not admit a closed-form analytic expression. These corrections turn out to be quite difficult to compute using the standard free addition formula, which in principle holds only in the limit $N \to \infty$.

Next, in Section 6.3 we analyze the behavior of the *level compressibility* $\chi(E)$, which is a simple indicator of the degree of level repulsion and is defined as follows [273]. We first introduce the empirical density of the (real) eigenvalues λ_i of $\mathcal{H}$, defined as

$$\rho_N(\lambda) = \frac{1}{N}\sum_{i=1}^{N} \delta(\lambda \quad \lambda_i). \tag{6.11}$$

Note that $\rho_N(\lambda)$ is normalized to unity. Let

$$I_N[\ \ ,\beta] \equiv N \int^{\beta} \mathrm{d}\lambda\, \rho_N(\lambda) \tag{6.12}$$

denote the number of eigenvalues lying in the interval $[\ \ ,\beta] \subseteq \mathbb{R}$, which is a random variable. Then

$$\chi(E) \equiv \frac{\kappa_2(E)}{\kappa_1(E)} = \frac{\left\langle I_N^2[\ \ E,E]\right\rangle \quad \langle I_N[\ \ E,E]\rangle^2}{\langle I_N[\ \ E,E]\rangle} = \frac{\left\langle I_N^2[\ \ E,E]\right\rangle_c}{\langle I_N[\ \ E,E]\rangle}, \tag{6.13}$$

where κ_1 and κ_2 are the first two cumulants of I_N. For Poisson statistics, one has $\kappa_2(E) \simeq \kappa_1(E)$ for small E, and then $\chi(E) \simeq 1$ (see Appendix F.2). On the contrary, for a rigid spectrum like that of the GOE matrix B in Eq. (6.1), the mean number of eigenvalues behaves as $\langle I_N[\ \ E,E]\rangle \propto \tilde{E}$, with $\tilde{E} \equiv N\rho_N(0)E$ and where $[N\rho_N(0)]^{\ -1}$ is the mean level spacing close to $E = 0$, while $\left\langle I_N^2[\ \ E,E]\right\rangle_c \propto \ln \tilde{E}$ for large $\tilde{E}$. Hence in the GOE case one finds $\chi(E) \to 0$ for $\tilde{E} \to \infty$, i.e., for $E \gg [N\rho_N(0)]^{\ -1}$ (but still much smaller than $E \sim O(1)$).

In Section 6.3.3 we provide the cumulant generating function of the variable $I_N[\ \ ,\beta]$ at leading order for large N. For a symmetric interval $[\ \ E,E]$ and a symmetric distribution $p_a(a)$, the result reads

$$\mathcal{F}_{[\ \ E,E]}(s) \equiv \frac{1}{N}\ln\left\langle e^{\ sI_N[\ \ E,E]}\right\rangle = \quad ms + \ln\left\langle e^{\ sf(a)}\right\rangle_a + O(\eta/N), \tag{6.14}$$

[1] It is known in statistics under the name of "Fano factor" [270], and it has been studied recently in physics in the context of extremes and record statistics of time series [271, 272].

where

$$m = \frac{2\eta}{\pi}\,\mathrm{Im}\left[\mathcal{G}_a\left(\ iA^{-1}\right)\right]^2, \qquad f(a) \equiv \frac{1}{\pi}\arctan\left(\frac{\sin 2\theta}{a^2 r^2 + \cos 2\theta}\right) \in [0,1], \tag{6.15}$$

and $\Delta(E) = r(E)e^{i\theta(E)}$ has to be determined by solving the self-consistency equation

$$\Delta^{-1} = \varepsilon \quad iE \quad 2i\eta\mathcal{G}_a\left(\ iA^{-1}\right), \tag{6.16}$$

before sending $\varepsilon \to 0$. Again, we show that a closed-form solution can be found in some particular cases. Our results are supported by the comparison with the numerical diagonalization of large random matrices.

The ratio of the first two cumulants of $I_N[\ E, E]$ gives the level compressibility $\chi(E)$ introduced in Eq. (6.13). In agreement with the picture presented above for the region $1 < \gamma < 2$, and having identified $E_T \propto \eta \propto N^{1-\gamma}$ as the Thouless energy of the system, we explicitly verify in Section 6.3.5 that $\chi(E) \sim 0$ for $E \ll E_T$ — but still much larger than the mean level spacing $\delta_N \propto N^{-1}$ — corresponding to level repulsion, while $\chi(E)$ follows the Poisson statistics for $E \gg E_T$. However, in the scaling limit $E = 2\pi p_a(0)\eta \cdot y$ with $N^{-1} \ll \eta \ll 1$, we show that $\chi(E)$ takes the universal form

$$\chi(E) \simeq \chi_T\left(y = \frac{E}{2\pi p_a(0)\eta}\right), \qquad \chi_T(y) = \frac{1}{\pi y}\left[2y\arctan(y) \quad \ln\left(1+y^2\right)\right], \tag{6.17}$$

where the scaling function $\chi_T(y)$ is independent of the specific choice of $p_a(a)$. This function is plotted in Fig. 6.5: it behaves as $\chi_T(y) \simeq y/\pi$ for small y, while it tends to 1 for large y. Note that the crossover energy scale $2\pi p_a(0)\eta$ coincides (apart from a factor of 4) with the width of the mini-bands identified in Eq. (6.4) using the Fermi golden rule, which allows us to put the intuitive arguments given above on the structure of spectral correlations on a much firmer basis.

Interestingly, using results from Refs. [225] and [238], we show that the same scaling function χ_T also describes the crossover for Hermitian B matrices — while the level compressibilities for the real and the Hermitian GRP ensembles differ outside of this energy regime. We do so by relating the level compressibility to the 2-level spectral correlation function of the Hermitian GRP model, previously derived in [225, 238] by means of the Harish-Chandra-Itzykson-Zuber integral (which notably does not admit a counterpart for matrices with real entries).

In Section 6.3.6 we finally inspect, using extensive numerical diagonalization of large random real matrices, the low-energy region where E is chosen on the scale of the Thouless energy. The scaling form of $\chi(E)$ presented in Eq. (6.17) is thus shown to represent a universal crossover between the classical GOE result $\chi(E \sim N^{-1}) \simeq \chi_{\mathrm{GOE}}(E)$ for energies of the order of the mean level spacing (and much smaller than the Thouless energy, see Eq. (6.113)), and the model-dependent prediction of Eqs. (6.13) and (6.14), valid for energies of the order of the total spectral band-width, i.e., $E \sim O(1)$.

6.2 Average spectral density

Let us begin by considering the density of states of the matrix $\mathcal{H}$ in Eq. (6.11). Its mean value can be obtained by means of the Edwards-Jones (E-J) formula [49, 274], which we briefly recall

here. One starts from the Plemelj-Sokhotski relation: if $f(x)$ is a complex-valued function that is continuous on the real axis, and given $\quad < 0 < \beta$, then

$$\lim_{\varepsilon\to 0^+} \int^{\beta} \mathrm{d}x\, \frac{f(x)}{x \pm i\varepsilon} = \mp i\pi f(0) + \mathcal{P}\int^{\beta} \mathrm{d}x\, \frac{f(x)}{x}, \tag{6.18}$$

where $\mathcal{P}$ indicates the Cauchy principal value of the integral. From Eq. (6.11) we then have

$$\langle \rho_N(\lambda)\rangle = \frac{1}{\pi N} \lim_{\varepsilon\to 0^+} \mathrm{Im} \left\langle \sum_{i=1}^{N} \frac{1}{\lambda \quad \lambda_i \quad i\varepsilon} \right\rangle = \frac{1}{\pi N} \lim_{\varepsilon\to 0^+} \mathrm{Im}\, \frac{\partial}{\partial\lambda} \left\langle \sum_{i=1}^{N} \ln(\lambda_i \quad \lambda + i\varepsilon) \right\rangle, \tag{6.19}$$

where the average is taken over the distribution of the entries of $\mathcal{H}$. In the last step we indicated by $\ln(\ )$ the principal branch of the complex logarithm. Using the properties of Gaussian integrals, we finally obtain the E-J formula [274]

$$\rho(\lambda) \equiv \langle \rho_N(\lambda)\rangle = \quad \frac{2}{\pi N} \lim_{\varepsilon\to 0^+} \mathrm{Im}\, \frac{\mathrm{d}}{\mathrm{d}\lambda} \langle \ln \mathcal{Z}(\lambda_\varepsilon)\rangle\,, \tag{6.20}$$

$$\mathcal{Z}(\lambda) \equiv \det(\mathcal{H} \quad \lambda\ )^{\ 1/2} = (2\pi i)^{\ N/2} \int_{\mathbb{R}^N} \mathrm{d}\mathbf{r}\, e^{\ \frac{i}{2}\mathbf{r}^T(\lambda \quad \mathcal{H})\mathbf{r}}, \tag{6.21}$$

where $\lambda_\varepsilon \equiv \lambda \quad i\varepsilon$ with $\varepsilon > 0$. Note that the negative imaginary part of λ_ε ensures the convergence of the integral in Eq. (6.21). The expectation value of the logarithm can then be handled by using the replica trick [51]

$$\langle \ln \mathcal{Z}(\lambda)\rangle = \lim_{n\to 0} \frac{1}{n} \ln \langle \mathcal{Z}^n(\lambda)\rangle\,, \tag{6.22}$$

which allows us to trade the *quenched* average on the left-hand-side for the *annealed* average on the right-hand-side. The latter can be evaluated by standard methods (see Appendix F.3) to give

$$\langle \mathcal{Z}^n(\lambda)\rangle \propto \int \mathcal{D}\mu \mathcal{D}\hat{\mu} e^{N\mathcal{S}_n[\mu,\hat{\mu};\lambda]}, \tag{6.23}$$

where the proportionality holds up to an irrelevant numerical constant, and where we introduced the action

$$\begin{aligned} \mathcal{S}_n[\mu,\hat{\mu};\lambda] \equiv \quad & i\int \mathrm{d}\vec{y}\, \mu(\vec{y})\hat{\mu}(\vec{y}) \quad \frac{\eta}{2}\int \mathrm{d}\vec{y}\, \mathrm{d}\vec{w}\, \mu(\vec{y})\mu(\vec{w}) \quad \vec{y}\cdot\vec{w})^2 \\ & + \ln \int \mathrm{d}\vec{y} \int \mathrm{d}a\, p_a(a) \exp\left[\quad \frac{i}{2}(\lambda \quad a)|\vec{y}|^2 + i\hat{\mu}(\vec{y}) \right]. \end{aligned} \tag{6.24}$$

The parameter η is defined in Eq. (6.3), while $\vec{y}, \vec{w}$ are n-dimensional vectors (one component for each of the replicas).

The strategy to obtain the finite-N averaged $\rho(\lambda)$ is the following:

1. For large N, we look for a saddle-point estimate of the path integral in Eq. (6.23) in the form

   $$\langle \mathcal{Z}^n(\lambda)\rangle \propto e^{N\mathcal{S}_n[\mu^*,\hat{\mu}^*;\lambda]+O(1)}, \tag{6.25}$$

   where the proportionality holds up to a λ-independent (even though possibly N-dependent) prefactor.

2. Using Eq. (6.20), we recover the spectral density via

$$\rho(\lambda) \simeq \frac{2}{\pi}\lim_{\varepsilon\to 0^+}\mathrm{Im}\lim_{n\to 0}\frac{1}{n}\frac{\mathrm{d}}{\mathrm{d}\lambda}\mathcal{S}_n[\mu^*,\hat{\mu}^*;\lambda_\varepsilon] \tag{6.26}$$
$$= \frac{1}{\pi}\lim_{\varepsilon\to 0^+}\mathrm{Im}\left\{\lim_{n\to 0}\frac{i}{n}\frac{\int \mathrm{d}\vec{y}\,|\vec{y}|^2\int \mathrm{d}a\,p_a(a)\exp\left[\ \frac{i}{2}(\lambda_\varepsilon\quad a)|\vec{y}|^2+i\hat{\mu}^*(\vec{y})\right]}{\int \mathrm{d}\vec{y}\int \mathrm{d}a\,p_a(a)\exp\left[\ \frac{i}{2}(\lambda_\varepsilon\quad a)|\vec{y}|^2+i\hat{\mu}^*(\vec{y})\right]}\right\}.$$

Indeed, only the third term in the action of Eq. (6.24) will contribute, because the dependence on λ in the first two terms is only implicit,

$$\frac{\mathrm{d}}{\mathrm{d}\lambda}\mathcal{S}_n[\mu,\hat{\mu};\lambda_\varepsilon] = \partial_\lambda\mathcal{S}_n + \int \mathrm{d}\vec{y}\left[\frac{\delta\mathcal{S}_n}{\delta\mu(\vec{y})}\frac{\mathrm{d}\mu(\vec{y})}{\mathrm{d}\lambda}+\frac{\delta\mathcal{S}_n}{\delta\hat{\mu}(\vec{y})}\frac{\mathrm{d}\hat{\mu}(\vec{y})}{\mathrm{d}\lambda}\right], \tag{6.27}$$

and the term under the integral vanishes at the saddle-point (where the action is stationary by construction). In turn this implies that, to compute $\rho(\lambda)$ from Eq. (6.26), we do not need to determine $\mu^*(\vec{y})$, but only $\hat{\mu}^*(\vec{y})$. Finally, by the $\simeq$ symbol in Eq. (6.26) we mean that the corrections are *at most* of $O(1/N)$.

6.2.1 Saddle-point equations and rotationally-invariant Ansatz

The leading contribution to Eq. (6.23) for large N can be found by minimizing the action in Eq. (6.24). Omitting (to ease the notations) the superscript $*$ from $\mu^*(\vec{y})$ and $\hat{\mu}^*(\vec{y})$, and understanding the dependencies on λ as computed in correspondence of λ_ε, the saddle-point equations read

$$0 \equiv \frac{\delta\mathcal{S}_n}{\delta\mu(\vec{x})} = i\hat{\mu}(\vec{x}) \quad \eta\int \mathrm{d}\vec{w}\,\mu(\vec{w})\ \ \vec{x}\cdot\vec{w}\big)^2, \tag{6.28}$$

$$0 \equiv \frac{\delta\mathcal{S}_n}{\delta\hat{\mu}(\vec{x})} = i\mu(\vec{x}) + i\frac{\int \mathrm{d}a\,p_a(a)\exp\left[\ \frac{i}{2}(\lambda\quad a)|\vec{x}|^2+i\hat{\mu}(\vec{x})\right]}{\int \mathrm{d}\vec{y}\int \mathrm{d}a\,p_a(a)\exp\left[\ \frac{i}{2}(\lambda\quad a)|\vec{y}|^2+i\hat{\mu}(\vec{y})\right]}. \tag{6.29}$$

Substituting the expression for $\mu(\vec{x})$ obtained from the second equation (6.29) in the first one (6.28), one obtains a closed equation for $\hat{\mu}(\vec{x})$ which reads

$$\hat{\mu}(\vec{x}) = i\eta\frac{\int \mathrm{d}\vec{y}\int \mathrm{d}a\,p_a(a)\exp\left[\ \frac{i}{2}(\lambda\quad a)|\vec{y}|^2+i\hat{\mu}(\vec{y})\right]\ \ \vec{x}\cdot\vec{y}\big)^2}{\int \mathrm{d}\vec{y}\int \mathrm{d}a\,p_a(a)\exp\left[\ \frac{i}{2}(\lambda\quad a)|\vec{y}|^2+i\hat{\mu}(\vec{y})\right]}. \tag{6.30}$$

To make progress, we plug in the Ansatz $\hat{\mu}(\vec{x}) = \hat{\mu}(x)$, with $x \equiv |\vec{x}|$, which is rotationally symmetric in the space of replicas (i.e., it is invariant under $O(n)$ transformations). Note that requiring invariance under $O(n)$ is a stronger request than the mere replica-symmetry (RS): indeed, the exchange between any pair of components of $\vec{x}$ can be obtained by means of a $O(n)$ transformation[2]. Stepping to spherical coordinates and using the identity

$$\int \mathrm{d}\Omega_n\ \ \vec{x}\cdot\vec{y}\big)^2 = \frac{(xy)^2}{n}\int \mathrm{d}\Omega_n\,, \tag{6.31}$$

[2] In the literature, multifractality has sometimes been associated with the breaking of replica-symmetry [275]. As we stressed in Section 6.1.1, the intermediate phase of the GRP model is *fractal*, but not *multifractal* [226]: it is then natural to look for, and remain with, a replica-symmetric solution, as we do here.

where $\mathrm{d}\Omega_n$ is the differential of the n-dimensional solid angle around $\vec{y}$, we find

$$\hat{\mu}(x) = i\frac{\eta}{n}\frac{\int_0^\infty \mathrm{d}y\, y^{n-1}\int \mathrm{d}a\, p_a(a)\exp\left[\frac{i}{2}(\lambda - a)y^2 + i\hat{\mu}(y)\right](xy)^2}{\int_0^\infty \mathrm{d}y\, y^{n-1}\int \mathrm{d}a\, p_a(a)\exp\left[\frac{i}{2}(\lambda - a)y^2 + i\hat{\mu}(y)\right]}. \tag{6.32}$$

Let us now introduce the auxiliary function

$$G(y;\lambda) \equiv \int \mathrm{d}a\, p_a(a)\exp\left[\frac{i}{2}(\lambda - a)y^2 + i\hat{\mu}(y)\right] = \exp\left[\frac{i}{2}\lambda y^2 + i\hat{\mu}(y)\right]\psi_a(-y^2/2), \tag{6.33}$$

where in the second equality we recognized the characteristic function of $p_a(a)$ (i.e., its Fourier transform), namely

$$\psi_a(k) = \int \mathrm{d}a\, p_a(a)e^{-ika}. \tag{6.34}$$

Equation (6.32) can readily be expressed in terms of $G(y;\lambda)$. We then integrate by parts in the denominator of Eq. (6.32), finding that boundary terms disappear at least as long as $\varepsilon > 0$ in $G(y;\lambda_\varepsilon)$ — we will check *a posteriori* that the presence of $\hat{\mu}(y)$ does not spoil the convergence. We thus get

$$\hat{\mu}(x) = -i\eta x^2\frac{\int_0^\infty \mathrm{d}y\, y^{n+1}G(y;\lambda)}{\int_0^\infty \mathrm{d}y\, y^n G'(y;\lambda)}, \tag{6.35}$$

where $G'(y;\lambda) = \partial_y G(y;\lambda)$. We can now take the limit $n \to 0$, which yields

$$i\hat{\mu}(x) = x^2\eta\frac{\int_0^\infty \mathrm{d}y\, yG(y;\lambda)}{\int_0^\infty \mathrm{d}y\, G'(y;\lambda)} \equiv x^2 C(\lambda). \tag{6.36}$$

The function $C(\lambda)$ must now be determined self-consistently via

$$C(\lambda) = \eta\frac{\int_0^\infty \mathrm{d}y\, yG(y;\lambda)}{\int_0^\infty \mathrm{d}y\, G'(y;\lambda)}, \tag{6.37}$$

where $G(y;\lambda)$ can be read from Eq. (6.33) upon setting $i\hat{\mu}(y) = y^2 C(\lambda)$.

6.2.2 General result

We now repeat the same steps at the level of the saddle-point action in Eq. (6.26): we plug in the rotationally symmetric Ansatz, we integrate by parts in the denominator and we finally take the limit $n \to 0$. This gives

$$\rho(\lambda) = \frac{1}{\pi}\lim_{\varepsilon\to 0^+}\mathrm{Re}\,\frac{\int_0^\infty \mathrm{d}y\, yG(y;\lambda_\varepsilon)}{\int_0^\infty \mathrm{d}y\, G'(y;\lambda_\varepsilon)} + O(1/N) = \frac{1}{\pi\eta}\lim_{\varepsilon\to 0^+}\mathrm{Re}\, C(\lambda_\varepsilon) + O(1/N). \tag{6.38}$$

We then go back to Eq. (6.37), which contains an exact differential in its denominator. If $\mathrm{Re}\, C(\lambda_\varepsilon) \leq 0$, then $G(y\to\infty;\lambda_\varepsilon) = 0$ and $G(0;\lambda_\varepsilon) = 1$, and we obtain a self-consistency equation for $C(\lambda_\varepsilon)$,

$$C(\lambda) = \eta\int_0^\infty \mathrm{d}\,\psi_a(-)e^{i\lambda+2C(\lambda)}, \tag{6.39}$$

where we recall that $\psi_a(x)$ is the characteristic function associated with $p_a(a)$ (see Eq. (6.34)). This determines $C(\lambda)$ implicitly. Equations (6.38) and (6.39) represent the main result of this section.

In Section 2.2.1 of Ref. [198] we check that, in the limit in which only the matrix A or B are retained in Eq. (6.1), Eq. (6.38) correctly returns $p_a(\lambda)$ or $\rho_{\mathrm{GOE}}(\lambda)$, respectively, with

$$\rho_{\mathrm{GOE}}(\lambda) = \frac{\sqrt{2 \quad \lambda^2}}{\pi} \Theta(\sqrt{2} \quad |\lambda|). \tag{6.40}$$

6.2.3 Resolvent formulation and connection with the Zee formula

One can observe that, under the same convergence hypotheses as above, the self-consistency equation (6.39) that determines $C(\lambda)$ can be rewritten as

$$C(\lambda) = i\eta \mathcal{G}_a \left[\lambda + 2iC(\lambda)\right], \tag{6.41}$$

where

$$\mathcal{G}_a(\ ) = \int \mathrm{d}a \, \frac{p_a(a)}{a} \tag{6.42}$$

is the resolvent (or Cauchy-Stieltjes transform) of the distribution $p_a(a)$. The resolvent can be inverted to give back

$$p_a(x) = \frac{1}{\pi} \lim_{\varepsilon \to 0^+} \mathrm{Im}\, \mathcal{G}_a(x \quad i\varepsilon), \tag{6.43}$$

which can be easily proved by using the Plemelj-Sokhotski formula in Eq. (6.18).

By comparing Eq. (6.43) with Eq. (6.38), one immediately realizes that our function $C(\lambda)$ is nothing but

$$C(\lambda) = i\eta \mathcal{G}(\lambda) + O(1/N), \tag{6.44}$$

where we denoted by $\mathcal{G}(\lambda)$ the resolvent of the spectral density $\rho(\lambda)$ of our model. Choosing $\gamma = 1$ (so that η in Eq. (6.3) becomes N-independent) and taking the limit $N \to \infty$, the correction in Eq. (6.44) vanishes, and Eq. (6.41) takes the form

$$\mathcal{G}(\lambda_\varepsilon) = \mathcal{G}_a(\lambda_\varepsilon \quad 2\eta \mathcal{G}(\lambda_\varepsilon)). \tag{6.45}$$

This is analogous to Eq. (148) in Ref. [240], which was derived in the case in which the matrix B belongs to the GUE (and not the GOE) ensemble, and it is consistent with the results of Ref. [242]. Moreover, in Appendix F.4 we show how Eq. (6.45) can be recovered by direct application of the Zee formula for the addition of two random matrices derived in Ref. [269].

One may legitimately wonder, at this point, whether our calculation is solely another way of obtaining Zee's result [269] for the particular case in which one of the two matrices being summed is a GOE matrix. In Section 6.2.4 we will analyze a few cases in which the self-consistency equation (6.39) (or (6.41)) can be solved exactly, so that from Eq. (6.38) one can find an expression for $\rho(\lambda)$ which is correct, up to $O(1/N)$, for any value of η. These cases are in fact the very same that could be cracked by applying the Zee formula to the deformed GOE matrix. The advantage of our framework is that, whenever η is N-dependent and decays slower than $1/N$

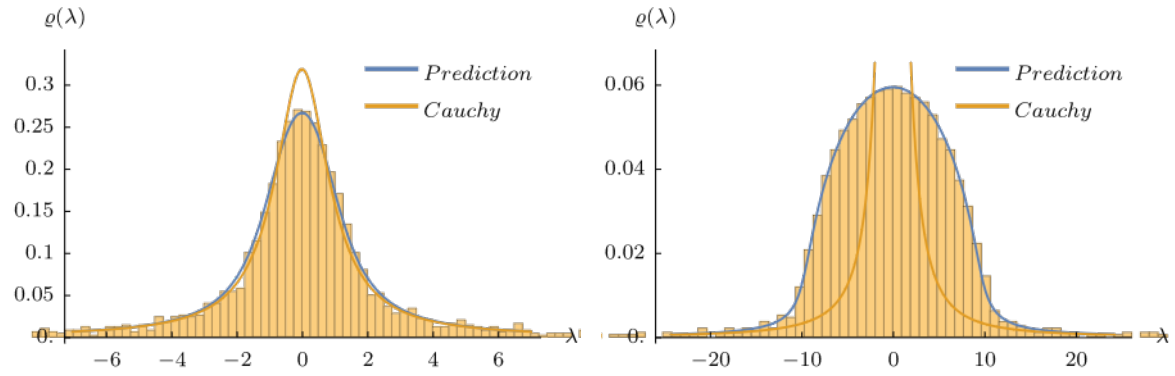

(a) (b)

Figure 6.2: Distribution of the eigenvalues $\rho(\lambda)$ in the case in which $p_a(a)$ is the Cauchy distribution (see Section 6.2.4.1). We show a numerical check of Eq. (6.48) in the regime of (a) small η (here $\eta = 0.12$) and (b) large η (here $\eta = 11.7$). The histogram was built using $\mu = 0$, $\omega = 1$, $\gamma = 1.1$ and $N = 2000$, with $\nu = 1$ in (a) and $\nu = 10$ in (b).

(as it happens, for instance, in Eq. (6.3) for $1 < \gamma < 2$), then we are still able to keep track of the finite-N corrections. Moreover, in Section 2.5 of Ref. [198] we provide approximate solutions which can be used whenever the resolvent $\mathcal{G}_a$ is not available in closed form, so that the Zee route is not viable.

6.2.4 Exactly solvable cases

In some particular cases, the self-consistency equation (6.39) admits an analytic solution, and we can access the limiting distribution $\rho(\lambda)$ for any value of η (i.e., not necessarily small). This happens whenever the following conditions are met:

(i) the resolvent $\mathcal{G}_a(\ )$ associated with $p_a(a)$ is known analytically, and

(ii) the self-consistency equation for $C(\lambda)$ resulting from Eq. (6.39) or Eq. (6.41) is not transcendental, so that we can solve for $C(\lambda)$.

Below we present two such examples, which will also prove useful in our discussion of the level compressibility presented later in Section 6.3.4.

6.2.4.1 Cauchy distributed a_i

Let us choose $p_a(a)$ to be a Lorentzian of width ω and centered at μ,

$$p_a(a) = \frac{1}{\pi\omega}\left[\frac{\omega^2}{(a \quad \mu)^2 + \omega^2}\right]. \tag{6.46}$$

Its characteristic function is an exponential, $\psi_a(\ ) = \exp(\ i\mu \quad \omega|\ |)$, and then by using Eq. (6.39) we can compute $C(\lambda)$ in closed form:

$$C(\lambda) = \frac{1}{4}\left\{\omega + i(\lambda \quad \mu) \pm \sqrt{[\omega + i(\lambda \quad \mu)]^2 + 8\eta}\right\}. \tag{6.47}$$

We choose the branch with the minus sign for which $\mathrm{Re}\, C(\lambda) \leq \omega/2$; using Eq. (6.38) yields

$$\rho(\lambda) = \frac{\omega \left\{4\omega^2(\lambda - \mu)^2 + \left[8\eta + \omega^2 - (\lambda - \mu)^2\right]^2\right\}^{1/4} \cos(\theta_\lambda/2)}{4\pi\eta} + O(1/N), \tag{6.48}$$

with $\theta_\lambda \equiv 2\{[\omega + i(\lambda - \mu)]^2 + 8\eta\}$. In Fig. 6.2a we plot Eq. (6.48) against numerical results in the small-η region: we find a good agreement with the theoretical prediction, as well as visible departures from the Cauchy distribution, especially in the bulk.

Another interesting limit is the one of large η, i.e., $\gamma = 1$ and ν large. It has been shown in Ref. [240] that, whenever $p_a(a)$ is rapidly decaying close to the edge of its finite support, then the spectral density $\rho(\lambda)$ interpolates between $p_a(a)$ and $\rho_{\mathrm{GOE}}(\lambda)$ as the value of ν is increased. Note, however, that in the present case $p_a(a)$ decays algebraically and its support is not compact, so the outcome is less clear. The correct way of taking this limit is to rescale the eigenvalues as $\kappa \equiv \lambda/\sqrt{4\eta}$ and look for the distribution $\rho_\kappa(\kappa) = \sqrt{4\eta}\rho(\sqrt{4\eta}\kappa)$. From Eq. (6.47) we see that, if $\eta \gg \omega, \mu$, then

$$C(\sqrt{4\eta}\kappa) = \frac{\sqrt{\eta}}{2}\left[i\kappa - \sqrt{2 - \kappa^2}\right] + O\left(\eta^0, 1/N\right), \tag{6.49}$$

and for large N we get from Eq. (6.38) that $\rho_\kappa(\kappa) \to \rho_{\mathrm{GOE}}(\kappa)$ (see Eq. (6.40)). For large but finite η and $N \to \infty$, on the other hand, the bulk distribution of κ looks like a semicircle (as in the GOE ensemble), but with fat tails whose width grows with ω (see Fig. 6.3a). Moreover, the whole distribution shifts rigidly by changing its center $\mu/\sqrt{4\eta}$. Numerical results in the large-η region are again nicely reproduced by Eq. (6.48), as shown in Fig. 6.2b.

Note that one can equivalently get to Eq. (6.47) by first computing the resolvent associated with the Lorentzian distribution in Eq. (6.46), i.e.,

$$\mathcal{G}_{\mathrm{Cauchy}}(\lambda) = \frac{1}{\lambda - \mu \pm i\omega}, \tag{6.50}$$

where the $\pm$ branches correspond to $\mathrm{Im}\{\lambda\} > 0$ or $\mathrm{Im}\{\lambda\} < 0$, respectively. This can be obtained by explicitly performing the complex integral in Eq. (6.42), which only entails simple poles for a Cauchy distribution. One can then easily solve the self-consistency equation (6.41), which turns out to be quadratic, and thus recover Eq. (6.47).

6.2.4.2 Wigner distributed a_i

Another simple case is the one in which $p_a(a)$ is chosen as the (μ-centered) Wigner distribution

$$p_a(a) \equiv \frac{2}{\pi\sigma^2}\sqrt{\sigma^2 - (a - \mu)^2}, \tag{6.51}$$

whose corresponding resolvent is

$$\mathcal{G}_a(\lambda) = \frac{2}{\sigma^2}\left[\lambda - \mu - \sqrt{(\lambda - \mu)^2 - \sigma^2}\right]. \tag{6.52}$$

The self-consistency equation (6.41) is again quadratic and it yields

$$C(\lambda) = 2\eta\frac{i(\lambda - \mu) \pm \sqrt{\sigma^2 + 8\eta - (\lambda - \mu)^2}}{\sigma^2 + 8\eta}, \tag{6.53}$$

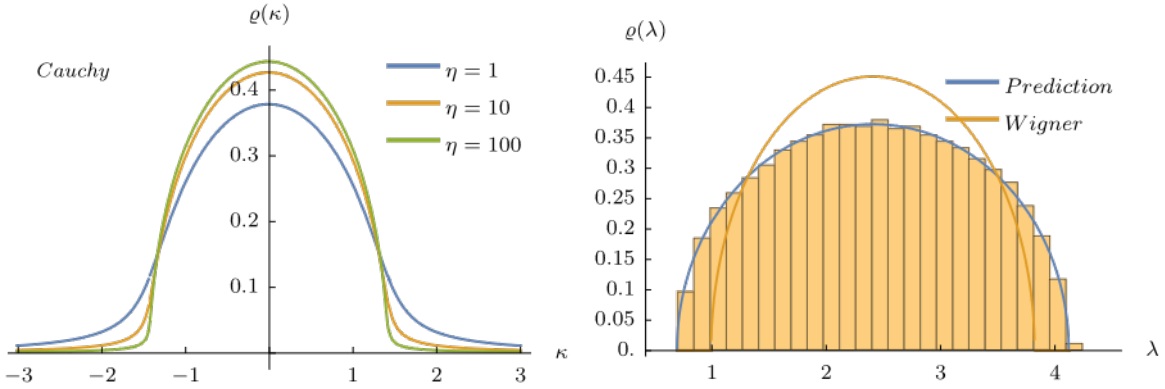

(a) (b)

Figure 6.3: (a) Limiting distribution of the rescaled eigenvalues $\kappa = \lambda/\sqrt{4\eta}$, with $\rho(\lambda)$ given in Eq. (6.48) for the Cauchy case (see Section 6.2.4.1). In this plot we used $\mu = 0$ and $\omega = 0.5$. (b) Distribution of the eigenvalues $\rho(\lambda)$ in the case in which $p_a(a)$ is the Wigner semicircle distribution (see Section 6.2.4.2), and numerical check of the prediction in Eq. (6.54). The histogram was built using $\sigma = \sqrt{2}$, $\mu = 1 + \sqrt{2}$, $\nu = 1$, $\gamma = 1.1$ and $N = 2000$.

so that by choosing the branch with the minus sign and using Eq. (6.38) we find

$$\rho(\lambda) = \frac{2\sqrt{\sigma^2 + 8\eta \quad (\lambda \quad \mu)^2}}{\pi(\sigma^2 + 8\eta)} \Theta\left(\sigma^2 + 8\eta \quad (\lambda \quad \mu)^2\right) + O(1/N). \tag{6.54}$$

As expected, this is still a Wigner distribution centered in $\lambda = \mu$, but its width gets corrected as $\sigma^2 \to \sigma^2 + 8\eta$.

6.3 Number of eigenvalues in an interval and level compressibility

In this Section we consider the number of eigenvalues $I_N[\ \ , \beta]$ in a finite interval $[\ \ , \beta]$, as given by Eq. (6.12), and compute its cumulant generating function. This, in turn, can be used to access the level compressibility $\chi(E)$ defined in Eq. (6.13). As we explained in the Introduction, $\chi(E)$ represents a simple measure of the rigidity of the spectrum, which in turn allows us to distinguish between the phases of the model.

This program can be achieved by following the replica-based procedure introduced and exploited in Refs. [276, 277], which we briefly outline here. Starting from the definition of the spectral density in Eq. (6.11), we first rewrite Eq. (6.12) as

$$I_N[\ \ , \beta] = \sum_{i=1}^{N} [\Theta(\beta \quad \lambda_i) \quad \Theta(\quad \lambda_i)] \,. \tag{6.55}$$

Now we recall that the Heaviside function can be represented in terms of the discontinuity of the complex logarithm,

$$\Theta(\ \ x) = \frac{1}{2\pi i} \lim_{\varepsilon \to 0^+} [\ln(x + i\varepsilon) \quad \ln(x \quad i\varepsilon)] \,, \tag{6.56}$$

so that we interpret

$$\sum_{i=1}^{N} \Theta(\quad \lambda_i) = \frac{1}{2\pi i} \lim_{\varepsilon \to 0^+} [\ln \det(\mathcal{H} \quad _\varepsilon) \quad \ln \det(\mathcal{H} \quad ^*_\varepsilon)] \,, \tag{6.57}$$

where we called as before $_\varepsilon \equiv \quad i\varepsilon$ with $\varepsilon > 0$. This allows us to express $I_N[\ ,\beta]$ in terms of the partition function given in Eq. (6.21), which leads to[3]

$$I_N[\ ,\beta] = \frac{1}{\pi i} \lim_{\varepsilon \to 0^+} \ln \left[\frac{\mathcal{Z}(\beta_\varepsilon)\mathcal{Z}(\ ^*_\varepsilon)}{\mathcal{Z}(\beta^*_\varepsilon)\mathcal{Z}(\ _\varepsilon)} \right] . \tag{6.58}$$

In order to compute the moments of I_N, we first address its cumulant generating function

$$\mathcal{F}_{[\ ,\beta]}(s) \equiv \frac{1}{N} \ln \left\langle e^{\ sI_N[\ ,\beta]} \right\rangle = \frac{1}{N} \ln \langle e^{\frac{s}{\pi i} \lim_{\varepsilon \to 0^+} \ln\{\mathcal{Z}(\beta_\epsilon)\mathcal{Z}(\ ^*_\epsilon)[\mathcal{Z}(\beta^*_\epsilon)\mathcal{Z}(\ _\epsilon)]^{\ 1}\}} \rangle \,. \tag{6.59}$$

Assuming now that one can move the limit $\varepsilon \to 0^+$ at the front of this expression, we obtain

$$\mathcal{F}_{[\ ,\beta]}(s) = \lim_{\varepsilon \to 0^+} \frac{1}{N} \ln Q_{[\ ,\beta]}(s), \tag{6.60}$$

where we introduced

$$Q_{[\ ,\beta]}(s) \equiv \left\langle [\mathcal{Z}(\beta^*_\varepsilon)\mathcal{Z}(\ _\varepsilon)]^{is/\pi} \, [\mathcal{Z}(\beta_\varepsilon)\mathcal{Z}(\ ^*_\varepsilon)]^{\ is/\pi} \right\rangle . \tag{6.61}$$

The latter can be accessed by first evaluating

$$Q_{[\ ,\beta]}(n_\pm) \equiv \left\langle [\mathcal{Z}(\beta^*_\varepsilon)\mathcal{Z}(\ _\varepsilon)]^{n_+} \, [\mathcal{Z}(\beta_\varepsilon)\mathcal{Z}(\ ^*_\varepsilon)]^{n_-} \right\rangle \tag{6.62}$$

within the replica formalism with $n_\pm$ integer, and then performing its analytic continuation

$$Q_{[\ ,\beta]}(s) = \lim_{n_\pm \to \pm is/\pi} Q_{[\ ,\beta]}(n_\pm). \tag{6.63}$$

To obtain the level compressibility in Eq. (6.13), we finally compute the cumulants

$$\frac{\kappa_j[\ ,\beta]}{N} = (\ \ 1)^j \, \partial_s^j \mathcal{F}_{[\ ,\beta]}(s)\Big|_{s=0} \,, \tag{6.64}$$

and we evaluate them at $\quad = \quad E, \beta = E$.

We remark that the average spectral density $\rho(E)$ is formally proportional to the derivative with respect to E of the first cumulant $\kappa_1(E) = \langle \mathcal{I}[\ \ E, E] \rangle$ (see Eq. (6.12)), thus providing an alternative way to compute $\rho(E)$ which does not rely on the Edwards-Jones formula in Eq. (6.20).

[3] It should be noted that Eq. (6.58) was obtained by naively adopting the identity $\ln(ab) = \ln a + \ln b$, which is however not satisfied in general by the complex logarithm (whose principal branch is bounded within $(\ \ \pi, \pi]$ — see Ref. [278]). As a result, the right-hand-side of Eq. (6.58) is not extensive, and thus seemingly unfit to count the number of eigenvalues in an interval for a single realization of $\mathcal{H}$ [277]. The introduction of replicas (see Eq. (6.62) and Appendix F.5.1) is essential in order to restore the extensivity of the ensemble-averaged moments of $\mathcal{I}_N$. This remarkable fact was dubbed *folding-unfolding mechanism* in Ref. [279].

6.3.1 Replica action and saddle-point equations

The details of this derivation are reported in Appendix F.5.1. In analogy with Section 6.2, here we express

$$Q_{[\ \ ,\beta]}(n_\pm) \propto \int \mathcal{D}(i\varphi) \exp\{N \mathcal{S}_{n_\pm}[\varphi; \hat{\Lambda}]\}, \tag{6.65}$$

$$\mathcal{S}_{n_\pm}[\varphi; \hat{\Lambda}] \equiv \frac{1}{2\eta} \int \mathrm{d}\vec{\tau}\, \mathrm{d}\vec{\tau}'\, \varphi(\vec{\tau}) M(\vec{\tau}, \vec{\tau}') \varphi(\vec{\tau}') + \ln \int \mathrm{d}\vec{\tau} \exp\left[\frac{i}{2} \vec{\tau} \hat{\Lambda}\, \vec{\tau} \int \mathrm{d}\vec{\tau}'\, M(\vec{\tau}, \vec{\tau}') \varphi(\vec{\tau}') \right] \psi_a \left(\frac{1}{2} \vec{\tau} \hat{L} \vec{\tau} \right), \tag{6.66}$$

where the replica vectors $\vec{\tau} \in \mathbb{R}^n$ live in dimension $n = 2(n_+ + n\ \ )$. Each of the four replica sets corresponds to one sector in the block matrices

$$\hat{\Lambda} \equiv \begin{pmatrix} \varepsilon\ \ n_+ & & & \\ & \bar{\beta}_\varepsilon\ \ n_+ & & \\ & & \beta_{\varepsilon\ \ n} & \\ & & & \bar{}_{\varepsilon\ \ n} \end{pmatrix}, \qquad \hat{L} \equiv \begin{pmatrix} n_+ & & & \\ & n_+ & & \\ & & n & \\ & & & n \end{pmatrix}, \tag{6.67}$$

where we called $\bar{}_\varepsilon = \ \ ^*_\varepsilon$, and similarly for $\bar{\beta}_\epsilon$. Finally, in Eq. (6.66) we introduced

$$M(\vec{\tau}, \vec{\tau}') \equiv \left(\vec{\tau} \hat{L} \vec{\tau}' \right)^2, \tag{6.68}$$

while we recall that $\psi_a(\ \ )$ was given in (6.34). Next, we need to compute the functional integration over $\mathcal{D}(i\varphi)$ in Eq. (6.65) in the limit of large N. From Eq. (6.66), the saddle-point equation follows simply as

$$\varphi_0(\vec{\tau}) = \frac{\eta}{Z_\varphi} \exp\left[\frac{i}{2} \vec{\tau} \hat{\Lambda}\, \vec{\tau} \int \mathrm{d}\vec{\tau}'\, M(\vec{\tau}, \vec{\tau}') \varphi_0(\vec{\tau}') \right] \psi_a \left(\frac{1}{2} \vec{\tau} \hat{L} \vec{\tau} \right), \tag{6.69}$$

with

$$Z_\varphi \equiv \int \mathrm{d}\vec{\tau} \exp\left[\frac{i}{2} \vec{\tau} \hat{\Lambda}\, \vec{\tau} \int \mathrm{d}\vec{\tau}'\, M(\vec{\tau}, \vec{\tau}') \varphi_0(\vec{\tau}') \right] \psi_a \left(\frac{1}{2} \vec{\tau} \hat{L} \vec{\tau} \right). \tag{6.70}$$

In order to better quantify the finite-size corrections and to make contact with the calculation performed in Ref. [277] for the pure GOE case, in Appendix F.5.2 we also compute the Gaussian fluctuations around the saddle-point $\varphi_0(\vec{\tau})$, leading to

$$Q_{[\ \ ,\beta]}(n_\pm) = \exp\left\{ N \mathcal{S}_{n_\pm}[\varphi_0; \hat{\Lambda}] + \frac{1}{2} \sum_{k=1}^{\infty} \frac{(\ \ 1)^k}{k} \operatorname{Tr} T^k \right\} + \mathcal{O}\left(1/N^2\right), \tag{6.71}$$

with

$$T(\vec{\tau}_1, \vec{\tau}_2) \equiv \varphi_0(\vec{\tau}_1) \left[M(\vec{\tau}_1, \vec{\tau}_2) \quad \frac{1}{\eta} \int \mathrm{d}\vec{\tau}'\, M(\vec{\tau}_2, \vec{\tau}') \varphi_0(\vec{\tau}') \right]. \tag{6.72}$$

Note that $\varphi_0(\vec{\tau}) \sim \mathcal{O}(\eta)$ (see Eq. (6.69)), so that the function $T(\vec{\tau}_1, \vec{\tau}_2)$ itself is also of $\mathcal{O}(\eta)$.

6.3.2 Rotationally-invariant Ansatz

In the pure GOE case (which is recovered, for instance, by setting $\psi_a(\ ) = 1$ identically in the expressions above), the saddle-point equation (6.69) suggests to look for a replica-symmetric solution in the form of a Gaussian, i.e.,

$$\varphi_0(\vec{\tau}) = \mathcal{N} \exp\left(\ \frac{1}{2}\vec{\tau}\hat{C}^{\ -1}\vec{\tau}\right), \tag{6.73}$$

where $\hat{C}$ is another block-diagonal matrix of the form

$$\hat{C} \equiv \begin{pmatrix} \Delta & n_+ & & & & & \\ & & \bar{\Delta}_\beta & n_+ & & & \\ & & & & \Delta_\beta & n & \\ & & & & & & \bar{\Delta} \quad n \end{pmatrix}. \tag{6.74}$$

The parameters Δ , $\bar{\Delta}$, Δ_β and $\bar{\Delta}_\beta$ are to be fixed, together with the prefactor $\mathcal{N}$ in Eq. (6.73), by substituting the Ansatz in Eq. (6.73) back into the saddle-point equation (6.69).

This strategy has proven effective in Ref. [277] and, for completeness, in Appendix F.6 we sketch the entire calculation for the GOE case. However, in the presence of a nontrivial $\psi_a(\ )$ in Eq. (6.69), there is no reason why the Ansatz in Eq. (6.73) should work: the structure of Eq. (6.69) suggests instead to extend it to the form

$$\varphi_0(\vec{\tau}) = \mathcal{N} \exp\left(\ \frac{1}{2}\vec{\tau}\hat{C}^{\ -1}\vec{\tau}\right)\psi_a\left(\ \frac{1}{2}\vec{\tau}\hat{L}\vec{\tau}\right). \tag{6.75}$$

This can be plugged into Eq. (6.69) to first obtain $\mathcal{N} = \eta/Z_\varphi$, where $Z_\varphi = \int \mathrm{d}\vec{\tau}\, \varphi_0(\vec{\tau})$. By using Gaussian integration one can then show that

$$\int \mathrm{d}\vec{\tau}'\, M(\vec{\tau}, \vec{\tau}')\varphi_0(\vec{\tau}') = \eta\vec{\tau}\hat{K}\vec{\tau}, \tag{6.76}$$

where $\hat{K}$ is a diagonal matrix given by

$$\hat{K} = \ i\hat{L}\mathcal{G}_a\left((i\hat{L}\hat{C})^{\ -1}\right), \tag{6.77}$$

$\mathcal{G}_a$ is the resolvent in Eq. (6.42), and $\hat{L}$ is given in Eq. (6.67). The remaining free parameters in Eq. (6.73) can be determined by solving the set of four self-consistency equations that follow from Eq. (6.69), i.e.,

$$\hat{C}^{\ -1} = 2\eta\hat{K} + i\hat{\Lambda}. \tag{6.78}$$

Finally, both the action and its Gaussian fluctuation matrix T (see Eq. (6.72)) can be computed by using the saddle-point solution in Eq. (6.75). First, notice that the action in Eq. (6.66) takes the form

$$\begin{aligned} \mathcal{S}_{n_\pm}[\varphi_0; \hat{\Lambda}] &= \frac{1}{2}\int \mathrm{d}\vec{\tau}\left(\vec{\tau}\hat{K}\vec{\tau}\right)\varphi_0(\vec{\tau}) + \ln Z_\varphi \\ &= \frac{\eta}{2}\sum_i K_{ii}^2 + \ln\int_\infty^\infty \mathrm{d}a\, p_a(a) \exp\left\{ \ \frac{1}{2}\,\mathrm{Tr}\ln[(i\hat{L}\hat{C})^{\ -1} \quad a]\right\} + \text{const.}. \end{aligned} \tag{6.79}$$

The constant term vanishes upon taking the analytic continuation $n_\pm \to \pm is/\pi$, yielding

$$\mathcal{S}_{\pm\frac{is}{\pi}}[\varphi_0;\hat{\Lambda}] = \frac{is\eta}{2\pi}\left(k^2 + \bar{k}_\beta^2 \quad k_\beta^2 \quad \bar{k}^2\right) + \ln\int_\infty^\infty \mathrm{d}a\, p_a(a)\exp\left\{\frac{is}{2\pi}\ln\left[\frac{(\bar{\Delta}_\beta{}^1 + ia)(\Delta^{\ 1} \quad ia)}{(\bar{\Delta}^{\ 1} + ia)(\Delta_\beta{}^1 \quad ia)}\right]\right\}, \tag{6.80}$$

where we introduced for brevity $\hat{K} \equiv \mathrm{diag}(k_{\quad n_+}, \bar{k}_{\beta\ n_+}, k_{\beta\ n}, \bar{k}_{\quad n})$. Note that this action coincides at leading order with the cumulant generating function in Eq. (6.60), i.e.,

$$\mathcal{F}_{[\ ,\beta]}(s) = \lim_{\varepsilon\to 0^+}\mathcal{S}_{\pm\frac{is}{\pi}}[\varphi_0;\hat{\Lambda}] + O(\eta/N), \tag{6.81}$$

where we used Eq. (6.71) (the estimate of the large-N correction will soon be justified). In the next Section we will make this result more explicit in the case of an interval that is symmetric around the origin.

The Gaussian fluctuations around the saddle-point are studied in Appendix F.5.2. A closed-form result is not available in this case (in contrast to the GOE case, see Appendix F.6), because the calculation involves increasingly complex generalizations of the resolvent $\mathcal{G}_a(\ )$ that encode higher order correlations (see Eq. (F.41)). However, we can show that the Gaussian fluctuations add to the leading order term in Eq. (6.81) a correction of $O(\eta/N) = O(N^{\ \gamma})$, which is strongly suppressed for large N in the region $\gamma > 1$ which we focus on here.

6.3.3 General result in the case of a symmetric interval

We consider now the simpler case in which $\quad = \quad E$ and $\beta = E$, and we take a symmetric distribution $p_a(a)$. From Eqs. (6.77) and (6.78) one can deduce that the entries of the matrix $\hat{C}$ are related by the following symmetries:

$$\Delta_{\ } \equiv \Delta \equiv re^{i\theta}, \qquad \bar{\Delta}_{\ } = \Delta^* = \Delta_\beta, \qquad \bar{\Delta}_\beta = \Delta_\beta^*. \tag{6.82}$$

The same holds for the entries of $\hat{K}$ (see Eq. (6.77)), hence we will simply call $k_{\ } \equiv k$. The problem is then reduced to computing one single unknown, namely Δ: from Eqs. (6.77) and (6.78), this amounts to solving the self-consistency equations

$$\begin{cases} \Delta^{\ 1} = \varepsilon \quad iE + 2\eta k, \\ k = \quad i\mathcal{G}_a\left(\ i\Delta^{\ 1}\right). \end{cases} \tag{6.83}$$

The action in Eq. (6.80) then takes the form

$$\mathcal{S}[\varphi_0;\hat{\Lambda}] = \quad \frac{2\eta s}{\pi}\,\mathrm{Im}\{k^2\} + \ln\int_\infty^\infty \mathrm{d}a\, p_a(a)\exp\left[\ \frac{s}{\pi}\arctan\left(\frac{\sin 2\theta}{a^2r^2 + \cos 2\theta}\right)\right], \tag{6.84}$$

where the branch of the arctan is chosen so that it returns an angle in $[0,\pi]$. From Eq. (6.60) we can then read the leading order contribution to the rate function, namely

$$\mathcal{F}_{[\ E,E]}(s) = \mathcal{S}[\varphi_0;\hat{\Lambda}] + O(\eta/N) = \quad ms + \ln\left\langle e^{\ sf(a)}\right\rangle_a + O(\eta/N). \tag{6.85}$$

Here we used the notation $\langle \bullet \rangle_a$ to indicate the average over $p_a(a)$, and we introduced

$$m \equiv \frac{2\eta}{\pi} \mathrm{Im}\{k^2\} = \frac{2\eta}{\pi} \mathrm{Im}\left[\mathcal{G}_a\left(i\Delta^{-1}\right)\right]^2, \tag{6.86}$$

$$f(a) \equiv \frac{1}{\pi} \arctan\left(\frac{\sin 2\theta}{a^2 r^2 + \cos 2\theta}\right) \in [0,1], \tag{6.87}$$

where in the first line we used Eq. (6.83). The cumulant generating function in Eq. (6.85), together with the self-consistency equations (6.83), represent our second main result. As we stressed above, when η is given by Eq. (6.3), the correction to Eq. (6.85) is of $O(\eta/N) = O(N^{-\gamma})$, which is strongly suppressed for large N in the region $\gamma > 1$.

Expanding Eq. (6.85) in powers of s we get

$$\mathcal{F}_{[E,E]}(s) \simeq s\left[m + \langle f(a)\rangle_a\right] + \frac{s^2}{2}\left[\left\langle f^2(a)\right\rangle_a - \langle f(a)\rangle_a^2\right] + O\left(s^3, \eta/N\right), \tag{6.88}$$

and by comparison with Eq. (6.64) we can identify the first two cumulants

$$\frac{\kappa_1}{N} = m + \langle f(a)\rangle_a + O(\eta/N), \qquad \frac{\kappa_2}{N} = \left\langle f^2(a)\right\rangle_a - \langle f(a)\rangle_a^2 + O(\eta/N). \tag{6.89}$$

From Eq. (6.13), we finally obtain the level compressibility

$$\chi(E) = \frac{\left\langle f^2(a)\right\rangle_a - \langle f(a)\rangle_a^2}{m + \langle f(a)\rangle_a} + O(\eta/N). \tag{6.90}$$

We remark that not only the level compressibility, but actually all the moments of $I_N[E,E]$ can be simply computed starting from Eq. (6.85): they read (at leading order for large N)

$$\langle (I_N[E,E])^m \rangle \simeq N \langle [f(a)]^m \rangle_a, \quad m \geq 2\,. \tag{6.91}$$

6.3.3.1 Limit of a pure diagonal matrix with random i.i.d. entries

It is instructive, at this point, to consider the limit $\eta \to 0$. In this case the GOE part of Eq. (6.1) is neglected, and the spectral properties are completely determined by the matrix A, whose entries are independent and identically distributed according to $p_a(a)$. The self-consistency equation (6.78) then reduces to

$$\hat{C} = (i\hat{\Lambda})^{-1}, \tag{6.92}$$

whence

$$\Delta = \Delta\Big|_{=E} = \frac{iE + \varepsilon}{E^2 + \varepsilon^2} \equiv r e^{i\theta}, \tag{6.93}$$

and there is no need to determine the entries of $\hat{K}$ since it does not enter the expression of the saddle-point action (6.84) for $\eta = 0$. From Eq. (6.84) we obtain, for $\varepsilon \to 0^+$,

$$\mathcal{S}[\varphi_0; \hat{\Lambda}] = \ln \int_{\infty}^{\infty} da\, p_a(a) \exp\left\{\frac{s}{\pi} \arctan\left[\frac{0^+}{(a/E)^2 - 1}\right]\right\} = \ln\left[1 + (e^{s} - 1)\int_E^E da\, p_a(a)\right], \tag{6.94}$$

where we used that the branch of arctan( ) $\in [0, \pi]$ has a discontinuity in = 0, i.e., it jumps from π to 0 as becomes positive. From Eqs. (6.12) and (6.85), we can then read out the cumulant generating function

$$\mathcal{F}_{[\ E,E]}(s) = \ln\left[1 + (e^{\ s} \quad 1)\frac{\langle I_N[\ E, E]\rangle_a}{N}\right]. \tag{6.95}$$

In this way we recover the standard textbook result for the cumulant generating function in the case of i.i.d. random variables, which we sketch for completeness in Appendix F.2. In particular, the level compressibility in Eq. (6.13) reads in this case

$$\chi(E) = 1 \quad \frac{\langle I_N[\ E, E]\rangle_a}{N}, \tag{6.96}$$

so that in general $\chi(E) \sim 1$ for small E, and $\chi(E) \to 0$ for large E. Finally, we note that Eq. (6.95) is exact, because we have stressed above that the Gaussian fluctuations around the saddle-point are at least of $O(\eta)$ and so they vanish in the limit $\eta \to 0$.

6.3.3.2 Limit of a pure GOE matrix

The opposite limit in which A is neglected in Eq. (6.1) is obtained by setting $p_a(a) = \delta(a)$, whose corresponding resolvent is $\mathcal{G}_a(\ ) = 1/$ (indeed, summing zeros to the matrix B in Eq. (6.1) does not change its spectrum). Equation (6.77) then implies $\hat{K} = \hat{C}$, where we used $\hat{L}^2 =$ (see Eq. (6.67)). The self-consistency equations (6.78) are then seen to coincide with Eq. (F.43), corresponding to the GOE case studied in Ref. [277] and here revisited in Appendix F.6. From Eq. (6.84) we obtain, in terms of r and θ introduced in Eq. (6.82),

$$\mathcal{S}[\varphi_0; \hat{\Lambda}] = \quad \frac{2\eta r^2 s}{\pi} \sin 2\theta \quad \frac{2s\theta}{\pi}, \tag{6.97}$$

which is linear in s: we deduce that the cumulants higher than the average $\langle I_N[\ E, E]\rangle$ are subleading for large N, and they are only accessible by explicitly computing the Gaussian fluctuations around the saddle-point (see Appendix F.5.2). Still, the leading order term in the first cumulant (see Eq. (F.55)) is correctly reproduced by Eq. (6.97).

6.3.4 Exactly solvable cases

The cumulant generating function we found in Eq. (6.85) is formal, in that $\Delta = re^{i\theta}$ must first be determined by solving the self-consistency equation (6.78). In Appendix F.7 we present two cases in which the result can be expressed in closed form, namely those in which $p_a(a)$ is the Cauchy or the Wigner distribution, see Eqs. (6.46) and (6.51), respectively. While the former presents fat tails and is thus slowly decaying, the latter has a compact support and a well-defined edge.

The resulting level compressibility $\chi(E)$ (see Eq. (6.90)) is plotted in Fig. 6.4, and it is compared to numerical results showing excellent agreement. We show in the same plot the level compressibility under the hypothesis that the level statistics is of the Poisson type, i.e., that the energy levels do not repel each other. This is given by Eq. (6.96) upon interpreting the average $\langle \bullet \rangle$ as taken over the average eigenvalue density $\rho(\lambda)$ for the case in which the matrix A has

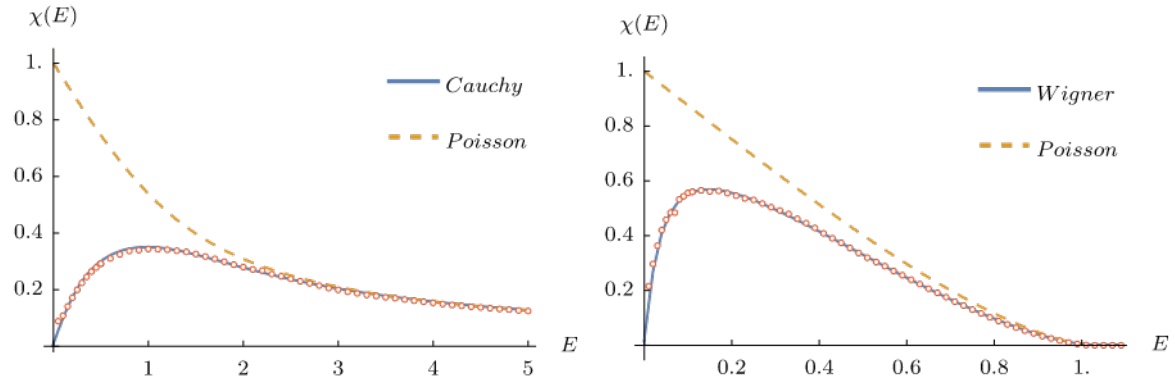

Figure 6.4: Numerical check of the level compressibility $\chi(E)$ predicted in Eq. (6.90) (solid blue line), for the case in which the elements of the diagonal matrix A belong to the (a) Cauchy, or (b) Wigner distribution. Numerical data (symbols) are obtained from the numerical diagonalization of $N_{\rm tot} = 1000$ random matrices of size $N = 5000$. The (dashed yellow) line denoted by *Poisson* shows the level compressibility as it would be in the absence of level repulsion — see the main text. In both plots we used the parameters $\mu = 0$, $\gamma = 1.1$. In (a) we chose $\omega = 1$ and $\nu = 1$, corresponding to $\eta = 0.125$, while in (b) we set $\sigma = 1$ and $\nu = 0.2$, yielding $\eta = 0.005$.

Cauchy/Wigner-distributed entries: this has been found previously in Eqs. (6.48) and (6.54), respectively. Even for very small values of η, the behavior at low energies E of the compressibility $\chi(E)$ is qualitatively very different: in the Poisson case we have $\chi(E) \sim 1$, while in the GRP model it is $\chi(E) \sim 0$. The latter $\chi(E)$ increases up to a maximum, whose position $E_{\rm max}(\eta)$ grows monotonically (and sublinearly) with η.

6.3.5 Scaling limit and Thouless energy

In this Section we focus on the limit in which $E = x\eta^\delta$ and $\eta \ll 1$, while $x \sim O(1)$. We can envision a different behavior depending on whether the exponent $\delta > 1$, $\delta < 1$ or $\delta = 1$. The latter case turns out to be particularly interesting: we will show that the level compressibility computed in $\chi(E = x\eta^\delta)$ assumes for $\delta = 1$ a *universal* scaling form, which is independent of the particular choice of the distribution $p_a(a)$ of the entries of the diagonal matrix A.

To this end, let us go back to the self-consistency equations (6.83), which we can rewrite for $\delta = 1$ and $\eta \ll 1$ as

$$\Delta^{-1} = \varepsilon - ix\eta - 2i\eta \mathcal{G}_a\left(-i\Delta^{-1}\right) \simeq \varepsilon - ix\eta - 2i\eta \mathcal{G}_a\left(-i\varepsilon + O(\eta)\right), \tag{6.98}$$

where again $\Delta = re^{i\theta}$. By taking the complex conjugate of Eq. (6.98) and by summing and subtracting the two equations, we obtain the two conditions

$$r^{-1}\cos\theta = \varepsilon + 2\eta\,\mathrm{Im}\,\mathcal{G}_a\left(-i\varepsilon + O(\eta)\right) \overset{\substack{\eta\ll 1\\ \varepsilon\to 0^+}}{\longrightarrow} 2\pi\eta p_a(0), \tag{6.99}$$

$$r^{-1}\sin\theta = x\eta + 2\eta\,\mathrm{Re}\,\mathcal{G}_a\left(-i\varepsilon + O(\eta)\right) \overset{\substack{\eta\ll 1\\ \varepsilon\to 0^+}}{\longrightarrow} x\eta, \tag{6.100}$$

where we used the Plemelj-Sokhotski formula recalled in Eq. (6.18), and the fact that for a symmetric distribution $p_a(a)$ one has

$$\mathcal{P}\int \mathrm{d}a\, \frac{p_a(a)}{a} = 0. \tag{6.101}$$

One then easily obtains, at leading order for small η (and with $x = E/\eta$),

$$\tan\theta \simeq \frac{x}{2\pi p_a(0)} \equiv y, \qquad r^{-1} \simeq 2\pi\eta p_a(0)\sqrt{1+y^2}. \tag{6.102}$$

Note that these manipulations are only possible under the additional assumption that the distribution $p_a(a)$ behaves regularly close to $a = 0$, and that $p_a(0) \neq 0$.

We can now estimate the level compressibility in this limit. First, note that $\mathcal{G}_a(-i\Delta^{-1}) = i\pi p_a(0) + O(\eta)$, so that from Eq. (6.86) we read

$$m = \frac{2\eta}{\pi}\,\mathrm{Im}\left[\mathcal{G}_a(-i\Delta^{-1})\right]^2 = O\left(\eta^2\right). \tag{6.103}$$

From Eq. (6.89), the first cumulant κ_1 thus reduces to

$$\frac{\kappa_1}{N} \simeq \langle f(a)\rangle_a = \int \mathrm{d}a\, p_a(a) f(a) \simeq \frac{p_a(0)}{r}\int_\infty^\infty \mathrm{d}u\, f(u/r) = \frac{p_a(0)}{r}\frac{2y}{\sqrt{1+y^2}} = 2p_a(0)x\eta, \tag{6.104}$$

where in the first line we changed variable to $u = ra$ and we used the fact that $r^{-1} \sim O(\eta)$ (see Eq. (6.102)), while in the second line we explicitly computed the integral

$$\frac{1}{\pi}\int_0^\infty \mathrm{d}u\, \arctan\left(\frac{\sin 2\theta}{u^2+\cos 2\theta}\right) = \frac{\tan\theta}{\sqrt{1+\tan^2\theta}} = \sin\theta, \qquad \theta \in \left[0, \frac{\pi}{2}\right], \tag{6.105}$$

and we inserted the expression for r found in Eq. (6.102) (note that $f(u/r)$ is actually r-independent — see Eq. (6.87)). One could alternatively compute κ_1 by taking the average of Eq. (6.12): this leads to the same result upon expanding for small E and η, since $\rho(\lambda) = p_a(\lambda) + O(\eta)$. The same steps can be repeated for the second (and possibly any other) cumulant κ_2, yielding

$$\frac{\kappa_2}{N} \simeq \left\langle f^2(a)\right\rangle_a \simeq \frac{p_a(0)}{r}\int_\infty^\infty \mathrm{d}u\, f^2(u/r). \tag{6.106}$$

From Eq. (6.90) we thus obtain the leading order estimate for the level compressibility when $\eta \ll 1$, which takes the universal scaling form

$$\begin{aligned}\chi(E) &\simeq \chi_T\left(y = \frac{E}{2\pi p_a(0)\eta}\right),\\ \chi_T(y) &\equiv \frac{\sqrt{1+y^2}}{\pi^2 y}\int_0^\infty \mathrm{d}u\left\{\arctan\left[\frac{2y}{u^2(1+y^2)+1-y^2}\right]\right\}^2,\end{aligned} \tag{6.107}$$

where we stress that we have chosen the branch $\arctan(-) \in [0,\pi]$. Upon integrating by parts and performing some algebra [280, 281], the integral over u can be computed explicitly to give

$$\chi_T(y) = \frac{1}{\pi y}\left[2y\arctan(y) - \ln\left(1+y^2\right)\right]. \tag{6.108}$$

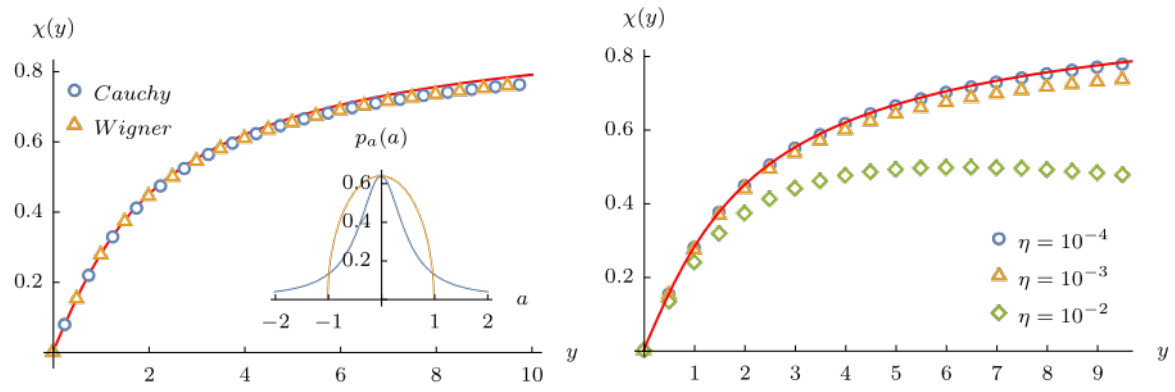

(a) (b)

Figure 6.5: Scaling form of the level compressibility, in the limit in which $E \propto y\eta$ and $\eta \ll 1$. In (a) we compare the universal prediction in Eq. (6.108) (solid red line) with the two exactly solvable cases studied in Section 6.3.4 (symbols), showing a good agreement at low energies $y = E/[2\pi p_a(0)\eta]$ (i.e., the condition under which Eq. (6.108) was derived). We chose $\eta = 5 \cdot 10^{-4}$ and $\omega = 0.5$, $\sigma = 1$, so that $p_a(0)$ assumes the same value for the two distributions (see inset). In (b) we exemplify in the Cauchy case how the curves corresponding to different values of η collapse onto the same master curve, when plotted as a function of $y \propto E/\eta$ for $\eta \ll 1$.

The function $\chi_T(y)$ grows monotonically from 0 to 1 as we increase y, and it is plotted in Fig. 6.5a together with the level compressibility for the two cases explicitly solved above, i.e., Cauchy and Wigner. We find a good agreement at low energies y, while we observe a departure at large energies: here the scaling prediction keeps growing, while the actual compressibility must hit a maximum and start decreasing — see Fig. 6.4. The same trend can be observed in Fig. 6.5b, where we evaluate the level compressibility for different values of η, and show that they collapse on a common master curve when they are plotted as a function of $y \propto E/\eta$.

The other two cases ($\delta > 1$ or $\delta < 1$) can be easily addressed by the same token. When $\delta > 1$, by studying the self-consistency equations as in Eq. (6.98) we obtain at leading order

$$\tan\theta \simeq y\eta^{\delta\ 1}, \qquad r^{\ 1} \simeq 2\pi\eta p_a(0). \tag{6.109}$$

It can be readily seen that $\kappa_1/N \simeq 2p_a(0)x\eta^\delta$ and $\kappa_2/N \sim O\left(\eta^{2\delta\ 1}\right)$, so that in this limit

$$\chi(E = x\eta^\delta) \sim O\left(\eta^{\delta\ 1}\right), \qquad \delta > 1,\ \eta \ll 1. \tag{6.110}$$

This resembles the behavior of $\chi(E)$ in the case of a pure GOE matrix, see Section 6.3.3.2 and Appendix F.6. Conversely, for $\delta < 1$ the self-consistency equations (6.83) reduce to $\Delta^{\ 1} \simeq \varepsilon \quad ix\eta^\delta$, and, by comparison with Eq. (6.92), we identify this limit as that in which the eigenvalues behave as i.i.d. random variables. In particular (compare with Eq. (6.96)),

$$\chi(E = x\eta^\delta) \simeq 1 \quad \frac{\langle I_N[\ E, E]\rangle_a}{N}, \qquad \delta < 1,\ \eta \ll 1. \tag{6.111}$$

The above analysis suggests to interpret the quantity $E_T \sim 2\pi p_a(0)\eta$ as the *Thouless energy* of the system. Indeed, consider again the limit in which $\eta \ll 1$, and let $E \propto \eta^\delta$. For $E \ll E_T$

(i.e., $\delta > 1$), the eigenvalues organize in multiplets (or mini-bands [225]) and they repel each other as in the GOE ensemble — as a result, the level compressibility is zero at leading order (see Eq. (6.110)). For $E \gg E_T$ ($\delta < 1$), on the other hand, the various multiplets no longer interact, and we recover the Poisson statistics — see Eq. (6.111). Finally, the case $\delta = 1$ marks a crossover in which the level compressibility $\chi(E/E_T)$ assumes the universal scaling form given in Eq. (6.108). Indeed, the asymptotics of the function $\chi_T(y)$ in Eq. (6.108) can be checked to give

$$\chi_T(y) \simeq \begin{cases} y/\pi, & y \ll 1, \\ 1 - \dfrac{2(1+\ln y)}{\pi y}, & y \gg 1, \end{cases} \tag{6.112}$$

showing that $\chi_T(y)$ interpolates between Wigner-Dyson statistics at low energy, and Poisson statistics at higher energy.

We finally note that a close relative of the level compressibility, namely the *two-level spectral correlation function* $C(t,t')$ — see Eqs. (F.63) and (F.64) for its definition — was computed in Ref. [225] for the Hermitian GRP model. In the latter, the GOE matrix B in Eq. (6.1) is replaced by a GUE matrix with complex entries, so that additional analytical techniques (notably the Harish-Chandra-Itzykson-Zuber integral [48]) are available. In particular, $C(t,t')$ is shown in Ref. [225] to assume a universal scaling form within the fractal region $1 < \gamma < 2$, and for large N. In Appendix F.8 we show that the corresponding scaling form of the level compressibility coincides, in the crossover regime in which $E \sim E_T$, with $\chi_T(y)$ in Eq. (6.108). This is quite remarkable, since these are in fact two distinct random matrix ensembles — and indeed their level compressibilities do not coincide for $E \gg E_T$ or $E \ll E_T$. This identification suggests that $\chi_T(y)$ originates from the structural properties of the model, rather than from the specific choice of the matrix B (e.g., GOE, GUE, but also possibly Wishart or sparse random matrices).

6.3.6 Behavior for small E

In this final Section we use extensive numerical exact diagonalization of large random matrices in order to inspect the low-energy behavior of the level compressibility $\chi(E)$. Indeed, our prediction in Section 6.3.5 is expected to break down for energies of the order of the mean level spacing δ_N of the finite-sized matrix $\mathcal{H}$, which is given by $\delta_N \simeq [N p_a(0)]^{-1}$, Eq. (6.5). Equivalently, we expect that the leading-order term in the saddle-point approximation adopted in our replica calculation (see Eqs. (6.60) and (6.71)) provides the correct result in the $N \to \infty$ limit, while for a matrix of size N and for sufficiently small E we should eventually recover the exact GOE result [48, 273, 282–287]

$$\begin{aligned} \chi_{\rm GOE}(y) = \frac{1}{2\pi^2 y}\Big\{ & [\mathrm{Si}(2\pi y)]^2 \quad 2\,\mathrm{Ci}(4\pi y) \quad \pi\,\mathrm{Si}(2\pi y) \\ & + 2\Big[\quad 4\pi y\,\mathrm{Si}(4\pi y) + 2\pi^2 y + \log(4\pi y) \quad \cos(4\pi y) + \gamma_E + 1\Big]\Big\}, \end{aligned} \tag{6.113}$$

whose derivation is reported in Appendix E.3 of Ref. [198]. The overall picture is thus the one we present in Fig. 6.6, and which we support by numerical results. The region $E \lesssim \delta_N$ is described

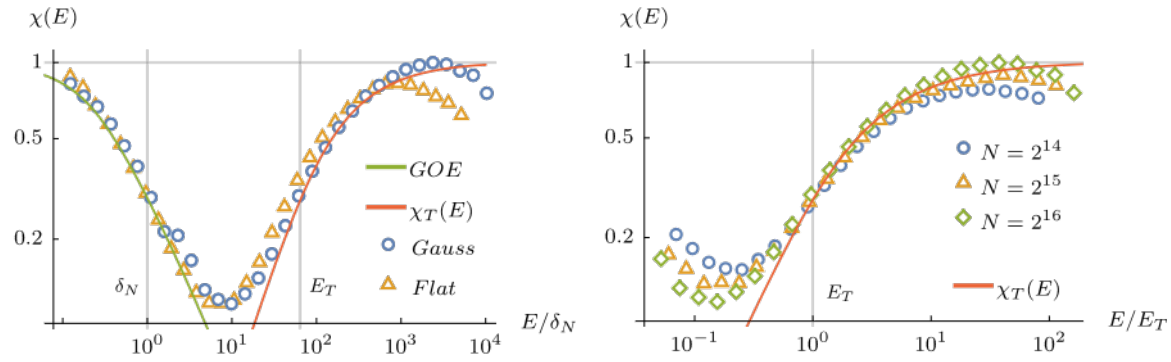

Figure 6.6: Behavior of the level compressibility $\chi(E)$ at low energies. The symbols correspond to numerical results, and we indicated with vertical lines the mean level spacing δ_N (see Eq. (6.5)) and the Thouless energy $E_T \sim N^{1-\gamma}$. In panel (a), $p_a(a)$ is chosen Gaussian with unit variance or uniform, and $N = 2^{16}$. The region $E \lesssim \delta_N$ is described by the GOE prediction in Eq. (6.113), while the crossover region $E \sim E_T$ is described by the universal scaling form in Eq. (6.108). In panel (b), $p_a(a)$ is Gaussian, and we show the approach to the universal curve $\chi_T(E)$ for increasing values of the matrix size N. We used $\gamma = 1.5$ throughout, and the simulations with $N = 2^{14}, 2^{15}$, or 2^{16} are averaged over $N_{\text{tot}} = 256, 64$, or 32 samples, respectively.

by the GOE prediction in Eq. (6.113). For $1 < \gamma < 2$ the Thouless energy $E_T \sim N^{1-\gamma}$ is such that $\delta_N \ll E_T \ll 1$, so that the crossover region with $E \sim E_T$ is described by the universal function $\chi_T(E)$ given in Eq. (6.108). For larger E $O(1)$, the level compressibility becomes model-dependent and it is described by Eq. (6.90) (see also Fig. 6.4).

The datapoints[4] presented in panel (a) of Fig. 6.6 correspond to the choices of $p_a(a)$ Gaussian or uniform, which supports our claim of universality of $\chi_T(E)$ in the region $E \sim E_T$. Note, in fact, that the data follow the predicted curves (up to finite-size effects) with no adjustable parameters (i.e., no fitting was needed). The datapoints are eventually observed to deviate from the scaling prediction, as they reach a maximum in correspondence of $E_{\max}(\eta) \gg E_{\text{T}}$, and then start decaying to zero as in Fig. 6.4. By increasing N, however, this maximum is observed to shift towards larger values of E, and the plateau around $\chi(E) \sim 1$ broadens accordingly.

6.4 Summary of this Chapter

In this Chapter we used the replica method to study the average spectral density (Section 6.2) and the local level statistics (Section 6.3) of a deformed GOE random matrix ensemble known as the generalized Rosenzweig-Porter model. We focused on its fractal intermediate phase (with $1 < \gamma < 2$, see Eq. (6.1) and Ref. [225]), which is conveniently characterized in terms of the level

[4] Although the scaling function in Eq. (6.108) has been derived under the assumption that the spectral density is symmetric, the numerical results are obtained by averaging the cumulants of the number of eigenvalues within many energy windows across the whole bandwidth, for which the symmetry with respect to the center of the window is lost. However, on the scale of the Thouless energy $E \simeq E_T \propto \eta$, the corrections due to the fact that $p_a(\ E) \neq p_a(E)$ are of $O(\eta)$, and therefore yield a contribution that is of the same order as the finite-size corrections, and which can be neglected for sufficiently large N.

compressibility $\chi(E)$ (see Eq. (6.13)). We showed that $\chi(E)$ assumes a universal form $\chi_T(E/E_T)$ independently of the character $p_a(a)$ of the deformation matrix A (see Eq. (6.1)), provided that the system is probed over energy scales of the order of the Thouless energy E_T (see Section 6.3.5).

It is natural to conjecture that this universal regime should persist in structurally similar random matrix ensembles (even more so, since we showed that the *same* scaling function $\chi_T(y)$ can be recovered for the Hermitian GRP model — see Appendix F.8). For instance, one could numerically inspect the case in which the GOE matrix is replaced by a Wigner matrix (i.e., any real symmetric matrix with i.i.d. random entries taken from a probability distribution with finite variance), whose limiting average spectral density is still given by the semi-circle law [288]. Similarly, it would be interesting to study the effect of the diagonal deformation matrix A on a Wishart matrix [289], or on a sparse (rather than dense) matrix B, such as those describing the Erdös-Rényi random graph [290–292], which can still be treated analytically (at least to some extent); if the average connectivity is chosen to be finite, the spectral density of Erdös-Rényi is no longer a semi-circle, but the local statistics is still of the Wigner-Dyson type.

Along our derivation, we heavily relied on the *independence* of the elements a_i characterizing the diagonal disorder (as usually assumed in standard formulations of the GRP model). However, the introduction of short-ranged correlations between the levels a_i seems within reach of the replica method. In particular, the analysis of Ref. [293] suggests that changing the power d with which the distance between sorted diagonal elements $a_n < a_{n+1}$ grows, e.g., $(a_{n+k} \quad a_n) \propto k^d$, has important implications on the phase diagram. Moreover, in Section 6.3.5 we assumed a regular behavior of $p_a(a)$ for $a \to 0$, while it would be interesting to check the fate of the universal scaling form $\chi_T(E)$ upon choosing a singular (but normalizable) distribution $p_a(a)$. Similarly, the analysis in Section 6.3.5 suggests that the particular choice of a distribution $p_a(a)$ such that $p_a(0) = 0$ may produce nontrivial consequences.

Finally, it is worth mentioning that the spectral properties of the intermediate phase of the generalized RP model are particularly simple: differently from realistic interacting quantum systems, the mini-bands are compact and the eigenvectors are fractal but not *multi*fractal (meaning that all the moments of the wave-functions amplitudes are described by the same fractal exponent $D_\gamma = 2 \quad \gamma$). In order to go beyond this case, several extensions of the RP model have been proposed in the last few years, featuring either log-normal [246, 247] or power-law [249] distributed off-diagonal matrix elements. Recent developments suggest, however, that the only way to obtain multifractality is to introduce correlations between the matrix elements of $\mathcal{H}$ (either the diagonal or the off-diagonal ones [294]). It would therefore be illuminating to study the behavior of the level compressibility at small energy in these generalizations of the RP model, and check whether or not the universal form discussed here is robust with respect to these modifications.

Conclusions and outlook

The core of this thesis has been devoted to examining a minimal model for the dynamics of a particle in a fluctuating correlated environment, featuring a spatially-resolved and time-evolving order parameter field reciprocally coupled to the particle coordinate. Here we have primarily focused on the case of a scalar Gaussian field, and used analytical (mostly perturbative) calculations and numerical simulations to describe the particle dynamics in a variety of equilibrium and nonequilibrium conditions. In particular, we investigated the relaxation towards equilibrium in a harmonic trap (Chapter 2), the field-induced response under periodic driving (Chapter 3), the stochastic thermodynamics and memory-induced oscillations in nonequilibrium steady states (Chapter 4), and the effective dynamics and stationary distributions under confinement (Chapter 5).

Several questions have been left unanswered; some of them, which are specific to the problems considered in each particular Chapter, have already been discussed in the corresponding summary. Here we will give instead an overview of the most compelling and promising directions for future research:

- First and foremost, experimental verification of the phenomena described in this thesis would be highly desirable, at least qualitatively. Above we have indicated the setup of colloidal particles in near-critical binary liquid mixtures as the most promising candidate: indeed, this type of systems is already accessible experimentally [32–36], and correlation lengths of the order of microns (which is the typical size of a colloidal particle) can nowadays be obtained by using, e.g., micellar solutions. In Appendices B.9 and D.5.1 we provided a rough estimate of the range of experimental parameters within which the novel phenomena discussed here (and due to correlations) may become observable: in general, they are only expected to become sizable if the correlation length of the medium exceeds the particle size.

- To make quantitative contact with actual fluid media, it is necessary to reinstate hydrodynamic effects in our description, which instead have been neglected in the simplified model discussed above. The velocity field of the underlying fluid is expected to couple both to the particle coordinate, and to the order parameter (whose transport is typically described by model H, in the nomenclature of Ref. [59]). Moreover, to approach the critical point we are naturally led to go beyond the Gaussian approximation and consider, instead, a scalar ϕ^4 theory as the starting point for our analysis. Due to the introduction of additional nonlinearities, this analysis will most likely rely on large-scale numerical simulations.

- It would be interesting to explore the possible role of *activity*, and its interplay with correlations in extensions of the present setting. There are in principle two ways to include the activity in our model: the first (which we have already started exploring) is to study the dynamics of an active particle (e.g., *run-and-tumble* or *active Ornstein-Uhlenbeck* [295, 296]) coupled to a fluctuating field as in Chapter 2; the second is to assume that the medium itself is active, i.e., that its fluctuations break detailed balance [297–299]. In particular, the active field theory of Ref. [299] seems an ideal starting point, as it hinges on colored noise rather than on introducing nonlinear and nonderivative terms in the dynamics of the field (as it is instead the case for more popular active field theories such as *active model B* [297]).

- Different types of coupling between the field and the particle(s) could be considered, other than a linear one — which we have instead adopted in most of the calculations above, mainly because it does not introduce nonlinearities in the equation of motion of the field. Similarly, an appropriate choice of the coupling potential $V(\mathbf{x})$ in Eq. (2.3) may be used to model an anisotropic particle, which is expected to bring in new phenomena.

- The extension of our model to many-particle systems has been outlined in Section 3.6 and Appendix C.9, where we established that no *multibody* effects can appear (even out of equilibrium) if the field-particle coupling is linear. However, the many-body problem could be revisited with different types of couplings to the field, and/or in the presence of activity (see, e.g., Refs. [92, 93, 300]). The thermodynamic framework we introduced in Chapter 4 could also be further enhanced by extending its applicability towards systems involving multiple particles in a common correlated (active) environment, with possibly non-quadratic Hamiltonians.

In the last Chapter of this thesis we have instead applied spin-glass techniques (notably the replica method) to derive novel predictions about the level spacing statistics of the generalized Rosenzweig-Porter random matrix ensemble [225], in particular revealing some universal properties of its intermediate partially-delocalized phase. As anticipated in Section 6.4, it is quite natural to ask whether such universality persists in structurally similar random matrix ensembles, which could be tackled using the same analytical methods; it would also be interesting to investigate how diagonal disorder can affect the spectral statistics of sparse random matrices. The latter have been in the focus of my recent follow-up work with the co-authors of Ref. [198], where we are applying another spin-glass technique, namely the *cavity* method, to tackle the localization properties of diluted Erdös-Rényi graphs. Finally, another long-standing question which it would be exciting to pursue further concerns the precise connection between the replica method we adopted in Chapter 6, and the supersymmetric formalism frequently used in random matrix theory [301, 302].

Bibliography

[1] A. Einstein, "On the theory of the Brownian movement", Ann. Phys. **324**, 371–381 (1906).

[2] M. Smoluchowski, *Essai d'une théorie cinétique du mouvement Brownien et des milieux troubles* (Acad. Litterarum Cracoviensis, 1906).

[3] K. Huang, *Statistical mechanics* (Wiley, 1988).

[4] P. W. Anderson, "More is different", Science **177**, 393–396 (1972).

[5] K. G. Wilson, "Problems in physics with many scales of length", Sci. Am. **241**, 158–179 (1979).

[6] H. E. Stanley, "Scaling, universality, and renormalization: three pillars of modern critical phenomena", Rev. Mod. Phys. **71**, S358–S366 (1999).

[7] R. Zwanzig, *Nonequilibrium statistical mechanics* (Oxford University Press, 2001).

[8] M. te Vrugt and R. Wittkowski, "Projection operators in statistical mechanics: a pedagogical approach", Eur. J. Phys. **41**, 045101 (2020).

[9] K. Kaneko, "Adiabatic elimination by the eigenfunction expansion method", Prog. Theor. Phys. **66**, 129–142 (1981).

[10] J. Łuczka, "Non-Markovian stochastic processes: Colored noise", Chaos **15**, 026107 (2005).

[11] C. Gardiner, *Stochastic Methods: A Handbook for the Natural and Social Sciences*, 4th ed. (Springer, Berlin, 2009).

[12] P. Langevin, "Sur la théorie du mouvement Brownien", C. R. Acad. Sci. (Paris) **146**, 530–533 (1908).

[13] T. Franosch, M. Grimm, M. Belushkin, F. M. Mor, G. Foffi, L. Forró, and S. Jeney, "Resonances arising from hydrodynamic memory in Brownian motion", Nature **478**, 85–88 (2011).

[14] B. J. Alder and T. E. Wainwright, "Velocity autocorrelations for hard spheres", Phys. Rev. Lett. **18**, 988–990 (1967).

[15] S. Jeney, B. Lukić, J. A. Kraus, T. Franosch, and L. Forró, "Anisotropic memory effects in confined colloidal diffusion", Phys. Rev. Lett. **100**, 240604 (2008).

[16] R. Larson, *The structure and rheology of complex fluids* (Oxford University Press, USA, 1999).

[17] E. Reister and U. Seifert, "Lateral diffusion of a protein on a fluctuating membrane", Europhys. Lett. **71**, 859 (2005).

[18] E. Reister-Gottfried, S. M. Leitenberger, and U. Seifert, "Diffusing proteins on a fluctuating membrane: Analytical theory and simulations", Phys. Rev. E **81**, 031903 (2010).

[19]B. A. Camley and F. L. H. Brown, "Contributions to membrane-embedded-protein diffusion beyond hydrodynamic theories", Phys. Rev. E **85**, 061921 (2012).

[20]B. A. Camley and F. L. H. Brown, "Fluctuating hydrodynamics of multicomponent membranes with embedded proteins", J. Chem. Phys. **141**, 075103 (2014).

[21]B. H. Stumpf, P. Nowakowski, C. Eggeling, A. Maciołek, and A.-S. Smith, "Protein induced lipid demixing in homogeneous membranes", Phys. Rev. Research **3**, L042013 (2021).

[22]G. Gompper and M. Hennes, "Sound attenuation and dispersion in microemulsions", Europhys. Lett. **25**, 193–198 (1994).

[23]M. Hennes and G. Gompper, "Dynamical behavior of microemulsion and sponge phases in thermal equilibrium", Phys. Rev. E **54**, 3811–3831 (1996).

[24]G. Gonnella, E. Orlandini, and J. M. Yeomans, "Spinodal decomposition to a lamellar phase: effects of hydrodynamic flow", Phys. Rev. Lett. **78**, 1695–1698 (1997).

[25]G. Gonnella, E. Orlandini, and J. M. Yeomans, "Lattice Boltzmann simulations of lamellar and droplet phases", Phys. Rev. E **58**, 480–485 (1998).

[26]V. Démery and D. S. Dean, "Drag forces in classical fields", Phys. Rev. Lett. **104**, 080601 (2010).

[27]V. Démery and D. S. Dean, "Drag forces on inclusions in classical fields with dissipative dynamics", Eur. Phys. J. E **32**, 377–390 (2010).

[28]V. Démery and D. S. Dean, "Thermal Casimir drag in fluctuating classical fields", Phys. Rev. E **84**, 010103 (2011).

[29]V. Démery and D. S. Dean, "Perturbative path-integral study of active- and passive-tracer diffusion in fluctuating fields", Phys. Rev. E **84**, 011148 (2011).

[30]D. S. Dean and V. Démery, "Diffusion of active tracers in fluctuating fields", J. Phys.: Condens. Matter **23**, 234114 (2011).

[31]V. Démery, "Diffusion of a particle quadratically coupled to a thermally fluctuating field", Phys. Rev. E **87**, 052105 (2013).

[32]C. Hertlein, L. Helden, A. Gambassi, S. Dietrich, and C. Bechinger, "Direct measurement of critical Casimir forces", Nature **451**, 172–175 (2008).

[33]A. Gambassi, A. Maciołek, C. Hertlein, U. Nellen, L. Helden, C. Bechinger, and S. Dietrich, "Critical Casimir effect in classical binary liquid mixtures", Phys. Rev. E **80**, 061143 (2009).

[34]S. Paladugu, A. Callegari, Y. Tuna, L. Barth, S. Dietrich, A. Gambassi, and G. Volpe, "Nonadditivity of critical Casimir forces", Nat. Commun. **7**, 11403 (2016).

[35]I. A. Martínez, C. Devailly, A. Petrosyan, and S. Ciliberto, "Energy transfer between colloids via critical interactions", Entropy **19**, 77 (2017).

[36]A. Magazzù, A. Callegari, J. P. Staforelli, A. Gambassi, S. Dietrich, and G. Volpe, "Controlling the dynamics of colloidal particles by critical Casimir forces", Soft Matter **15**, 2152–2162 (2019).

[37]G. Volpe, I. Buttinoni, D. Vogt, H.-J. Kümmerer, and C. Bechinger, "Microswimmers in patterned environments", Soft Matter **7**, 8810 (2011).

[38]H. Mori, "Transport, collective motion, and Brownian motion", Progr. Theor. Phys. **33**, 423–455 (1965).

[39]H. B. G. Casimir, "On the attraction between two perfectly conducting plates", Kon. Ned. Akad. Wetensch. Proc. **51**, 793–795 (1948).

[40]M. Krech, *The Casimir effect in critical systems* (World Scientific, 1994).

[41]M. Kardar and R. Golestanian, "The "friction" of vacuum, and other fluctuation-induced forces", Rev. Mod. Phys. **71**, 1233–1245 (1999).

[42]J. G. Brankov, D. M. Danchev, and N. S. Tonchev, *Theory of critical phenomena in finite-size systems* (World Scientific, 2000).

[43]A. Gambassi, "The Casimir effect: From quantum to critical fluctuations", J. Phys.: Conf. Ser. **161**, 012037 (2009).

[44]A. Maciołek and S. Dietrich, "Collective behavior of colloids due to critical Casimir interactions", Rev. Mod. Phys. **90**, 045001 (2018).

[45]D. Dantchev and S. Dietrich, "Critical Casimir effect: exact results", Phys. Rep. **1005**, 1–130 (2023).

[46]S. Ciliberto, "Experiments in stochastic thermodynamics: short history and perspectives", Phys. Rev. X **7**, 021051 (2017).

[47]J. Berner, B. Müller, J. R. Gomez-Solano, M. Krüger, and C. Bechinger, "Oscillating modes of driven colloids in overdamped systems", Nat. Commun. **9**, 999 (2018).

[48]M. L. Mehta, *Random matrices*, 3rd ed. (Academic Press, New York, 2004).

[49]G. Livan, M. Novaes, and P. Vivo, *Introduction to random matrices* (Springer International Publishing, 2018).

[50]E. P. Wigner, "On the statistical distribution of the widths and spacings of nuclear resonance levels", Math. Proc. Cambridge **47**, 790–798 (1951).

[51]M. Mézard, G. Parisi, and M. Virasoro, *Spin glass theory and beyond* (World Scientific, 1987).

[52]D. Venturelli, "Dynamical response to local perturbations of an active matter system with polar order", Master's thesis (2019).

[53]H. Risken, *The Fokker-Planck equation: methods of solution and applications* (Springer Berlin Heidelberg, 1996).

[54]U. C. Täuber, *Critical dynamics: a field theory approach to equilibrium and non-equilibrium scaling behavior* (Cambridge University Press, 2014).

[55]W. Horsthemke and R. Lefever, *Noise-induced transitions* (Springer Berlin Heidelberg, 2006).

[56]C. Aron, G. Biroli, and L. F. Cugliandolo, "Symmetries of generating functionals of Langevin processes with colored multiplicative noise", J. Stat. Mech. **2010**, P11018 (2010).

[57]C. Aron, D. G. Barci, L. F. Cugliandolo, Z. G. Arenas, and G. S. Lozano, "Dynamical symmetries of Markov processes with multiplicative white noise", J. Stat. Mech. **2016**, 053207 (2016).

[58]L. Giuggioli and Z. Neu, "Fokker-Planck representations of non-Markov Langevin equations: application to delayed systems", Philos. T. R. Soc. A **377**, 20180131 (2019).

[59]P. C. Hohenberg and B. I. Halperin, "Theory of dynamic critical phenomena", Rev. Mod. Phys. **49**, 435–479 (1977).

[60]A. M. Sudupe and R. F. Alvarez-Estrada, "Field-theoretic study of the nonlinear Fokker-Planck equation", J. Phys. A: Math. Gen. **16**, 3049–3064 (1983).

[61]L. M. A. Bettencourt, "Properties of the Langevin and Fokker-Planck equations for scalar fields and their application to the dynamics of second order phase transitions", Phys. Rev. D **63**, 045020 (2001).

[62]M. Le Bellac, *Quantum and statistical field theory* (Clarendon Press, 1991).

[63]*NIST Digital Library of Mathematical Functions*, Release 1.1.8, 2022.

[64]M. Gross, "Dynamics and steady states of a tracer particle in a confined critical fluid", J. Stat. Mech. **2021**, 063209 (2021).

[65]D. Venturelli and M. Gross, "Tracer particle in a confined correlated medium: an adiabatic elimination method", J. Stat. Mech. **2022**, 123210 (2022).

[66]H. K. Janssen, B. Schaub, and B. Schmittmann, "New universal short-time scaling behaviour of critical relaxation processes", Z. Phys. B **73**, 539–549 (1989).

[67]N. van Kampen, "Remarks on non-Markov processes", Braz. J. Phys. **28**, 90–96 (1998).

[68]G. W. Ford, M. Kac, and P. Mazur, "Statistical mechanics of assemblies of coupled oscillators", J. Math. Phys. **6**, 504–515 (1965).

[69]L. Onsager and S. Machlup, "Fluctuations and irreversible processes", Phys. Rev. **91**, 1505–1512 (1953).

[70]P. C. Martin, E. D. Siggia, and H. A. Rose, "Statistical dynamics of classical systems", Phys. Rev. A **8**, 423–437 (1973).

[71]C. De Dominicis, "Dynamics as a substitute for replicas in systems with quenched random impurities", Phys. Rev. B **18**, 4913–4919 (1978).

[72]H.-K. Janssen, "On a Lagrangean for classical field dynamics and renormalization group calculations of dynamical critical properties", Z. Phys. B **23**, 377–380 (1976).

[73]D. Hochberg, C. Molina-París, J. Pérez-Mercader, and M. Visser, "Effective action for stochastic partial differential equations", Phys. Rev. E **60**, 6343–6360 (1999).

[74]J.-S. Gagnon, D. Hochberg, and J. Pérez-Mercader, "Renormalization of stochastic differential equations with multiplicative noise using effective potential methods", Phys. Rev. E **102**, 062142 (2020).

[75]J. Zinn-Justin, *Quantum field theory and critical phenomena* (Oxford University Press, 2002).

[76]T. M. Squires and J. F. Brady, "A simple paradigm for active and nonlinear microrheology", Phys. Fluids **17**, 073101 (2005).

[77]R. N. Zia and J. F. Brady, "Stress development, relaxation, and memory in colloidal dispersions: transient nonlinear microrheology", J. Rheol. **57**, 457–492 (2013).

[78]Y. Fujitani, "Fluctuation amplitude of a trapped rigid sphere immersed in a near-critical binary fluid mixture within the regime of the Gaussian model", J. Phys. Soc. Jpn **85**, 044401 (2016).

[79]Y. Fujitani, "Osmotic suppression of positional fluctuation of a trapped particle in a near-critical binary fluid mixture in the regime of the Gaussian model", J. Phys. Soc. Jpn **86**, 114602 (2017).

[80]U. Basu, V. Démery, and A. Gambassi, "Dynamics of a colloidal particle coupled to a Gaussian field: from a confinement-dependent to a non-linear memory", SciPost Phys. **13**, 078 (2022).

[81]D. Venturelli, F. Ferraro, and A. Gambassi, "Nonequilibrium relaxation of a trapped particle in a near-critical Gaussian field", Phys. Rev. E **105**, 054125 (2022).

[82]F. Glatzel and T. Schilling, "The interplay between memory and potentials of mean force: a discussion on the structure of equations of motion for coarse-grained observables", Europhys. Lett. **136**, 36001 (2021).

[83]G. Jung, "Non-Markovian systems out of equilibrium: exact results for two routes of coarse graining", J. Phys.: Condens. Matter **34**, 204004 (2022).

[84]W. Theiss and U. Titulaer, "The systematic adiabatic elimination of fast variables from a many-dimensional fokker-planck equation", Physica A **130**, 123–142 (1985).

[85]W. Theiss and U. M. Titulaer, "Some remarks on the adiabatic elimination of fast variables from coupled Langevin equations", Physica A **130**, 143–154 (1985).

[86]D. Dalvit, P. Milonni, D. Roberts, and F. Rosa, *Casimir physics* (Springer Berlin, Heidelberg, 2011).

[87]A. Ajdari, L. Peliti, and J. Prost, "Fluctuation-induced long-range forces in liquid crystals", Phys. Rev. Lett. **66**, 1481–1484 (1991).

[88]R. Golestanian, "Fluctuation-induced forces in and out of equilibrium", Pramana **64**, 1029–1038 (2005).

[89]T. R. Kirkpatrick, J. M. O. de Zárate, and J. V. Sengers, "Fluctuation-induced pressures in fluids in thermal nonequilibrium steady states", Phys. Rev. E **89**, 022145 (2014).

[90]A. Aminov, Y. Kafri, and M. Kardar, "Fluctuation-induced forces in nonequilibrium diffusive dynamics", Phys. Rev. Lett. **114**, 230602 (2015).

[91]M. Krech, "Fluctuation-induced forces in critical fluids", J. Phys.: Condens. Matter **11**, R391–R412 (1999).

[92]J.-B. Fournier, "Field-mediated interactions of passive and conformation-active particles: multi-body and retardation effects", Soft Matter **18**, 2634–2645 (2022).

[93]J.-B. Fournier, "Dynamics of the force exchanged between membrane inclusions", Phys. Rev. Lett. **112**, 128101 (2014).

[94]M. Rahman and M. Saghir, "Thermodiffusion or Soret effect: historical review", Int. J. Heat Mass Tran. **73**, 693–705 (2014).

[95]C. Maes, "Fluctuating motion in an active environment", Phys. Rev. Lett. **125**, 208001 (2020).

[96]O. Granek, Y. Kafri, and J. Tailleur, "Anomalous transport of tracers in active baths", Phys. Rev. Lett. **129**, 038001 (2022).

[97]C. A. Guevara-Valadez, R. Marathe, and J. R. Gomez-Solano, "A Brownian cyclic engine operating in a viscoelastic active suspension", Physica A **609**, 128342 (2023).

[98]I. Santra, "Dynamical fluctuations of a tracer coupled to active and passive particles", J. Phys. Complex. **4**, 015013 (2023).

[99]K. Symanzik, "Schrödinger representation and Casimir effect in renormalizable quantum field theory", Nucl. Phys. B **190**, 1–44 (1981).

[100]H.-W. Diehl, "Field-theoretical approach to critical behaviour at surfaces", in *Phase transitions and critical phenomena*, Vol. 10 (Academic Press, London, 1986), p. 75.

[101]H. W. Diehl, "The theory of boundary critical phenomena", Int. J. Mod. Phys. B **11**, 3503–3523 (1997).

[102]A. Furukawa, A. Gambassi, S. Dietrich, and H. Tanaka, "Nonequilibrium critical Casimir effect in binary fluids", Phys. Rev. Lett. **111**, 055701 (2013).

[103]F. Schlesener, A. Hanke, and S. Dietrich, "Critical Casimir forces in colloidal suspensions", J. Stat. Phys. **110**, 981–1013 (2003).

[104]D. Venturelli and A. Gambassi, "Inducing oscillations of trapped particles in a near-critical Gaussian field", Phys. Rev. E **106**, 044112 (2022).

[105]P. Hänggi, "Correlation functions and masterequations of generalized (non-Markovian) Langevin equations", Z. Phys. B **31**, 407–416 (1978).

[106]G. Bimonte, T. Emig, N. Graham, and M. Kardar, "Something can come of nothing: surface approaches to quantum fluctuations and the Casimir force", Ann. Rev. Nucl. Part. Sci. **72**, 93–118 (2022).

[107]A. Hanke, F. Schlesener, E. Eisenriegler, and S. Dietrich, "Critical Casimir forces between spherical particles in fluids", Phys. Rev. Lett. **81**, 1885–1888 (1998).

[108]L. Peliti and S. Pigolotti, *Stochastic thermodynamics: an introduction* (Princeton University Press, 2021).

[109]U. Seifert, "Stochastic thermodynamics, fluctuation theorems and molecular machines", Rep. Prog. Phys. **75**, 126001 (2012).

[110]P. Jones, O. Maragò, and G. Volpe, *Optical tweezers: principles and applications* (Cambridge University Press, 2015).

[111]J. R. Gomez-Solano and C. Bechinger, "Probing linear and nonlinear microrheology of viscoelastic fluids", Europhys. Lett. **108**, 54008 (2014).

[112]J. S. Lintuvuori, K. Stratford, M. E. Cates, and D. Marenduzzo, "Colloids in cholesterics: size-dependent defects and non-Stokesian microrheology", Phys. Rev. Lett. **105**, 178302 (2010).

[113]D. Venturelli and A. Gambassi, "Memory-induced oscillations of a driven particle in a dissipative correlated medium", New J. Phys. **25**, 093025 (2023).

[114]D. Venturelli, S. A. M. Loos, B. Walter, É. Roldán, and A. Gambassi, "Stochastic thermodynamics of a probe in a fluctuating correlated field", arXiv:2305.16235 (2023).

[115]K. Sekimoto, *Stochastic energetics* (Springer Berlin Heidelberg, 2010).

[116]C. V. den Broeck and M. Esposito, "Ensemble and trajectory thermodynamics: a brief introduction", Physica A **418**, 6–16 (2015).

[117]S. Bo and A. Celani, "Multiple-scale stochastic processes: decimation, averaging and beyond", Phys. Rep. **670**, 1–59 (2017).

[118]É. Roldán, I. Neri, R. Chetrite, S. Gupta, S. Pigolotti, F. Jülicher, and K. Sekimoto, "Martingales for physicists", arXiv:2210.09983 (2022).

[119]C. Maes and K. Netocný, "Time-reversal and entropy", J. Stat. Phys. **110**, 269–310 (2003).

[120]P. Gaspard, "Time-reversed dynamical entropy and irreversibility in Markovian random processes", J. Stat. Phys. **117**, 599–615 (2004).

[121]J. M. R. Parrondo, C. V. den Broeck, and R. Kawai, "Entropy production and the arrow of time", New J. Phys. **11**, 073008 (2009).

[122]É. Roldán and J. M. R. Parrondo, "Estimating dissipation from single stationary trajectories", Phys. Rev. Lett. **105**, 150607 (2010).

[123]G. Falasco, R. Rao, and M. Esposito, "Information thermodynamics of Turing patterns", Phys. Rev. Lett. **121**, 108301 (2018).

[124]T. Suchanek, K. Kroy, and S. A. M. Loos, "Entropy production in the nonreciprocal Cahn-Hilliard model", arXiv:2305.00744 (2023).

[125]G. Pruessner and R. Garcia-Millan, "Field theories of active particle systems and their entropy production", arXiv:2211.11906 (2022).

[126]T. Suchanek, K. Kroy, and S. A. M. Loos, "Irreversible mesoscale fluctuations herald the emergence of dynamical phases", arXiv:2303.16701 (2023).

[127]M. Campisi and R. Fazio, "The power of a critical heat engine", Nat. Commun. **7**, 11895 (2016).

[128]V. Holubec and A. Ryabov, "Work and power fluctuations in a critical heat engine", Phys. Rev. E **96**, 030102 (2017).

[129]T. Herpich, T. Cossetto, G. Falasco, and M. Esposito, "Stochastic thermodynamics of all-to-all interacting many-body systems", New J. Phys. **22**, 063005 (2020).

[130]F. Caballero and M. E. Cates, "Stealth entropy production in active field theories near Ising critical points", Phys. Rev. Lett. **124**, 240604 (2020).

[131]Y. I. Li and M. E. Cates, "Steady state entropy production rate for scalar Langevin field theories", J. Stat. Mech. **2021**, 013211 (2021).

[132]C. Nardini, É. Fodor, E. Tjhung, F. van Wijland, J. Tailleur, and M. E. Cates, "Entropy production in field theories without time-reversal symmetry: quantifying the non-equilibrium character of active matter", Phys. Rev. X **7**, 021007 (2017).

[133]T. Markovich, É. Fodor, E. Tjhung, and M. E. Cates, "Thermodynamics of active field theories: energetic cost of coupling to reservoirs", Phys. Rev. X **11**, 021057 (2021).

[134]I. Di Terlizzi, M. Gironella, D. Herráez-Aguilar, T. Betz, F. Monroy, M. Baiesi, and F. Ritort, "Variance sum rule for entropy production", arXiv:2302.08565 (2023).

[135]C. Bechinger, R. Di Leonardo, H. Löwen, C. Reichhardt, G. Volpe, and G. Volpe, "Active particles in complex and crowded environments", Rev. Mod. Phys. **88**, 045006 (2016).

[136]S. Ro, B. Guo, A. Shih, T. V. Phan, R. H. Austin, D. Levine, P. M. Chaikin, and S. Martiniani, "Model-free measurement of local entropy production and extractable work in active matter", Phys. Rev. Lett. **129**, 220601 (2022).

[137]C. Battle, C. P. Broedersz, N. Fakhri, V. F. Geyer, J. Howard, C. F. Schmidt, and F. C. MacKintosh, "Broken detailed balance at mesoscopic scales in active biological systems", Science **352**, 604–607 (2016).

[138]P. Mestres, I. A. Martínez, A. Ortiz-Ambriz, R. A. Rica, and É. Roldán, "Realization of nonequilibrium thermodynamic processes using external colored noise", Phys. Rev. E **90**, 032116 (2014).

[139]T. Speck and U. Seifert, "The Jarzynski relation, fluctuation theorems, and stochastic thermodynamics for non-Markovian processes", J. Stat. Mech. **2007**, L09002 (2007).

[140]T. Mai and A. Dhar, "Nonequilibrium work fluctuations for oscillators in non-Markovian baths", Phys. Rev. E **75**, 061101 (2007).

[141]A. Plati, A. Puglisi, and A. Sarracino, "Thermodynamic bounds for diffusion in nonequilibrium systems with multiple timescales", Phys. Rev. E **107**, 044132 (2023).

[142]I. D. Terlizzi and M. Baiesi, "A thermodynamic uncertainty relation for a system with memory", J. Phys. A: Math. Theor. **53**, 474002 (2020).

[143]A. Puglisi and D. Villamaina, "Irreversible effects of memory", Europhys. Lett. **88**, 30004 (2009).

[144]T. Ohkuma and T. Ohta, "Fluctuation theorems for non-linear generalized Langevin systems", J. Stat. Mech. **2007**, P10010 (2007).

[145]S. A. Loos, *Stochastic systems with time delay* (Springer International Publishing, 2021).

[146]B. I. Shraiman and E. D. Siggia, "Scalar turbulence", Nature **405**, 639–646 (2000).

[147]G. Falkovich, K. Gawedzki, and M. Vergassola, "Particles and fields in fluid turbulence", Rev. Mod. Phys. **73**, 913–975 (2001).

[148]V. Démery and É. Fodor, "Driven probe under harmonic confinement in a colloidal bath", J. Stat. Mech. **2019**, 033202 (2019).

[149]I. Gazuz, A. M. Puertas, T. Voigtmann, and M. Fuchs, "Active and nonlinear microrheology in dense colloidal suspensions", Phys. Rev. Lett. **102**, 248302 (2009).

[150]J. R. Gomez-Solano and C. Bechinger, "Transient dynamics of a colloidal particle driven through a viscoelastic fluid", New J. Phys. **17**, 103032 (2015).

[151]R. Jain, F. Ginot, and M. Krüger, "Micro-rheology of a particle in a nonlinear bath: Stochastic Prandtl–Tomlinson model", Phys. Fluids **33**, 103101 (2021).

[152]R. Jain, F. Ginot, J. Berner, C. Bechinger, and M. Krüger, "Two step micro-rheological behavior in a viscoelastic fluid", J. Chem. Phys. **154**, 184904 (2021).

[153]J. Dhont, *An introduction to dynamics of colloids* (Elsevier Science, 1996).

[154]H. Mori, T. Morita, and K. T. Mashiyama, "Contraction of state variables in non-equilibrium open systems. I", Prog. Theor. Phys. **63**, 1865–1884 (1980).

[155]T. Morita, H. Mori, and K. T. Mashiyama, "Contraction of state variables in non-equilibrium open systems. II", Prog. Theor. Phys. **64**, 500–521 (1980).

[156]J. Schiff, *The Laplace transform: theory and applications* (Springer New York, 1999).

[157]I. Di Terlizzi, F. Ritort, and M. Baiesi, "Explicit solution of the generalised Langevin equation", J. Stat. Phys. **181**, 1609–1635 (2020).

[158]A. J. Roberts, "Modify the improved Euler scheme to integrate stochastic differential equations", arXiv:1210.0933 (2012).

[159]G. I. Barenblatt, *Scaling, self-similarity, and intermediate asymptotics: dimensional analysis and intermediate asymptotics* (Cambridge University Press, 1996).

[160]R. L. Stratonovich, *Topics in the theory of random noise* (Gordon and Breach, New York, 1963).

[161]M. san Miguel and J. M. Sancho, "A colored-noise approach to Brownian motion in position space. Corrections to the Smoluchowski equation", J. Stat. Phys. **22**, 605–624 (1980).

[162]P. Hanggi and P. Jung, "Colored Noise in Dynamical Systems", Adv. Chem. Phys. **89**, 239–326 (1995).

[163]G. A. Pavliotis, *Stochastic Processes and Applications: Diffusion Processes, the Fokker-Planck and Langevin Equations* (Springer, New York, 2014).

[164]A. Naji, P. J. Atzberger, and F. L. H. Brown, "Hybrid elastic and discrete-particle approach to biomembrane dynamics with application to the mobility of curved integral membrane proteins", Phys. Rev. Lett. **102**, 138102 (2009).

[165]C. W. Gardiner, "Adiabatic elimination in stochastic systems. I. Formulation of methods and application to few-variable systems", Phys. Rev. A **29**, 2814–2822 (1984).

[166]M. E. Cates and J. Tailleur, "When are active Brownian particles and run-and-tumble particles equivalent? Consequences for motility-induced phase separation", Europhys. Lett. **101**, 20010 (2013).

[167]A. P. Solon, M. E. Cates, and J. Tailleur, "Active Brownian particles and run-and-tumble particles: A comparative study", Eur. Phys. J. ST **224**, 1231–1262 (2015).

[168]A. Singh Vishen, J.-F. Rupprecht, G. V. Shivashankar, J. Prost, and M. Rao, "Soft inclusion in a confined fluctuating active gel", Phys. Rev. E **97**, 032602 (2018).

[169]K. B. Petersen and M. S. Pedersen, *The Matrix Cookbook* (Technical University of Denmark, 2012).

[170]W. Helfrich, "Elastic properties of lipid bilayers: theory and possible experiments", Z. Naturforsch. C **28**, 693–703 (1973).

[171]F. Campelo, C. Arnarez, S. J. Marrink, and M. M. Kozlov, "Helfrich model of membrane bending: From Gibbs theory of liquid interfaces to membranes as thick anisotropic elastic layers", Adv. Coll. Int. Sci. **208**, 25–33 (2014).

[172]U. Seifert, "Configurations of fluid membranes and vesicles", Adv. Phys. **46**, 13–137 (1997).

[173]G. Pätzold and K. Dawson, "Numerical simulation of phase separation in the presence of surfactants and hydrodynamics", Phys. Rev. E **52**, 6908–6911 (1995).

[174]I. Pawłow and W. M. Zajaczkowski, "A sixth order Cahn-Hilliard type equation arising in oil-water-surfactant mixtures", Comm. Pure Appl. Anal. **10**, 1823–1847 (2011).

[175]G. Schimperna and I. Pawlow, "On a class of Cahn–Hilliard models with nonlinear diffusion", SIAM J. Math. Anal. **45**, 31–63 (2013).

[176]X. Yang, "Numerical approximations for the Cahn–Hilliard phase field model of the binary fluid-surfactant system", J. Sci. Comp. **74**, 1533–1553 (2018).

[177]A. Naji and F. L. H. Brown, "Diffusion on ruffled membrane surfaces", J. Chem. Phys. **126**, 235103 (2007).

[178]L. C.-L. Lin and F. L. H. Brown, "Brownian dynamics in fourier space: membrane simulations over long length and time scales", Phys. Rev. Lett. **93**, 256001 (2004).

[179]H. W. Diehl and H. K. Janssen, "Boundary conditions for the field theory of dynamic critical behavior in semi-infinite systems with conserved order parameter", Phys. Rev. A **45**, 7145–7155 (1992).

[180]M. Gross, C. M. Rohwer, and S. Dietrich, "Dynamics of the critical Casimir force for a conserved order parameter after a critical quench", Phys. Rev. E **100**, 012114 (2019).

[181]M. Gross, "First-passage dynamics of linear stochastic interface models: numerical simulations and entropic repulsion effect", J. Stat. Mech. **2018**, 033212 (2018).

[182]B. Bransden and C. Joachain, *Physics of atoms and molecules* (Addison-Wesley, 2014).

[183]R. Bellman, *Introduction to matrix analysis*, 2nd ed. (Society for Industrial & Applied Mathematics (SIAM), 1997).

[184]J. Łuczka, P. Hänggi, and A. Gadomski, "Non-Markovian process driven by quadratic noise: Kramers-Moyal expansion and Fokker-Planck modeling", Phys. Rev. E **51**, 2933–2938 (1995).

[185]J. Luczka, "A stochastic process driven by the quadratic Ornstein-Uhlenbeck noise: generator, propagators and all that", J. Phys. A: Math. Gen. **21**, 3063–3077 (1988).

[186]D. S. Dean and A. Gopinathan, "The non-equilibrium behavior of pseudo-Casimir forces", J. Stat. Mech. **2009**, L08001 (2009).

[187]D. S. Dean and A. Gopinathan, "Out-of-equilibrium behavior of Casimir-type fluctuation-induced forces for free classical fields", Phys. Rev. E **81**, 041126 (2010).

[188]A. Gambassi and S. Dietrich, "Critical dynamics in thin films", J. Stat. Phys. **123**, 929–1005 (2006).

[189]C. M. Rohwer, M. Kardar, and M. Krüger, "Transient Casimir forces from quenches in thermal and active matter", Phys. Rev. Lett. **118**, 015702 (2017).

[190]M. Gross, A. Gambassi, and S. Dietrich, "Surface-induced nonequilibrium dynamics and critical Casimir forces for model B in film geometry", Phys. Rev. E **98**, 032103 (2018).

[191]M. Gross, A. Gambassi, and S. Dietrich, "Fluctuations of the critical Casimir force", Phys. Rev. E **103**, 062118 (2021).

[192]T. G. Mattos, L. Harnau, and S. Dietrich, "Many-body effects for critical Casimir forces", J. Chem. Phys. **138**, 074704 (2013).

[193]H. Hobrecht and A. Hucht, "Many-body critical Casimir interactions in colloidal suspensions", Phys. Rev. E **92**, 042315 (2015).

[194]R. Zakine, J.-B. Fournier, and F. van Wijland, "Spatial organization of active particles with field-mediated interactions", Phys. Rev. E **101**, 022105 (2020).

[195]A. Squarcini, A. Maciołek, E. Eisenriegler, and S. Dietrich, "Critical Casimir interaction between colloidal Janus-type particles in two spatial dimensions", J. Stat. Mech. **2020**, 043208 (2020).

[196]R. M. May, "Will a large complex system be stable?", Nature **238**, 413–414 (1972).

[197]H. Ikeda, "Bose–Einstein-like condensation of deformed random matrix: a replica approach", J. Stat. Mech. **2023**, 023302 (2023).

[198]D. Venturelli, L. F. Cugliandolo, G. Schehr, and M. Tarzia, "Replica approach to the generalized Rosenzweig-Porter model", SciPost Phys. **14**, 110 (2023).

[199]P. W. Anderson, "Absence of diffusion in certain random lattices", Phys. Rev. **109**, 1492–1505 (1958).

[200]F. Wegner, "Inverse participation ratio in 2+ ε dimensions", Z. Phys. B **36**, 209–214 (1980).

[201]A. Rodriguez, L. J. Vasquez, K. Slevin, and R. A. Römer, "Multifractal finite-size scaling and universality at the Anderson transition", Phys. Rev. B **84**, 134209 (2011).

[202]M. Srednicki, "Chaos and quantum thermalization", Phys. Rev. E **50**, 888–901 (1994).

[203]M. Rigol, V. Dunjko, and M. Olshanii, "Thermalization and its mechanism for generic isolated quantum systems", Nature **452**, 854–858 (2008).

[204]N. Macé, F. Alet, and N. Laflorencie, "Multifractal scalings across the many-body localization transition", Phys. Rev. Lett. **123**, 180601 (2019).

[205]G. De Tomasi, I. M. Khaymovich, F. Pollmann, and S. Warzel, "Rare thermal bubbles at the many-body localization transition from the Fock space point of view", Phys. Rev. B **104**, 024202 (2021).

[206]I. Gornyi, A. Mirlin, D. Polyakov, and A. Burin, "Spectral diffusion and scaling of many-body delocalization transitions", Ann. Phys. **529**, 1600360 (2017).

[207]M. Tarzia, "Many-body localization transition in Hilbert space", Phys. Rev. B **102**, 014208 (2020).

[208]D. J. Luitz, N. Laflorencie, and F. Alet, "Many-body localization edge in the random-field Heisenberg chain", Phys. Rev. B **91**, 081103 (2015).

[209]M. Serbyn, Z. Papic, and D. A. Abanin, "Thouless energy and multifractality across the many-body localization transition", Phys. Rev. B **96**, 104201 (2017).

[210]K. S. Tikhonov and A. D. Mirlin, "Many-body localization transition with power-law interactions: statistics of eigenstates", Phys. Rev. B **97**, 214205 (2018).

[211]D. J. Luitz, I. M. Khaymovich, and Y. B. Lev, "Multifractality and its role in anomalous transport in the disordered XXZ spin-chain", SciPost Phys. Core **2**, 006 (2020).

[212]D. M. Basko, I. L. Aleiner, and B. L. Altshuler, "Metal–insulator transition in a weakly interacting many-electron system with localized single-particle states", Ann. Phys. **321**, 1126–1205 (2006).

[213]B. L. Altshuler, Y. Gefen, A. Kamenev, and L. S. Levitov, "Quasiparticle lifetime in a finite system: a nonperturbative approach", Phys. Rev. Lett. **78**, 2803–2806 (1997).

[214]L. Faoro, M. V. Feigel'man, and L. Ioffe, "Non-ergodic extended phase of the quantum random energy model", Ann. Phys. **409**, 167916 (2019).

[215]C. L. Baldwin and C. R. Laumann, "Quantum algorithm for energy matching in hard optimization problems", Phys. Rev. B **97**, 224201 (2018).

[216]G. Biroli, D. Facoetti, M. Schiró, M. Tarzia, and P. Vivo, "Out-of-equilibrium phase diagram of the quantum random energy model", Phys. Rev. B **103**, 014204 (2021).

[217]T. Parolini and G. Mossi, "Multifractal dynamics of the QREM", arXiv:2007.00315 (2020).

[218]K. Kechedzhi, V. Smelyanskiy, J. R. McClean, V. S. Denchev, M. Mohseni, S. Isakov, S. Boixo, B. Altshuler, and H. Neven, "Efficient population transfer via non-ergodic extended states in quantum spin glass", arXiv:1807.04792 (2018).

[219]M. Pino, V. E. Kravtsov, B. L. Altshuler, and L. B. Ioffe, "Multifractal metal in a disordered Josephson junctions array", Phys. Rev. B **96**, 214205 (2017).

[220]M. Pino, L. B. Ioffe, and B. L. Altshuler, "Nonergodic metallic and insulating phases of Josephson junction chains", Proc. Natl. Acad. Sci. USA **113**, 536–541 (2016).

[221]V. N. Smelyanskiy, K. Kechedzhi, S. Boixo, S. V. Isakov, H. Neven, and B. Altshuler, "Nonergodic delocalized states for efficient population transfer within a narrow band of the energy landscape", Phys. Rev. X **10**, 011017 (2020).

[222]T. Micklitz, F. Monteiro, and A. Altland, "Nonergodic extended states in the Sachdev-Ye-Kitaev model", Phys. Rev. Lett. **123**, 125701 (2019).

[223]F. Monteiro, T. Micklitz, M. Tezuka, and A. Altland, "Minimal model of many-body localization", Phys. Rev. Research **3**, 013023 (2021).

[224]N. Rosenzweig and C. E. Porter, "Repulsion of energy levels in complex atomic spectra", Phys. Rev. **120**, 1698–1714 (1960).

[225]V. E. Kravtsov, I. M. Khaymovich, E. Cuevas, and M. Amini, "A random matrix model with localization and ergodic transitions", New J. Phys. **17**, 122002 (2015).

[226]P. von Soosten and S. Warzel, "Non-ergodic delocalization in the Rosenzweig–Porter model", Lett. Math. Phys. **109**, 905–922 (2019).

[227]D. Facoetti, P. Vivo, and G. Biroli, "From non-ergodic eigenvectors to local resolvent statistics and back: a random matrix perspective", Europhys. Lett. **115**, 47003 (2016).

[228]K. Truong and A. Ossipov, "Eigenvectors under a generic perturbation: non-perturbative results from the random matrix approach", Europhys. Lett. **116**, 37002 (2016).

[229]E. Bogomolny and M. Sieber, "Eigenfunction distribution for the Rosenzweig-Porter model", Phys. Rev. E **98**, 032139 (2018).

[230]G. D. Tomasi, M. Amini, S. Bera, I. M. Khaymovich, and V. E. Kravtsov, "Survival probability in generalized Rosenzweig-Porter random matrix ensemble", SciPost Phys. **6**, 14 (2019).

[231]M. Amini, "Spread of wave packets in disordered hierarchical lattices", Europhy. Lett. **117**, 30003 (2017).

[232]M. Pino, J. Tabanera, and P. Serna, "From ergodic to non-ergodic chaos in Rosenzweig-Porter model", J. Phys. A: Mat. Theor. **52**, 475101 (2019).

[233]R. Berkovits, "Super-Poissonian behavior of the Rosenzweig-Porter model in the nonergodic extended regime", Phys. Rev. B **102**, 165140 (2020).

[234]A. Pandey, "Brownian-motion model of discrete spectra", Chaos Soliton. Frac. **5**, 1275–1285 (1995).

[235]T. Guhr, "Transition from Poisson regularity to chaos in a time-reversal noninvariant system", Phys. Rev. Lett. **76**, 2258–2261 (1996).

[236]T. Guhr and A. Müller-Groeling, "Spectral correlations in the crossover between GUE and Poisson regularity: on the identification of scales", J. Math. Phys. **38**, 1870–1887 (1997).

[237]E. Brézin and S. Hikami, "Correlations of nearby levels induced by a random potential", Nucl. Phys. B **479**, 697–706 (1996).

[238]H. Kunz and B. Shapiro, "Transition from Poisson to Gaussian unitary statistics: the two-point correlation function", Phys. Rev. E **58**, 400–406 (1998).

[239]A. Altland, M. Janssen, and B. Shapiro, "Perturbation theory for the Rosenzweig-Porter matrix model", Phys. Rev. E **56**, 1471–1475 (1997).

[240]A. Krajenbrink, P. Le Doussal, and N. O'Connell, "Tilted elastic lines with columnar and point disorder, non-Hermitian quantum mechanics, and spiked random matrices: pinning and localization", Phys. Rev. E **103**, 042120 (2021).

[241]P. Mergny and S. N. Majumdar, "Stability of large complex systems with heterogeneous relaxation dynamics", J. Stat. Mech. **2021**, 123301 (2021).

[242]J.-P. Bouchaud, "Random matrix theory and (big) data analysis", in *Stochastic processes and random matrices: lecture notes of the Les Houches summer school 2015* (Oxford University Press, 2017).

[243]T. Claeys, A. B. J. Kuijlaars, K. Liechty, and D. Wang, "Propagation of singular behavior for Gaussian perturbations of random matrices", Commun. Math. Phys. **362**, 1–54 (2018).

[244]B. Altshuler and B. Shklovskii, "Repulsion of energy levels and conductivity of small metal samples", Sov. Phys. JETP **64**, 127–135 (1986).

[245]E. Cuevas and V. E. Kravtsov, "Two-eigenfunction correlation in a multifractal metal and insulator", Phys. Rev. B **76**, 235119 (2007).

[246]V. E. Kravtsov, I. M. Khaymovich, B. L. Altshuler, and L. B. Ioffe, "Localization transition on the Random Regular Graph as an unstable tricritical point in a log-normal Rosenzweig-Porter random matrix ensemble", arXiv:2002.02979 (2020).

[247]I. M. Khaymovich, V. E. Kravtsov, B. L. Altshuler, and L. B. Ioffe, "Fragile extended phases in the log-normal Rosenzweig-Porter model", Phys. Rev. Res. **2**, 043346 (2020).

[248]C. Monthus, "Multifractality of eigenstates in the delocalized non-ergodic phase of some random matrix models: Wigner–Weisskopf approach", J. Phys. A: Mat. Theor. **50**, 295101 (2017).

[249]G. Biroli and M. Tarzia, "Lévy-Rosenzweig-Porter random matrix ensemble", Phys. Rev. B **103**, 104205 (2021).

[250]W. Buijsman and Y. Bar Lev, "Circular Rosenzweig-Porter random matrix ensemble", SciPost Phys. **12**, 082 (2022).

[251]I. M. Khaymovich and V. E. Kravtsov, "Dynamical phases in a "multifractal" Rosenzweig-Porter model", SciPost Phys. **11**, 045 (2021).

[252]M. Sarkar, R. Ghosh, A. Sen, and K. Sengupta, "Mobility edge and multifractality in a periodically driven Aubry-André model", Phys. Rev. B **103**, 184309 (2021).

[253]M. A. Skvortsov, M. Amini, and V. E. Kravtsov, "Sensitivity of (multi)fractal eigenstates to a perturbation of the Hamiltonian", Phys. Rev. B **106**, 054208 (2022).

[254]X. Cai, L.-J. Lang, S. Chen, and Y. Wang, "Topological superconductor to Anderson localization transition in one-dimensional incommensurate lattices", Phys. Rev. Lett. **110**, 176403 (2013).

[255]W. DeGottardi, D. Sen, and S. Vishveshwara, "Majorana fermions in superconducting 1d systems having periodic, quasiperiodic, and disordered potentials", Phys. Rev. Lett. **110**, 146404 (2013).

[256]F. Liu, S. Ghosh, and Y. D. Chong, "Localization and adiabatic pumping in a generalized Aubry-André-Harper model", Phys. Rev. B **91**, 014108 (2015).

[257]A. K. Das and A. Ghosh, "Nonergodic extended states in the β ensemble", Phys. Rev. E **105**, 054121 (2022).

[258]A. Ahmed, A. Ramachandran, I. M. Khaymovich, and A. Sharma, "Flat band based multifractality in the all-band-flat diamond chain", Phys. Rev. B **106**, 205119 (2022).

[259]S. Lee, A. Andreanov, and S. Flach, "Critical-to-insulator transitions and fractality edges in perturbed flat bands", Phys. Rev. B **107**, 014204 (2023).

[260]S. Roy, I. M. Khaymovich, A. Das, and R. Moessner, "Multifractality without fine-tuning in a Floquet quasiperiodic chain", SciPost Phys. **4**, 025 (2018).

[261]J. Wang, X.-J. Liu, G. Xianlong, and H. Hu, "Phase diagram of a non-Abelian Aubry-André-Harper model with p-wave superfluidity", Phys. Rev. B **93**, 104504 (2016).

[262]P. A. Nosov, I. M. Khaymovich, and V. E. Kravtsov, "Correlation-induced localization", Phys. Rev. B **99**, 104203 (2019).

[263]A. Duthie, S. Roy, and D. E. Logan, "Anomalous multifractality in quantum chains with strongly correlated disorder", Phys. Rev. B **106**, L020201 (2022).

[264]A. G. Kutlin and I. M. Khaymovich, "Emergent fractal phase in energy stratified random models", SciPost Phys. **11**, 101 (2021).

[265]V. R. Motamarri, A. S. Gorsky, and I. M. Khaymovich, "Localization and fractality in disordered Russian Doll model", SciPost Phys. **13**, 117 (2022).

[266]W. Tang and I. M. Khaymovich, "Non-ergodic delocalized phase with Poisson level statistics", Quantum **6**, 733 (2022).

[267]M. Tarzia, "Fully localized and partially delocalized states in the tails of Erdös-Rényi graphs in the critical regime", Phys. Rev. B **105**, 174201 (2022).

[268]D. V. Voiculescu, K. J. Dykema, and A. Nica, *Free random variables* (American Mathematical Soc., 1992).

[269]A. Zee, "Law of addition in random matrix theory", Nucl. Phys. B **474**, 726–744 (1996).

[270]U. Fano, "Ionization yield of radiations. II. The fluctuations of the number of ions", Phys. Rev. **72**, 26–29 (1947).

[271]S. N. Majumdar, P. von Bomhard, and J. Krug, "Exactly solvable record model for rainfall", Phys. Rev. Lett. **122**, 158702 (2019).

[272]S. N. Majumdar, P. Mounaix, and G. Schehr, "Universal record statistics for random walks and Lévy flights with a nonzero staying probability", J. Phys. A: Math. Theor. **54**, 315002 (2021).

[273]A. D. Mirlin, "Statistics of energy levels and eigenfunctions in disordered systems", Phys. Rep. **326**, 259–382 (2000).

[274]S. F. Edwards and R. C. Jones, "The eigenvalue spectrum of a large symmetric random matrix", J. Phys. A: Math. Gen. **9**, 1595–1603 (1976).

[275]V. Kravtsov, B. Altshuler, and L. Ioffe, "Non-ergodic delocalized phase in Anderson model on Bethe lattice and regular graph", Ann. Phys. **389**, 148–191 (2018).

[276]F. L. Metz and I. Pérez Castillo, "Large deviation function for the number of eigenvalues of sparse random graphs inside an interval", Phys. Rev. Lett. **117**, 104101 (2016).

[277]F. L. Metz, "Replica-symmetric approach to the typical eigenvalue fluctuations of Gaussian random matrices", J. Phys. A: Math. Theor. **50**, 495002 (2017).

[278]P. Vivo, "Index of a matrix, complex logarithms, and multidimensional Fresnel integrals", J. Phys. A: Math. Theor. **54**, 025002 (2020).

[279]I. P. Castillo and F. L. Metz, "Large-deviation theory for diluted Wishart random matrices", Phys. Rev. E **97**, 032124 (2018).

[280]D. H., "Asymptotic expansion of integral involving an ArcTan", Mathematics Stack Exchange (2022).

[281]I. S. Gradshteyn and I. M. Ryzhik, *Table of integrals, series, and products* (Elsevier, 2015).

[282]F. J. Dyson, "Statistical Theory of the Energy Levels of Complex Systems. I", J. Math. Phys. **3**, 140–156 (1962).

[283]F. J. Dyson and M. L. Mehta, "Statistical Theory of the Energy Levels of Complex Systems. IV", J. Math. Phys. **4**, 701–712 (1963).

[284]P. J. Forrester, *Log-gases and random matrices* (Princeton University Press, 2010).

[285]R. Marino, S. N. Majumdar, G. Schehr, and P. Vivo, "Phase transitions and edge scaling of number variance in Gaussian random matrices", Phys. Rev. Lett. **112**, 254101 (2014).

[286]R. Marino, S. N. Majumdar, G. Schehr, and P. Vivo, "Number statistics for β-ensembles of random matrices: applications to trapped fermions at zero temperature", Phys. Rev. E **94**, 032115 (2016).

[287]K. S. Tikhonov and A. D. Mirlin, "Statistics of eigenstates near the localization transition on random regular graphs", Phys. Rev. B **99**, 024202 (2019).

[288]G. B. Arous and A. Guionnet, "Wigner matrices", in *The Oxford Handbook of Random Matrix Theory* (Oxford University Press, 2015).

[289]M. Potters and J.-P. Bouchaud, *A first course in random matrix theory: for physicists, engineers and data scientists* (Cambridge University Press, 2020).

[290]G. Semerjian and L. F. Cugliandolo, "Sparse random matrices: the eigenvalue spectrum revisited", J. Phys. A: Math. Gen. **35**, 4837–4851 (2002).

[291]T. Rogers, I. Pérez Castillo, R. Kühn, and K. Takeda, "Cavity approach to the spectral density of sparse symmetric random matrices", Phys. Rev. E **78**, 031116 (2008).

[292]F. L. Metz, G. Parisi, and L. Leuzzi, "Finite-size corrections to the spectrum of regular random graphs: an analytical solution", Phys. Rev. E **90**, 052109 (2014).

[293]G. De Tomasi and I. M. Khaymovich, "Non-Hermitian Rosenzweig-Porter random-matrix ensemble: Obstruction to the fractal phase", Phys. Rev. B **106**, 094204 (2022).

[294]A. Kutlin and I. M. Khaymovich, "Anatomy of the eigenstates distribution: a quest for a genuine multifractality", arXiv:2309.06468 (2023).

[295]J. Tailleur and M. E. Cates, "Statistical mechanics of interacting run-and-tumble bacteria", Phys. Rev. Lett. **100**, 218103 (2008).

[296]D. Martin, J. O'Byrne, M. E. Cates, É. Fodor, C. Nardini, J. Tailleur, and F. van Wijland, "Statistical mechanics of active Ornstein-Uhlenbeck particles", Phys. Rev. E **103**, 032607 (2021).

[297]R. Wittkowski, A. Tiribocchi, J. Stenhammar, R. J. Allen, D. Marenduzzo, and M. E. Cates, "Scalar φ^4 field theory for active-particle phase separation", Nat. Commun. **5**, 4351 (2014).

[298]M. E. Cates, "Active field theories", in *Active matter and nonequilibrium statistical physics: lecture notes of the Les Houches summer school 2018* (Oxford University PressOxford, 2022), pp. 180–216.

[299]C. Maggi, N. Gnan, M. Paoluzzi, E. Zaccarelli, and A. Crisanti, "Critical active dynamics is captured by a colored-noise driven field theory", Commun. Phys. **5**, 55 (2022).

[300]R. Zakine, J.-B. Fournier, and F. van Wijland, "Field-embedded particles driven by active flips", Phys. Rev. Lett. **121**, 028001 (2018).

[301]P. Akara-pipattana and O. Evnin, "Random matrices with row constraints and eigenvalue distributions of graph Laplacians", J. Phys. A: Math. Theor. **56**, 295001 (2023).

[302]K. Efetov, *Supersymmetry in disorder and chaos* (Cambridge University Press, 1996).

[303]G. Arfken, *Mathematical methods for physicists*, 3rd ed. (Academic Press, San Diego, 1985).

[304]D. Frenkel and B. Smit, *Understanding molecular simulation: from algorithms to applications*, 2nd ed., Vol. 1 (Academic Press, San Diego, 2002).

[305]R. L. Honeycutt, "Stochastic Runge-Kutta algorithms. I. White noise", Phys. Rev. A **45**, 600–603 (1992).

[306]D. Venturelli and B. Walter, *Source code for a particle in a scalar field*, `https://github.com/sonarventu/field_and_particle`, 2021.

[307]A. Onuki, *Phase transition dynamics* (Cambridge University Press, 2002).

[308]E. A. Novikov, "Functionals and the random-force method in turbulence theory", Sov. Phys. JETP **20**, 1290–1294 (1965).

[309]C. M. Bender and S. A. Orszag, *Advanced Mathematical Methods for Scientists and Engineers* (McGraw-Hill, 1978).

[310]U. Seifert, "Entropy production along a stochastic trajectory and an integral fluctuation theorem", Phys. Rev. Lett. **95**, 040602 (2005).

[311]F. Zamponi, F. Bonetto, L. F. Cugliandolo, and J. Kurchan, "A fluctuation theorem for non-equilibrium relaxational systems driven by external forces", J. Stat. Mech. **2005**, P09013 (2005).

[312]T. E. Hull and C. Froese, "Asymptotic behaviour of the inverse of a Laplace transform", Canadian J. Math. **7**, 116–125 (1955).

[313]S. Redner, *A guide to first-passage processes* (Cambridge University Press, 2001).

[314]R. Morgado, F. A. Oliveira, G. G. Batrouni, and A. Hansen, "Relation between anomalous and normal diffusion in systems with memory", Phys. Rev. Lett. **89**, 100601 (2002).

[315]Y. L. Raikher, V. V. Rusakov, and R. Perzynski, "Brownian motion in a viscoelastic medium modelled by a Jeffreys fluid", Soft Matter **9**, 10857 (2013).

[316]J. Mayer, K. Khairy, and J. Howard, "Drawing an elephant with four complex parameters", Am. J. Phys. **78**, 648–649 (2010).

[317]P. Sollich, "Rheological constitutive equation for a model of soft glassy materials", Phys. Rev. E **58**, 738–759 (1998).

[318]S. M. Fielding, P. Sollich, and M. E. Cates, "Aging and rheology in soft materials", J. Rheol. **44**, 323–369 (2000).

[319]M. Fuchs and M. E. Cates, "Schematic models for dynamic yielding of sheared colloidal glasses", Faraday Discuss. **123**, 267–286 (2002).

[320]M. L. Falk and J. Langer, "Deformation and failure of amorphous, solidlike materials", Ann. Rev. Condens. Matter Phys. **2**, 353–373 (2011).

[321]C. P. Amann, M. Siebenbürger, M. Krüger, F. Weysser, M. Ballauff, and M. Fuchs, "Overshoots in stress-strain curves: colloid experiments and schematic mode coupling theory", J. Rheol. **57**, 149–175 (2013).

[322]N. W. Ashcroft and N. D. Mermin, *Solid State Physics* (Holt-Saunders, 1976).

[323]D. Voiculescu, "Limit laws for random matrices and free products", Invent. Math. **104**, 201–220 (1991).

[324]P. Biane, "On the free convolution with a semi-circular distribution", Indiana U. Math. J. **46**, 705–718 (1997).

[325]F. J. Dyson, "Statistical theory of the energy levels of complex systems. III", J. Math. Phys. **3**, 166–175 (1962).

[326]A. Cavagna, J. P. Garrahan, and I. Giardina, "Index distribution of random matrices with an application to disordered systems", Phys. Rev. B **61**, 3960–3970 (2000).

[327]S. N. Majumdar, C. Nadal, A. Scardicchio, and P. Vivo, "Index distribution of Gaussian random matrices", Phys. Rev. Lett. **103**, 220603 (2009).

[328]S. N. Majumdar, C. Nadal, A. Scardicchio, and P. Vivo, "How many eigenvalues of a Gaussian random matrix are positive?", Phys. Rev. E **83**, 041105 (2011).

[329]I. Pérez Castillo, "Spectral order statistics of Gaussian random matrices: Large deviations for trapped fermions and associated phase transitions", Phys. Rev. E **90**, 040102 (2014).

A

Markovian embedding and effective equation

In this Appendix we present a simple example of a coupled 2-variables system, where the first variable can be explicitly integrated out in order to obtain an effective equation for the other. The inverse process is known as *Markovian embedding*. This will clarify the meaning of the above mentioned effective equation, and the construction of its path-integral representation, which will serve as a prototype for the model of a particle coupled to a field discussed in Chapter 2 (and anticipated in Appendix A.2).

A.1 A toy model

Consider the Hamiltonian involving the two variables X and Y,

$$\mathcal{H}(X,Y) = \mathcal{U}(X) + \frac{\kappa_y}{2}Y^2 \quad \lambda\mathcal{V}(X,Y), \qquad \text{with} \qquad \mathcal{V}(x,y) \equiv y f(x), \tag{A.1}$$

where $f(x)$ is in general a *nonlinear* function of x. Assume that X and Y evolve as

$$\dot{X} = \quad \nu_x \frac{\partial \mathcal{H}}{\partial X} + \eta_x, \qquad \dot{Y} = \quad \nu_y \frac{\partial \mathcal{H}}{\partial Y} + \eta_y, \tag{A.2}$$

where the two η_i's are white uncorrelated Gaussian noises with zero mean and

$$\langle \eta_i(t)\eta_i(s)\rangle = 2\nu_i k_B T \delta(t \quad s) \equiv \Omega_i \delta(t \quad s)\ . \tag{A.3}$$

We are interested in the effective dynamics of $X(t)$ once the Y-coordinate is integrated out.

A.1.1 Effective equation

Since the Hamiltonian is quadratic in Y and the coupling potential $\mathcal{V}(x,y)$ is linear in y, the equation of motion for $Y(t)$ can be solved by means of its linear response function

$$G_y(t,s) \equiv \Theta(t \quad s) e^{\ \gamma_y(t \ \ s)}, \tag{A.4}$$

[1] One should understand X as the position of the particle, and Y as one of the field Fourier modes with which the particle interacts in the full problem discussed in Chapter 2 and Appendix A.2.

where $\gamma_y \equiv \nu_y \kappa_y$, and the result can be plugged back into Eq. (A.2) to obtain the effective equation

$$\begin{aligned}\dot{X}(t) = \quad & \nu_x \mathcal{U}'(X(t)) + \lambda^2 \nu_x f'(X(t)) \int_{t_0}^{t} \mathrm{d}s\, \chi_y(t,s) f(X(s)) \\ & + \eta_x(t) + \lambda f'(X(t)) \underbrace{\nu_x \int_{t_0}^{t} \mathrm{d}s\, G_y(t,s) \eta_y(s)}_{\zeta_y(t)} . \end{aligned} \tag{A.5}$$

Above we assumed for simplicity $Y(t = t_0) = 0$, and we introduced the linear susceptibility $\chi_y(t,s) \equiv \nu_y G_y(t,s)$. The effect of the coupling to Y on the dynamics of X is encoded in a memory term in the first line, plus a colored and multiplicative noise term in the second line. We can indeed identify the colored noise $\zeta_y(t)$, which is Gaussian with zero mean and correlation $\langle \zeta_y(t)\zeta_y(s)\rangle = \nu_x^2 C_y(t,s)$, where C_y is the (equilibrium) correlator of Y (see Eq. (1.13)), i.e.,

$$C_y(t,s) = \frac{\Omega_y}{2\gamma_y} e^{-\gamma_y |t-s|}. \tag{A.6}$$

Upon introducing the combinations

$$\mathcal{F}(x,y;t-s) \equiv \lambda^2 \nu_x f'(x) \chi_y(t-s) f'(y), \tag{A.7}$$

$$\Xi(x,t) \equiv \eta_x(t) + \lambda f'(x) \zeta_y(t), \tag{A.8}$$

we may formally rewrite Eq. (A.5) as

$$\dot{X}(t) = \nu_x \mathcal{U}'(X(t)) + \int_{t_0}^{t} \mathrm{d}s\, \mathcal{F}(X(t), X(s); t-s) + \Xi(X(t), t). \tag{A.9}$$

Of course the quantity $\Xi(X(t),t)$ — seen as an effective multiplicative noise, which is a function of the trajectory $X(t)$ — is in general *not* Gaussian and there is no reason for it to have zero mean. Note, however, that considering instead $\Xi(x,t)$ as a random function of time t alone, with an additional parametric dependence on x, would formally render $\langle \Xi(x,t)\rangle = 0$ *for any fixed value of* x (i.e., not along the trajectory $X(t)$), and

$$\begin{aligned}\langle \Xi(x_1,t)\Xi(x_2,s)\rangle &= \langle \eta_x(t)\eta_x(s)\rangle + \lambda^2 f'(x_1) f'(x_2) \left\langle \zeta_y(t)\zeta_y(s)\right\rangle \\ &= \Omega_x \delta(t-s) + \lambda^2 f'(x_1) f'(x_2) \nu_x^2 C_y(t,s) \equiv C_\Xi(x_1,x_2;t,s), \end{aligned} \tag{A.10}$$

where in the second line we have used the fact that η_x and ζ_y are independent.

A.1.2 Path integral representation

Stepping from the effective equation (A.5) to its path integral formulation is a priori nontrivial: the presence of multiplicative noise can in general produce additional drift terms depending on the integration convention we choose (Itô, Stratonovich), which have to be included in the dynamical functional [57]. An unambiguous way of proceeding is to start from the dynamical

functionals (see Section 1.5) describing the joint stochastic dynamics of the two variables:

$$\mathcal{S}[X,\tilde{X},Y,\tilde{Y}] = \mathcal{S}_0[X,\tilde{X}] + \mathcal{S}_1[Y,\tilde{Y}] \quad \lambda\mathcal{S}_{\text{int}}[X,\tilde{X},Y,\tilde{Y}], \tag{A.11}$$

$$\mathcal{S}_0[X,\tilde{X}] = \int \mathrm{d}t \left\{ \tilde{X}(t)\left[\dot{X}(t) + \nu_x \mathcal{U}'(X(t))\right] \quad \frac{\Omega_x}{2}\tilde{X}^2(t)\right\}, \tag{A.12}$$

$$\mathcal{S}_1[Y,\tilde{Y}] = \int \mathrm{d}t \left\{ \tilde{Y}(t)\left[\dot{Y}(t) + \gamma_y Y(t)\right] \quad \frac{\Omega_y}{2}\tilde{Y}^2(t)\right\}, \tag{A.13}$$

$$\mathcal{S}_{\text{int}}[X,\tilde{X},Y,\tilde{Y}] = \int \mathrm{d}t \left[\tilde{X}(t)\nu_x Y(t) f'(X(t)) + \tilde{Y}(t)\nu_y f(X(t))\right]. \tag{A.14}$$

These can be obtained by standard methods and no ambiguity (see Section 1.5), because the initial equations (A.2) only feature additive noise, which is insensitive to the integration convention[2]. Performing the Gaussian functional integral

$$\iint \mathcal{D}Y\,\mathcal{D}\tilde{Y}\, e^{\ \mathcal{S}[X,\tilde{X},Y,\tilde{Y}]} \equiv e^{\ \mathcal{S}_{\text{eff}}[X,\tilde{X}]} \tag{A.15}$$

then gives the effective action

$$\mathcal{S}_{\text{eff}}[X,\tilde{X}] = \int \mathrm{d}t\, \tilde{X}(t)\left[\dot{X}(t) + \nu_x \mathcal{U}'(X(t)) \quad \int \mathrm{d}s\, F(X(t),X(s);t \quad s)\right] \\ \frac{1}{2}\iint \mathrm{d}t\,\mathrm{d}s\, \tilde{X}(t) C_\Xi(X(t),X(s);t,s)\tilde{X}(s), \tag{A.16}$$

where the functions $\mathcal{F}$ and C_Ξ were defined in Eqs. (A.7) and (A.10), respectively. Comparing Eq. (A.16) with the effective equation (A.5) shows why it was useful to formally introduce C_Ξ as in Eq. (A.10): indeed, the dynamical action in Eq. (A.16) has the exact same form one would guess *by sight* from Eq. (A.5), as if the noise Ξ were Gaussian and additive — see Eq. (1.47).

It turns out that the effective equation (A.5) can in fact be mapped onto the more general one studied in Ref. [56], and that the corresponding dynamical functional coincides with the one in Eq. (A.16). The general dynamical action given in Ref. [56] is independent of the integration convention as long as the noise is colored, which appears physically intuitive now that we know where this noise comes from.

A.2 Particle coupled to a field

The toy model described above can be easily generalized to the case of $(n+1)$ variables with Hamiltonian

$$\mathcal{H}(X,\{Y_i\}_{i=1}^n) = \mathcal{U}(X) + \sum_{i=1}^n \frac{\kappa_i}{2}Y_i^2 \quad \lambda\mathcal{V}(X,\{Y_i\}), \qquad \mathcal{V}(x,\{y_i\}) \equiv \sum_{i=1}^n V_i y_i f_i(x), \tag{A.17}$$

with "weights" V_i. The problem described in Chapter 2 of a particle coupled to a field, i.e., to the continuum of its Fourier modes labelled by $\mathbf{q}$, can be easily understood on the same footing

[2] Here we chose the Itô convention only to suppress spurious terms deriving from the Jacobian in Eq. (1.40), but which do not modify the equations of motion [54].

by considering the Hamiltonian[3]

$$\mathcal{H}(\mathbf{X}, \{\phi_q\}) = \mathcal{U}(\mathbf{X}) + \int \frac{\mathrm{d}^d q}{(2\pi)^d} \frac{q^2 + r}{2} \phi_q \phi_{\ q} \quad \lambda \mathcal{V}(\mathbf{X}, \{\phi_q\}), \tag{A.18}$$

$$\mathcal{V}(\mathbf{x}, \{\phi_q\}) \equiv \int \frac{\mathrm{d}^d q}{(2\pi)^d} V_{\ q} \phi_q e^{i\mathbf{q}\cdot\mathbf{x}}, \tag{A.19}$$

where the $V_{\ q}$'s play the role of the weights introduced above. The dynamical action given later in Eqs. (3.74) and (C.109) can in this sense be understood as a generalization of the one in Eq. (A.16).

[3]One should really separate the real and imaginary parts of ϕ_q in order to obtain full decoupling; we did not do it here for simplicity, but we will discuss this subtlety in Section 2.3.1.

B

Calculations of Chapter 2

B.1 n-time correlation functions of the non-interacting particle

The knowledge of the one- and two-time correlation functions is sufficient to write the generating functional $\mathcal{Z}[j]$ for any Gaussian process: for each scalar component $X_i(t) \mapsto x(t)$, it reads

$$\begin{aligned}\mathcal{Z}[j] &= \left\langle \exp\left[\int \mathrm{d}s\, j(s)x(s)\right]\right\rangle = \int \mathcal{D}x(s) e^{\ \mathcal{S}_{\mathrm{OM}}[x(\tau)]+\int \mathrm{d}s j(s)x(s)} \\ &= \exp\left[\frac{1}{2}\int \mathrm{d}s_1\, \mathrm{d}s_2\, j(s_1)C(s_1,s_2)j(s_2) + \int \mathrm{d}s\, j(s)m(s)\right], \end{aligned} \tag{B.1}$$

where we averaged the source term $j(x)$ over the Onsager-Machlup dynamical functional (see Section 1.5)

$$\mathcal{S}_{\mathrm{OM}}[x(\tau)] \equiv \frac{1}{2}\int \mathrm{d}s_1\, \mathrm{d}s_2\, [x(s_1) \quad m(s_1)]C^{\ -1}(s_1,s_2)[x(s_2) \quad m(s_2)], \tag{B.2}$$

and we normalized the integration measure $\mathcal{D}x(s)$ so that $\mathcal{Z}[j=0]=1$. Here the functions $m(s)$ and $C(s_1,s_2)$ are the average and 2-point function of the Ornstein-Uhlenbeck particle discussed in Section 1.2 — see Eqs. (1.10) and (1.13), respectively. We can use the generating functional to compute a generic n-time expectation value over the independent process, and in particular $Q_{\mathbf{q}}(s_1,s_2)$ defined in Eq. (2.14). Notice first that, due to the statistical independence of the process along the various spatial coordinates,

$$Q_{\mathbf{q}}(s_1,s_2) = \prod_{n=1}^{d} \left\langle e^{iq_n[X_n^{(0)}(s_2) \quad X_n^{(0)}(s_1)]}\right\rangle . \tag{B.3}$$

Each of these factors can be simply obtained from $\mathcal{Z}[j]$ in Eq. (B.1) by setting $j = j^*(s) \equiv iq_n\,[\delta(s \quad s_2) \quad \delta(s \quad s_1)]$, which yields

$$Q_{\mathbf{q}}(s_1,s_2) = \exp\left\{ i\mathbf{q}\cdot[\mathbf{m}(s_2) \quad \mathbf{m}(s_1)] \quad \frac{q^2}{2}\,[C(s_1,s_1)+C(s_2,s_2) \quad 2C(s_1,s_2)]\right\}. \tag{B.4}$$

In order to specialize this formula to our problem, let again the particle leave the initial position $\mathbf{X}_0$ at time $t = t_0$; the effect of having $\mathbf{X}_0 \neq 0$ enters solely in the expression of $\mathbf{m}(t)$ given in Eq. (1.10) (with $\mathbf{X}_F(t) \equiv 0$). We may write explicitly, in terms of the two-time function $C(s_1,s_2)$ defined in Eq. (1.13),

$$e^{\ \frac{q^2}{2}[C(s_1,s_1)+C(s_2,s_2) \ \ 2C(s_1,s_2)]} = \begin{cases} \exp\left\{ \ \frac{Tq^2}{\kappa}\left[1 \quad e^{\ \gamma|s_2 \ \ s_1|} \quad \frac{(e^{\ \gamma s_1} \ e^{\ \gamma s_2})^2}{2}\right]\right\} & \text{for } t_0 = 0, \\ \exp\left[\ \frac{Tq^2}{\kappa}\left(1 \quad e^{\ \gamma|s_2 \ \ s_1|}\right)\right] & \text{for } t_0 \to \ \infty. \end{cases} \tag{B.5}$$

In particular, for $t_0 = 0$,

$$\mathbf{m}(s_2) \quad \mathbf{m}(s_1) = \mathbf{X}_0 \left(e^{\ \gamma s_2} \quad e^{\ \gamma s_1}\right), \tag{B.6}$$

while $\mathbf{m}(t)$ vanishes for $t_0 \to \quad \infty$.

In the perturbative calculations discussed further below, we also need the expressions for the averages

$$\langle e^{i\mathbf{q}\cdot\mathbf{X}^{(0)}(t)}\rangle = \prod_{n=1}^{d} \langle e^{iq_n X_n^{(0)}(t)}\rangle\,, \tag{B.7}$$

$$\langle X_j^{(0)}(s_2) e^{i\mathbf{q}\cdot\mathbf{X}^{(0)}(s_1)}\rangle = \langle X_j^{(0)}(s_2) e^{iq_j X_j^{(0)}(s_1)}\rangle \prod_{n\neq j}^{d} \langle e^{iq_n X_n^{(0)}(s_2)}\rangle\,. \tag{B.8}$$

These quantities can be similarly calculated by using the generating functional in Eq. (B.1):

$$\left\langle e^{iq_j X_j^{(0)}(t)}\right\rangle = \mathcal{Z}\left[j(s) = iq_j\delta(s \quad t)\right] = e^{\ \frac{1}{2}q_j^2 C(t,t)} e^{iq_j m_j(t)}, \tag{B.9}$$

$$\left\langle X_j^{(0)}(s_2) e^{iq_j X_j^{(0)}(s_1)}\right\rangle = \frac{\delta}{\delta j(s_2)}\mathcal{Z}[j]\Big|_{j(s)=iq_j\delta(s\ \ s_1)} = \left[m_j(s_2) + iq_j C(s_1,s_2)\right]\ \langle e^{iq_j X_j^{(0)}(s_1)}\rangle\,, \tag{B.10}$$

whence

$$\langle e^{i\mathbf{q}\cdot\mathbf{X}^{(0)}(t)}\rangle = e^{\ \frac{1}{2}q^2 C(t,t)} e^{i\mathbf{q}\cdot\mathbf{m}(t)}, \tag{B.11}$$

$$\langle \mathbf{X}^{(0)}(s_2) e^{i\mathbf{q}\cdot\mathbf{X}^{(0)}(s_1)}\rangle = \left[\mathbf{m}(s_2) + i\mathbf{q}C(s_1,s_2)\right]\ \langle e^{i\mathbf{q}\cdot\mathbf{X}^{(0)}(s_1)}\rangle\,. \tag{B.12}$$

B.2 Marginal equilibrium distribution of the particle

The equilibrium distribution of the system composed by the particle in interaction with the field, the field itself and the thermal bath which provides the thermal noise is given by the Boltzmann distribution

$$P_{\rm eq}[\phi,\mathbf{X}] \propto \exp\quad \beta\mathcal{H}[\phi,\mathbf{X}]\big), \tag{B.13}$$

where β is the inverse temperature of the bath and $\mathcal{H}$ is the Hamiltonian. Assume that the latter has the generic form

$$\mathcal{H}[\phi,\mathbf{X}] = \mathcal{H}_\phi[\phi] + \mathcal{U}(\mathbf{X}) + \mathcal{H}_{\rm int}[\phi,\mathbf{X}], \tag{B.14}$$

where $\mathcal{H}_\phi[\phi]$ describes the field in the bulk and is not necessarily Gaussian, while $\mathcal{U}(\mathbf{X})$ is a confining potential for the particle, e.g., $\mathcal{U}(\mathbf{X}) = (\kappa/2)\mathbf{X}^2$ in the case considered in Chapter 2. Finally, $\mathcal{H}_{\rm int}$ describes the interaction between the particle and the field via a possibly nonlinear coupling

$$\mathcal{H}_{\rm int}[\phi,\mathbf{X}] = \int \mathrm{d}^d x\, F[\phi(\mathbf{x})] V(\mathbf{x} \quad \mathbf{X}), \tag{B.15}$$

where $F[\phi(\mathbf{x})]$ is a quasi-local functional of ϕ. Importantly, we require $\mathcal{H}_{\rm int}$ to be translationally invariant, in the sense that

$$\mathcal{H}_{\rm int}[\phi(\mathbf{x}),\mathbf{X}] = \mathcal{H}_{\rm int}[\phi(\mathbf{x} \quad \mathbf{a}),\mathbf{X}+\mathbf{a}]\,. \tag{B.16}$$

Note that the interacting Hamiltonian in Eq. (2.3) satisfies these requirements, while the one in, c.f., Eq. (5.2) does not, due to the confinement.

The equilibrium distribution of the particle follows as

$$P_{\rm eq}(\mathbf{X}) \propto \int \mathcal{D}\phi\, e^{-\beta\mathcal{H}[\phi,\mathbf{X}]} = e^{-\beta\mathcal{U}(\mathbf{X})} \int \mathcal{D}\phi\, e^{-\beta\{\mathcal{H}_\phi[\phi]+\mathcal{H}_{\rm int}[\phi,\mathbf{X}]\}}, \tag{B.17}$$

and our aim is to show that the functional integral on the right-hand-side does not actually depend on $\mathbf{X}$, i.e., that the interaction with the field does not affect the equilibrium distribution $P_{\rm eq}(\mathbf{X}) \propto \exp[-\beta\mathcal{U}(\mathbf{X})]$ of the particle. The argument goes as follows: introduce $\mathbf{z} = \mathbf{x} - \mathbf{X}$ and define a new shifted field $\varphi(\mathbf{z}) \equiv \phi(\mathbf{z}+\mathbf{X})$. Since the field is in the bulk, then $\mathcal{H}_\phi[\phi] = \mathcal{H}_\phi[\varphi]$, while $\mathcal{H}_{\rm int}$ in Eq. (B.15) becomes

$$\mathcal{H}_{\rm int}[\phi,\mathbf{X}] \to \int \mathrm{d}^d\mathbf{z}\; F[\varphi(\mathbf{z})]V(\mathbf{z}). \tag{B.18}$$

The proof is concluded by noting that the integration measure $\mathcal{D}\phi$ in Eq. (B.17) remains the same under a translation by $\mathbf{X}$ in space.

We emphasize that this argument fails if the system is not translationally invariant, as it happens, for instance, in the presence of boundaries or confinement [64, 65]. Moreover, it does not imply the factorization of $P_{\rm eq}[\phi,\mathbf{X}]$ into two independent parts at long times. In fact, the marginal equilibrium distribution of the field ϕ, which may be obtained by integrating out $\mathbf{X}$ in Eq. (B.13), is actually modified by the presence of the particle. For a linear field-particle coupling such as that of Eq. (2.1), for instance, we physically expect at equilibrium the field to be enhanced around the particle, i.e., around the minima of its confining potential $\mathcal{U}(\mathbf{x})$.

B.3 Perturbative calculation of the average particle position

Here we compute the correction to the average particle position, to the lowest nontrivial order in the coupling λ, due to the presence of the field. To this end, we first insert the perturbative expansions given in Eq. (2.11) into Eq. (2.6) for the particle, thus getting, order by order in the coupling λ,

$$\dot{\mathbf{X}}^{(0)}(t) = -\nu k\mathbf{X}^{(0)}(t) + \boldsymbol{\xi}(t), \tag{B.19}$$

$$\dot{\mathbf{X}}^{(n)}(t) = -\nu k\mathbf{X}^{(n)}(t) + \nu\mathbf{f}^{(n-1)}(t), \tag{B.20}$$

where we introduced

$$\mathbf{f}^{(n)}(t) \equiv \frac{1}{n!}\frac{\mathrm{d}^n}{\mathrm{d}\lambda^n}\bigg|_{\lambda=0}\mathbf{f}(t). \tag{B.21}$$

At $O(\lambda^0)$, Eq. (B.19) is solved by the Ornstein-Uhlenbeck process, recalled in Section 1.2. The higher-order corrections $\mathbf{X}^{(n)}$ can be formally expressed as

$$\mathbf{X}^{(n)}(t) = \nu\int_{t_0}^{t}\mathrm{d}s\, e^{-\gamma(t-s)}\mathbf{f}^{(n-1)}(s), \tag{B.22}$$

where t_0 is the time at which the initial condition $\mathbf{X}^{(0)}(t = t_0) = \mathbf{X}_0$ is imposed. Similarly, the Langevin equation (2.8) for the field in Fourier space renders

$$\partial_t \phi_{\mathbf{q}}^{(0)}(t) = \quad {}_q\phi_{\mathbf{q}}^{(0)}(t) + \eta_{\mathbf{q}}(t), \tag{B.23}$$

$$\partial_t \phi_{\mathbf{q}}^{(n)}(t) = \quad {}_q\phi_{\mathbf{q}}^{(n)}(t) + \frac{Dq \;\; V_q}{(n \quad 1)} \frac{\mathrm{d}^{n \;\; 1}}{\mathrm{d}\lambda^{n \;\; 1}}\bigg|_{\lambda=0} e^{\;\; i\mathbf{q}\cdot\mathbf{X}}, \tag{B.24}$$

where $\mathbf{X}$ on the r.h.s. of Eq. (B.24) is written in powers of λ as in Eq. (2.11). The function V_q is the Fourier transform of the interaction potential $V(\mathbf{x})$, and it only depends on $|\mathbf{q}|$ if we take $V(\mathbf{x})$ to be isotropic, i.e., a function of $|\mathbf{x}|$. The properties of the uncoupled field $\phi_{\mathbf{q}}^{(0)}(t)$ were discussed in Section 1.3, while the equation of motion of the field at $O(\lambda)$ can be formally solved as

$$\phi_{\mathbf{q}}^{(1)}(s) = Dq \;\; V_q \int_{t_0}^{s} \mathrm{d}\tau \, e^{\;\; {}_q(s \;\; \tau)} e^{\;\; i\mathbf{q}\cdot\mathbf{X}^{(0)}(\tau)}. \tag{B.25}$$

If we assumed the field to be initially in thermal equilibrium *in contact* with the particle, then a second term accounting for the initial condition of the field would appear in Eq. (B.25) in the form $G_q(t \quad t_0)\phi_{\mathbf{q}}^{(1)}(t_0)$, where the function $G_q(\tau)$ is the free-field propagator defined in Eq. (1.27). However, such a term turns out *a posteriori* to be irrelevant for what concerns the long-time properties of the tracer particle (while it greatly impacts its short-time properties, as we explore in Chapter 4). For the sake of simplicity, here we will thus assume that the initial condition of the field $\phi_{\mathbf{q}}(t_0)$ is extracted from its stationary distribution reached *before* the particle is put in contact with the field.

The first nontrivial correction $\langle \mathbf{X}^{(2)}(t) \rangle$ to the average particle position (see Eq. (2.12)) can then be computed starting from

$$\begin{aligned}
\mathbf{f}^{(0)}(s_1) &= \int \frac{\mathrm{d}^d q}{(2\pi)^d} i\mathbf{q} V \;\; {}_q\phi_{\mathbf{q}}^{(0)}(s_1) e^{i\mathbf{q}\cdot\mathbf{X}^{(0)}(s_1)}, \\
\mathbf{f}^{(1)}(s_2) &= \int \frac{\mathrm{d}^d q}{(2\pi)^d} i\mathbf{q} V \;\; {}_q e^{i\mathbf{q}\cdot\mathbf{X}^{(0)}(s_2)} \left[\phi_{\mathbf{q}}^{(1)}(s_2) + i\mathbf{q}\cdot\mathbf{X}^{(1)}(s_2)\phi_{\mathbf{q}}^{(0)}(s_2) \right],
\end{aligned} \tag{B.26}$$

while bearing in mind that, as we take the expectation values over the realizations of the noises $\eta_{\mathbf{q}}(t)$ and $\xi(t)$,

$$\langle \phi_{\mathbf{q}}^{(0)}(s_2)\phi_{\mathbf{q}}^{(0)}(s_1) e^{i\mathbf{q}\cdot[\mathbf{X}^{(0)}(s_2) \;\; \mathbf{X}^{(0)}(s_1)]} \rangle = \langle \phi_{\mathbf{q}}^{(0)}(s_2)\phi_{\mathbf{q}}^{(0)}(s_1) \rangle \, \langle e^{i\mathbf{q}\cdot[\mathbf{X}^{(0)}(s_2) \;\; \mathbf{X}^{(0)}(s_1)]} \rangle \,, \tag{B.27}$$

because at $O\left(\lambda^0\right)$ the two processes $\phi_{\mathbf{q}}^{(0)}(t)$ and $\mathbf{X}^{(0)}(t)$ are independent. Using $V_{\;\; q} = V_q^*$ because $V(\mathbf{x})$ is real, we find the expression reported in Eq. (2.13) in the main text.

B.4 Long-time behavior of the average position

In this section we derive the asymptotic behaviour of the second-order correction to the average position in Eq. (2.13) at long times by considering separately the cases of model A and model B field dynamics. A more general calculation, which comprises both cases close to criticality, is provided later in Appendix B.5.

By rotational symmetry, we can choose the initial position to have a single non-vanishing coordinate, i.e., $\mathbf{X}_0(t) = X_0\,\hat{}$, where $\hat{}$ is the unit vector of the j-th Cartesian axis. The resulting average position $\langle \mathbf{X}(t) \rangle$ will then vanish at all times for all but the j-th component. The latter can be written, upon using Eqs. (1.30), (1.31), (B.4) and (B.5), as

$$\langle X_j^{(2)}(t) \rangle = \frac{\nu}{T} \int \frac{\mathrm{d}^d q}{(2\pi)^d} q_j |V_q|^2 \int_0^t \mathrm{d}s_2\, e^{\ \gamma(t\ \ s_2)} \int_0^{s_2} \mathrm{d}s_1 \left[\ _{\mathbf{q}} + \nu T q^2 e^{\ \gamma(s_2\ \ s_1)} \right] \times C_q(s_2 \quad s_1) \sin\ q_j X_{0j} (e^{\ \gamma s_1} \quad e^{\ \gamma s_2}) \big)\, e^{\ R(s_2, s_1) q^2}, \tag{B.28}$$

where we introduced, for brevity,

$$R(s_2, s_1) \equiv \frac{T}{k} \left[1 \quad e^{\ \gamma |s_2\ \ s_1|} \quad \frac{1}{2} (e^{\ \gamma s_2} \quad e^{\ \gamma s_1})^2 \right]. \tag{B.29}$$

The more general case in which the particle is linearly coupled to the n-th even derivative of the field, as it does in Eq. (2.15), can be simply accounted for as follows. Note first that Eq. (2.15) can be rewritten in Fourier space for even n as

$$\mathcal{H}_{\text{int}} = \ \lambda \int \frac{\mathrm{d}^d q}{(2\pi)^d} \phi\ _{\mathbf{q}}(t) (iq)^n V_q e^{\ i\mathbf{q}\cdot\mathbf{X}(t)}. \tag{B.30}$$

It is then sufficient to replace V_q in Eq. (B.28) with $\tilde{V}_q \equiv (iq)^n V_q$. Since $V(\mathbf{x})$ is normalized, we can expand the Fourier transform of the rotationally-invariant potential V_q as $|V_q|^2 = 1 + c_2 q^2 + \dots$, whence $|\tilde{V}_q|^2 = q^{2n} + c_2 q^{2(n+1)} + \dots$. Without loss of generality, $\langle X_j^{(2)}(t) \rangle$ can then be expressed as a sum of expressions identical to Eq. (B.28), but with q^{2n} in place of $|V_q|^2$. Accordingly, in the following we consider the specific case of a potential with $|V_q|^2 = q^{2n}$ and we will show that each term in this sum becomes increasingly subleading at long times upon increasing n.

B.4.1 Field with model A dynamics

In the case of model A, we start by rescaling $s_1' = s_1/t$, $s_2' = s_2/t$ and $q \to t^{1/2} q$ so as to write Eq. (B.28) into the equivalent form

$$\langle X_j^{(2)}(t) \rangle = t^{\ (d/2+n\ \ 3/2)} \frac{\nu}{T} \int \frac{\mathrm{d}^d q}{(2\pi)^d} q_j q^{2n} \int_0^1 \mathrm{d}s_2'\, e^{\ \gamma t(1\ \ s_2')} \int_0^{s_2'} \mathrm{d}s_1'\, e^{\ R(ts_2', ts_1')t\ \ ^1 q^2} \times \left[\ _{t\ ^{1/2}q} + \nu T t\ \ ^1 q^2 e^{\ \gamma t(s_2'\ \ s_1')} \right] C_{t\ ^{1/2}q}(t(s_2' \quad s_1')) \sin \left(t\ \ ^{1/2} q_j X_{0,j} (e^{\ \gamma t s_1'} \quad e^{\ \gamma t s_2'}) \right). \tag{B.31}$$

In this way we removed the time dependence from the integration limits and left it in the integrand only; this is more convenient for considering the limit $t \to \infty$. To this end, let us briefly discuss the asymptotic behaviour for $t \to \infty$ of each term in the integrand. The first term in brackets tends to

$$_{t\ ^{1/2}q} + \nu t\ \ ^1 T q^2 e^{\ \gamma t(s_2'\ \ s_1')} = \begin{cases} Dr & \text{for } r > 0 \\ Dq^2 t\ \ ^1 & \text{for } r = 0 \end{cases} + \ \ h.o., \tag{B.32}$$

where we noticed that in both cases the second addendum is subleading with respect to the first for large t. Here and in what follows, $h.o.$ denotes additional terms that are subleading in the limit $t \to \infty$. The field correlator tends to

$$C_{t\ 1/2q}(t(s_2'\quad s_1')) = \begin{cases} Tr\ ^1e^{\ D(rt+q^2)(s_2'\ s_1')} & \text{for } r>0 \\ Ttq\ ^2e^{\ Dq^2(s_2'\ s_1')} & \text{for } r=0 \end{cases} \quad + \quad h.o.. \tag{B.33}$$

The argument of the sine tends to zero at long times, so that we can expand $\sin x \simeq x$ to leading order. Finally, $R(ts_2', ts_1')t^{\ 1}q^2$ tends to zero at long times.

Let us now focus on the case $r > 0$. The correction to the average position of the particle is then asymptotic to

$$\langle X_j^{(2)}(t)\rangle \simeq \nu D X_{0,j} C_d t^{\ (d/2+n\ \ 1)} e^{\ \gamma t} \int_0^\infty \mathrm{d}q \int_0^1 \mathrm{d}s_2' \int_0^{s_2'} \mathrm{d}s_1'\, q^{d+2n+1} e^{\ D(rt+q^2)(s_2'\ s_1')} \left[e^{\gamma t(s_2'\ s_1')} \quad 1\right], \tag{B.34}$$

where we performed the integration over the angular q variables. The constant $C_d = c_d/d$ comes from the integration of the solid angle in d dimensions, being

$$c_d \equiv \int \frac{\mathrm{d}\Omega_d}{(2\pi)^d} = \frac{2^{1\ \ d}}{\pi^{d/2}\ (d/2)}, \tag{B.35}$$

and where we noted that we can replace $q_j^2 \to q^2/d$ in the integral. At this point the integration over s_2' and s_1' can be performed explicitly and we immediately obtain

$$\langle X_j^{(2)}(t \to \infty)\rangle \propto \begin{cases} te^{\ \nu\kappa t} & \text{for } \nu\kappa < Dr, \\ t^{\ (1+d/2+n)} e^{\ Drt} & \text{for } \nu\kappa > Dr. \end{cases} \tag{B.36}$$

For $r = 0$ the asymptotics in Eqs. (B.32)) and (B.33) are different from the non-critical case $r > 0$, and this affects the asymptotics of Eq. (B.31), which now reads (at leading order)

$$\langle X_j^{(2)}(t)\rangle \simeq \nu D^2 X_{0,j} C_d t^{\ (d/2+n\ \ 1)} e^{\ \gamma t} \int_0^\infty \mathrm{d}q \int_0^1 \mathrm{d}s_2' \int_0^{s_2'} \mathrm{d}s_1'\, q^{d+2n+1} e^{\ Dq^2(s_2'\ s_1')} \left[e^{\gamma t(s_2'\ s_1')} \quad 1\right]. \tag{B.37}$$

As before, by performing the integration over s_1' and s_2' one gets

$$\langle X_j^{(2)}(t)\rangle \propto t^{\ (d/2+n+1)}. \tag{B.38}$$

We conclude that, in model A dynamics, an algebraic behavior of the tracer particle is observed at long times only in the critical case $r = 0$. These results are summarized in Eq. (2.16) of the main text.

B.4.2 Field with model B dynamics

We now turn to the long-time asymptotic behaviour of the average position of the particle in the case of a field with model B dynamics. For $r > 0$, we rescale s_2, s_1 and q as we did in Section

B.4.1 in order to obtain Eq. (B.31). In this case, however, the asymptotic behaviour of the first two terms are

$$ {}_{t\ 1/2}{}_q + \nu T t\ {}^1q^2 e\ {}^{\gamma t(s_2'\ \ s_1')} = \left[Dr + \nu T e\ {}^{\gamma t(s_2'\ \ s_1')} \right] t\ {}^1q^2 \quad + \quad h.o., \tag{B.39} $$

and

$$ C_{t\ 1/2q}(t(s_2' \quad s_1')) = Tr\ {}^1e\ {}^{Drq^2(s_2'\ \ s_1')} \quad + \quad h.o., \tag{B.40} $$

thus leading to

$$ \begin{aligned} \langle X_j^{(2)}(t) \rangle = \nu X_{0,j} C_d t\ {}^{(d/2+n)} e\ {}^{\gamma t} \int_0^\infty \mathrm{d}q \int_0^1 \mathrm{d}s_2' \int_0^{s_2'} \mathrm{d}s_1'\, q^{d+2n+3} e\ {}^{Drq^2(s_2'\ \ s_1')} \\ \times \left[e^{\gamma t(s_2'\ \ s_1')} \quad 1 \right] \left[D + r\ {}^1\nu T e\ {}^{\gamma t(s_2'\ \ s_1')} \right] \quad + \quad h.o.. \end{aligned} \tag{B.41} $$

As before, the integration over s_2' and s_1' becomes trivial and we obtain

$$ \langle X_j^{(2)}(t) \rangle \propto t\ {}^{(d/2+n+2)}. \tag{B.42} $$

The case $r = 0$ requires, in contrast with the previous ones, that momenta are rescaled in Eq. (B.28) as $q \to t^{1/4} q$. In this way we get the equivalent expression

$$ \begin{aligned} \langle X_j^{(2)}(t) \rangle = t\ {}^{(d/4+n/2\ \ 7/4)} \frac{\nu}{T} \int \frac{\mathrm{d}^d q}{(2\pi)^d} q_j q^{2n} \int_0^1 \mathrm{d}s_2'\, e\ {}^{\gamma t(1\ \ s_2')} \int_0^{s_2'} \mathrm{d}s_1'\, e\ {}^{R(ts_2', ts_1')t\ {}^{1/2}q^2} \\ \times \left[{}_{t\ 1/4}{}_q + \nu T t\ {}^{1/2}q^2 e\ {}^{\gamma t(s_2'\ \ s_1')} \right] C_{t\ 1/4q}(t(s_2' \quad s_1')) \sin\left(t\ {}^{1/4} q_j X_{0,j}(e\ {}^{\gamma t s_2'} \quad e\ {}^{\gamma t s_1'}) \right). \end{aligned} \tag{B.43} $$

Since for $r = 0$

$$ {}_{t\ 1/4}{}_q + \nu T t\ {}^{1/2}q^2 e\ {}^{\gamma t(s_2'\ \ s_1')} = t\ {}^{1/2} \left[Dt\ {}^{1/2}q^4 + \nu T e\ {}^{\nu k t(s_2'\ \ s_1')} \right] \quad + \quad h.o. \tag{B.44} $$

and

$$ C_{t\ 1/4q}(t(s_2' \quad s_1')) = Tt^{1/2} q\ {}^2 e\ {}^{Dq^4(s_2'\ \ s_1')} \quad + \quad h.o., \tag{B.45} $$

one has

$$ \begin{aligned} \langle X_j^{(2)}(t) \rangle = \nu X_{0,j} C_d t\ {}^{(d/4+n/2\ \ 3/2)} e\ {}^{\gamma t} \int_0^\infty \mathrm{d}q \int_0^1 \mathrm{d}s_2' \int_0^{s_2'} \mathrm{d}s_1'\, q^{d+2n}\ {}^1e\ {}^{Dq^4(s_2'\ \ s_1')} \\ \times \left[e^{\gamma t(s_2'\ \ s_1')} \quad 1 \right] \left[Dt\ {}^{1/2}q^4 + \nu T e\ {}^{\gamma t(s_2'\ \ s_1')} \right] \quad + \quad h.o.. \end{aligned} \tag{B.46} $$

At this point the integration over s_1' and s_2' is again straightforward and we get

$$ \langle X_j^{(2)}(t) \rangle \propto t\ {}^{(d/4+n/2+1)}. \tag{B.47} $$

We thus conclude that, in model B dynamics, an algebraic behavior of the tracer particle is observed at long times both in the critical case ($r = 0$) and off-criticality ($r > 0$). These results are summarized in Eq. (2.17) in the main text.

B.5 Asymptotic behavior of the particle from the critical properties of the field

We are now in the position to relate the decay exponents of the average particle coordinate that we obtained at criticality to the dynamical critical exponent of the underlying free-field theory. The key is to introduce the general scaling form of the dynamical susceptibility and two-time function, as recalled in Eq. (1.35).

In order to address the long-time behavior of the average position, we start again from Eq. (2.13), in which we identify

$$\chi_x(t) \equiv \nu\theta(t)e^{-\gamma t} \tag{B.48}$$

as the susceptibility of the particle. We then rescale time as $s = s't$ and momenta as $p = qt^{1/z}$, as suggested by the scaling forms in Eqs. (1.35). This gives

$$\begin{aligned}\langle X_j^{(2)}(t)\rangle = t^{2-(d+1)/z} \int \frac{\mathrm{d}^d p}{(2\pi)^d} i p_j |V_{pt^{1/z}}|^2 \int_0^1 \mathrm{d}s_2' \int_0^{s_2'} \mathrm{d}s_1' \, \chi_x\left(t(1-s_2')\right) Q_{pt^{1/z}}\left(ts_1', ts_2'\right) \\ \times \left[\chi_\phi\left(pt^{1/z}, t(s_2'-s_1')\right) + (pt^{1/z})^2 \chi_x\left(t(s_2'-s_1')\right) C_\phi\left(pt^{1/z}, t(s_2'-s_1')\right)\right],\end{aligned} \tag{B.49}$$

where

$$Q_{\mathbf{q}}(s_1, s_2) = e^{i\mathbf{q}\cdot\mathbf{X_0}(e^{-\gamma s_2} - e^{-\gamma s_1}) - q^2 R(s_1,s_2)}, \tag{B.50}$$

and $R(s_1, s_2)$ was defined in Eq. (B.29). It is easy to check that $p^2 t^{2/z} R(ts_1', ts_2') \underset{\gamma t \gg 1}{\longrightarrow} 0$, thus

$$Q_{pt^{1/z}}(ts_1', ts_2') \simeq 1 + it^{1/z}\, \mathbf{p}\cdot\mathbf{X}_0 \left(e^{-\gamma t s_2'} - e^{-\gamma t s_1'}\right), \tag{B.51}$$

$$i\chi_x\left(t(1-s_2')\right) Q_{pt^{1/z}}\left(ts_1', ts_2'\right) \simeq \nu t^{1/z}\, \mathbf{p}\cdot\mathbf{X}_0 \left(e^{-\gamma t(s_2'-s_1')} - 1\right), \tag{B.52}$$

where we omitted an imaginary term from the right-hand-side of the last equation because it would vanish by symmetry when we integrate over $\mathbf{p}$ in Eq. (B.49). The integrand in Eq. (B.49) now only depends on $u \equiv s_2' - s_1'$, so that $v \equiv s_2' + s_1'$ can be integrated out yielding

$$\begin{aligned}\langle X_j^{(2)}(t)\rangle \simeq \nu t^{2-(d+2)/z} e^{-\gamma t} \int \frac{\mathrm{d}^d p}{(2\pi)^d} p_j |V_{pt^{1/z}}|^2 \mathbf{p}\cdot\mathbf{X}_0 \\ \times \int_0^1 \mathrm{d}u\, f(u) \left\{\chi_\phi\left(pt^{1/z}, tu\right) + (pt^{1/z})^2 \chi_x(tu)\, C_\phi\left(pt^{1/z}, tu\right)\right\},\end{aligned} \tag{B.53}$$

where we defined the function

$$f(u) \equiv (1-u)\left(e^{\gamma t u} - 1\right). \tag{B.54}$$

We now look for a saddle-point estimate of the integral over u in Eq. (B.53), bearing in mind that we are after terms that can counterbalance the exponential factor $\exp(-\gamma t)$ in front of the integrals, so as to produce an algebraic behavior of $\langle X_j^{(2)}(t)\rangle$ for large t. We can already drop a subleading term from

$$f(u) \simeq (1-u)e^{\gamma t u} = \exp\left\{t\left[\gamma u + \frac{1}{t}\ln(1-u)\right]\right\} \equiv e^{t g(u)}, \tag{B.55}$$

where the function $g(u)$ has its maximum in $u^* = 1 \quad (\gamma t)^{\ 1}$. The integrands χ_ϕ and C_ϕ are both decreasing functions of their second argument and they decay with the relaxation timescale τ_ϕ of the field: we thus expect them not to affect the position of the saddle point whenever $\tau_\phi \gg \tau_\kappa$, i.e., in the presence of slow field modes (with hindsight, we actually know that this argument only fails in model A when we are sufficiently far from criticality so that $Dr > \gamma$). Moreover, due to the additional factor $\chi_x(tu) \sim e^{\ \gamma tu}$ in front, the term containing C_ϕ in Eq. (B.53) is *a priori* subleading for large t. We thus obtain

$$\begin{aligned}
&\int_0^1 \mathrm{d}u\, f(u) \left[\chi_\phi\left(pt^{\ 1/\ }, tu\right) + (pt^{\ 1/\ })^2 \chi_x(tu)\, C_\phi\left(pt^{\ 1/\ }, tu\right)\right] \\
&\simeq \int_0^1 \mathrm{d}u\, e^{tg(u)} \chi_\phi\left(pt^{\ 1/\ }, tu\right) \simeq \frac{e^{\gamma t}\ ^1}{\gamma t} \chi_\phi\left(pt^{\ 1/\ }, tu^*\right) \int_{\mathbb{R}} \mathrm{d}u \exp\left[\ \frac{\gamma^2 t^2}{2}(u \quad u^*)^2\right] \\
&= \frac{\sqrt{2\pi}}{(\gamma t)^2} e^{\gamma t\ ^1} \chi_\phi\left(pt^{\ 1/\ }, t \quad 1/\gamma\right),
\end{aligned} \tag{B.56}$$

from which one reads the general asymptotic result

$$\langle X_j^{(2)}(t)\rangle \simeq \frac{\sqrt{2\pi}\nu}{e\gamma^2} t^{\ (d+2)/\ } \int \frac{\mathrm{d}^d p}{(2\pi)^d} p_j |V_{pt^{\ 1/\ }}|^2 (\mathbf{p}\cdot\mathbf{X}_0)\, \chi_\phi\left(pt^{\ 1/\ }, t \quad 1/\gamma\right). \tag{B.57}$$

This expression is in general model-dependent, through the specific form of the field susceptibility $\chi_\phi(q,t)$. Close to criticality, however, we can plug in the scaling form Eq. (1.35) to get

$$\langle X_j^{(2)}(t)\rangle \simeq t^{\ 1\ (d+2n)/\ } \int \frac{\mathrm{d}^d p}{(2\pi)^d} p_j p^{2n\ 2+} (\mathbf{p}\cdot\mathbf{X}_0)\, \chi_\pm\left(pt^{\ 1/\ } \xi, \frac{Da_0}{\xi}(t \quad 1/\gamma)\right), \tag{B.58}$$

where we set $\eta = 0$ since we are dealing with a free theory, and we generically assumed $V_q \sim q^n$ for small q; this also accounts for the case of a linear coupling to the n-th even derivative of the field as in Eq. (2.15) (see discussion in Appendix B.4). When $\xi \to \infty$, the t dependence drops out of the $\mathrm{d}^d p$ integral and we recover the universal long-time scaling at criticality, see Eq. (2.19).

Using the free-field susceptibility in Eq. (1.31) allows to write explicitly, for model A and B at criticality ($r = 0$) and within the Gaussian approximation, the asymptotic estimate

$$\langle X_j(t)\rangle \simeq \frac{\sqrt{2\pi} c_d}{e\, d} \left(1 + \frac{d+2n}{\quad}\right) \frac{\lambda^2 X_0}{k} (\gamma t)^{\ 1} (Dt)^{\ (d+2n)/\ }, \tag{B.59}$$

where the constant c_d was defined in Eq. (B.35), and (x) is the Euler Gamma function. This determines the asymptotic amplitude of the average particle position. A similar calculation gives, for the off-critical model B,

$$\langle X_j(t)\rangle \simeq \frac{\sqrt{\pi/2}\, c_d}{e\, d} \left(1 + \frac{d+2n}{\quad}\right) \frac{\lambda^2 X_0 D}{k\gamma} (Dr)^{\ (2+n+d/2)} t^{\ 2\ (d+n)/2}, \tag{B.60}$$

where we noted that the free-field susceptibility simplifies because $(p^2 t^{\ 2/\ } + r) \simeq r$ at long times, and we changed the integration variable to $y = Drp^2\sqrt{t}$ in Eq. (B.57).

We emphasize that, in order to derive our expression for the average position of the particle in Eq. (B.49), we used explicitly the fact that the Hamiltonian of the field is Gaussian: this makes the

equation of motion for $\phi_{\mathbf{q}}(t)$ linear and thus exactly solvable via its linear response propagator. This prevents a direct application of our final scaling result, Eq. (B.58), to an interacting field theory. We postpone the investigation of a possible extension in this direction to future works.

B.6 Nonlinear transient behavior for large initial displacements

In this Appendix we investigate the transient behavior displayed by the perturbative solution in Eq. (2.13) when the initial displacement X_0 is chosen sufficiently large so as to depart from the linear response regime. Our analysis is based on the phenomenological observation that a transient regime exists, in which the average displacement of the particle decays algebraically, but with a characteristic intermediate exponent different from the one displayed at longer times. One then observes, for some time t_c, a crossover to the asymptotic behavior predicted by Eqs. (2.16) and (2.17); the value of t_c grows as we increase the initial displacement X_0. Interestingly enough, the amplitude of the average position in the intermediate regime turns out to be independent of the value of X_0 itself. This behavior is well confirmed by numerical simulations of the system (see, e.g., Fig. 2.6b) and it is already visible at zero temperature; we thus focus here, for simplicity, on the noiseless case ($T = 0$).

Consider first the critical case $r = 0$. Here the field propagator $\chi_q(t)$ defined in Eq. (1.31) can be expressed, both for model A and B dynamics, in the compact form

$$\chi_q(t) = Dq^{\quad 2} e^{-Dq^{\quad}t}\Theta(t), \tag{B.61}$$

where $\quad = 2+\quad$ is the dynamical critical exponent. Stepping to dimensionless variables $s_1 \to s_1/t$, $s_2 \to s_2/t$ in Eq. (2.13) and rescaling momenta as $p = qX_0$, we can rewrite our perturbative solution for the average tracer position as [159]

$$\langle X_j^{(2)}(t)\rangle = \frac{X_0^{1\quad d}}{k}\Phi\left(\gamma t, \frac{t}{t_c}\right), \tag{B.62}$$

$$\begin{aligned}\Phi(\Pi_1,\Pi_2) = \Pi_1\Pi_2 \int \frac{\mathrm{d}^d p}{(2\pi)^d} ip_j p^{\quad} \left|V_{p/X_0}\right|^2 \int_0^1 \mathrm{d}s_2 \int_0^{s_2} \mathrm{d}s_1\, e^{-\Pi_1(1-\quad s_2)-\quad \Pi_2 p^{\quad}(s_2-\quad s_1)} \\ \times \exp\left[ip_j\left(e^{-\Pi_1 s_2}-\quad e^{-\Pi_1 s_1}\right)\right],\end{aligned} \tag{B.63}$$

where we set $t_0 = 0$ and we identified the crossover time $t_c \equiv X_0/D$. This has to be compared with the asymptotic expression we found in Eq. (2.19) which, upon setting $n = 0$, can be expressed in terms of t_c as

$$\langle X_j^{(2)}(t)\rangle \simeq \frac{c_1 X_0^{1\quad d}}{k}(\gamma t)^{\quad 1}(t/t_c)^{\quad d/\quad}. \tag{B.64}$$

The latter is, in fact, linear in X_0, so that at long times we can write

$$\langle X_j(t)\rangle \simeq c_\infty X_0\, t^{\quad \infty}, \tag{B.65}$$

where we introduced $\quad_\infty \equiv 1 + d/\quad$ and $c_\infty \propto \lambda^2/(\gamma k D^{d/\quad})$ up to a numerical constant (see Eq. (B.59) in Appendix B.5).

We already noted that the correction in Eq. (2.13) to the average position vanishes at time $t = 0$ (as well as for $t \to \infty$), and thus the function $\Phi(\Pi_1, \Pi_2)$ vanishes for $\Pi_1 = \Pi_2 = 0$. However, studying such function analytically is difficult, mostly because Π_1 and Π_2 cannot really be treated as independent variables. Note, moreover, that a residual dependence on X_0 is left into the integral over the variable p in Eq. (B.63) even after introducing dimensionless variables, thus complicating the analysis even further. Some progress can be made by assuming that, when $t_c \gg \tau_\kappa = \gamma^{-1}$ and the leading order $O(\lambda^0)$ exponential term has become negligible, the average position of the particle evolves according to a different scaling form, namely Eq. (2.39) of the main text. This second ansatz incorporates the phenomenological observation that the amplitude of the average position is independent of X_0 within the transient region $t \lesssim t_c$, while the behavior as a function of time t remains algebraic with an exponent $\theta_0 \neq \theta_\infty$. The underlying physical intuition is the following. At time $t = 0$ the particle is put in contact with the field at position $X(0) = X_0$, and at short times it is dragged primarily by the restoring force of the harmonic trap, so that $\dot{X} \simeq -\gamma X_0$. On a timescale given by $\tau_\kappa = \gamma^{-1}$ the particle covers a distance ΔX of the order of $\Delta X \sim X_0$, so that it becomes relevant to take into account the time $t_c(X_0)$ taken by the field to rearrange over such a distance. This allows us to identify $t_c(X_0) \equiv \tau_\phi(q \sim 1/X_0)$ in the language of Eq. (1.25), which tells us in particular that when $r = 0$ this timescale is given by $t_c = X_0/D$. When X_0 is small, on the other hand, we enter the regime in which $t_c \ll \tau_\kappa$, and no crossover is observed within the asymptotic region $t \gg \tau_\kappa$.

The intermediate algebraic decay exponent θ_0 can be determined by comparing the asymptotic form of Eq. (2.39) with Eq. (B.65) and by matching powers of X_0 in the two expressions. This gives $\beta_0 = 1/\theta_\infty$, and thus

$$\theta_0 = \theta_\infty \beta_0 = 1 + \frac{d-1}{2}. \tag{B.66}$$

This matching additionally instructs on which parameters control the amplitude of the average particle position within the transient regime, yielding, up to some numerical constant,

$$c_0 \propto D^{1/\theta_\infty} \, c_\infty \propto \frac{\lambda^2}{\gamma k} D^{(1-d)/\theta_\infty} . \tag{B.67}$$

We verified that Eq. (B.66) correctly predicts the intermediate exponent in numerical plots of Eq. (2.13) and in numerical simulations of the system in various spatial dimensions d. Alternatively, we can rephrase Eq. (2.39) as

$$\langle X_j(t) \rangle \simeq c_0 t_c^{\theta_0} f_2(\tau) , \tag{B.68}$$

which is a function of the parameter $\tau = t/t_c$ only, having identified $f_2(\tau) \equiv \tau^{\theta_0} f(\tau)$. In the inset of Fig. 2.6b we thus plot $t_c^{-\theta_0} \langle X_j(t) \rangle \propto f_2(\tau)$ in order to observe this scaling function from the collapse of numerical curves obtained for different values of the initial displacement X_0.

Above we presented the argument for the critical case $r = 0$, but it can be easily extended so as to cover the off-critical case in model B, which also displays an eventual algebraic decay. From Eq. (1.25) with $q \sim 1/X_0$ we read the crossover time $t_c \sim X_0^2/(Dr)$, valid for $r^{-1/2} = \xi \ll X_0$. The asymptotic matching of Eq. (2.39) with the long-time decay exponents given in Eq. (2.17)

for $r > 0$, i.e., $\quad_\infty = 2 + d/2$, yields the prediction $\quad_0 = 2 + (d \quad 1)/2$ for the intermediate decay exponent, and

$$c_0 \propto \sqrt{Dr}\, c_\infty \propto \frac{\lambda^2 D}{\gamma k} (Dr)^{\ (d+3)/2}. \tag{B.69}$$

This correctly describes the transient behavior observed in numerical simulations for the off-critical case in model B.

B.7 Adiabatic elimination of the field degrees of freedom

Following Refs. [9, 53], we derive an adiabatic approximation of the dynamics of the system by integrating out the field degrees of freedom from the Fokker-Planck equation (2.31), under the assumption that they relax much faster than the position $\mathbf{X}(t)$ of the particle. Since we have denoted by D and ν the mobility of the field and the particle respectively, which set the timescales for their relaxation, we will initially use their ratio ν/D as a small parameter for our expansion. A later comparison with the weak-coupling solution discussed in Section 2.2 will lead us to conclude that the adiabatic approximation is in fact only reliable for a dissipative field dynamics (model A) and sufficiently far from the critical point so that $Dr \gg \gamma \equiv \nu\kappa$, being $\tau_\kappa = \gamma^{\ 1}$ the relaxation timescale of the particle.

To simplify the notation, let us first rewrite the Langevin equations (2.27) and (2.28) as

$$\dot{\mathbf{X}} = \quad \nu\kappa\mathbf{X} + \sum_{\sigma=R,I} \int_{\mathbb{R}^d} \frac{\mathrm{d}^d q}{(2\pi)^d} \mathbf{f}^\sigma_{\mathbf{q}} \phi^\sigma_{\mathbf{q}} + \boldsymbol{\xi}(t) \ \equiv \ \mathbf{F}(\mathbf{X}, \phi; t) + \boldsymbol{\xi}(t), \tag{B.70}$$

$$\dot{\phi}^\sigma_{\mathbf{q}} = \quad _{\mathbf{q}} \phi^\sigma_{\mathbf{q}} + D\lambda q \ \ g^\sigma_{\mathbf{q}} + \eta^\sigma_{\mathbf{q}} \ \equiv \quad a\phi^\sigma_{\mathbf{q}} \quad b + \eta^\sigma_{\mathbf{q}}, \tag{B.71}$$

where $\sigma = R, I$ indicate the real or the imaginary part, respectively. Here we introduced $g_{\mathbf{q}}(\mathbf{X}) \equiv V_q \exp(\ \ i\mathbf{q}\cdot\mathbf{X})$ as in Section 2.3.1, while

$$\begin{cases} a \equiv \ _{\mathbf{q}} = Dq \ \ (q^2 + r), \\ b \equiv \ D\lambda q \ \ g^\sigma_{\mathbf{q}}, \\ c \equiv \ _\phi/2 = DTq \ \ , \end{cases} \tag{B.72}$$

and $\mathbf{f}^\sigma_{\mathbf{q}} \equiv \nu\lambda\mathbf{q} \begin{pmatrix} g^I_{\mathbf{q}} \\ g^R_{\mathbf{q}} \end{pmatrix}$. The noise amplitudes can be obtained from Eqs. (1.2) and (1.17),

$$\langle \xi_i(t)\xi_j(t')\rangle = 2\nu T\delta_{ij}\delta(t \quad t') \equiv \ _x\delta_{ij}\delta(t \quad t'), \tag{B.73}$$

$$\langle \eta^\sigma_{\mathbf{q}}(t)\eta^\sigma_{\mathbf{q}'}(t')\rangle = \frac{\phi}{2}\left[\delta^d(\mathbf{q} \quad \mathbf{q}') \pm \delta^d(\mathbf{q}+\mathbf{q}')\right]\delta(t \quad t'), \tag{B.74}$$

where the plus sign in Eq. (B.74) is assumed for the real part $\sigma = R$, and the minus sign for $\sigma = I$. The average values of all the noises involved here vanish, and so do the cross correlations such as $\langle \eta^R_{\mathbf{q}}(t)\eta^I_{\mathbf{q}'}(t')\rangle$ or $\langle \eta^\sigma_{\mathbf{q}}(t)\xi_j(t')\rangle$. We note that rescaling time in Eq. (B.70) as $t \to \nu t$ is tantamount to setting $\nu \equiv 1$ and replacing $D \to \widetilde{D} = D/\nu$ in all the above relations; we will henceforth use $\widetilde{D}^{\ 1}$ as an adiabaticity parameter.

In this notation, the Fokker-Planck equation for the joint probability distribution $\mathcal{P}\left[\phi, \mathbf{X}, t\right]$ becomes

$$\partial_t \mathcal{P} = \left[\mathcal{L}_X + \sum_{\sigma=R,I} \int_{\mathbb{R}^d} \frac{\mathrm{d}^d q}{(2\pi)^d} \mathcal{L}^\sigma_{\mathbf{q}}\right] \mathcal{P}, \tag{B.75}$$

where, recalling the definition of $\mathbf{F}$ in Eq. (B.70), we introduced

$$\mathcal{L}_X = \quad \nabla \quad \mathbf{F} + \frac{x}{2}\nabla^2, \qquad \mathcal{L}^\sigma_{\mathbf{q}} = \partial_\phi(a\phi + b) + c\partial^2_\phi, \tag{B.76}$$

with $\partial_\phi \equiv \frac{\delta}{\delta \phi^\sigma_{\mathbf{q}}}$. Let us also denote, for brevity,

$$\int' \mathrm{d}^d q \equiv \sum_{\sigma=R,I} \int_{\mathbb{R}^d} \frac{\mathrm{d}^d q}{(2\pi)^d}, \tag{B.77}$$

and omit the indication of the superscript σ from now on: a further dependence on σ will be understood whenever a quantity depends on $\mathbf{q}$.

The approach described below resembles the Born-Oppenheimer approximation for solving the Schrödinger equation for an atom under the assumption that the dynamics of the nucleus is much slower than that of the surrounding electrons. For each fixed $\mathbf{X}$, we consider the eigenfunctions $\varphi_{n_{\mathbf{q}}}(\phi_{\mathbf{q}}; \mathbf{X})$ of the operators $\mathcal{L}_{\mathbf{q}}$ defined in Eq. (B.76), each satisfying an eigenvalue equation

$$\lambda_{n_{\mathbf{q}}}(\mathbf{X})\varphi_{n_{\mathbf{q}}}(\phi_{\mathbf{q}}; \mathbf{X}) = \quad \mathcal{L}_{\mathbf{q}}\varphi_{n_{\mathbf{q}}}(\phi_{\mathbf{q}}; \mathbf{X}). \tag{B.78}$$

We can expand the joint probability density $\mathcal{P}\left[\phi, \mathbf{X}, t\right]$ as

$$\mathcal{P}\left[\phi, \mathbf{X}, t\right] = \sum_{\mathbf{n}} P_{\mathbf{n}}(\mathbf{X}, t)\Phi_{\mathbf{n}}\left[\phi; \mathbf{X}\right], \qquad \Phi_{\mathbf{n}}\left[\phi; \mathbf{X}\right] \equiv \prod_{\mathbf{q}\in\mathbb{R}^d}{}' \varphi_{n_{\mathbf{q}}} \ \ \phi_{\mathbf{q}}; \mathbf{X}), \tag{B.79}$$

where $\mathbf{n} = \{n_{\mathbf{q}}\}$ is the collection of the excitation numbers for each mode, and the prime sign again indicates a further product over real and imaginary parts. Using the property [53]

$$\int \mathcal{D}\phi\, \Phi_{\mathbf{n}}\left[\phi; \mathbf{X}\right] = \delta_{\mathbf{n}\mathbf{0}}, \tag{B.80}$$

one can show that the marginal probability distribution $P_0(\mathbf{X}, t)$ of the position of the particle can be obtained as

$$P_0(\mathbf{X}, t) = \int \mathcal{D}\phi\, \mathcal{P}\left[\phi, \mathbf{X}, t\right]. \tag{B.81}$$

In the following, we will thus derive an effective evolution equation for $P_0(\mathbf{X}, t)$.

B.7.1 Transformation to a Schrödinger-type operator

It is well known (see, e.g., Ref. [53]) that a Fokker-Planck operator $\mathcal{L}_{\mathrm{FP}}$ acting on a probability distribution P can be brought, under suitable conditions, into a self-adjoint form via a similarity transformation

$$\mathcal{H}_{\mathrm{FP}} = e^{\Phi_{\mathrm{st}}/2}\mathcal{L}_{\mathrm{FP}}e^{\ \Phi_{\mathrm{st}}/2}. \tag{B.82}$$

In the case of natural boundary conditions [53], the function $\Phi_{\rm st}$ is simply related to the stationary distribution $P_{\rm st} = \mathcal{N}\exp\{-\Phi_{\rm st}\}$, where $\mathcal{N}$ is a normalization constant. This way the Fokker-Planck equation

$$\partial_t P = \mathcal{L}_{\rm FP} P \qquad \leftrightarrow \qquad \partial_t \widetilde{P} = \mathcal{H}_{\rm FP}\widetilde{P} \tag{B.83}$$

takes the form of a time-dependent Schrödinger equation in imaginary time for the transformed $\widetilde{P} = e^{\Phi_{\rm st}/2}P$. One can check that its eigenfunctions ψ_n defined by

$$\varphi_n = \psi_n\psi_0, \quad \text{with} \quad \psi_0^2 = P_{\rm st}, \tag{B.84}$$

have the same eigenvalues as $\mathcal{L}_{\rm FP}$ and form an orthonormal set,

$$\int \psi_n\psi_m = \delta_{nm}. \tag{B.85}$$

Now we observe that each of the operators $\mathcal{L}^{\sigma}_{\mathbf{q}}$ defined in Eq. (B.76) can be mapped onto

$$\mathcal{H}_{\rm FP} = c\partial_\phi^2 - W(\phi) \equiv -a\hat{a}^\dagger\hat{a} \tag{B.86}$$

using the similarity transformation in Eq. (B.82). Here

$$W(\phi) = \frac{a^2}{4c}\left(\phi + \frac{b}{a}\right)^2 - \frac{a}{2} \tag{B.87}$$

is a simple harmonic potential, while $\hat{a}^\dagger$ and $\hat{a}$ are the raising and lowering bosonic operators defined by

$$\hat{a} = \sqrt{\frac{a}{4c}}\left(\tilde{\phi} + \frac{2c}{a}\partial_{\tilde{\phi}}\right), \qquad \hat{a}^\dagger = \sqrt{\frac{a}{4c}}\left(\tilde{\phi} - \frac{2c}{a}\partial_{\tilde{\phi}}\right), \tag{B.88}$$

where we introduced

$$\tilde{\phi} \equiv \phi + \frac{b}{a} = \sqrt{\frac{c}{a}}\left(\hat{a} + \hat{a}^\dagger\right). \tag{B.89}$$

The solution to the eigenvalue problem (analogous to Eq. (B.78))

$$\lambda_n\psi_n = -\mathcal{H}_{\rm FP}\psi_n \tag{B.90}$$

is then given by the set of eigenvalues $\lambda_n = a\,n$, and the corresponding eigenfunctions are

$$\psi_n(\tilde{\phi}) = \frac{1}{\sqrt{2^n n}}H_n\left(\sqrt{\frac{a}{2c}}\tilde{\phi}\right)\psi_0(\tilde{\phi}), \qquad \psi_0(\tilde{\phi}) = \left(\frac{a}{2\pi c}\right)^{1/4} e^{-a\tilde{\phi}^2/(4c)}, \tag{B.91}$$

where $H_n(\ )$ are Hermite polynomials [303]. Note that using $P_{\rm st} = \psi_0^2(\tilde{\phi})$, as prescribed by Eq. (B.84), correctly renders the $(\mathbf{q},\sigma)$-dependent part of the stationary distribution of the field at fixed particle position $\mathbf{X}$, which is in our case the canonical one. Indeed, rewriting the Hamiltonian in Eq. (2.1) in Fourier space we get

$$\begin{aligned}\mathcal{P}_{\rm st}(\phi;x) \propto e^{-\beta\mathcal{H}} &\propto \exp\left\{-\beta\int\frac{\mathrm{d}^d q}{(2\pi)^d}\left[\frac{1}{2}(q^2+r)\phi_{\mathbf{q}}\phi_{-\mathbf{q}} - \lambda V_q e^{-i\mathbf{q}\cdot\mathbf{X}}\phi_{\mathbf{q}}\right]\right\} \\ &= \exp\left\{-\beta\int\frac{\mathrm{d}^d q}{(2\pi)^d}\left[\frac{1}{2}(q^2+r)\left((\phi^R_{\mathbf{q}})^2 + (\phi^I_{\mathbf{q}})^2\right) - \lambda\left(\phi^R_{\mathbf{q}}g^R_{\mathbf{q}} + \phi^I_{\mathbf{q}}g^I_{\mathbf{q}}\right)\right]\right\},\end{aligned} \tag{B.92}$$

which factorizes over the modes and their real and imaginary parts. This coincides with $P_{\rm st} = \psi_0^2(\tilde{\phi})$ upon substituting the definition of $\tilde{\phi}$ in Eq. (B.89) and of a, b, c in Eq. (B.72).

B.7.2 Effective Fokker-Planck equation

Following Ref. [9], we now generalize that approach from two to an infinite set of coupled Langevin equations. In order to obtain an evolution equation for each of the $P_{\mathbf{n}}(\mathbf{X}, t)$, we first substitute the expansion of $\mathcal{P}\left[\phi, \mathbf{X}, t\right]$ in Eq. (B.79) into the Fokker-Planck equation (B.75) and we multiply both sides by $\Psi_{\mathbf{m}}/\Psi_{\mathbf{0}}$, where (recall $\Phi_{\mathbf{m}} = \Psi_{\mathbf{m}}\Psi_0$)

$$\Psi_{\mathbf{m}}\left[\phi; \mathbf{X}\right] = \prod_{\mathbf{q}\in\mathbb{R}^d}{}' \psi_{m_{\mathbf{q}}}\ \ \phi_{\mathbf{q}}; \mathbf{X}\big)\,. \tag{B.93}$$

Then we take the functional integral over $\mathcal{D}\phi$ and use the orthogonality relation

$$\int \mathcal{D}\phi \Psi_{\mathbf{m}}\Psi_{\mathbf{n}} = \delta_{\mathbf{mn}}, \tag{B.94}$$

which follows from Eq. (B.85). We now notice that the eigenvalue equation (B.78) implies

$$\int' \mathrm{d}^d q\, \mathcal{L}_{\mathbf{q}}\Phi_{\mathbf{n}}\left[\phi; \mathbf{X}\right] = \int' \mathrm{d}^d q\, \lambda_{n_{\mathbf{q}}}[\mathbf{X}]\, \Phi_{\mathbf{n}}\left[\phi; \mathbf{X}\right] = \lambda_{\mathbf{n}}\Phi_{\mathbf{n}}\left[\phi; \mathbf{X}\right], \tag{B.95}$$

where we introduced

$$\lambda_{\mathbf{n}} \equiv \int' \mathrm{d}^d q\, \lambda_{n_{\mathbf{q}}} = \int' \mathrm{d}^d q\, n_{\mathbf{q}} a_{\mathbf{q}}. \tag{B.96}$$

(Note that we reintroduced the $\mathbf{q}$-dependence in a defined in Eq. (B.72), which had so far been omitted for brevity). Some straightforward algebra [9] then gives (omitting the various functional dependencies from $P_{\mathbf{n}} = P_{\mathbf{n}}(\mathbf{X}, t)$)

$$\partial_t P_{\mathbf{m}} = \sum_{\mathbf{n}} \left\langle \frac{\Psi_{\mathbf{n}}}{\Psi_{\mathbf{0}}} \mathcal{L}_X \Phi_{\mathbf{n}} \right\rangle P_{\mathbf{n}} \quad \lambda_{\mathbf{m}} P_{\mathbf{m}}, \tag{B.97}$$

where by the average symbol we mean

$$\langle \cdots \rangle = \int \mathcal{D}\phi\, (\cdots) = \int \prod_{\mathbf{q}\in\mathbb{R}^d}{}' \mathrm{d}\phi_{\mathbf{q}}\, (\cdots). \tag{B.98}$$

In particular, the marginal distribution of the particle position defined in Eq. (B.81) evolves according to

$$\partial_t P_{\mathbf{0}} = \langle \mathcal{L}_X \Phi_{\mathbf{0}} \rangle\, P_{\mathbf{0}} + \sum_{\mathbf{n}\neq\mathbf{0}} \langle \mathcal{L}_X \Phi_{\mathbf{n}} \rangle\, P_{\mathbf{n}}, \tag{B.99}$$

because $\lambda_{\mathbf{0}} = 0$ (we proved this in Sec. B.7.1). By $\mathbf{n} \neq 0$ in the sum above we mean that the numbers $n_{\mathbf{q}}$ cannot be all zero simultaneously. Since all the other $P_{\mathbf{m}}$'s decay on timescales $\lambda_{\mathbf{m}}{}^1 \propto \widetilde{D}^{\ 1}$, we can solve for $P_{\mathbf{m}}$ up to $O\left(\widetilde{D}^{\ 1}\right)$ by setting $\partial_t P_{\mathbf{m}} = \delta_{\mathbf{m0}}$ in Eq. (B.97) and keeping only the term $\mathbf{n} = 0$ in the sum, whence

$$P_{\mathbf{m}} = \frac{1}{\lambda_{\mathbf{m}}} \left\langle \frac{\Psi_{\mathbf{m}}}{\Psi_{\mathbf{0}}} \mathcal{L}_X \Phi_{\mathbf{0}} \right\rangle P_{\mathbf{0}} + O\left(\frac{1}{\widetilde{D}^2}\right). \tag{B.100}$$

Plugging this result back into Eq. (B.99) and using the fact that $\langle \nabla^2 \Phi_{\mathbf{n}} \rangle = 0$ because of Eq. (B.80), we get an evolution equation for the reduced probability density

$$\partial_t P_0(\mathbf{X}, t) = \mathcal{L}^{\mathrm{eff}} P_0(\mathbf{X}, t), \tag{B.101}$$

where

$$\mathcal{L}^{\text{eff}} = \quad \nabla \quad \langle \mathbf{F}\Psi_{\mathbf{0}}^2 \rangle + \frac{x}{2}\nabla^2 + \sum_{\mathbf{n}\neq 0} \nabla \quad \langle \Psi_{\mathbf{n}}\mathbf{F}\Psi_{\mathbf{0}} \rangle \frac{1}{\lambda_{\mathbf{n}}} \Bigg[\nabla \quad \langle \Psi_{\mathbf{n}}\mathbf{F}\Psi_{\mathbf{0}} \rangle \quad \left\langle \Psi_{\mathbf{0}}^2 \mathbf{F} \cdot \left(\nabla \frac{\Psi_{\mathbf{n}}}{\Psi_{\mathbf{0}}} \right) \right\rangle$$
$$2 \ _x \langle \Psi_{\mathbf{n}} \nabla \Psi_{\mathbf{0}} \rangle \cdot \nabla \quad \frac{x}{2} \left\langle \frac{\Psi_{\mathbf{n}}}{\Psi_{\mathbf{0}}} \left(\nabla^2 \Psi_{\mathbf{0}}^2 \right) \right\rangle \Bigg] + \mathcal{O}\left(\frac{1}{\widetilde{D}^2} \right). \tag{B.102}$$

Recall that in general $\lambda_{\mathbf{n}} = \lambda_{\mathbf{n}}[\mathbf{X}]$ (although not in our specific case), while we did not indicate the dependence on $\mathbf{X}$ and ϕ of $\mathbf{F}$ and $\Psi_{\mathbf{n}}$, so as to lighten the notation. The result in Eq. (B.101) is analogous to Eq. (2.13) in Ref. [9], which was derived for the simple case of two coupled scalar equations (but note that the analog of the second term in braces in Eq. (B.102) was reported with the wrong sign in Ref. [9]).

In order to compute the averages that appear in Eq. (B.102), we can make explicit use of the fact that $\mathbf{F}$ is linear in each of the $\phi_{\mathbf{q}}$, hence also in the bosonic creation and annihilation operators $\hat{a}_{\mathbf{q}}^\dagger$ and $\hat{a}_{\mathbf{q}}$. Let us inspect explicitly one of these terms:

$$\begin{aligned}
\langle \Psi_{\mathbf{n}}\mathbf{F}\Psi_{\mathbf{0}} \rangle &= \quad \nu k \mathbf{X} \langle \Psi_{\mathbf{n}}\Psi_{\mathbf{0}} \rangle + \int \frac{\mathrm{d}^d q}{(2\pi)^d} \mathbf{f}_{\mathbf{q}} \langle \Psi_{\mathbf{n}} | \tilde{\phi}_{\mathbf{q}} \quad \frac{b_{\mathbf{q}}}{a_{\mathbf{q}}} | \Psi_{\mathbf{0}} \rangle \\
&= \quad \nu k \mathbf{X} \delta_{\mathbf{n}0} + \int \frac{\mathrm{d}^d q}{(2\pi)^d} \mathbf{f}_{\mathbf{q}} \left[\sqrt{\frac{c_{\mathbf{q}}}{a_{\mathbf{q}}}} \langle \Psi_{\mathbf{n}} | \hat{a}_{\mathbf{q}} + \hat{a}_{\mathbf{q}}^\dagger | \Psi_{\mathbf{0}} \rangle \quad \frac{b_{\mathbf{q}}}{a_{\mathbf{q}}} \langle \Psi_{\mathbf{n}}\Psi_{\mathbf{0}} \rangle \right] \\
&= \quad \nu k \mathbf{X} \delta_{\mathbf{n}0} + \int \frac{\mathrm{d}^d q}{(2\pi)^d} \mathbf{f}_{\mathbf{q}} \left[\sqrt{\frac{c_{\mathbf{q}}}{a_{\mathbf{q}}}} \delta_{\mathbf{n}\mathbf{q}} \quad \frac{b_{\mathbf{q}}}{a_{\mathbf{q}}} \delta_{\mathbf{n}0} \right],
\end{aligned} \tag{B.103}$$

where we used the definition of $\tilde{\phi}_{\mathbf{q}}$ in Eq. (B.89); the $\delta_{\mathbf{n}\mathbf{q}}$ in the last line selects the element $\mathbf{n}$ with $n_{\mathbf{p}} = \delta_{\mathbf{p}\mathbf{q}}$, while $\delta_{\mathbf{n}0}$ selects the "ground state" with $n_{\mathbf{p}} = 0$ for every $\mathbf{p}$. Next, note that

$$\nabla \quad \langle \Psi_{\mathbf{n}}\mathbf{F}\Psi_{\mathbf{0}} \rangle \frac{1}{\lambda_{\mathbf{n}}} \nabla \quad \langle \Psi_{\mathbf{n}}\mathbf{F}\Psi_{\mathbf{0}} \rangle = \sum_{i,j} \partial_i \langle \Psi_{\mathbf{n}} F_i \Psi_{\mathbf{0}} \rangle \frac{1}{\lambda_{\mathbf{n}}} \partial_j \langle \Psi_{\mathbf{n}} F_j \Psi_{\mathbf{0}} \rangle , \tag{B.104}$$

and for the sake of simplicity we will assume isotropy of the interaction potential (i.e., V_q depends only on $q = |\mathbf{q}|$). This implies that no mixed derivative of the form $\partial_i \partial_j$ will survive the $\mathrm{d}^d q$ integration, so that a δ_{ij} can be understood in the sum. Similar considerations apply to the other averages in Eq. (B.102), which can be dealt with using the properties of Hermite polynomials (or equivalently the bosonic algebra); it is crucial at some point to reinstate the dependence on σ, because many of the contributions cancel out when taking $\sum_\sigma$. A lengthy but simple computation gives, once reinstating the original parameters ν and D,

$$\mathcal{L}^{\text{eff}} = \sum_{j=1}^{d} \left[\partial_j \quad \chi_j \nu k X_j \right) + \chi_j \nu T \partial_j^2 \Big] + \mathcal{O}\left(\left(\frac{\nu}{D} \right)^2 \right), \tag{B.105}$$

where

$$\chi_j \equiv 1 \quad \frac{\lambda^2 \nu}{D} \int_{\mathbb{R}} \frac{\mathrm{d}^d q}{(2\pi)^d} \frac{q_j^2}{q \quad (q^2 + r)^2} |V_q|^2. \tag{B.106}$$

As we had already assumed V_q to be isotropic, then $\chi_j = \chi$ is the same for all the components (i.e., it is independent of the index j). It can be easily computed by replacing $q_j^2 \to q^2/d$ in the integral, leading to the final result in Eq. (2.34).

We conclude by noting that our effective equation (2.34) is heuristically consistent with the results of Refs. [84, 85]. Similarly, we can consider several copies of the effective Fokker-Planck operator obtained in Ref. [9] (let us call it $\mathcal{L}_{\rm K}^{\rm eff}$), one for each of the field modes $(\mathbf{q}, \sigma)$ and particle components j. Calling then each of these copies $\mathcal{L}_{\rm K}^{\rm eff} \equiv \mathcal{L}_j^{\sigma,\mathbf{q}}$, one can recover our result $\mathcal{L}^{\rm eff}$ as

$$\mathcal{L}^{\rm eff} = \sum_{j=1}^{d} \sum_{\sigma=R,I} \int \frac{\mathrm{d}^d q}{(2\pi)^d} \mathcal{L}_j^{\sigma,\mathbf{q}}. \tag{B.107}$$

B.8 Numerical simulation

Numerical simulations are performed by direct integration of the coupled Langevin equations of motion (2.5) and (2.6). Field variables are discretized as $\{\phi_i(t)\}_{i=1}^N$ with $\phi_i(t) \equiv \phi(\mathbf{x}_i, t) \in \mathbb{R}$, and they sit on the $N = L^d$ sites of a d-dimensional hypercubic lattice of side length L. Distances are measured in units of the lattice spacing a, which we retain for clarity in the following formulas, but which will be eventually set to unity. The coordinate $\mathbf{X}(t) \in \mathbb{R}^d$ of the center of the particle is taken to be real-valued, i.e., the particle is not constrained to move on the lattice sites only. Upon integration by parts, the equation of motion of the particle can be rewritten as

$$\dot{\mathbf{X}}(t) = \quad \nu k \mathbf{X} + \nu\lambda \int \mathrm{d}^d x \, V(\mathbf{x} \quad \mathbf{X}) \nabla\phi(\mathbf{x}) + \boldsymbol{\xi}(t) \simeq \quad \nu k \mathbf{X} + \nu\lambda \sum_{i=1}^{N} V(\mathbf{x}_i \quad \mathbf{X}) \widetilde{\nabla}\phi_i + \boldsymbol{\xi}(t), \tag{B.108}$$

where we introduced the discrete gradient

$$\widetilde{\nabla}_j \phi_i = \frac{\phi(\mathbf{x}_i + \hat{\boldsymbol{\mu}}_j) \quad \phi(\mathbf{x}_i \quad \hat{\boldsymbol{\mu}}_j)}{2a}, \tag{B.109}$$

with $\hat{\boldsymbol{\mu}}_j$ locating the position of the 2 neighbouring sites of each $\mathbf{x}_i$ along direction j. The discretized equation of motion for the field ϕ_i in model A reads

$$\partial_t \phi_i(t) = \quad D \left[(r \quad \widetilde{\Delta}) \phi_i(t) \quad \lambda V(\mathbf{x}_i \quad \mathbf{X}(t)) \right] + \eta_i(t), \tag{B.110}$$

where $\eta_i(t)$ is a Gaussian random variable with variance $\langle \eta_i(t) \eta_j(t') \rangle = 2DTa \quad {}^1\delta_{ij} \delta(t \quad t')$. We also defined the discrete Laplacian

$$\widetilde{\Delta} \phi_i = \frac{1}{a^2} \sum_{\langle k,i \rangle} \quad \phi_k \quad \phi_i \big) \,, \tag{B.111}$$

where the sum runs over the $2d$ neighbouring sites of $\mathbf{x}_i$. Similarly, the discretized equation of motion for the field in model B reads

$$\partial_t \phi_i(t) = D \widetilde{\Delta} \left[(r \quad \widetilde{\Delta}) \phi_i(t) \quad \lambda V(\mathbf{x}_i \quad \mathbf{X}(t)) \right] + \widetilde{\nabla} \cdot \boldsymbol{\eta}_i(t) \tag{B.112}$$

where $\boldsymbol{\eta}_i(t)$ is a vectorial noise with zero mean and variance

$$\langle \eta_i^{(\ )}(t) \eta_j^{(\beta)}(t') \rangle = 2DTa \quad {}^1\delta_{ij} \delta \quad {}_\beta \delta(t \quad t'), \tag{B.113}$$

and we take its discrete divergence as $\widetilde{\nabla}\ \eta_i^{(\ )}(t)$. We chose in both cases a Gaussian interaction potential as in Eq. (2.4), which yields a smooth expression for its Laplacian

$$\nabla^2 V_{\mathrm{G}}(\mathbf{x}) = \frac{|\mathbf{x}|^2 \quad R^2 d}{R^4} V_{\mathrm{G}}(\mathbf{x}). \tag{B.114}$$

Equations (B.108) and (B.110) (or (B.112)) represent a set of $(N+d)$ ordinary stochastic differential equations which can be integrated by standard methods in real space [304]. We choose a simple Euler-Maruyama scheme (order $\Delta t^{1/2}$) for the evolution of the field variables and a more refined method, i.e., the Stochastic Runge-Kutta (order $\Delta t^{3/2}$, see Ref. [305]), for the particle coordinate. We expect this to improve the stability of the particle dynamics in spite of the lower-order algorithm adopted for the field, because the latter only contributes at $O(\lambda \ll 1)$ to the evolution of the particle.

At the beginning of each trial, we prepare the field in its equilibrium distribution at temperature T in Fourier space and then move back to real space using a discrete Fourier transform. We then add the particle at position $X_0 \neq 0$, and record its relaxation trajectory as it moves towards the center of the harmonic trap. Simulations performed at temperature $T \sim O\ 10^{\ 1})$ on a lattice with side $L \sim O\ 10^3)$, such as the one shown in Fig. 2.6a, require $O\ 10^8 \quad 10^9)$ trials in order to obtain a clear sample of the algebraic decay of the average particle position. Indeed, the signal/noise ratio becomes increasingly small at long times, which is the region we are mostly interested in. The complete code written in C is available open source on GitHub [306].

B.9 A first quantitative estimate

In this Appendix we attempt a comparison between our model with off-critical model B dynamics, and experiments performed on colloidal particles in binary liquid mixtures. Even though our model is not meant to give a realistic description of such a physical system (for instance, hydrodynamic effects are ignored), it is still interesting to inspect the typical orders of magnitude and check how large the algebraic behavior of the average particle position can be made, compared with its radius R.

Following Sections 2.4.1 and 2.4.2, we start by choosing the value of the initial displacement X_0 in order to maximize the amplitude of the particle position at the crossover time t_c. This was given in Eq. (2.44), which suggests to take X_0 as small as possible, but still sufficiently large so that the assumption $t_c > \tau_\kappa$ we made in Section 2.4.1 is still satisfied. Recall that t_c is the time taken by the field in order to relax over a length scale $\sim X_0$, and it can be identified in the off-critical model B with $t_c \sim X_0^2/Dr$.

What is the typical size of t_c? While $r = \xi^{\ 1/2}$ and it is simple to plug in typical values for the correlation length ξ which can be obtained in experiments, it is not obvious how large a realistic D is. Within model B, we learn from Eq. (1.25) that $\tau_\phi^{\ 1} \simeq Drq^2$ for wavelengths $q \ll r^{1/2} = 1/\xi$. However, real binary fluid mixtures are generally described by model H [54, 59], where the field relaxation time for $q\xi \ll 1$ is given within mode-coupling theory by $\tau_\phi^{\ 1} \simeq D_\xi q^2$, with [307]

$$D_\xi = \frac{k_B T}{6\pi\eta\xi}, \tag{B.115}$$

being η the fluid viscosity. Note the similarity with the free diffusion coefficient of the colloid $\left\langle X^2(t)\right\rangle \simeq D_R t$,

$$D_R = \frac{k_B T}{6\pi\eta R}. \tag{B.116}$$

Typical colloid radii are of the order of $R \simeq 1\mu$m, while typical correlation lengths obtainable with a water-lutidine mixture are or the order of a few tens of nanometers [35, 36]. To give a heuristic estimate of D, we compare the diffusion coefficient of the order parameter fluctuations in model B with that of model H, thus identifying $Dr \simeq D_\xi$, which renders $t_c \simeq X_0^2/D_\xi$.

Equation (2.44) still contains the dimensionless parameter g, which sets the strength of the interaction between the field and the particle. Its amplitude will depend on the specific coupling mechanism realized in a certain experiment, and clearly the overall effect will be enhanced if g can be made larger. However, here we take $g \sim 1$ in order to remain within the perturbative regime, under which most of the analyses in this work were carried out.

To fix the ideas, we take $t_c \sim 4\tau_\kappa$, whence $X_0 \simeq \sqrt{2\tau_\kappa D_\xi}$. From Eq. (2.44) we read

$$\frac{\langle X_j(t_c)\rangle}{R} \sim \left(\frac{4\tau_\kappa D_\xi}{R^2}\right)^{(1\ \ d\ \ )/2} \sim \left(\frac{200\tau_\kappa D_R}{R^2}\right)^{(d+3)/2}, \tag{B.117}$$

where in the last step we inserted the realistic estimate $\xi \sim R/50$ and we set $\quad = 4$. Now we note that $\tau_d \sim R^2/D_R$ is the timescale of thermal diffusion of the colloid over a distance of the order of its own radius. A typical value for the free diffusion coefficent is $D_R \simeq 0.22(\mu m)^2 s^{\ 1}$ [36], whence $\tau_d \sim 4 \quad 5$s. We can conclude that

$$\frac{\langle X_j(t_c)\rangle}{R} \sim \left(\frac{\tau_d}{200\tau_\kappa}\right)^{(d+3)/2}. \tag{B.118}$$

Typical timescales τ_κ of relaxation of colloidal particles trapped by optical tweezers are of the order of a few tens of milliseconds [35]. It then appears that $\langle X(t_c)\rangle$, measured in units of the colloid radius R, can be made as large as $10^{\ 1}$ at least. It should be stressed that digital video-microscopic observation of 2μm-sized silica particles immersed in binary liquid mixtures currently allows to resolve displacements of up to 5nm. We are thus led to conclude that, even if $\langle X(t_c)\rangle$ is indeed small compared to the colloid radius, the effect we predicted could still be detected experimentally.

C

Calculations of Chapter 3

C.1 Brownian motion in an oscillating harmonic potential

The motion of a Brownian particle in a (possibly moving) harmonic potential is ruled by the Ornstein-Uhlenbeck process, recalled in Section 1.2. Here we specialize the expressions derived therein to the case in which $\mathbf{X}(t) \mapsto \mathbf{Z}(t)$ is forced sinusoidally as in Eq. (3.12). Setting $\mathbf{X}_0 = 0$, it is straightforward to obtain

$$\begin{aligned}\mathbf{m}(t) = \langle \mathbf{Z}(t) \rangle_0 &= \boldsymbol{\Delta} \left[1 \quad e^{\quad \gamma \ (t \quad t_0)} \right] + \mathbf{A} \left[\sin(\Omega t \quad \theta \ ) \quad \sin(\Omega t_0 \quad \theta \ ) e^{\quad \gamma \ (t \quad t_0)} \right] \\ &\underset{t_0 \to \quad \infty}{\longrightarrow} \boldsymbol{\Delta} + \mathbf{A} \sin(\Omega t \quad \theta \ ),\end{aligned} \tag{C.1}$$

where we defined the phase shift θ as in Eq. (3.28). In the deterministic limit where $\kappa \ \longrightarrow \infty$, the particle simply follows the external forcing with no delay ($\theta \ \longrightarrow 0$) and we recover $\langle \mathbf{Z}(t) \rangle_0 = \mathbf{z}_F(t)$.

Proceeding as in Appendix B.1, we can compute any generic n-point average over the independent process — see in particular Eqs. (B.4) and (B.11). These are denoted as $\langle \ldots \rangle_0$ in the main text of Chapter 3, e.g., $\langle \exp\left[i\mathbf{q} \cdot \mathbf{X}^{(0)}(t) \right] \rangle \mapsto \langle \exp[i\mathbf{q} \cdot \mathbf{X}(t)] \rangle_0$ with reference to Appendix B.1.

C.2 Master equation

In this Appendix we provide details on the derivation and solution of the master equation for $P_1(\mathbf{y}, t)$ discussed in Section 3.2.

C.2.1 Derivation of the master equation

The master equation (3.15) can be derived from Eq. (3.14) by evaluating each of the terms that appear on its RHS. The first one reads simply

$$\langle \delta(\mathbf{y} \quad \mathbf{Y}(t)) \mathbf{Y}(t) \rangle = \mathbf{y} P_1(\mathbf{y}, t), \tag{C.2}$$

where the average is intended over all possible realizations of the stochastic noises $\eta_{\mathbf{q}}(t)$ and $\boldsymbol{\xi}^{(y, \ )}(t)$, and similarly

$$\left\langle \delta(\mathbf{y} \quad \mathbf{Y}(t)) e^{i\mathbf{q} \cdot \mathbf{Y}(t)} \right\rangle = e^{i\mathbf{q} \cdot \mathbf{y}} P_1(\mathbf{y}, t). \tag{C.3}$$

In order to obtain the first nontrivial correction of $O\ \lambda^2)$, it is sufficient to compute up to $O\ \lambda^0)$ the term

$$\left\langle \delta(\mathbf{y} \quad \mathbf{Y}(t)) e^{i\mathbf{q} \cdot \mathbf{Z}(s)} \right\rangle_0 = \left\langle e^{i\mathbf{q} \cdot \mathbf{Z}(s)} \right\rangle_0 P_1(\mathbf{y}, t), \tag{C.4}$$

where we used the fact that the processes for $\mathbf{Y}$ and $\mathbf{Z}$ with $\lambda = 0$ are independent, and the remaining average on the r.h.s. of Eq. (C.4) is meant over the noise $\boldsymbol{\xi}^{(\ )}(t)$ only. Expectation values involving the noises $\boldsymbol{\xi}^{(y)}(t)$ and $\eta(t)$ can be handled by taking path-integrals over the stochastic actions [54]

$$\mathcal{S}_\xi[\boldsymbol{\xi}] = \frac{1}{2\Omega_y}\sum_{i=1}^{d}\int \mathrm{d}\tau\, \xi_i^2(\tau), \qquad \mathcal{S}_\eta[\eta] = \frac{1}{2}\int \frac{\mathrm{d}^d q}{(2\pi)^d}\int \mathrm{d}\tau\, \frac{\eta_{\mathbf{q}}(\tau)\eta_{\ \mathbf{q}}(\tau)}{\Omega_\phi(q)}, \tag{C.5}$$

with $\Omega_y \equiv 2\nu_y T$, and $\Omega_\phi(q)$ as in Eq. (1.24). For instance,

$$\begin{aligned}\left\langle \delta(\mathbf{y} \quad \mathbf{Y}(t))\xi_i^{(y)}(t)\right\rangle &= \left\langle \int \mathcal{D}\boldsymbol{\xi}^{(y)}\, \delta(\mathbf{y} \quad \mathbf{Y}(t))\xi_i^{(y)}(t) e^{\ \mathcal{S}_\xi[\boldsymbol{\xi}^{(y)}]}\right\rangle_{\eta,\boldsymbol{\xi}^{(\ )}} \\ &= \Omega_y \left\langle \int \mathcal{D}\boldsymbol{\xi}^{(y)}\, \delta(\mathbf{y} \quad \mathbf{Y}(t))\frac{\delta}{\delta\xi_i^{(y)}(t)} e^{\ \mathcal{S}_\xi[\boldsymbol{\xi}^{(y)}]}\right\rangle_{\eta,\boldsymbol{\xi}^{(\ )}} \\ &= \Omega_y \left\langle \frac{\delta}{\delta\xi_i^{(y)}(t)}\delta(\mathbf{y} \quad \mathbf{Y}(t))\right\rangle = \Omega_y \nabla_{\mathbf{y}}\cdot\left\langle \delta(\mathbf{y} \quad \mathbf{Y}(t))\frac{\delta \mathbf{Y}(t)}{\delta\xi_i^{(y)}(t)}\right\rangle,\end{aligned} \tag{C.6}$$

where we basically retraced the steps that prove the Novikov theorem [10, 308]. Using the equation of motion (3.6) for $\mathbf{Y}(t)$, one gets

$$\mathbf{Y}(t) = \mathbf{Y}(t_0) + \int_{t_0}^{t} \mathrm{d}s\, e^{\ \gamma_y(t\ \ s)}\left[\boldsymbol{\xi}^{(y)}(s) + \lambda\nu_y \mathbf{f}_y(\mathbf{Y},\phi,s)\right], \tag{C.7}$$

whence

$$\frac{\delta Y_j(t)}{\delta\xi_i^{(y)}(t)} = \int_{t_0}^{t}\mathrm{d}s\, e^{\ \gamma_y(t\ \ s)}\delta_{ij}\delta(t \quad s) = \frac{1}{2}\delta_{ij}. \tag{C.8}$$

In the last step we have adopted the Stratonovich convention, but this does not affect the resulting Fokker-Planck equation, because the noise $\boldsymbol{\xi}^{(y)}$ enters additively in the Langevin equation (3.6) for the particle $\mathbf{Y}$ [53]. Note that in Eq. (C.8) we have neglected the term $\mathbf{f}_y(\mathbf{Y},\phi,s)$, while in principle it contains an implicit dependence on $\boldsymbol{\xi}^{(y)}(t)$. However, one can check that it brings no additional contributions, morally because after taking the functional derivative with respect to $\xi_i^{(y)}(t)$ one finds a vanishing term in the form $\int_{t_0}^{t}\mathrm{d}s\int_{t_0}^{s}\mathrm{d}\tau\,(\dots)\delta(t \quad \tau) = 0$, independently of the convention adopted. From Eq. (C.6) we then find

$$\left\langle \delta(\mathbf{y} \quad \mathbf{Y}(t))\boldsymbol{\xi}^{(y)}(t)\right\rangle = \frac{\Omega_y}{2}\nabla_{\mathbf{y}} P_1(\mathbf{y},t). \tag{C.9}$$

Similarly to Eq. (C.6), we can then calculate

$$\begin{aligned}\left\langle \delta(\mathbf{y} \quad \mathbf{Y}(t))\eta_{\mathbf{q}}(s)\right\rangle &= \Omega_\phi(q)\left\langle \int \mathcal{D}\eta\, \delta(\mathbf{y} \quad \mathbf{Y}(t))\frac{\delta}{\delta\eta_{\ \mathbf{q}}(s)} e^{\ \mathcal{S}_\eta[\eta]}\right\rangle_{\boldsymbol{\xi}^{(y)},\boldsymbol{\xi}^{(\ )}} \\ &= \Omega_\phi(q)\nabla_{\mathbf{y}}\cdot\left\langle \delta(\mathbf{y} \quad \mathbf{Y}(t))\frac{\delta\mathbf{Y}(t)}{\delta\eta_{\ \mathbf{q}}(s)}\right\rangle,\end{aligned} \tag{C.10}$$

[1] Note that Eq. (C.7) is *exact*, even if $\mathbf{f}_y(\mathbf{Y},\phi,t)$ in Eq. (3.6) is nonlinear in $\mathbf{Y}$. This can be easily checked by Fourier transforming Eq. (3.6) with respect to t.

and using the effective Langevin equation for $\mathbf{Y}(t)$ one obtains

$$\frac{\delta \mathbf{Y}(t)}{\delta \eta_{\mathbf{q}}(s)} = i v_y \lambda \int_{t_0}^{t} \mathrm{d}s_2\, e^{\gamma_y(t-s_2)} \int \frac{\mathrm{d}^d p}{(2\pi)^d} \mathbf{p} V_p^{(y)} \frac{\delta}{\delta \eta_{\mathbf{q}}(s)} \left[\phi_{\mathbf{p}}(s_2) e^{i\mathbf{p}\cdot\mathbf{Y}(s_2)}\right]. \tag{C.11}$$

From Eqs. (3.6) and (3.13) it follows that

$$\begin{aligned} &\frac{\delta}{\delta \eta_{\mathbf{q}}(s)} \left[\phi_{\mathbf{p}}(s_2) e^{i\mathbf{p}\cdot\mathbf{Y}(s_2)}\right] = e^{i\mathbf{p}\cdot\mathbf{Y}(s_2)} \frac{\delta \phi_{\mathbf{p}}(s_2)}{\delta \eta_{\mathbf{q}}(s)} + O(\lambda) \\ &= e^{i\mathbf{p}\cdot\mathbf{Y}(s_2)} \int_{t_0}^{s_2} \mathrm{d}s_1\, G_p(s_2 - s_1) \delta^d(p+q) \delta(s_1 - s) + O(\lambda) = e^{i\mathbf{p}\cdot\mathbf{Y}(s_2)} G_p(s_2 - s) \delta^d(p+q) + O(\lambda), \end{aligned} \tag{C.12}$$

so we can express

$$\begin{aligned} \left\langle \delta(\mathbf{y} - \mathbf{Y}(t)) \eta_{\mathbf{q}}(s) \right\rangle = i v_y \lambda \Omega_\phi(q) V_q^{(y)} \mathbf{q} \int_{t_0}^{t} \mathrm{d}s_2\, e^{\gamma_y(t-s_2)} G_q(s_2 - s) \nabla_{\mathbf{y}} \left\langle \delta(\mathbf{y} - \mathbf{Y}(t)) e^{i\mathbf{q}\cdot\mathbf{Y}(s_2)} \right\rangle \\ + O\left(\lambda^2\right). \end{aligned} \tag{C.13}$$

Note that in the calculation above there has been no need to specify the Itô or Stratonovich interpretation, because the noise $\eta_q(s)$ gets integrated over the past times in the effective Langevin equation for $\mathbf{Y}$ derived as explained in Section 3.2.1: the non-Markovianity renders such a specification unnecessary [56, 57]. Finally, we interpret

$$\left\langle \delta(\mathbf{y} - \mathbf{Y}(t)) e^{i\mathbf{q}\cdot\mathbf{Y}(s)} \right\rangle = \int_{\mathbf{Y}(t)=\mathbf{y}} \mathcal{D}\mathbf{Y}(\tau)\, e^{i\mathbf{q}\cdot\mathbf{Y}(s)} = \int \mathrm{d}\mathbf{x}\, e^{i\mathbf{q}\cdot\mathbf{x}} P_2(\mathbf{y}, t; \mathbf{x}, s), \tag{C.14}$$

where the path integral is intended over all possible realizations of the process $\mathbf{Y}(\tau)$, conditioned to the constraint $\mathbf{Y}(t) = \mathbf{y}$. Putting together the various terms in Eqs. (C.2) to (C.4), (C.9), (C.13) and (C.14), and using Eq. (1.33), we arrive at the master equation in Eq. (3.15). Note that a term of $O\left(\lambda^3\right)$ in the marginal distribution $P(\mathbf{y}, t)$ is forbidden by the symmetry $\{\lambda \leftrightarrow -\lambda\,,\ \phi \leftrightarrow -\phi\}$, so that the next perturbative correction is at least of $O\left(\lambda^4\right)$.

A hierarchy of master equations linking the n-time correlation function P_n with P_{n+1} can be obtained starting from the definition [58]

$$P_n(\mathbf{x}_n, t_n; \ldots; \mathbf{x}_1, t_1) = \langle \delta(\mathbf{x}_n - \mathbf{Y}(t_n)) \ldots \delta(\mathbf{x}_1 - \mathbf{Y}(t_1)) \rangle \tag{C.15}$$

and acting as

$$\partial_{t_j} P_n(\mathbf{x}_n, t_n; \ldots; \mathbf{y}, t_j; \ldots; \mathbf{x}_1, t_1) = -\nabla_{\mathbf{y}} \cdot \left\langle \delta(\mathbf{x}_n - \mathbf{Y}(t_n)) \ldots \delta(\mathbf{x}_1 - \mathbf{Y}(t_1)) \dot{\mathbf{Y}}(t_j) \right\rangle. \tag{C.16}$$

The result of this procedure is completely analogous to Eq. (3.15) upon replacing $P_1 \to P_n$ and $P_2 \to P_{n+1}$.

In order to check the accuracy of the master equation (3.15), we can use it to predict the expectation value of the position $\langle \mathbf{Y}(t) \rangle$ when $\mathbf{Y}(t = t_0) \neq 0$ and the second particle $\mathbf{Z}$ is decoupled from the system (i.e., with $V_q^{(\ )} = 0$). Recall that we derived this same quantity in Section 2.2 via a weak-coupling expansion. Within the effective master equation derived here, one starts instead by replacing the two-point function $P_2(\mathbf{y}, t; \mathbf{x}, s)$ in Eq. (3.15) by its $O\left(\lambda^0\right)$ approximation,

$$P_2(\mathbf{y}, t; \mathbf{x}, s) = P_{1|1}(\mathbf{y}, t|\mathbf{x}, s) P_1(\mathbf{x}, s) + O\left(\lambda^2\right), \tag{C.17}$$

where we used the fact that the independent ($\lambda = 0$) process is Markovian, $P_{1|1}$ is the Ornstein-Uhlenbeck propagator given in Section 1.2, and $P_1(\mathbf{x}, s)$ is chosen to be the thermal equilibrium distribution of the particle $\mathbf{Y}$ in its harmonic trap (see, c.f., Eq. (C.22)). By using Eq. (C.17), the master equation (3.15) becomes a Fokker-Planck equation which can be used to compute $\langle \mathbf{Y}(t) \rangle$: a straightforward calculation renders the same result as in Eq. (2.13), as expected.

C.2.2 Irrelevance of the memory kernel in the periodic state up to $O\left(\lambda^2\right)$

Here we prove that the non-Markovian term in the master equation (3.15) containing the memory kernel $\mathcal{L}(t \quad s)$ can be discarded in the periodic state. In order to do this, we need to use the result derived in Appendix B.2, namely that — under suitable hypotheses of translational invariance — the marginal equilibrium distribution of a single particle coupled to the field reads simply $P_{\mathrm{eq}}(\mathbf{X}) \propto \exp[\ \beta \mathcal{U}(\mathbf{X})]$, i.e., it is unaffected by the interaction.

We then consider the master equation for $\mathbf{Y}(t)$ in Eq. (3.15), and set initially $V_q^{(\ )} \equiv 0$, so that the second particle is decoupled from the problem. The master equation then reads at long times

$$\partial_t P_1(\mathbf{y}, t) = \mathcal{L}_0 P_1(\mathbf{y}, t) + \lambda^2 \int_0^\infty \mathrm{d}u \int \mathrm{d}\mathbf{x}\, \mathcal{L}(\mathbf{y}, \mathbf{x}; u) P_2(\mathbf{y}, t; \mathbf{x}, t \quad u) + O\Big(\lambda^4\Big), \tag{C.18}$$

where we called $u \equiv t \quad s$ and sent $t_0 \to \quad \infty$, and where the operators $\mathcal{L}_0$ and $\mathcal{L}$ were given in Eqs. (3.16) and (3.19), respectively. In the absence of any external forcing, the system will reach a state of thermal equilibrium with a stationary probability distribution $P_{1,\mathrm{eq}}$ satisfying $\partial_t P_{1,\mathrm{eq}}(\mathbf{y}) \equiv 0$: this has to be the case order by order in the coupling constant λ. In particular, we read at $O\left(\lambda^2\right)$

$$0 \equiv \ \mathcal{L}_0 P^{(2)}_{1,\mathrm{eq}}(\mathbf{y}) + \int_0^\infty \mathrm{d}u \int \mathrm{d}\mathbf{x}\, \mathcal{L}(\mathbf{y}, \mathbf{x}; u) P^{(0)}_{2,\mathrm{eq}}(\mathbf{y}, t; \mathbf{x}, t \quad u), \tag{C.19}$$

where the superscript indicates the order in the expansion in powers of λ. On the other hand, we know *a priori* (see discussion above) that the stationary distribution of a single particle in thermal equilibrium with a fluctuating field reads simply

$$P_{1,\mathrm{eq}}(\mathbf{Y}) \propto \int \mathcal{D}\phi\, e^{\ \beta \mathcal{H}[\phi, \mathbf{Y}]} \propto e^{\ \beta \kappa_y Y^2/2}. \tag{C.20}$$

Here we deduce in particular that $P^{(2)}_{1,\mathrm{eq}}(\mathbf{y}) = 0$, and thus we can conclude that

$$\int_0^\infty \mathrm{d}u \int \mathrm{d}\mathbf{x}\, \mathcal{L}(\mathbf{y}, \mathbf{x}; u) P^{(0)}_{2,\mathrm{eq}}(\mathbf{y}, t; \mathbf{x}, t \quad u) \equiv 0. \tag{C.21}$$

Switching on the coupling $V_q^{(\ )}$, so as to include the second particle into the problem, has actually no effect on $P_{2,\mathrm{eq}}(\mathbf{y}, t; \mathbf{x}, t \quad u)$ at $O\left(\lambda^0\right)$ — this can be deduced by looking at its master equation, see Appendix C.2.1. Accordingly, we conclude that Eq. (C.21) must still hold true in the periodic state, up to $O\left(\lambda^2\right)$.

C.2.3 Solution of the master equation in the periodic state

In this Appendix we look for a perturbative solution of the master equation (3.20) in powers of the coupling constant λ. To lighten the notation, we will drop the subscript y from the constants ν and κ, and simply add the subscript $\quad$ when we are referring to the second particle $\mathbf{Z}$. Notice first that Eq. (3.20) is solved at the lowest order by the stationary distribution of the Ornstein-Uhlenbeck process (see Appendix C.1):

$$P_1^{(0)}(\mathbf{y}) = (2\pi T/\kappa)^{\ d/2} \exp\Big(\ \kappa y^2/2T\Big). \tag{C.22}$$

The effect of the external perturbation only appears at the next perturbative order as

$$\partial_t P_1^{(2)}(\mathbf{y},t) = \mathcal{L}_0 P_1^{(2)}(\mathbf{y},t) + \mathcal{L}\ (t) P_1^{(0)}(\mathbf{y},t), \tag{C.23}$$

with $\mathcal{L}_0$ and $\mathcal{L}$ given in Eqs. (3.16) and (3.17), respectively. The Green function of the operator $\mathcal{L}_{\rm OU} \equiv \partial_t \quad \mathcal{L}_0$ is simply the Ornstein-Uhlenbeck propagator in Eq. (1.9), henceforth denoted as $P^{(0)}_{1|1}$, so that the solution of Eq. (C.23) after an initial transient will read

$$P_1^{(2)}(\mathbf{y},t) = \int \mathrm{d}\mathbf{x} \int_{\infty}^{t} \mathrm{d}t'\, P^{(0)}_{1|1}(\mathbf{y},t|\mathbf{x},t') f_s(\mathbf{x},t'), \tag{C.24}$$

where we introduced the source term

$$f_s(\mathbf{y},t) \equiv \mathcal{L}\ (t) P_1^{(0)}(\mathbf{y},t). \tag{C.25}$$

Using the definition of $\mathcal{L}\ (t)$ given in Eq. (3.17) and integrating by parts, it is straightforward to check that $\int \mathrm{d}\mathbf{y}\, P_1^{(2)}(\mathbf{y},t) = 0$, which shows that the normalization condition $\int \mathrm{d}\mathbf{y}\, P_1(\mathbf{y},t) = 1$ is still satisfied.

Since the operator $\mathcal{L}_{\rm OU}$ is time-translational invariant, then so will be its propagator

$$P^{(0)}_{1|1}(\mathbf{y},t|\mathbf{x},t') = P^{(0)}_{1|1}(\mathbf{y},\tau \equiv t \quad t'|\mathbf{x},0). \tag{C.26}$$

As a result, Eq. (C.24) takes the form of a convolution over the time domain. The integration over the spatial degrees of freedom can be readily performed by noting that

$$\int \mathrm{d}\mathbf{x}\, P^{(0)}_{1|1}(\mathbf{y},\tau|\mathbf{x},0) \nabla_{\mathbf{x}} \Big[e^{\ i\mathbf{q}\cdot\mathbf{x}} P_1^{(0)}(\mathbf{x})\Big] = \int \mathrm{d}\mathbf{x}\, e^{\ i\mathbf{q}\cdot\mathbf{x}} P_1^{(0)}(\mathbf{x}) \nabla_{\mathbf{x}} P^{(0)}_{1|1}(\mathbf{y},\tau|\mathbf{x},0) \tag{C.27}$$
$$= e^{\ \gamma\tau} \nabla_{\mathbf{y}} \int \mathrm{d}\mathbf{x}\, e^{\ i\mathbf{q}\cdot\mathbf{x}} P_1^{(0)}(\mathbf{x}) P^{(0)}_{1|1}(\mathbf{y},\tau|\mathbf{x},0) = e^{\ \gamma\tau} \nabla_{\mathbf{y}} P_1^{(0)}(\mathbf{y}) \exp\Big[\ i\mathbf{q}\cdot\mathbf{y} e^{\ \gamma\tau} \quad q^2\sigma^2(\tau)/2\Big],$$

where $\sigma(\tau)$ is given in Eq. (1.11) and where we used Gaussian integration in the last line. We thus find

$$P_1^{(2)}(\mathbf{y},t) = \nabla_{\mathbf{y}} \cdot \left[\nu P_1^{(0)}(\mathbf{y}) \int \frac{\mathrm{d}^d q}{(2\pi)^d} i\mathbf{q} v(\mathbf{q}) \int_{\infty}^{t} \mathrm{d}t'\, F_{\mathbf{q}}^{(\ )}(t') e^{\ \gamma\tau} e^{\ i\mathbf{q}\cdot\mathbf{y} e^{\ \gamma\tau}\ \ q^2\sigma^2(\tau)/2} \right], \tag{C.28}$$

with $F_{\mathbf{q}}^{(\ )}(t)$ and $v(\mathbf{q})$ defined in Eqs. (3.21) and (3.24), respectively.

As usual, knowing $P_1(\mathbf{y},t)$ allows to compute averages of one-time observables $O(\mathbf{Y})$ as

$$\langle O(\mathbf{Y})(t)\rangle = \int \mathrm{d}\mathbf{y}\, O(\mathbf{y}) \Big[P_1^{(0)}(\mathbf{y}) + \lambda^2 P_1^{(2)}(\mathbf{y},t)\Big] + \mathcal{O}\Big(\lambda^3\Big). \tag{C.29}$$

Thus, the preliminary result in Eq. (C.28) can be used in practical calculations for a generic choice of $F_{\mathbf{q}}^{(\ )}(t)$. Below we will focus instead on the particular case of periodic driving.

C.2.3.1 Periodic driving

We have already observed that the time integral in Eq. (C.28) is a convolution between $F_{\mathbf{q}}^{(\ )}(t)$ and a non-periodic function which we will denote as

$$H(\tau) \equiv \Theta(\tau)h(\tau) \equiv \Theta(\tau)e^{\ \gamma\tau}e^{\ i\mathbf{q}\cdot\mathbf{y}e^{\ \gamma\tau}\ q^2\sigma^2(\tau)/2}, \tag{C.30}$$

the Fourier transform of which reads

$$\tilde{H}(\omega) \equiv \int_{\infty}^{\infty} \mathrm{d}\tau\, e^{\ i\omega\tau}h(\tau)\Theta(\tau) = \int_{0}^{\infty} \mathrm{d}\tau\, e^{\ i\omega\tau}h(\tau). \tag{C.31}$$

Now let us choose $F_{\mathbf{q}}^{(\ )}(t)$ to be periodic with period $T = 2\pi/\Omega$, so that we can expand it in Fourier series as

$$F_{\mathbf{q}}^{(\ )}(t) = \sum_{n\in\mathbb{Z}} a_n(\mathbf{q})e^{in\Omega t}, \tag{C.32}$$

where the values of the coefficients $a_n(\mathbf{q})$ depend on the specific form of the external forcing applied to the particle $\mathbf{Z}(t)$ in Eq. (3.21) (further below we will focus on the specific case of monochromatic forcing). The Fourier transform of $F_{\mathbf{q}}^{(\ )}(t)$ will then read

$$F(\omega) = \sum_{n\in\mathbb{Z}} a_n(\mathbf{q})\delta(\omega \quad n\Omega), \tag{C.33}$$

so we can transform the convolution in Eq. (C.28) into a product in Fourier space:

$$\begin{aligned} P_1^{(2)}(\mathbf{y},t) &= \boldsymbol{\nabla}_{\mathbf{y}}\cdot\left[\nu P_1^{(0)}(\mathbf{y})\int\frac{\mathrm{d}^d q}{(2\pi)^d}i\mathbf{q}v(\mathbf{q})\int_{\infty}^{\infty}\mathrm{d}t'\,F_{\mathbf{q}}^{(\ )}(t')H(t \quad t')\right] \\ &= \boldsymbol{\nabla}_{\mathbf{y}}\cdot\left[\nu P_1^{(0)}(\mathbf{y})\int\frac{\mathrm{d}^d q}{(2\pi)^d}i\mathbf{q}v(\mathbf{q})\int\frac{\mathrm{d}\omega}{2\pi}\sum_n a_n(\mathbf{q})\delta(\omega \quad n\Omega)\tilde{H}(\omega)e^{i\omega t}\right] \\ &= \sum_{n\in\mathbb{Z}}\left[\boldsymbol{\nabla}_{\mathbf{y}}\cdot\nu P_1^{(0)}(\mathbf{y})\int\frac{\mathrm{d}^d q}{(2\pi)^d}i\mathbf{q}v(\mathbf{q})a_n(\mathbf{q})\tilde{H}(n\Omega)\right]e^{in\Omega t}, \end{aligned} \tag{C.34}$$

where in $\tilde{H}(\omega)$ we understand a further dependence on $\mathbf{q}$ and $\mathbf{y}$. One can also obtain an expression for the moment generating function by using Gaussian integration,

$$\left\langle e^{\ i\mathbf{p}\cdot\boldsymbol{\Upsilon}(t)}\right\rangle = e^{\ \frac{Tp^2}{2k}}\left[1 \quad \nu\lambda^2\sum_n C_n(\mathbf{p})e^{in\Omega t}\right] + O\left(\lambda^4\right), \tag{C.35}$$

where we introduced

$$C_n(\mathbf{p}) \equiv \int\frac{\mathrm{d}^d q}{(2\pi)^d}e^{\ \frac{Tq^2}{2k}}v(\mathbf{q})a_n(\mathbf{q})A_n(\mathbf{p}\cdot\mathbf{q}), \tag{C.36}$$

and where the function $A_n(\mathbf{p}\cdot\mathbf{q})$ was given in Eq. (3.26). We can use the moment generating function to compute the mean displacement of the particle,

$$\langle\boldsymbol{\Upsilon}(t)\rangle = i\,\boldsymbol{\nabla}_{\mathbf{p}}\left\langle e^{\ i\mathbf{p}\cdot\boldsymbol{\Upsilon}(t)}\right\rangle\Big|_{\mathbf{p}=0} \simeq \quad \nu\lambda^2\sum_{n\in\mathbb{Z}}\left[\int\frac{\mathrm{d}^d q}{(2\pi)^d}i\mathbf{q}e^{\ \frac{Tq^2}{2k}}v(\mathbf{q})\frac{a_n(\mathbf{q})}{\gamma + in\Omega}\right]e^{in\Omega t}. \tag{C.37}$$

Connected correlations can be obtained from the cumulant generating function, which reads, up to the first nontrivial order in λ,

$$\ln\left\langle e^{\ i\mathbf{p}\cdot\boldsymbol{\Upsilon}(t)}\right\rangle \simeq \quad \frac{Tp^2}{2k} \quad \nu\lambda^2\sum_{n\in\mathbb{Z}}C_n(\mathbf{p})e^{in\Omega t}. \tag{C.38}$$

C.2.3.2 Monochromatic forcing

Motivated by the setting described in Section 3.1, we consider here a sinusoidal forcing term $\mathbf{z}_F(t)$ as in Eq. (3.12). In order to calculate explicitly the various quantities discussed above, we need first the coefficients of the Fourier series of the function $F_{\mathbf{q}}^{(\ )}(t)$:

$$a_n(\mathbf{q}) \equiv \left(e^{in\Omega t},\, F_{\mathbf{q}}^{(\ )}(t)\right), \tag{C.39}$$

where we introduced the scalar product

$$(f(t),\, g(t)) = \frac{\Omega}{2\pi}\int_0^{2\pi/\Omega} \mathrm{d}t\, f^*(t)g(t). \tag{C.40}$$

Recall the definition of $F_{\mathbf{q}}^{(\ )}(t)$ in Eq. (3.21), where the term $\langle \exp[i\mathbf{q}\cdot\mathbf{Z}(t)]\rangle_0$ was computed in Appendix C.1 and is given in Eq. (3.27) for the case of a sinusoidal forcing. Using the properties of the Bessel functions of the first kind $J_n(\ )$ [281], one can prove the relation

$$\left(e^{in\Omega t},\, e^{i\ \sin(\Omega(t\ \ u))}\right) = e^{\ in\Omega u} J_n(\ ), \tag{C.41}$$

so that the Fourier coefficients in Eq. (C.39) take the form

$$a_n(\mathbf{q}) = Dq\ \ \frac{J_n(\mathbf{q}\cdot\mathbf{A})}{q + in\Omega} e^{i\mathbf{q}\cdot\Delta} \exp\left(\ \ \frac{Tq^2}{2\kappa}\ \ \ in\theta\ \right). \tag{C.42}$$

For $n = 0$ the coefficient does not depend on the dynamics of the field ($= 0$ or $= 2$), and one recovers the adiabatic mean value in Eq. (3.51). Notice also that, in the deterministic limit $\kappa \ \to \infty$, one has $\exp\left[\ \ Tq^2/(2\kappa\ )\ \ \ in\theta\ \right] \to 1$.

C.3 Effective field picture

In this Appendix we analyze the dynamics of the particle $\mathbf{Y}$ as if it were immersed into the effective field

$$\phi_{\mathbf{q}}^{\mathrm{eff}}(t) = \int_{\infty}^{t} \mathrm{d}s\, G_q(t\ \ \ s)\left[\lambda Dq\ \ V_q^{(\ )} e^{\ i\mathbf{q}\cdot\mathbf{Z}(s)} + \eta_{\mathbf{q}}(s)\right]. \tag{C.43}$$

In this expression the second particle $\mathbf{Z}(t)$ is treated as a source, on the same footing as the noise $\eta_{\mathbf{q}}(t)$. We take for simplicity the deterministic limit $\kappa \ \to \infty$ for the motion of the second particle, so that it appears clearly that the field in Eq. (C.43) is Gaussian with mean value

$$\langle \phi_{\mathbf{q}}^{\mathrm{eff}}(t)\rangle = \lambda V_q^{(\ )} \int_0^{\infty} \mathrm{d}u\, \chi_q(u) e^{\ i\mathbf{q}\cdot\mathbf{z}_F(t\ \ u)} = \lambda V_q^{(\ )} F^{(\ )}{}_{\mathbf{q}}(t), \tag{C.44}$$

and (connected) correlations that are analogous to those of the free-field (see Appendix 1.3). The function $F^{(\ )}{}_{\mathbf{q}}(t)$ was defined in Eq. (3.21). Plugging this expression for the average field $\langle \phi_{\mathbf{q}}^{\mathrm{eff}}(t)\rangle$ into the Langevin equation (3.6) for the particle $\mathbf{Y}$, we get

$$\dot{\mathbf{Y}}(t) = \ \ \gamma_y \mathbf{Y}(t) + \xi^{(y)}(t) + \nu_y \lambda \int \frac{\mathrm{d}^d q}{(2\pi)^d} i\mathbf{q} V_q^{(y)} \langle \phi_q^{\mathrm{eff}}(t)\rangle\, e^{i\mathbf{q}\cdot\mathbf{Y}(t)}. \tag{C.45}$$

Note that we are treating the field ϕ^{eff} as if it were independent of the variable $\mathbf{Y}(t)$, and that by using $\langle\phi_q^{\text{eff}}(t)\rangle$ in place of $\phi_q^{\text{eff}}(t)$ we are practically ignoring its thermal fluctuations. It is however rather straightforward (see, e.g., Ref. [53]) to show that Eq. (C.45) is equivalent to the Fokker-Planck equation (3.20) satisfied by the particle up to $O(\lambda^2)$ in the periodic state. That the thermal fluctuations of the field do not enter at all the Fokker-Planck equation (up to and including $O(\lambda^2)$) may look surprising at first sight. However, this is actually consistent with the fact that such fluctuations do not modify the equilibrium distribution of the particle in the absence of any external forcing (see discussion in Appendix C.2.2). Indeed, the field does not know that the particle $\mathbf{Y}$ is not in equilibrium, being its displacement already of $O(\lambda^2)$: any feedback effect would only appear at higher perturbative orders in the coupling constant.

C.4 Upper bound on the value of λ

In Section 3.2.2 we derived an expression for the variance of the particle position, Eq. (3.30), which takes the form

$$\left\langle Y_j^2(t)\right\rangle_c = \frac{T}{\kappa_y}\left(1 \quad \lambda^2\mathcal{A}\right) \tag{C.46}$$

upon calling

$$\mathcal{A} \equiv \sum_{n\in\mathbb{Z}} \frac{vD}{2\gamma_y + in\Omega} e^{in(\Omega t \quad \theta)} \left[\int \frac{\mathrm{d}^d q}{(2\pi)^d} \frac{q_j^2 q \quad v(\mathbf{q}) J_n(\mathbf{q}\cdot\mathbf{A})}{\quad q + in\Omega} e^{\frac{Tq^2}{2k_p} + i\mathbf{q}\cdot} \right]. \tag{C.47}$$

Up to this order in λ, a necessary condition for the variance to be positive is $\lambda^2\mathcal{A} \leq 1$. Calling $g(\mathbf{q}) \equiv q_j^2 v(\mathbf{q}) \exp\left[\quad Tq^2/(2k_p)\right]$, it is simple to derive an upper bound for

$$\begin{aligned} |\mathcal{A}| &\leq \sum_{n\in\mathbb{Z}} \int \frac{\mathrm{d}^d q}{(2\pi)^d} \frac{Dq \quad g(\mathbf{q}) J_n(\mathbf{q}\cdot\mathbf{A})}{\sqrt{\frac{2}{q} + (n\Omega)^2}\sqrt{(2\gamma_y)^2 + (n\Omega)^2}} \\ &\leq \int \frac{\mathrm{d}^d q}{(2\pi)^d} \frac{Dq \quad g(\mathbf{q})}{2\gamma_y \quad q} \sum_{n\in\mathbb{Z}} J_n(\mathbf{q}\cdot\mathbf{A}) = \frac{1}{2\gamma_y}\int \frac{\mathrm{d}^d q}{(2\pi)^d} \frac{g(\mathbf{q})}{q^2 + r}, \end{aligned} \tag{C.48}$$

where in the second line we set $\Omega = 0$, and in the third we used the identity $\sum_{n=\ \infty}^{\infty} J_n(x) = 1$ [281]. The last integral in Eq. (C.48) is a decreasing function of the parameter r and it can be computed in closed form for some elementary functional forms of the interaction potentials $V_q^{(a)}$ contained in $v(\mathbf{q})$ (see Eq. (3.24)). Choosing, for instance, Gaussian interacting potentials as in Eq. (2.4) and setting $r = 0$ (for which the integral is maximum), we get the upper bound reported in Eq. (3.32). For λ smaller than this upper bound it is guaranteed that the variance in Eq. (C.46) is positive, a necessary condition for the perturbative expansion to provide meaningful results.

C.5 Equilibrium effective potential

In this Appendix we study the effective induced interaction between the two particles due to the presence of the field.

C.5.1 Derivation of the potential

Let us start by considering the joint probability distribution of the two particles, which at equilibrium is the canonical one given in Eq. (3.36). Under the functional integral we recognize, up to a normalization factor, the stationary distribution of the field at fixed particles positions

$$\begin{aligned}\mathcal{P}_{\rm st}\left[\phi|\mathbf{Y},\mathbf{Z}\right] &= \frac{1}{\mathcal{Z}_{\rm st}(\mathbf{Y},\mathbf{Z})}e^{\ \beta\left(\mathcal{H}_\phi+\mathcal{H}_{\rm int}\right)} \\ &= \frac{1}{\mathcal{Z}_{\rm st}}\exp\left\{\ \ \beta\int\frac{\mathrm{d}^d q}{(2\pi)^d}\left[\frac{1}{2}(q^2+r)\phi_{\mathbf{q}}\phi_{\ \mathbf{q}}\quad\lambda\phi_{\mathbf{q}}\left(V^{(y)}_q e^{i\mathbf{q}\cdot\mathbf{Y}}+V^{(\ )}_q e^{i\mathbf{q}\cdot\mathbf{Z}}\right)\right]\right\}.\end{aligned} \tag{C.49}$$

The coupling to the field is linear, so the Gaussian functional integral over $\mathcal{P}_{\rm st}\left[\phi|\mathbf{Y},\mathbf{Z}\right]$ in Eq. (3.36) can be calculated exactly. To this end, we first bring it in the form

$$\int\mathcal{D}\phi\, e^{\ \beta\left(\mathcal{H}_\phi+\mathcal{H}_{\rm int}\right)}=\int\mathcal{D}\phi\, e^{\ \frac{\beta}{2}\left(\phi,\hat{A}\phi\right)+\beta\lambda\left(h^{(y)}+h^{(\ )},\phi\right)}\propto\exp\left[\frac{\beta\lambda^2}{2}\left(h^{(y)}+h^{(\ )},\ \hat{A}^{\ 1}(h^{(y)}+h^{(\ )})\right)\right], \tag{C.50}$$

where we introduced the vectors $h^{(a)}(\mathbf{x})\equiv V^{(a)}(\mathbf{x}\quad\mathbf{X}_a)$ and the scalar product

$$(f,\ g)=\int\mathrm{d}^d x\, f(\mathbf{x})g(\mathbf{x}). \tag{C.51}$$

The operator $\hat{A}$ is defined by its kernel

$$A(\mathbf{x},\mathbf{y})=\left(\ \ \nabla^2+r\right)\delta(\mathbf{x}\quad\mathbf{y}),\qquad\hat{A}\phi(\mathbf{x})=\int\mathrm{d}^d y\, A(\mathbf{x},\mathbf{y})\phi(\mathbf{y}). \tag{C.52}$$

In Fourier space, these become $\tilde{h}^{(a)}(\mathbf{q})=V^{(a)}_q\exp[\ \ i\mathbf{q}\cdot\mathbf{X}_a(t)]$ and

$$\tilde{A}(\mathbf{q},\mathbf{p})=\left(q^2+r\right)\delta(\mathbf{q}+\mathbf{p})\qquad\rightarrow\qquad\tilde{A}^{\ 1}(\mathbf{q},\mathbf{p})=\frac{\delta(\mathbf{q}+\mathbf{p})}{q^2+r}. \tag{C.53}$$

Integrating over the dummy variables (momenta) as

$$\left(f,\ \hat{A}g\right)=\int\frac{\mathrm{d}^d q\,\mathrm{d}^d p}{(2\pi)^{2d}}\tilde{f}(\ \ \mathbf{q})\tilde{A}(\mathbf{q},\ \ \mathbf{p})\tilde{g}(\mathbf{p}), \tag{C.54}$$

we finally get the effective Hamiltonian $\mathcal{H}_{\rm eff}(\mathbf{Y},\mathbf{Z})$ given in Eq. (3.38), featuring the field-induced interaction potential $V_c(\mathbf{Y}\quad\mathbf{Z})$ of Eq. (3.39) (up to a constant that we fix by requiring $V_c(\mathbf{x}\to\infty)=0$). We notice that $V_c(\mathbf{x})$ is translational invariant, as expected, so that the induced force is given by $\mathbf{F}_c(\mathbf{x})=\ \ \lambda^2\boldsymbol{\nabla}_{\mathbf{x}}V_c(\mathbf{x})$. The latter is in general a non-monotonic function of $\mathbf{x}$, and the location of its extremal points $\mathbf{x}=\mathbf{x}_*$ along the various spatial directions is found by inspecting the Hessian matrix

$$0\equiv\left.\frac{\partial^2 V_c(\mathbf{x})}{\partial x_i\partial x_j}\right|_{\mathbf{x}=\mathbf{x}_*}=\int\frac{\mathrm{d}^d q}{(2\pi)^d}\frac{v(\mathbf{q})}{q^2+r}q_i q_j e^{i\mathbf{q}\cdot\mathbf{x}_*}. \tag{C.55}$$

C.5.2 Analysis of the induced potential for the isotropic case

If the interaction potentials of the two particles are equal, i.e., $V_q^{(y)} = V_q^{(\ )} \equiv V_q$, then $v(\mathbf{q}) \equiv |V_q|^2$ (see Eq. (3.24)). Moreover, if $V(\mathbf{x})$ is isotropic (which is a sensible requirement if the particles are assumed to be spherically symmetric), then $v(\mathbf{q}) = v(q)$, and we can rewrite Eq. (3.39) in polar coordinates as

$$V_c(x) = \int_0^\infty \mathrm{d}q \, \frac{q^{d\ 1}}{q^2 + r} v(q) \int \frac{\mathrm{d}\Omega_d}{(2\pi)^d} e^{i\mathbf{q}\cdot\mathbf{x}}. \tag{C.56}$$

Using the property of the Bessel functions [281], one can prove that

$$\int \frac{\mathrm{d}\Omega_d}{(2\pi)^d} e^{i\mathbf{q}\cdot\mathbf{x}} = \frac{J_{d/2\ 1}(qx)}{(2\pi)^{d/2}(qx)^{d/2\ 1}}, \tag{C.57}$$

and introducing the dimensionless variable $\equiv qx$ we find

$$V_c(x) = \frac{x^{2\ d}}{(2\pi)^{d/2}} \int_0^\infty \mathrm{d}\ \ ^{d/2}{}_{2 + rx^2} v(\ /x) J_{d/2\ 1}(\ ). \tag{C.58}$$

If we assume for V_q a Gaussian form as in Eq. (2.4), then this expression becomes

$$V_c(x) = R^{2\ d} f(x/\xi, x/R), \tag{C.59}$$

where the scaling function

$$f(\Theta, \Lambda) \equiv \frac{\Lambda^{2\ d}}{(2\pi)^{d/2}} \int_0^\infty \mathrm{d}\ \ ^{d/2} e^{(\ /\Lambda)^2}{}_{2 + \Theta^2} J_{d/2\ 1}(\ ) \tag{C.60}$$

depends on the dimensionless parameters $\Theta = x\sqrt{r} = x/\xi$ and $\Lambda = x/R$ (in accordance with the scaling form in Eq. (1) of Ref. [107]). Note that Θ and Λ actually play the role of an IR and a UV cutoff, respectively. Similarly, the resulting induced force is

$$\mathbf{F}_c(x) = \lambda^2 \nabla_{\mathbf{x}} V_c(x) = \mathbf{x}\lambda^2 R^{1\ d} f'\left(\frac{x}{\xi}, \frac{x}{R}\right), \tag{C.61}$$

with

$$f'(\Theta, \Lambda) \equiv \frac{\Lambda^{1\ d}}{(2\pi)^{d/2}} \int_0^\infty \mathrm{d}\ \ ^{d/2+1} e^{(\ /\Lambda)^2}{}_{2 + \Theta^2} J_{d/2}(\ ). \tag{C.62}$$

We now look for the asymptotic behavior for large x of the induced potential in Eq. (3.39) with the Gaussian interaction potential $v(q) = \exp\ q^2R^2)$. This can be obtained by using the identity [62]

$$\frac{1}{q^2 + r} = \int_0^\infty \mathrm{d}\mu \, e^{\ \mu(q^2+r)}, \tag{C.63}$$

and performing the Gaussian integration in $\mathrm{d}^d q$. Changing variables to $s \equiv (\mu + R^2)/x$ gives[2]

$$V_c(x) = \frac{x^{1\ d/2}}{(4\pi)^{d/2}} e^{R^2 r} \int_{R^2/x}^\infty \frac{\mathrm{d}s}{s^{d/2}} e^{\ x[rs+1/(4s)]}. \tag{C.64}$$

[2] See Ref. [309], *Laplace's method for integrals with movable maxima*.

Finally, the integral over s can be estimated for large x using the Laplace method, whence

$$V_c(x) \sim \frac{(2\pi x)^{(1-d)/2}}{2r^{(3-d)/4}} e^{R^2 r - x\sqrt{r}}, \tag{C.65}$$

which presents the familiar exponential tails $\sim \exp(-x/\xi)$, being $\xi = r^{-1/2}$ the field correlation length. One can check that a similar asymptotic behavior is shared by the induced force, since for large x one finds $\mathbf{F}_c(x) \sim \mathbf{x}\lambda^2\sqrt{r}V_c(x)$.

In $d = 1$, the expressions above become

$$V_c(x) = \frac{x}{\pi}\int_0^\infty \mathrm{d}\, \frac{\cos(-x)e^{-2(R/x)^2}}{2 + rx^2}, \tag{C.66}$$

$$F_c(x) = \frac{\lambda^2}{\pi}\int_0^\infty \mathrm{d}\, \frac{\sin(-x)e^{-2(R/x)^2}}{2 + rx^2}, \tag{C.67}$$

which are plotted in Fig. 3.2a (rescaled by the R-dependent part of their asymptotic amplitude found in Eq. (C.65)). It appears that the induced force is small for both small and large x, while it presents a maximum defined by the condition

$$\partial_x F_c(x)\Big|_{x_{\max}} \propto \int_{-\infty}^{\infty} \mathrm{d}q\, \frac{q^2 e^{-q^2R^2}}{q^2 + r} e^{iqx_{\max}} \equiv 0. \tag{C.68}$$

Note that the induced potential in Eq. (C.66) diverges for $r = 0$, but the force in Eq. (C.67) does not. Equivalently, the induced potential in Eq. (C.66) is regularized by subtracting its value in $x = 0$,

$$V_c(x = 0) = \frac{1}{\pi}\int_0^\infty \mathrm{d}q\, \frac{v(q)}{q^2 + r}, \tag{C.69}$$

which is just a constant shift in energy. However, the induced force $F_c(x)$ in $d = 1$ and for $r = 0$ is still somewhat pathological, in that it saturates to a constant value at large x instead of decaying to zero. To understand why, we note that at large distances x the cutoff R in the induced potential $V_c(\mathbf{x})$ is expected to play no role (apart from taming possible UV divergences which can arise for sufficiently large d). If we set $R \simeq 0$ in Eq. (3.39), we obtain

$$V_c(\mathbf{x}) \simeq \int \frac{\mathrm{d}^d q}{(2\pi)^d} \frac{1}{q^2 + r} e^{i\mathbf{q}\cdot\mathbf{x}} = \langle\phi(\mathbf{x})\phi(0)\rangle\,, \tag{C.70}$$

where we recognized the two-point correlation function of a scalar Gaussian field in d spatial dimensions [62]. At the critical point $r = 0$, this behaves generically as $\langle\phi(\mathbf{x})\phi(\mathbf{0})\rangle \sim |\mathbf{x}|^{2-d}$, and in particular in $d = 1$ it grows linearly with x. This explains why the force $F_c(x) \propto \partial_x V_c(x)$ saturates to a constant value for large x. However, we will simply interpret this phenomenon as a pathology of the model for $d = 1$ and $r = 0$, which does not affect our results since we always assume the field to have a (possibly small but) finite correlation length $\xi = r^{-1/2}$.

Different choices of the interaction potential $V(x)$ lead to qualitatively similar results. For instance, a more realistic representation of a spherical particle requires

$$V(\mathbf{x}) = \frac{1}{V_d}\Theta(R - |\mathbf{x}|) \quad \leftrightarrow \quad V_q = \left(\frac{2}{qR}\right)^{d/2} \left(\frac{d}{2} + 1\right) J_{d/2}(qR), \tag{C.71}$$

where V_d is the volume of a d-dimensional sphere and $\Theta(\ )$ is the Heaviside distribution. This leads to the same scaling forms as in Eqs. (C.59) and (C.61) for the induced potential and force, with different scaling functions

$$f_2(\Theta,\Lambda) \equiv \Lambda^2 c_d \int_0^\infty \mathrm{d}\ \frac{^{d/2} J_{d/2\ 1}(\ )}{^2+\Theta^2}\left[J_{d/2}\left(\frac{}{\Lambda}\right)\right]^2, \tag{C.72}$$

$$f_2'(\Theta,\Lambda) \equiv \Lambda c_d \int_0^\infty \mathrm{d}\ \frac{^1\ ^{d/2} J_{d/2}(\ )}{^2+\Theta^2}\left[J_{d/2}\left(\frac{}{\Lambda}\right)\right]^2, \tag{C.73}$$

$$c_d \equiv (2/\pi)^{d/2}[\ (d/2+1)]^2, \tag{C.74}$$

which are qualitatively similar to the Gaussian case shown in Fig. 3.2a. In particular, the induced force still presents a maximum as a function of the distance x, which can give rise to the phenomenon of frequency doubling in the adiabatic response (see Section 3.3.3.2 and Appendix C.6.3).

C.6 Particle dynamics within the adiabatic approximation

In this Appendix we derive the particle dynamics at lowest order within the adiabatic approximation. This is achieved by averaging the equations of motion (3.6) and (3.7) of $\mathbf{Y}(t)$ and $\mathbf{Z}(t)$, respectively, over the stationary distribution $\mathcal{P}_{\rm st}\left[\phi|\mathbf{Y},\mathbf{Z}\right]$ of the field ϕ at fixed particles positions given in Eq. (3.34). This is analogous to the Born-Oppenheimer approximation in condensed matter physics, where the wavefunction of the electrons orbiting around a nucleus is obtained by exploiting the separation of their dynamical timescales.

C.6.1 Langevin equation within the adiabatic approximation

Let us focus on the motion of $\mathbf{Y}(t)$, the particle in the fixed trap, which is ruled by Eq. (3.6). We average each of the terms that appear in Eq. (3.6) over the stationary distribution in Eq. (3.34). The terms proportional to $\mathbf{Y}(t)$ and $\dot{\mathbf{Y}}(t)$ yield trivially

$$\langle \mathbf{Y}(t)\rangle_{\rm st} = \int \mathcal{D}\phi\, \mathbf{Y}(t)\mathcal{P}_{\rm st}\left[\phi|\mathbf{Y},\mathbf{Z}\right] = \mathbf{Y}(t), \tag{C.75}$$

and similarly for $\dot{\mathbf{Y}}(t)$, while

$$\begin{aligned}\left\langle \lambda \mathbf{f}_y\right\rangle_{\rm st} = \left\langle \nabla_y \mathcal{H}_{\rm int}\right\rangle_{\rm st} &= \frac{1}{\mathcal{Z}_{\rm st}}\int \mathcal{D}\phi\, \nabla_y \mathcal{H}_{\rm int} e^{\ \beta\left(\mathcal{H}_\phi+\mathcal{H}_{\rm int}\right)} \\ &= \frac{1}{\beta}\nabla_y \log \mathcal{Z}_{\rm st} = \lambda^2 \nabla_y V_c(\mathbf{Y},\mathbf{Z}),\end{aligned} \tag{C.76}$$

where in the last step we used Eq. (3.37). This yields the effective Langevin equation (3.40).

Now we look for a perturbative solution of Eq. (3.40) that is valid up to $O\ \lambda^2)$, and which we will denote as $\mathbf{Y}_{\rm ad}(t)$. To this end, we average each of its terms over the noises $\xi^{(y)}(t)$ and $\xi^{(\ )}(t)$, bearing in mind that

$$\left\langle e^{i\mathbf{q}\cdot(\mathbf{Z}(t)\ \ \mathbf{Y}(t))}\right\rangle = \left\langle e^{i\mathbf{q}\cdot(\mathbf{Z}(t)\ \ \mathbf{Y}(t))}\right\rangle_0 + O(\lambda) = \left\langle e^{i\mathbf{q}\cdot\mathbf{Z}(t)}\right\rangle_0 \left\langle e^{\ i\mathbf{q}\cdot\mathbf{Y}(t)}\right\rangle_0 + O(\lambda), \tag{C.77}$$

where we used the fact that the two independent processes for $\mathbf{Y}(t)$ and $\mathbf{Z}(t)$ factorize. Specializing Eq. (B.11) to the present case gives

$$\left\langle e^{\ i\mathbf{q}\cdot\mathbf{Y}(t)}\right\rangle_0 = \exp\left[\ \ Tq^2/(2\kappa_y)\right], \tag{C.78}$$

which leads to

$$\partial_t \left\langle \mathbf{Y}_{\rm ad}\right\rangle = \ \ \nu_y\kappa_y \left\langle \mathbf{Y}_{\rm ad}\right\rangle \ \ \ \nu_y\lambda^2 \int \frac{\mathrm{d}^d q}{(2\pi)^d}\frac{i\mathbf{q}v(\mathbf{q})}{q^2+r} e^{\ \frac{Tq^2}{2\kappa_y}} \left\langle e^{i\mathbf{q}\cdot\mathbf{Z}}\right\rangle_0 . \tag{C.79}$$

Solving this differential equation with the initial condition $\langle \mathbf{Y}_{\rm ad}(t=t_0)\rangle = 0$, we finally obtain Eq. (3.41).

C.6.2 Adiabatic limit from the master equation

Consider the free-field susceptibility $\chi_q(t \quad s)$ in Eq. (1.31) and assume $\ _q \neq 0$ (see Eq. (1.25)). One can take the formal limit $D \to \infty$, finding

$$\chi_q(t \quad s) \underset{D\to\infty}{\to} \frac{\delta(t \quad s)}{q^2+r}. \tag{C.80}$$

Inserting this expression into Eq. (3.23) for the average displacement of the particle, we immediately recover its adiabatic approximation in Eq. (3.41).

Conversely (and more generally), it is straightforward to check [53] that the Fokker-Planck equation corresponding to the adiabatic Langevin equation (3.40) is exactly the master equation (3.20). To see this, one can use the adiabatic limit in Eq. (C.80) in the expression (3.21) for the function $F_{\mathbf{q}}(t)$, which appears in the operator $\mathcal{L}\ (t)$ of the master equation. The key observation is then that

$$F_{\mathbf{q}}^{(\ )}(t) \underset{D\to\infty}{\to} \frac{\langle e^{i\mathbf{q}\cdot\mathbf{Z}(t)}\rangle_0}{q^2+r}. \tag{C.81}$$

C.6.3 Frequency doubling in the adiabatic response

Looking at the Fourier coefficients of the adiabatic response in Eq. (3.49), it appears that $|\mathbf{b}_1| = 0$ in correspondence of a certain value r_1 of the parameter r. This value can be approximately found, in $d = 1$, by writing

$$\frac{q}{q^2+r} = \frac{1}{q}\left(1 \quad \frac{r}{q^2+r}\right) \tag{C.82}$$

in the condition $|b_1| = 0$, which gives

$$\begin{aligned}\int \mathrm{d}q\, e^{\ q^2\widetilde{R}^2}\frac{J_1(qA)}{q}\cos(q\Delta) &= r_1 \int \mathrm{d}q\, e^{\ q^2\widetilde{R}^2}\frac{J_1(qA)}{q(q^2+r_1)}\cos(q\Delta)\\ &= \int \mathrm{d}y \exp\Big(\ \ y^2\widetilde{R}^2 r_1\Big)\frac{J_1(yA\sqrt{r_1})}{y(y^2+1)}\cos\ y\Delta\sqrt{r_1}\Big),\end{aligned} \tag{C.83}$$

where we changed variable as $q = y\sqrt{r_1}$ in the last line. Assuming r_1 to be small, which can be verified *a posteriori*, one can expand for small r_1, finding

$$r_1 = \left[\frac{4}{\pi A}\int_0^\infty \mathrm{d}q\, e^{\ q^2\widetilde{R}^2}\frac{J_1(qA)}{q}\cos(q\Delta)\right]^2 + O\left(r_1^{3/2}\right). \tag{C.84}$$

One can check numerically that r_1 determined above is an increasing function of the driving amplitude A. A further expansion for small A gives

$$r_1 \simeq \frac{e^{\Delta^2/(2\widetilde{R}^2)}}{\pi\widetilde{R}^2} + O\left(r_1^{3/2}\right), \tag{C.85}$$

which is finite even for $A = 0$, in agreement with the physical interpretation we proposed in Section 3.3.3.

C.7 Phase of the dynamical response

Here we derive some of the results concerning the phase of the dynamical response anticipated in Section 3.4.2.2.

C.7.1 Large-Ω behavior

Let us focus first on the limit in which the frequency Ω of the external driving is large: then the Fourier coefficients in Eq. (3.48) become

$$\mathbf{c}_n e^{in\theta} \sim i\frac{\lambda^2 \nu_y D}{(n\Omega)^2} \int \frac{\mathrm{d}^d q}{(2\pi)^d} \mathbf{q} q \; J_n(\mathbf{q}\cdot\mathbf{A}) e^{q^2\widetilde{R}^2 + i\mathbf{q}\cdot\Delta}, \tag{C.86}$$

where we factored out the phase θ of the driven particle. As explained in the main text, this approximation works if the condition in Eq. (3.65) is met. Notice that the quantity on the r.h.s. of Eq. (C.86) is purely imaginary, which means that for large Ω the dynamical response of $\mathbf{Y}$ is either in phase or in counterphase with the motion of the particle $\mathbf{Z}(t)$ (see Eq. (3.55)). To determine its sign, one has to evaluate the integral in Eq. (C.86). In $d = 1$ and focusing on the first harmonic $n = 1$, we can rescale $\equiv q\Delta$ and write

$$c_1 e^{i\theta} \propto \frac{i}{\Omega^2} \int_0^\infty \mathrm{d} \quad {}^{+1} \cos(\;) J_1(\;\beta_1) e^{(\;\beta_2)^2}, \tag{C.87}$$

where we called $\beta_1 \equiv \widetilde{R}/\Delta$ and $\beta_2 \equiv A/\Delta$ the small parameters of our problem (see setup in Fig. 3.1). Figure C.1a shows that, for β_1 and $\beta_2 \ll 1$, this integral is positive for model B ($= 2$) and negative for model A ($= 0$). This corresponds to the behavior of the phase observed in Fig. 3.6a. Although the sign may change in $d > 1$, one would in any case observe a $\pi/2$ phase shift with respect to the adiabatic prediction at large Ω (see Fig. 3.3b).

C.7.2 Dependence of the phase φ_1 on Δ

Let us now study the dependence of the phase φ_1 of the dynamical response defined in Eq. (3.61) on the average separation Δ between the two traps. To this end, we will consider the case of model A ($= 0$) and examine the behavior for large Δ of the integral I_1 that appears in Eq. (3.62). Focusing on the component j parallel to $\mathbf{A}$ and , we note that Eq. (3.62) can be rewritten, up to first order in the driving amplitude A, as

$$I_1 = \frac{A}{2DR^{d+4}} \frac{\partial^2}{\partial x^2} \int \frac{\mathrm{d}^d y}{(2\pi)^d} \frac{e^{y^2 + i y_j x}}{y^2 + R^2 r + i\Omega/\Omega_0}, \tag{C.88}$$

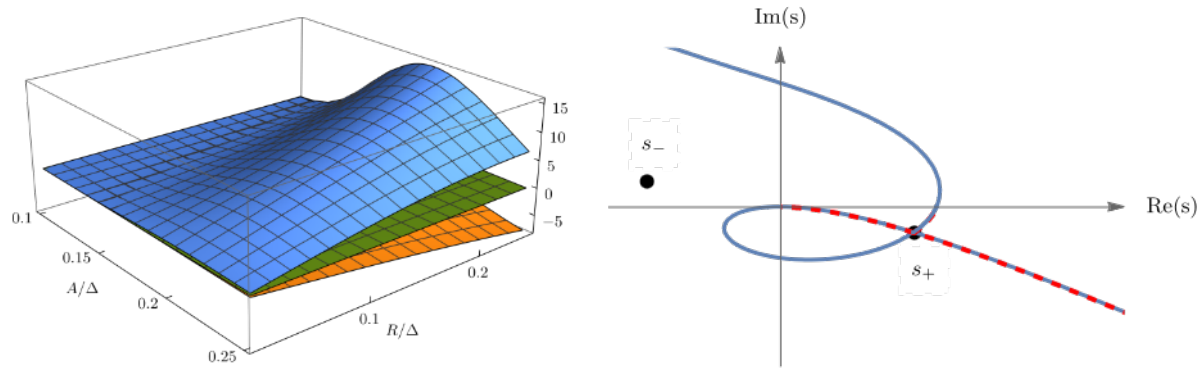

(a) (b)

Figure C.1: **a)** Plot of the integral in Eq. (C.87) in the case of model A (orange, below, rescaled for graphical convenience) and model B (blue, above), compared with the plane = 0 (green, center) to check the zero crossings. **b)** Integration contour for the function in Eq. (C.91) analytically continued to the complex plane s. The black dots indicate the stationary points $s_\pm$ of $f(s)$, and we plotted in solid blue the contour lines of $v(s) = \mathrm{Im}[f(s)]$ passing through s_+. We deform the original integration contour, i.e., the positive real axis, to a portion of the curve above indicated by the red-dashed line. Indeed, the integrand in Eq. (C.91) vanishes for large $|s|$ in the region $\{\mathrm{Re}(s) > 0, \mathrm{Im}(s) < 0\}$, so the integration contour can be closed at infinity and the Cauchy theorem applies. In this plot we set all the parameters in $f(s)$ to unity, for the sake of illustration.

where we used $J_1(x) \simeq x/2$, and we rescaled momenta as $q = y/R$. One can check *a posteriori* that including higher orders in A does not change our conclusions as long as $A \ll \Delta$. In Eq. (C.88) we have introduced the quantities $x \equiv \Delta/R$, and $\Omega_0 \equiv D/R^2$, which we recognize from Eq. (1.25) as the inverse timescale of relaxation of the field ϕ over a length scale $\sim R$. The integral in I_1 finally contains a further dependence on $R^2 r = (R/\xi)^2$. Using again Eq. (C.63) and computing the Gaussian integral we find

$$I_1 = \frac{A}{2DR^{d+4}} \frac{\partial^2}{\partial x^2} \int_0^\infty \mathrm{d}\mu \, \frac{e^{\ \mu c\ \ x^2/4(1+\mu)}}{[4\pi(1+\mu)]^{d/2}}, \tag{C.89}$$

where we defined $c \equiv R^2 r + i\Omega/\Omega_0$. In order to avoid the trivial saddle-point $\mu = \infty$, we change variables as $\mu = sx$, leading to

$$I_1 = \frac{A}{2DR^{d+4}} \frac{\partial^2}{\partial x^2} \left[\frac{x^{1\ \ d/2}}{(4\pi)^{d/2}} Q(x) \right], \tag{C.90}$$

$$Q(x) = \int_0^\infty \mathrm{d}s \, g(s) e^{\ xf(s)}, \tag{C.91}$$

with

$$f(s) \equiv sc \quad \frac{1}{4s}, \qquad g(s) \equiv (s + 1/x)^{\ d/2} \exp\left[\frac{x}{4s(sx+1)} \right]. \tag{C.92}$$

Since the function $g(s)$ is regular and x-independent for large x, the integral in Eq. (C.91) can be estimated using the method of steepest descent [309]. To this end, one considers the analytic continuation in the complex plane $s = a + ib$ of the function $f(s) = u(a,b) + iv(a,b)$, and then

deforms the original integration path (i.e., the positive real axis) to a level curve of $v(a,b)$ passing through a stationary point of $u(a,b)$. By the Cauchy-Riemann conditions, these stationary points are necessarily saddle-points for $u(a,b)$, and they coincide with the extrema of the function $f(s)$, given by $s_\pm = \pm 1/(2\sqrt{c})$. The relevant integration contour is shown in Fig. C.1b, and it passes through the saddle-point s_+. By standard methods, one then finds

$$Q(x) \simeq \sqrt{\frac{2\pi}{x|f''(s_+)|}} g(s_+) e^{\ xf(s_+)\ \ i3\theta/2}, \tag{C.93}$$

where $f(s_+) = \sqrt{c} \equiv \rho \exp(i\theta)$, and we introduced

$$\rho = R\left[r^2 + (\Omega/D)^2\right]^{1/4}, \qquad \theta = \frac{1}{2}\arctan\left(\frac{\Omega}{Dr}\right). \tag{C.94}$$

The angle $3\theta/2$ in Eq. (C.93) stems from selecting the path along which s_+ is a maximum (and not minimum) point for $u(a,b)$. We also see that $|f''(s_+)| = 1/(2\rho^6)$, while

$$g(s_+) = (s + 1/x)^{\ d/2} \exp\left[\frac{x}{4s(sx+1)}\right]. \tag{C.95}$$

Note that $g(s_+)$ still contains x, and this may have affected the position of the saddle-point. We must then make sure *a posteriori* that x is sufficiently large so that $g(s)$ has saturated to its asymptotic value, $g(s) \to s^{\ d/2} \exp\left[1/(4s^2)\right]$, at the saddle-point $s = s_+$. From Eq. (C.95), this amounts at requiring $x \gg 2|\sqrt{c}|$, or equivalently $\Delta \gg 2R\rho(\Omega)$. When r is negligible, this condition becomes $\Omega \ll \Omega_0(\Delta/R)^2$: this sets a limit to the values of Ω for which the saddle-point estimate is valid. We finally plug Eq. (C.93) back into Eq. (C.90) to get

$$I_1 \propto e^{\ ix\,\mathrm{Im}[f(s_+)]} = e^{\ ix\rho\sin\theta}, \tag{C.96}$$

where we omitted a complex prefactor and extracted the Δ-dependent part of the phase. This justifies the result reported in Eq. (3.66).

C.8 Numerical simulations

Numerical simulations are performed by direct integration of the coupled Langevin equations of motion (3.4) and (3.6) in real space, with a procedure analogous to the one described in Appendix B.8. The second particle, $\mathbf{Z}(t)$, is instead moved deterministically as in the infinite trap strength limit $\kappa \to \infty$. The discretized equation of motion for the field (see Eqs. (3.4), (B.110) and (B.112)) are straightforwardly generalized as

$$\partial_t \phi_i(t) = D\left[(r - \widetilde{\Delta})\phi_i(t) - \lambda V(\mathbf{x}_i - \mathbf{Y}(t)) - \lambda V(\mathbf{x}_i - \mathbf{Z}(t))\right] + \eta_i(t), \tag{C.97}$$

$$\partial_t \phi_i(t) = D\widetilde{\Delta}\left[(r - \widetilde{\Delta})\phi_i(t) - \lambda V(\mathbf{x}_i - \mathbf{Y}(t)) - \lambda V(\mathbf{x}_i - \mathbf{Z}(t))\right] + \widetilde{\nabla}\cdot\boldsymbol{\eta}_i(t), \tag{C.98}$$

for model A or model B dynamics, respectively.

Once we start the simulation, we need to wait until the system has reached its long-time periodic state, which can be recognized by the fact that the mean value of the oscillations of $\mathbf{Y}(t)$

stops growing, and from its independence from the field dynamics (model A or B). This process takes longer as we approach criticality ($r \to 0$), but it is never infinite because the system size L is finite. We may estimate the relaxation time by using Eq. (1.25) and inserting $q \simeq 2\pi/L$. Once the non-equilibrium periodic state is reached, we record the trajectory of $\mathbf{Y}(t)$ and use its periodicity in order to average the relevant observables over each period $T = 2\pi/\Omega$. This allows to improve the statistics without the need to repeat the initial relaxation for each run.

C.9 Dynamical functional for the many-particle problem

In this Appendix we derive the Martin–Siggia–Rose (or Janssen–De Dominicis–Peliti) dynamical functional [70–72] that describes the many-particle problem introduced in Section 3.6. The dynamical functionals corresponding to Eqs. (3.4) and (3.70) can be obtained by standard methods (see Ref. [54] and Section 1.5), leading in the case $\lambda = 0$ to

$$\mathcal{S}_a[\mathbf{X}_a, \widetilde{\mathbf{X}}_a] = \int \mathrm{d}t \left\{ \widetilde{\mathbf{X}}_a(t) \left[\dot{\mathbf{X}}_a(t) \quad \mathbf{F}_a(\mathbf{X}_a(t), t) \right] \quad \frac{\Omega_a}{2} |\widetilde{\mathbf{X}}_a(t)|^2 \right\}, \tag{C.99}$$

for the particles, and to $\mathcal{S}_\phi[\phi, \tilde{\phi}]$ given in Eq. (1.49) for the field. Above we have introduced $\Omega_a \equiv 2\nu_a T$, while $\widetilde{\mathbf{X}}_a$, $\tilde{\phi}$ are the auxiliary variables (response fields [54]) conjugate to $\mathbf{X}_a$ and ϕ, respectively. Choosing $\lambda \neq 0$ leads to the total action

$$\mathcal{S}[\phi, \tilde{\phi}, \{\mathbf{X}_a, \widetilde{\mathbf{X}}_a\}] = \sum_{a=1}^{N} \mathcal{S}_a[\mathbf{X}_a, \widetilde{\mathbf{X}}_a] + \mathcal{S}_\phi[\phi, \tilde{\phi}] \quad \lambda \mathcal{S}_{\mathrm{int}}[\phi, \tilde{\phi}, \{\mathbf{X}_a, \widetilde{\mathbf{X}}_a\}], \tag{C.100}$$

where the interaction terms proportional to the coupling λ gave rise to

$$\mathcal{S}_{\mathrm{int}}[\phi, \tilde{\phi}, \{\mathbf{X}_a, \widetilde{\mathbf{X}}_a\}] = \sum_{a=1}^{N} \int \mathrm{d}t \int \frac{\mathrm{d}^d q}{(2\pi)^d} \Big[Dq \quad \tilde{\phi}_{\mathbf{q}}(t) + i\nu_a \phi_{\mathbf{q}}(t)\, \mathbf{q} \cdot \widetilde{\mathbf{X}}_a(t) \Big] V_q^{(a)} e^{i\mathbf{q}\cdot\mathbf{X}_a(t)}. \tag{C.101}$$

It is useful at this point to introduce the vector notation

$$\mathbf{\Psi} = \mathbf{\Psi}_q(t) \equiv \begin{pmatrix} \phi_{\mathbf{q}}(t) \\ \tilde{\phi}_{\mathbf{q}}(t) \end{pmatrix}, \qquad \mathbf{\Psi}^T \equiv \begin{pmatrix} \phi \ _{\mathbf{q}}(t) & \tilde{\phi} \ _{\mathbf{q}}(t) \end{pmatrix}, \tag{C.102}$$

so as to rewrite in a compact form

$$\mathcal{S}_\phi[\phi, \tilde{\phi}] = \frac{1}{2} \mathbf{\Psi}^T \hat{A} \mathbf{\Psi}, \qquad \mathcal{S}_{\mathrm{int}}[\phi, \tilde{\phi}, \{\mathbf{X}_a, \widetilde{\mathbf{X}}_a\}] = \frac{1}{\lambda} \mathbf{b}^T \mathbf{\Psi}, \tag{C.103}$$

where we introduced the matrix (see Eq. (1.49))

$$\hat{A}_{q,p}(t, t') = \begin{pmatrix} 0 & \partial_t + \ _q \\ \partial_t + \ _q & \Omega(q) \end{pmatrix} \delta^d(\mathbf{q} + \mathbf{p}) \delta(t \quad t'), \tag{C.104}$$

and the vector

$$\mathbf{b}_q(t) \equiv \sum_{a=1}^{N} \begin{pmatrix} i\nu_a \mathbf{q} \cdot \widetilde{\mathbf{X}}_a(t) \\ Dq \end{pmatrix} V_q^{(a)} e^{\ i\mathbf{q}\cdot\mathbf{X}_a(t)}. \tag{C.105}$$

The effective action $\mathcal{S}_{\text{eff}}[\{\mathbf{X}_a, \widetilde{\mathbf{X}}_a\}]$ that describes the particles alone will have the form of Eq. (3.72), where the free part $\mathcal{S}_0[\{\mathbf{X}_a, \widetilde{\mathbf{X}}_a\}]$ is simply the sum of the single-particle actions $\mathcal{S}_a[\mathbf{X}_a, \widetilde{\mathbf{X}}_a]$ given in Eq. (C.99). In order to obtain the interacting part $\mathcal{S}_\lambda[\{\mathbf{X}_a, \widetilde{\mathbf{X}}_a\}]$, we marginalize over the field ϕ and its conjugate variable $\tilde{\phi}$ as

$$e^{\ \mathcal{S}_\lambda[\{\mathbf{X}_a, \widetilde{\mathbf{X}}_a\}]} \equiv \int \mathcal{D}\phi\, \mathcal{D}\tilde{\phi}\, e^{\ \mathcal{S}_\phi + \lambda \mathcal{S}_{\text{int}}} = \int \mathcal{D}\phi\, \mathcal{D}\tilde{\phi}\, e^{\ \frac{1}{2}\boldsymbol{\Psi}^T \hat{A} \boldsymbol{\Psi} + \mathbf{b}^T \boldsymbol{\Psi}} \propto e^{\frac{1}{2}\mathbf{b}^T \hat{A}^{\ -1}\mathbf{b}}. \tag{C.106}$$

The result of the Gaussian integration involves the inverse matrix [54]

$$\hat{A}^{\ 1}_{q,p}(t,t') = \begin{pmatrix} C_q(t,t') & G_q(t \quad t') \\ G_q(t' \quad t) & 0 \end{pmatrix} \delta^d(\mathbf{q}+\mathbf{p}), \tag{C.107}$$

where $G_q(t)$ and $C_q(t,t')$ are the linear response function and the correlator of the free field given in Eqs. (1.27) and (1.30), respectively. Equation (C.106) is only formal, but it can be made explicit by integrating over the dummy variables (times and momenta) as

$$\mathbf{b}^T \hat{A}^{\ -1}\mathbf{b} \equiv \int \frac{\mathrm{d}^d q\, \mathrm{d}^d p}{(2\pi)^{2d}} \int \mathrm{d}t\, \mathrm{d}t'\, \mathbf{b}_{\ q}(t) \hat{A}^{\ 1}_{q,\ p}(t,t') \mathbf{b}_p(t'). \tag{C.108}$$

The resulting $\mathcal{S}_\lambda[\{\mathbf{X}_a, \widetilde{\mathbf{X}}_a\}]$ can then be expressed as in Eq. (3.74), with

$$\begin{aligned} \mathcal{S}_{ab}[\mathbf{X}_a, \widetilde{\mathbf{X}}_a, \mathbf{X}_b, \widetilde{\mathbf{X}}_b] = \nu_a \int \frac{\mathrm{d}^d q}{(2\pi)^d} V_q^{(b)} V_q^{(a)} \int \mathrm{d}t \int \mathrm{d}t'\, [\mathbf{q}\cdot\widetilde{\mathbf{X}}_a(t)]\, e^{i\mathbf{q}\cdot[\mathbf{X}_a(t) \ \ \mathbf{X}_b(t')]} \\ \times \left\{ i\chi_q(t \quad t') + \frac{\nu_b}{2} C_q(t,t')[\mathbf{q}\cdot\widetilde{\mathbf{X}}_b(t')] \right\}, \end{aligned} \tag{C.109}$$

and where $\chi_q(t)$ is the linear susceptibility of the field given in Eq. (1.31). We note that the terms with $a = b$ in Eq. (3.74) describe the self-interaction of the particle $\mathbf{X}_a$ mediated by the field ϕ, while the terms with $a \neq b$ describe the field-induced interaction between pairs of particles. Finally, we recognize in Eq. (C.109) a *drift* term (i.e., the one containing $\chi_q(t \quad t')$) which is non-local in time, and a colored *noise* term (i.e., the one containing $C_q(t,t')$): they both result from having integrated out the field degrees of freedom from the dynamics.

D

Calculations of Chapter 4

D.1 Stochastic entropy production rate

The irreversibility $\Delta S_{\rm tot}[\{\mathbf{Y},\phi\}_{t_{\rm i}}^{t_{\rm f}}]$ associated with an individual, joint (probe+field) trajectory was given in Eq. (4.17). Due to the Gaussian statistics of the noise, the path weights therein are proportional to the exponential of the Onsager–Machlup action $\mathcal{A}$ [69, 132], i.e.,

$$\mathcal{P} \propto \rho_{\mathbf{Y},\phi}[\mathbf{Y}(t_{\rm i}),\phi(\mathbf{x},t_{\rm i})]e^{\ \mathcal{A}}, \tag{D.1}$$

where $\rho_{\mathbf{Y},\phi}$ is the joint field–particle probability density. Since the noises acting on the probe and the field are independent from each other, the total action of the joint process is the sum of the actions of the probe and the field, reading [132]

$$\begin{aligned}\mathcal{A} = &\frac{1}{4\gamma_y T}\int_{t_{\rm i}}^{t_{\rm f}} {\rm d}t\,(\gamma_y\dot{\mathbf{Y}} + \boldsymbol{\nabla}_{\mathbf{Y}}\mathcal{H}^{\rm int} + \boldsymbol{\nabla}_{\mathbf{Y}}\mathcal{U} \quad \mathbf{F}_{\rm ext})^2 \\ &+ \frac{1}{4\gamma_\phi T}\int_{t_{\rm i}}^{t_{\rm f}}{\rm d}t\int {\rm d}^d\mathbf{x}\ \ \gamma_\phi\dot{\phi} + \boldsymbol{\nabla}\ \ \mathbf{J}_{\rm d})\,(\ \ \nabla^2)\quad^{/2}\ \gamma_\phi\dot{\phi} + \boldsymbol{\nabla}\ \ \mathbf{J}_{\rm d})\,,\end{aligned} \tag{D.2}$$

where we defined

$$\boldsymbol{\nabla}\ \ \mathbf{J}_{\rm d} = (\ \ \nabla^2)\ ^{/2}\frac{\delta\mathcal{H}}{\delta\phi}, \tag{D.3}$$

with $\quad = 0$ for non-conserved dynamics and $\quad = 2$ for conserved dynamics. All the stochastic integrals in this section [such as the one in Eq. (D.2)] are intended in the Stratonovich sense, but we will omit the $\circ$ sign to ease the notation [1]. The term $\boldsymbol{\nabla}\ \ \mathbf{J}_{\rm d}$ in Eq. (D.3) is the deterministic dynamical operator of the field dynamics (4.3), i.e., $\boldsymbol{\nabla}\ \ \mathbf{J}_{\rm d} = \gamma_\phi\dot{\phi}\quad\eta$. The action of the time-reversed process is, accordingly, given by

$$\begin{aligned}\mathcal{A}^{\rm R} = &\frac{1}{4\gamma_y T}\int_{t_{\rm i}}^{t_{\rm f}} {\rm d}t\,(\ \ \gamma_y\dot{\mathbf{Y}} + \boldsymbol{\nabla}_{\mathbf{Y}}\mathcal{H}^{\rm int} + \boldsymbol{\nabla}_{\mathbf{Y}}\mathcal{U} \quad \mathbf{F}_{\rm ext})^2 \\ &+ \frac{1}{4\gamma_\phi T}\int_{t_{\rm i}}^{t_{\rm f}}{\rm d}t\int {\rm d}^d\mathbf{x}\quad\ \gamma_\phi\dot{\phi} + \boldsymbol{\nabla}\ \ \mathbf{J}_{\rm d})\,(\ \ \nabla^2)\quad^{/2}\quad\gamma_\phi\dot{\phi} + \boldsymbol{\nabla}\ \ \mathbf{J}_{\rm d})\,.\end{aligned} \tag{D.4}$$

Inserting the path probabilities into Eq. (4.17) yields

$$\Delta S_{\rm tot} = \ln\frac{\rho_{\mathbf{Y},\phi}[\mathbf{Y}(t_{\rm i}),\phi(t_{\rm i})]}{\rho_{\mathbf{Y},\phi}[\mathbf{Y}(t_{\rm f}),\phi(t_{\rm f})]} + \mathcal{A}^{\rm R}\quad\mathcal{A} \equiv \Delta S^{\rm sh}_{y,\phi} + \mathcal{A}^{\rm R}\quad\mathcal{A}, \tag{D.5}$$

[1] Note that for $\quad = 2$ the operator $(\ \ \nabla^2)\ ^{/2}$ is nonlocal, hence, in the last term on the r.h.s. of Eq. (D.2), we use $\int {\rm d}^d\mathbf{x}\,A(\mathbf{x})(\ \ \nabla^2)\quad^{/2}B(\mathbf{x})$ as a shorthand for $\int {\rm d}^d\mathbf{x}\int {\rm d}^d\mathbf{x}'\,A(\mathbf{x})(\ \ \nabla^2)\quad^{/2}(\mathbf{x},\mathbf{x}')B(\mathbf{x}')$.

where the we identified the term $\Delta S^{\rm sh}_{y,\phi}$ as the change, along the considered time interval, of the Shannon entropy $S^{\rm sh}_{y,\phi} \propto \ln \rho_{\mathbf{Y},\phi}$ associated with the initial/final configuration $\rho_{\mathbf{Y},\phi}$ of the joint process (i.e., considering both the probe and the field). Furthermore, the second term on the r.h.s. of Eq. (D.5) can be simplified to

$$\begin{aligned}\mathcal{A}^{\rm R} \quad \mathcal{A} &= \frac{1}{\gamma_y T}\int_{t_{\rm i}}^{t_{\rm f}} {\rm d}t\,\gamma_y \dot{\mathbf{Y}}\,\big(\underbrace{\boldsymbol{\nabla}_{\mathbf{Y}}\mathcal{H}^{\rm int} + \boldsymbol{\nabla}_{\mathbf{Y}}\mathcal{U}}_{=(\xi\ \ \gamma_y\dot{\mathbf{Y}})} \quad \mathbf{F}_{\rm ext}\big) + \frac{1}{\gamma_\phi T}\int {\rm d}^d\mathbf{x}\int_{t_{\rm i}}^{t_{\rm f}} {\rm d}t\,\gamma_\phi\dot{\phi}\,(\ \ \nabla^2)\ \ ^{/2}\ \underbrace{\boldsymbol{\nabla}\ \mathbf{J}_{\rm d}}_{=(\eta\ \ \gamma_\phi\dot{\phi})}\\ &= \frac{1}{T}\int_{\{\mathbf{Y},\phi\}_{t_{\rm i}}^{t_{\rm f}}} \xi\quad \gamma_y\dot{\mathbf{Y}})\,{\rm d}\mathbf{Y} + \frac{1}{T}\int {\rm d}^d\mathbf{x}\int_{\{\mathbf{Y},\phi\}_{t_{\rm i}}^{t_{\rm f}}} {\rm d}\phi(\mathbf{x})\,(\ \ \nabla^{\ 2})\ ^{/2}\ \eta\quad \gamma_\phi\dot{\phi})\,. \end{aligned} \tag{D.6}$$

In the last step, we have inserted the equations of motion (4.2) and (4.3), and we converted the integrals over time into line integrals along the trajectory $\{\mathbf{Y},\phi\}_{t_{\rm i}}^{t_{\rm f}}$. As a final step, we identify in Eq. (D.6) the heat flows as given in Eqs. (4.12) and (4.16), and therefore we obtain Eq. (4.18), consistently with the thermodynamic definition of entropy.

D.1.1 Proof of the second law

It is well known that the definition of $\Delta S_{\rm tot}$ given in Eq. (4.17) implies, after taking an ensemble average, that the total entropy production is constrained by the second law, i.e., $\langle \Delta S_{\rm tot}\rangle \geq 0$ [109, 310]. One way to show this is to prove first the integral fluctuation theorem [109, 145, 311], i.e.,

$$\left\langle e^{\ -\Delta S_{\rm tot}[\{\mathbf{Y},\phi\}]}\right\rangle = \int \mathcal{D}\{\mathbf{Y},\phi\}\,\mathcal{P}[\{\mathbf{Y},\phi\}]e^{\ -\Delta S_{\rm tot}[\{\mathbf{Y},\phi\}]} = \int \mathcal{D}\{\mathbf{Y},\phi\}\,\mathcal{P}^{\rm R}[\{\mathbf{Y}^{\rm R},\phi^{\rm R}\}] = 1, \tag{D.7}$$

where in the second line we inserted the definition of $\Delta S_{\rm tot}$ given in Eq. (4.17), while in the third line we assumed that the integration measure is invariant under time-reversal, i.e., $\mathcal{D}\{\mathbf{Y},\phi\} = \mathcal{D}\{\mathbf{Y}^{\rm R},\phi^{\rm R}\}$. Using $\ln x \leq x\quad 1$, $\forall x > 0$, the second law follows as

$$\langle\ \ \Delta S_{\rm tot}\rangle = \left\langle \ln e^{\ \Delta S_{\rm tot}}\right\rangle \leq \left\langle e^{\ \Delta S_{\rm tot}}\right\rangle\quad 1 = 0, \tag{D.8}$$

where in the last step we used Eq. (D.7). The fluctuations of $\Delta S_{\rm tot}$ can also be shown to obey, by construction, the detailed fluctuation theorem $p[\Delta S_{\rm tot}]/p[\ \ \Delta S_{\rm tot}] = e^{\ \Delta S_{\rm tot}}$ [109, 310]. Along long trajectories with $t_{\rm f} \gg t_{\rm i}$, this further implies that the total dissipation $Q = \int {\rm d}\mathbf{x}\, Q_\phi(\mathbf{x}) + Q_y$ asymptotically also fulfills these relations, because $\Delta S^{\rm sh}_{y,\phi}$ — contrary to Q_ϕ and Q_y — does not grow upon increasing time (i.e., it is not "extensive").

D.2 Comparison with the dissipated power predicted by a GLE

An established approach [139–144] to study the thermodynamics of driven particles in complex environments is based on using generalized Langevin equations (GLEs) [7, 38]. Within this description, the effect of the (slowly relaxing) medium on the particle is described by a friction kernel and a colored noise, as discussed in Section 1.4. However, GLEs generally capture only temporal correlations of the medium, but not dynamically-varying spatial correlations. In this section, we consider the conditions under which a GLE may capture the various dependencies

on the drag velocity v of the mean dissipation rate, which are discussed in Section 4.3.4 — see, e.g., Fig. 4.4(b). In particular, consider a generic linear (overdamped) GLE of the form

$$\gamma_y \dot{Y} = \int_{\infty}^{t} \mathrm{d}t' \quad (t \quad t')\dot{Y}(t') \quad \kappa(Y \quad vt) + \mu, \tag{D.9}$$

with a certain friction kernel (which we do not need to specify further here) and a zero-mean Gaussian colored noise[2] μ. We consider a nonequilibrium steady-state of the system with $v \neq 0$, and we are particularly interested in the mean position (relative to the center of the trap), from which we can access the mean power [see Eq. (4.22)].

By averaging the GLE (D.9) over the possible realizations of the noise, one finds

$$\gamma_y \dot{u} = \int_{\infty}^{t} \mathrm{d}t' \quad (t \quad t')\dot{u}(t') \quad \kappa(u \quad vt), \tag{D.10}$$

with $u(t) \equiv \langle Y(t) \rangle$. In the steady state, the average velocity $\dot{u}(t)$ of the particle does not depend on time t. Accordingly, we can further simplify the previous equation as

$$\gamma_y \dot{u} = G_{\mathrm{m}} \dot{u} \quad \kappa(u \quad vt), \tag{D.11}$$

where we have introduced the constant $G_{\mathrm{m}} = \int_{\infty}^{t} \mathrm{d}t' \quad (t \quad t')$. The solution of Eq. (D.11) is

$$u = vt + C, \quad \text{with} \quad C = \quad (\gamma_y + G_{\mathrm{m}})v/\kappa. \tag{D.12}$$

Together with Eq. (4.34), this implies that, for *any* linear GLE, with arbitrary friction kernel, the correction to the average dissipated power is

$$\langle \dot{W} \rangle = \quad \kappa v \left[\langle Y(t) \rangle \quad vt + v\gamma_y/\kappa \right] = \quad \kappa v \quad C + v\gamma_y/\kappa \big) = G_{\mathrm{m}} v^2. \tag{D.13}$$

This expression, being quadratic in v, corresponds to the first regime among those shown in Fig. 4.4(b), and to the usual Stokes friction. We conclude that the other regimes discussed in Section 4.3.4 and displayed in Fig. 4.4(b) can only possibly emerge in the presence of a nonlinear friction term in the effective evolution equation of the probe. Choosing heuristically a form of the friction term in Eq. (D.9) other than linear seems difficult to justify on phenomenological grounds alone. In contrast, by systematically integrating out the field degrees of freedom $\phi(\mathbf{x}, t)$ from the joint field–particle dynamics [given by Eqs. (4.2) and (4.3)], we can obtain an effective description for the motion of the particle in the form of a nonlinear GLE [see, c.f., Eq. (4.63)]. This will be discussed in the next two sections within this Appendix.

D.3 Moment generating function of the particle position

Here we provide the derivation of the cumulant generating function of the particle position reported in Eq. (4.31). We start from the coupled equations of motion for the variables $\mathbf{Z}(t)$ and

[2] The fluctuations of μ do not in general satisfy a fluctuation-dissipation theorem, because the term $\propto vt$ in Eq. (D.9) drives the system out of equilibrium.

$\varphi(\mathbf{z}, t)$, i.e., Eqs. (4.25) and (4.26). Assuming the coupling constant λ to be small, it is possible to derive a (forward) evolution equation which describes the marginal probability distribution $P_1(\mathbf{z}, t)$ of the particle coordinate alone. The derivation is analogous to the one presented in Appendix C.2.1, where a more general case was treated, in which a second particle also interacts with the field via an interaction potential $V_p^{(\ )}$; the present case corresponds to $V_p^{(\ )} \mapsto 0$. We report here only the final result:

$$\partial_t P_1(\mathbf{z}, t) = \mathcal{L}_0(\mathbf{z}) P_1(\mathbf{z}, t) + \lambda^2 \int_\infty^t \mathrm{d}s \int \mathrm{d}\mathbf{x}\, \mathcal{L}(\mathbf{z}, \mathbf{x}; t \quad s) P_2(\mathbf{z}, t; \mathbf{x}, s) + O\Big(\lambda^4\Big). \tag{D.14}$$

Here $\mathcal{L}_0$ is the Fokker-Planck operator for an Ornstein-Uhlenbeck particle [53],

$$\mathcal{L}_0 \equiv \boldsymbol{\nabla}_\mathbf{z} \cdot (\gamma \mathbf{z} + \nu T \boldsymbol{\nabla}_\mathbf{z}) \,, \tag{D.15}$$

while the memory term $\mathcal{L}$, analogous to the one in Eq. (3.19), reads

$$\mathcal{L}(\mathbf{z}, \mathbf{x}; u) \equiv \nu \nabla_\mathbf{z}^l \int \frac{\mathrm{d}^d p}{(2\pi)^d} i p_l |V_p|^2 e^{\ i\mathbf{p}\cdot(\mathbf{z}\ \ \mathbf{x})} \Big[\chi_\mathbf{p}^{(\mathbf{v})}(u) \quad i\nu C_\mathbf{p}^{(\mathbf{v})}(u) e^{\ \gamma u} p_j \nabla_\mathbf{z}^j \Big] \,, \tag{D.16}$$

where $\chi_\mathbf{p}^{(\mathbf{v})}$ and $C_\mathbf{p}^{(\mathbf{v})}$ were given in Eqs. (4.27) and (4.28).

We want to use Eq. (D.14) to find an expression for the characteristic function

$$g(\mathbf{k}, t) \equiv \langle e^{\ i\mathbf{k}\cdot\mathbf{Z}(t)} \rangle = \int \mathrm{d}\mathbf{z}\, e^{\ i\mathbf{k}\cdot\mathbf{z}} P_1(\mathbf{z}, t). \tag{D.17}$$

We start by taking the Fourier transform of the various terms in the master equation (D.14), which leads to

$$\big[\partial_t \quad \mathcal{L}_0^\dagger(\mathbf{k})\big] g(\mathbf{k}, t) = f(\mathbf{k}, t) + O\Big(\lambda^4\Big), \tag{D.18}$$

where, from Eq. (D.15),

$$\mathcal{L}_0^\dagger(\mathbf{k}) = \quad \gamma \mathbf{k} \cdot \boldsymbol{\nabla}_\mathbf{k} \quad \nu T k^2, \tag{D.19}$$

and we have introduced

$$f(\mathbf{k}, t) \equiv \lambda^2 \int_\infty^t \mathrm{d}s \int \mathrm{d}\mathbf{x}\, \mathrm{d}\mathbf{z}\, e^{\ i\mathbf{k}\cdot\mathbf{z}} \mathcal{L}(\mathbf{z}, \mathbf{x}; t \quad s) P_2(\mathbf{z}, t; \mathbf{x}, s). \tag{D.20}$$

The solution of Eq. (D.18) is formally given, at the lowest nontrivial order in λ, by

$$g(\mathbf{k}, t) = g^{(0)}(\mathbf{k}) + \int_\infty^t \mathrm{d}t' \int \frac{\mathrm{d}^d k'}{(2\pi)^d} g_{1|1}(\mathbf{k}, t|\mathbf{k}', t') f(\mathbf{k}', t') + O\Big(\lambda^4\Big), \tag{D.21}$$

where we introduced

$$g^{(0)}(\mathbf{p}) \equiv \exp\Big(\quad p^2 T / 2\kappa \Big), \tag{D.22}$$

i.e., the moment generating function of the uncoupled ($\lambda = 0$) particle, and where we indicated by $g_{1|1}$ the propagator of the Ornstein-Uhlenbeck process in momentum space. The latter is easily found by solving the homogeneous part of Eq. (D.18) via the method of characteristics [309], or even by simply Fourier transforming the real space propagator given in Eq. (1.9): both ways lead to

$$g_{1|1}(\mathbf{k}, t|\mathbf{k}', t') = e^{\ (k^2/2)\sigma^2(t \ \ t')} \delta^d(\mathbf{k}' + \mathbf{k} e^{\ \gamma(t \ \ t')}), \tag{D.23}$$

where $\sigma(t \quad t')$ was introduced in Eq. (1.11).

Let us now focus on the stationary state, for which

$$g(\mathbf{k},t) \to g(\mathbf{k}), \quad g_{1|1}(\mathbf{k},t|\mathbf{k}',t') \to g_{1|1}(\mathbf{k},t \quad t'|\mathbf{k}',0), \quad P_2(\mathbf{z},t;\mathbf{x},s) \to P_2(\mathbf{z},t \quad s;\mathbf{x},0). \tag{D.24}$$

Equation (D.21) then becomes

$$\begin{aligned} g(\mathbf{k}) &= g^{(0)}(\mathbf{k}) + \int_0^\infty \mathrm{d}u' \int \frac{\mathrm{d}^d k'}{(2\pi)^d} g_{1|1}(\mathbf{k},u'|\mathbf{k}',0) f(\mathbf{k}') + O\left(\lambda^4\right) \\ &= g^{(0)}(\mathbf{k}) + \int_0^\infty \mathrm{d}u'\, e^{\ (k^2/2)\sigma^2(u')} f\left(\ \ \mathbf{k}e^{\ \gamma u'}\right) + O\left(\lambda^4\right), \end{aligned} \tag{D.25}$$

where in the second line we used Eq. (D.23). Manipulating Eqs. (D.16) and (D.20) renders

$$f(\mathbf{k}) = \ \ \nu\lambda^2 \int_0^\infty \mathrm{d}u \int \frac{\mathrm{d}^d p}{(2\pi)^d} |V_p|^2(\mathbf{p}\cdot\mathbf{k}) \left[\chi_{\mathbf{p}}^{(\mathbf{v})}(u) + \nu\mathbf{p}\cdot(\mathbf{p}+\mathbf{k}) C_{\mathbf{p}}^{(\mathbf{v})}(u) e^{\ \gamma u}\right] \widetilde{P}_2(\mathbf{p}+\mathbf{k},u;\ \ \mathbf{p},0) \tag{D.26}$$

in terms of the double Fourier transform $\widetilde{P}_2$ of the two-point probability distribution P_2, with respect to both its spatial arguments. Since we are neglecting terms of order higher than λ^2, then P_2 above can be replaced by its expression for $\lambda = 0$, i.e.,

$$P_2(\mathbf{z},t;\mathbf{x},s) = P_{1|1}(\mathbf{z},t|\mathbf{x},s) P_1(\mathbf{x},s) + O\left(\lambda^2\right), \tag{D.27}$$

where $P_{1|1}$ is the Ornstein-Uhlenbeck propagator given in Eq. (1.14), with Fourier transform $g_{1|1}$ provided in Eq. (D.23). In the long-time limit, we can replace $P_1(\mathbf{x},s)$ by the stationary distribution $P_1^{\mathrm{st}}(\mathbf{x})$ eventually attained by the uncoupled particle in its harmonic trap, see Eq. (1.14). We recall that the Fourier transform of $P_1^{\mathrm{st}}(\mathbf{x})$ is the function $g^{(0)}(\mathbf{p})$ given in Eq. (D.22). This yields

$$\widetilde{P}_2(\mathbf{p}_2,t;\mathbf{p}_1,0) \simeq \int \frac{\mathrm{d}^d p_0}{(2\pi)^d} g_{1|1}(\mathbf{p}_2,t|\mathbf{p}_1 \quad \mathbf{p}_0,0) g^{(0)}(\mathbf{p}_0) = g^{(0)}(\mathbf{p}_1+\mathbf{p}_2 e^{\ \gamma t}) e^{\ p_2^2\sigma^2(t)/2}. \tag{D.28}$$

Equation (D.26) can be further simplified by noting that, for any u-independent value A [and, in particular, for $A \equiv \mathbf{p}\cdot(\mathbf{p}+\mathbf{k})$], we can rewrite [81]

$$\left[\chi_p(u) + \nu A C_p(u) e^{\ \gamma u}\right] = \ \ \frac{e^{A\sigma_2^2(u)}}{p} \frac{\partial}{\partial u}\left[\chi_p(u) e^{\ A\sigma_2^2(u)}\right], \tag{D.29}$$

where we recall that $\chi_p(u)$ and $C_p(u)$ differ from the corresponding $\chi_{\mathbf{p}}^{(\mathbf{v})}(u)$ and $C_{\mathbf{p}}^{(\mathbf{v})}(u)$ only by a multiplicative factor $\exp(i\mathbf{p}\cdot\mathbf{v}\,u)$ for $u > 0$ [see Eqs. (4.27) and (4.28)], and where we introduced

$$\sigma_2^2(u) \equiv \sigma^2(u/2), \tag{D.30}$$

with σ given in Eq. (1.11). Equation (D.29) readily follows as a direct consequence of the fluctuation-dissipation theorem for the free-field, recalled in Eq. (1.32). From Eq. (D.26), after integrating by parts in u, we thus get

$$f(\mathbf{k}) = \ \ i\nu\lambda^2 g^{(0)}(\mathbf{k}) \int_0^\infty \mathrm{d}u \int \frac{\mathrm{d}^d p}{(2\pi)^d} \frac{|V_p|^2(\mathbf{p}\cdot\mathbf{k})(\mathbf{p}\cdot\mathbf{v})}{p^2+r} G_{\mathbf{p}}^{(\mathbf{v})}(u) e^{\ \mathbf{p}\cdot(\mathbf{p}+\mathbf{k})\sigma_2^2(u)}, \tag{D.31}$$

with $G_{\mathbf{p}}^{(\mathbf{v})}(u)$ given in Eq. (4.28). We finally substitute the expression of $f(\mathbf{k})$ given in Eq. (D.31) into Eq. (D.25) for $g(\mathbf{k})$, and we simplify the integral over u' by recognizing that

$$(\mathbf{p}\cdot\mathbf{k})e^{\gamma u'}\exp\left[(\mathbf{p}\cdot\mathbf{k})\sigma_2^2(u)e^{\gamma u'}\right] = \frac{1}{\gamma\sigma_2^2(u)}\frac{\partial}{\partial u'}\exp\left[(\mathbf{p}\cdot\mathbf{k})\sigma_2^2(u)e^{\gamma u'}\right]. \tag{D.32}$$

This gives the moment generating function

$$g(\mathbf{k}) = g^{(0)}(\mathbf{k})\left\{1+\frac{i\lambda^2}{\kappa}\int_0^\infty\frac{\mathrm{d}u}{\sigma_2^2(u)}\int\frac{\mathrm{d}^d p}{(2\pi)^d}\frac{(\mathbf{p}\cdot\mathbf{v})}{p^2+r}|V_p|^2 G_{\mathbf{p}}^{(\mathbf{v})}(u)e^{p^2\sigma_2^2(u)}\left[1 \quad e^{(\mathbf{p}\cdot\mathbf{k})\sigma_2^2(u)}\right]\right\} + \mathcal{O}\left(\lambda^4\right). \tag{D.33}$$

Upon taking the logarithm of Eq. (D.33) and expanding for small λ, we obtain the cumulant generating function reported in Eq. (4.31). In particular, computing $\nabla_{\mathbf{q}}^2 g(\mathbf{q})|_{\mathbf{q}=\mathbf{0}}$ gives the correlation function

$$\langle Z_l Z_m\rangle_c = \frac{T}{\kappa}\delta_{lm} + \frac{\lambda^2}{\kappa}\int\frac{\mathrm{d}^d p}{(2\pi)^d}\frac{ip_l p_m\,(\mathbf{p}\cdot\mathbf{v})}{p^2+r}|V_p|^2\int_0^\infty \mathrm{d}u\, G_{\mathbf{p}}^{(\mathbf{v})}(u)\sigma_2^2(u)e^{p^2\sigma_2^2(u)}. \tag{D.34}$$

We note that the contribution $\propto \lambda^2$ actually vanishes for $l \neq m$, as it follows from the fact that, otherwise, the integrand would be an odd function of some component of the vector $\mathbf{p}$. It thus appears that no cross-correlations arise between the various orthogonal components of the displacement, i.e., $\langle Z_l Z_m\rangle_c \propto \delta_{lm}$, but the variance is anisotropically modified along the directions parallel and perpendicular to the trap velocity $\mathbf{v}$ (see also Fig. D.1). In the critical case, as well as for small velocities or small thermal fluctuations, it is possible to prove analytically that the correction in Eq. (D.34) is positive. Note that in the absence of the field (i.e., for $\lambda = 0$) the variance *does not* change, at finite v, compared to the case $v = 0$.

D.4 Average particle position and dissipation rate

In this Appendix, we analyze the behavior of the average particle position $\langle\mathbf{Z}\rangle$ reported in Eq. (4.32), together with its consequences on the dissipation rate discussed Section 4.3.4, focusing on the case of non-conserved dynamics.

D.4.1 Behavior as a function of the drag speed v

The average position $\langle Z\rangle$ in the steady state is plotted in the inset of Fig. 4.4(b) as a function of the trap velocity v, for the case of non-conserved dynamics in $d = 1$. For any finite value of r, i.e., of the correlation length $\xi = r^{1/2}$, one can generically identify three regimes and a crossover:

- *Low-velocity adiabatic) regime*, for $0 < v \lesssim v_I$. When $v = 0$ the system is in equilibrium, and the average particle position is not modified by the presence of the field [81], thus yielding $\langle Z(v=0)\rangle = 0$. Inspecting Eq. (4.32) shows that $\langle Z\rangle \propto v$, i.e., a linear dependence of $\langle Z\rangle$ on v for small v.

- *Intermediate crossover*, for $v_I \lesssim v \lesssim v_{II}$. Here $|\langle Z \rangle|$ reaches a maximum and behaves in a possibly non-monotonic way (depending on the choice of the various parameters).
- *High-velocity adiabatic) regime*, for $v_{II} \lesssim v \lesssim v_{III}$. The amplitude of the average position starts decaying as $|\langle Z \rangle| \propto v^{-1}$.
- *"Depinning" regime*, for $v \gtrsim v_{III}$. At very high speeds, one can check that $\langle Z \rangle$ tends to a small but finite value.

These regimes correspond to those observed for the correction $\propto \lambda^2$ to the dissipation rate $\langle \dot{W} \rangle_\lambda \propto v \langle Z \rangle$ in Fig. 4.4(b), which grows like $\propto v^2$ for small v (as it is the case for the usual Stokes friction), while it is v-independent for intermediate v, and finally grows like $\propto v$ in the last regime.

We can understand these behaviors starting from the effective equation of motion for the particle coordinate $\mathbf{Z}(t)$, which is given in Eq. (4.63). The latter is markedly non-Markovian because of the presence of a (nonlinear) memory term [i.e., the term that is proportional to $\chi^{(\mathbf{v})}_{\mathbf{p}}(u)$], and a colored multiplicative noise term $\zeta_{\mathbf{p}}(t)$. In the limits of very small and very large drag speed v, however, we physically expect to recover an approximately Markovian description. First, for very small v, the field is fast enough to equilibrate with the particle being fixed at its actual position, so that an adiabatic approximation is applicable [64, 65, 81, 104]. Second, for very large v, the evolution of the field is so slow that the particle effectively encounters a field landscape that is effectively static, i.e., quenched.

To make these statements more substantial, it is interesting to investigate the properties of the nonequilibrium steady state of the field, characterized by the formation of a comoving stationary profile around the particle, which we dubbed *shadow* in Section 4.3.3. Its analytical expression is found by averaging Eq. (4.26) over thermal fluctuations and by setting $\partial_t \langle \varphi_{\mathbf{p}} \rangle = 0$, which yields, at the leading order in λ [148],

$$\langle \varphi_{\mathbf{p}} \rangle_{\rm st} = \lambda \frac{D p \; V_p \exp\big[\; T p^2/(2\kappa)\big]}{_p \quad i\mathbf{p}\cdot\mathbf{v}}, \tag{D.35}$$

where we used Eq. (4.31), for $\lambda = 0$, in order to express the average $\langle \exp(\; i\mathbf{p}\cdot\mathbf{Z})\rangle = g(\mathbf{p})$ at the numerator of the resulting expression. The shadow is plotted in Fig. 4.4(a) for the case of $d = 1$ and non-conserved dynamics. Qualitatively, as the value of the speed v increases, the shadow becomes increasingly asymmetric (with its wavefront becoming steeper and its wake longer), and its overall amplitude decreases towards zero. In the limit of a point-like particle — which is obtained by choosing an interaction potential $V(\mathbf{x}) = \delta(\mathbf{x})$ — one can explicitly compute the inverse Fourier transform of Eq. (D.35) in $d = 1$ non-conserved dynamics by complex integration, finding

$$\langle \varphi(\;\;) \rangle_{\rm st} = \frac{\lambda}{\sqrt{(v/D)^2 + (2/\xi)^2}} \exp\left\{ \;\; \frac{v}{2D} \left[\;\; + | \;\; | \sqrt{1 + \left(\frac{2D}{v\xi}\right)^2} \right] \right\}. \tag{D.36}$$

Accordingly, the shadow decays exponentially, in front or behind the particle (i.e., for $\to \pm\infty$), over two generically distinct length scales $\ell_\pm$, respectively, as reported in Eq. (4.30). From this

expression of $\ell_\pm$ it appears that D/ξ is a natural velocity scale of this problem and, in fact, we shall see below that it coincides with the velocity v_I under which the dynamics is adiabatic. Close to equilibrium, i.e., for $v \ll v_I = D/\xi$, Eq. (D.36) reduces to

$$\langle \varphi(\ ) \rangle_{\rm st} \simeq \frac{\lambda \xi}{2} e^{\ |\ |/\xi}, \tag{D.37}$$

which is symmetric as expected, and extends over distances of $O(\xi)$. Conversely, for large speeds $v \gg v_I$ the amplitude of the shadow decreases as $1/v$, and decays in its front over a typical length $D/v \ll \xi$, and in its wake over the length $\xi^2 v/D \gg \xi$. Notably, by using a more realistic interaction potential $V(\mathbf{x})$ that takes into account the finite particle radius $R \ll \xi$, Eq. (D.36) would still describe the tails of the shadow, i.e., its behavior for $|\ | \gg R$.

As we emphasized in Chapter 2, choosing positive values of the coupling constant λ and $V(\mathbf{x})$ in Eq. (2.3) results in an effective attraction between the particle and the shadow; we are interested here in how this attraction modifies the steady-state average particle position $\langle \mathbf{Z} \rangle$. Let us assume initially that this *deterministic* attraction dominates over the (non-Gaussian) thermal fluctuations induced by the field, which are encoded in the noise term $\zeta_{\mathbf{p}}(t)$ in Eq. (4.64). Focusing on the two Markovian limits described above, we can approximately replace the field $\varphi_{\mathbf{p}}$ in Eq. (4.25) by its mean value, i.e., by the shadow given in Eq. (D.35). This approximation implies that

$$v\ {}^1\partial_t \langle \mathbf{Z}(t) \rangle \simeq\ \ \kappa \langle \mathbf{Z} \rangle + \lambda \int \frac{\mathrm{d}^d p}{(2\pi)^d} i\mathbf{p} \left\langle e^{i\mathbf{p}\cdot\mathbf{Z}} \right\rangle \left\langle \varphi_{\mathbf{p}} \right\rangle_{\rm st}. \tag{D.38}$$

The second term on the right hand side represents a field-induced effective force which, in the steady state defined by $\partial_t \langle \mathbf{Z}(t) \rangle = 0$, counterbalances the restoring force $\kappa \langle \mathbf{Z} \rangle$ of the harmonic trap. For small speeds v, the shadow is essentially symmetric [see Eq. (D.37)] around its center which we will denote as $\ _p$. Linearizing Eq. (D.38) around the unperturbed position $\langle Z \rangle = 0$ (for simplicity, we consider below the case $d = 1$) renders in general

$$v\ {}^1\partial_t \langle Z \rangle \simeq\ \ \kappa \langle Z \rangle\ \ \ \lambda^2 \kappa_\phi\ \langle Z \rangle\ \ \ \ _p\big), \tag{D.39}$$

where the expression of the effective linear strength κ_ϕ and of $\ _p$ introduced above can be found on the basis of the expression of the shadow in Eq. (D.35) — as they are not necessary for our argument, we do not provide them here. In the steady state and at leading order in the coupling λ, we thus find

$$\langle Z \rangle \simeq \lambda^2 \frac{\kappa_\phi}{\kappa}\ \ _p. \tag{D.40}$$

At small but nonzero v, one expects the center of the shadow to lag behind the average particle position (which effectively "drags" the shadow), i.e., $\ _p = av + O\ v^2\big)$ with some $a < 0$. Accordingly, Eq. (D.40) with this expression for $\ _p$ predicts that $|\langle Z \rangle|$ has a linear dependence on v for small velocities, as observed in Fig. 4.4(b) (see the inset), and as discussed above.

The simplified description presented above is expected to become less accurate as v increases, because the rearrangement of the field can no longer be assumed to be instantaneous, and the particle actually moves considerably (due to the dragging) while the shadow forms. The spatial extension of the shadow is of $O(\xi)$ in this regime [see Eq. (D.37)], so it builds over a timescale

$\tau_\xi \simeq \xi^2/D$ in the case of non-conserved dynamics. This timescale should be compared with the time τ taken by the trap to span a distance of the order of the field correlation length ξ, i.e., $\tau \simeq \xi/v$. The two timescales balance at

$$v_I \simeq D/\xi, \tag{D.41}$$

which we identify as the end of the first regime, i.e., the beginning of the crossover in Fig. 4.4(b). This estimate assumes also that $\tau_\xi \ll \tau_\kappa$, i.e., that the field relaxes faster than the typical timescale set by the harmonic trap (which is typically the case in experimental realizations with colloidal particles — see Appendix D.5.1).

For intermediate velocities $v_I \leq v \leq v_{II}$, the behavior of $\langle Z \rangle$ is fully determined by non-Markovian effects which, contrary to the previous regimes, cannot be explained in terms of a simplified model. Conversely, for $v > v_{II}$, we can again replace the field by its expectation value as in Eq. (D.38). In this high-velocity regime, the shadow is so asymmetric [see Fig. 4.4(a)] that it is no longer meaningful to treat it as a point-particle concentrated in its center $\quad_p$ [as we essentially did in Eq. (D.39)]. In spite of this difficulty, it actually turns out that its form can still be determined analytically. In particular, from Eq. (D.35) one can first compute

$$\begin{aligned}\partial_x \langle \varphi(x) \rangle_{\rm st} &= \partial_x \int \frac{\mathrm{d}p}{2\pi} \langle \varphi_p \rangle_{\rm st} e^{ipx} = \lambda D \int \frac{\mathrm{d}p}{2\pi} \frac{ipV_p e^{\quad Tp^2/(2\kappa)}}{\quad_p \quad ipv} e^{ipx} \\ &\simeq \frac{\lambda D}{v} \int \frac{\mathrm{d}p}{2\pi} V_p e^{\quad Tp^2/(2\kappa)} e^{ipx},\end{aligned} \tag{D.42}$$

where the approximation introduced in the last equality is expected to be valid when v exceeds *all* the relevant ratios of length and time scales of the system. This requires, inter alia, that

$$\tau_v \ll \tau_\kappa \tag{D.43}$$

[see Eqs. (1.12) and (4.45)], which justifies the replacement of the field $\varphi_{\mathbf{p}}$ by its mean value in Eq. (D.38). Moreover, we assume (as done above and in Section 4.3.4) that the interaction potential $V(x)$ is characterized by a single length scale R (i.e., the particle radius), so that V_p provides an effective cutoff over momenta $p \gg 1/R$. In the denominator of Eq. (D.42), we can thus impose the large velocity condition $\quad_p \ll pv$ in correspondence of $p \sim 1/R$, so that this condition is satisfied for all values of $p \leq 1/R$: this gives [with reference to Eqs. (4.44) and (4.45)]

$$\tau_v \ll \tau_R. \tag{D.44}$$

Accordingly, the second threshold velocity v_{II} is expected to be provided by the smallest velocity v for which both conditions in Eq. (D.43) and (D.44) are satisfied, which depends on the particular choice of parameters and specific details of the system. In Eq. (D.42) we also recognize the term $\widetilde{V}_p \equiv V_p \exp\big[\ Tp^2/(2\kappa)\big]$, featuring the Fourier transform of the interaction potential $V(x)$, corrected by a factor which takes into account the mean squared displacement of the particle in the harmonic trap induced by the thermal fluctuations. Accordingly, in this limit, the shadow becomes

$$\langle \varphi(x) \rangle_{\rm st} \simeq \frac{\lambda D}{v} \int_\infty^x \mathrm{d}x' \, \widetilde{V}(x'). \tag{D.45}$$

[Here we assumed that $\langle\varphi(x)\rangle_{\rm st} \to 0$ for $|x| \to +\infty$, as expected from Fig. 4.4(a).] As a consequence, the effective force term in Eq. (D.38) scales in this regime as v^{-1}, which produces an analogous dependence on v for the average particle position $\langle Z\rangle$ in the steady state. Due to this very v^{-1} dependence, we expect this *deterministic* effect to die out for very large v. In this last ("depinning") regime, the field is so slow with respect to the particle motion that no shadow can build up, and the particle effectively sees a rough landscape whose features are solely determined by the thermal fluctuations of the field. In order to describe this situation, we have to go back to the particle effective equation (4.63), the average over thermal fluctuations of which yields

$$\langle\dot{\mathbf{Z}}\rangle = -\gamma\,\langle\mathbf{Z}\rangle + \lambda v\int\frac{\mathrm{d}^d p}{(2\pi)^d}\,i\mathbf{p}V_{-p}\left[\left\langle\zeta_{\mathbf{p}}(t)e^{i\mathbf{p}\cdot\mathbf{Z}(t)}\right\rangle + \lambda V_p\int_0^\infty \mathrm{d}u\,\chi^{(\mathbf{v})}_{\mathbf{p}}(u)\left\langle e^{i\mathbf{p}\cdot[\mathbf{Z}(t)-\mathbf{Z}(t-u)]}\right\rangle\right]. \tag{D.46}$$

By using Novikov's theorem [10, 308]

$$\langle\zeta(t)F[\zeta]\rangle = \int\mathrm{d}s\,\langle\zeta(t)\zeta(s)\rangle\left\langle\frac{\delta F[\zeta]}{\delta\zeta(s)}\right\rangle, \tag{D.47}$$

where $F[\zeta]$ is any functional of the (Gaussian) noise ζ, we can compute the expectation value

$$\begin{aligned}\left\langle\zeta_{\mathbf{p}}(t)e^{i\mathbf{p}\cdot\mathbf{Z}(t)}\right\rangle &= i\mathbf{p}\int\mathrm{d}s\,C^{(\mathbf{v})}_{\mathbf{p}}(t-s)\left\langle e^{i\mathbf{p}\cdot\mathbf{Z}(t)}\frac{\delta\mathbf{Z}(t)}{\delta\zeta_{-p}(s)}\right\rangle\\ &\simeq \lambda v p^2 V_p\int_{-\infty}^{t}\mathrm{d}s\,e^{-\gamma(t-s)}C^{(\mathbf{v})}_{\mathbf{p}}(t-s)\left\langle e^{i\mathbf{p}\cdot[\mathbf{Z}(t)-\mathbf{Z}(s)]}\right\rangle_0,\end{aligned} \tag{D.48}$$

where in the last step we used the equation of motion (4.63) of $\mathbf{Z}(t)$, we indicated by $\langle\ldots\rangle_0$ the expectation value over the unperturbed process with $\lambda = 0$, and we discarded higher-order terms in λ. The leading-order expression for the dynamical structure factor

$$\left\langle e^{i\mathbf{p}\cdot[\mathbf{Z}(t)-\mathbf{Z}(t-u)]}\right\rangle_0 \underset{t\to+\infty}{\longrightarrow} e^{-p^2\sigma_2^2(u)} \tag{D.49}$$

was computed in Appendix B.1, with $\sigma_2(u)$ given in Eq. (D.30) — this is sufficient to evaluate the r.h.s. of Eq. (D.46) at the lowest non-trivial order in λ, i.e., at $O(\lambda^2)$. Setting $\partial_t\langle\mathbf{Z}\rangle = 0$ in Eq. (D.46) and taking the limit for $t\to+\infty$ on its r.h.s. then yields the steady-state average position

$$\langle\mathbf{Z}\rangle = \frac{\lambda^2}{\kappa}\int\frac{\mathrm{d}^d p}{(2\pi)^d}\,i\mathbf{p}|V_p|^2\int_0^\infty\mathrm{d}u\left[\chi^{(\mathbf{v})}_{\mathbf{p}}(u) + \nu p^2 e^{-\gamma u}C^{(\mathbf{v})}_{\mathbf{p}}(u)\right]e^{-p^2\sigma_2^2(u)} + O\left(\lambda^4\right). \tag{D.50}$$

This last expression indeed coincides with Eq. (4.32), *for any finite temperature* $T > 0$, which can be seen upon integrating by parts in $\mathrm{d}u$ and by using the fluctuation-dissipation theorem in the form of Eq. (D.29). It is simple to verify that the term proportional to $\chi^{(\mathbf{v})}_{\mathbf{p}}(u)$ in Eq. (D.50) decays as $1/v$ for large v, as it encodes the deterministic effect of the shadow. At large v, the only term that contributes is the one originating from the noise $\zeta_{\mathbf{p}}(t)$ and proportional to the field correlator $C^{(\mathbf{v})}_{\mathbf{p}}(u)$, which explicitly becomes

$$\langle\mathbf{Z}\rangle = \frac{\lambda^2\nu T}{\kappa}\int\frac{\mathrm{d}^d p}{(2\pi)^d}\,\frac{i\mathbf{p}\,p^2|V_p|^2}{p^2+r}\int_0^\infty\mathrm{d}u\exp\left[(i\mathbf{p}\cdot\mathbf{v}-\gamma-\nu p^2)u - p^2\sigma_2^2(u)\right] + O\left(\lambda^4\right). \tag{D.51}$$

This term is proportional to the strength T of the thermal fluctuations and the coupling λ^2 to the field, in agreement with the interpretation we provided earlier in this section — i.e., that the features of the field landscape encountered by the particle in this regime are determined by the critical fluctuations of the former. The identification of the value v_{III} of the velocity v at which this regime begins is, however, not straightforward: it marks the value at which the field-induced thermal fluctuations start to dominate over its deterministic attraction. Since these fluctuations exhibit a rather strong dependence on the distance r from the critical point [as it appears by inspecting the field correlator $C_{\mathbf{p}}^{(\mathbf{v})}(u)$ in Eq. (4.27)], then v_{III} also shows a similar dependence on the correlation length $\xi = r^{1/2}$ (as well as on the temperature T). In particular, Fig. 4.4(b) shows that v_{III} decreases upon approaching the critical point $r = 0$, while the extents of the first and second velocity regimes decrease.

D.4.2 The case of critical non-conserved dynamics

It is instructive, at this point, to inspect the case of critical non-conserved dynamics, i.e., to consider $r = 0$ and $\quad = 0$. In $d = 1$ and with a Gaussian interaction potential V_p (with zero mean and variance R), the average particle position given in Eq. (4.32) can be simplified as

$$\langle Z \rangle = \frac{\lambda^2 v}{\kappa} \int_0^\infty \frac{\mathrm{d}u}{\sqrt{4\pi}\Sigma(u)} \exp\left[\frac{(vu)^2}{4\Sigma^2(u)} \right] \leq 0, \qquad \Sigma^2(u) \equiv R^2 + u/\gamma_\phi + \sigma_2^2(u). \tag{D.52}$$

The corresponding curve for the dissipation rate is plotted in Fig. 4.4(b) (solid green line with $\xi = \infty$). As the critical point is approached, we note that the crossover velocity v_I described in Appendix D.4.1 decreases; exactly at criticality, the entire low-velocity (adiabatic) regime disappears, in agreement with the expression of v_I given in Eq. (D.41). Furthermore, for $r \to 0$, critical fluctuations are found to play a major role, as signaled by the fact that the crossover velocity v_{III} also decreases considerably.

Interestingly, we note that the expression of $\langle Z \rangle$ for $r = 0$ in Eq. (D.52) has a finite, non-vanishing limit for $v \to 0$, while Eq. (4.32), in the same limit but with a generic value of r, correctly vanishes independently of $r \neq 0$; in fact, at equilibrium, the presence of the field does not modify the equilibrium distribution of the particle [81]. We are thus led to the conclusion that the limits $r \to 0$ and $v \to 0$ do not commute: the physical interpretation is that, when $r \to 0$, the relaxation timescale τ_ξ of the field diverges [see Eq. (4.35)] and therefore the system is out of equilibrium for any finite value of v, no matter how small.

D.5 Numerical simulation of the stochastic dynamics

The numerical integration scheme we adopt to simulate the coupled stochastic dynamics of field and particle is similar to the one described in Appendix B.8; further details can be found in the Supplemental Material of Ref. [114] (see Section VII), together with a technical description of the numerical measurement of the heat dissipation field

$$đQ_\phi = \left[\frac{\delta \mathcal{H}_\phi}{\delta \phi} + \frac{\delta \mathcal{H}^{\mathrm{int}}}{\delta \phi} \right] \circ \mathrm{d}\phi(\mathbf{x}, t) = \left[\left(\nabla^2 + r \right) \phi(\mathbf{x}, t) + \lambda V(\mathbf{x} \quad \mathbf{Y}(t)) \right] \circ \mathrm{d}\phi\,(\mathbf{x}, t), \tag{D.53}$$

as displayed in Fig. 4.3. Below we only focus on the choice of the parameters to be used in the simulation, and on the measurement of the distribution of the particle position.

D.5.1 Choice of parameters

Here we discuss the choice of the values of the parameters of the model to be used in the numerical simulations, so that they eventually correspond to the typical time and length scales observed in experiments with colloidal particles. As a prototypical example, we consider the case of a μm–sized colloidal particle immersed in a binary liquid mixture close to its demixing transition [32–36], so that the field ϕ represents the relative concentration of the two species that compose the mixture. It must be emphasized, however, that our model is not meant to reproduce quantitatively the results of such experiments (for which hydrodynamic effects would need to be taken into account), but rather to highlight the role played by spatial correlations. Moreover, other very diverse physical systems (such as inclusions in lipid membranes [17–20], microemulsions [22–25], or defects in ferromagnetic systems [26–31]) also fall within the scopes of our model, and they may entail very different time and length scales.

Binary liquid mixtures can undergo a demixing phase transition close to room temperature [43], in correspondence of which the correlation length $\xi = \xi(T)$ diverges. In real experiments, achieving large values of ξ is generally challenging, as it requires a fine-tuning and highly accurate control of the temperature across the experimental sample. However, in the following we will assume that ξ can indeed be made much larger than the particle radius R, in order to magnify the qualitative effects of spatially extended correlations, which are the central topic of this Chapter.

Note that our model features several parameters, but only a limited number of physical units (i.e., mass, length, time and temperature). As detailed in Section 4.6.2, close to the critical point the system can be conveniently described in terms of a reduced set of dimensionless parameters, which correspond to ratios of the typical time and length scales of the system. These are

$$w \equiv \frac{\tau_R}{2\tau_v}, \qquad \rho \equiv \tau_R/\tau_\kappa, \qquad g \equiv \frac{\lambda^2}{\kappa R^d}, \qquad \text{and} \qquad \epsilon \equiv \frac{l}{R}. \tag{D.54}$$

The first is the Weissenberg number $w = \mathrm{Wi}$ (see Eq. (4.57)), which compares the shear rate due to dragging with the typical relaxation time of the field τ_R, over length scales of the order of the particle radius R. The second parameter, ρ (see Eq. (4.52)), compares the relaxation time τ_R of the field with the time scale τ_κ set by the harmonic trap. The effective coupling g (see Eq. (4.50)) quantifies the strength of the interaction between the particle and the field. Finally, ϵ is the ratio between the thermal length l (i.e., the mean-squared displacement of the particle in the trap according to equipartition in equilibrium, see Eq. (4.68)) and the particle radius R. Specializing these expressions to the case of critical non-conserved dynamics in $d = 2$ yields $g = \lambda^2/(\kappa R^2)$, $w = Rv/(2D)$, and $\rho = \kappa R^2 \nu/D$.

Having identified the relevant parameters in Eq. (D.54), we now discuss which of their values are within experimental reach. The typical magnitude of the thermal length l can be estimated at room temperature $T \simeq 300\,\mathrm{K}$ by assuming a typical value of the optical trap strength

$\kappa \simeq 0.5\,\mathrm{pN}/\mu\mathrm{m}$ [34], yielding $l \simeq 100\,\mathrm{nm}$, and hence $\epsilon \simeq 0.1$ for a μm-sized particle. Next, the typical relaxation time scale τ_ϕ of a near-critical binary mixture can be estimated by using model H [59]. Within mode-coupling theory and for momenta p such that $p\xi \ll 1$ (i.e., for small ξ, which has been the case in past experiments [32–36]), the relaxation timescale of the field is given by [307]

$$\tau_\phi{}^{1}(p) \simeq D_\xi\, p^2, \tag{D.55}$$

where $D_\xi = k_B T/(6\pi\eta\xi)$, and η is the fluid viscosity. By comparison with the diffusion coefficient D_R of the particle [36]

$$D_R = \frac{k_B T}{6\pi\eta R} \simeq 0.22(\mu\mathrm{m})^2\mathrm{s}^{\ 1}, \tag{D.56}$$

one can estimate the relaxation time scale of the field over distances of the order of the particle radius as

$$\tau_R \simeq \tau_\phi(p \sim \pi/R) \simeq \frac{R\xi}{\pi^2 D_R} \simeq 10\mathrm{ms}, \tag{D.57}$$

where we chose $\xi \simeq R/50$ (which is common for water-lutidine mixtures [35, 36]). Since the typical relaxation time τ_κ of optical traps is of the order of a few tens of ms [35], this gives $\rho \simeq 10^{\ 1}$. This value is expected to increase if the correlation length ξ can be made larger, since this generally entails longer relaxation times τ_ϕ [54]. Next, with typical drag speeds up to a few tens of μm/s [150], one can explore Weissenberg numbers up to $w \simeq 10^{\ 1}$. On the other hand, the effective coupling g quantifies the strength of the interaction between the particle and the field, and its amplitude thus depends on the specific coupling mechanism realized in a certain experiment. At present, it is still unclear how to estimate its order of magnitude on the basis of past experimental data, but we clearly expect any overall qualitative effect to be enhanced if g can be made larger. We finally keep an eye for consistency on the ratio $\Theta \equiv \tau_v/\tau_\kappa = \rho/(2w)$ [see Eq. (D.54)] of the shear rate to the trap time scale which, based on the estimates above for ρ and w, is typically of $O(1)$.

The experimentally accessible values of the parameters in Eq. (D.54) discussed above are reproduced in numerical simulations by choosing the following set of values of the model parameters:

$$T = 0.7, \quad \kappa = 0.2, \quad v = 5, \quad R = 2, \quad \lambda = 10, \quad r = 10^{\ 4}, \quad D = 20, \quad \text{and} \quad \nu = 5, \tag{D.58}$$

where space is expressed in units of the lattice spacing Δx, and we furthermore chose a discretized time step $\Delta t = 10^{\ 2}$. This choice corresponds, in fact, to $w = 0.25$, $\rho = 0.2$, $\epsilon = 0.66$, $\Theta = 0.4$, and $g = 125$. The lattice size $L = 128$ is chosen sufficiently large so as to accommodate the tails of the field shadow [see Fig. 4.4(a)], and to avoid spurious field currents due to the *stirring* that the particle would generate if it were dragged around the periodic boundaries [see Section 4.6.2].

D.5.2 Distribution of the particle position

Using the parameters described above, we determined the statistics of the particle position, shown in Fig. D.1. In particular, for a field in $d = 2$ with non-conserved dynamics, the upper

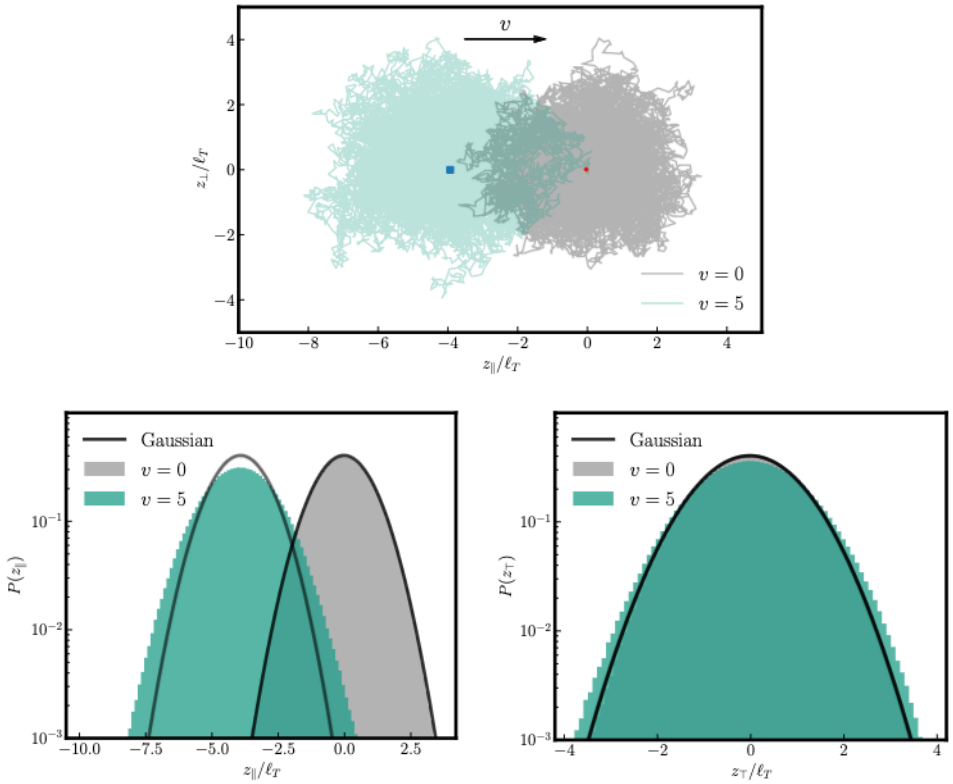

Figure D.1: **Upper panel:** scatter plot of the particle position, in the comoving frame, as measured in numerical simulations in $d = 2$ and for a field with non-conserved dynamics. The average positions for $v = 0$ and $v = 5$ are indicated with a red dot and a blue square, respectively. **Lower panels:** histograms of the particle position along the directions parallel ($_{\parallel}$) and perpendicular ($_{\perp}$) to the trap velocity $\mathbf{v}$. In the simulations we used the parameter set given in Eq. (D.58), with $\ell_T^2 \equiv R^2 + T/\kappa$ being the effective particle radius. In the plot, we indicated with a solid black line the Gaussian distribution, which is recovered for $v = 0$ (boundary of the gray regions) or in the absence of particle-field interactions, i.e., for $\lambda = 0$ (leftmost curve in the left panel).

panel of Fig D.1 presents a scatter plot of the particle position $\mathbf{Z}$ measured in the comoving frame. This shows clearly two of the main features already emerging from the cumulant generating function, predicted perturbatively (i.e., for small λ) in Eq. (4.31), namely:

1. At finite v, the steady-state average position (blue square in Fig. D.1) lags behind the one obtained for $v = 0$ (red dot). Note that the latter coincides with the average position found at $\lambda = 0$, i.e., $\langle \mathbf{Z} \rangle = 0$, because the coupling to the field does not modify the one-time properties of the particle position statistics at equilibrium (this result was proven non-perturbatively in Appendix B.2).

2. The variance of the particle position increases in the directions parallel and perpendicular to $\mathbf{v}$ by a different amount. Note that in the absence of the field (i.e., for $\lambda = 0$) the particle variance would be $\langle Z_l Z_m \rangle_c = (T/\kappa)\delta_{lm}$ [see Eq. (D.34)], independently of the value of v. Accordingly, the observed anisotropic change of the variance of the particle position is the

result of the combined effect of the presence of the field and of the dragging.

The lower panels of Fig. D.1 show histograms of the distribution of the particle positions $_{\parallel}$ and $_{\perp}$ along the directions parallel (left) and perpendicular (right) to the trap velocity $\mathbf{v}$, respectively, compared to the case with $\mathbf{v} = 0$ (gray shading). Note that the distribution for $\mathbf{v} \neq \mathbf{0}$ is non-Gaussian, although the non-Gaussian character is not immediately apparent for the values of the parameters used in this figure. However, this non-Gaussianity is evident at the lowest perturbative order in λ, as we discussed in Section 4.3.3 [see Eq. (4.31)].

D.6 Long-time behavior from the Laplace transform

The features of the long-time behavior of a function $f(t)$ can be inferred from the analytic structure of its Laplace transform $\hat{f}(s)$. This kind of relations are referred to as *Haar's Tauberian theorems* in the mathematical literature [312]. In this Appendix we recap and summarize some useful related results which are applied in Section 4.5.

Simple poles. — Consider, first of all, the textbook case [156] in which $\hat{f}(s)$ is a meromorphic function in the complex s plane:

$$\hat{f}(s) = g(s) \prod_{j=1}^{n} \frac{1}{s \quad s_j}, \tag{D.59}$$

where $g(s)$ is an analytic function, and the n poles $\{s_1, s_2, \dots, s_n\}$ are located at $s_j = \quad \delta_j + i\Omega_j$. We order the poles so that $0 \leq \delta_1 < \cdots < \delta_n$. By using the Cauchy residue theorem we then easily obtain

$$f(t) = \sum_{j=1}^{n} g(s_j) e^{\quad \delta_j t + i\Omega_j t} \prod_{k \neq j} \frac{1}{s_j \quad s_k} g(s_1) \left(\prod_{k \neq 1} \frac{1}{s_1 \quad s_k} \right) e^{\quad \delta_1 t + i\Omega_1 t}, \tag{D.60}$$

where in the last step we retained the dominant term at long $t > 0$. This shows that the rightmost pole s_1 of $\hat{f}(s)$ (i.e., the closest to the imaginary axis) determines the long-time behavior of $f(t)$, which exhibits damped oscillations with frequency Ω_1 if s_1 has a nonzero imaginary part.

Branch cuts. — Next, assume that $\hat{f}(s)$ is no longer meromorphic, but rather displays a branch cut with branch point s_0 (for instance, in Fig. 4.7a the branch cut develops along the real axis for $\mathrm{Re}\{s\} < \quad w$, with $s_0 = \quad w$). In this case, we can generally expand $\hat{f}(s)$ around the branch point s_0 as

$$\hat{f}(s) \sim \sum_j a_j (s \quad s_0)^{\lambda_j}, \tag{D.61}$$

for some (possibly non integer) λ_j, and take the inverse Laplace transform term by term as in Eq. (4.60) to obtain

$$f(t) \sim e^{s_0 t} \sum_j \frac{a_j}{_E(\quad \lambda_j)\, t^{1+\lambda_j}}. \tag{D.62}$$

In the presence of poles alongside the branch cut (as in Fig. 4.7a), the contribution in Eq. (D.62) simply adds up to that in Eq. (D.60). Again, the long-time behavior of $f(t)$ is determined by the rightmost among the poles s_j and the branching point s_0.

Algebraic decays. — We describe for completeness the case in which $f(t)$ does not exhibit an oscillatory behavior, but rather an asymptotic algebraic decay of the form

$$f(t) \sim A t^{-\mu}, \quad \text{for} \quad t \geq t_c \gg 1, \tag{D.63}$$

where $\mu \geq 0$ and t_c is a crossover time [3]. The strategy to obtain the corresponding Laplace transform is to divide the integration domain as

$$\hat{f}(s) = \int_0^{t_c} \mathrm{d}t\, e^{-st} f(t) + A \int_{t_c}^{\infty} \mathrm{d}t\, e^{-st} t^{-\mu}. \tag{D.64}$$

The first term is regular, i.e., it can be expanded in a power series containing only integer powers of s. The integration in the second term of Eq. (D.64) can be further split into [4]

$$\begin{aligned} \int_{t_c}^{\infty} \mathrm{d}t\, e^{-st} t^{-\mu} &= \int_{t_c}^{1/s} \mathrm{d}t\, e^{-st} t^{-\mu} + \int_{1/s}^{\infty} \mathrm{d}t\, e^{-st} t^{-\mu} \\ &= \int_{t_c}^{1/s} \mathrm{d}t\, e^{-st} t^{-\mu} + s^{\mu-1} \int_1^{\infty} \mathrm{d}\tau\, e^{-\tau} \tau^{-1}. \end{aligned} \tag{D.65}$$

The first term on the r.h.s. of Eq. (D.65) can be shown to involve both a regular and a non-regular part. To see this, we expand the exponential in power series and integrate term by term to find

$$\mathcal{I} \equiv \int_{t_c}^{1/s} \mathrm{d}t\, e^{-st} t^{-\mu} = \sum_{n=0}^{\infty} \frac{(-1)^n \left(s^{\mu-1} - s^n t_c^{n-\mu+1}\right)}{(n-\mu+1)n}. \tag{D.66}$$

For μ not integer, the second term in the series is regular. The first term $\sim s^{\mu-1}$, together with the last term in Eq. (D.65), reconstructs the Euler gamma function via its integral representation (for $-\mu \neq 0, -1, -2, \ldots$ [63])

$$\Gamma_E(-\mu) = \int_1^{\infty} \mathrm{d}\tau\, \tau^{-\mu-1} e^{-\tau} + \sum_{n=0}^{\infty} \frac{(-1)^n}{(n-\mu)n}. \tag{D.67}$$

If instead $\mu \in \mathbb{N}^+$, let us first set $\mu = p + \varepsilon$, with $p \in \mathbb{N}^+$ and $\varepsilon \ll 1$, and isolate the diverging term in Eq. (D.66) as

$$\mathcal{I} = \sum_{n \neq (p-1)}^{\infty} (\ldots)\Big|_{\mu=p} \quad \lim_{\varepsilon \to 0} \frac{(-s)^{p-1}}{(p-1)!\,\varepsilon} (s^{\varepsilon} - t_c^{\varepsilon}) = \sum_{n \neq (p-1)}^{\infty} (\ldots)\Big|_{\mu=p} \quad \frac{(-s)^{p-1}}{(p-1)!} \ln(s\, t_c), \tag{D.68}$$

where we used $x^{\varepsilon} = e^{\varepsilon \ln x} \simeq 1 + \varepsilon \ln x$. Note that the remaining series may still produce terms proportional to $s^m \ln s$, with $m > p - 1$, but these are subleading for small s.

Including all the terms in Eq. (D.64) we thus finally get

$$\hat{f}(s) = \hat{f}_r(s) + \begin{cases} A\, \Gamma_E(1-\mu)\, s^{\mu-1}, & \mu \in [0,\infty) - \mathbb{N}^+, \\ \dfrac{A(-1)^{\mu}}{(\mu-1)!} \ln(s\, t_c) s^{\mu-1} + \mathcal{O}(s^{\mu} \ln s), & \mu \in \mathbb{N}^+, \end{cases} \tag{D.69}$$

[3] Simpler heuristic arguments can be found in the literature for the case $0 \leq \mu < 1$ [313, 314].

[4] For the sake of the argument we are assuming here $s \in \mathbb{R}$, but the resulting series expansion in Eq. (D.69) is well defined on a compact region of the real axis, and it can thus be analytically continued to all $s \in \mathbb{C}$.

where $\hat{f}_r(s)$ is the regular part of $\hat{f}(s)$. Thus, to unveil a long-time asymptotic power-law decay of $f(t)$ as in Eq. (D.63), one can expand its Laplace transform $\hat{f}(s)$ in series for small s, and check for the presence of a term $\sim \ln(st_c)s^{\mu\ 1}$ (with μ a positive integer), or $\sim s^{\mu\ 1}$ (with $\mu \geq 0$ not integer). An application of these last relations is presented in Appendix D.7.

D.7 Relaxation towards equilibrium

We consider here the problem of the relaxation towards equilibrium of a particle in contact with a scalar Gaussian field, in a *fixed* harmonic trap, and which is subject to a small initial displacement $\mathbf{X}_0 \neq 0$ at time $t = 0$. Indeed, in the absence of external dragging the steady state reached by the system at long times is actually an equilibrium state [81].

The problem is analogous to the one we analyzed in Section 4.5 upon setting $v = 0$, and thus the solution $\hat{X}_j(s)$ for $T = 0$ (noiseless case), and within the linear-response approximation, is given by Eq. (4.43). In particular, the memory kernel in Eqs. (4.47) and (4.48) reduces to

$$\hat{}_j(s) = \lambda^2 \nu D \int \frac{\mathrm{d}^d q}{(2\pi)^d} \frac{q_j^2 q\ |V_q|^2}{s + \ _q}. \tag{D.70}$$

At the critical point $r = 0$ of the medium one has $\ _q = Dq\ $ (see Eq. (1.25)), so that, using polar coordinates and changing variables to $y = Dq\ /s$, one finds

$$\hat{}_j(s) = \lambda^2 \nu c_d (sD)^{d/\ } \int_0^\infty \frac{\mathrm{d}y\ y^{d/\ }}{1+y} |V_{(sy/D)^{1/\ }}|^2 \sim s^{d/\ }\ . \tag{D.71}$$

Here c_d is a numerical constant accounting for the integration over the angular variables, while in the last step we expanded the expression for small s by using the normalization condition $V_q = 1 + O(q)$ of the interaction potential. Expanding the denominator of Eq. (4.43) in a geometric series now gives

$$\hat{X}_j(s) = X_0 \sum_{n=0}^{\infty} \left[\hat{}_j(s) \quad s\right]^n \left[\hat{}_j(0) + \gamma\right]^{\ (n+1)}. \tag{D.72}$$

Comparing with Eq. (D.71), we deduce that the power series of $\hat{X}_j(s)$ contains a term $\sim s^{d/\ }$, which is non-regular whenever the ratio $d/\ $ is not integer. From our discussion in Appendix D.6, this corresponds to an algebraic asymptotic decay of $X_j(t) \sim t^{\ \mu}$, with $\mu = 1 + d/\ $. Note that the terms $\sim s^{nd/\ }$ contained in the series of Eq. (D.72) may also be non-regular, but they correspond to subleading algebraic contributions to $X_j(t)$ at long times.

Similarly, for critical model B one has $\ _q = Dq^2(q^2 + r)$ (see Eq. (1.25)). Accordingly, by following the same steps as those that led from Eq. (D.70) to Eq. (D.71), one finds

$$\hat{}_j(s) = \lambda^2 \nu c_d \int_0^\infty \frac{\mathrm{d}y\ |V_{(sy/D)^{1/2}}|^2}{1 + y(r + sy/D)} \left(\frac{sy}{D}\right)^{1+d/2} \sim s^{1+d/2}, \tag{D.73}$$

where we set $y \equiv Dq^2/s$. Comparing with Eq. (D.72) one eventually concludes that $X_j(t) \sim t^{\ \mu}$ with the decay exponent $\mu = 2 + d/2$.

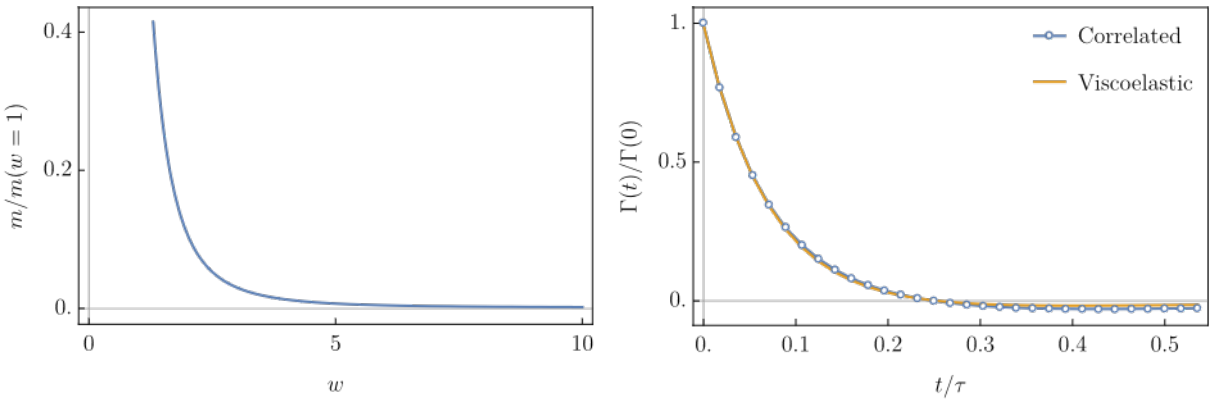

(a) (b)

Figure D.2: Comparison with the phenomenological model for viscoelastic fluids of Ref. [47]. **a)** Effective mass m given in Eq. (D.82) as a function of w (see the main text for details). **b)** Comparison between the memory kernel (t) of a viscoelastic fluid (solid yellow line, obtained as $(t) = \nu\mathcal{K}'(t)$ from Eq. (D.76)) and the one of the model studied in this work (blue line with symbols, corresponding to Eq. (D.84) for $d = 1$ model A). The parameters of the former kernel were chosen as in Ref. [47] (see the main text). For illustrative purposes, in Eq. (D.84) we set $\tau_\xi = \infty$ (i.e., we consider the field at criticality), while τ_R and τ_v for the latter kernel have been fixed by matching the leading behavior of the former (t) at short times, and the crossing point of the horizontal axis. Both curves eventually approach zero from below as $t \to \infty$.

The powers of the algebraic decays of $X_j(t)$ agree with those previously found in Ref. [81] — see Eqs. (33) and (34) therein. The approach used in Ref. [81] in order to derive these predictions differs, however, from the one used here and in Section 4.5: in particular, the former relies on a weak-coupling expansion for small λ, while it assumes $T \neq 0$ and it does not require the linear-response approximation (thus it also allows the investigation of an intermediate nonlinear dynamical crossover, see Ref. [81] for details). Although limited to the noiseless case $T = 0$, the analysis presented here and in Section 4.5 of the present work makes, instead, no assumption concerning the magnitude of λ. This suggests that the exponents of the algebraic decays determined above may in fact be nonperturbative in λ, as it was conjectured in Ref. [81] based on the evidence provided by numerical simulations.

D.8 Comparison with a phenomenological model for viscoelastic fluids

The underdamped oscillations of a colloidal particle dragged through a viscoelastic fluid reported in Ref. [47] have been described therein in terms of the linear, generalized Langevin equation

$$\gamma_\infty \dot{X}(t) + \int_\infty^t \mathrm{d}u\, \mathcal{K}(t \quad u)\dot{X}(u) = \quad \kappa X(t) + f^{(\mathrm{v})}(t)\,, \tag{D.74}$$

where γ_∞ is the friction coefficient at infinite frequency, while $f^{(\mathrm{v})}(t)$ is a stochastic correlated noise term with vanishing average. Using that both $\langle X(t)\rangle$ and $\langle \dot{X}(t)\rangle$ vanish for $t < 0$ and

integrating by parts, one can check that Eq. (D.74) is formally equivalent to the effective equation in (4.65) upon identifying

$$\gamma_\infty \equiv 1/v, \quad \text{and} \quad (t) \equiv \quad v\mathcal{K}'(t). \tag{D.75}$$

Finally, the memory kernel is assumed in Ref. [47] to be of the form

$$\mathcal{K}(t) = \frac{\gamma_0 \quad \gamma_\infty}{\tau} e^{\ t/\tau} + \sum_i \left(\frac{\gamma_i}{\tau_i} e^{\ t/\tau_i} \quad \frac{\gamma_i}{\tau} e^{\ t/\tau} \right), \tag{D.76}$$

where $\gamma_0 > \gamma_\infty$ is the *zero-frequency* friction coefficient, while γ_i and τ_i are phenomenological parameters introduced to fit the experimental data. The kernel in Eq. (D.76) reduces to that of a Jeffrey's fluid [315] for $\gamma_i \equiv 0$, which is shown in Ref. [47] to appropriately describe the particle dynamics in a static trap, i.e., for $v = 0$. For $v > 0$, instead, one can rationalize the experimental data by considering one or more additional relaxation timescales $\tau_i > \tau$, weighted as in Eq. (D.76) by some suitable coefficients $\gamma_i < 0$. It actually turns out that an increasing number of pairs (γ_i, τ_i) is needed for fitting the experimental data upon increasing the dragging velocity v, hence the Weissenberg number [316].

Integrating by parts the second term on the l.h.s. of Eq. (D.74) and introducing $\mathcal{M}(t) \equiv \int_t^\infty \mathrm{d}u\, \mathcal{K}(u)$, one can cast Eq. (D.74) in the form

$$\int_\infty^t \mathrm{d}u\, \mathcal{M}(t \quad u)\ddot{X}(u) = \quad \gamma_0 \dot{X}(t) \quad \kappa X(t) + f^{(\mathbf{v})}(t)\,. \tag{D.77}$$

At long times, the l.h.s. may be further approximated as

$$\begin{aligned}\int_\infty^t \mathrm{d}u_0\, \mathcal{M}(t \quad u_0)\ddot{X}(u_0) &= \int_0^\infty \mathrm{d}u\, \mathcal{M}(u) \left[\ddot{X}(t) \quad u\frac{\mathrm{d}^3X(t)}{\mathrm{d}t^3} + \frac{u^2}{2}\frac{\mathrm{d}^4X(t)}{\mathrm{d}t^4} + \dots \right] \\ &= \hat{\mathcal{M}}(0)\ddot{X}(t) + \hat{\mathcal{M}}'(0)\frac{\mathrm{d}^3X(t)}{\mathrm{d}t^3} + \frac{1}{2}\hat{\mathcal{M}}''(0)\frac{\mathrm{d}^4X(t)}{\mathrm{d}t^4} + \dots \end{aligned} \tag{D.78}$$

where

$$\hat{\mathcal{M}}(s) = [\hat{\mathcal{K}}(s) \quad \hat{\mathcal{K}}(0)]/s \tag{D.79}$$

denotes as usual the Laplace transform of $\mathcal{M}(t)$. By retaining only the first term $\hat{\mathcal{M}}(0)\ddot{X}(t)$ in the expansion of Eq. (D.78), then Eq. (D.77) reduces to that of an underdamped harmonic oscillator with mass

$$m \equiv \hat{\mathcal{M}}(0) = \quad \left(\gamma_0 \quad \gamma_\infty \quad \sum_i \gamma_i \right) \tau \quad \sum_i \gamma_i \tau_i\,. \tag{D.80}$$

One normally finds $m < 0$ when $\gamma_i \equiv 0$ (corresponding to exponentially decaying solutions for $\langle X(t) \rangle$), while an appropriate choice of the coefficients $\gamma_i < 0$ can render $m > 0$, i.e., a bona-fide inertia which may explain the emergence of oscillations within the system. An oscillating behavior of $\langle X(t) \rangle$ with frequency

$$\Omega = \frac{1}{2m}\sqrt{4m\kappa \quad \gamma_0^2} > 0 \tag{D.81}$$

is then expected for $\gamma_0 < 2\sqrt{m\kappa}$.

It is interesting to check if the analogy with a harmonic oscillator holds for our model as well, via the mapping in Eq. (D.75). Considering for instance critical model A (see Section 4.5.2) and using Eqs. (4.58) and (D.79), one formally finds a (zero-frequency) mass

$$m = \hat{\mathcal{M}}(0) = \frac{\lambda^2 \tau_R^2}{8R} \left[\frac{1}{w^3} \quad \frac{2(5+4w)}{(1+2w)^4} \right], \tag{D.82}$$

as a function of the Weissenberg number w (see Eq. (4.57)). This effective mass is plotted in Fig. D.2a and it appears to be always positive, while it increases and diverges upon reducing the value of w towards zero. This behavior can be rationalized by comparing with the dynamical phase diagram in the strong-confinement limit shown in Fig. 4.7b. In fact, we note that $\Omega \simeq 0$ in the latter as soon as the complex poles appear for small values of w and g, after which Ω is a growing function of w (for any value of g). Inverting Eq. (D.81) yields in fact, consistently, $m \sim 1/\Omega^2$ — i.e., heavier objects oscillate more slowly.

It is now tempting to use the condition stated in Eq. (D.81) in order to predict the boundaries within the phase diagram in Fig. 4.7b. In the strong-confinement limit of critical model A, however, the argument outlined above renders a friction coefficient γ_0 in Eq. (D.77) equal to

$$\gamma_0 \to \quad \frac{\lambda^2 \tau_R}{4R} \frac{3+2w}{(1+2w)^3}, \tag{D.83}$$

which is negative for all values of w. Accordingly, this indicates that the approximation used in Eq. (D.80) — corresponding to keeping only the first order term in the expansion for small s in Eq. (D.78) — is no longer accurate in our case. In fact, it turns out that the nontrivial analytic structure of the memory kernel in Eq. (4.58) (see Fig. 4.7) prevents us from simply expanding $\hat{}(s)$ (and hence $\hat{\mathcal{M}}(s)$) in a Taylor series around $s = 0$. In order to check this, one can numerically invert $\hat{X}(s)$ in Eq. (4.43) after replacing $\hat{}(s)$ by its n-th order Taylor expansion: the amplitude of the corresponding approximation to $X(t)$ turns out to diverge upon increasing t (unlike the actual solution, which is expected to be bounded).

In conclusion, contrary to the phenomenological model presented in Ref. [47] — which explains the origin of the observed oscillations in terms of the emergence of an effective harmonic oscillator — the dynamics investigated here does not admit such a simplified explanation. Still, it is interesting to compare the qualitative features of the memory kernels (t) that emerge in these two cases. To be concrete, we consider a field with model A dynamics in $d = 1$ and we choose a Gaussian interaction potential $V_q = \exp\ q^2R^2/2)$, so that the integral in Eq. (4.41) can be computed in closed form, yielding

$$(t) = \frac{\lambda^2 \nu}{4\sqrt{\pi} R\, \tau_R} \frac{1 + t/\tau_R \quad \frac{1}{2}(t/\tau_v)^2}{(1+t/\tau_R)^{5/2}} \exp\left[\frac{t}{\tau_\xi} \quad \frac{(t/\tau_v)^2}{4(1+t/\tau_R)} \right]. \tag{D.84}$$

We note that this function, which is positive for $t = 0$, becomes negative upon increasing t and, for $t \to \infty$, it approaches zero from below, provided that the dragging speed v does not vanish (hence $\tau_v < \infty$, see Eq. (4.45)).

The kernel (t) in Eq. (D.84) is plotted in Fig. D.2b, where we compare it to the one of Ref. [47]. The latter, which encodes the interaction with the viscoelastic fluid, can be readily

obtained by combining Eqs. (D.75) and (D.76). As we show in Fig. D.2b, choices of the values of the parameters γ_i and τ_i exist such that this second (t) also becomes negative for sufficiently large t. In particular, in Fig. D.2b we used two timescales τ_i, with $i \in \{1, 2\}$, as reported in Tab. 1 of Ref. [47] for Wi = 0.17. We thus conclude that, in both models, the memory kernel (t) features *anti*-correlations at long times. This is reminiscent of the *negative memory* often found in the context of rheology of complex fluids [317–321], and suggests that the underdamped modes displayed by the particle are indeed due to the negative response of the surrounding non-equilibrium environment [47], independently of its actual physical origin (i.e., due to either correlations or viscoelasticity).

E

Calculations of Chapter 5

E.1 Lyapunov route to the *super adiabatic* approximation

In the reactive case, one can obtain the $O(\chi^0)$ part of the effective Fokker-Planck equation for the tracer particle, Eq. (5.53), without invoking the quasi-equilibrium distribution as done in Section 5.3.1, but instead directly from the adiabatic elimination equations (5.46) derived in Section 5.3. We start from Eq. (5.46b), which gives to lowest order in χ

$$B_{nm} q_m^{(1)} = s_n Q^{(0)} \quad \Longrightarrow \quad q_n^{(1)} = Q^{(0)} B^{-1}_{nm} s_m = Q^{(0)} \, {}^{1}_{nm}\tau_m, \tag{E.1}$$

where the very last step holds in the reactive case with $\zeta = 1$ — see Eqs. (5.39) and (5.44). Next, from Eq. (5.46c) we infer

$$B_{nj} q_{jm}^{(2)} + B_{mj} q_{jn}^{(2)} = s_n q_m^{(1)} + s_m q_n^{(1)} + 2L_n \delta_{nm} Q^{(0)}, \tag{E.2}$$

where in general the matrix B_{nj} is non-diagonal because of the $O(c)$ terms (see its definition in Eq. (5.40)). We recognize in Eq. (E.2) a matrix Lyapunov equation in the form

$$B\mathcal{M} + \mathcal{M}B^T = C, \tag{E.3}$$

with $\mathcal{M}_{ij} = q_{ij}^{(2)}$, and we need to search for a symmetric solution $\mathcal{M} = \mathcal{M}^T$. Such a solution is unique whenever the whole spectrum of the matrix B has a definite sign [183]. Under this symmetry assumption (which will be checked below), we rewrite Eq. (E.3) as

$$B\mathcal{M} + (B\mathcal{M})^T = C. \tag{E.4}$$

Since C is a symmetric matrix in our case, we deduce that the solution should read

$$B\mathcal{M} = \frac{1}{2} C + \mathcal{A}, \tag{E.5}$$

where $\mathcal{A}$ is an anti-symmetric matrix. Choosing $\mathcal{A} = 0$, we obtain

$$\mathcal{M} = \frac{1}{2} B^{-1} C, \tag{E.6}$$

which indeed is a symmetric matrix owing to the non-trivial property $CB^T = BC$, which holds in our case. We thus identify Eq. (E.6) as the solution we are searching for. This coincides with $q_{ij}^{(2)}$ given in Eq. (5.52), but we did not have to resort to Wick's theorem in order to obtain it. In particular, it holds true also for $T_x \neq T_\phi$, in which case the one in Eq. (5.19) is *not* the correct stationary distribution.

Now we turn to the spectrum of the matrix B. From the theorems on the Sylvester equation [183], it is sufficient to prove that the matrices B and $\quad B$ have no common eigenvalues in order for the matrix equation (E.2) to admit a unique symmetric solution $\mathcal{M}_{ij}$. For $c = 0$ this is trivially true, while for $c \neq 0$ one can give an argument akin to the non-crossing rule in condensed matter physics [322]: indeed, the perturbation c_{ij} to the matrix B_{ij} is a function of the parameter X — i.e., the tracer position, see Eq. (5.40) — so that any "crossing" between eigenvalues can only be accidental and does not provide additional solutions that are valid for any choice of X.

E.2 Calculations for the passive quadratic case

In the following we consider the quadratic coupling case described in Section 5.3.2.2, providing all the intermediate steps in the derivation.

In this case $s_n = t_n = 0$ in Eq. (5.46), so that we only need the evolution equations for the even moments $Q^{(2n)}$. In particular, Eq. (5.46a) implies that we need to determine the fourth moment $q^{(4)}_{ijnm}$ at the lowest order in χ. However, in the passive case the system does not satisfy detailed balance, and thus the correct stationary distribution is not given by Eq. (5.19) but instead follows by solving the corresponding dynamical equation. Analogously to the approach leading to Eq. (5.46), we can derive

$$\begin{aligned}\partial_t Q^{(4)}_{nmpq} = \quad & \chi^{\ 1}\left[B_{nl}Q^{(4)}_{mpql} + B_{ml}Q^{(4)}_{npql} + B_{pl}Q^{(4)}_{nmql} + B_{ql}Q^{(4)}_{nmpl}\right] + O(\chi^0) \\ + 2\chi^{\ 1}&\left[L_n\delta_{nm}Q^{(2)}_{pq} + L_m\delta_{mp}Q^{(2)}_{np} + L_p\delta_{pq}Q^{(2)}_{nm} + L_q\delta_{qm}Q^{(2)}_{np} + L_n\delta_{np}Q^{(2)}_{mp} + L_n\delta_{nq}Q^{(2)}_{mp}\right].\end{aligned} \tag{E.7}$$

Since $B_{nm} = b_n\delta_{nm}$ is diagonal, from Eqs. (5.46c) and (E.7) we find the $O(\chi^0)$ solutions

$$q^{(2)}_{nm} = \frac{T_\phi}{\beta_n}\delta_{nm}Q^{(0)}, \tag{E.8}$$

$$\begin{aligned}q^{(4)}_{mnpq} &= 2T_\phi\frac{L_n\delta_{nm}q^{(2)}_{pq} + L_m\delta_{mp}q^{(2)}_{nq} + L_p\delta_{pq}q^{(2)}_{nm} + L_q\delta_{qm}q^{(2)}_{np} + L_n\delta_{np}q^{(2)}_{mq} + L_n\delta_{nq}q^{(2)}_{mp}}{L_n\beta_n + L_m\beta_m + L_p\beta_p + L_q\beta_q} \\ &= T_\phi^2\left[\frac{\delta_{nm}\delta_{pq}}{\beta_n\beta_q} + \frac{\delta_{mp}\delta_{nq} + \delta_{mq}\delta_{np}}{\beta_n\beta_m}\right].\end{aligned} \tag{E.9}$$

In order to evaluate Eq. (5.46c) at $O(\chi^0)$, we need to determine $\partial_t q^{(2)}$ using Eqs. (5.46a) and (E.8), which yields

$$\begin{aligned}\tilde{q}^{(2)}_{nm} &= \frac{1}{c\,(b_n + b_m)}\left[\frac{T_\phi^2}{\beta_n}\delta_{nm}\sum_p \partial_X\frac{A_{pp}}{\beta_p}Q^{(0)} + \sum_{pq}\partial_X A_{pq}Q^{(4)}_{nmpq}\right] \\ &= \frac{T_\phi^2}{c\,(b_n + b_m)}\sum_p \partial_X\left[\frac{A_{pn}\delta_{mp}}{\beta_p\beta_n} + \frac{A_{pm}\delta_{np}}{\beta_p\beta_m}\right]Q^{(0)}.\end{aligned} \tag{E.10}$$

Finally, inserting Eqs. (E.8) and (E.10) into Eq. (5.46a) renders the effective Fokker-Planck equation reported in Eq. (5.71).

E.3 Comparison with previous results in the bulk

In this Appendix we check the consistency of our results with the effective particle dynamics derived in Refs. [29–31] for the same model that we described in Section 5.1, but in the absence of confinement, i.e., in the *bulk* limit. Throughout the main text, we have assumed that the OP field satisfies either Neumann or Dirichlet boundary conditions (see Section 5.1), while we did not address explicitly the case of periodic BCs. In fact, this case is arguably less interesting than the other two, since the effective drift and diffusion coefficients $\mu(X)$, $D(X)$ of the particle become X-independent at leading order in the adiabatic expansion (see Ref. [64]). Moreover, the case of PBCs can often be addressed by starting from the results for Neumann and Dirichlet BCs, as we will detail below.

Attempting to recover the bulk limit of the coefficients $\mu(X)$, $D(X)$ by simply sending $L \to \infty$ in the final expressions corresponding to Neumann/Dirichlet BCs would render, in general, a wrong result. Heuristically, this is because only *half* of the modes of the OP field present in a bulk system are retained when dealing with Neumann/Dirichlet BCs. Indeed, a periodic function $f(\ )$ on the interval $[\ \ L, L]$ admits the expansion

$$f(\ ) = \frac{1}{\sqrt{L}}\left[\frac{a_0}{2} + \sum_{n=1}^{\infty}\left(a_n \cos\frac{n\pi}{L} + b_n \sin\frac{n\pi}{L}\right)\right], \tag{E.11}$$

where the Fourier coefficients are given as usual by

$$a_n = \frac{1}{\sqrt{L}}\int_{L}^{L} \mathrm{d}\ \ f(\ )\cos\frac{n\pi}{L}, \qquad b_n = \frac{1}{\sqrt{L}}\int_{L}^{L} \mathrm{d}\ \ f(\ )\sin\frac{n\pi}{L}. \tag{E.12}$$

Equation (E.11) essentially contains a sum of Neumann and Dirichlet eigenmodes, as we can write, using Eq. (5.31):

$$f(\ ) = \frac{1}{\sqrt{2}}\left[\sum_{n=0}^{\infty} a_n \sigma_n^{(\mathrm{N})}(\ ) + \sum_{n=1}^{\infty} b_n \sigma_n^{(\mathrm{D})}(\ )\right] \equiv \sum_{n=\ \ \infty}^{\infty} c_n \sigma_n^{(\mathrm{P})}(\ ), \tag{E.13}$$

where $\sigma_n^{(\mathrm{P})}(\ )$ was introduced in Eq. (5.34), while

$$c_n \equiv \begin{cases} a_{\ n}, & n = 0,\ \ 1,\ \ 2, \dots \\ b_n, & n = 1, 2, 3, \dots \end{cases} \tag{E.14}$$

We then turn to the comparison with previous bulk results by starting with the linearly coupled case. The effective particle dynamics has been obtained in the adiabatic limit in Ref. [30] in the form of a Langevin equation. While the associated bulk drift term has been found to vanish, $\mu_b(X) = 0$, the diffusion coefficient $D_b(X)$ takes a nontrivial form as reported in Eqs. (22) and (23) therein. Upon expressing $D_b(X) = T\quad \chi T M_b(X)$ as we did in Eq. (5.58), and by calling $\chi \equiv \kappa/\kappa_\phi$ the adiabaticity parameter (i.e., the ratio of the particle/field mobilities in the notation of Ref. [30]), the bulk result reads

$$M_b(X) = (2\zeta\quad 1)\frac{h^2}{d}\int \frac{d^d q}{(2\pi)^d}\frac{q^2\tilde{\mathcal{K}}_1^2(q)}{\tilde{\Delta}(q)\tilde{\Lambda}(q)} \tag{E.15}$$

up to $O(\chi)$. This is valid in any dimension d, and the tilde stands for the Fourier transform of the operators introduced in Section 5.1. Since $\zeta = 0/1$ for a passive/reactive tracer respectively, the correction to the diffusion coefficient is the same in these two cases, but with the opposite sign (in particular, diffusion is enhanced in the passive case and hindered in the reactive case). Note that the same result, Eq. (E.15), can be recovered by taking the *adiabatic* limit $\kappa_\phi \gg \kappa$ in Eq. (43) of Ref. [29].

Comparing these with our results, we note the following points:

- The correction to the diffusion coefficient $M_b(X)$ in Eq. (E.15) reduces, for $d = 1$, to $M(X)$ given in Eq. (5.59) for a reactive tracer, provided that in the latter one replaces the term $[\partial_X v_n(X)]^2$ by $|\partial_X v_n(X)|^2$, and chooses plane waves $\sigma_n(\ ) = \exp(\mathrm{i}k_n\ )/\sqrt{2L}$, with $k_n = \pi n/L$, $n \in \mathbb{Z}$, as the eigenbasis. In this way, the X-dependence evidently drops out of the integral over q. [Note, however, that this prescription is equivalent to choosing real periodic eigenfunctions as in Eq. (5.34)]. The equivalence between the two expressions in Eqs. (5.59) and (E.15) can then be recognized by replacing the Fourier transforms of the operators $\Delta, \Lambda, \mathcal{K}_1$ introduced in Section 5.1 by their corresponding Fourier coefficients β_n, L_n and v_n [see Section 5.2.1], and the integral by a sum according to $\int_{\mathbb{R}} \mathrm{d}q \to \frac{1}{2L}\sum_{n\in\mathbb{Z}}$. Recall that the same function $M(X)$ controls the diffusion coefficient also in the passive case [see Eq. (5.69)].

- The vanishing bulk drift term $\mu_b(X) = 0$ is consistent with the flattening of the stationary effective potentials and of the diffusion coefficient in the bulk limit, i.e., $V(X), W(X), D(X) \to$ const. for $L \to \infty$. Indeed, the drift coefficient $\mu(X)$ is generally proportional to their derivative with respect to X [see Eqs. (5.53), (5.58), (5.66), (5.69) and (5.72)]. We have already noted in Section 5.3.2.3 that $V(X), W(X)$ defined in Section 5.2.2 must become X-independent in the bulk by translational invariance (this has been checked explicitly in Section 5.4.1 for the off-critical LG model). At the critical point, $V(X)$ and $W(X)$ may reduce in the bulk limit to a structureless, IR diverging constant, which however does not affect their derivatives and thus the drift coefficient.

To be more concrete, let us analyze the case of the Gaussian LG Hamiltonian with model A dynamics addressed in Ref. [30]. In the limit $L \to \infty$, our expression in Eq. (E.33) becomes

$$M_{D/N}(X) \to \frac{h^2}{4}\left[\xi \pm e^{\ 2X/\xi}(\xi \quad 2X)\right], \tag{E.16}$$

where the $\pm$ sign corresponds to Dirichlet/Neumann BCs, respectively. Using Eq. (E.13) together with the definition of $M(X)$ in Eq. (5.59), we can obtain the bulk result as

$$M_b(X) = \frac{1}{2}[M_N(X) + M_D(X)] = \frac{h^2\xi}{4}, \tag{E.17}$$

which coincides with the expression reported in Eq. (37) in Ref. [30] (with $d = 1$ and $m \equiv 1/\xi$).

We remark that, for the LG Hamiltonian with model B dynamics, the adiabatic limit and the bulk limit are incompatible (see also Ref. [81] and Section 2.3). The reason is that in model B a

continuum of slow OP modes builds up at the wavenumber scale $q \sim 1/L$ when approaching the bulk limit, so that the OP field can never be considered *fast* (while in model A even the slowest mode has a finite relaxation time, as long as the correlation length ξ remains finite). This is a direct consequence of the conservation of the OP field in model B dynamics. In our formalism, this translates into the divergence of the effective adiabaticity parameter $\tilde{\chi}$ in Eq. (5.36) in the bulk limit, being $d_\Lambda = \quad 2$ for model B (while $d_\Lambda = 0$ for model A).

Let us finally address the quadratically coupled case. The correction to the diffusion coefficient has been obtained in the bulk under the *weak-coupling* approximation in Ref. [31], see Eq. (66) therein. Its *adiabatic* limit can again be recovered by inspecting the limit for $\kappa_\phi \gg \kappa$, which renders

$$M_b(X) = (2\zeta \quad 1)\frac{h^2}{2d}\int \frac{d^d q\, d^d q}{(2\pi)^{2d}} \frac{(\mathbf{q}+\mathbf{p})^2 \tilde{\mathcal{K}}_2^2(\mathbf{q})\tilde{\mathcal{K}}_2^2(\mathbf{p})}{\tilde{\Delta}(\mathbf{q})\tilde{\Delta}(\mathbf{p})\left[\tilde{\Lambda}(\mathbf{q})\tilde{\Delta}(\mathbf{q}) + \tilde{\Lambda}(\mathbf{p})\tilde{\Delta}(\mathbf{p})\right]}. \tag{E.18}$$

This again compares very well with the correction to the diffusion coefficient presented in Eq. (5.73) for the passive case, upon replacing A_{nm}^2 by $|A_{nm}|^2$ and choosing plane waves for the eigenmodes (while we have shown in Section 5.3.2.3 that the correction in the reactive case reduces in the bulk limit to that of the passive case, up to a minus sign). No explicit forms have been obtained for the diffusion coefficient of specific models in the quadratic case (either in this manuscript or in Ref. [31]), but we have still checked their overall qualitative agreement (see Section 5.4).

E.4 Effective noise in the passive-quadratic case

In the passive case and in the absence of linear couplings or boundary fields, the dynamics of the field modes ϕ_n given in Eq. (5.38) reduces to

$$\partial_t \phi_n = \quad \chi \ ^1 b_n \phi_n + \chi \ ^{1/2}\xi_n, \tag{E.19}$$

where the correlations of ξ_n are given in Eq. (5.42). At long times we thus have

$$\left\langle \phi_n(t)\phi_m(t')\right\rangle = \delta_{nm}\frac{L_n}{b_n} e^{\ b_n|t\ \ t'|/\chi} = \delta_{nm}\frac{T_\phi}{\beta_n} e^{\ b_n|t\ \ t'|/\chi}. \tag{E.20}$$

Similarly, the Langevin equation (5.37) for the passive tracer can be cast in the form

$$\partial_t X(t) = \quad \sum_{nm} A_{nm}(X)\phi_n(t)\phi_m(t) + \eta(t) \equiv \quad \sum_n \varphi_n(X,t) + \eta(t) \equiv \Pi_c(X,t) + \eta(t), \tag{E.21}$$

where following Ref. [64] we introduced the effective noise

$$\Pi_c(X,t) \equiv \quad \sum_n \varphi_n(X,t) \equiv \quad \sum_{nm} A_{nm}(X)\phi_n(t)\phi_m(t). \tag{E.22}$$

Using Wick's theorem, it is simple to show that

$$\langle \varphi_n(t)\rangle = A_{nm}(X)\frac{T_\phi}{\beta_n}, \tag{E.23}$$

$$\langle \varphi_n(t)\varphi_k(t')\rangle_c = A_{nk}A_{kn}\frac{T_\phi^2}{\beta_n\beta_k} e^{\ (b_n+b_k)|t\ \ t'|/\chi} + \delta_{nk}\frac{T_\phi^2}{\beta_n}\sum_m \frac{A_{nm}^2}{\beta_m} e^{\ (b_n+b_m)|t\ \ t'|/\chi}, \tag{E.24}$$

whence

$$\langle \Pi_c(X,t)\Pi_c(X,t')\rangle_c = T_\phi^2 \sum_{nm} \frac{A_{nm}^2 + A_{nm}A_{mn}}{\beta_n \beta_m} e^{-(b_n+b_m)|t-t'|/\chi}. \tag{E.25}$$

By comparing the latter with the effective diffusion coefficient $D(X)$ in Eq. (5.72), we finally obtain the Green-Kubo relation in Eq. (5.77).

E.5 Details of the calculation of the stationary potentials

In this Appendix we give further details on the derivations presented in Section 5.4.

Let us start from the LG model, and consider the computation of $V(X)$ in the quadratic case [see Eqs. (5.22) and (5.80)]: if $0 \le x \le \pi$, we can use the relations [281]

$$\sum_{k=1}^{\infty} \frac{\cos^2(kx)}{k^2+a^2} = \frac{a\pi\,\mathrm{csch}(a\pi)\,[\cosh(a\pi)+\cosh(a(\pi-2x))]-2}{4a^2}, \tag{E.26}$$

$$\sum_{k=1}^{\infty} \frac{\sin^2(kx)}{k^2+a^2} = \frac{\pi\,\mathrm{csch}(a\pi)\sinh(a(\pi-x))\sinh(ax)}{2a}, \tag{E.27}$$

and identify $ax \to x/\xi$, $a\pi \to L/\xi$.

Next, whenever the result is still a convergent series, we can compute derivatives as

$$\sum_{k=1}^{\infty} \frac{\cos^2(kx)}{(k^2+a^2)^2} = -\frac{\partial}{\partial(a^2)} \sum_{k=1}^{\infty} \frac{\cos^2(kx)}{k^2+a^2}. \tag{E.28}$$

In this way, we can obtain a closed-form expression for $M(X)$ in the linearly coupled case: specializing Eq. (5.59) to the LG model with linear coupling, one has

$$M(X) = \frac{2h^2}{L} \sum_n \frac{k_n^2\,[\cos/\sin(k_n X)]^2}{(k_n^2+r)^2 k_n}, \tag{E.29}$$

for Dirichlet/Neumann BCs, respectively. For model B ($r=2$), this reduces to the series in Eq. (E.28), yielding Eq. (5.86) in the case of Neumann BCs, and

$$M(X)_{\mathrm{Dir}} = \left[\frac{h\xi e^{L/\xi}}{2(e^{2L/\xi}-1)}\right]^2 \left\{\frac{4}{L}\left[L^2+2\xi^2+LX\cosh\frac{2}{\xi}(L-X)+L(L-X)\cosh\frac{2X}{\xi}\right] + 2\xi\left[\sinh\frac{2}{\xi}(L-X)+\sinh\frac{2X}{\xi}+\sinh\frac{2L}{\xi}-\frac{4\xi}{L}\cosh\frac{2L}{\xi}\right]\right\} \tag{E.30}$$

in the case of Dirichlet BCs (reported here mainly for formal reasons, since model B dynamics with a globally conserved OP field is incompatible with Dirichlet BCs — see Section 5.2.3). For model A ($r=0$), we can add and subtract r at the numerator to write

$$M(X) = \frac{2h^2}{L}\left\{\sum_n \frac{[\cos/\sin(k_n X)]^2}{k_n^2+r} - r\sum_n \frac{[\cos/\sin(k_n X)]^2}{(k_n^2+r)^2}\right\}. \tag{E.31}$$

The first term is identical to Eqs. (E.26) and (E.27), while the second is analogous to model B. The two series reported above in Eqs. (E.26) and (E.27) start from $n = 1$, so the zero mode $n = 0$ has to be added by hand when considering Neumann BCs — see Eq. (5.31b). Overall, this gives

$$\begin{aligned} M(X)_{\rm Dir} &= h^2\xi\left\{\frac{1}{2}\,\mathrm{csch}(L/\xi)\left[\cosh(L/\xi)+\cosh\left(\frac{L\quad 2X}{\xi}\right)\right]\quad\frac{\xi}{L}\right\}\quad\frac{1}{\xi^2}M(X)^{\text{model B}}_{\rm Dir},\\ M(X)_{\rm Neum} &= h^2\xi\,\mathrm{csch}(L/\xi)\sinh(X/\xi)\sinh\left(\frac{L\quad X}{\xi}\right)\quad\frac{1}{\xi^2}M(X)^{\text{model B}}_{\rm Neum}, \end{aligned} \tag{E.32}$$

which simplify to

$$\begin{aligned} M(X)_{\rm Dir} &= \frac{h^2}{8\sinh^2(L/\xi)}\left\{2(X\quad L)\cosh\left(\frac{2X}{\xi}\right)\quad 2X\cosh\left(\frac{2(L\quad X)}{\xi}\right)\quad 2L\right.\\ &\qquad\left.+\,\xi\left[\sinh\left(\frac{2X}{\xi}\right)+\sinh\left(\frac{2L}{\xi}\right)+\sinh\left(\frac{2(L\quad X)}{\xi}\right)\right]\right\},\\ M(X)_{\rm Neum} &= \frac{h^2}{8\sinh^2(L/\xi)}\left\{\quad 2\sinh\left(\frac{L}{\xi}\right)\left[\xi\cosh\left(\frac{L\quad 2X}{\xi}\right)\quad 2X\sinh\left(\frac{L\quad 2X}{\xi}\right)\right]\right.\\ &\qquad\left.+\,4L\sinh^2\left(\frac{X}{\xi}\right)+\xi\sinh\left(\frac{2L}{\xi}\right)\right\}. \end{aligned} \tag{E.33}$$

Finally, in order to compute the part of $W(X)$ proportional to h_1 [see Eqs. (5.84) and (5.87)], we make use of the Werner's formulas and the relation [281]

$$\sum_{k=1}^{\infty}\frac{\cos(kx)}{k^2+a^2}=\frac{\pi\cosh a(\pi\quad x)}{2a\sinh a\pi}\quad\frac{1}{2a^2}. \tag{E.34}$$

For the critical GS model, we make use of the known relation [281]

$$f_{2n}(x)\equiv\sum_{k=1}^{\infty}\frac{\cos kx}{k^{2n}}=\frac{(\quad 1)^n\ \ 1(2\pi)^{2n}}{2(2n)}B_{2n}\left(\frac{x}{2\pi}\right), \tag{E.35}$$

where $B_n(x)$ is the n-th Bernoulli polynomial [281], and $x\in[0,2\pi]$. For instance, one has

$$\begin{aligned} f_4(x) &= \frac{1}{720}(8\pi^4\quad 60\pi^2x^2+60\pi x^3\quad 15x^4),\\ f_6(x) &= \frac{1}{30240}(32\pi^6\quad 168\pi^4x^2+210\pi^2x^4\quad 126\pi x^5+21x^6),\\ f_8(x) &= \frac{1}{1209600}(128\pi^8\quad 640\pi^6x^2+560\pi^4x^4\quad 280\pi^2x^6+120\pi x^7\quad 15x^8). \end{aligned} \tag{E.36}$$

F

Calculations of Chapter 6

F.1 Connection with the May model for ecology

Within the May model for complex ecosystems [196], we can let $\mathbf{P}(t) \in \mathbb{R}^N$ represent N populations, and $\mathbf{n}(t) = \mathbf{P}(t) \quad \mathbf{P}^*$ be the fluctuation with respect to their equilibrium value. The latter is assumed to evolve according to

$$\dot{\mathbf{n}}(t) = \quad H\mathbf{n}(t), \qquad H = A + \sqrt{T}M, \tag{F.1}$$

where A is a diagonal matrix (which coincides with the identity in the original May model), while M is a GOE matrix with limiting eigenvalue spectrum supported in $[\ \ 2, 2]$. This can be mapped on the model described in Section 6.1.1 upon identifying $T \equiv 2\eta$. In the limit $N \to \infty$ the spectrum of M becomes a Wigner semicircle (see Eq. (6.40)); if $p_a(a)$ has a compact support, then the limiting support of H itself will thus be compact. If part of this support falls within the negative semiaxis, then the dynamical system in Eq. (F.1) becomes unstable: this transition is expected to occur for a critical value of $T = T_c$.

Different choices of $p_a(a)$ will in general affect the position of T_c [241]. We could for example choose $p_a(a)$ to be a Wigner semicircle whose left edge is at $a = 1$ (see Fig. 6.3b), which is obtained by setting $\mu = 1 + \sigma$ in Eq. (6.51). With the identification $T = 2\eta$, the limiting spectral distribution of H follows from Eq. (6.54) as

$$\rho_N(\lambda) = \frac{2\sqrt{\sigma^2 + 4T \quad (\lambda \quad 1 \quad \sigma)^2}}{\pi(\sigma^2 + 4T)} \Theta\left(\sigma^2 + 4T \quad (\lambda \quad 1 \quad \sigma)^2\right) + O(1/N)\ . \tag{F.2}$$

The support is in $\lambda \quad \leq \lambda \leq \lambda_+$, where $\lambda_\pm = 1 + \sigma \pm \sqrt{\sigma^2 + 4T}$, so that in the limit $N \to \infty$ a stable-unstable transition is predicted for $T_c = \sigma/2 + 1/4$. For $\sigma \to 0$ we recover the original result of May, $T_c = 1/4$ [196].

F.2 Number of i.i.d. variables in an interval

In this Appendix we revise the standard textbook result for the statistics of the number of eigenvalues in a finite interval, when such eigenvalues behave as independent and identically distributed random variables. This will help clarifying the behavior of the level compressibility $\chi(E)$ in the case of Poisson level statistics.

Given N random variables a_i distributed according to $p_a(a_i)$ (e.g., the eigenvalues of the matrix A in Eq. (6.1)), the number of variables contained in the interval $[\ ,\beta]$ can be written as

$$I_N[\ ,\beta] = \sum_{i=1}^{N} \theta_i, \tag{F.3}$$

where we introduced the indicator function

$$\theta_i \equiv \ _{[\ ,\beta]}(a_i), \qquad \ _{[\ ,\beta]}(x) = \begin{cases} 1 & x \in [\ ,\beta], \\ 0 & x \notin [\ ,\beta]. \end{cases} \tag{F.4}$$

Its cumulant generating function can be constructed by noting that

$$e^{\ sI_N[\ ,\beta]} = \prod_{i=1}^{N} e^{\ s\theta_i} = \prod_{i=1}^{N} [1 + (e^{\ s} \quad 1)\theta_i], \tag{F.5}$$

and then

$$\ln \left\langle e^{\ sI_N[\ ,\beta]} \right\rangle = \sum_{i=1}^{N} \ln \left[1 + (e^{\ s} \quad 1) \int^{\beta} \mathrm{d}a\, p_a(a) \right] = N \ln \left[1 + (e^{\ s} \quad 1) \frac{\langle I_N[\ ,\beta] \rangle}{N} \right]. \tag{F.6}$$

Note that this coincides with the limiting case in Eq. (6.95) of our general result.

By expanding in powers of s the two sides of Eq. (F.6) and comparing with Eqs. (6.60) and (6.64), we can in particular extract the first two cumulants

$$\kappa_1 = \langle I_N[\ ,\beta] \rangle, \qquad \kappa_2 = \langle I_N[\ ,\beta] \rangle \left(1 \quad \frac{\langle I_N[\ ,\beta] \rangle}{N} \right), \tag{F.7}$$

and from Eq. (6.13) we obtain the level compressibility

$$\chi(E) = 1 \quad \frac{\langle I_N[\ E, E] \rangle}{N}. \tag{F.8}$$

We thus generically expect $\chi(E) \sim 1$ for small E, and $\chi(E) \to 0$ for large E.

F.3 Details of the replica calculation of the spectral density

In this Appendix we fill in the missing steps that lead from Eq. (6.22) to Eq. (6.23) in Section 6.2. A replica-based calculation for the pure GOE ensemble can be found in Ref. [49], from which we partially adopt the notation. We start by expressing the average of the replicated partition function as

$$\langle \mathcal{Z}^n(\lambda) \rangle \propto \left\langle \int_{\mathbb{R}^{Nn}} \left(\prod_{=1}^{n} \mathrm{d}\mathbf{r} \ \right) \exp \left[\ \frac{i}{2} \sum_{i,j=1}^{N} \sum_{=1}^{n} r_i \ (\lambda_\varepsilon \delta_{ij} \quad h_{ij}) r_j \ \right] \right\rangle_{A,B}, \tag{F.9}$$

where we indicated by $h_{ij} \equiv a_i \delta_{ij} + J b_{ij}$ the elements of the random matrix $\mathcal{H}$ given in Eq. (6.1), and $J = J(N) \equiv \nu N^{\ \gamma/2}$. The average symbol means

$$\langle \bullet \rangle_{A,B} \equiv \int_{\mathbb{R}^N} \left(\prod_{i \le j}^{N} \mathrm{d}b_{ij} \right) p_B(\{b_{ij}\}) \left(\prod_{i=1}^{N} \int \mathrm{d}a_i\, p_a(a_i) \right) (\bullet), \tag{F.10}$$

where the probability distribution of the elements b_{ij} of the GOE matrix B reads

$$p_B(\{b_{ij}\}) = \prod_{i=1}^{N} \frac{e^{\,b_{ii}^2/2}}{\sqrt{2\pi}} \prod_{i<j} \frac{e^{\,b_{ij}^2}}{\sqrt{\pi}}. \tag{F.11}$$

Here and henceforth, Latin indices run up to N in real space, while Greek indices run up to n in replica space. Computing the Gaussian integrals over b_{ij} gives (up to a numerical constant)

$$\begin{aligned}\langle \mathcal{Z}^n(\lambda)\rangle \propto \int_{\mathbb{R}^{Nn}} \left(\prod_{\alpha=1}^{n} \mathrm{d}\mathbf{r}_\alpha\right) \left\langle \exp\left[\ \frac{i}{2}\sum_{i=1}^{N}\sum_{\alpha=1}^{n}(\lambda_\alpha - a_i) r_{i\alpha}^2\ \right]\right\rangle_A \\ \times \exp\left\{\ \frac{J^2}{4}\left[\frac{1}{2}\sum_{i=1}^{N}\left(\sum_{\alpha=1}^{n} r_{i\alpha}^2\right)^2 + \sum_{i<j}\left(\sum_{\alpha=1}^{n} r_{i\alpha}\, r_{j\alpha}\right)^2\right]\right\},\end{aligned} \tag{F.12}$$

where $\langle \bullet \rangle_A$ indicates the reduced averaged over the entries of A — see Eq. (F.10). The interacting term in the second line can be usually decoupled by means of the Hubbard-Stratonovich transformation [51], which is however ineffective in our case, for a generic choice of $p_a(a)$. We introduce instead the normalized density

$$\mu(\vec{y}) \equiv \frac{1}{N}\sum_{i=1}^{N}\prod_{\alpha=1}^{n} \delta(y_\alpha - r_{i\alpha}), \tag{F.13}$$

where $\vec{y} \in \mathbb{R}^n$ has components $y_\alpha \in \mathbb{R}$, and we insert into Eq. (F.12) the functional integral representation of the identity

$$1 = N^{\dim(\mu)} \int \mathcal{D}\mu\, \mathcal{D}\hat{\mu}\, \exp\left\{\ i\int \mathrm{d}\vec{y}\, \hat{\mu}(\vec{y})\left[N\mu(\vec{y}) - \sum_{i=1}^{N}\prod_{\alpha=1}^{n}\delta(y_\alpha - r_{i\alpha})\right]\right\}. \tag{F.14}$$

Here $\dim(\mu)$ is the dimension of the field μ, which renders the prefactor on the right hand side formally infinite — this will be of no consequence in the following calculation, since this prefactor is λ-independent. Equation (F.14) is useful because it allows us to rewrite

$$\begin{aligned}&\frac{1}{2}\sum_{i=1}^{N}\left(\sum_{\alpha=1}^{n} r_{i\alpha}^2\right)^2 + \sum_{i<j}\left(\sum_{\alpha=1}^{n} r_{i\alpha}\, r_{j\alpha}\right)^2 = \frac{1}{2}\sum_{i,j=1}^{N}\left(\sum_{\alpha=1}^{n} r_{i\alpha}\, r_{j\alpha}\right)^2 \\ &= \frac{N^2}{2}\int \mathrm{d}\vec{y}\,\mathrm{d}\vec{w}\,\mu(\vec{y})\mu(\vec{w})\left(\sum_{\alpha=1}^{n} y_\alpha\, w_\alpha\right)^2 = \frac{N^2}{2}\int \mathrm{d}\vec{y}\,\mathrm{d}\vec{w}\,\mu(\vec{y})\mu(\vec{w})\ (\vec{y}\cdot\vec{w})^2,\end{aligned} \tag{F.15}$$

so that inserting the identity in Eq. (F.14) into Eq. (F.12) leads to

$$\begin{aligned}\langle \mathcal{Z}^n(\lambda)\rangle \propto \int \mathcal{D}\mu\, \mathcal{D}\hat{\mu}\, \exp\left\{\ iN\int \mathrm{d}\vec{y}\,\hat{\mu}(\vec{y})\mu(\vec{y}) - \frac{(JN)^2}{8}\int \mathrm{d}\vec{y}\,\mathrm{d}\vec{w}\,\mu(\vec{y})\mu(\vec{w})\ (\vec{y}\cdot\vec{w})^2\right\} \\ \times \int_{\mathbb{R}^{Nn}}\left(\prod_{\alpha=1}^{n}\mathrm{d}\mathbf{r}_\alpha\right)\left\langle \exp\left[\ \frac{i}{2}\sum_{i=1}^{N}\sum_{\alpha=1}^{n}(\lambda_\alpha - a_i) r_{i\alpha}^2 + i\sum_{i=1}^{N}\int \mathrm{d}\vec{w}\,\hat{\mu}(\vec{w})\prod_{\alpha=1}^{n}\delta(w_\alpha - r_{i\alpha})\right]\right\rangle_A.\end{aligned} \tag{F.16}$$

Staring at Eq. (F.16) for long enough, one realizes that the second line contains N copies of the same integral,

$$\begin{aligned}
&\int_{\mathbb{R}^{Nn}} \left(\prod_{=1}^{n} \mathrm{d}\mathbf{r} \quad \right) \left\langle \exp\left[\quad \frac{i}{2} \sum_{i=1}^{N} \sum_{=1}^{n} (\lambda_\varepsilon \quad a_i) r_i^2 \; + i \sum_{i=1}^{N} \int \mathrm{d}\vec{w}\, \hat{\mu}(\vec{w}) \prod_{=1}^{n} \delta(w \qquad r_i \;) \right] \right\rangle_A \\
&= \left\{ \int_{\mathbb{R}^n} \mathrm{d}\vec{y} \int \mathrm{d}a\, p_a(a) \exp\left[\quad \frac{i}{2} \sum_{=1}^{n} (\lambda_\varepsilon \quad a) y^2 + i \int \mathrm{d}\vec{w}\, \hat{\mu}(\vec{w}) \prod_{=1}^{n} \delta(w \qquad y \;) \right] \right\}^N \\
&= \left\{ \int_{\mathbb{R}^n} \mathrm{d}\vec{y} \int \mathrm{d}a\, p_a(a) \exp\left[\quad \frac{i}{2} (\lambda_\varepsilon \quad a) |\vec{y}|^2 + i \hat{\mu}(\vec{y}) \right] \right\}^N . \qquad \text{(F.17)}
\end{aligned}$$

Note that it was crucial to assume independent entries a_i, so that their distribution in Eq. (F.10) is factorized. Plugging this expression back into Eq. (F.16) allows us to rewrite $\langle \mathcal{Z}^n(\lambda) \rangle$ as reported in Eq. (6.23) of the main text.

F.4 Connection with the Zee formula

In this Appendix we show why Eq. (6.45) is hiddenly the Zee formula. In Ref. [269], the recipe for computing the spectrum $\rho_{1+2}(\lambda)$ of the sum of two random matrices $M_1 + M_2$ is given as follows:

(i) Compute the resolvents (or Green's functions) associated to $\rho_1(\lambda)$ and $\rho_2(\lambda)$, i.e., $\mathcal{G}_1(\ )$ and $\mathcal{G}_2(\ )$.

(ii) Compute their functional inverses $B_1(\ )$ and $B_2(\ )$, or Blue's functions, via $B(\mathcal{G}(\ )) = \quad$.

(iii) Apply the sum rule

$$B_{1+2}(\ ) = B_1(\ ) + B_2(\ ) \quad 1/\ . \qquad \text{(F.18)}$$

(iv) Invert the result back (see Eq. (6.43)) to find

$$B_{1+2}(\ ) \to \mathcal{G}_{1+2}(\ ) \to \rho_{1+2}(\lambda). \qquad \text{(F.19)}$$

Another interesting object is however the R-function, which is simply defined as

$$R(\ ) \equiv B(\ ) \quad 1/\ , \qquad \text{(F.20)}$$

and which is easily seen to satisfy the free-sum rule [49, 268, 323]

$$R_{1+2}(\ ) = R_1(\ ) + R_2(\ ). \qquad \text{(F.21)}$$

It follows that

$$B_1(x) = B_{1+2}(x) \quad R_2(x), \qquad \text{(F.22)}$$

which we can choose to apply in particular on $x = \mathcal{G}_{1+2}(\ )$, yielding by construction

$$B_1(\mathcal{G}_{1+2}(\ )) = \qquad R_2(\mathcal{G}_{1+2}(\ )). \qquad \text{(F.23)}$$

Applying $\mathcal{G}_1$ on both sides finally yields

$$\mathcal{G}_{1+2}(\ \ ) = \mathcal{G}_1(\qquad R_2(\mathcal{G}_{1+2}(\ \ ))). \tag{F.24}$$

The analogy with Eq. (6.45) is readily established once we recall that, if M_2 is a GOE matrix, then its R-function is simply $R_2(\ \ ) = \quad$ [324].

F.5 Details of the replica calculation of the level compressibility

In this Appendix we provide the technical steps for the derivation of the cumulant generating function and the level compressibility presented in Section 6.3. A similar calculation for the pure GOE/GUE ensemble can be found in Ref. [277], while the derivation in the case of the Erdös-Rényi graph and the Anderson model on a random regular graph was reported in Ref. [276].

F.5.1 Functional representation

The target of this Section is to express $Q_{[\ \ ,\beta]}(n_\pm)$ given in Eq. (6.62) within the replica formalism, as we did in Appendix F.3. The first step is to choose a suitable representation for the partition function $\mathcal{Z}(\ \ )$ that appears in Eq. (6.62): indeed, the one we introduced in Eq. (6.21) is only appropriate if $\mathrm{Im}\{\ \ \} < 0$, being the integral not convergent otherwise. If on the contrary $\mathrm{Im}\{\ \ \} > 0$, then one should choose instead

$$\mathcal{Z}_+(\ \ ) \equiv \left(\frac{i}{2\pi}\right)^{N/2} \int_{\mathbb{R}^N} \mathrm{d}\mathbf{r}\, e^{\frac{i}{2}\mathbf{r}^T(\quad \mathcal{H})\mathbf{r}}. \tag{F.25}$$

Since the various prefactors in front of the integral in Eq. (6.21) will cancel out in Eq. (6.62) after we take the analytic continuation to $n_\pm \to \pm is/\pi$, we will not need to keep track of them in the following.

In analogy with the representation in Eq. (F.9), we can still write

$$Q_{[\ \ ,\beta]}(n_\pm) \propto \left\langle \int_{\mathbb{R}^{Nn}} \left(\prod_{\sigma=1}^{n} \mathrm{d}\mathbf{r}_\sigma\right) \exp\left[\ \ \frac{i}{2}\sum_{i,j=1}^{N}\sum_{\sigma=1}^{n} r_{i\sigma}(\Lambda_{\sigma\sigma}\delta_{ij} \quad L_{\sigma\sigma}h_{ij})r_{j\sigma}\right]\right\rangle_{A,B}, \tag{F.26}$$

but now we interpret

$$n = 2(n_+ + n\ \ ), \tag{F.27}$$

because each of the four partition functions in Eq. (6.62) requires its own set of replicas (here labelled by the Greek index σ, to avoid confusion with the left boundary $\quad$ of the interval). We have also replaced the eigenvalue λ_ε by the block matrix $\hat{\Lambda}$, which is defined in Eq. (6.67) together with the block matrix $\hat{L}$. Notice that the elements $^{-}_{\varepsilon} = \quad ^{*}_{\varepsilon}$ of the matrix $\hat{\Lambda}$ follow from the representation in Eq. (F.25).

The same steps that in Appendix F.3 led us to Eq. (6.23) of the main text now give

$$Q_{[\ \ ,\beta]}(n_\pm) \propto \int \mathcal{D}\mu\, \mathcal{D}\hat{\mu}\, \exp\{N\mathcal{S}_{n_\pm}[\mu,\hat{\mu};\hat{\Lambda}]\}, \tag{F.28}$$

with the action

$$\mathcal{S}_{n_\pm}[\mu,\hat{\mu};\hat{\Lambda}] \equiv \quad i\int \mathrm{d}\vec{\tau}\,\mu(\vec{\tau})\hat{\mu}(\vec{\tau}) \quad \frac{\eta}{2}\int \mathrm{d}\vec{\tau}\,\mathrm{d}\vec{\tau}'\,\mu(\vec{\tau})\mu(\vec{\tau}')\left(\vec{\tau}\,\hat{L}\,\vec{\tau}'\right)^2 \\ + \ln\int \mathrm{d}\vec{\tau}\exp\left[\ \frac{i}{2}\vec{\tau}\,\hat{\Lambda}\,\vec{\tau} + i\hat{\mu}(\vec{\tau})\right]\int \mathrm{d}a\,p_a(a)\exp\left(\frac{i}{2}a\vec{\tau}\,\hat{L}\,\vec{\tau}\right). \tag{F.29}$$

This generalizes the action in Eq. (6.24), and the vector $\vec{\tau}\in\mathbb{R}^n$ plays the same role as the vector $\vec{y}$ but in an extended replica space, with n given in Eq. (F.27). By noting that the action in Eq. (F.29) is quadratic in μ, we can evaluate the Gaussian functional integral in $\mathcal{D}\mu$ to obtain

$$Q_{[\ ,\beta]}(n_\pm) \propto \int \mathcal{D}\hat{\mu}\,\exp\{N\mathcal{S}_{n_\pm}[\hat{\mu};\hat{\Lambda}]\}, \tag{F.30}$$

$$\mathcal{S}_{n_\pm}[\hat{\mu};\hat{\Lambda}] \equiv \quad \frac{1}{2\eta}\int \mathrm{d}\vec{\tau}\,\mathrm{d}\vec{\tau}'\,\hat{\mu}(\vec{\tau})M^{\ -1}(\vec{\tau},\vec{\tau}')\hat{\mu}(\vec{\tau}') + \ln\int \mathrm{d}\vec{\tau}\exp\left[\ \frac{i}{2}\vec{\tau}\,\hat{\Lambda}\,\vec{\tau} + i\hat{\mu}(\vec{\tau})\right]\psi_a\left(\ \frac{1}{2}\vec{\tau}\,\hat{L}\,\vec{\tau}\right), \tag{F.31}$$

where $\psi_a(\ )$ was given in Eq. (6.34), and we introduced the function $M(\vec{\tau},\vec{\tau}')$ as in Eq. (6.68). We omitted from Eq. (F.30) a $\hat{\Lambda}$ independent prefactor coming from the Gaussian integration, which will in general depend on n. However, one can check that all the prefactors cancel out smoothly by including the Jacobian of the variable transformations (see later), and after taking the functional integral over the Gaussian fluctuations in Appendix F.5.2. We will thus avoid reporting these prefactors, so as to lighten the notation.

The saddle-point equation follows simply from Eq. (F.31) as

$$\hat{\mu}(\vec{\tau}) = i\eta\frac{\int \mathrm{d}\vec{\tau}'\,M(\vec{\tau},\vec{\tau}')\exp\left[\ \frac{i}{2}\vec{\tau}'\,\hat{\Lambda}\,\vec{\tau}' + i\hat{\mu}(\vec{\tau}')\right]\psi_a\left(\ \frac{1}{2}\vec{\tau}'\,\hat{L}\,\vec{\tau}'\right)}{\int \mathrm{d}\vec{\tau}'\exp\left[\ \frac{i}{2}\vec{\tau}'\,\hat{\Lambda}\,\vec{\tau}' + i\hat{\mu}(\vec{\tau}')\right]\psi_a\left(\ \frac{1}{2}\vec{\tau}'\,\hat{L}\,\vec{\tau}'\right)}, \tag{F.32}$$

which is analogous to Eq. (6.30). In the following, we will look for a rotationally-invariant solution: to this end, it is useful to introduce the new variable $\varphi(\vec{\tau})$ defined via

$$\hat{\mu}(\vec{\tau}) = i\int \mathrm{d}\vec{\tau}'\,M(\vec{\tau},\vec{\tau}')\varphi(\vec{\tau}'). \tag{F.33}$$

Changing variables from $\hat{\mu}$ to φ in Eq. (F.30) leads to the expression reported in Eq. (6.66).

F.5.2 Gaussian fluctuations around the saddle-point

In order to go beyond the saddle-point approximation, we introduce the fluctuation $\phi(\vec{\tau})$ around the saddle-point solution $\varphi_0(\vec{\tau})$ in the form $\varphi(\vec{\tau}) = \varphi_0(\vec{\tau}) + \phi(\vec{\tau})$. Calling for brevity $\mathcal{S}_{n_\pm}[\varphi;\hat{\Lambda}] \equiv \mathcal{S}[\varphi]$, we then have up to $O\ N^{\ -2}$)

$$Q_{[\ ,\beta]}(n_\pm) \propto e^{N\mathcal{S}[\varphi_0]}\int \mathcal{D}(i\phi)\exp\left\{\frac{N}{2}\int \mathrm{d}\vec{\tau}_1\,\mathrm{d}\vec{\tau}_2\,\phi(\vec{\tau}_1)\left.\frac{\delta^2\mathcal{S}[\varphi]}{\delta\varphi(\vec{\tau}_1)\delta\varphi(\vec{\tau}_2)}\right|_{\varphi=\varphi_0}\phi(\vec{\tau}_2)\right\}, \tag{F.34}$$

and one can check that we can express

$$\left.\frac{\delta^2\mathcal{S}[\varphi]}{\delta\varphi(\vec{\tau}_1)\delta\varphi(\vec{\tau}_2)}\right|_{\varphi=\varphi_0} = \frac{1}{\eta}M(\vec{\tau}_1,\vec{\tau}_2)\left[\ (\vec{\tau}_1,\vec{\tau}_2) + T(\vec{\tau}_1,\vec{\tau}_2)\right] \tag{F.35}$$

in terms of the functions M and T given in Eqs. (6.68) and (6.72), respectively. Computing the Gaussian integral in Eq. (F.34) we thus find

$$Q_{[\ \ ,\beta]}(n_\pm) = \exp\left\{N\mathcal{S}[\varphi_0] \quad \frac{1}{2}\ln\det(\ \ + T)\right\} + \mathcal{O}\left(1/N^2\right). \tag{F.36}$$

Expanding the logarithm in series as

$$\ln(1+x) = \sum_{k=1}^{\infty} \frac{(\ \ x)^k}{k}, \tag{F.37}$$

we finally get Eq. (6.71), where the trace and matrix operations are intended over the replica vectors as

$$\mathrm{Tr}\, T = \int \mathrm{d}\vec{\tau}\ T(\vec{\tau},\ \ \vec{\tau}), \qquad T^2(\vec{\tau}_1,\vec{\tau}_2) = \int \mathrm{d}\vec{\tau}\ T(\vec{\tau}_1,\vec{\tau})T(\vec{\tau},\vec{\tau}_2). \tag{F.38}$$

We may try to specialize Eq. (6.71) to the rotationally invariant Ansatz in Eq. (6.75). The fluctuation matrix in Eq. (F.35) becomes

$$T(\vec{\tau}_1,\vec{\tau}_2) = \varphi_0(\vec{\tau}_1)\left[\left(\vec{\tau}_1\,\hat{L}\,\vec{\tau}_2\right)^2 \quad \left(\vec{\tau}_2\,\hat{K}\,\vec{\tau}_2\right)\right], \tag{F.39}$$

and by using Wick's theorem together with Eq. (6.76) we obtain, for instance,

$$\mathrm{Tr}\, T = \int \mathrm{d}\vec{\tau}\, T(\vec{\tau},\vec{\tau}) = \eta\left[\sum_i \left(2K^{(2)}_{ii} \quad K^2_{ii}\right) + \sum_{ij} L_{ii}L_{jj}K^{(2)}_{ij}\right], \tag{F.40}$$

where we introduced the matrix

$$K^{(2)}_{ij} \equiv \int \mathrm{d}a\, p_a(a)\left(\frac{\hat{C}}{1 \quad ia\hat{L}\hat{C}}\right)_{ii}\left(\frac{\hat{C}}{1 \quad ia\hat{L}\hat{C}}\right)_{jj}. \tag{F.41}$$

We recognize in the last expression a generalization of the resolvent (see Eq. (6.42)) that encodes higher order correlations. The next terms $\mathrm{Tr}\, T^k$ with $k > 1$ in the series of Eq. (6.71) will involve some matrices $K^{(k+1)}_{ij}$ with increasingly higher order correlations, which are nontrivial to compute in general. However, it is straightforward to show that $\mathrm{Tr}\, T^k = \mathcal{O}\ \eta^k)$, so that when η is small the series in Eq. (6.71) is dominated by its first few terms. To the best of our efforts, it has not been possible to resum the whole series in Eq. (6.71), as it happens instead in the pure GOE case — see Appendix F.6 and Ref. [277].

F.6 Level compressibility in the pure GOE case

In this Appendix we recover the results of Ref. [277] concerning the level compressibility for a GOE matrix. This allows us to inspect the similarities and the differences with respect to the GRP case analyzed in this manuscript. In Appendix E.3 of Ref. [198] we repeat the derivation of $\chi_{\mathrm{GOE}}(E)$ using more standard techniques in order to address the low-energy region $E \ll \delta_N$ (see Eq. (6.5) and Section 6.3.6).

The pure GOE case can be formally obtained from Eq. (6.1) by letting the distribution $p_a(a)$ of the diagonal elements of the matrix A tend to a delta function, so that $\psi_a(\ ) \to 1$. The calculation then becomes analogous to that reported in Ref. [277], whose main steps we detail here for completeness. By replacing the replica-symmetric Ansatz of Eq. (6.73) into the saddle-point equation (6.69) one first obtains $\mathcal{N} = \eta/Z_\varphi$, where $Z_\varphi = \int \mathrm{d}\vec{\tau}\, \varphi_0(\vec{\tau})$. By using Gaussian integration one can then show that

$$\int \mathrm{d}\vec{\tau}'\, M(\vec{\tau}, \vec{\tau}')\varphi_0(\vec{\tau}') = \eta \vec{\tau}\, \hat{C}\, \vec{\tau}, \tag{F.42}$$

and thus the remaining free parameters in Eq. (6.73) can be determined by solving the set of four self-consistency equations that follow from Eq. (6.69) as

$$\hat{C}^{\ -1} = 2\eta\, \hat{C} + i\, \hat{\Lambda}. \tag{F.43}$$

Note that this can be recovered from Eqs. (6.77) and (6.78) by using the fact that the resolvent corresponding to $p_a(a) = \delta(a)$ is $\mathcal{G}_a(\ ) = 1/\ \ .$

F.6.1 Action and fluctuations around the saddle-point

Both the action and its Gaussian fluctuation matrix T can now be computed in correspondence of the saddle-point solution in Eq. (6.73). By using the definition of the action given in Eq. (6.66) together with the saddle-point equation (6.69) and the property in Eq. (F.42), one deduces

$$\begin{aligned}\mathcal{S}_{n_\pm}[\varphi_0; \hat{\Lambda}] = \frac{\eta}{2}\left[n_+\left(\Delta^2 + \bar{\Delta}_\beta^2\right) + n\ \ \left(\Delta_\beta^2 + \bar{\Delta}^2\right)\right] + \frac{1}{2}(n_+ + n\ )\ln(2\pi) \\ + \frac{1}{2}n_+ \ln\ \Delta\ \ \bar{\Delta}_\beta) + \frac{1}{2}n\ \ \ln\ \Delta_\beta\bar{\Delta}\ \ ).\end{aligned} \tag{F.44}$$

The computation of $\mathrm{Tr}\, T^k$ in Eq. (6.71) requires more work. First, we rewrite in correspondence of the Ansatz in Eq. (6.73)

$$T(\vec{\tau}_1, \vec{\tau}_2) = \varphi_0(\vec{\tau}_1)\left[\left(\vec{\tau}_1\, \hat{L}\, \vec{\tau}_2\right)^2 \quad \left(\vec{\tau}_2\, \hat{C}\, \vec{\tau}_2\right)\right], \tag{F.45}$$

where we have used the definition of the function $M(\vec{\tau}_1, \vec{\tau}_2)$ in Eq. (6.68) and the property in Eq. (F.42). The first few powers of T can then be computed by applying Wick's theorem: by introducing the notation

$$\langle \bullet \rangle_1 \equiv \frac{1}{\eta}\int \mathrm{d}\vec{\tau}_1\, (\bullet)\varphi_0(\vec{\tau}_1), \tag{F.46}$$

we note that $\left\langle \tau_{1i}\tau_{1j}\right\rangle_1 = C_{ij}$, so that more complicated averages can be handled as

$$\left\langle \tau_{1i}\tau_{1j}\tau_{1k}\tau_{1l}\right\rangle_1 = C_{ij}C_{kl} + C_{ik}C_{jl} + C_{il}C_{jk}. \tag{F.47}$$

Upon noting that $\hat{L}^2 = \ \ _n$, one can then prove by induction the relation

$$T^{k+1}(\vec{\tau}_1, \vec{\tau}_2) = (2\eta)^k \varphi_0(\vec{\tau}_1)\left[\left(\vec{\tau}_1\, \hat{L}^{k+1}\, \hat{C}^k\, \vec{\tau}_2\right)^2 \quad \left(\vec{\tau}_2\, \hat{C}^{2k+1}\, \vec{\tau}_2\right)\right]. \tag{F.48}$$

Using Eq. (F.38) now yields

$$\mathrm{Tr}\, T^k = 2^k\ {}^1\eta^k \left[\left(\sum_i L_{ii}^k C_{ii}^k \right)^2 + \sum_i C_{ii}^{2k} \right], \tag{F.49}$$

and inserting the definition of the matrices $\hat{L}$ and $\hat{C}$ given in Eqs. (6.67) and (6.74) gives

$$\mathrm{Tr}\, T^k = 2^k\ {}^1\eta^k \left\{ \left[n_+ \left(\Delta^k + (\ \ \bar{\Delta}_\beta)^k \right) + n\ \ \left(\Delta_\beta^k + (\ \ \bar{\Delta}\ \ )^k \right) \right]^2 + n_+ \left(\Delta^{2k} + \bar{\Delta}_\beta^{2k} \right) + n\ \ \left(\Delta_\beta^{2k} + \bar{\Delta}^{2k} \right) \right\}. \tag{F.50}$$

Taking the limit $n_\pm \to \pm is/\pi$ in Eqs. (F.44) and (F.50) then results in

$$\mathcal{S}_{\pm \frac{is}{\pi}}[\varphi_0; \hat{\Lambda}] = \frac{is}{2\pi} \left[\eta \left(\Delta^2 + \bar{\Delta}_\beta^2 \quad \Delta_\beta^2 \quad \bar{\Delta}^2 \right) + \ln \left(\frac{\Delta\ \ \bar{\Delta}_\beta}{\Delta_\beta \bar{\Delta}} \right) \right], \tag{F.51}$$

$$\mathrm{Tr}\, T^k \Big|_{\varphi=\varphi_0} = 2^k\ {}^1\eta^k \left\{ \frac{is}{\pi} \left(\Delta^{2k} + \bar{\Delta}_\beta^{2k} \quad \Delta_\beta^{2k} \quad \bar{\Delta}^{2k} \right) \quad \frac{s^2}{\pi^2} \left[\Delta^k + (\ \ \bar{\Delta}_\beta)^k \quad \Delta_\beta^k \quad (\ \ \bar{\Delta}\ \ )^k \right]^2 \right\}. \tag{F.52}$$

Comparing with the definitions of the cumulant generating function and the cumulants in Eqs. (6.60) and (6.64), respectively, we can finally identify

$$\begin{aligned} \frac{\kappa_1}{N} &= \frac{i}{2\pi} \left[\eta \left(\Delta^2 + \bar{\Delta}_\beta^2 \quad \Delta_\beta^2 \quad \bar{\Delta}^2 \right) + \ln \left(\frac{\Delta\ \ \bar{\Delta}_\beta}{\Delta_\beta \bar{\Delta}} \right) \right] \quad \frac{i}{4\pi N} \sum_{k=1}^{\infty} \frac{(\ \ 2\eta)^k}{k} \left(\Delta^{2k} + \bar{\Delta}_\beta^{2k} \quad \Delta_\beta^{2k} \quad \bar{\Delta}^{2k} \right), \\ \frac{\kappa_2}{N} &= \frac{i}{2\pi^2 N} \sum_{k=1}^{\infty} \frac{(\ \ 2\eta)^k}{k} \left[\Delta^k + (\ \ \bar{\Delta}_\beta)^k \quad \Delta_\beta^k \quad (\ \ \bar{\Delta}\ \ )^k \right]^2. \end{aligned} \tag{F.53}$$

In the next Section we will specialize these results to the case in which the interval $[\ \ , \beta]$ is symmetric.

F.6.2 Case of a symmetric interval

We consider here the case in which $\ \ = \ \ E$ and $\beta = E$. With this choice, solving Eq. (F.43) gives

$$\Delta \Big|_{a=\ \ E} = \frac{1}{4\eta} \left[\ \ (\varepsilon \quad iE) \pm \sqrt{8\eta + (\varepsilon \quad iE)^2} \right] \equiv r e^{i\theta}, \tag{F.54}$$

where we choose the positive branch of the square root so that $\mathrm{Re}\, \Delta \ \ \geq 0$ for any positive η (recall that $\Delta\ \ $ represents the variance of a Gaussian distribution, see Eq. (6.73)). Similarly, from Eq. (F.43) one finds for the entries of $\hat{C}$ the same symmetries as in Eq. (6.82). The first two cumulants in Eq. (F.53) are then found to yield

$$\frac{\kappa_1}{N} = \frac{x}{\pi} \sin 2\theta + \frac{2\theta}{\pi} + \frac{i}{2\pi N} \ln \left(\frac{1 + x e^{2i\theta}}{1 + x e^{\ \ 2i\theta}} \right), \tag{F.55}$$

$$\frac{\kappa_2}{N} = \frac{1}{\pi^2 N} \ln \left[1 + \left(\frac{2x \sin 2\theta}{1 \quad x^2} \right)^2 \right], \tag{F.56}$$

[1] The angle θ should be compared with θ_L in Ref. [277].

where we called $x \equiv 2\eta r^2$. As a first check, one can easily verify that both $\kappa_1, \kappa_2 \to 0$ in the limit of a vanishing interval $E \to 0$.

By choosing $2\eta = 1$, we obtain in the $N \to \infty$ limit an eigenvalue spectrum distributed within the interval $[-2, 2]$. Sending $\varepsilon \to 0^+$ as prescribed by Eq. (6.60), one can check that $r \to 1$ (hence $x \to 1$), while

$$\theta \underset{\varepsilon \to 0^+}{\to} \theta_0 \equiv \arctan\left(\frac{E}{\sqrt{4 - E^2}}\right) \in \left[-\frac{\pi}{2}, \frac{\pi}{2}\right]. \tag{F.57}$$

This concludes the calculation of κ_1 (see Eq. (F.55)), which includes both the leading order term and its $O(N^0)$ correction (note that the latter is actually real-valued). However, the second cumulant κ_2 is seen to diverge in the limit $\varepsilon \to 0^+$; the problem is addressed in Ref. [277] by introducing a N-dependent regularization of the infinite sum that appears in Eq. (F.53). Nonetheless, we have shown that such infinite sum (and hence κ_2 itself in Eq. (F.56)) does *not* diverge for any finite value of ε. This hints at the well-known fact that the limit $\varepsilon \to 0^+$ and that for $N \to \infty$ in Eq. (6.60) are not interchangeable. It is then useful to expand for small ε

$$x = r^2 \simeq 1 - \frac{2\varepsilon}{\sqrt{4 - E^2}} \qquad \to \qquad \kappa_2 \simeq \frac{2}{\pi^2} \ln\left[\frac{\sqrt{4 - E^2}\sin 2\theta}{2\varepsilon}\right]. \tag{F.58}$$

In order to recover the leading order result $\kappa_2 \sim \ln N$ found in previous literature [325–329], one has to assume some type of functional relation $\varepsilon = \varepsilon(N)$, so that the limit $\varepsilon \to 0^+$ is taken by controlling the product εN [326]. This goes however beyond the scope of the present paper.

F.7 Level compressibility in two exactly solvable cases

In this Appendix we provide analytical expressions for the quantities discussed in Section 6.3.4 and plotted in Fig. 6.4.

F.7.0.1 Cauchy distributed a_i

Let us start from the case in which $p_a(a)$ is the Cauchy distribution, see Eq. (6.46). We set $\mu = 0$, so that the problem remains symmetric around the origin. Using the expression of $\mathcal{G}_a(\ )$ in Eq. (6.50), from Eq. (6.77) we get $\hat{K} = \hat{C}/(1 + \omega\hat{C})$. Solving the self-consistency equation (6.78) then yields

$$\Delta = \Delta\Big|_{=E} = 2\left[\varepsilon - iE - \omega + \sqrt{8\eta + (\varepsilon - iE + \omega)^2}\right]^{-1} \equiv re^{i\theta}, \tag{F.59}$$

where we chose the positive branch of the square root so that $\mathrm{Re}\,\Delta > 0$. After this choice, the constant ε can be safely sent to zero. The resulting cumulant generating function is given in Eq. (6.85), where the averages are taken over the Cauchy distribution in Eq. (6.46), and the coefficient of the term linear in s reads

$$m = \frac{4\eta r^2 \sin\theta\,(r\omega + \cos\theta)}{\pi\left[1 + (r\omega)^2 + 2r\omega\cos\theta\right]^2}. \tag{F.60}$$

F.7.0.2 Wigner distributed a_i

Let us now consider the case in which $p_a(a)$ is the Wigner distribution, see Eq. (6.51). Again we set $\mu = 0$, so that the problem remains symmetric around the origin. Using the expression of $\mathcal{G}_a(\ )$ in Eq. (6.52), the quantity $\hat{K}$ in Eq. (6.77) becomes

$$\hat{K} = \frac{2}{\sigma^2 \hat{C}} \left[1 \quad \sqrt{1 + (\sigma \hat{C})^2} \right]. \tag{F.61}$$

Solving the self-consistency equation (6.78) yields, after choosing the positive branch of the square root so that $\mathrm{Re}\,\Delta \quad > 0$ and letting $\varepsilon \to 0$,

$$\Delta = \Delta \Big|_{\quad = E} = \frac{iE(\sigma^2 + 4\eta) + 4\eta\sqrt{\sigma^2 + 8\eta \quad E^2}}{16\eta^2 + \sigma^2 E^2} \equiv r e^{i\theta}. \tag{F.62}$$

The resulting cumulant generating function is again given in Eq. (6.85), where the averages are taken over the Wigner distribution in Eq. (6.51). The analytical expression of the quantity m in Eq. (6.86) is cumbersome, but it follows readily from Eq. (F.61).

F.8 Scaling function for the Hermitian GRP model

In this Appendix we consider the case in which the matrix B has complex (rather than real) entries, i.e., it belongs to the GUE ensemble. In this case, powerful analytical tools such as the Harish-Chandra-Itzykson-Zuber integral are available [48]. Following the method introduced in Ref. [238], the authors of Ref. [275] demonstrated that the two-level spectral correlation function assumes a universal form in the fractal regime $1 < \gamma < 2$, and for large N. Our aim here is to link their result to the level compressibility $\chi(E)$, and to show that the latter assumes in the fractal regime the *same* universal form as in the real symmetric case (i.e., in the deformed GOE ensemble studied in this manuscript).

Let us begin by defining, as in Ref. [238] (see Eqs. (2.9) and (3.1) therein),

$$C_1(t) \equiv \sum_n e^{it\lambda_n}, \qquad C_2(t,t') \equiv \sum_{n \neq m} e^{it\lambda_m + it'\lambda_n}, \tag{F.63}$$

$$N C(t,t') \equiv \langle C_2(t,t') \rangle \quad \langle C_1(t) \rangle \, \langle C_1(t') \rangle \,, \tag{F.64}$$

where $C(t,t')$ is the *spectral form factor*, and the average is intended over the entries of the matrix $\mathcal{H}$. Inserting the identity in the form of $1 = \int \mathrm{d}\lambda \, \delta(\lambda \quad \lambda_n)$ and using Eq. (6.11), one gets

$$\langle C_1(t) \rangle = N \int \mathrm{d}\lambda \, e^{it\lambda} \, \langle \rho_N(\lambda) \rangle \,, \tag{F.65}$$

$$\langle C_2(t,t') \rangle = N^2 \int \mathrm{d}\lambda \int \mathrm{d}\lambda' \, e^{it\lambda + it'\lambda'} \, \langle \rho_N(\lambda) \rho_N(\lambda') \rangle \quad N \int \mathrm{d}\lambda \, e^{i(t+t')\lambda} \, \langle \rho_N(\lambda) \rangle \,. \tag{F.66}$$

We now introduce the Fourier transform of the spectral form factor

$$\hat{C}(\omega, \omega') \equiv \int \frac{\mathrm{d}t}{2\pi} \int \frac{\mathrm{d}t'}{2\pi} e^{\ i\omega t \ \ i\omega' t'} C(t,t') = N \, \langle \rho_N(\omega) \rho_N(\omega') \rangle_c \quad \langle \rho_N(\omega) \rangle \, \delta(\omega \quad \omega'), \tag{F.67}$$

so that using Eq. (6.12) we can express

$$N \int_E^E d\omega \int_E^E d\omega' \, \hat{C}(\omega, \omega') = \left\langle I_N^2[\ \ E, E] \right\rangle_c \quad \langle I_N[\ \ E, E] \rangle \,. \tag{F.68}$$

Comparing Eqs. (F.67) and (F.68), we deduce that the *non-singular* part of $\hat{C}(\omega, \omega')$ determines the variance of the number of eigenvalues $I_N[\ \ E, E]$ within the interval $[\ \ E, E]$.

The function $C(t, t')$ was computed in Ref. [225] for the Hermitian GRP model with $\left\langle |\mathcal{H}_{i \neq j}|^2 \right\rangle = v^2/(4N^\gamma)$, and it reads[2]

$$C(t, t') = 2\pi p_a(0) \delta(t + t') \left[S\left(\frac{t \quad t'}{2} E_{\rm Th} \right) \quad 1 \right], \tag{F.69}$$

where in the large N limit and for $1 < \gamma < 2$ the function $S(u)$ assumes the simple form

$$S(u) = e^{\ 2\pi\Lambda^2 |u|}. \tag{F.70}$$

We have introduced (as in [225]) the quantities

$$E_{\rm Th} \equiv \delta_N N^{2\ \gamma} = \frac{2E_T}{\pi [v p_a(0)]^2} = \frac{E_T}{\pi \Lambda^2}, \qquad \Lambda \equiv v p_a(0)/\sqrt{2}, \tag{F.71}$$

where $\delta_N \simeq [N p_a(0)]^{\ 1}$ is the mean level spacing (see Section 6.3.6), while $E_T \simeq 2\pi p_a(0) \eta$ is the Thouless energy as we introduced it in Section 6.3.5 (with η given in Eq. (6.3)). It follows that

$$\hat{C}(\omega, \omega') = \frac{p_a(0)}{E_{\rm Th}} \hat{S}\left(\frac{\omega \quad \omega'}{E_{\rm Th}} \right) \quad p_a(0)\, \delta(\omega \quad \omega'), \tag{F.72}$$

where

$$\hat{S}(\omega) = \frac{1}{\pi} \frac{2\pi\Lambda^2}{\omega^2 + (2\pi\Lambda^2)^2} \tag{F.73}$$

is the Fourier transform of $S(u)$ in Eq. (F.70). Using Eq. (F.68), we thus obtain

$$\begin{aligned} \left\langle I_N^2[\ \ E, E] \right\rangle_c &= \frac{N p_a(0)}{E_{\rm Th}} \int_E^E d\omega \int_E^E d\omega' \, \hat{S}\left(\frac{\omega \quad \omega'}{E_{\rm Th}} \right) = \frac{N p_a(0)}{E_{\rm Th}} \int_{2E}^{2E} dx \, (2E \quad |x|) \, \hat{S}\left(\frac{x}{E_{\rm Th}} \right) \\ &= 2NE p_a(0) \cdot \chi_T\left(\frac{E}{\pi \Lambda^2 E_{\rm Th}} \right) = 2NE p_a(0) \cdot \chi_T\left(E/E_T \right), \end{aligned} \tag{F.74}$$

where in the second line we changed variables to $x = (\omega \quad \omega')$, $\quad = (\omega + \omega' + 2E)$, and we integrated out $\quad$, while in the third line we used Eqs. (F.71) and (F.73) and we recognized the scaling function $\chi_T(y)$ given in Eq. (6.108).

The result in Eq. (F.74) should be compared with the one we found in Section 6.3.5 for the real GRP model: using Eq. (6.104) and Section 6.3.5 yields in fact

$$\kappa_2(E) = \left\langle I_N^2[\ \ E, E] \right\rangle_c = 2NE p_a(0) \chi_T\left(E/E_T \right). \tag{F.75}$$

Quite interestingly, the same scaling function χ_T appears both in the deformed GUE and GOE ensembles.

[2] Note that in Ref. [225] this function was instead identified with $C_2(t, t')$ given in Eq. (F.63). A factor of $p_a(0)$ was also missing.